INTERNATIONAL COUNCIL FOR RESEARCH AND INNOVATION
IN BUILDING AND CONSTRUCTION

WORKING COMMISSION W18 - TIMBER STRUCTURES

CIB - W18

Proceedings

Meeting 46

26 -29 August 2013

Vancouver, Canada

Edited by Rainer Görlacher

Timber Scientific Publishing
KIT Holzbau und Baukonstruktionen
Karlsruhe, Germany
2013

Publisher:
Timber Scientific Publishing
KIT Holzbau und Baukonstruktionen
Reinhard-Baumeister-Platz 1
76131 Karlsruhe
Germany
2013

ISSN 1864-1784

Table of Contents

1 List of Participants

AUSTRIA	
A Thiel	Competence Centre holz.bau forschungs gmbh, Graz
U Hübner	Association of the Austrian Wood Industries
G Schickhofer	Institute of Timber Engineering and Wood Technology, Graz
CANADA	
J Barrett	University of British Columbia, Vancouver
Zhiyong Chen	University of New Brunswick
R Foschi	University of British Columbia, Vancouver
T Haukaas	University of British Columbia, Vancouver
F Lam	University of British Columbia, Vancouver
Minghao Li	University of British Columbia, Vancouver
Chun Ni	FPInnovations, Vancouver
M Popovski	FPInnovations, Vancouver
Hyung Suk Lim	University of British Columbia, Vancouver
T Tannert	University of British Columbia, Vancouver
CROATIA	
M Stepinac	Faculty of Civil Engineering, University of Zagreb
DENMARK	
J Munch-Andersen	Danish Timber Information, Lyngby
ESTONIA	
A Just	Tallinn University of Technology
FRANCE	
C Faye	FCBA
F Rouger	FCBA
GERMANY	
S Aicher	MPA University Stuttgart
H J Blaß	Karlsruhe Institute of Technology (KIT)
P Dietsch	Technical University of Munich
M Enders-Comberg	Karlsruhe Institute of Technology (KIT)
M Flaig	Karlsruhe Institute of Technology (KIT)
M Frese	Karlsruhe Institute of Technology (KIT)
R Görlacher	Karlsruhe Institute of Technology (KIT)
U Kuhlmann	University Suttgart
K-U Schober	Mainz University of Applied Sciences
W Seim	University Kassel
J-W van de Kuilen	Technical University of Munich
S Winter	Technical University of Munich

ITALY

A Ceccotti	CNR-IVALSA
M Fragiacomo	University of Sassari, Alghero
R Scotta	University of Padova

JAPAN

K Kobayashi	Shizuoka University
M Yasumura	Shizuoka University

NEW ZEALAND

A H Buchanan	University of Canterbury, Christchurch
W van Beerschoten	University of Canterbury, Christchurch
D Moroder	University of Canterbury, Christchurch
P Quenneville	University of Auckland
F Sarti	University of Canterbury, Christchurch

SWEDEN

J Schmid	SP Wood Technology
E Serrano	Linnéuniversitetet

SWITZERLAND

L Boccadoro	ETH Zurich
G Fink	ETH Zurich
A Frangi	ETH Zürich
R Jockwer	EMPA Dübendorf
P Kobel	ETH Zürich
C Sigrist	Berner Fachhochschule, Biel

THE NETHERLANDS

A J M Leijten	Eindhoven University of Technology

UNITED KINGDOM

R Harris	University of Bath
K K Ranasinghe	TRADA, High Wycombe
T Reynolds	University of Bath
Wen-Shao Chang	University of Bath

USA

T Skaggs	American Plywood Association, Tacoma
B Yeh	American Plywood Association, Tacoma

2 Minutes of the Meeting (by F Lam)

CHAIRMAN'S INTRODUCTION

Prof. Hans Blass welcomed the delegates to the 46th CIB W18 Meeting in Vancouver, Canada. The chair relayed kind greetings from K. Crews who cannot attend this year's meeting. Special greetings were also received from C. Stieda (past Chair of CIB W18). The Chair thanked Frank Lam (UBC) for hosting the 46th CIB W18 meeting. This is the fifth meeting in Canada. The first four meetings in Canada took place in Vancouver (1978), Parkville (1988), Vancouver (1997), and St. Andrews (2007).

There are 23 papers accepted for this meeting. Papers brought directly to the meeting would not be accepted for presentation, discussions, or publication. The same rule applies to papers where none of the authors is present or papers which are not defended by one of the authors. The papers were selected based on the review process for abstracts. The four acceptance criteria are: state of the art; originality; (assumed) content; and relation to codes or standards. Each criterion was judged with a scale of 0 (bad) to 5 (very good) leading to an overall grade. Reviewing was performed by 13 reviewers and a total of 15 submitted abstracts were not accepted.

The presentations are limited to 20 minutes each, allowing time for meaningful discussions after each presentation. The Chair asked the presenters to conclude the presentation with a general proposal or statements concerning impact of the research results on existing or future potential applications and development in codes and standards. R Görlacher will deal with questions regarding the meeting proceedings.

There are 6 topics covered in this meeting: Stresses for solid timber (1), Timber joints and fasteners (9), Laminated members (4), Structural stability (7), Fire (1), and Serviceability (1). Numbers in parentheses are the number of papers presented within each topic.

The participants have the possibility of presenting notes towards the end of the technical session. R Görlacher has brought a list of intended note presentations. Participants intending to present notes that are not on the list should notify R Görlacher accordingly.

Questions regarding the proceedings should be directed towards R. Görlacher. An address list of the participants will be circulated for verification of accuracy.

GENERAL TOPICS

The Chair further discussed the circulated email from the General Secretariat of CIB, W Bakens, concerning newly adopted CIB strategy, membership and fee structure. The new fee system includes a maximum number of free commission memberships per type of CIB member. If a CIB member wants more commission membership, extra payment will be required on top of the annual membership fee. CIB board will not allow non-members of CIB to attend commission meetings except one trial meeting to assess whether or not one wants to obtain a CIB membership. Modes of intervention will be established for noncompliance starting 2014. In the next CIB W18 meeting in Bath, non CIB members will not be accepted to attend the CIB W18 meeting except on a trial meeting basis. Individual membership fee has been decreased to €200 and no fees will need to be paid for the remaining year when one applies after September 2013.

P Quenneville received clarification that membership will be probably checked at the time of abstract submission. R Harris would like to have further discussion on Thursday for the purpose of organization of next year's meeting as this could impact the number of participants. M. Fragiacomo received clarification that in cases of multiple authors all attendants of the meeting need to be CIB members. JW van de Kuilen received clarification that universities may be members and this has been expanded to allow associate members within a University.

Since ISI publications are becoming increasingly important, conference proceedings status is being sought for the CIB W18 proceedings with Thomson Reuters Web of Knowledge. Conference proceedings status is being sought for the CIB W18 proceedings for the past four years with pending decisions. The format of the proceedings needs to be changed with keywords for each paper and a continuous numbering system.

F. Lam welcomed the participants and presented logistic information and organizational matters for the meeting.

3STRESSES FOR SOLID TIMBER

46 - 6 - 1 *Enhanced Design Approach for Reinforced Notched Beams* - **R Jockwer, A Frangi, E Serrano, R Steiger**

Presented by R Jockwer

P Quenneville asked whether it matters where the reinforcing screws are located. R Jockwer responded yes and it is most effective to install them close to the notch corner but limited by the end distance requirements. P. Quenneville asked whether 5 cm distance could create crack problems. R Jockwer responded no.

H. Blass stated that for large notch ratios, it is difficult to get large enough anchorage length because the height of the notched part is so small. R Jockwer agreed. H Blass further commented that axial stiffness values from testing of different types of screws available for technical approval are valid for low anchorage depths. R Jockwer responded that the higher the stiffness the better the behaviour so the matter is valid. H Blass commented that glued on plates may be more appropriate because of the importance of stiffness. R. Jockwer agreed but stated that there could be bond line failures. H Blass commented that the test configuration on the left where the screw is pulled has a shear force component in reality; as the mechanism of load transfer is different and higher stiffness may result in real applications. R. Jockwer agreed and stated that there are always combined stresses in both directions.

S. Winter received confirmation that the test specimen on the right side is three pieces jointed together with Teflon sheets installed in between to reduce friction.

A Buchanan asked when predrill is needed and if the screws would be broken without predrilling. R. Jockwer stated in general predrilling was not needed. However close to end grain one may have a splitting problem. In large diameter thread rods where drill tips were not available predrilling would be needed. H Blass stated that close to end grain one should predrill. He stated that with density of 450 kg/m^3 it should be okay without predrilling. In LVL with density in the range of 600 kg/m^3 one would have problems. A Buchanan agreed.

TIMBER JOINTS AND FASTENERS

46 - 7 - 1 *Comparison of Design Rules for Glued-in rods and Design Rule Proposal for Implementation in European Standards* - **M Stepinac, F Hunger, R Tomasi, E Serrano, V Rajcic, J-W van de Kuilen**

Presented by M Stepinac

A Buchanan congratulated the authors about the work and look forward to additional information in the future.

A Frangi asked whether a unified approach is needed as good technical approval procedures are available. He stated that quality assurance would be the most important factor for glued in rods and engineers should choose a reputable firm for installation of these connectors. M Stepinac stated that technical guidelines would be needed. A Frangi further discussed the importance of quality control and assurance and stated that one might be giving an illusion with a codified approach.

S Aicher stated that glued in rod performance depends on adhesive and quality control. M Stepinac stated clear design rules would also be needed along with good quality control; otherwise one would not be able to consider glued in rods for implementation at an international level and its use would be stuck at a national level only.

H Blass stated one needs technical approval and it should be a combination of technical approval and code provisions.

S Winter stated principal rules given in code and European technical approval would be the correct combination. Also the influence of common understanding of testing details, climate change influence (temperature and relative humidity) would be important issues of study.

S Aicher stated European work group on glued in rod and adhesive is available.

46 - 7 - 2 *In-service Dynamic Stiffness of Dowel-type Connections* - **T Reynolds, R Harris Wen-Shao Chang**

Presented by T Reynolds

A Leijten stated in European standard procedure there is a loop in the loading protocol and asked for clarification. T Reynolds answered that in the standard test method load goes up to 40% and down to 10% on a yield basis. The amplitude is too big compared to, for example, foot fall loading. With large amplitude of movement, too much nonlinearity would lead to lower dynamic stiffness.

J W van de Kuilen stated that the Eurocode 5 approach to estimate initial stiffness was incorrectly applied in this study. Apart from the load range, which was assumed between 0 % and 40 % of the maximum load instead of the correct range between 10 % and 40 %, recovery period between dowel loadings seemed not to be taken into consideration. T Reynolds stated that the frequency of loading is 1 Hz which is similar to wind induced frequency for tall building systems.

F Lam commented that half-hole and full-hole tests would yield different results as the dowel would be allowed to bend in the full hole tests.

A Frangi commented that the load path is different between the compressive and tension tests. T Reynolds stated that in terms of design method it would seem unreasonable to allow different stiffness in tension and compression. The approach taken in this study is pragmatic.

A Ceccotti received confirmation that the dynamic stiffness is five times the value calculated from Eurocode 5. T Reynolds further stated that the initial loading is dominated by the plastic loading of a small region. This was the reason that they believed the finding was significant.

M Fragiacomo asked whether different frequencies were considered. T Reynolds stated that different frequencies of loading were tried and the resulting difference was in the range of 10% to 15%. With large cycles, creep crushing of the contact surface contributed a lot to the initial stiffness.

E Serrano asked whether friction behaviour was included. T Reynolds responded that friction was considered for the distribution of load calculations but did not have strong effects on stiffness.

46 - 7 - 3 *Design Procedure to Determine the Capacity of Timber Connections under Potential Brittle, Mixed and Ductile Failure Modes* - **P Zarnani, P Quenneville**

Presented by P Quenneville

U Kuhlmann asked if the calculations were made based on a measured yield point of steel. She stated that the distinction between different modes of failures would depend on the real yield point of steel. After discussion it was clarified that the yield strength of the steel rivets were checked.

M Fragiacomo asked about the ductility value of the mixed failure mode and asked if some energy dissipation can be expected. P Quenneville answered that the mixed failure mode will be brittle with little energy dissipation.

BJ Yeh asked if one wants to avoid block tear out, could one install the rivets with the fasteners turned 90 degree, i.e., the major axis perpendicular to the wood grain. P Quenneville answered no, this is not recommended and one should use nails if one would want ductile failure mode.

C Sigrist asked about the purpose of the study since small penetration length of nails was considered. It would make more sense and be better to use longer nails. P Quenneville answered that we are researchers so the study was configured to force a particular mode of failure to check the prediction method. He agreed with C Sigrist's comments. The study checked the calculation method with nails even though it might not be the most optimal use of the fasteners.

H Blass commented the rivet yielding shape depicted in some of the figures (slide 17) was incorrect. P Quenneville agreed.

A Li asked and received clarification of how to evaluate the failure mode for different penetration depth of the fasteners.

46 - 7 - 4 *Withdrawal Strength of Self-tapping Screws in Hardwoods* - **U Hübner**

Presented by U Hübner

A Frangi commented about the load duration behaviour and different COV as a function of diameter and asked if there were any physical reasons. U Hübner responded that with larger diameter screws reinforcing specimens against splitting perpendicular to grain was needed and that this was a very complicated failure mechanism with mixture of failure modes. Also it was very difficult to distinguish what governed at which angle. Also tests from Graz and Karlsruhe with screws installed parallel to grain and loaded at 70% of the short-term failure load indicated failure within 1 week. More research is needed.

F Lam commented that installation at less than 30 degree parallel to grain can be risky especially in cyclic moisture conditions.

J Munch Andersen commented that in terms of comparison with code equations it would be better to compare with softwood.

J W van de Kuilen commented that the density of hardwood can range from 100 kg/m³ to 1200 kg/m³ and received clarification of the density of wood studied as 550 kg/m³ to 900 kg/m³ as medium density hardwood from central Europe.

H Blass received confirmation that these screws would be intended for reinforcing hardwood and predrilling diameter would not be larger than the core screw diameter. H Blass stated that high insertion moment/torque can develop in the longer screws.

J W van de Kuilen received confirmation that the density dependency model was used for different wood species. He questioned whether the density model worked for only one species, for example, beech. U Hübner responded that calculation model was developed for European Ash first and adding another species increased COV a little and there was not too much difference between species.

J Munch Andersen received confirmation that the graphs were based on mean values.

46 - 7 - 5 *Wood Splitting Capacity in Timber Connections Loaded Transversely: Riveted Joint Strength for Full and Partial Width Failure Modes* - **P Zarnani, P Quenneville**

Presented by P Quenneville

A Leijten commented that on slide 11 about the test set up the force was high and the span to beam depth was small. He questioned whether some of the applied force could go directly into the supports. P Quenneville clarified about the span and stated that one would need to verify that some of the forces did not go directly into the supports.

JW van de Kuilen received clarification that the LVL was not cross banded and splitting would not happen in cross banded LVL.

F Lam received clarification that the sample size for LVL and glulam was 3 and 5, respectively and COV information was in the paper.

46 - 7 - 6 *Design Approach for the Splitting Failure of Dowel-type Connections Loaded Perpendicular to Grain*- **B Franke, P Quenneville**

Presented by P Quenneville

C Sigrist asked for clarification of how the loads in the dowels were monitored. P Quenneville stated the Plexiglas plate was strain gauged and calibrated, and even though the method was not precise, it gave a good indication. C Sigrist further asked whether optical method could be used. P Quenneville stated yes although the method was considered outdated.

S Aicher commented that the numerical solution depended on fracture energy normalized to available tested material. He asked to what extent these numerical models could be extended to other material. P Quenneville agreed with the comments and was not sure if the models could be extended to other material.

A Leijten commented that in slide 15 two cracks existed. With reference to the test results at Delft he questioned whether it was possible that gaps between the bolt and the bolt hole existed might have an influence on the results. He further questioned the validity of the unit of Ge' being N/mm^2. P Quenneville did not believe the units were wrong but will check and could provide example calculations. S Aicher confirmed the correctness of the units in the paper. A Leijten further commented that the spacing of dowels was increased for scientific interest but in practice one would want to have minimal spacing. P Quenneville responded that the spacing was kept the same in the study and the information was used for model.

A Frangi discussed existing rules for loaded edge distance and in European technical approval database splitting was observed even though the rules were followed. P Quenneville stated that if you have very big bolts one should check carefully as mixed mode of failure could happen.

A Frangi asked if one could have a ductile failure, would the Johansen approach be still correct for this type of connection given the stress variation between bolts. P Quenneville stated that the Johansen approach would be valid as there is redistribution of loads once plasticity was reached in one of the bolts.

C Sigrist discussed the choice of slenderness of dowel which was chosen to check splitting failure mode. He commented that it would not be possible to check the issue of ductile behaviour raised by A Frangi.

46 - 7 - 7 *Beams Loaded Perpendicular to Grain by Connections* - **J C M Schoenmakers, A J M Leijten, A J M Jorissen**

Presented by A Leijten

H Blass asked how would one define a double or triple connection and asked why not every column considered as a connection. He further commented that if spacing was taken as minimum would they not be considered as individual connection. He stated the reason for the question was that one needed to give limit to the results so that they can be applied. A Leijten discussed the capacity would be influenced by distance and they did not do tests by varying spacing. In standards if the spacing is more than 2 times the depth, they can be considered as individual connection.

J W van de Kuilen asked what kind of moisture adjustment factor would one apply? A Leijten stated the same as Eurocode 5. He discussed that as the number of connections increased, the results showed that it was not proportional.

W Seim asked if a minimum height could be used to avoid such an effect. A Leijten stated that higher than 70% of the depth one should see bending failures.

J W van de Kuilen questioned about the influence of growth rings. A Leijten stated that no significant influence was found.

46 - 7 - 8 *Influence of Fasteners in the Compression Area of Timber Members* - **M Enders-Comberg, H J Blaß**

Presented by M Enders-Comberg

P Quenneville asked about the smallest diameter. M Enders-Comberg stated self-tapping screws had 6.5 mm inner thread diameter. P Quenneville asked what would be the case if 2 to 3 mm diameter nails were used. M Enders-Comberg stated they do not know.

S Winter received confirmation that smooth surface normal dowel was used. M Enders-Comberg and S Winter further discussed that glue in rod did not show any influence as stresses can be transferred by the glue and glue can be regarded as local reinforcement.

S Winter received clarification that the glue used was epoxy. S Winter asked what would happen if screws were included in service class 2. M Enders-Comberg stated that there would be less reduction.

G Schickhofer received confirmation about the screw inner thread diameter.

C Sigrist stated that he was not 100% convinced as the study only dealt with defect free wood and standard quality wood would not see this level of reduction. M Enders-Comberg and H Blass showed pictures where the wood considered was a normal standard quality timber.

T Reynolds commented on the issue that a perfectly fitted connection was not possible. M Enders-Comberg stated that contact element was used in the model and its surface was studied.

E Serrano received clarification of local reduction for glued-in threaded rod connection.

K Ranasinghe questioned about the closeness of the fasteners. M Enders-Comberg stated that spacing rules were followed.

J W van de Kuilen received clarification that moisture content influence was done with glulam.

W Seim received an example that this connection can be used in a truss chord. W Seim commented that one should apply this specific example in Eurocode 5. H Blass commented that in practice this has not surfaced as a problem in service class 1 as there is a large buffer in service class 1 for compressive strength. This is not the same for service class 2.

S Aicher made an analogy to reinforced concrete and matrix basis.

A Frangi asked if the same result would be obtained if one considers it as a wood steel wood connection. M Enders-Comberg stated that it was not applicable.

A Buchanan asked if there were also results for tension loaded specimens. M Enders-Comberg stated that yes it was done in Karlsruhe Institute of Technology.

46 - 7 - 9 *Design of Shear Reinforcement for Timber Beams* - **P Dietsch, H Kreuzinger, S Winter**

Presented by P Dietsch

P Dietsch discussed the question whether the thesis covered cases where shear cracks followed a step pattern and did not follow a horizontal line. P Dietsch stated the model could consider such cases however friction could come into play in a step pattern which would not be considered.

M Fragiacomo stated it would be a good idea to pre-stress. P Dietsch stated that pre-stressing could be lost due to creep. M Fragiacomo suggested using a spring to maintain pre-stressing. P Dietsch stated this might not be the best idea.

A Frangi questioned whether minimum stiffness of the screw can be given. P Dietsch stated that a general method was presented without presenting a minimum value. He further discussed results from TU Munich and Karlsruhe Institute of Technology where different connectors were considered and large glued in rods achieved higher stiffness compared to self-tapping wood screws. H Blass commented that stiffness per unit length should be considered. P Dietsch commented that 45 degree inclined screw angle made the best option for shear reinforcement.

F Lam asked about availability of information for stiffness as a function of inclined angle. P Dietsch responded that not much information is available although the Karlsruhe data indicated a trend that the stiffness increased as the angle decreased.

U Kuhlmann stated that rehabilitation of existing structures could be an interesting field of study. P Dietsch agreed and stated there are many practical examples for such applications.

M Fragiacomo asked whether one can achieve full capacity using screws to reinforce a fully cracked beam. P Dietsch stated very close screw spacing would be needed to achieve full capacity.

LAMINATED MEMBERS

46 - 12 - 1 Modelling the Bending Strength of Glued Laminated Timber - Considering the Natural Growth Characteristics of Timber - **G Fink, A Frangi, J Köhler**

Presented by G Fink

M Li asked about the basis for justifying the assumption on tension strength of finger joints. G Fink stated the finger joint was considered as 0.2 KAR. Finger joint strength would be dependent on the strength of the wood as well as the manufacturing process.

E Serrano received clarification that the resolution of FEM was 50 mm and transverse direction was taken as an element. They tried more elements but not much effect.

R Görlacher clarified that in the research performed at Karlsruhe Institute of Technology knot clusters were never divided into two (corrected by the author in the published paper)

R Foschi stated he likes the approach of using model to predict performance since a verified model can be used to study size effect and quality control techniques. In UBC he worked with industry to develop similar models. He asked for clarification how failures were defined and when failed elements were removed to continue the analysis. The majority of failure was defined as first failure.

F Lam commented that since finger joint failure dominated the failure mode it would make sense to obtain experimental data on finger joint strength rather than relying on assumptions.

JW van de Kuilen commented that the laminate E seemed to have low variability. G Fink stated that it seemed to be consistent with other studies.

H Blass stated that model can be used to consider timber from different regions to expand the variability of the resource.

R Harris commented that the model considered only tension failure and did not consider cases where compression failure initiated the failure. G Fink stated that the influence from model of such effect would be small.

A Buchanan agreed the usefulness of the approach but commented that with other species this work would need to start again. G Fink agreed.

46 - 12 - 2 In-Plane Shear Strength of Cross Laminated Timber (CLT): Test Configuration, Quantification and Influencing Parameters - **R Brandner, T Bogensperger, G Schickhofer**

Presented by G Schickhofer

H Blass commented that the interaction of shear and compression perpendicular to grain should be interaction of shear and compression parallel to grain.

BJ Yeh asked how to relate the test results of the inclined test and whether one could use this for beams and header applications. G Schickhofer stated that it was very difficult to get shear failure (in-plane) for CLT. The in-plane shear strength of 5.5 MPa was conservative based on a referenced shear element. BJ Yeh asked if there was volume effect in shear and how one could relate the information to beam results. G Schickhofer stated that this study was very different from the beam situation where other stresses would be present.

C Sigrist asked whether this method could be used for quality control. G Schickhofer stated no and perhaps it could be considered as a later option. The current study was intended to get basic information.

M Fragiacomo and G Schickhofer discussed the existence of different failure modes within the specimens and the results might depend on which mode governed more. Glue area failure happened first and there could be thickness effect.

J Schmid asked about the process of standardization of laminate thickness to 20, 30 and 40 mm. G Schickhofer stated that it would be important for the industry to have standardised laminate thickness. U Hübner added that this ongoing process would take time to arrive at an agreement. It would not be possible to arrive at a change over a very short time.

46 - 12 - 3 *Shear Strength and Shear Stiffness of CLT-beams Loaded in Plane* - **M Flaig, H J Blaß**

Presented by M Flaig

M Fragiacomo asked in which application shear deformation would be important. M Flaig stated that in glulam the shear deformation might be in the range of 3 to 6 %, but in CLT as a beam the shear deformation might be in the range of 10%; therefore, shear component would be more important for CLT used as a beam.

G Schickhofer asked and received clarification about the failure mode of CLT elements. Typical elements were discussed in relationship to the realistic failure modes.

A Buchanan asked about the rolling shear failure and whether it was indeed rolling shear failure. M Flaig stated that torsion shear strength would be higher than that of rolling shear strength and discussed the small area of thickness near the glue interface and stated it was indeed rolling shear failure.

F Lam asked about past work of using CLT as beam by I Bejtka. M Flaig stated that they are aware of the work.

S Aicher received clarification about the low shear modulus slip value in equation 13.

BJ Yeh asked about the influence of gaps, laminate thickness etc. on shear strength and stiffness. M Flaig stated single basic strength value was used in the model without consideration of the gaps and laminate thickness.

M Popovski stated that the FPinnovations results showed that shear strength of beams varied from 2 to 6 MPa. Method was needed to account for the large variations and the method presented could explain the varying test results.

A Aicher asked if edge glued material was used and what k value would one use. M Flaig responded k would be assumed as ∞ resulting in Geff,bsp=Glam; therefore no torsion in between.

46 - 12 - 4 Stiffness of Screw-Reinforced LVL in Compression Perpendicular to the Grain **- C Watson, W van Beerschoten, T Smith, S Pampanin, A H Buchanan**

Presented by A Buchanan

H Blass commented that when they studied this issue, buckling of the screws and push in failure of the screws were observed. Also there were compression perpendicular to grain failures at the tip of the screws. He asked whether the compression failures were observed in this study. A Buchanan responded that this study was about stiffness and did not look into this aspect.

F Lam received confirmation that the tests were under load control.

H Blass asked about the compression perpendicular to strength of LVL. A Buchanan responded ~5 MPa typically. If stress spreading was included, ~ 12 MPa and 8 MPa in blocks.

G Schickhofer received clarification that the material was cross banded. They were 36 mm thick with 12 veneers out of which 2 were in the orthogonal direction. Five pieces were glued together to form the test specimens.

K Ranasinghe asked why three different lengths of screws considered. A Buchanan stated that long screws could hit each other if they were driven in from other sides. Also predrilling up to 300 mm was performed because of splitting issues.

C Sigrist asked if this solution was cheaper than other options. A Buchanan stated that there is no right or wrong answers but this was introduced as one option. When working with steel there could be tolerance issues even though screws are not cheap. In general screws could be commonly available and therefore economical. S Winter stated in Germany for a practical design solution if one could avoid steel and use screw, the solution would be typically 50% cheaper.

E Serrano received confirmation that typical loading until 8 MPa. In some cases higher loading was used.

R Harris commented that this would be an intuitive way to carry loads across to the joint. Reinforcement of surface allowed the load to spread through the timber but creep might be important. A Buchanan agreed and they will look into the creep issue.

STRUCTURAL STABILITY

46 - 15 - 1 Experimental Investigations on Seismic Behaviour of Conventional Timber Frame Wall with OSB Sheathing - Proposal of Behaviour Factor **- C Faye, L Le Magorou, P Garcia, J-C Duccini**

Presented by C Faye

M Fragiacomo stated that q of 3 seemed to be very conservative for timber walls and if one moves from wall components to system, higher values of q would be expected. C Faye responded that the results showed OSB has similar q as plywood even though it might be conservative. She agreed that consideration of other building components could lead to higher q.

W Seim stated the results would be helpful. He received clarification that three different typical earthquakes were considered with No. 1 and No. 2 from French zone and No. 3 simulated. He commented that the earthquakes from the French zone might need to be scaled to consider higher level of acceleration. Discussions were taken about comparing results from different earthquakes.

A Ceccotti commented that the study seemed to rely on experiments to estimate q and did not perform analytical work. C Faye stated that FEM models are being developed. A Ceccotti asked how one would reach the PGA near collapse. C Faye stated that FEM models would be needed.

F Lam commented that the statement of no damage was inaccurate as there was permanent deformation. He commented that coupling with model is important for establishing q but the database of shake table test results is very valuable especially for model verification. D Moroder stated that the statement should be no visible damage rather than no damage.

M Li asked whether nail connection tests were performed. C Faye stated that connection tests were performed only on 12 mm OSB.

46 - 15 - 2 *Capacity Seismic Design of X-Lam Wall Systems Based on Connection Mechanical Properties* - **I Gavric, M Fragiacomo, A Ceccotti**

Presented by I Gavric

A Buchanan commented that the principal concern with the approach was that the location where ductility is to take place needs to be identified. He asked whether there was any thought on how to regain strength and stiffness after an earthquake, especially a large earthquake. I Gavric responded that installation of additional energy dissipation elements would be possible and there should not be huge effort to replace elements if damaged.

F Sarti discussed about the rocking mechanism and self centering mechanism of CLT buildings. M Fragiacomo stated that shake table tests of CLT buildings showed no severe damage was concentrated in a few points.

A Buchanan further commented that coupled wall and properly designed joints including corner joints are critical. He received confirmation that in the corner of a building, connections in perpendicular walls could cause uplift of the perpendicular walls.

D Moroder stated that overstrength factor of 1.6 might be too conservative and that there were so many overstrength factors which could result in non-economical designs.

46 - 15 - 3 *An Approach to Derive System Seismic Force Modification Factor for Buildings Containing Different LLRS's* - **Z Chen, C Ni, Y-H Chui, G Doudak, M Mohammad**

Presented by Z Chen

F Lam commented that he was confused by the presentation and asked for clarification of the spring analogy used in the analysis. Z Chen stated that a spring represented hybrid walls which were assumed to undergo the same lateral movements due to rigid diaphragm assumptions. F Lam questioned the generality of the assumption.

A Ceccotti asked for clarification and 3D sketches of the Vancouver buildings studied. They were not available as they were not real buildings but design of buildings that could be used in Vancouver.

C Moroder commented that for frame and wall large forces could be present in diaphragm therefore modeling of the deformability of the diaphragm would be important.

46 - 15 - 4 Connections and Anchoring for Wall and Slab Elements in Seismic Design - **M Schick, T Vogt, W Seim**

Presented by W Seim

M Fragiacomo asked which embedment strength was used in the equation. W Seim stated that experimental mean values were used. M Fragiacomo commented that using the predicted embedment strength might be better because the designers could find the information easier.

A Buchanan commented that a hierarchic failure process was needed to get the desirable failure and this was a rational approach.

I Gavric received clarification that the mean values for metal connections came from experiments.

T Reynolds asked how to define the expected probability of failure. W Seim responded that this would be similar to a safety consideration with the comparison of fractile of demand and resistance and introduction of safety factors.

J Munch Andersen commented that the factor of 1.15 in the Johansen-type equation should not be used for the mean strength. S Seim agreed.

46 - 15 - 5 Analytical Formulation Based on Extensive Numerical Simulations of Behavior Factor q for CLT buildings - **L Pozza, R Scotta, D Trutalli, A Ceccotti, A Polastri**

Presented by R Scotta

M Popovski agreed that using more joints can lead to higher ductility.

46 - 15 - 6 Proposal for the q-factor of Moment Resisting Timber Frames with High Ductility Dowel Connectors - **D Wrzesniak, G Rinaldin, M Fragiacomo, C Amadio**

Presented by M Fragiacomo

H Blass asked how to distinguish between single bay and multiple bay frames as there would be a huge difference in number of connections in the two cases. M Fragiacomo agreed that this could be an issue and will look into it further.

A Ceccotti discussed the issue of calculation of q factor. Two methods were presented in this study based on the definition of ductility. This was the approach he used in the past to find the “intrinsic” value of behaviour factor. Recently based on research of CLT buildings and shake table tests in Tsukuba and Miki, a different way of considering q as a ratio between PGA corresponding to ultimate limit state and PGA given by code seemed to be more rational. Also for designers, a single factor - Ceccotti calls it a “design” q factor - would be better without having to consider the ductility of the structure - that is always difficult to identify in wooden structures, differently from steel structures, for example. This q factor will be code-dependent of course, but this is what designers need. M Fragiacomo responded there were two concerns. For the portal frames the design was governed by snow instead of seismic loads. For a single DOF system, the two approaches will theoretically coincide. In multi-story buildings, he believed the base shear approach would be more appropriate.

A Buchanan raised a code related question as there were research based debates and code based debates. He questioned what the intent was and whether different q would be needed for different systems. He also asked whether similar issues exist for N. America.

M. Fragiacomo stated in Eurocode different q values would be needed for different systems. In Canadian code, R would be a product of several factors like Rd, Ro. Trying to split the q into different factors would involve large approximations. This would not be proposed for Eurocode as one has to consider different materials and systems.

46-15 - 7 Wind Tunnel Tests for Wood Structural Panels Used as Nailable Sheathing - **B Yeh, A Cope, E Keith**

Presented by BJ Yeh

H Blass received confirmation that no foam was used as outer thermal insulation of the building. He commented that if foam was used nails would have to bridge and question whether the nails would then have to carry vertical loads also. BJ Yeh responded that these could be next stages of the research. For example, heavier siding could be considered which might be able to resist higher wind loads. H Blass stated calculation model for laterally loaded dowel-type fasteners with interlayer was available. Also heavier cladding could impose a higher vertical load.

S Winter received clarification that smooth shanked instead of ring shanked nails were used. S Winter stated nailing through OSB normally causes break out on the other side of OSB and discussed possible increase of capacity with other types of fasteners. BJ Yeh agreed that other types of fasteners could achieve higher capacity; however, contractors do not like screw guns and screw shank nails and prefer using normal nail guns.

J Munch Andersen commented that the wind pressure between the inside and outside of the siding would be different and whether such issues were considered. BJ Yeh agreed that this was an interesting point. They have information based on pressure tape but information was not reported here.

A Ceccotti asked how much was the test cost. BJ Yeh responded the test cost ~US$20k for two walls. The project was a collaborative effort, so there was a discount. A Ceccotti asked what height could be reached in the test facility. BJ Yeh responded 18 m ~ 3 stories.

S Aicher asked whether loosening of the nail was considered as a result of reversed cyclic loads. BJ Yeh stated that this issue was considered and therefore rigid siding rather than more flexible vinyl siding was used.

U Hübner commented that dynamic loading on smooth shank nails would be more realistic. BJ Yeh explained that the applied wind load was not constant as turbulences were created and wind direction of 20 degree was found to be most critical.

7 FIRE

46 - 16 - 1 Comparison of the Fire Resistance of Timber Members in Tests and Calculation Models - **J Schmid, M Klippel, A Just, A Frangi**

Presented by J Schmid

S Winter received clarification that the compression side lost most of the strength under fire. This was not their test results but based on backward calculations. It could be the compression side that was governing in bending and it could be more sensitive to steam and moisture transfer. S Winter commented that buckling would be the issue in compression. He questioned the assumed relationship between real strength and stiffness properties. Based on his experience and their test results, d0= 7 mm fitted with the tabulated data more or less. Also in practice there are no damages or collapses in fire if this design process was correctly taken into consideration. J Schmid responded that standard fire is not likely to happen in reality. He further responded that just to say it never happened would not be a good excuse and one should look at the test data.

G Schickhofer and J Schmid discussed the negative value of the zero strength layer indicated that the prediction of material properties might be too variable. J Schmid agreed that the consideration is uncertain and more data is needed. As a next step there would be more work to consider test and analysis of members in compression.

A Buchanan questioned the zero strength layer increased with increase of member size. J Schmid explained that the use of 30% load ratio was connected to failure time. Larger member implies longer time before failure. A Buchanan asked about a slab with large width and stated that there was large variability therefore reliability of performance of timber members in real fire needs to be studied. J Schmid stated we are not there yet.

SERVICEABILITY

46 - 20 - 1 CLT and Floor Vibrations: a Comparison of Design Methods - **A Thiel, S Zimmer, M Augustin, G Schickhofer**

Presented by A Thiel

JW van de Kuilen received clarification that static MOE values instead of dynamic MOE was used.

T Reynolds asked about the relationship between amplitude of vibration and damping and whether this could explain the difference observed from heel drop tests. A Thiel stated in heel drop tests, the person was on the floor and the person also acted as a damper to the system. P Dietsch asked about the difference between sandbag and heel drop tests. A Thiel stated results from Hamm/Richter did consider this issue.

K Ranasinghe questioned the usefulness of standard heel drop tests.

M Fragiacomo suggested the use of dynamic shaker.

H Blass stated this might not be an issue as vibration affects people and people need to be on the floor to be affected.

NOTES

Two technical notes were presented

ANY OTHER BUSINESS

The chair discussed the issue of CIB membership with the new CIB fee system and strategy as it could impact the number of participants in future meetings. This group functioned in the past as an independent group and did not rely on CIB except for the use of its name. There were suggestions from participants during the last few days that the group could leave CIB and form its own group. The chair sought comments and suggestions from meeting participants.

J Schmid would be interested to find out how many would not be able to joint CIB. P Quenneville questioned what would be the point of joining CIB if there is no advantage or benefit from the CIB membership. H Blass stated that CIB could be considered as a brand name.

S Winter asked whether CIB membership will help to get proceedings rated. H Blass stated that this is an independent issue. Rating of the proceedings for this year is already in an advanced discussion stage. One issue is that these are yearly proceedings. Creating a different group, the proceedings can also be rated. P Quenneville stated the WCTE proceeding have no problems in getting the rating. E Serrano discussed an innovative solution, namely the group rather than individual members becomes a member of CIB. H Blass stated that up to 30 people can participate as a group at a cost of 8000 euro. The math does not add up at individual membership fees of 200 euro. J Munch Andersen stated although the first appearance is for free, industry will need to send people within the CIB rule; they may not support this extra membership cost.

U Kuhlmann suggested changing the heading organization to, for example, IABSE. IABSE can easily form a working group with a specific heading. H Blass questioned whether fees will need to be paid. S Winter stated not likely.

R Harris stated that CIB not allowing non-members to attend meetings is a real issue especially for hosts of meetings. He commented CIB does not organize the meeting and yet it imposes such rules which are difficult to accept. He suggested the group should have its own ID with minimal cost.

BJ Yeh stated that this would not be an issue for APA as they have membership already.

E Serrano asked if there would be any advantages from CIB. H Blass stated CIB offered proceedings preparation services which we do not need or use. The service would likely have a cost involved. Also as chair there are other administrative issues associated with CIB which cost time. J Schmid received confirmation that home page and paper would still be available either way.

BJ Yeh asked if this group left CIB, would CIB continue to have CIB W18. H Blass stated that is possible as other people might register.

S Winter stated that we could try to be independent but IABSE is a good option as it is under a well-known organization which could lead to some benefits. R Harris said that as a member of IASBE you get the Structural Engineering International (SEI) journal also.

P Quenneville suggested that we should form our own group. G Schickhofer agreed.

H Blass suggested that he could write an email to the general secretary of CIB with the statement that unless we are allowed to continue as we used to, we will leave CIB. R Harris asked about the next CIB W18 meeting in regards to the new CIB membership and participation rules. H Blass stated we would defer making any decision about forming a new group or joining a new organization until the next CIB W18 meeting and would accept non-members to attend the next CIB W18 meeting.

S Winter stated that IABSE never forced people to join for attendance of meetings. P Dietsch stated that IASBE could give us an avenue to reach out to other materials.

A Frangi stated that the idea to join IABSE is fine but we can be an independent group of international timber engineering experts which has advantages also.

A Ceccotti stated that IABSE journal with impact factor is an advantage.

S Winter stated since we belong to the CIB for 46 years it would be fair to go back to CIB and negotiate with them. If they are not willing to change we will take action. BJ Yeh agreed that the decision can be made next year.

H Blass will inform CIB General Secretariat about the discussion.

A Ceccotti will replace HJ Larsen to take care of the home page of CIB W18.

VENUE AND PROGRAMME FOR NEXT MEETING

The venues for the next series of CIB W18 meetings are noted as Bath 2014, Croatia 2015, Graz 2016 and Asia 2017.

R Harris, K Ranasinghe, and WS Chang presented an invitation to the participants to the 2014 CIB W18 meeting in Bath, UK.

CLOSE

Chairman thanked F Lam and the supporting group for hosting and organizing the excellent meeting.

3 Peer review of papers for the CIB-W18 Proceedings

Experts involved:

Members of the CIB-W18 “Timber Structures” group are a community of experts in the field of timber engineering.

Procedure of peer review

- Submission of manuscripts: all members of the CIB-W18 group attending the meeting receive the manuscripts of the papers at least four weeks before the meeting. Everyone is invited to read and review the manuscripts especially in their respective fields of competence and interest.

- Presentation of the paper during the meeting by the author

- Comments and recommendations of the experts, discussion of the paper

- Comments, discussion and recommendations of the experts are documented in the minutes of the meeting and are printed on the front page of each paper.

- Final acceptance of the paper for the proceedings with
    - no changes
    - minor changes
    - major changes
    - or reject

- Revised papers are to be sent to the editor of the proceedings and the chairman of the CIB-W18 group

- Editor and chairman check, whether the requested changes have been carried out.

4 Current List of CIB W18(A) Papers

Technical papers presented to CIB-W18(A) are identified by a code CIB-W18(A)/a-b-c, where:

a denotes the meeting at which the paper was presented.

1 Princes Risborough, England; March 1973
2 Copenhagen, Denmark; October 1973
3 Delft, Netherlands; June 1974
4 Paris, France; February 1975
5 Karlsruhe, Federal Republic of Germany; October 1975
6 Aalborg, Denmark; June 1976
7 Stockholm, Sweden; February/March 1977
8 Brussels, Belgium; October 1977
9 Perth, Scotland; June 1978
10 Vancouver, Canada; August 1978
11 Vienna, Austria; March 1979
12 Bordeaux, France; October 1979
13 Otaniemi, Finland; June 1980
14 Warsaw, Poland; May 1981
15 Karlsruhe, Federal Republic of Germany; June 1982
16 Lillehammer, Norway; May/June 1983
17 Rapperswil, Switzerland; May 1984
18 Beit Oren, Israel; June 1985
19 Florence, Italy; September 1986
20 Dublin, Ireland; September 1987
21 Parksville, Canada; September 1988
22 Berlin, German Democratic Republic; September 1989
23 Lisbon, Portugal; September 1990
24 Oxford, United Kingdom; September 1991
25 Åhus, Sweden; August 1992
26 Athens, USA; August 1993
27 Sydney, Australia; July 1994
28 Copenhagen, Denmark; April 1995
29 Bordeaux, France; August 1996
30 Vancouver, Canada; August 1997
31 Savonlinna, Finland; August 1998
32 Graz, Austria, August 1999
33 Delft, The Netherlands; August 2000
34 Venice, Italy; August 2001
35 Kyoto, Japan; September 2002
36 Colorado, USA; August 2003
37 Edinburgh, Scotland, August 2004
38 Karlsruhe, Germany, August 2005
39 Florence, Italy, August 2006
40 Bled, Slovenia, August 2007
41 St. Andrews, Canada 2008
42 Dübendorf, Switzerland 2009

43 Nelson, New Zealand 2010
44 Alghero, Italy 2011
45 Växjö,Sweden 2012
46 Vancouver, Canada 2013

b denotes the subject:

1 Limit State Design
2 Timber Columns
3 Symbols
4 Plywood
5 Stress Grading
6 Stresses for Solid Timber
7 Timber Joints and Fasteners
8 Load Sharing
9 Duration of Load
10 Timber Beams
11 Environmental Conditions
12 Laminated Members
13 Particle and Fibre Building Boards
14 Trussed Rafters
15 Structural Stability
16 Fire
17 Statistics and Data Analysis
18 Glued Joints
19 Fracture Mechanics
20 Serviceability
21 Test Methods
100 CIB Timber Code
101 Loading Codes
102 Structural Design Codes
103 International Standards Organisation
104 Joint Committee on Structural Safety
105 CIB Programme, Policy and Meetings
106 International Union of Forestry Research Organisations

c is simply a number given to the papers in the order in which they appear:

Example: CIB-W18/4-102-5 refers to paper 5 on subject 102 presented at the fourth meeting of W18.

Listed below, by subjects, are all papers that have to date been presented to W18. When appropriate some papers are listed under more than one subject heading.

LIMIT STATE DESIGN

1-1-1	Limit State Design - H J Larsen
1-1-2	The Use of Partial Safety Factors in the New Norwegian Design Code for Timber Structures - O Brynildsen
1-1-3	Swedish Code Revision Concerning Timber Structures - B Noren
1-1-4	Working Stresses Report to British Standards Institution Committee BLCP/17/2
6-1-1	On the Application of the Uncertainty Theoretical Methods for the Definition of the Fundamental Concepts of Structural Safety - K Skov and O Ditlevsen
11-1-1	Safety Design of Timber Structures - H J Larsen
18-1-1	Notes on the Development of a UK Limit States Design Code for Timber - A R Fewell and C B Pierce
18-1-2	Eurocode 5, Timber Structures - H J Larsen
19-1-1	Duration of Load Effects and Reliability Based Design (Single Member) - R O Foschi and Z C Yao
21-102-1	Research Activities Towards a New GDR Timber Design Code Based on Limit States Design - W Rug and M Badstube
22-1-1	Reliability-Theoretical Investigation into Timber Components Proposal for a Supplement of the Design Concept - M Badstube, W Rug and R Plessow
23-1-1	Some Remarks about the Safety of Timber Structures - J Kuipers
23-1-2	Reliability of Wood Structural Elements: A Probabilistic Method to Eurocode 5 Calibration - F Rouger, N Lheritier, P Racher and M Fogli
31-1-1	A Limit States Design Approach to Timber Framed Walls - C J Mettem, R Bainbridge and J A Gordon
32 -1-1	Determination of Partial Coefficients and Modification Factors- H J Larsen, S Svensson and S Thelandersson
32 -1-2	Design by Testing of Structural Timber Components - V Enjily and L Whale
33-1-1	Aspects on Reliability Calibration of Safety Factors for Timber Structures – S Svensson and S Thelandersson
33-1-2	Sensitivity studies on the reliability of timber structures – A Ranta-Maunus, M Fonselius, J Kurkela and T Toratti
41-1–1	On the Role of Stiffness Properties for Ultimate Limit State Design of Slender Columns– J Köhler, A Frangi, R Steiger

TIMBER COLUMNS

2-2-1	The Design of Solid Timber Columns - H J Larsen
3-2-1	The Design of Built-Up Timber Columns - H J Larsen
4-2-1	Tests with Centrally Loaded Timber Columns - H J Larsen and S S Pedersen
4-2-2	Lateral-Torsional Buckling of Eccentrically Loaded Timber Columns- B Johansson
5-9-1	Strength of a Wood Column in Combined Compression and Bending with Respect to Creep - B Källsner and B Norén
5-100-1	Design of Solid Timber Columns (First Draft) - H J Larsen
6-100-1	Comments on Document 5-100-1, Design of Solid Timber Columns - H J Larsen and E Theilgaard
6-2-1	Lattice Columns - H J Larsen

6-2-2	A Mathematical Basis for Design Aids for Timber Columns - H J Burgess
6-2-3	Comparison of Larsen and Perry Formulas for Solid Timber Columns- H J Burgess
7-2-1	Lateral Bracing of Timber Struts - J A Simon
8-15-1	Laterally Loaded Timber Columns: Tests and Theory - H J Larsen
17-2-1	Model for Timber Strength under Axial Load and Moment - T Poutanen
18-2-1	Column Design Methods for Timber Engineering - A H Buchanan, K C Johns, B Madsen
19-2-1	Creep Buckling Strength of Timber Beams and Columns - R H Leicester
19-12-2	Strength Model for Glulam Columns - H J Blaß
20-2-1	Lateral Buckling Theory for Rectangular Section Deep Beam-Columns- H J Burgess
20-2-2	Design of Timber Columns - H J Blaß
21-2-1	Format for Buckling Strength - R H Leicester
21-2-2	Beam-Column Formulae for Design Codes - R H Leicester
21-15-1	Rectangular Section Deep Beam - Columns with Continuous Lateral Restraint - H J Burgess
21-15-2	Buckling Modes and Permissible Axial Loads for Continuously Braced Columns - H J Burgess
21-15-3	Simple Approaches for Column Bracing Calculations - H J Burgess
21-15-4	Calculations for Discrete Column Restraints - H J Burgess
22-2-1	Buckling and Reliability Checking of Timber Columns - S Huang, P M Yu and J Y Hong
22-2-2	Proposal for the Design of Compressed Timber Members by Adopting the Second-Order Stress Theory - P Kaiser
30-2-1	Beam-Column Formula for Specific Truss Applications - W Lau, F Lam and J D Barrett
31-2-1	Deformation and Stability of Columns of Viscoelastic Material Wood - P Becker and K Rautenstrauch
34-2-1	Long-Term Experiments with Columns: Results and Possible Consequences on Column Design – W Moorkamp, W Schelling, P Becker, K Rautenstrauch
34-2-2	Proposal for Compressive Member Design Based on Long-Term Simulation Studies – P Becker, K Rautenstrauch
35-2-1	Computer Simulations on the Reliability of Timber Columns Regarding Hygrothermal Effects- R Hartnack, K-U Schober, K Rautenstrauch
36-2-1	The Reliability of Timber Columns Based on Stochastical Principles - K Rautenstrauch, R Hartnack
38-2-1	Long-term Load Bearing of Wooden Columns Influenced by Climate – View on Code - R Hartnack, K Rautenstrauch
45-2-1	Design of Timber Columns Based on 2nd Order Structural Analysis - M Theiler, A Frangi, R Steiger

SYMBOLS

PLYWOOD

STRESS GRADING

STRESSES FOR SOLID TIMBER

7-6-1 Strength and Long-term Behaviour of Lumber and Glued Laminated Timber under Torsion Loads - K Möhler

9-6-1 Classification of Structural Timber - H J Larsen

9-6-2 Code Rules for Tension Perpendicular to Grain - H J Larsen

9-6-3 Tension at an Angle to the Grain - K Möhler

9-6-4 Consideration of Combined Stresses for Lumber and Glued Laminated Timber - K Möhler

11-6-1 Evaluation of Lumber Properties in the United States - W L Galligan and J H Haskell

11-6-2 Stresses Perpendicular to Grain - K Möhler

11-6-3 Consideration of Combined Stresses for Lumber and Glued Laminated Timber (addition to Paper CIB-W18/9-6-4) - K Möhler

12-6-1 Strength Classifications for Timber Engineering Codes - R H Leicester and W G Keating

12-6-2 Strength Classes for British Standard BS 5268 - J R Tory

13-6-1 Strength Classes for the CIB Code - J R Tory

13-6-2 Consideration of Size Effects and Longitudinal Shear Strength for Uncracked Beams - R O Foschi and J D Barrett

13-6-3 Consideration of Shear Strength on End-Cracked Beams - J D Barrett and R O Foschi

15-6-1 Characteristic Strength Values for the ECE Standard for Timber - J G Sunley

16-6-1 Size Factors for Timber Bending and Tension Stresses - A R Fewell

16-6-2 Strength Classes for International Codes - A R Fewell and J G Sunley

17-6-1 The Determination of Grade Stresses from Characteristic Stresses for BS 5268: Part 2 - A R Fewell

17-6-2 The Determination of Softwood Strength Properties for Grades, Strength Classes and Laminated Timber for BS 5268: Part 2 - A R Fewell

18-6-1 Comment on Papers: 18-6-2 and 18-6-3 - R H Leicester

18-6-2 Configuration Factors for the Bending Strength of Timber - R H Leicester

18-6-3 Notes on Sampling Factors for Characteristic Values - R H Leicester

18-6-4 Size Effects in Timber Explained by a Modified Weakest Link Theory- B Madsen and A H Buchanan

18-6-5 Placement and Selection of Growth Defects in Test Specimens - H Riberholt

18-6-6 Partial Safety-Coefficients for the Load-Carrying Capacity of Timber Structures - B Norén and J-0 Nylander

19-6-1 Effect of Age and/or Load on Timber Strength - J Kuipers

19-6-2 Confidence in Estimates of Characteristic Values - R H Leicester

19-6-3 Fracture Toughness of Wood - Mode I - K Wright and M Fonselius

19-6-4 Fracture Toughness of Pine - Mode II - K Wright

19-6-5 Drying Stresses in Round Timber - A Ranta-Maunus

19-6-6 A Dynamic Method for Determining Elastic Properties of Wood - R Görlacher

20-6-1 A Comparative Investigation of the Engineering Properties of "Whitewoods" Imported to Israel from Various Origins - U Korin

20-6-2 Effects of Yield Class, Tree Section, Forest and Size on Strength of Home Grown Sitka Spruce - V Picardo

20-6-3 Determination of Shear Strength and Strength Perpendicular to Grain - H J Larsen

21-6-1 Draft Australian Standard: Methods for Evaluation of Strength and Stiffness of Graded Timber - R H Leicester

21-6-2 The Determination of Characteristic Strength Values for Stress Grades of Structural Timber. Part 1 - A R Fewell and P Glos

21-6-3 Shear Strength in Bending of Timber - U Korin

22-6-1 Size Effects and Property Relationships for Canadian 2-inch Dimension Lumber - J D Barrett and H Griffin

22-6-2 Moisture Content Adjustements for In-Grade Data - J D Barrett and W Lau

22-6-3 A Discussion of Lumber Property Relationships in Eurocode 5 - D W Green and D E Kretschmann

22-6-4 Effect of Wood Preservatives on the Strength Properties of Wood - F Ronai

23-6-1 Timber in Compression Perpendicular to Grain - U Korin

24-6-1 Discussion of the Failure Criterion for Combined Bending and Compression - T A C M van der Put

24-6-3 Effect of Within Member Variability on Bending Strength of Structural Timber - I Czmoch, S Thelandersson and H J Larsen

24-6-4 Protection of Structural Timber Against Fungal Attack Requirements and Testing- K Jaworska, M Rylko and W Nozynski

24-6-5 Derivation of the Characteristic Bending Strength of Solid Timber According to CEN-Document prEN 384 - A J M Leijten

25-6-1 Moment Configuration Factors for Simple Beams- T D G Canisius

25-6-3 Bearing Capacity of Timber - U Korin

25-6-4 On Design Criteria for Tension Perpendicular to Grain - H Petersson

25-6-5 Size Effects in Visually Graded Softwood Structural Lumber - J D Barrett, F Lam and W Lau

26-6-1 Discussion and Proposal of a General Failure Criterion for Wood - T A C M van der Put

27-6-1 Development of the "Critical Bearing": Design Clause in CSA-086.1 - C Lum and E Karacabeyli

27-6-2 Size Effects in Timber: Novelty Never Ends - F Rouger and T Fewell

27-6-3 Comparison of Full-Size Sugi (Cryptomeria japonica D.Don) Structural Performance in Bending of Round Timber, Two Surfaces Sawn Timber and Square Sawn Timber - T Nakai, H Nagao and T Tanaka

28-6-1 Shear Strength of Canadian Softwood Structural Lumber - F Lam, H Yee and J D Barrett

28-6-2 Shear Strength of Douglas Fir Timbers - B Madsen

28-6-3 On the Influence of the Loading Head Profiles on Determined Bending Strength - L Muszyñsky and R Szukala

28-6-4 Effect of Test Standard, Length and Load Configuration on Bending Strength of Structural Timber- T Isaksson and S Thelandersson

28-6-5 Grading Machine Readings and their Use in the Calculation of Moment Configuration Factors - T Canisius, T Isaksson and S Thelandersson

28-6-6 End Conditions for Tension Testing of Solid Timber Perpendicular to Grain - T Canisius

29-6-1 Effect of Size on Tensile Strength of Timber - N Burger and P Glos

29-6-2 Equivalence of In-Grade Testing Standards - R H Leicester, H O Breitinger and H F Fordham

30-6-1 Strength Relationships in Structural Timber Subjected to Bending and Tension - N Burger and P Glos

30-6-2 Characteristic Design Stresses in Tension for Radiata Pine Grown in Canterbury - A Tsehaye, J C F Walker and A H Buchanan

30-6-3 Timber as a Natural Composite: Explanation of Some Peculiarities in the Mechanical Behaviour - E Gehri

31-6-1 Length and Moment Configuration Factors - T Isaksson

31-6-2 Tensile Strength Perpendicular to Grain According to EN 1193 - H J Blaß and M Schmid

31-6-3 Strength of Small Diameter Round Timber - A Ranta-Maunus, U Saarelainen and H Boren

31-6-4 Compression Strength Perpendicular to Grain of Structural Timber and Glulam - L Damkilde, P Hoffmeyer and T N Pedersen

31-6-5 Bearing Strength of Timber Beams - R H Leicester, H Fordham and H Breitinger

32-6-1 Development of High-Resistance Glued Robinia Products and an Attempt to Assign Such Products to the European System of Strength Classes - G Schickhofer and B Obermayr

32-6-2 Length and Load Configuration Effects in the Code Format - T Isaksson

32-6-3 Length Effect on the Tensile Strength of Truss Chord Members - F Lam

32-6-4 Tensile Strength Perpendicular to Grain of Glued Laminated Timber - H J Blaß and M Schmid

32-6-5 On the Reliability-based Strength Adjustment Factors for Timber Design - T D G Canisius

34-6-1 Material Strength Properties for Canadian Species Used in Japanese Post and Beam Construction - J D Barrett, F Lam, S Nakajima

35-6-1 Evaluation of Different Size Effect Models for Tension Perpendicular to Grain Design - S Aicher, G Dill-Langer

35-6-2 Tensile Strength of Glulam Perpendicular to Grain - Effects of Moisture Gradients - J Jönsson, S Thelandersson

36-6-1 Characteristic Shear Strength Values Based on Tests According to EN 1193 - P Glos, J Denzler

37-6-1 Tensile Strength of Nordic Birch - K H Solli

37-6-2 Effect of Test Piece Orientation on Characteristic Bending Strength of Structural Timber - P Glos, J K Denzler

37-6-3 Strength and Stiffness Behaviour of Beech Laminations for High Strength Glulam - P Glos, J K Denzler, P W Linsenmann

37-6-4 A Review of Existing Standards Related to Calculation of Characteristic Values of Timber - F Rouger

37-6-5 Influence of the Rolling-Shear Modulus on the Strength and Stiffness of Structural Bonded Timber Elements - P Fellmoser, H J Blass

38-6-1 Design Specifications for Notched Beams in AS:1720 - R H Leicester

38-6-2 Characteristic Bending Strength of Beech Glulam - H J Blaß, M Frese

38-6-3 Shear Strength of Glued Laminated Timber - H Klapp, H Brüninghoff

39-6-1 Allocation of Central European hardwoods into EN 1912 - P Glos, J K Denzler

39-6-2 Revisiting EN 338 and EN 384 Basics and Procedures - R Steiger, M Arnold, M Fontana

40-6-1 Bearing Strength Perpendicular to the Grain of Locally Loaded Timber Blocks - A J M Leijten, J C M Schoenmakers

40-6-2 Experimental Study of Compression and Shear Strength of Spruce Timber - M Poussa, P Tukiainen, A Ranta-Maunus

40-6-3 Analysis of Tension and Bending strength of Graded Spruce Timber - A Hanhijärvi, A Ranta-Maunus, H Sarkama, M Kohsaku, M Poussa, J Puttonen

41-6-1 Design of Inclined Glulam Members with an End Notch on the Tension Face - A Asiz, I Smith

41-6-2 A New Design Approach for End-notched Beams - View on Code - K Rautenstrauch, B Franke, S Franke, K U Schober

41-6-3 The Design Rules in Eurocode 5 for Compression Perpendicular to the Grain - Continuous Supported Beams - H J Larsen, T A C M van der Put, A J M Leijten

41-6-4 Size Effects in Bending – J K Denzler, P Glos

42-6-1 Variability of Strength of European Spruce - A Ranta-Maunus, J K Denzler

42-6-2 Impact Loaded Structural Timber Elements Made from Swiss Grown Norway Spruce - R Widmann, R Steiger

42-6-3 Modelling the Bending Strength of Timber Components –Implications to Test Standards - J Köhler, M Sandomeer, T Isaksson, B Källsner

43-6-1 The Bearing Strength of Timber Beams on Discrete Supports - A Jorissen, B de Leijer, A Leijten

44-6-1 Impact of Material Properties on the Fracture Mechanics Design Approach for Notched Beams in Eurocode 5 - R Jockwer, R Steiger, A Frangi, J Köhler

44-6-2 Interaction of Shear Stresses and Stresses Perpendicular to the Grain - R Steiger, E Gehri

46-6-1 Enhanced Design Approach for Reinforced Notched Beams - R Jockwer, A Frangi, E Serrano, R Steiger

TIMBER JOINTS AND FASTENERS

1-7-1 Mechanical Fasteners and Fastenings in Timber Structures - E G Stern

4-7-1 Proposal for a Basic Test Method for the Evaluation of Structural Timber Joints with Mechanical Fasteners and Connectors - RILEM 3TT Committee

4-7-2 Test Methods for Wood Fasteners - K Möhler

5-7-1 Influence of Loading Procedure on Strength and Slip-Behaviour in Testing Timber Joints - K Möhler

5-7-2 Recommendations for Testing Methods for Joints with Mechanical Fasteners and Connectors in Load-Bearing Timber Structures - RILEM 3 TT Committee

5-7-3 CIB-Recommendations for the Evaluation of Results of Tests on Joints with Mechanical Fasteners and Connectors used in Load-Bearing Timber Structures - J Kuipers

6-7-1 Recommendations for Testing Methods for Joints with Mechanical Fasteners and Connectors in Load-Bearing Timber Structures (seventh draft) - RILEM 3 TT Committee

6-7-2 Proposal for Testing Integral Nail Plates as Timber Joints - K Möhler

6-7-3 Rules for Evaluation of Values of Strength and Deformation from Test Results - Mechanical Timber Joints - M Johansen, J Kuipers, B Norén

6-7-4 Comments to Rules for Testing Timber Joints and Derivation of Characteristic Values for Rigidity and Strength - B Norén

7-7-1 Testing of Integral Nail Plates as Timber Joints - K Möhler

7-7-2	Long Duration Tests on Timber Joints - J Kuipers
7-7-3	Tests with Mechanically Jointed Beams with a Varying Spacing of Fasteners - K Möhler
7-100-1	CIB-Timber Code Chapter 5.3 Mechanical Fasteners;CIB-Timber Standard 06 and 07 - H J Larsen
9-7-1	Design of Truss Plate Joints - F J Keenan
9-7-2	Staples - K Möhler
11-7-1	A Draft Proposal for International Standard: ISO Document ISO/TC 165N 38E
12-7-1	Load-Carrying Capacity and Deformation Characteristics of Nailed Joints - J Ehlbeck
12-7-2	Design of Bolted Joints - H J Larsen
12-7-3	Design of Joints with Nail Plates - B Norén
13-7-1	Polish Standard BN-80/7159-04: Parts 00-01-02-03-04-05. "Structures from Wood and Wood-based Materials. Methods of Test and Strength Criteria for Joints with Mechanical Fasteners"
13-7-2	Investigation of the Effect of Number of Nails in a Joint on its Load Carrying Ability - W Nozynski
13-7-3	International Acceptance of Manufacture, Marking and Control of Finger-jointed Structural Timber - B Norén
13-7-4	Design of Joints with Nail Plates - Calculation of Slip - B Norén
13-7-5	Design of Joints with Nail Plates - The Heel Joint - B Källsner
13-7-6	Nail Deflection Data for Design - H J Burgess
13-7-7	Test on Bolted Joints - P Vermeyden
13-7-8	Comments to paper CIB-W18/12-7-3 "Design of Joints with Nail Plates"- B Norén
13-7-9	Strength of Finger Joints - H J Larsen
13-100-4	CIB Structural Timber Design Code. Proposal for Section 6.1.5 Nail Plates - N I Bovim
14-7-1	Design of Joints with Nail Plates (second edition) - B Norén
14-7-2	Method of Testing Nails in Wood (second draft, August 1980) - B Norén
14-7-3	Load-Slip Relationship of Nailed Joints - J Ehlbeck and H J Larsen
14-7-4	Wood Failure in Joints with Nail Plates - B Norén
14-7-5	The Effect of Support Eccentricity on the Design of W- and WW-Trussed with Nail Plate Connectors - B Källsner
14-7-6	Derivation of the Allowable Load in Case of Nail Plate Joints Perpendicular to Grain - K Möhler
14-7-7	Comments on CIB-W18/14-7-1 - T A C M van der Put
15-7-1	Final Recommendation TT-1A: Testing Methods for Joints with Mechanical Fasteners in Load-Bearing Timber Structures. Annex A Punched Metal Plate Fasteners - Joint Committee RILEM/CIB-3TT
16-7-1	Load Carrying Capacity of Dowels - E Gehri
16-7-2	Bolted Timber Joints: A Literature Survey - N Harding
16-7-3	Bolted Timber Joints: Practical Aspects of Construction and Design; a Survey - N Harding

22-7-1 End Grain Connections with Laterally Loaded Steel Bolts A draft proposal for design rules in the CIB Code - J Ehlbeck and M Gerold

22-7-2 Determination of Perpendicular-to-Grain Tensile Stresses in Joints with Dowel-Type Fasteners - A draft proposal for design rules - J Ehlbeck, R Görlacher and H Werner

22-7-3 Design of Double-Shear Joints with Non-Metallic Dowels A proposal for a supplement of the design concept - J Ehlbeck and O Eberhart

22-7-4 The Effect of Load on Strength of Timber Joints at high Working Load Level - A J M Leijten

22-7-5 Plasticity Requirements for Portal Frame Corners - R Gunnewijk and A J M Leijten

22-7-6 Background Information on Design of Glulam Rivet Connections in CSA/CAN3-086.1-M89 - A proposal for a supplement of the design concept - E Karacabeyli and D P Janssens

22-7-7 Mechanical Properties of Joints in Glued-Laminated Beams under Reversed Cyclic Loading - M Yasumura

22-7-8 Strength of Glued Lap Timber Joints - P Glos and H Horstmann

22-7-9 Toothed Rings Type Bistyp 075 at the Joints of Fir Wood - J Kerste

22-7-10 Calculation of Joints and Fastenings as Compared with the International State - K Zimmer and K Lissner

22-7-11 Joints on Glued-in Steel Bars Present Relatively New and Progressive Solution in Terms of Timber Structure Design - G N Zubarev, F A Boitemirov and V M Golovina

22-7-12 The Development of Design Codes for Timber Structures made of Compositive Bars with Plate Joints based on Cyclindrical Nails - Y V Piskunov

22-7-13 Designing of Glued Wood Structures Joints on Glued-in Bars - S B Turkovsky

23-7-1 Proposal for a Design Code for Nail Plates - E Aasheim and K H Solli

23-7-2 Load Distribution in Nailed Joints - H J Blass

24-7-1 Theoretical and Experimental Tension and Shear Capacity of Nail Plate Connections - B Källsner and J Kangas

24-7-2 Testing Method and Determination of Basic Working Loads for Timber Joints with Mechanical Fasteners - Y Hirashima and F Kamiya

24-7-3 Anchorage Capacity of Nail Plate - J Kangas

25-7-2 Softwood and Hardwood Embedding Strength for Dowel type Fasteners - J Ehlbeck and H Werner

25-7-4 A Guide for Application of Quality Indexes for Driven Fasteners Used in Connections in Wood Structures - E G Stern

25-7-5 35 Years of Experience with Certain Types of Connectors and Connector Plates Used for the Assembly of Wood Structures and their Components- E G Stern

25-7-6 Characteristic Strength of Split-ring and Shear-plate Connections - H J Blass, J Ehlbeck and M Schlager

25-7-7 Characteristic Strength of Tooth-plate Connector Joints - H J Blass, J Ehlbeck and M Schlager

25-7-8 Extending Yield Theory to Screw Connections - T E McLain

25-7-9 Determination of k_{def} for Nailed Joints - J W G van de Kuilen

25-7-10 Characteristic Strength of UK Timber Connectors - A V Page and C J Mettem

25-7-11	Multiple-fastener Dowel-type Joints, a Selected Review of Research and Codes - C J Mettem and A V Page
25-7-12	Load Distributions in Multiple-fastener Bolted Joints in European Whitewood Glulam, with Steel Side Plates - C J Mettem and A V Page
26-7-1	Proposed Test Method for Dynamic Properties of Connections Assembled with Mechanical Fasteners - J D Dolan
26-7-2	Validatory Tests and Proposed Design Formulae for the Load-Carrying Capacity of Toothed-Plate Connectored Joints - C J Mettem, A V Page and G Davis
26-7-3	Definitions of Terms and Multi-Language Terminology Pertaining to Metal Connector Plates - E G Stern
26-7-4	Design of Joints Based on in V-Shape Glued-in Rods - J Kangas
26-7-5	Tests on Timber Concrete Composite Structural Elements (TCCs) - A U Meierhofer
27-7-1	Glulam Arch Bridge and Design of it's Moment-Resisting Joints - K Komatsu and S Usuku
27-7-2	Characteristic Load - Carrying Capacity of Joints with Dowel - type Fasteners in Regard to the System Properties - H Werner
27-7-3	Steel Failure Design in Truss Plate Joints - T Poutanen
28-7-1	Expanded Tube Joint in Locally DP Reinforced Timber - A J M Leijten, P Ragupathy and K S Virdi
28-7-2	A Strength and Stiffness Model for the Expanded Tube Joint - A J M Leijten
28-7-3	Load-carrying Capacity of Steel-to Timber Joints with Annular Ring Shanked Nails. A Comparison with the EC5 Design Method - R Görlacher
28-7-4	Dynamic Effects on Metal-Plate Connected Wood Truss Joints - S Kent, R Gupta and T Miller
28-7-5	Failure of the Timber Bolted Joints Subjected to Lateral Load Perpendicular to Grain - M Yasumura and L Daudeville
28-7-6	Design Procedure for Locally Reinforced Joints with Dowel-type Fasteners - H Werner
28-7-7	Variability and Effects of Moisture Content on the Withdrawal Characteristics for Lumber as Opposed to Clear Wood - J D Dolan and J W Stelmokas
28-7-8	Nail Plate Capacity in Joint Line - A Kevarinmäki and J Kangas
28-7-9	Axial Strength of Glued-In Bolts - Calculation Model Based on Non-Linear Fracture Mechanics - A Preliminary Study - C J Johansson, E Serrano, P J Gustafsson and B Enquist
28-7-10	Cyclic Lateral Dowel Connection Tests for seismic and Wind Evaluation - J D Dolan
29-7-1	A Simple Method for Lateral Load-Carrying Capacity of Dowel-Type Fasteners - J Kangas and J Kurkela
29-7-2	Nail Plate Joint Behaviour at Low Versus High Load Level - T Poutanen
29-7-3	The Moment Resistance of Tee and Butt - Joint Nail Plate Test Specimens - A Comparison with Current Design Methods - A Reffold, L R J Whale and B S Choo
29-7-4	A Critical Review of the Moment Rotation Test Method Proposed in prEN 1075 - M Bettison, B S Choo and L R J Whale
29-7-5	Explanation of the Translation and Rotation Behaviour of Prestressed Moment Timber Joints - A J M Leijten
29-7-6	Design of Joints and Frame Corners using Dowel-Type Fasteners - E Gehri

29-7-7 Quasi-Static Reversed-Cyclic Testing of Nailed Joints - E Karacabeyli and A Ceccotti

29-7-8 Failure of Bolted Joints Loaded Parallel to the Grain: Experiment and Simulation - L Davenne, L Daudeville and M Yasumura

30-7-1 Flexural Behaviour of GLT Beams End-Jointed by Glued-in Hardwood Dowels - K Komatsu, A Koizumi, J Jensen, T Sasaki and Y Iijima

30-7-2 Modelling of the Block Tearing Failure in Nailed Steel-to-Timber Joints - J Kangas, K Aalto and A Kevarinmäki

30-7-3 Cyclic Testing of Joints with Dowels and Slotted-in Steel Plates - E Aasheim

30-7-4 A Steel-to-Timber Dowelled Joint of High Performance in Combination with a High Strength Wood Composite (Parallam) - E Gehri

30-7-5 Multiple Fastener Timber Connections with Dowel Type Fasteners - A Jorissen

30-7-6 Influence of Ductility on Load-Carrying Capacity of Joints with Dowel-Type Fasteners - A Mischler

31-7-1 Mechanical Properties of Dowel Type Joints under Reversed Cyclic Lateral Loading - M Yasumura

31-7-2 Design of Joints with Laterally Loaded Dowels - A Mischler

31-7-3 Flexural Behaviour of Glulam Beams Edge-Jointed by Lagscrews with Steel Splice Plates - K Komatsu

31-7-4 Design on Timber Capacity in Nailed Steel-to-Timber Joints - J Kangas and J Vesa

31-7-5 Timber Contact in Chord Splices of Nail Plate Structures - A Kevarinmäki

31-7-6 The Fastener Yield Strength in Bending - A Jorissen and H J Blaß

31-7-7 A Proposal for Simplification of Johansen`s Formulae, Dealing With the Design of Dowelled-Type Fasteners - F Rouger

31-7-8 Simplified Design of Connections with Dowel-type fasteners - H J Blaß and J Ehlbeck

32-7-1 Behaviour of Wood-Steel-Wood Bolted Glulam Connections - M Mohammad and J H P Quenneville

32-7-2 A new set of experimental tests on beams loaded perpendicular-to-grain by dowel-type joints- M Ballerini

32-7-3 Design and Analysis of Bolted Timber Joints under Lateral Force Perpendicular to Grain - M Yasumura and L Daudeville

32-7-4 Predicting Capacities of Joints with Laterally Loaded Nails - I Smith and P Quenneville

32-7-5 Strength Reduction Rules for Multiple Fastener Joints - A Mischler and E Gehri

32-7-6 The Stiffness of Multiple Bolted Connections - A Jorissen

32-7-7 Concentric Loading Tests on Girder Truss Components - T N Reynolds, A Reffold, V Enjily and L Whale

32-7-8 Dowel Type Connections with Slotted-In Steel Plates - M U Pedersen, C O Clorius, L Damkilde, P Hoffmeyer and L Esklidsen

32-7-9 Creep of Nail Plate Reinforced Bolt Joints - J Vesa and A Kevarinmäki

32-7-10 The Behaviour of Timber Joints with Ring Connectors - E Gehri and A Mischler

32-7-11 Non-Metallic, Adhesiveless Joints for Timber Structures - R D Drake, M P Ansell, C J Mettem and R Bainbridge

32-7-12 Effect of Spacing and Edge Distance on the Axial Strength of Glued-in Rods - H J Blaß and B Laskewitz

32-7-13 Evaluation of Material Combinations for Bonded in Rods to Achieve Improved Timber Connections - C J Mettem, R J Bainbridge, K Harvey, M P Ansell, J G Broughton and A R Hutchinson

33-7-1 Determination of Yield Strength and Ultimate Strength of Dowel-Type Timber Joints – M Yasumura and K Sawata

33-7-2 Lateral Shear Capacity of Nailed Joints – U Korin

33-7-3 Height-Adjustable Connector for Composite Beams – Y V Piskunov and E G Stern

33-7-4 Engineering Ductility Assessment for a Nailed Slotted-In Steel Connection in Glulam– L Stehn and H Johansson

33-7-5 Effective Bending Capacity of Dowel-Type Fasteners - H J Blaß, A Bienhaus and V Krämer

33-7-6 Load-Carrying Capacity of Joints with Dowel-Type Fasteners and Interlayers - H J Blaß and B Laskewitz

33-7-7 Evaluation of Perpendicular to Grain Failure of Beams caused by Concentrated Loads of Joints – T A C M van der Put and A J M Leijten

33-7-8 Test Methods for Glued-In Rods for Timber Structures – C Bengtsson and C J Johansson

33-7-9 Stiffness Analysis of Nail Plates – P Ellegaard

33-7-10 Capacity, Fire Resistance and Gluing Pattern of the Rods in V-Connections – J Kangas

33-7-11 Bonded-In Pultrusions for Moment-Resisting Timber Connections – K Harvey, M P Ansell, C J Mettem, R J Bainbridge and N Alexandre

33-7-12 Fatigue Performance of Bonded-In Rods in Glulam, Using Three Adhesive Types - R J Bainbridge, K Harvey, C J Mettem and M P Ansell

34-7-1 Splitting Strength of Beams Loaded by Connections Perpendicular to Grain, Model Validation – A J M Leijten, A Jorissen

34-7-2 Numerical LEFM analyses for the evaluation of failure loads of beams loaded perpendicular-to-grain by single-dowel connections – M Ballerini, R Bezzi

34-7-3 Dowel joints loaded perpendicular to grain - H J Larsen, P J Gustafsson

34-7-4 Quality Control of Connections based on in V-shape glued-in Steel Rods – J Kangas, A Kevarinmäki

34-7-5 Testing Connector Types for Laminated-Timber-Concrete Composite Elements – M Grosse, S Lehmann, K Rautenstrauch

34-7-6 Behaviour of Axially Loaded Glued-in Rods - Requirements and Resistance, Especially for Spruce Timber Perpendicular to the Grain Direction – A Bernasconi

34-7-7 Embedding characteristics on fibre reinforcement and densified timber joints - P Haller, J Wehsener, T Birk

34-7-8 GIROD – Glued-in Rods for Timber Structures – C Bengtsson, C-J Johansson

34-7-9 Criteria for Damage and Failure of Dowel-Type Joints Subjected to Force Perpendicular to the Grain – M Yasumura

34-7-10 Interaction Between Splitting and Block Shear Failure of Joints – A J M Leijten, A Jorissen, J Kuipers

34-7-11 Limit states design of dowel-fastener joints – Placement of modification factors and partial factors, and calculation of variability in resistance – I Smith, G Foliente

34-7-12 Design and Modelling of Knee Joints - J Nielsen, P Ellegaard

34-7-13 Timber-Steel Shot Fired Nail Connections at Ultimate Limit States - R J Bainbridge, P Larsen, C J Mettem, P Alam, M P Ansell

35-7-1 New Estimating Method of Bolted Cross-lapped Joints with Timber Side Members - M Noguchi, K Komatsu

35-7-2 Analysis on Multiple Lag Screwed Timber Joints with Timber Side Members - K Komatsu, S Takino, M Nakatani, H Tateishi

35-7-3 Joints with Inclined Screws - A Kevarinmäki

35-7-4 Joints with Inclined Screws - I Bejtka, H J Blaß

35-7-5 Effect of distances, Spacing and Number of Dowels in a Row an the Load Carrying Capacity of Connections with Dowels failing by Splitting - M Schmid, R Frasson, H J Blaß

35-7 6 Effect of Row Spacing on the Capacity of Bolted Timber Connections Loaded Perpendicular-to-grain - P Quenneville, M Kasim

35-7-7 Splitting Strength of Beams Loaded by Connections, Model Comparison - A J M Leijten

35-7-8 Load-Carrying Capacity of Perpendicular to the Grain Loaded Timber Joints with Multiple Fasteners - O Borth, K U Schober, K Rautenstrauch

35-7-9 Determination of fracture parameter for dowel-type joints loaded perpendicular to wooden grain and its application - M Yasumura

35-7-10 Analysis and Design of Modified Attic Trusses with Punched Metal Plate Fasteners - P Ellegaard

35-7-11 Joint Properties of Plybamboo Sheets in Prefabricated Housing - G E Gonzalez

35-7-12 Fiber-Reinforced Beam-to-Column Connections for Seismic Applications - B Kasal, A Heiduschke, P Haller

36-7-1 Shear Tests in Timber-LWAC with Screw-Type Connections - L Jorge, H Cruz, S Lopes

36-7-2 Plug Shear Failure in Nailed Timber Connections: Experimental Studies - H Johnsson

36-7-3 Nail-Laminated Timber Elements in Natural Surface-Composite with Mineral Bound Layer - S Lehmann, K Rautenstrauch

36-7-4 Mechanical Properties of Timber-Concrete Joints Made With Steel Dowels - A Dias, J W G van de Kuilen, H Cruz

36-7-5 Comparison of Hysteresis Responses of Different Sheating to Framing Joints - B Dujič, R Zarnić

36-7- 6 Evaluation and Estimation of the Performance of the Nail Joints and Shear Walls under Dry/Humid Cyclic Climate - S Nakajima

36-7-7 Beams Transversally Loaded by Dowel-Type Joints: Influence on Splitting Strength of Beam Thickness and Dowel Size - M Ballerini, A Giovanella

36-7-8 Splitting Strength of Beams Loaded by Connections - J L Jensen

36-7-9 A Tensile Fracture Model for Joints with Rods or Dowels loaded Perpendicular-to-Grain - J L Jensen, P J Gustafsson, H J Larsen

36-7-10 A Numerical Model to Simulate the Load-Displacement Time-History of Mutiple-Bolt Connections Subjected to Various Loadings - C P Heine, J D Dolan

36-7-11 Reliability of Timber Structures, Theory and Dowel-Type Connection Failures - A Ranta-Maunus, A Kevarinmäki

37-7-1 Development of the "Displaced Volume Model" to Predict Failure for Multiple-Bolt Timber Joints - D M Carradine, J D Dolan, C P Heine

37-7-2 Mechanical Models of the Knee Joints with Cross-Lapped Glued Joints and Glued in Steel Rods - M Noguchi, K Komatsu

37-7-3 Simplification of the Neural Network Model for Predicting the Load-Carrying Capacity of Dowel-Type Connections - A Cointe, F Rouger

37-7-4 Bolted Wood Connections Loaded Perpendicular-to-Grain- A Proposed Design Approach - M C G Lehoux, J H P Quenneville

40-7-4 A EYM Based Simplified Design Formula for the Load-carrying Capacity of Dowel-type Connections - M Ballerini

40-7-5 Evaluation of the Slip Modulus for Ultimate Limit State Verifications of Timber-Concrete Composite Structures - E Lukaszewska, M Fragiacomo, A Frangi

40-7-6 Models for the Predictions of the Ductile and Brittle Failure Modes (Parallel-to-Grain) of Timber Rivet Connections - M Marjerrison, P Quenneville

40-7-7 Creep of Timber and Timber-Concrete Joints. - J W G van de Kuilen, A M P G Dias

40-7-8 Lag Screwed Timber Joints with Timber Side Members- K Komatsu, S Takino, H Tateishi

41-7-1 Applicability of Existing Design Approaches to Mechanical Joints in Structural Composite Lumber - M Snow, I Smith, A Asiz, M Ballerini

41-7-2 Validation of the Canadian Bolted Connection Design Proposal - P Quenneville, J Jensen

41-7-3 Ductility of Moment Resisting Dowelled Joints in Heavy Timber Structures - A Polastri, R Tomasi, M Piazza, I Smith

41-7-4 Mechanical Behaviour of Traditional Timber Connections: Proposals for Design, Based on Experimental and Numerical Investigations. Part I: Birdsmouth - C Faye, P Garcia, L Le Magorou, F Rouger

41-7-5 Embedding Strength of European Hardwoods - U Hübner, T Bogensperger, G Schickhofer

42-7-1 Base Parameters of Self-tapping Screws - G Pirnbacher, R Brandner, G Schickhofer

42-7-2 Joints with Inclined Screws and Steel Plates as Outer Members - H Krenn, G Schickhofer

42-7-3 Models for the Calculation of the Withdrawal Capacity of Self-tapping Screws - M Frese, H J Blaß

42-7-4 Embedding Strength of New Zealand Timber and Recommendation for the NZ Standard - S Franke, P Quenneville

42-7-5 Load Carrying Capacity of Timber-Wood Fiber Insulation Board – Joints with Dowel Type Fasteners - G Gebhardt, H J Blaß

42-7-6 Prediction of the Fatigue Resistance of Timber-Concrete-Composite Connections - U Kuhlmann, P Aldi

42-7-7 Using Screws for Structural Applications in Laminated Veneer Lumber - D M Carradine, M P Newcombe, A H Buchanan

42-7-8 Influence of Fastener Spacings on Joint Performance - Experimental Results and Codification - E Gehri

42-7-9 Connections with Glued-in Hardwood Rods Subjected to Combined Bending and Shear Actions - J L Jensen, P Quenneville

43-7-1 Probabilistic Capacity Prediction of Timber Joints under Brittle Failure Modes - T Tannert, T Vallée, and F Lam

43-7-2 Ductility in Timber Structures - A Jorissen, M Fragiacomo

43-7-3 Design of Mechanically Jointed Concrete-Timber Beams Taking into Account the Plastic Behaviour of the Fasteners - H J Larsen, H Riberholt, A Ceccotti

43-7-4 Design of Timber-Concrete Composite Beams with Notched Connections - M Fragiacomo, D Yeoh

43-7-5 Development of Design Procedures for Timber Concrete Composite Floors in Australia and New Zealand - K Crews, C Gerber

43-7-6 Failure Behaviour and Resistance of Dowel-Type Connections Loaded Perpendicular to Grain - B Franke, P Quenneville

43-7-7 Predicting Time Dependent Effects in Unbonded Post-Tensioned Timber Beams and Frames - S Giorgini, A Neale, A Palermo, D Carradine, S Pampanin, A H Buchanan

43-7-8 Simplified Design of Post-tensioned Timber Frames - M Newcombe, M Cusiel, S Pampanin, A Palermo, A H Buchanan

44-7-1 Pull-through Capacity in Plywood and OSB - J Munch-Andersen, J D Sørensen

44-7-2 Design Concept for CLT - Reinforced with Self-Tapping Screws - P Mestek, H Kreuzinger, S Winter

44-7-3 Fatigue Behaviour of the Stud Connector Used for Timber-Concrete Composite Bridges – K Rautenstrauch, J Mueller

44-7-4 The Stiffness of Beam to Column Connections in Post-Tensioned Timber Frames – T Smith, W van Beerschoten, A Palermo, S Pampanin, F C Ponzo

44-7-5 Design Approach for the Splitting Failure of Dowel-Type Connections Loaded Perpendicular to Grain - Bettina Franke, Pierre Quenneville

45-7-1 A Stiffness-based Analytical Model for Wood Strength in Timber Connections loaded Parallel to Grain: Riveted Joint Capacity in Brittle and Mixed Failure - P Zarnani, P Quenneville

45-7-2 Beams Loaded Perpendicular to Grain by Connections – Combined Effect of Edge and End Distance - J L Jensen, P Quenneville, U A Girhammar, B Källsner

45-7-3 L Block Failure of Dowelled Connections Subject to Bending Reinforced with Threaded Rods - J-F Bocquet, C Barthram, A Pineur

45-7-4 Block Shear Failure of Wooden Dowel Connections - G Stapf, S Aicher, N Zisi

45-7-5 Requirements on Ductility in Timber Structures - F Brühl, U Kuhlmann

46-7-1 Comparison of Design Rules for Glued-in rods and Design Rule Proposal for Implementation in European Standards - M Stepinac, F Hunger, R Tomasi, E Serrano, V Rajcic, J-W van de Kuilen

46-7-2 In-service Dynamic Stiffness of Dowel-type Connections - T Reynolds, R Harris Wen-Shao Chang

46-7-3 Design Procedure to Determine the Capacity of Timber Connections under Potential Brittle, Mixed and Ductile Failure Modes - P Zarnani, P Quenneville

46-7-4 Withdrawal Strength of Self-tapping Screws in Hardwoods - Ulrich Hübner

46-7-5 Wood Splitting Capacity in Timber Connections Loaded Transversely: Riveted Joint Strength for Full and Partial Width Failure Modes - P Zarnani, P Quenneville

46-7-6 Design Approach for the Splitting Failure of Dowel-type Connections Loaded Perpendicular to Grain- B Franke, P Quenneville

46-7-7 Beams Loaded Perpendicular to Grain by Connections - J C M Schoenmakers, A J M Leijten, A J M Jorissen

46-7-8 Influence of Fasteners in the Compression Area of Timber Members - M Enders-Comberg, H J Blaß

46-7-9 Design of Shear Reinforcement for Timber Beams - P Dietsch, H Kreuzinger, S Winter

LOAD SHARING

3-8-1 Load Sharing - An Investigation on the State of Research and Development of Design Criteria - E Levin

4-8-1 A Review of Load-Sharing in Theory and Practice - E Levin

4-8-2 Load Sharing - B Norén

19-8-1 Predicting the Natural Frequencies of Light-Weight Wooden Floors - I Smith and Y H Chui

20-8-1 Proposed Code Requirements for Vibrational Serviceability of Timber Floors - Y H Chui and I Smith

21-8-1 An Addendum to Paper 20-8-1 - Proposed Code Requirements for Vibrational Serviceability of Timber Floors - Y H Chui and I Smith

21-8-2 Floor Vibrational Serviceability and the CIB Model Code - S Ohlsson

22-8-1 Reliability Analysis of Viscoelastic Floors - F Rouger, J D Barrett and R O Foschi

24-8-1 On the Possibility of Applying Neutral Vibrational Serviceability Criteria to Joisted Wood Floors - I Smith and Y H Chui

25-8-1 Analysis of Glulam Semi-rigid Portal Frames under Long-term Load - K Komatsu and N Kawamoto

34-8-1 System Effect in Sheathed Parallel Timber Beam Structures – M Hansson, T Isaksson

35-8-1 System Effects in Sheathed Parallel Timber Beam Structures part II. - M Hansson, T Isaksson

39-8-1 Overview of a new Canadian Approach to Handling System Effects in Timber Structures - I Smith, Y H Chui, P Quenneville

DURATION OF LOAD

3-9-1 Definitions of Long Term Loading for the Code of Practice - B Norén

4-9-1 Long Term Loading of Trussed Rafters with Different Connection Systems - T Feldborg and M Johansen

5-9-1 Strength of a Wood Column in Combined Compression and Bending with Respect to Creep - B Källsner and B Norén

6-9-1 Long Term Loading for the Code of Practice (Part 2) - B Norén

6-9-2 Long Term Loading - K Möhler

6-9-3 Deflection of Trussed Rafters under Alternating Loading during a Year - T Feldborg and M Johansen

7-6-1 Strength and Long Term Behaviour of Lumber and Glued-Laminated Timber under Torsion Loads - K Möhler

7-9-1 Code Rules Concerning Strength and Loading Time - H J Larsen and E Theilgaard

17-9-1 On the Long-Term Carrying Capacity of Wood Structures - Y M Ivanov and Y Y Slavic

18-9-1 Prediction of Creep Deformations of Joints - J Kuipers

19-9-1 Another Look at Three Duration of Load Models - R O Foschi and Z C Yao

19-9-2 Duration of Load Effects for Spruce Timber with Special Reference to Moisture Influence - A Status Report - P Hoffmeyer

19-9-3 A Model of Deformation and Damage Processes Based on the Reaction Kinetics of Bond Exchange - T A C M van der Put

19-9-4 Non-Linear Creep Superposition - U Korin

19-9-5 Determination of Creep Data for the Component Parts of Stressed-Skin Panels - R Kliger

19-9-6 Creep an Lifetime of Timber Loaded in Tension and Compression - P Glos

19-1-1 Duration of Load Effects and Reliability Based Design (Single Member) - R O Foschi and Z C Yao

19-6-1 Effect of Age and/or Load on Timber Strength - J Kuipers

19-7-4 The Prediction of the Long-Term Load Carrying Capacity of Joints in Wood Structures - Y M Ivanov and Y Y Slavic

19-7-5 Slip in Joints under Long-Term Loading - T Feldborg and M Johansen

20-7-2 Slip in Joints under Long-Term Loading - T Feldborg and M Johansen

22-9-1 Long-Term Tests with Glued Laminated Timber Girders - M Badstube, W Rug and W Schöne

22-9-2 Strength of One-Layer solid and Lengthways Glued Elements of Wood Structures and its Alteration from Sustained Load - L M Kovaltchuk, I N Boitemirova and G B Uspenskaya

24-9-1 Long Term Bending Creep of Wood - T Toratti

24-9-2 Collection of Creep Data of Timber - A Ranta-Maunus

24-9-3 Deformation Modification Factors for Calculating Built-up Wood-Based Structures - I R Kliger

25-9-2 DVM Analysis of Wood. Lifetime, Residual Strength and Quality - L F Nielsen

26-9-1 Long Term Deformations in Wood Based Panels under Natural Climate Conditions. A Comparative Study - S Thelandersson, J Nordh, T Nordh and S Sandahl

28-9-1 Evaluation of Creep Behavior of Structural Lumber in Natural Environment - R Gupta and R Shen

30-9-1 DOL Effect in Tension Perpendicular to the Grain of Glulam Depending on Service Classes and Volume - S Aicher and G Dill-Langer

30-9-2 Damage Modelling of Glulam in Tension Perpendicular to Grain in Variable Climate - G Dill-Langer and S Aicher

31-9-1 Duration of Load Effect in Tension Perpendicular to Grain in Curved Glulam - A Ranta-Maunus

32-9-1 Bending-Stress-Redistribution Caused by Different Creep in Tension and Compression and Resulting DOL-Effect - P Becker and K Rautenstrauch

32-9-2 The Long Term Performance of Ply-Web Beams - R Grantham and V Enjily

36-9-1 Load Duration Factors for Instantaneous Loads - A J M Leijten, B Jansson

39-9-1 Simplified Approach for the Long-Term Behaviour of Timber-Concrete Composite Beams According to the Eurocode 5 Provisions - M Fragiacomo, A Ceccotti

TIMBER BEAMS

4-10-1 The Design of Simple Beams - H J Burgess

4-10-2 Calculation of Timber Beams Subjected to Bending and Normal Force - H J Larsen

5-10-1 The Design of Timber Beams - H J Larsen

9-10-1 The Distribution of Shear Stresses in Timber Beams - F J Keenan

9-10-2 Beams Notched at the Ends - K Möhler

11-10-1 Tapered Timber Beams - H Riberholt

13-6-2 Consideration of Size Effects in Longitudinal Shear Strength for Uncracked Beams - R O Foschi and J D Barrett

13-6-3 Consideration of Shear Strength on End-Cracked Beams - J D Barrett and R O Foschi

18-10-1 Submission to the CIB-W18 Committee on the Design of Ply Web Beams by Consideration of the Type of Stress in the Flanges - J A Baird

18-10-2 Longitudinal Shear Design of Glued Laminated Beams - R O Foschi

19-10-1 Possible Code Approaches to Lateral Buckling in Beams - H J Burgess

19-2-1 Creep Buckling Strength of Timber Beams and Columns - R H Leicester

20-2-1 Lateral Buckling Theory for Rectangular Section Deep Beam-Columns - H J Burgess

20-10-1 Draft Clause for CIB Code for Beams with Initial Imperfections - H J Burgess

20-10-2 Space Joists in Irish Timber - W J Robinson

20-10-3 Composite Structure of Timber Joists and Concrete Slab - T Poutanen

21-10-1 A Study of Strength of Notched Beams - P J Gustafsson

22-10-1 Design of Endnotched Beams - H J Larsen and P J Gustafsson

22-10-2 Dimensions of Wooden Flexural Members under Constant Loads - A Pozgai

22-10-3 Thin-Walled Wood-Based Flanges in Composite Beams - J König

22-10-4 The Calculation of Wooden Bars with flexible Joints in Accordance with the Polish Standart Code and Strict Theoretical Methods - Z Mielczarek

23-10-1 Tension Perpendicular to the Grain at Notches and Joints - T A C M van der Put

23-10-2 Dimensioning of Beams with Cracks, Notches and Holes. An Application of Fracture Mechanics - K Riipola

23-10-3 Size Factors for the Bending and Tension Strength of Structural Timber - J D Barret and A R Fewell

23-12-1 Bending Strength of Glulam Beams, a Design Proposal - J Ehlbeck and F Colling

23-12-3 Glulam Beams, Bending Strength in Relation to the Bending Strength of the Finger Joints - H Riberholt

24-10-1 Shear Strength of Continuous Beams - R H Leicester and F G Young

25-10-1 The Strength of Norwegian Glued Laminated Beams - K Solli, E Aasheim and R H Falk

25-10-2 The Influence of the Elastic Modulus on the Simulated Bending Strength of Hyperstatic Timber Beams - T D G Canisius

27-10-1 Determination of Shear Modulus - R Görlacher and J Kürth

29-10-1 Time Dependent Lateral Buckling of Timber Beams - F Rouger

29-10-2 Determination of Modulus of Elasticity in Bending According to EN 408 - K H Solli

29-10-3 On Determination of Modulus of Elasticity in Bending - L Boström, S Ormarsson and O Dahlblom

29-10-4 Relation of Moduli of Elasticity in Flatwise and Edgewise Bending of Solid Timber - C J Johansson, A Steffen and E W Wormuth

30-10-1 Nondestructive Evaluation of Wood-based Members and Structures with the Help of Modal Analysis - P Kuklik

30-10-2 Measurement of Modulus of Elasticity in Bending - L Boström

30-10-3 A Weak Zone Model for Timber in Bending - B Källsner, K Salmela and O Ditlevsen

30-10-4 Load Carrying Capacity of Timber Beams with Narrow Moment Peaks - T Isaksson and J Freysoldt

37-10-1 Design of Rim Boards for Use with I-Joists Framing Systems - B Yeh, T G Williamson

40-10- 1 Extension of EC5 Annex B Formulas for the Design of Timber-concrete Composite Structures - J Schänzlin, M Fragiacomo

40-10-2 Simplified Design Method for Mechanically Jointed Beams - U A Girhammar

41-10-1 Composite Action of I-Joist Floor Systems - T G Williamson, B Yeh

41-10-2 Evaluation of the Prestressing Losses in Timber Members Prestressed with Unbonded Tendons - M Fragiacomo, M Davies

41-10-3 Relationship Between Global and Local MOE – J K Denzler, P Stapel, P Glos

42-10-1 Relationships Between Local, Global and Dynamic Modulus of Elasticity for Soft- and Hardwoods – G J P Ravenshorst, J W G van de Kuilen

ENVIRONMENTAL CONDITIONS

5-11-1 Climate Grading for the Code of Practice - B Norén

6-11-1 Climate Grading (2) - B Norén

9-11-1 Climate Classes for Timber Design - F J Keenan

19-11-1 Experimental Analysis on Ancient Downgraded Timber Structures - B Leggeri and L Paolini

19-6-5 Drying Stresses in Round Timber - A Ranta-Maunus

22-11-1 Corrosion and Adaptation Factors for Chemically Aggressive Media with Timber Structures - K Erler

29-11-1 Load Duration Effect on Structural Beams under Varying Climate Influence of Size and Shape - P Galimard and P Morlier

30-11-1 Probabilistic Design Models for the Durability of Timber Constructions - R H Leicester

36-11-1 Structural Durability of Timber in Ground Contact – R H Leicester, C H Wang, M N Nguyen, G C Foliente, C McKenzie

38-11-1 Design Specifications for the Durability of Timber – R H Leicester, C-H Wang, M Nguyen, G C Foliente

38-11-2 Consideration of Moisture Exposure of Timber Structures as an Action - M Häglund, S Thelandersson

45-11-1 Building Climate – Long-term Measurements to Determine the Effect on the Moisture Gradient in Large-span Timber Structures - P Dietsch, A Gamper, M Merk, S Winter

LAMINATED MEMBERS

6-12-1 Directives for the Fabrication of Load-Bearing Structures of Glued Timber - A van der Velden and J Kuipers

8-12-1 Testing of Big Glulam Timber Beams - H Kolb and P Frech

8-12-2 Instruction for the Reinforcement of Apertures in Glulam Beams - H Kolb and P Frech

8-12-3 Glulam Standard Part 1: Glued Timber Structures; Requirements for Timber (Second Draft)

9-12-1 Experiments to Provide for Elevated Forces at the Supports of Wooden Beams with Particular Regard to Shearing Stresses and Long-Term Loadings - F Wassipaul and R Lackner

9-12-2 Two Laminated Timber Arch Railway Bridges Built in Perth in 1849 - L G Booth

9-6-4 Consideration of Combined Stresses for Lumber and Glued Laminated Timber - K Möhler

11-6-3 Consideration of Combined Stresses for Lumber and Glued Laminated Timber (addition to Paper CIB-W18/9-6-4) - K Möhler

12-12-1 Glulam Standard Part 2: Glued Timber Structures; Rating (3rd draft)

12-12-2 Glulam Standard Part 3: Glued Timber Structures; Performance (3 rd draft)

13-12-1 Glulam Standard Part 3: Glued Timber Structures; Performance (4th draft)

14-12-1 Proposals for CEI-Bois/CIB-W18 Glulam Standards - H J Larsen

14-12-2 Guidelines for the Manufacturing of Glued Load-Bearing Timber Structures - Stevin Laboratory

14-12-3 Double Tapered Curved Glulam Beams - H Riberholt

14-12-4 Comment on CIB-W18/14-12-3 - E Gehri

18-12-1 Report on European Glulam Control and Production Standard - H Riberholt

18-10-2 Longitudinal Shear Design of Glued Laminated Beams - R O Foschi

19-12-1 Strength of Glued Laminated Timber - J Ehlbeck and F Colling

19-12-2 Strength Model for Glulam Columns - H J Blaß

19-12-3 Influence of Volume and Stress Distribution on the Shear Strength and Tensile Strength Perpendicular to Grain - F Colling

19-12-4 Time-Dependent Behaviour of Glued-Laminated Beams - F Zaupa

21-12-1 Modulus of Rupture of Glulam Beam Composed of Arbitrary Laminae - K Komatsu and N Kawamoto

21-12-2 An Appraisal of the Young's Modulus Values Specified for Glulam in Eurocode 5- L R J Whale, B O Hilson and P D Rodd

21-12-3 The Strength of Glued Laminated Timber (Glulam): Influence of Lamination Qualities and Strength of Finger Joints - J Ehlbeck and F Colling

21-12-4 Comparison of a Shear Strength Design Method in Eurocode 5 and a More Traditional One - H Riberholt

22-12-1 The Dependence of the Bending Strength on the Glued Laminated Timber Girder Depth - M Badstube, W Rug and W Schöne

22-12-2 Acid Deterioration of Glulam Beams in Buildings from the Early Half of the 1960s - Prelimination summary of the research project; Overhead pictures - B A Hedlund

22-12-3 Experimental Investigation of normal Stress Distribution in Glue Laminated Wooden Arches - Z Mielczarek and W Chanaj

22-12-4 Ultimate Strength of Wooden Beams with Tension Reinforcement as a Function of Random Material Properties - R Candowicz and T Dziuba

23-12-1 Bending Strength of Glulam Beams, a Design Proposal - J Ehlbeck and F Colling

23-12-2 Probability Based Design Method for Glued Laminated Timber - M F Stone

23-12-3 Glulam Beams, Bending Strength in Relation to the Bending Strength of the Finger Joints - H Riberholt

23-12-4 Glued Laminated Timber - Strength Classes and Determination of Characteristic Properties - H Riberholt, J Ehlbeck and A Fewell

24-12-1 Contribution to the Determination of the Bending Strength of Glulam Beams - F Colling, J Ehlbeck and R Görlacher

24-12-2 Influence of Perpendicular-to-Grain Stressed Volume on the Load-Carrying Capacity of Curved and Tapered Glulam Beams - J Ehlbeck and J Kürth

25-12-1	Determination of Characteristic Bending Values of Glued Laminated Timber. EN-Approach and Reality - E Gehri
26-12-1	Norwegian Bending Tests with Glued Laminated Beams-Comparative Calculations with the "Karlsruhe Calculation Model" - E Aasheim, K Solli, F Colling, R H Falk, J Ehlbeck and R Görlacher
26-12-2	Simulation Analysis of Norwegian Spruce Glued-Laminated Timber - R Hernandez and R H Falk
26-12-3	Investigation of Laminating Effects in Glued-Laminated Timber - F Colling and R H Falk
26-12-4	Comparing Design Results for Glulam Beams According to Eurocode 5 and to the French Working Stress Design Code (CB71) - F Rouger
27-12-1	State of the Art Report: Glulam Timber Bridge Design in the U.S. - M A Ritter and T G Williamson
27-12-2	Common Design Practice for Timber Bridges in the United Kingdom - C J Mettem, J P Marcroft and G Davis
27-12-3	Influence of Weak Zones on Stress Distribution in Glulam Beams - E Serrano and H J Larsen
28-12-1	Determination of Characteristic Bending Strength of Glued Laminated Timber - E Gehri
28-12-2	Size Factor of Norwegian Glued Laminated Beams - E Aasheim and K H Solli
28-12-3	Design of Glulam Beams with Holes - K Riipola
28-12-4	Compression Resistance of Glued Laminated Timber Short Columns- U Korin
29-12-1	Development of Efficient Glued Laminated Timber - G Schickhofer
30-12-1	Experimental Investigation and Analysis of Reinforced Glulam Beams - K Oiger
31-12-1	Depth Factor for Glued Laminated Timber-Discussion of the Eurocode 5 Approach - B Källsner, O Carling and C J Johansson
32-12-1	The bending stiffness of nail-laminated timber elements in transverse direction- T Wolf and O Schäfer
33-12-1	Internal Stresses in the Cross-Grain Direction of Wood Induced by Climate Variation – J Jönsson and S Svensson
34-12-1	High-Strength I-Joist Compatible Glulam Manufactured with LVL Tension Laminations – B Yeh, T G Williamson
34-12-2	Evaluation of Glulam Shear Strength Using A Full-Size Four-Point Test Method – B Yeh, T G Williamson
34-12-3	Design Model for FRP Reinforced Glulam Beams – M Romani, H J Blaß
34-12-4	Moisture induced stresses in glulam cross sections – J Jönsson
34-12-5	Load Carrying Capacity of Nail-Laminated Timber under Concentrated Loads – V Krämer, H J Blaß
34-12-6	Determination of Shear Strength Values for GLT Using Visual and Machine Graded Spruce Laminations – G Schickhofer
34-12-7	Mechanically Jointed Beams: Possibilities of Analysis and some special Problems – H Kreuzinger
35-12-1	Glulam Beams with Round Holes – a Comparison of Different Design Approaches vs. Test Data - S Aicher L Höfflin
36-12-1	Problems with Shear and Bearing Strength of LVL in Highly Loaded Structures - H Bier
36-12-2	Weibull Based Design of Round Holes in Glulam - L Höfflin, S Aicher

37-12-1 Development of Structural LVL from Tropical Wood and Evaluation of Their Performance for the Structural Components of Wooden Houses. Part-1. Application of Tropical LVL to a Roof Truss - K Komatsu, Y Idris, S Yuwasdiki, B Subiyakto, A Firmanti

37-12-2 Reinforcement of LVL Beams With Bonded-in Plates and Rods - Effect of Placement of Steel and FRP Reinforcements on Beam Strength and Stiffness - P Alam, M P Ansell, D Smedley

39-12-1 Recommended Procedures for Determination of Distribution Widths in the Design of Stress Laminated Timber Plate Decks - K Crews

39-12-2 In-situ Strengthening of Timber Structures with CFRP - K U Schober, S Franke, K Rautenstrauch

39-12-3 Effect of Checking and Non-Glued Edge Joints on the Shear Strength of Structural Glued Laminated Timber Beams - B Yeh, T G Williamson, Z A Martin

39-12-4 A Contribution to the Design and System Effect of Cross Laminated Timber (CLT) - R Jöbstl, T Moosbrugger, T Bogensperger, G Schickhofer

39-12-5 Behaviour of Glulam in Compression Perpendicular to Grain in Different Strength Grades and Load Configurations - M Augustin, A Ruli, R Brandner, G Schickhofer

40-12-1 Development of New Constructions of Glulam Beams in Canada - F Lam, N Mohadevan

40-12-2 Determination of Modulus of Shear and Elasticity of Glued Laminated Timber and Related Examination - R Brandner, E Gehri, T Bogensperger, G Schickhofer

40-12-3 Comparative Examination of Creep of GTL and CLT-Slabs in Bending - R A Jöbstl, G Schickhofer,

40-12-4 Standard Practice for the Derivation of Design Properties of Structural Glued Laminated Timber in the United States - T G Williamson, B Yeh

40-12-5 Creep and Creep-Rupture Behaviour of Structural Composite Lumber Evaluated in Accordance with ASTM D 6815 - B Yeh, T G Williamson.

40-12-6 Bending Strength of Combined Beech-Spruce Glulam - M Frese, H J Blaß

40-12-7 Quality Control of Glulam: Shear Tests of Glue Lines - R Steiger, E Gehri

41-12-1 Paper withdrawn by the author

41-12-2 Bending Strength of Spruce Glulam: New Models for the Characteristic Bending Strength - M Frese, H J Blass,

41-12-3 In-Plane Shear Strength of Cross Laminated Timber - R A Joebstl, T Bogensperger, G Schickhofer

41-12-4 Strength of Glulam Beams with Holes - Tests of Quadratic Holes and Literature Test Results Compilation - H Danielsson, P J Gustafsson

42-12-1 Glulam Beams with Holes Reinforced by Steel Bars – S Aicher, L Höfflin

42-12-2 Analysis of X-lam Panel-to-Panel Connections under Monotonic and Cyclic Loading - C Sandhaas, L Boukes, J W G van de Kuilen, A Ceccotti

42-12-3 Laminating Lumber and End Joint Properties for FRP-Reinforced Glulam Beams - T G Williamson, B Yeh

43-12-4 Validity of Bending Tests on Strip-Shaped Specimens to Derive Bending Strength and Stiffness Properties of Cross-Laminated Solid Timber (CLT) - R Steiger, A Gülzow

42-12-5 Mechanical Properties of Stress Laminated Timber Decks - Experimental Study - K Karlsson, R Crocetti, R Kliger

43-12-1 Fatigue Behaviour of Finger Jointed Lumber - S Aicher, G Stapf

43-12-2 Experimental and Numercial Investigation on the Shear Strength of Glulam - R Crocetti, P J Gustafsson, H Danielsson, A Emilsson, S Ormarsson

43-12-3 System Effects in Glued Laminated Timber in Tension and Bending - M Frese, H J Blaß

43-12-4 Experimental Investigations on Mechanical Behaviour of Glued Solid timber - C Faye, F Rouger, P Garcia

44-12-1 Properties of CLT-Panels Exposed to Compression Perpendicular to their Plane- T Bogensperger, M Augustin, G Schickhofer

44-12-2 Strength of Spruce Glulam Subjected to Longitudinal Compression – M Frese, M Enders-Comberg, H J Blaß, P Glos

44-12-3 Glued Laminated Timber: A proposal for New Beam Layups - F Rouger, P Garcia

44-12-4 Glulam Beams with Internally and Externally Reinforced Holes – Test, Detailing and Design – S Aicher

44-12-5 Size Effect of Bending Strength in Glulam Beam - F Lam

45-12-1 Asymmetrically Combined Glulam - Simplified Verification of the Bending Strength - M Frese, H J Blaß

45-12-2 Determination of Shear Strength of Structural and Glued Laminated Timber - R Brandner, W Gatternig, G Schickhofer

45-12-3 Shear Resistance of Glulam Beams with Cracks - A Pousette, M Ekevad

45-12-4 Experimental Investigation on in-plane Behaviour of Cross-laminated Timber Elements - M Andreolli, A Polastri, R Tomasi

46-12-1 Modelling the Bending Strength of Glued Laminated Timber - Considering the Natural Growth Characteristics of Timber - G Fink, A Frangi, J Kohler

46-12-2 In-Plane Shear Strength of Cross Laminated Timber (CLT): Test Configuration, Quantification and Influencing Parameters - R Brandner, T Bogensperger, G Schickhofer

46-12-3 Shear Strength and Shear Stiffness of CLT-beams Loaded in Plane - M Flaig, H J Blaß

46-12-4 Stiffness of Screw-Reinforced LVL in Compression Perpendicular to the Grain - C Watson, W van Beerschoten, T Smith, S Pampanin, A H Buchanan

PARTICLE AND FIBRE BUILDING BOARDS

7-13-1 Fibre Building Boards for CIB Timber Code (First Draft)- O Brynildsen

9-13-1 Determination of the Bearing Strength and the Load-Deformation Characteristics of Particleboard - K Möhler, T Budianto and J Ehlbeck

9-13-2 The Structural Use of Tempered Hardboard - W W L Chan

11-13-1 Tests on Laminated Beams from Hardboard under Short- and Longterm Load - W Nozynski

11-13-2 Determination of Deformation of Special Densified Hardboard under Long-term Load and Varying Temperature and Humidity Conditions - W Halfar

11-13-3 Determination of Deformation of Hardboard under Long-term Load in Changing Climate - W Halfar

14-4-1 An Introduction to Performance Standards for Wood-Base Panel Products - D H Brown

14-4-2 Proposal for Presenting Data on the Properties of Structural Panels - T Schmidt

16-13-1 Effect of Test Piece Size on Panel Bending Properties - P W Post

20-4-1 Considerations of Reliability - Based Design for Structural Composite Products - M R O'Halloran, J A Johnson, E G Elias and T P Cunningham

20-13-1 Classification Systems for Structural Wood-Based Sheet Materials - V C Kearley and A R Abbott

21-13-1 Design Values for Nailed Chipboard - Timber Joints - A R Abbott

25-13-1 Bending Strength and Stiffness of Izopanel Plates - Z Mielczarek

28-13-1 Background Information for "Design Rated Oriented Strand Board (OSB)" in CSA Standards - Summary of Short-term Test Results - E Karacabeyli, P Lau, C R Henderson, F V Meakes and W Deacon

28-13-2 Torsional Stiffness of Wood-Hardboard Composed I-Beam - P Olejniczak

TRUSSED RAFTERS

4-9-1 Long-term Loading of Trussed Rafters with Different Connection Systems - T Feldborg and M Johansen

6-9-3 Deflection of Trussed Rafters under Alternating Loading During a Year - T Feldborg and M Johansen

7-2-1 Lateral Bracing of Timber Struts - J A Simon

9-14-1 Timber Trusses - Code Related Problems - T F Williams

9-7-1 Design of Truss Plate Joints - F J Keenan

10-14-1 Design of Roof Bracing - The State of the Art in South Africa - P A V Bryant and J A Simon

11-14-1 Design of Metal Plate Connected Wood Trusses - A R Egerup

12-14-1 A Simple Design Method for Standard Trusses - A R Egerup

13-14-1 Truss Design Method for CIB Timber Code - A R Egerup

13-14-2 Trussed Rafters, Static Models - H Riberholt

13-14-3 Comparison of 3 Truss Models Designed by Different Assumptions for Slip and E-Modulus - K Möhler

14-14-1 Wood Trussed Rafter Design - T Feldborg and M Johansen

14-14-2 Truss-Plate Modelling in the Analysis of Trusses - R O Foschi

14-14-3 Cantilevered Timber Trusses - A R Egerup

14-7-5 The Effect of Support Eccentricity on the Design of W- and WW-Trusses with Nail Plate Connectors - B Källsner

15-14-1 Guidelines for Static Models of Trussed Rafters - H Riberholt

15-14-2 The Influence of Various Factors on the Accuracy of the Structural Analysis of Timber Roof Trusses - F R P Pienaar

15-14-3 Bracing Calculations for Trussed Rafter Roofs - H J Burgess

15-14-4 The Design of Continuous Members in Timber Trussed Rafters with Punched Metal Connector Plates - P O Reece

15-14-5 A Rafter Design Method Matching U.K. Test Results for Trussed Rafters - H J Burgess

16-14-1 Full-Scale Tests on Timber Fink Trusses Made from Irish Grown Sitka Spruce - V Picardo

17-14-1 Data from Full Scale Tests on Prefabricated Trussed Rafters - V Picardo

17-14-2 Simplified Static Analysis and Dimensioning of Trussed Rafters - H Riberholt

17-14-3 Simplified Calculation Method for W-Trusses - B Källsner

18-14-1 Simplified Calculation Method for W-Trusses (Part 2) - B Källsner

18-14-2 Model for Trussed Rafter Design - T Poutanen

19-14-1 Annex on Simplified Design of W-Trusses - H J Larsen

19-14-2 Simplified Static Analysis and Dimensioning of Trussed Rafters - Part 2 - H Riberholt

19-14-3 Joint Eccentricity in Trussed Rafters - T Poutanen

20-14-1 Some Notes about Testing Nail Plates Subjected to Moment Load - T Poutanen

20-14-2 Moment Distribution in Trussed Rafters - T Poutanen

20-14-3 Practical Design Methods for Trussed Rafters - A R Egerup

22-14-1 Guidelines for Design of Timber Trussed Rafters - H Riberholt

23-14-1 Analyses of Timber Trussed Rafters of the W-Type - H Riberholt

23-14-2 Proposal for Eurocode 5 Text on Timber Trussed Rafters - H Riberholt

24-14-1 Capacity of Support Areas Reinforced with Nail Plates in Trussed Rafters - A Kevarinmäki

25-14-1 Moment Anchorage Capacity of Nail Plates in Shear Tests - A Kevarinmaki and J. Kangas

25-14-2 Design Values of Anchorage Strength of Nail Plate Joints by 2-curve Method and Interpolation - J Kangas and A Kevarinmaki

26-14-1 Test of Nail Plates Subjected to Moment - E Aasheim

26-14-2 Moment Anchorage Capacity of Nail Plates - A Kevarinmäki and J Kangas

26-14-3 Rotational Stiffness of Nail Plates in Moment Anchorage - A Kevarinmäki and J Kangas

26-14-4 Solution of Plastic Moment Anchorage Stress in Nail Plates - A Kevarinmäki

26-14-5 Testing of Metal-Plate-Connected Wood-Truss Joints - R Gupta

26-14-6 Simulated Accidental Events on a Trussed Rafter Roofed Building - C J Mettem and J P Marcroft

30-14-1 The Stability Behaviour of Timber Trussed Rafter Roofs - Studies Based on Eurocode 5 and Full Scale Testing - R J Bainbridge, C J Mettern, A Reffold and T Studer

32-14-1 Analysis of Timber Reinforced with Punched Metal Plate Fasteners- J Nielsen

33-14-1 Moment Capacity of Timber Beams Loaded in Four-Point Bending and Reinforced with Punched Metal Plate Fasteners – J Nielsen

36-14-1 Effect of Chord Splice Joints on Force Distribution in Trusses with Punched Metal Plate Fasteners - P Ellegaard

36-14-2 Monte Carlo Simulation and Reliability Analysis of Roof Trusses with Punched Metal Plate Fasteners - M Hansson, P Ellegaard

36-14-3 Truss Trouble – R H Leicester, J Goldfinch, P Paevere, G C Foliente

40-14-1 Timber Trusses with Punched Metal Plate Fasteners - Design for Transport and Erection - H J Blaß

45-14-1 Robustness Analysis of Timber Truss Systems - D Čizmar, V Rajčić

STRUCTURAL STABILITY

8-15-1 Laterally Loaded Timber Columns: Tests and Theory - H J Larsen

13-15-1 Timber and Wood-Based Products Structures. Panels for Roof Coverings. Methods of Testing and Strength Assessment Criteria. Polish Standard BN-78/7159-03

16-15-1 Determination of Bracing Structures for Compression Members and Beams - H Brüninghoff

17-15-1 Proposal for Chapter 7.4 Bracing - H Brüninghoff

17-15-2 Seismic Design of Small Wood Framed Houses - K F Hansen

18-15-1 Full-Scale Structures in Glued Laminated Timber, Dynamic Tests: Theoretical and Experimental Studies - A Ceccotti and A Vignoli

18-15-2 Stabilizing Bracings - H Brüninghoff

19-15-1 Connections Deformability in Timber Structures: a Theoretical Evaluation of its Influence on Seismic Effects - A Ceccotti and A Vignoli

19-15-2 The Bracing of Trussed Beams - M H Kessel and J Natterer

19-15-3 Racking Resistance of Wooden Frame Walls with Various Openings - M Yasumura

19-15-4 Some Experiences of Restoration of Timber Structures for Country Buildings - G Cardinale and P Spinelli

19-15-5 Non-Destructive Vibration Tests on Existing Wooden Dwellings - Y Hirashima

20-15-1 Behaviour Factor of Timber Structures in Seismic Zones. - A Ceccotti and A Vignoli

21-15-1 Rectangular Section Deep Beam - Columns with Continuous Lateral Restraint - H J Burgess

21-15-2 Buckling Modes and Permissible Axial Loads for Continuously Braced Columns- H J Burgess

21-15-3 Simple Approaches for Column Bracing Calculations - H J Burgess

21-15-4 Calculations for Discrete Column Restraints - H J Burgess

21-15-5 Behaviour Factor of Timber Structures in Seismic Zones (Part Two) - A Ceccotti and A Vignoli

22-15-1 Suggested Changes in Code Bracing Recommendations for Beams and Columns - H J Burgess

22-15-2 Research and Development of Timber Frame Structures for Agriculture in Poland- S Kus and J Kerste

22-15-3 Ensuring of Three-Dimensional Stiffness of Buildings with Wood Structures - A K Shenghelia

22-15-5 Seismic Behavior of Arched Frames in Timber Construction - M Yasumura

22-15-6 The Robustness of Timber Structures - C J Mettem and J P Marcroft

22-15-7 Influence of Geometrical and Structural Imperfections on the Limit Load of Wood Columns - P Dutko

23-15-1 Calculation of a Wind Girder Loaded also by Discretely Spaced Braces for Roof Members - H J Burgess

23-15-2 Stability Design and Code Rules for Straight Timber Beams - T A C M van der Put

23-15-3 A Brief Description of Formula of Beam-Columns in China Code - S Y Huang

23-15-4 Seismic Behavior of Braced Frames in Timber Construction - M Yasumara

23-15-5 On a Better Evaluation of the Seismic Behavior Factor of Low-Dissipative Timber Structures - A Ceccotti and A Vignoli

23-15-6 Disproportionate Collapse of Timber Structures - C J Mettem and J P Marcroft

23-15-7 Performance of Timber Frame Structures During the Loma Prieta California Earthquake - M R O'Halloran and E G Elias

24-15-2 Discussion About the Description of Timber Beam-Column Formula - S Y Huang

24-15-3	Seismic Behavior of Wood-Framed Shear Walls - M Yasumura
25-15-1	Structural Assessment of Timber Framed Building Systems - U Korin
25-15-3	Mechanical Properties of Wood-framed Shear Walls Subjected to Reversed Cyclic Lateral Loading - M Yasumura
26-15-1	Bracing Requirements to Prevent Lateral Buckling in Trussed Rafters - C J Mettem and P J Moss
26-15-2	Eurocode 8 - Part 1.3 - Chapter 5 - Specific Rules for Timber Buildings in Seismic Regions - K Becker, A Ceccotti, H Charlier, E Katsaragakis, H J Larsen and H Zeitter
26-15-3	Hurricane Andrew - Structural Performance of Buildings in South Florida - M R O'Halloran, E L Keith, J D Rose and T P Cunningham
29-15-1	Lateral Resistance of Wood Based Shear Walls with Oversized Sheathing Panels - F Lam, H G L Prion and M He
29-15-2	Damage of Wooden Buildings Caused by the 1995 Hyogo-Ken Nanbu Earthquake - M Yasumura, N Kawai, N Yamaguchi and S Nakajima
29-15-3	The Racking Resistance of Timber Frame Walls: Design by Test and Calculation - D R Griffiths, C J Mettem, V Enjily, P J Steer
29-15-4	Current Developments in Medium-Rise Timber Frame Buildings in the UK - C J Mettem, G C Pitts, P J Steer, V Enjily
29-15-5	Natural Frequency Prediction for Timber Floors - R J Bainbridge, and C J Mettem
30-15-1	Cyclic Performance of Perforated Wood Shear Walls with Oversize Oriented Strand Board Panels - Ming He, H Magnusson, F Lam, and H G L Prion
30-15-2	A Numerical Analysis of Shear Walls Structural Performances - L Davenne, L Daudeville, N Kawai and M Yasumura
30-15-3	Seismic Force Modification Factors for the Design of Multi-Storey Wood-Frame Platform Construction - E Karacabeyli and A Ceccotti
30-15-4	Evaluation of Wood Framed Shear Walls Subjected to Lateral Load - M Yasumura and N Kawai
31-15-1	Seismic Performance Testing On Wood-Framed Shear Wall - N Kawai
31-15-2	Robustness Principles in the Design of Medium-Rise Timber-Framed Buildings - C J Mettem, M W Milner, R J Bainbridge and V. Enjily
31-15-3	Numerical Simulation of Pseudo-Dynamic Tests Performed to Shear Walls - L Daudeville, L Davenne, N Richard, N Kawai and M Yasumura
31-15-4	Force Modification Factors for Braced Timber Frames - H G L Prion, M Popovski and E Karacabeyli
32-15-1	Three-Dimensional Interaction in Stabilisation of Multi-Storey Timber Frame Buildings - S Andreasson
32-15-2	Application of Capacity Spectrum Method to Timber Houses - N Kawai
32-15-3	Design Methods for Shear Walls with Openings - C Ni, E Karacabeyli and A Ceccotti
32-15-4	Static Cyclic Lateral Loading Tests on Nailed Plywood Shear Walls - K Komatsu, K H Hwang and Y Itou
33-15-1	Lateral Load Capacities of Horizontally Sheathed Unblocked Shear Walls – C Ni, E Karacabeyli and A Ceccotti
33-15-2	Prediction of Earthquake Response of Timber Houses Considering Shear Deformation of Horizontal Frames – N Kawai
33-15-3	Eurocode 5 Rules for Bracing – H J Larsen

34-15-1 A simplified plastic model for design of partially anchored wood-framed shear walls – B Källsner, U A Girhammar, Liping Wu

34-15-2 The Effect of the Moisture Content on the Performance of the Shear Walls – S Nakajima

34-15-3 Evaluation of Damping Capacity of Timber Structures for Seismic Design – M Yasumura

35-15-1 On test methods for determining racking strength and stiffness of wood-framed shear walls - B Källsner, U A Girhammar, L Wu

35-15-2 A Plastic Design Model for Partially Anchored Wood-framed Shear Walls with Openings - U A Girhammar, L Wu, B Källsner

35-15-3 Evaluation and Estimation of the Performance of the Shear Walls in Humid Climate - S Nakajima

35-15-4 Influence of Vertical Load on Lateral Resistance of Timber Frame Walls - B Dujič, R Žarnić

35-15-5 Cyclic and Seismic Performances of a Timber-Concrete System - Local and Full Scale Experimental Results - E Fournely, P Racher

35-15-6 Design of timber-concrete composite structures according to EC5 - 2002 version - A Ceccotti, M Fragiacomo, R M Gutkowski

35-15-7 Design of timber structures in seismic zones according to EC8- 2002 version - A Ceccotti, T Toratti, B Dujič

35-15-8 Design Methods to Prevent Premature Failure of Joints at Shear Wall Corners - N Kawai, H Okiura

36-15-1 Monitoring Light-Frame Timber Buildings: Environmental Loads and Load Paths – I Smith et al.

36-15-2 Applicability of Design Methods to Prevent Premature Failure of Joints at Shear Wall Corners in Case of Post and Beam Construction - N Kawai, H Isoda

36-15-3 Effects of Screw Spacing and Edge Boards on the Cyclic Performance of Timber Frame and Structural Insulated Panel Roof Systems - D M Carradine, J D Dolan, F E Woeste

36-15-4 Pseudo-Dynamic Tests on Conventional Timber Structures with Shear Walls - M Yasumura

36-15-5 Experimental Investigation of Laminated Timber Frames with Fiber-reinforced Connections under Earthquake Loads - B Kasal, P Haller, S Pospisil, I Jirovsky, A Heiduschke, M Drdacky

36-15-6 Effect of Test Configurations and Protocols on the Performance of Shear Walls - F Lam, D Jossen, J Gu, N Yamaguchi, H G L Prion

36-15-7 Comparison of Monotonic and Cyclic Performance of Light-Frame Shear Walls - J D Dolan, A J Toothman

37-15-1 Estimating 3D Behavior of Conventional Timber Structures with Shear Walls by Pseudodynamic Tests - M Yasumura, M Uesugi, L Davenne

37-15-2 Testing of Racking Behavior of Massive Wooden Wall Panels - B Dujič, J Pucelj, R Žarnić

37-15-3 Influence of Framing Joints on Plastic Capacity of Partially Anchored Wood-Framed Shear Walls - B Källsner, U A Girhammar

37-15-4 Bracing of Timber Members in Compression - J Munch-Andersen

37-15-5 Acceptance Criteria for the Use of Structural Insulated Panels in High Risk Seismic Areas - B Yeh, T D Skaggs, T G Williamson Z A Martin

37-15-6 Predicting Load Paths in Shearwalls - Hongyong Mi, Ying-Hei Chui, I Smith, M Mohammad

38-15-1 Background Information on ISO STANDARD 16670 for Cyclic Testing of Connections - E Karacabeyli, M Yasumura, G C Foliente, A Ceccotti

38-15-2 Testing & Product Standards – a Comparison of EN to ASTM, AS/NZ and ISO Standards – A Ranta-Maunus, V Enjily

38-15-3 Framework for Lateral Load Design Provisions for Engineered Wood Structures in Canada - M Popovski, E Karacabeyli

38-15-4 Design of Shear Walls without Hold-Downs - Chun Ni, E Karacabeyli

38-15-5 Plastic design of partially anchored wood-framed wall diaphragms with and without openings - B Källsner, U A Girhammar

38-15-6 Racking of Wooden Walls Exposed to Different Boundary Conditions - B Dujič, S Aicher, R Žarnić

38-15-7 A Portal Frame Design for Raised Wood Floor Applications - T G Williamson, Z A Martin, B Yeh

38-15-8 Linear Elastic Design Method for Timber Framed Ceiling, Floor and Wall Diaphragms - Jarmo Leskelä

38-15-9 A Unified Design Method for the Racking Resistance of Timber Framed Walls for Inclusion in EUROCODE 5 - R Griffiths, B Källsner, H J Blass, V Enjily

39-15-1 Effect of Transverse Walls on Capacity of Wood-Framed Wall Diaphragms - U A Girhammar, B Källsner

39-15-2 Which Seismic Behaviour Factor for Multi-Storey Buildings made of Cross-Laminated Wooden Panels? - M Follesa, M P Lauriola, C Minowa, N Kawai, C Sandhaas, M Yasumura, A Ceccotti

39-15-3 Laminated Timber Frames under dynamic Loadings - A Heiduschke, B Kasal, P Haller

39-15-4 Code Provisions for Seismic Design of Multi-storey Post-tensioned Timber Buildings - S Pampanin, A Palermo, A Buchanan, M Fragiacomo, B Deam

40-15-1 Design of Safe Timber Structures – How Can we Learn from Structural Failures? - S Thelandersson, E Frühwald

40-15-2 Effect of Transverse Walls on Capacity of Wood-Framed Wall Diaphragms—Part 2 - U A Girhammar, B Källsner

40-15-3 Midply Wood Shear Wall System: Concept, Performance and Code Implementation - Chun Ni, M Popovski, E Karacabeyli, E Varoglu, S Stiemer

40-15-4 Seismic Behaviour of Tall Wood-Frame Walls - M Popovski, A Peterson, E Karacabeyli

40-15-5 International Standard Development of Lateral Load Test Method for Shear Walls - M Yasumura, E Karacabeyli

40-15-6 Influence of Openings on Shear Capacity of Wooden Walls - B Dujič, S Klobcar, R Žarnić

41-15-1 Need for a Harmonized Approach for Calculations of Ductility of Timber Assemblies - W Muñoz, M Mohammad, A Salenikovich, P Quenneville

41-15-2 Plastic Design of Wood Frame Wall Diaphragms in Low and Medium Rise Buildings - B Källsner, U A Girhammar

41 15-3 Failure Analysis of Light Wood Frame Structures under Wind Load - A Asiz, Y H Chui, I Smith

41-15-4 Combined Shear and Wind Uplift Resistance of Wood Structural Panel Shearwalls B Yeh, T G Williamson

41-15-5 Behaviour of Prefabricated Timber Wall Elements under Static and Cyclic Loading – P Schädle, H J Blass

42-15-1 Design Aspects on Anchoring the Bottom Rail in Partially Anchored Wood-Framed Shear Walls - U A Girhammar, B Källsner

42-15-2 New Seismic Design Provisions for Shearwalls and Diaphragms in the Canadian Standard for Engineering Design in Wood - M Popovski, E Karacabeyli, Chun Ni, P Lepper, G Doudak

42-15-3 Stability Capacity and Lateral Bracing Force of Metal Plate Connected Wood Truss Assemblies - Xiaobin Song, F Lam, Hao Huang, Minjuan He

42-15-4 Improved Method for Determining Braced Wall Requirements for Conventional Wood-Frame Buildings - Chun Ni, H Rainer, E Karacabeyli

43-15-1 Influence of the Boundary Conditions on the Racking Strength of Shear Walls with an Opening - M Yasumura

43-15-2 Influence of Different Standards on the Determination of Earthquake Properties of Timber Shear Wall Systems - P Schädle, H J Blaß

43-15-3 Full-Scale Shear Wall Tests for Force Transfer Around Openings - T Skaggs, B Yeh, F Lam

43-15-4 Optimized Anchor-Bolt Spacing for Structural Panel Shearwalls Subjected to Combined Shear and Wind Uplift Forces - B Yeh, E Keith, T Skaggs

44-15-1 A Proposal for Revision of the Current Timber Part (Section 8) of Eurocode 8 Part 1 - M Follesa, M Fragiacomo, M P Lauriola

44-15-2 Influence of Vertical Loads on Lateral Resistance and Deflections of Light-Frame Shear Walls - M Payeur, A Salenikovich, W Muñoz

44-15-3 Modelling Force Transfer Around Openings of Full-Scale Shear Walls - T Skaggs, B Yeh, F Lam, Minghao Li, D Rammer, J Wacker

44-15-4 Design of Bottom Rails in Partially Anchored Shear Walls Using Fracture Mechanics - E Serrano, J Vessby, A Olsson, U A Girhammar, B Källsner

44-15-5 Notes on Deformation and Ductility Requirements in Timber Structures. - K A Malo, P Ellingsbø, C Stamatopoulos

44-15-6 Enhanced Model of the Nonlinear Load-bearing Behaviour of Wood Shear Walls and Diaphragms - M H Kessel, C Hall

44-15-7 Seismic Performance of Cross-Laminated Wood Panels - M Popovski, E Karacabeyli

44-15-8 Evaluation of Plywood Sheathed Shear Walls with Screwed Joints Tested According to ISO 21581 - K Kobayashi, M Yasumura

44-15-9 Influence of Connection Properties on the Ductility and Seismic Resistance of Multi-Storey Cross-Lam Buildings - I Sustersic, M Fragiacomo, B Dujic

45-15-1 Performance Based Design and Force Modification Factors for CLT Structures - S Pei, M Popovski, J van de Lindt

45-15-2 Seismic Behaviour of Wood-Concrete Frame Shear-wall System and Comparison with Code Provisions - L Pozza, R Scotta, A Polastri, A Ceccotti

45-15-3 Determination of Failure Mechanism of CLT Shear Walls Subjected to Seismic Action - M Yasumura

45-15-4 Seismic Response of Timber Frames with Laminated Glass Glass Infill - V Rajčić, R Žarnić

45-15-5 Modeling Wood Structural Panel Portal Frame Response - T Skaggs, B Yeh

45-15-6 Simplified Cross-laminated Timber Wall Modeling for Linear-elastic Seismic Analysis - I Sustersic, B Dujic

46-15-1 Experimental Investigations on Seismic Behaviour of Conventional Timber Frame Wall with OSB Sheathing - Proposal of Behaviour Factor - C Faye, L Le Magorou, P Garcia, J-C Duccini

46-15-2 Capacity Seismic Design of X-Lam Wall Systems Based on Connection Mechanical Properties - I Gavric, M Fragiacomo, A Ceccotti

46-15-3 An Approach to Derive System Seismic Force Modification Factor for Buildings Containing Different LLRS's - Z Chen, C Ni, Y-H Chui, G Doudak, M Mohammad

46-15-4 Connections and Anchoring for Wall and Slab Elements in Seismic Design - M Schick, T Vogt, W Seim

46-15-5 Analytical Formulation Based on Extensive Numerical Simulations of Behavior Factor q for CLT buildings - L Pozza, R Scotta, D Trutalli, A Ceccotti, A Polastri

46-15-6 Proposal for the q-factor of Moment Resisting Timber Frames with High Ductility Dowel Connectors - D Wrzesniak, G Rinaldin, M Fragiacomo, C Amadio

46-15-7 Wind Tunnel Tests for Wood Structural Panels Used as Nailable Sheathing - B Yeh, A Cope, E Keith

FIRE

12-16-1 British Standard BS 5268 the Structural Use of Timber: Part 4 Fire Resistance of Timber Structures

13-100-2 CIB Structural Timber Design Code. Chapter 9. Performance in Fire

19-16-1 Simulation of Fire in Tests of Axially Loaded Wood Wall Studs - J König

24-16-1 Modelling the Effective Cross Section of Timber Frame Members Exposed to Fire - J König

25-16-1 The Effect of Density on Charring and Loss of Bending Strength in Fire - J König

25-16-2 Tests on Glued-Laminated Beams in Bending Exposed to Natural Fires - F Bolonius Olesen and J König

26-16-1 Structural Fire Design According to Eurocode 5, Part 1.2 - J König

31-16-1 Revision of ENV 1995-1-2: Charring and Degradation of Strength and Stiffness - J König

33-16-1 A Design Model for Load-carrying Timber Frame Members in Walls and Floors Exposed to Fire - J König

33-16-2 A Review of Component Additive Methods Used for the Determination of Fire Resistance of Separating Light Timber Frame Construction - J König, T Oksanen and K Towler

33-16-3 Thermal and Mechanical Properties of Timber and Some Other Materials Used in Light Timber Frame Construction - B Källsner and J König

34-16-1 Influence of the Strength Determining Factors on the Fire Resistance Capability of Timber Structural Members – I Totev, D Dakov

34-16-2 Cross section properties of fire exposed rectangular timber members - J König, B Källsner

34-16-3 Pull-Out Tests on Glued-in Rods at High Temperatures – A Mischler, A Frangi

35-16-1 Basic and Notional Charring Rates - J König

37 - 16 - 1 Effective Values of Thermal Properties of Timber and Thermal Actions During the Decay Phase of Natural Fires - J König

37 - 16 - 2 Fire Tests on Timber Connections with Dowel-type Fasteners - A Frangi, A Mischler

38-16-1 Fire Behaviour of Multiple Shear Steel-to-Timber Connections with Dowels - C Erchinger, A Frangi, A Mischler

38-16-2 Fire Tests on Light Timber Frame Wall Assemblies - V Schleifer, A Frangi

39-16-1 Fire Performance of FRP Reinforced Glulam - T G Williamson, B Yeh

39-16-2 An Easy-to-use Model for the Design of Wooden I-joists in Fire - J König, B Källsner

39-16-3 A Design Model for Timber Slabs Made of Hollow Core Elements in Fire - A Frangi, M Fontana

40-16-1 Bonded Timber Deck Plates in Fire - J König, J Schmid

40-16-2 Design of Timber Frame Floor Assemblies in Fire - A Frangi, C Erchinger

41-16-1 Effect of Adhesives on Finger Joint Performance in Fire - J König, J Norén, M Sterley

42-16-1 Advanced Calculation Method for the Fire Resistance of Timber Framed Walls -S Winter, W Meyn

42-16-2 Fire Design Model for Multiple Shear Steel-to-Timber Dowelled Connections - C Erchinger, A Frangi, M Fontana

42-16-3 Comparison between the Conductive Model of Eurocode 5 and the Temperature Distribution Within a Timber Cross-section Exposed to Fire - M Fragiacomo, A Menis, P Moss, A Buchanan, I Clemente

43-16-1 Light Timber Frame Construction with Solid Timber Members – Application of the Reduced Cross-section Method - J König, J Schmid

43-16-2 Fire Exposed Cross-Laminated Timber - Modelling and Tests - J Schmid, J König, J Köhler

43-16-3 Timber-Concrete Composite Floors in Fire - J O'Neill, D Carradine, R Dhakal, P J Moss, A H Buchanan, M Fragiacomo

44-16-1 Gypsum Plasterboards and Gypsum Fibreboards – Protective Times for Fire Safety Design of Timber Structures –A Just, J Schmid, J König

45-16-1 The Reduced Cross Section Method for Timber Members Subjected to Compression, Tension and Bending in Fire - M Klippel, J Schmid, A Frangi

46-16-1 Comparison of the Fire Resistance of Timber Members in Tests and Calculation Models - J Schmid, M Klippel, A Just, A Frangi

STATISTICS AND DATA ANALYSIS

13-17-1 On Testing Whether a Prescribed Exclusion Limit is Attained - W G Warren

16-17-1 Notes on Sampling and Strength Prediction of Stress Graded Structural Timber - P Glos

16-17-2 Sampling to Predict by Testing the Capacity of Joints, Components and Structures - B Norén

16-17-3 Discussion of Sampling and Analysis Procedures - P W Post

17-17-1 Sampling of Wood for Joint Tests on the Basis of Density - I Smith, L R J Whale

17-17-2 Sampling Strategy for Physical and Mechanical Properties of Irish Grown Sitka Spruce - V Picardo

18-17-1 Sampling of Timber in Structural Sizes - P Glos

18-6-3 Notes on Sampling Factors for Characteristic Values - R H Leicester

19-17-1 Load Factors for Proof and Prototype Testing - R H Leicester

19-6-2 Confidence in Estimates of Characteristic Values - R H Leicester

21-6-1 Draft Australian Standard: Methods for Evaluation of Strength and Stiffness of Graded Timber - R H Leicester

21-6-2 The Determination of Characteristic Strength Values for Stress Grades of Structural Timber. Part 1 - A R Fewell and P Glos

22-17-1 Comment on the Strength Classes in Eurocode 5 by an Analysis of a Stochastic Model of Grading - A proposal for a supplement of the design concept - M Kiesel

24-17-1 Use of Small Samples for In-Service Strength Measurement - R H Leicester and F G Young

24-17-2 Equivalence of Characteristic Values - R H Leicester and F G Young

24-17-3 Effect of Sampling Size on Accuracy of Characteristic Values of Machine Grades - Y H Chui, R Turner and I Smith

24-17-4 Harmonisation of LSD Codes - R H Leicester

25-17-2 A Body for Confirming the Declaration of Characteristic Values - J Sunley

25-17-3 Moisture Content Adjustment Procedures for Engineering Standards - D W Green and J W Evans

27-17-1 Statistical Control of Timber Strength - R H Leicester and H O Breitinger

30-17-1 A New Statistical Method for the Establishment of Machine Settings - F Rouger

35-17-1 Probabilistic Modelling of Duration of Load Effects in Timber Structures - J Köhler, S Svenson

38-17-1 Analysis of Censored Data - Examples in Timber Engineering Research - R Steiger, J Köhler

39-17-1 Possible Canadian / ISO Approach to Deriving Design Values from Test Data - I Smith, A Asiz, M Snow, Y H Chui

44-17-1 Influence of Sample Size on Assigned Characteristic Strength Values – P Stapel, G J P Ravenshorst, J W G van de Kuilen

GLUED JOINTS

20-18-1 Wood Materials under Combined Mechanical and Hygral Loading - A Martensson and S Thelandersson

20-18-2 Analysis of Generalized Volkersen - Joints in Terms of Linear Fracture Mechanics - P J Gustafsson

20-18-3 The Complete Stress-Slip Curve of Wood-Adhesives in Pure Shear - H Wernersson and P J Gustafsson

22-18-1 Perspective Adhesives and Protective Coatings for Wood Structures - A S Freidin

34-18-1 Performance Based Classification of Adhesives for Structural Timber Applications - R J Bainbridge, C J Mettem, J G Broughton, A R Hutchinson

35-18-1 Creep Testing Wood Adhesives for Structural Use - C Bengtsson, B Källander

38-18-1 Adhesive Performance at Elevated Temperatures for Engineered Wood Products - B Yeh, B Herzog, T G Williamson

39-18-1 Comparison of the Pull–out Strength of Steel Bars Glued in Glulam Elements Obtained Experimentally and Numerically - V Rajčić, A Bjelanović, M Rak

39-18-2 The Influence of the Grading Method on the Finger Joint Bending Strength of Beech - M Frese, H J Blaß

43-18-1 Comparison of API, RF and MUF Adhesives Using a Draft Australian/New Zealand Standard - B Walford

FRACTURE MECHANICS

21-10-1 A Study of Strength of Notched Beams - P J Gustafsson

22-10-1 Design of Endnotched Beams - H J Larsen and P J Gustafsson

23-10-1	Tension Perpendicular to the Grain at Notches and Joints - T A C M van der Put
23-10-2	Dimensioning of Beams with Cracks, Notches and Holes. An Application of Fracture Mechanics - K Riipola
23-19-1	Determination of the Fracture Energie of Wood for Tension Perpendicular to the Grain - W Rug, M Badstube and W Schöne
23-19-2	The Fracture Energy of Wood in Tension Perpendicular to the Grain. Results from a Joint Testing Project - H J Larsen and P J Gustafsson
23-19-3	Application of Fracture Mechanics to Timber Structures - A Ranta-Maunus
24-19-1	The Fracture Energy of Wood in Tension Perpendicular to the Grain - H J Larsen and P J Gustafsson
28-19-1	Fracture of Wood in Tension Perpendicular to the Grain: Experiment and Numerical Simulation by Damage Mechanics - L Daudeville, M Yasumura and J D Lanvin
28-19-2	A New Method of Determining Fracture Energy in Forward Shear along the Grain - H D Mansfield-Williams
28-19-3	Fracture Design Analysis of Wooden Beams with Holes and Notches. Finite Element Analysis based on Energy Release Rate Approach - H Petersson
28-19-4	Design of Timber Beams with Holes by Means of Fracture Mechanics - S Aicher, J Schmidt and S Brunold
30-19-1	Failure Analysis of Single-Bolt Joints - L Daudeville, L Davenne and M Yasumura
37 - 19 - 1	Determination of Fracture Mechanics Parameters for Wood with the Help of Close Range Photogrammetry - S Franke, B Franke, K Rautenstrauch
39-19-1	First Evaluation Steps of Design Rules in the European and German codes of Transverse Tension Areas - S Franke, B Franke, K Rautenstrauch

SERVICEABILITY

27-20-1	Codification of Serviceability Criteria - R H Leicester
27-20-2	On the Experimental Determination of Factor k_{def} and Slip Modulus k_{ser} from Short- and Long-Term Tests on a Timber-Concrete Composite (TCC) Beam - S Capretti and A Ceccotti
27-20-3	Serviceability Limit States: A Proposal for Updating Eurocode 5 with Respect to Eurocode 1 - P Racher and F Rouger
27-20-4	Creep Behavior of Timber under External Conditions - C Le Govic, F Rouger, T Toratti and P Morlier
30-20-1	Design Principles for Timber in Compression Perpendicular to Grain - S Thelandersson and A Mårtensson
30-20-2	Serviceability Performance of Timber Floors - Eurocode 5 and Full Scale Testing - R J Bainbridge and C J Mettem
32-20-1	Floor Vibrations - B Mohr
37-20-1	A New Design Method to Control Vibrations Induced by Foot Steps in Timber Floors - Lin J Hu, Y H Chui
37-20-2	Serviceability Limit States of Wooden Footbridges. Vibrations Caused by Pedestrians - P Hamm
43-20-1	The Long Term Instrumentation of a Timber Building in Nelson NZ - the Need for Standardisation - H W Morris, S R Uma, K Gledhill, P Omenzetter, M Worth

46-20-1 CLT and Floor Vibrations: a Comparison of Design Methods - A Thiel, S Zimmer, M Augustin, G Schickhofer

TEST METHODS

31-21-1 Development of an Optimised Test Configuration to Determine Shear Strength of Glued Laminated Timber - G Schickhofer and B Obermayr

31-21-2 An Impact Strength Test Method for Structural Timber. The Theory and a Preliminary Study - T D G Canisius

35-21-1 Full-Scale Edgewise Shear Tests for Laminated Veneer Lumber- B Yeh, T G Williamson

39-21-1 Timber Density Restrictions for Timber Connection Tests According to EN28970/ISO8970 - A Leijten, J Köhler, A Jorissen

39-21-2 The Mechanical Inconsistence in the Evaluation of the Modulus of Elasticity According to EN384 - T Bogensperger, H Unterwieser, G Schickhofer

40-21-1 ASTM D198 - Interlaboratory Study for Modulus of Elasticity of Lumber in Bending - A Salenikovich

40-21-2 New Test Configuration for CLT-Wall-Elements under Shear Load - T Bogensperger, T Moosbrugger, G Schickhofer

41-21-1 Determination of Shear Modulus by Means of Standardized Four-Point Bending Tests - R Brandner, B Freytag, G Schickhofer

43-21-1 Estimation of Load-Bearing Capacity of Timber Connections - J Munch-Andersen, J D Sørensen, F Sørensen

43-21-2 A New Method to Determine Suitable Spacings and Distances for Self-tapping Screws - T Uibel, H J Blaß

45-21-1 Evaluation of Shear Modulus of Structural Timber Utilizing Dynamic Excitation and FE Analysis - A Olsson, B Källsner

CIB TIMBER CODE

2-100-1 A Framework for the Production of an International Code of Practice for the Structural Use of Timber - W T Curry

5-100-1 Design of Solid Timber Columns (First Draft) - H J Larsen

5-100-2 A Draft Outline of a Code for Timber Structures - L G Booth

6-100-1 Comments on Document 5-100-1; Design of Solid Timber Columns - H J Larsen and E Theilgaard

6-100-2 CIB Timber Code: CIB Timber Standards - H J Larsen and E Theilgaard

7-100-1 CIB Timber Code Chapter 5.3 Mechanical Fasteners; CIB Timber Standard 06 and 07 - H J Larsen

8-100-1 CIB Timber Code - List of Contents (Second Draft) - H J Larsen

9-100-1 The CIB Timber Code (Second Draft)

11-100-1 CIB Structural Timber Design Code (Third Draft)

11-100-2 Comments Received on the CIB Code - U Saarelainen; Y M Ivanov, R H Leicester, W Nozynski, W R A Meyer, P Beckmann; R Marsh

11-100-3 CIB Structural Timber Design Code; Chapter 3 - H J Larsen

12-100-1 Comment on the CIB Code - Sous-Commission Glulam

12-100-2	Comment on the CIB Code - R H Leicester
12-100-3	CIB Structural Timber Design Code (Fourth Draft)
13-100-1	Agreed Changes to CIB Structural Timber Design Code
13-100-2	CIB Structural Timber Design Code. Chapter 9: Performance in Fire
13-100-3a	Comments on CIB Structural Timber Design Code
13-100-3b	Comments on CIB Structural Timber Design Code - W R A Meyer
13-100-3c	Comments on CIB Structural Timber Design Code - British Standards Institution
13-100-4	CIB Structural Timber Design Code. Proposal for Section 6.1.5 Nail Plates - N I Bovim
14-103-2	Comments on the CIB Structural Timber Design Code - R H Leicester
15-103-1	Resolutions of TC 165-meeting in Athens 1981-10-12/13
21-100-1	CIB Structural Timber Design Code. Proposed Changes of Sections on Lateral Instability, Columns and Nails - H J Larsen
22-100-1	Proposal for Including an Updated Design Method for Bearing Stresses in CIB W18 - Structural Timber Design Code - B Madsen
22-100-2	Proposal for Including Size Effects in CIB W18A Timber Design Code - B Madsen
22-100-3	CIB Structural Timber Design Code - Proposed Changes of Section on Thin-Flanged Beams - J König
22-100-4	Modification Factor for "Aggressive Media" - a Proposal for a Supplement to the CIB Model Code - K Erler and W Rug
22-100-5	Timber Design Code in Czechoslovakia and Comparison with CIB Model Code - P Dutko and B Kozelouh

LOADING CODES

4-101-1	Loading Regulations - Nordic Committee for Building Regulations
4-101-2	Comments on the Loading Regulations - Nordic Committee for Building Regulations
37-101-1	Action Combination Processing for the Eurocodes Basis of Software to Assist the Engineer - Y Robert, A V Page, R Thépaut, C J Mettem
43-101-1	Dependant Versus Independent Loads in Structural Design - T Poutanen

STRUCTURAL DESIGN CODES

1-102-1	Survey of Status of Building Codes, Specifications etc., in USA - E G Stern
1-102-2	Australian Codes for Use of Timber in Structures - R H Leicester
1-102-3	Contemporary Concepts for Structural Timber Codes - R H Leicester
1-102-4	Revision of CP 112 - First Draft, July 1972 - British Standards Institution
4-102-1	Comparsion of Codes and Safety Requirements for Timber Structures in EEC Countries - Timber Research and Development Association
4-102-2	Nordic Proposals for Safety Code for Structures and Loading Code for Design of Structures - O A Brynildsen
4-102-3	Proposal for Safety Codes for Load-Carrying Structures - Nordic Committee for Building Regulations

4-102-4 Comments to Proposal for Safety Codes for Load-Carrying Structures - Nordic Committee for Building Regulations

4-102-5 Extract from Norwegian Standard NS 3470 "Timber Structures"

4-102-6 Draft for Revision of CP 112 "The Structural Use of Timber" - W T Curry

8-102-1 Polish Standard PN-73/B-03150: Timber Structures; Statistical Calculations and Designing

8-102-2 The Russian Timber Code: Summary of Contents

9-102-1 Svensk Byggnorm 1975 (2nd Edition); Chapter 27: Timber Construction

11-102-1 Eurocodes - H J Larsen

13-102-1 Program of Standardisation Work Involving Timber Structures and Wood-Based Products in Poland

17-102-1 Safety Principles - H J Larsen and H Riberholt

17-102-2 Partial Coefficients Limit States Design Codes for Structural Timberwork - I Smith

18-102-1 Antiseismic Rules for Timber Structures: an Italian Proposal - G Augusti and A Ceccotti

18-1-2 Eurocode 5, Timber Structures - H J Larsen

19-102-1 Eurocode 5 - Requirements to Timber - Drafting Panel Eurocode 5

19-102-2 Eurocode 5 and CIB Structural Timber Design Code - H J Larsen

19-102-3 Comments on the Format of Eurocode 5 - A R Fewell

19-102-4 New Developments of Limit States Design for the New GDR Timber Design Code - W Rug and M Badstube

19-7-3 Effectiveness of Multiple Fastener Joints According to National Codes and Eurocode 5 (Draft) - G Steck

19-7-6 The Derivation of Design Clauses for Nailed and Bolted Joints in Eurocode5 - L R J Whale and I Smith

19-14-1 Annex on Simplified Design of W-Trusses - H J Larsen

20-102-1 Development of a GDR Limit States Design Code for Timber Structures - W Rug and M Badstube

21-102-1 Research Activities Towards a New GDR Timber Design Code Based on Limit States Design - W Rug and M Badstube

22-102-1 New GDR Timber Design Code, State and Development - W Rug, M Badstube and W Kofent

22-102-2 Timber Strength Parameters for the New USSR Design Code and its Comparison with International Code - Y Y Slavik, N D Denesh and E B Ryumina

22-102-3 Norwegian Timber Design Code - Extract from a New Version - E Aasheim and K H Solli

23-7-1 Proposal for a Design Code for Nail Plates - E Aasheim and K H Solli

24-102-2 Timber Footbridges: A Comparison Between Static and Dynamic Design Criteria - A Ceccotti and N de Robertis

25-102-1 Latest Development of Eurocode 5 - H J Larsen

25-102-1A Annex to Paper CIB-W18/25-102-1. Eurocode 5 - Design of Notched Beams - H J Larsen, H Riberholt and P J Gustafsson

25-102-2 Control of Deflections in Timber Structures with Reference to Eurocode 5 - A Martensson and S Thelandersson

28-102-1	Eurocode 5 - Design of Timber Structures - Part 2: Bridges - D Bajolet, E Gehri, J König, H Kreuzinger, H J Larsen, R Mäkipuro and C Mettem
28-102-2	Racking Strength of Wall Diaphragms - Discussion of the Eurocode 5 Approach - B Källsner
29-102-1	Model Code for the Probabilistic Design of Timber Structures - H J Larsen, T Isaksson and S Thelandersson
30-102-1	Concepts for Drafting International Codes and Standards for Timber Constructions - R H Leicester
33-102-1	International Standards for Bamboo – J J A Janssen
35-102-1	Design Characteristics and Results According to EUROCODE 5 and SNiP Procedures - L Ozola, T Keskküla
35-102-2	Model Code for the Reliability-Based Design of Timber Structures - H J Larsen
36-102-1	Predicted Reliability of Elements and Classification of Timber Structures - L Ozola, T Keskküla
36-102-2	Calibration of Reliability-Based Timber Design Codes: Choosing a Fatigue Model - I Smith
38-102-1	A New Generation of Timber Design Practices and Code Provisions Linking System and Connection Design - A Asiz, I Smith
38-102-2	Uncertainties Involved in Structural Timber Design by Different Code Formats - L Ozola, T Keskküla
38-102-3	Comparison of the Eurocode 5 and Actual Croatian Codes for Wood Classification and Design With the Proposal for More Objective Way of Classification - V Rajcic A Bjelanovic
39-102-1	Calibration of Partial Factors in the Danish Timber Code - H Riberholt
41 - 102 - 1	Consequences of EC 5 for Danish Best Practise - J Munch-Andersen
41 - 102 - 2	Development of New Swiss standards for the Assessment of Existing Load Bearing Structures – R Steiger, J Köhler
41 – 102 - 3	Measuring the CO2 Footprint of Timber Buildings – A Buchanan, S John
45-102-1	Assessment of Relevant Eurocode Based Design Equations in Regard to Structural Reliability - J Köhler, R Steiger

INTERNATIONAL STANDARDS ORGANISATION

3-103-1	Method for the Preparation of Standards Concerning the Safety of Structures (ISO/DIS 3250) - International Standards Organisation ISO/TC98
4-103-1	A Proposal for Undertaking the Preparation of an International Standard on Timber Structures - International Standards Organisation
5-103-1	Comments on the Report of the Consultion with Member Bodies Concerning ISO/TC/P129 - Timber Structures - Dansk Ingeniorforening
7-103-1	ISO Technical Committees and Membership of ISO/TC 165
8-103-1	Draft Resolutions of ISO/TC 165
12-103-1	ISO/TC 165 Ottawa, September 1979
13-103-1	Report from ISO/TC 165 - A Sorensen
14-103-1	Comments on ISO/TC 165 N52 "Timber Structures; Solid Timber in Structural Sizes; Determination of Some Physical and Mechanical Properties"
14-103-2	Comments on the CIB Structural Timber Design Code - R H Leicester

21-103-1 Concept of a Complete Set of Standards - R H Leicester

JOINT COMMITTEE ON STRUCTURAL SAFETY

3-104-1 International System on Unified Standard Codes of Practice for Structures - Comité Européen du Béton (CEB)

7-104-1 Volume 1: Common Unified Rules for Different Types of Construction and Material - CEB

37-104-1 Proposal for a Probabilistic Model Code for Design of Timber Structures - J Köhler, H Faber

CIB PROGRAMME, POLICY AND MEETINGS

1-105-1 A Note on International Organisations Active in the Field of Utilisation of Timber - P Sonnemans

5-105-1 The Work and Objectives of CIB-W18-Timber Structures - J G Sunley

10-105-1 The Work of CIB-W18 Timber Structures - J G Sunley

15-105-1 Terms of Reference for Timber - Framed Housing Sub-Group of CIB-W18

19-105-1 Tropical and Hardwood Timbers Structures - R H Leicester

21-105-1 First Conference of CIB-W18B, Tropical and Hardwood Timber Structures Singapore, 26 - 28 October 1987 - R H Leicester

INTERNATIONAL UNION OF FORESTRY RESEARCH ORGANISATIONS

7-106-1 Time and Moisture Effects - CIB W18/IUFRO 55.02-03 Working Party

5 CIB-W18 Papers, Vancouver, Canada 2013

46 - 6 - 1 Enhanced Design Approach for Reinforced Notched Beams - **R Jockwer, A Frangi, E Serrano, R Steiger**

46 - 7 - 1 Comparison of Design Rules for Glued-in rods and Design Rule Proposal for Implementation in European Standards - **M Stepinac, F Hunger, R Tomasi, E Serrano, V Rajcic, J-W van de Kuilen**

46 - 7 - 2 In-service Dynamic Stiffness of Dowel-type Connections - **T Reynolds, R Harris, Wen-Shao Chang**

46 - 7 - 3 Design Procedure to Determine the Capacity of Timber Connections under Potential Brittle, Mixed and Ductile Failure Modes - **P Zarnani, P Quenneville**

46 - 7 - 4 Withdrawal Strength of Self-tapping Screws in Hardwoods - **Ulrich Hübner**

46 - 7 - 5 Wood Splitting Capacity in Timber Connections Loaded Transversely: Riveted Joint Strength for Full and Partial Width Failure Modes - **P Zarnani, P Quenneville**

46 - 7 - 6 Design Approach for the Splitting Failure of Dowel-type Connections Loaded Perpendicular to Grain- **B Franke, P Quenneville**

46 - 7 - 7 Beams Loaded Perpendicular to Grain by Connections - **J C M Schoenmakers, A J M Leijten, A J M Jorissen**

46 - 7 - 8 Influence of Fasteners in the Compression Area of Timber Members - **M Enders-Comberg, H J Blaß**

46 - 7 - 9 Design of Shear Reinforcement for Timber Beams - **P Dietsch, H Kreuzinger, S Winter**

46 - 12 - 1 Modelling the Bending Strength of Glued Laminated Timber - Considering the Natural Growth Characteristics of Timber - **G Fink, A Frangi, J Kohler**

46 - 12 - 2 In-Plane Shear Strength of Cross Laminated Timber (CLT): Test Configuration, Quantification and Influencing Parameters - **R Brandner, T Bogensperger, G Schickhofer**

46 - 12 - 3 Shear Strength and Shear Stiffness of CLT-beams Loaded in Plane - **M Flaig, H J Blaß**

46 - 12 - 4 Stiffness of Screw-Reinforced LVL in Compression Perpendicular to the Grain - **C Watson, W van Beerschoten, T Smith, S Pampanin, A H Buchanan**

46 - 15 - 1 Experimental Investigations on Seismic Behaviour of Conventional Timber Frame Wall with OSB Sheathing - Proposal of Behaviour Factor - **C Faye, L Le Magorou, P Garcia, J-C Duccini**

INTERNATIONAL COUNCIL FOR RESEARCH AND INNOVATION
IN BUILDING AND CONSTRUCTION

WORKING COMMISSION W18 - TIMBER STRUCTURES

ENHANCED DESIGN APPROACH FOR REINFORCED NOTCHED BEAMS

R Jockwer
Empa, Swiss Federal Laboratories for Materials Science and Technology, Dübendorf
ETH Zurich, Institute of Structural Engineering IBK, Zurich
A Frangi
ETH Zurich, Institute of Structural Engineering IBK, Zurich
R Steiger
Empa, Swiss Federal Laboratories for Materials Science and Technology, Dübendorf
SWITZERLAND
E Serrano
Linnaeus University, Department of Building and Energy Technology, Växjö
SWEDEN

Keywords: notch, reinforcement, reinforced notched beam, fracture mechanics, self-tapping screw, design approach, shear reinforcement, timber

---

Presented by R Jockwer

P Quenneville asked whether it matters where the reinforcing screws are located. R Jockwer responded yes and it is most effective to install them close to the notch corner but limited by the end distance requirements. P. Quenneville asked whether 5 cm distance could create crack problems. R Jockwer responded no.

H. Blass stated that for large notch ratios, it is difficult to get large enough anchorage length because the height of the notched part is so small. R Jockwer agreed. H Blass further commented that axial stiffness values from testing of different types of screws available for technical approval are valid for low anchorage depths. R Jockwer responded that the higher the stiffness the better the behaviour so the matter is valid. H Blass commented that glued on plates may be more appropriate because of the importance of stiffness. R. Jockwer agreed but stated that there could be bond line failures. H Blass commented that the test configuration on the left where the screw is pulled has a shear force component in reality; as the mechanism of load transfer is different and higher stiffness may result in real applications. R. Jockwer agreed and stated that there are always combined stresses in both directions.

S. Winter received confirmation that the test specimen on the right side is three pieces jointed together with Teflon sheets installed in between to reduce friction.

A Buchanan asked when predrill is needed and if the screws would be broken without predrilling. R. Jockwer stated in general predrilling was not needed. However close to end grain one may have a splitting problem. In large diameter thread rods where drill tips were not available predrilling would be needed. H Blass stated that close to end grain one should predrill. He stated that with density of 450 kg/m³ it should be okay without predrilling. In LVL with density in the range of 600 kg/m³ one would have problems. A Buchanan agreed.

Enhanced design approach for reinforced notched beams

Robert Jockwer[1,2)], Andrea Frangi[2)], Erik Serrano[3)], René Steiger[1)]
[1)] Empa, Swiss Federal Laboratories for Materials Science and Technology, Structural Engineering Research Laboratory, Dübendorf, Switzerland
[2)] ETH Zurich, Institute of Structural Engineering IBK, Zurich, Switzerland
[3)] Linnaeus University, Department of Building and Energy Technology, Växjö, Sweden

1 Introduction

Notches at the support (Fig. 1a) considerably reduce the load-carrying capacity of beams due to the stress concentrations around the notch corner. Recent design approaches based on fracture energy [9; 26] accordingly account for this reduction (EC5: EN 1995-1-1 [6], CSA O.86 [4]). In order to prevent brittle failure and to increase the load-carrying capacity, notches should be reinforced. The impact of different types of reinforcement on the load-carrying capacity of notched beams has been studied by various authors (e.g. Möhler and Mistler [19]). In general it was found that the load-carrying capacity could be increased significantly by the reinforcement.

Empirical equations e.g. by Scholten [23] represent a first step in the development of design approaches for notched beams. Later a bilinear approach has been developed [20] from more detailed analysis by means of Finite Element models and from further experimental tests. At the same time an approach based on linear elastic fracture mechanics (LEFM) was implemented in the Australian code for the design of timber structures AS1720 (AS CA 65 - 1972) [27] based on the studies by Leicester [16]. In the late 1980's a fracture mechanics design approach was developed by Gustafsson [9] and later made part of EC5 [6].

Shifted in time this development can be observed also in the design of reinforced notches. Initially only general rules for constructural reinforcement were required by e.g. DIN 1052:1969 before an empirical approach was proposed by Möhler and Mistler [19; 20]. Influences of orthotropy were accounted for in the studies by Henrici [10]. This approach was part of the German design code for timber structures DIN 1052:1988. However, discrepancies between the predicted load-carrying capacities of reinforced notched beams and test results (Fig. 1b) can be noticed. In order to well predict the load-carrying capacity of notched beams a more comprehensive understanding of the failure of reinforced notches is required. In this paper a model for the determination of the load-carrying capacity of reinforced notches in dependency of the stiffness of the reinforcement is presented. In addition, recommendations for an optimized reinforcement of notched beams are given.

2 Current design of reinforced notches

The design of the reinforcement when applied to notched beams is not specified in EC5, nor in CSA O.86 or AS 1720. However, approaches to determine the force acting in the reinforcement are given in the German standard DIN 1052:2008 (and also in the German National Annex of EC5) as well as in other handbooks (e.g. APA [4]): The tensile force perpendicular to the grain $F_{t,90,d}$ is set equal to the shear force V_d carried by the notched part of the cross-section $((1-\alpha)\cdot h)$ assuming a parabolic distribution of the shear stresses in

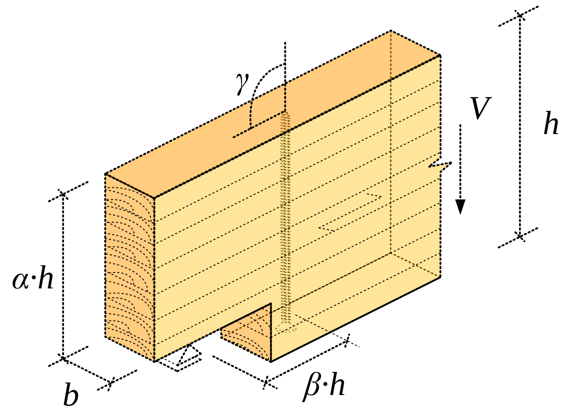

(a)

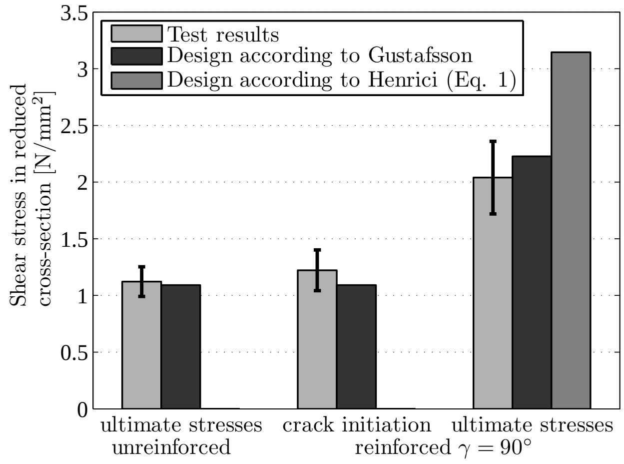

(b)

Fig. 1: Denotation used in this paper (a) and comparison of estimated load-carrying capacites with test results (b).

the full cross-section (Fig. 1a). V_d is increased by 1.3 in order to account for the orthotropy of the material and the notch length.

$$F_{t,90,d} = 1.3V_d \left[3\,(1-\alpha)^2 - 2\,(1-\alpha)^3\right] \tag{1}$$

A detailed explanation of the tensile force $F_\mathrm{t,90,d}$ acting in the reinforcement is given by Henrici [11], who performed extensive studies on the stress distribution around notches. From the total tensile force acting in the notch corner and the length of the region with tensile stresses perpendicular to the grain the factor 1.3 in the design equation was developed. However, this factor is conservative only for notch ratios $\alpha < 0.65$.

For the verification of notch strength the tensile force $F_\mathrm{t,90,d}$ that has to be carried by the reinforcement can be determined with the above design approach (Eq. 1). The reinforcement itself is designed with regard to tensile and withdrawal capacity (for inner reinforcement) or with regard to tensile and bond line capacity (for outer reinforcement). Reinforcing elements exhibiting high strength, like fully threaded self-tapping screws or adhered carbon fibre sheets, make it possible to achieve very high theoretical notch capacities. However, compared to predicted values in experiments reinforced notches exhibit much lower capacities (Fig. 1(b)).

The load-carrying capacity of notches without reinforcement can be predicted by means of Gustafsson's approach [9] when taking a reduced mode 1 fracture energy $G_{f,1}$ into account as discussed by Franke [8] and Jockwer [13].

Reinforced notches show an initial cracking, defined as the development of an apparent crack, that can be predicted by Gustafsson's approach. Further crack growth with mode 1 failure of the notch is prevented by the reinforcing element. The failure of the reinforced notch typically exhibits large deformations in shear. In experiments the load-carrying capacity of the reinforced notch was well predicted by Gustafsson's approach using the mode 2 fracture energy instead of the mode 1 fracture energy, which corresponds to an increase in strength by approximately a factor of 2 as compared to an unreinforced notch. The load-carrying capacity predicted by Eq. 1 is considerably higher compared to test results. This is due to the fact that shear failure of the reinforced notch is not accounted for in Eq. 1. Hence, a more detailed approach is needed in order to accurately predict the load-carrying capacity of reinforced notches with regard to shear and tensile perpendicular to grain failure.

3 Proposal for analytically modeling reinforced notches

The concept of fracture mechanics is commonly used to describe various fracture problems in timber engineering [24]. Hence, a model based on energy release rate is developed in order to get a more comprehensive understanding of the failure of a reinforced notch.

3.1 Energy release rate of an unreinforced notched beam

The approaches for the design of unreinforced notched beams in EC5 and CSA O.86 start from the calculation of energy release during crack growth at the notch corner. From equilibrium of the changes in potential ($W_{\text{potential}}$) and in internal elastic energies (W_{internal}) during unit area crack growth ΔA the energy release rate G can be calculated:

$$G = \frac{\partial W_{\text{total}}}{\partial A} = \frac{\partial W_{\text{potential}}}{\partial A} - \frac{\partial W_{\text{internal}}}{\partial A} \tag{2}$$

If G is equal or larger than a critical value G_c sufficient energy is available for the formation of a new crack surface. In a linear elastic fracture mechanics (LEFM) approach the change in potential energy $\Delta W_{\text{potential}}$ turns out to be twice the change in internal elastic energy $\Delta W_{\text{internal}}$. $\Delta W_{\text{internal}}$ can be calculated from the increase in deflection Δd of the notched beam during crack growth and therefore from the change in compliance ΔC and the applied load P (Eq. 3). The increase in crack surface can be expressed by an increase in crack length over the beam width $\Delta A = b\Delta l_{\text{crack}}$. Thus, the energy release rate G can be calculated from the derivation of the compliance C with respect to crack length l_{crack} (Eq. 4).

$$\Delta W_{\text{internal}} = \frac{1}{2}P\Delta d = \frac{1}{2}P^2\Delta C = Gb\Delta l_{\text{crack}} \tag{3}$$

$$G = \frac{P^2}{2b}\frac{\partial C}{\partial l_{\text{crack}}} \tag{4}$$

The compliance C is derived from the bending and shear deflection of the beam. In addition, Gustafsson [9] took into account a reduced stiffness at the connection between reduced and full cross-section to allow for a not fully rigid clamping at the intersection. Depending on the notch ratio α the beam part with reduced cross-section was increased by a length of up to approximately $1.5\alpha h$. This leads to a higher energy release rate $G_{\text{Gustafsson}}$ in the Gustafsson approach (Eq. 5) compared to other approaches not taking this reduction into account, like e.g. G_{Smith} by Smith and Springer [26] (Eq. 6).

$$G_{\text{Gustafsson}} = \frac{P^2}{b^2\alpha^2 h}\left(\sqrt{\frac{0.6\left(\alpha-\alpha^2\right)}{G_{xy}}} + \beta\sqrt{\frac{6\left(\frac{1}{\alpha}-\alpha^2\right)}{E_x}}\right)^2 \tag{5}$$

$$G_{\text{Smith}} = \frac{P^2}{b^2\alpha^2 h}\left(\frac{0.6\left(\alpha-\alpha^2\right)}{G_{xy}} + \beta\frac{6\left(\frac{1}{\alpha}-\alpha^2\right)}{E_x}\right) \tag{6}$$

Both approaches (5) and (6) estimate the total energy release rate of the notched beam for mixed mode failure occuring at the notch corner. Lum and Foschi [17] discussed the distribution of portions of mode 1 failure (crack opening) and mode 2 failure (in-plane shear) at notches. For the notched beam it can be found that mode 1 failure is the dominating fracture mode. That is why Gustafsson as well as Smith and Springer propose the mode 1 fracture energy to be the relevant strength criterion in the design. The influence of combined mode 1 and mode 2 actions at the notch was discussed analyzed Franke [8]. A reduction in the effectiv strength of the notch was found.

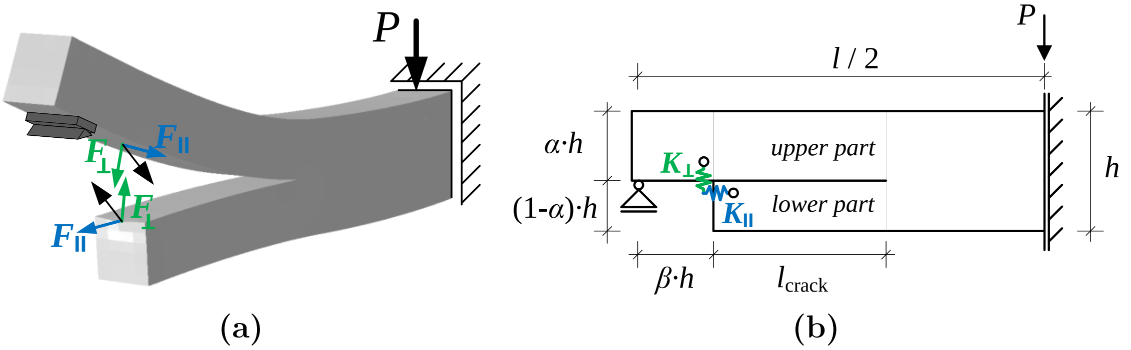

Fig. 2: Static model with acting forces induced by the reinforcement (a) and discretisation by means of springs (b).

Riipola [22] proposes to separate energy release rates with respect to the two failure modes. Mode 2 fracture is characterized by pure in-plane shear failure with zero crack opening of the crack surfaces. This corresponds to equal deflection and equal curvature κ of the upper and lower beam parts separated by the crack (Eq. 7) as explained in [29]. Riipola used the corresponding distribution of forces and moments during this pure shear fracture for the calculation of $G_{\mathrm{II,Riipola}}$. The mode 1 energy release rate G_{I} is the difference of the general mixed mode energy release rate G_{mixed} and the mode 2 energy release rate G_{II} (Eq. 8).

$$\frac{M_{upper}}{EI_{upper}} = \frac{M_{lower}}{EI_{lower}} \quad (7) \qquad\qquad G_{\mathrm{I}} = G_{\mathrm{mixed}} - G_{\mathrm{II}} \quad (8)$$

The resulting $G_{\mathrm{I,Riipola}}$ and $G_{\mathrm{II,Riipola}}$ in Eq. 9 and 10 are based on the compliance from bending and shear. Hence, the sum of $G_{\mathrm{I,Riipola}}$ and $G_{\mathrm{II,Riipola}}$ equals G_{Smith}. A comparison of all the approaches represented by Eq. 5, 6, 9 and 10 is shown in Figure 6a.

$$G_{\mathrm{I,Riipola}} = \frac{6}{b^2h^3E_x}(P\beta h)^2 \frac{(1-\alpha)^3}{\alpha^3\left(\alpha^3+(1-\alpha)^3\right)} + \frac{6}{b^2hG_{xy}}P^2\frac{(1-\alpha)}{10\alpha} \tag{9}$$

$$G_{\mathrm{II,Riipola}} = \frac{6}{b^2h^3E_x}(P\beta h)^2 \frac{3\left(\alpha-\alpha^2\right)}{\left(\alpha^3+(1-\alpha)^3\right)} \tag{10}$$

3.2 Energy release rate of a reinforced notched beam

The energy release rate of a reinforced notched beam can be calculated from the compliance of the beam according to Eq. 4. In contrast to the notched beam without reinforcement, the lower beam part contributes to the stiffness of the reinforced notched beam after crack initiation. The level of contribution of the lower beam part depends on the structural behaviour of the reinforcement with respect to the acting forces.

3.2.1 Forces in the reinforcement

The reinforcement leads to an exchange of forces between the upper and the lower part of the beam. Depending on the effect of the reinforcement and on the geometry of the notched beam, shear and normal forces and bending moment are induced in the lower beam part. The load transfer between upper and lower beam part depends on the type of reinforcement. Dowel type reinforcement like self-tapping, fully-threaded screws, threaded or glued in rods transfer load mainly in axial direction. Also unidirectional fibre reinforcement is most effective in fibre direction whereas shell type reinforcement made of e.g. plywood panels can transfer more

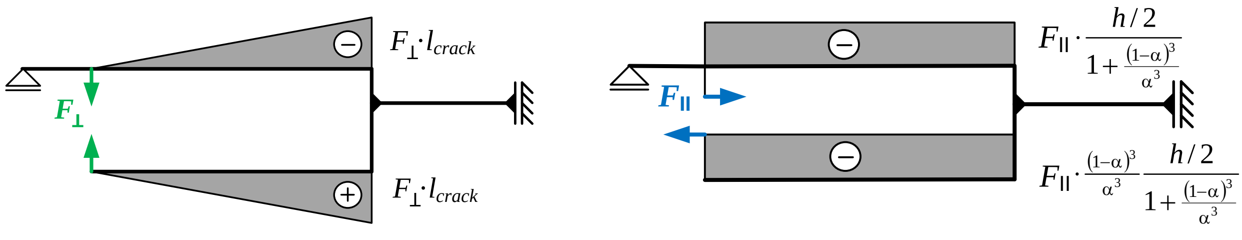

Fig. 3: Moment distribution in the bar model of Fig. 2 induced by spring forces in directions perpendicular (a) and parallel (b) to the crack plane.

complex stress distributions and moments. For the sake of simplicity the model is limited to dowel type reinforcement.

In order to account for different angles of inclination of reinforcement the force in the reinforcement at the intersection of the crack is split into two components $F_\perp$ and $F_{\shortparallel}$ in directions perpendicular and parallel to the crack plane (Fig. 2a). For the determination of the compliance the two components of the reinforcement are replaced by two springs with stiffness $K_\perp$ and $K_{\shortparallel}$ in direction perpendicular and parallel to the crack plane (Fig. 2b). The force $F_{\shortparallel}$ introduces a moment with a total lever arm of $h/2$ between upper and lower beam part. This moment is shared by the upper and the lower part of the beam according to their bending stiffness. The moment induced by $F_\perp$ is equal in the upper and lower beam part. The moment distributions resulting from $F_\perp$ and $F_{\shortparallel}$, are shown in Figure 3. The forces in the reinforcement and the resulting moment and shear force distribution of the second order statically indeterminate system can be calculated by applying the principle of virtual forces. The compliance $C_{\text{reinforced}}$ takes the stiffness of the springs according to Eq. 11 into account. Using $C_{\text{reinforced}}$ the mixed mode energy release rate of a reinforced notch beam $G_{\text{reinforced}}$ can be derived from Eq. 4.

$$C_{\text{reinforced}} = \frac{d}{P} = \frac{1}{P}\left\{\frac{M\bar{M}}{EI} + \frac{Q\bar{Q}}{GA} + \frac{N\bar{N}}{EA} + \frac{F_\perp \bar{F}_\perp}{K_\perp} + \frac{F_{\shortparallel}\bar{F}_{\shortparallel}}{K_{\shortparallel}}\right\} \tag{11}$$

With increasing stiffness $K_\perp$ and $K_{\shortparallel}$ the load contribution of the lower beam part increases. This leads to a reduction of the deflection of the beam and, hence, to a reduction of the energy release rate $G_{\text{reinforced}}$. Full activation of the cracked part could be achieved with infinitely stiff reinforcement.

The mode 2 energy release rate $G_{\text{II,reinforced}}$ is determined from the system with equal deflection and equal curvature κ of the upper and the lower beam part (Eq. 7). Consequently $G_{\text{II,reinforced}}$ depends on the stiffness of the reinforcement only in shearing direction $K_{\shortparallel}$. As a result the mode 1 energy release rate $G_{\text{I,reinforced}}$ as the difference of $G_{\text{mixed,reinforced}}$ and $G_{\text{II,reinforced}}$ depends on $K_\perp$. The energy release rates further are functions of the geometric parameters $\alpha, \beta, h, b, l_{\text{crack}}$ and on the load P. Due to the statically indeterminate system explicit calculation of $G_{\text{I,reinforced}}$ and $G_{\text{II,reinforced}}$ from the compliance according to Eq. 4 is rather tedious. Only for boundary conditions with zero reinforcement the solutions of $G_{\text{I,reinforced}}$ and $G_{\text{II,reinforced}}$ can be given, which coincide exactly with $G_{\text{I,Riipola}}$ and $G_{\text{II,Riipola}}$, respectively. The calcuations for the cases $K_{\shortparallel} \neq 0$ and $K_\perp \neq 0$ were performed using the software MAPLE.

3.2.2 Intersection of the members during crack growth

Depending on the stiffness ratio of the upper and the lower beam part and the stiffness $K_{\shortparallel}$ and $K_\perp$ of the reinforcement, it can happen, that in the simplified model (Fig. 2) the curvature of

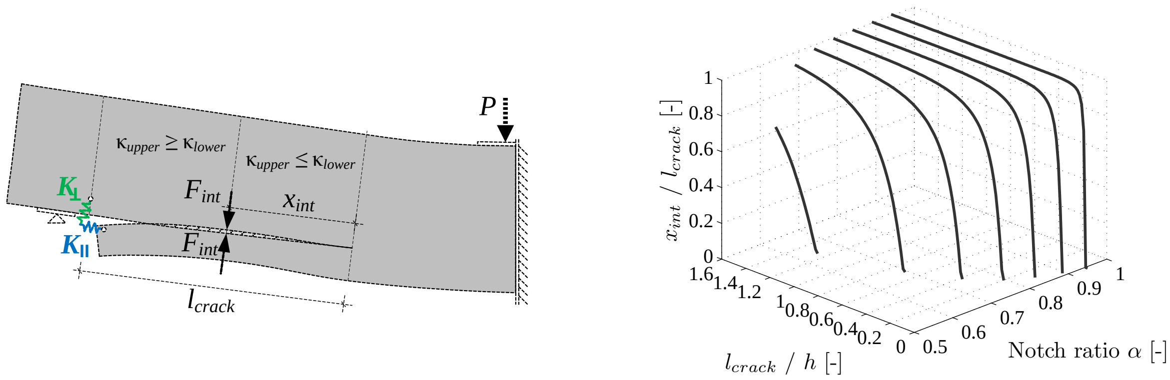

(a) (b)

Fig. 4: Sketch of the intersection of upper and lower beam part with $\kappa_{lower} \geq \kappa_{upper}$ and placement of the interaction force F_{int} at the position x_{int} in (a). The ratio of x_{int} to crack length l_{crack} in dependency of the notch ratio α is shown in (b) for a sample beam.

the lower beam part κ_{lower} is greater than the curvature of the upper beam part κ_{upper}. Due to the assumed linear distribution of the moment this would lead to an intersection of the upper and lower parts. In reality, besides non-linear stress distribution, a compression force is acting on the crack surface equalising the curvatures of the two parts. In Finite Element models with predifined contact properties along the crack path the interaction stresses can be calculated. The compression stresses are concentrated in the region of zero clearance. In order to account for this crack surface contact stresses an interaction force F_{int} was introduced into the analytical model working as a crack opening component at position x_{int} from the notch corner (Fig. 4a). Since the moment distribution of the two members is linear in the model the region of the intersection is defined as the region in which $\kappa_{lower} \geq \kappa_{upper}$. The moment and shear distribution changes due to F_{int} leading to a decrease in κ_{lower} and to an increase in κ_{upper}. The force F_{int} is chosen such that the curvature in the two members is equal. The magnitude F_{int} and the position x_{int} of the interaction force is found by iteration. Fig. 4b shows the ratio of position of intersection x_{int} to crack length l_{crack} for different notch ratios α along the crack path for a sample beam with $h = 600\mathrm{mm}$, $b = 140\mathrm{mm}$, $\beta = 0.25$, $E_{\mathrm{x}} = 11500\mathrm{N/mm}^2$, $G_{\mathrm{xy}} = 650\mathrm{N/mm}^2$ (corresponding to GL24h according to EN 14080 [7]) and $K_{\shortparallel} = K_{\perp} = 10^4\mathrm{N/mm}$. For larger notches with α around 0.5 and for short cracks mode 1 failure is dominant and no interaction occurs. For small notches with α around 0.9 and with long cracks the upper and lower beam part are interacting over a large extant of the crack length l_{crack}. These notches fail by peeling off of the notched part with dominant mode 2 failure.

3.3 Structural behaviour of the reinforced notched beam

A study of the structural behaviour of a reinforced notched beam was carried out on a sample beam with the following parameters: $h = 600\mathrm{mm}$, $b = 140\mathrm{mm}$, $\alpha = 0.6$, $\beta = 0.25$, $E_{\mathrm{x}} = 11500\mathrm{N/mm}^2$, $G_{\mathrm{xy}} = 650\mathrm{N/mm}^2$. The height and width of the beam are linearly connected to the influence of the stiffness of the reinforcement. Therefore, extrapolation to other dimensions is possible. The material properties Modulus of Elasticity E_{x} and shear modulus G_{xy} are linearly correlated to the influence of the stiffness of the reinforcement in direction parallel and perpendicular to the crack, respectively.

For a given configuration the influence of the reinforcement increases with increasing crack length. Figure 5 shows the influence of $K_{\perp}$ and $K_{\shortparallel}$ on the progression of $G_{\mathrm{I,reinforced}}$ and $G_{\mathrm{II,reinforced}}$, respectively, along the crack length l_{crack}. The values are normalized in relation

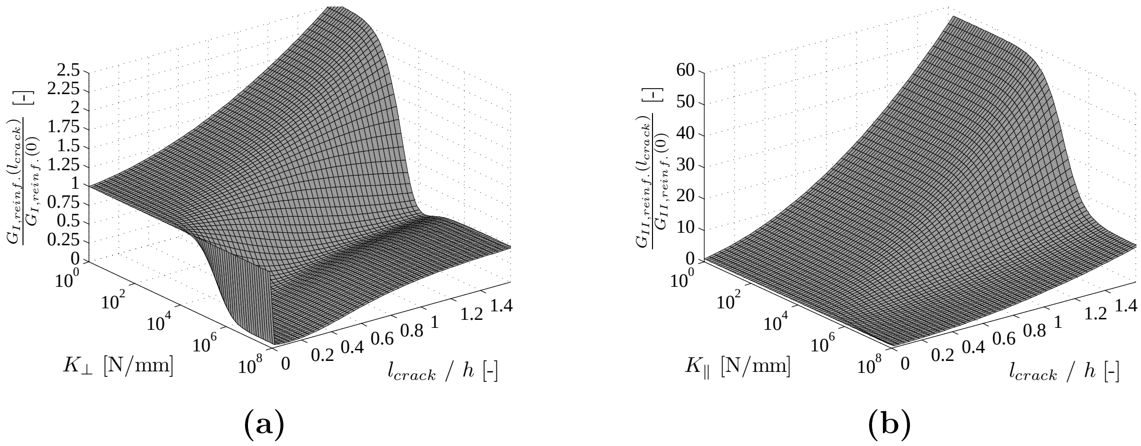

Fig. 5: Ratio of the energy release rates $G_{\mathrm{I,reinforced}}$ (a) and $G_{\mathrm{II,reinforced}}$ (b) at crack length l_{crack} to the energy release rates at zero crack length $G_{\mathrm{i,reinforced}}(0)$ for different stiffnesses $K_{\perp}$ (a) and $K_{\shortparallel}$ (b) (in logarithmic scale).

to the energy release rates at zero crack length. The reinforcement considerably reduces the progression of $G_{\mathrm{I,reinforced}}$ for $K_{\perp} > 10^3$ (Figure 5a). For higher stiffnesses $G_{\mathrm{I,reinforced}}$ approaches zero with increasing crack length. The influence of the parallel to crack stiffness on $G_{\mathrm{II,reinforced}}$ increases for $K_{\shortparallel} > 10^4$ (Fig. 5b). As can be seen in Fig. 6a the fracture of the reinforced notch is initiated by mode 1 failure, due to the much higher initial value of $G_{\mathrm{I,reinforced}}$ compared to $G_{\mathrm{II,reinforced}}$. This effect is intensified by the approximately 3 times lower value of $G_{\mathrm{I,c}}$ against mode 1 failure of the wood as compared to $G_{\mathrm{II,c}}$ of mode 2 failure (Chapter 4.3). If the reinforcement is designed to be of sufficient stiffness to reduce $G_{\mathrm{I,reinforced}}$ after crack initiation towards zero and to limit $G_{\mathrm{II,reinforced}}$ to a constant value, the load-carrying capacity and the structural behaviour of the reinforced notch can be enhanced considerably.

4 Benchmarking of the proposed analytical model

4.1 Comparison of the approaches in estimating G

The models represented by Eq. 5 and 6, which are part of the current design equations for unreinforced notched beams in EC5 and CSA O.86, serve for comparison with the model for zero crack length and no reinforcement. The model proposed by Riipola gives the separated fracture modes according to Eq. 9 and 10. The energy release rates of mode 1 and mode 2 according to Riipola and the ones of the model of this paper are equal for zero reinforcement and have the same basis as Equation 6. In Figure 6 the energy release rates in dependency of the notch ratio of the different approaches are compared for a sample beam.

Eq. 5 leads to higher values compared to Eq. 6 which results from Gustafsson's assumption of a reduced clamping stiffness at the notch corner. In all the other models no such assumption was made. The clamping effect increases in particular the mode 1 energy release rate. After initial crack growth, when both the upper and the lower beam part are contributing to the stiffness of the beam the impact of the reduced clamping decreases significantly. This leads to a theoretical stiffening of the beam and to a reduction in deflection, especially for short cracks. Negative fracture energies of the reinforced notched beam after an infinitesimal crack growth would be the result. Therefore the effect of reduced clamping was disregarded in the model for $G_{\mathrm{I,reinforced}}$ and $G_{\mathrm{II,reinforced}}$. However, $G_{\mathrm{Gustafsson}}$ can be used to calculate the initial cracking of the reinforced notched beam.

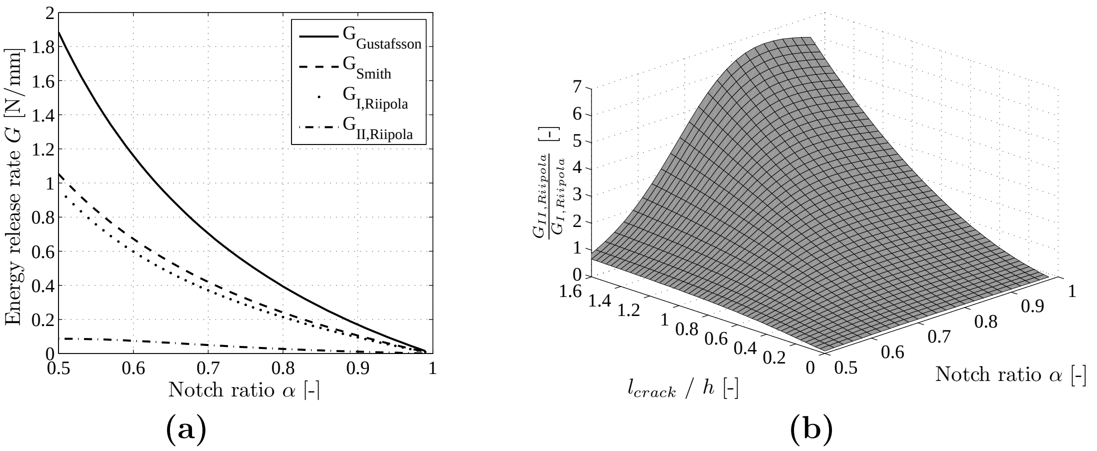

Fig. 6: Comparison of the approaches for mixed mode and mode separated energy release rates of the unreinforced notched beam (a) and progression of the ratio of $G_{\mathrm{II,Riipola}}$ to $G_{\mathrm{I,Riipola}}$ with l_{crack} and α (b). $G_{\mathrm{I,Riipola}}$ and $G_{\mathrm{II,Riipola}}$ are equal to $G_{\mathrm{I,reinforced}}$ and $G_{\mathrm{II,reinforced}}$ of the unreinforced notched beam.

Increasing crack length is equivalent to an increase in notch length in $G_{\mathrm{Gustafsson}}$ and G_{Smith}. During this crack growth the ratio of mode 2 to mode 1 energy release rate changes as displayed in Figure 6b. Mode 1 failure is dominating at zero crack length and for large notches with α around 0.5. For small notches (α around 0.9) and long crack length mode 2 failure becomes decisive.

4.2 Benchmarking of the proposed model to experimental data

The load-carrying capacity of the reinforced notch can be calculated applying a failure criterion to the model of energy release rates. Most exisiting failure criteria are based on stress intensity factors (SIF, fracture toughness, K_i). The Wu criterion [30] (Eq. 12) was found to be appropriate for describing failure in wood [18]. In order to use this criterion together with the above approach for energy release rates the relation between SIF and energy release rate as given by Sih et al. [25] is used. The resulting transformed Wu's criterion is given in Equation 13.

It has to be taken into account that $G_{\mathrm{I,reinforced}}$ when calculated as the difference between mixed mode and mode 2 energy release rate can be negative. If this is the case only the $G_{\mathrm{II,reinforced}}$ is used to determine the load-carrying capacity.

The ultimate load of the reinforced notched beam is determined by iterating the notch capacities along the crack from zero to ultimate length. In every step the respective forces in

Tab. 1: Parameters of tests performed on reinforced notched beams

Property			LNU Växjö	Empa Dübendorf
Sample size n			4 and 4	4 and 4
	γ	[°]	90 and 45	60 and 45
	d_{Screw}	[mm]	13	13
	α	[−]	0.65	0.8
	β	[−]	0.48	0.25
Height	h	[mm]	315	600
Width	b	[mm]	90	140
Length	l	[m]	3.15	2.9

$$\frac{K_I}{K_{Ic}} + \left(\frac{K_{II}}{K_{IIc}}\right)^2 \leq 1 \tag{12}$$

$$\sqrt{\frac{max\,\{G_I, 0\}}{Gc_I}} + \frac{G_{II}}{Gc_{II}} \leq 1 \tag{13}$$

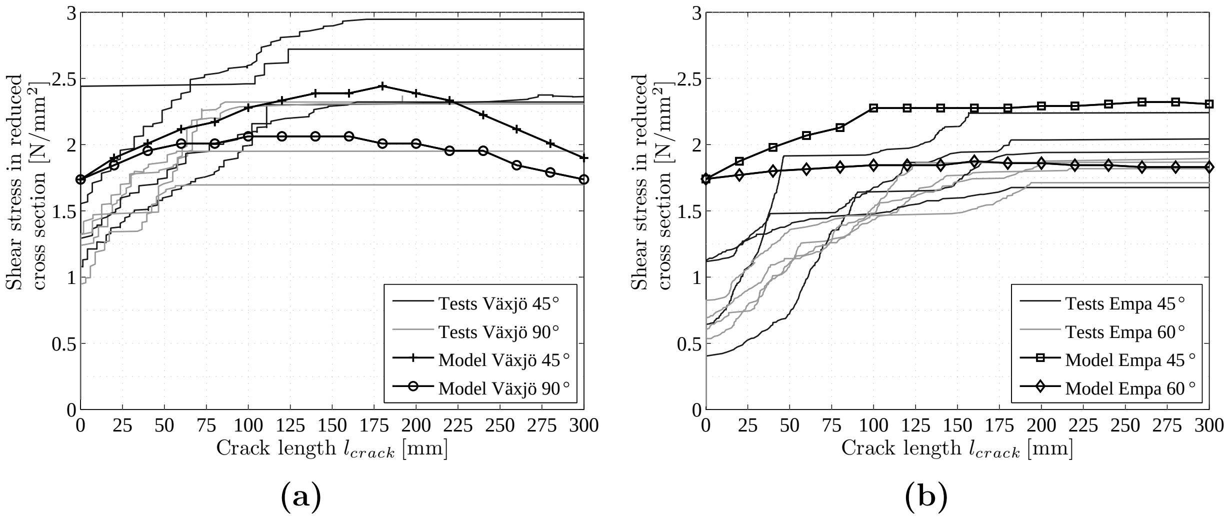

Fig. 7: Progression of shear stresses in the reduced cross section $b\alpha h$ force increasing crack length in experiments and according to the proposed model for the test carried out at LNU Växjö (a) and at Empa Dübendorf (b).

the reinforcement $F_{\perp}$ and $F_{\shortparallel}$, the resulting stiffness of the reinforcement $K_{\perp}$ and $K_{\shortparallel}$ and the interaction force F_{int} and position x_{int} are calculated. Non-linear stiffness of the reinforcement was considered as determined in experiments [12].

The model was finally benchmarked to results from tests on notched beams carried out at Linnaeus University Växjö, Sweden and at Empa Dübendorf, Switzerland (Tab. 1). The comparison of the results from experiments to those as predicted by the model is done by analysing the progression of crack length l_{crack} with increasing loads (Fig. 7). In the experiments strains and crack growth were recorded by means of the image correlation system ARAMIS. From the resulting strain distribution the crack length was identified at every step. In the analytical model the load-carrying capacity of a notch was determined by increasing the load until failure was reached.

The relative path of the curve calculated from the model is influenced by $K_{\perp}$ and $K_{\shortparallel}$, the absolut load value is governed by the assumed fracture energies $G_{\text{I,c}}$ and $G_{\text{II,c}}$. The values $G_{\text{I,c}} = 0.3\text{N/mm}$ and $G_{\text{II,c}} = 1.15\text{N/mm}$ were used in this study.

As can be seen in Fig. 7 the loads at crack initiation are overestimated by the model due to the effects discussed in Chapter 4.1. Nevertheless, progression of the crack and ultimate load are pedicted adequately.

4.3 Sensitivity analysis

In order to achieve a reliable estimate of the load-carrying capacity of reinforced notched beams it is crucial to have information about the sensitivity of the model with regard to the variation of the input parameters. Besides the geometry of the notch and the crack length, which are assumed to be deterministic variables, the stiffness of the reinforcement $K_{\perp}$ and $K_{\shortparallel}$ and the material properties MOE E_{x} and shear modulus G_{xy} of the timber impact the level of energy release rates $G_{\text{I,reinforced}}$ and $G_{\text{II,reinforced}}$. On the resistance side, critical fracture energies of mode 1 $G_{\text{I,c}}$ and mode 2 $G_{\text{II,c}}$ affect the load-carrying capacity of the notch. Even if graded into different strength classes the material properties of the timber are still strongly uncertain due to the natural structure of the wood. According to JCSS Probabilistic Model Code [14] MOE and shear modulus can be taken as lognormal distributed variables with a coefficient of variation $CoV = 13\%$, density ρ as normal distributed with $CoV = 10\%$. All

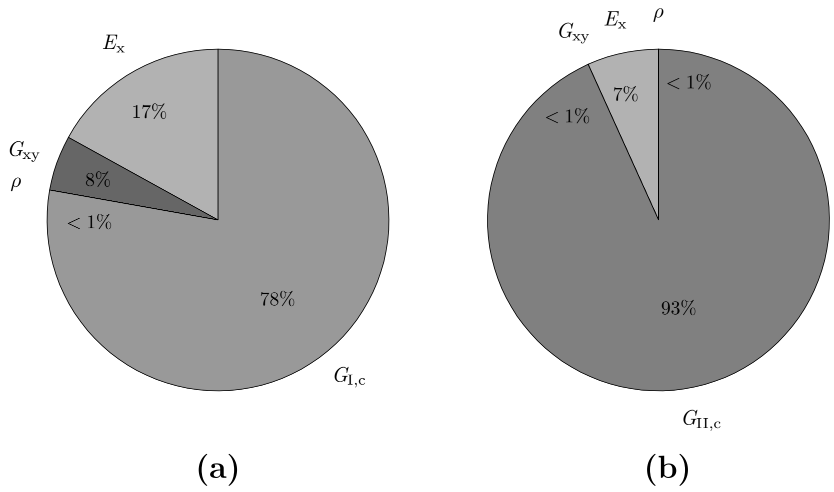

Fig. 8: Sensitivity of the load factor with regard to the random variables E_{x}, G_{xy}, ρ, $G_{\mathrm{I,c}}$ and $G_{\mathrm{II,c}}$ for predominantly mode 1 fracture (a) ($\alpha = 0.5, \beta = 0.25, l_{\mathrm{crack}} = 10\mathrm{mm}$) and mode 2 fracture (b) ($\alpha = 0.9, \beta = 1.0, l_{\mathrm{crack}} = 600\mathrm{mm}$).

of these properties are correlated to a medium extent (0.6). Density of the timber is known to have a large impact on the stiffness of screws [12]. The stiffness in lateral direction is specified with $K_v = \rho^{1.5}d/20$ N/mm in EC5. In [2] the stiffness in axial direction was found to be $K_{ax} = 234(\rho d)^{0.2} l_s^{0.4}$ N/mm based on a large number of experiments. In the sensitivity analysis an equal dependency $K_\perp$ and $K_{\shortparallel}$ from the density of $\rho^{1.5}$ is used, as it is supported by own tests on specimens of high and low density [12].

The determination of fracture energies $G_{\mathrm{I,c}}$ and $G_{\mathrm{II,c}}$ is laborious and not specified in standards. Influences on the variation of $G_{\mathrm{I,c}}$ are discussed in [13]. A lognormal distribution fits the experiments from literature well leading to a mean value $G_{\mathrm{I,c,mean}} = 0.3\mathrm{N/mm}$ (CoV = 20%). A method to determine $G_{\mathrm{II,c}}$ by means of an end notched flexural specimen [3] is described in [1]. However, not only the test method but also the evaluation of the data has a large impact on the results. Using the model as proposed in [1] the fracture energy was calculated from [1; 21; 28] for a sample of 214 specimens to be $G_{\mathrm{II,c,mean}} = 1.15\mathrm{N/mm}$. The data can be characterized by a lognormal distribution (CoV = 31%) with a fifth percentile value of $G_{\mathrm{II,c,05}} = 0.69\mathrm{N/mm}$.

In a sensitivity analysis the sensitivity factors were calculated for a sample beam with $h = 600\mathrm{mm}$ and $b = 140\mathrm{mm}$. The results are shown as the squares of the sensitivity factors in Fig. 8. The sensitivity factors can be interpreted as the relative importance of the individual random variables on the variation of the results [15]. The sum of the squares of the sensitivity factors is equal to 1. The sensitivity analysis was performed separately for the cases of predominantly mode 1 and mode 2 fracture. The fracture energy $G_{\mathrm{I,c}}$ and $G_{\mathrm{II,c}}$, respectively, have a dominating impact on the variation of load-carrying capacity of the reinforced notched beam. The magnitude of variation of the load-carrying capacity is in the order of 15% and 23% for predominantly mode 1 and mode 2 fracture, respectively, if fracture energies are represented by either characteristic or mean values.

5 How to optimize the reinforcement of notched beams?

An optimization of the structural behaviour of reinforced notched beams asks for an increase in load-carrying capacity and for turning brittle into ductile failure. In order to achieve a benefitial behaviour of reinforced notched beams, the total value and the relative proportion of the stiffness of the reinforcement in directions parallel and perpendicular to the grain can

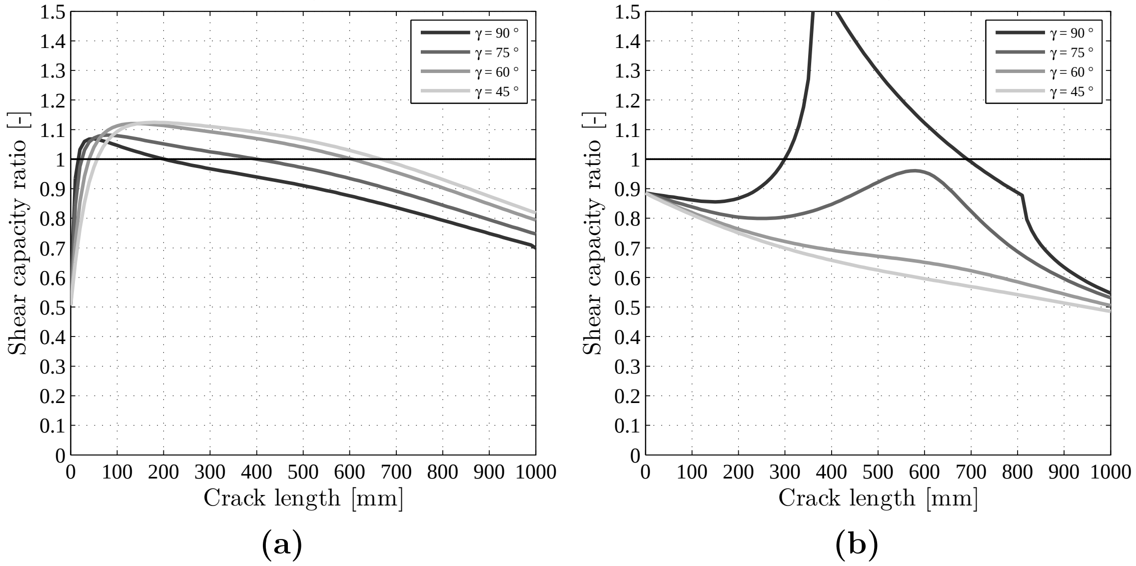

Fig. 9: The shear capacity ratio of a reinforced notched beam with $\alpha = 0.5$ (a) and $\alpha = 0.9$ (b) in dependency of the crack length l_{crack} for different inclination γ of the reinforcement. The reinforcement has a stiffness of $K_{ax} = 10^{6.4}$ and $K_v = 10^{5.4}$ in (a) and $K_{ax} = 10^{3.6}$ and $K_v = 10^{2.6}$ in (b).

be adjusted by applying different amount of reinforcement with different inclination, e.g. by means of self-tapping fully-threaded screws.

The structural behaviour of self-tapping fully-threaded screws is complex due to the interaction of withdrawal and embedment stiffnesses. The structural behaviour of inclined screws was discussed when loaded parallel to the grain in [2] and when loaded perpendicular to the grain in [12]. As a simplification $K_{\shortparallel,\gamma}$ can be taken as the sum of the portions of stiffness in axial (K_{ax}) and lateral (K_v) direction with respect to the inclination γ of the reinforcement (Eq. 14). The total stiffness $K_{\perp,\gamma}$ perpendicular to the grain is the inverse sum of K_{ax} and K_v (Eq. 15). From tests, e.g. [12], it is found that the stiffness in axial direction is approximetely 10 times the stiffness in lateral direction $K_{ax} = 10K_v$.

$$K_{\shortparallel,\gamma} = K_v sin^2\gamma + K_{ax} cos^2\gamma \qquad (14)$$

$$\frac{1}{K_{\perp,\gamma}} = \frac{cos^2\gamma}{K_v} + \frac{sin^2\gamma}{K_{ax}} \qquad (15)$$

When the load factor is calculated according to Eq. 13, no linear relation with the applied load is achieved in an optimisation study. That is why a square root interaction of $G_{\text{I,reinforced}}$ and $G_{\text{II,reinforced}}$ was used. According to [18] the corresponding failure criterion based on SIFs leads to conservative results compared to experiments. The results of the optimisation study as the ratio of the capacity of the reinforced notched beam at a certain crack length to the mean value of the shear capacity of the reduced cross-section $R_{\text{v,mean}} = f_{\text{v,mean}}\alpha hb$ are shown for $\alpha = 0.5$ and $\alpha = 0.9$ in Fig. 9. For the optimization study the sample beam from Chapter 3.3 was used.

The bigger notch with $\alpha = 0.5$ exhibits a more pronounced reduction of load-carrying capacity due to the higher energy release rate as already shown in Fig. 6a. Reinforcements with a high stiffness $K_\perp$ provoke a strong increase in $G_{\text{II,reinforced}}$. In order to reach the shear capacity of the reduced cross-section high stiffness in both directions $K_\perp$ and $K_{\shortparallel}$ is required. For self-tapping screws an inclination of $\gamma = 60 - 45°$ is most effective.

The beam with a smaller notch $\alpha = 0.9$ suffers only a slight reduction in load-carrying capacity (Fig. 6a). Though the ratio of $G_{\text{II,reinforced}}$ to $G_{\text{I,reinforced}}$ is higher compared to $\alpha = 0.5$, reinforcement with moderate $K_\perp$ is sufficient to reach the shear capacity of the reduced cross-section. For self-tapping screws an inclination of $\gamma = 90°$ is most effective.

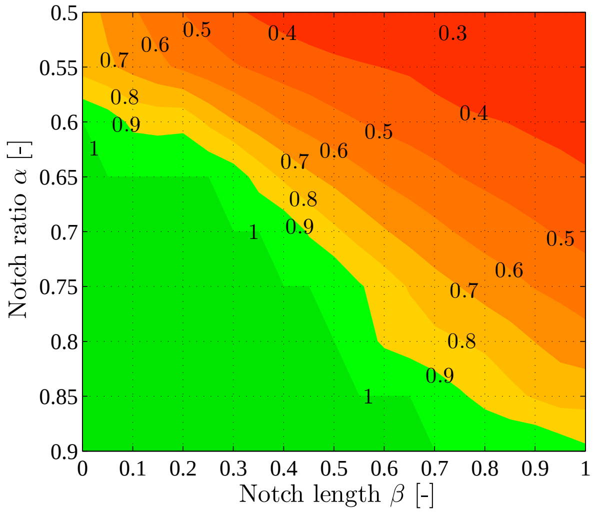

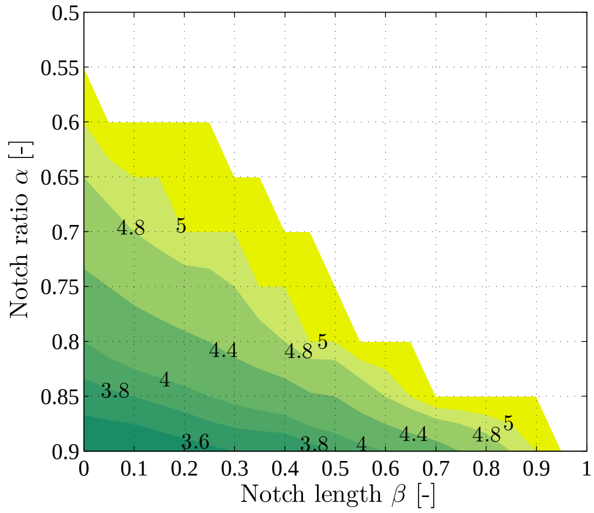

Fig. 10: Level of shear capacity of the reduced cross-section, that can be achieved by combined reinforcement with $K_\perp = 10^5$[N/mm] and $K_\shortparallel = 10^5$[N/mm] (a), and required stiffness of the reinforcement $K_\perp$[N/mm] and $K_\shortparallel$[N/mm] in order to reach the level of shear capacity of the reduced cross-section (b).

The loading of the reinforcement by the components $F_\perp$ and $F_\shortparallel$ changes during progression of the crack. An optimization of the reinforcement can be achieved by using a combination of reinforcement in directions $K_\perp$ and $K_\shortparallel$. This way the load-carrying capacity of the reinfocred notch can be enhanced for a broad range of geometries. The sample beam as described in Chapter 3.3 was studied for various notch length and notch ratios. In Fig. 10a the remaining level of shear capacity of the reduced cross-section is shown for a maximum stiffness of the reinforcement of $K_\perp = 10^5$[N/mm] and $K_\shortparallel = 10^5$[N/mm]. This stiffness can be achieved by means of threaded rods according to e.g. [5]. It can be seen, that for larger β and smaller α the impact of the notch on the reduction of strength can not be recovered by the reinforcement. Fig. 10b shows the required stiffness of combined reinforcement $K_\perp$ and $K_\shortparallel$ in order to retain the level of shear capacity of the reduced cross-section. For α around 0.9 and short notch length the stiffness of the reinforcement can be reduced.

6 Conclusions

The failure mechanism of reinforced notched beams is driven by both mode 1 and mode 2 fracture. If the notch is reinforced only in direction perpendicular to the grain against crack opening, the notch still can fail in shear (mode 2). Thus the capacity of the notch reinforced that way is limited to approximately twice the capacity of the unreinforced notch.

In order to reach higher capacities the reinforcement of the notch has to be optimized, allowing for loading in directions parallel and perpendicular to the crack. For that reason a model for the calculation of energy release rates of reinforced notch beams was developed accounting for the geometry of the notched beam, the stiffness of the reinforcement and the stiffness of the timber in shear and bending. By using e.g. the Wu failure criterion the load-carrying capacity of the reinforced notch can be calculated during the growth of a crack starting in the notch corner.

Depending on the stiffness of the reinforcement in directions parallel and perpendicular to the crack plane (resistance against mode 1 and mode 2 failure) the energy release rate of the notched beam is reduced considerably. In the case of short cracks and large notches with

$\alpha \approx 0.5$, the failure is dominated by mode 1 fracture. For this situations a high stiffness of the reinforcement in direction perpendicular to the crack is needed to prevent early failure. With increasing crack length mode 2 fracture is dominating the load-carrying capacity of the notch and a very stiff reinforcement in shear is needed to prevent excessive crack growth. For smaller notches with larger notch ratios $\alpha \approx 0.9$ mode 1 failure is dominating only crack initiation. Reinforcement with moderate stiffness in direction perpendicular to the crack is able to stop crack growth. The shear capacity of the reduced cross section is limiting the load-carrying capacity of these beams.

In order to achieve an optimal structural behaviour of the reinforced notched beam, reinforcement can be combined in both directions shear and tension perpendicular to the grain. To reach this benefitial behaviour stiffness of the reinforcement should be chosen according to the recommendations given in this paper.

References

[1] Aicher, S., Boström, L., Gierl, M., Kretschmann, D., Valentin, G.: Determination of fracture energy of wood in mode II - RILEM TC 133 Report. Tech. rep., SP-Swedish National Testing and Research Institute, Boras, Sweden (1997)

[2] Bejtka, I.: Verstärkung von Bauteilen aus Holz mit Vollgewindeschrauben. Ph.D. thesis, Universität Karlsruhe, Germany (2005)

[3] Boström, L.: Draft recommendation for determination of fracture energy in forward shear along the grain in wood. Materials and Structures **28**(8), 482–487 (1995)

[4] Canadian Standards Association CSA: O86-09: Engineering design of wood (2009)

[5] Deutsches Institut für Bautechnik, DIBt: Allgemeine bauaufsichtliche Zulassung Z-9.1-679 (2009)

[6] European Committee for Standardization CEN: EN 1995-1-1: Eurocode 5: Design of timber structures - Part 1-1: General - Common rules and rules for buildings (2004)

[7] European Committee for Standardization CEN: prEN 14080: Timber structures - Glued laminated timber and glued solid timber (2011)

[8] Franke, B.: Zur Bewertung der Tragfähigkeit von Trägerausklinkungen in Nadelholz. Ph.D. thesis, Bauhaus-Universität Weimar, Germany (2008)

[9] Gustafsson, P.J.: A study of strength of notched beams. In: Proceedings of the CIB-W18 Meeting 21, Parksville, Canada, Paper no. CIB-W18/21-10-1 (1988)

[10] Henrici, D.: Beitrag zur Spannungsermittlung in ausgeklinkten Biegeträgern aus Holz. Ph.D. thesis, Technische Universtität München, Germany (1984)

[11] Henrici, D.: Beitrag zur Bemessung ausgeklinkter Brettschichtholzträger. Bauen mit Holz **11**, 806–811 (1990)

[12] Jockwer, R., Steiger, R., Frangi, A.: Fully threaded self-tapping screws subjected to combined axial and lateral loading with different load to grain angles. In: Proceedings of the Rilem Conference - Materials and Joints in Timber Structures (2013). to be published October 2013

[13] Jockwer, R., Steiger, R., Frangi, A., Kohler, J.: Impact of material properties on the fracture mechanics design approach for notched beams in Eurocode 5. In: Proceedings of the CIB-W18 Meeting 44, Alghero, Italy, Paper no. CIB-W18/44-6-1 (2011)

[14] Joint Committee of Structural Safety: Probabilistic Model Code. http://www.jcss.byg.dtu.dk/ (2001)

[15] Kohler, J.: Reliability of timber structures. Ph.D. thesis, Institute of structural engineering IBK, ETH Zurich, Switzerland (2007)

[16] Leicester, R.H.: The size effect of notches. In: Proceedings of the 2nd Australasian Conference on Mechanics of Stuctures and Materials, pp. V4 1–20 (1969)

[17] Lum, C., Foschi, R.O.: Arbitrary V-notches in orthotropic plates. Journal of Engineering Mechanics **114**(4), 638–655 (1988)

[18] Mall, S., Murphy, J.F., Shottafer, J.E.: Criterion for mixed mode fracture in wood. Journal of Engineering Mechanics **109**(3), 680–690 (1983)

[19] Möhler, K., Mistler, H.L.: Untersuchungen über den Einfluss von Ausklinkungen im Auflagerbereich von Holzbiegeträgern auf die Tragfestigkeit, vol. F 1504. Fraunhofer IRB Verlag (1978)

[20] Mistler, H.L.: Die Tragfähigkeit des am Endauflager unten rechtwinklig ausgeklinkten Brettschichtträgers. Ph.D. thesis, Technische Hochschule Karlsruhe, Germany (1979)

[21] Riberholt, H., Enquist, B., Gustafsson, P.J., Jensen, R.B.: Timber beams notched at the support. Afdelingen for Baerende Konstruktioner, Lyngby, Denmark (1991)

[22] Riipola, K.: Design of glulam beams with holes. In: Proceedings of the CIB-W18 Meeting 28, Copenhagen, Denmark, Paper no. CIB-W18/28-12-3 (1995)
[23] Scholten: Rounding notches makes stronger joists. American Lumberman (1935)
[24] Serrano, E., Gustafsson, P.J.: Fracture mechanics in timber engineering - Strength analyses of components and joints. Materials and Structures **40**(1), 87–96 (2007)
[25] Sih, G.C., Paris, P.C., Irwin, G.R.: On cracks in rectilinearly anisotropic bodies. International Journal of Fracture Mechanics **1**(3), 189–203 (1965)
[26] Smith, I., Springer, G.: Consideration of Gustaffsson's proposed Eurocode 5 failure criterion for notched timber beams. Canadian Journal of Civil Engineering **20**(6), 1030–1036 (1993)
[27] Standards Association of Australia: AS CA65-1972, SAA Timber Engineering Code (1972)
[28] Stefansson, F.: Fracture analysis of orthotropic beams - linear elastic and nonlinear methods. Tech. rep., Division of Structural Mechanics, Lund University, Sweden (2001)
[29] Williams, J.: On the calculation of energy release rates for cracked laminates. International Journal of Fracture **36**(2), 101–119 (1988)
[30] Wu, E.M.: Application of fracture mechanics to anisotropic plates. Journal of Applied Mechanics **34**(4), 967–974 (1967)

INTERNATIONAL COUNCIL FOR RESEARCH AND INNOVATION IN BUILDING AND CONSTRUCTION

WORKING COMMISSION W18 - TIMBER STRUCTURES

COMPARISON OF DESIGN RULES FOR GLUED-IN RODS AND DESIGN RULE PROPOSAL FOR IMPLEMENTATION IN EUROPEAN STANDARDS

M Stepinac

University of Zagreb, Faculty of Civil Engineering, CROATIA

F Hunger

Technische Universität München, Holzforschung München, GERMANY

R Tomasi

University of Trento, ITALY

E Serrano

Linnaeus University, SWEDEN

V Rajcic

University of Zagreb, Faculty of Civil Engineering, CROATIA

J-W van de Kuilen

Technische Universität München, Holzforschung München, GERMANY

TU Delft, Faculty of Civil Engineering and Geosciences, THE NETHERLANDS

Keywords: glued-in steel rods, bonded-in rods, design rules, EN1995, structural timber connections, pull-out capacity, anchorage length, shear strength factor

---

Presented by M Stepinac

A Buchanan congratulated the authors about the work and look forward to additional information in the future.

A Frangi asked whether a unified approach is needed as good technical approval procedures are available. He stated that quality assurance would be the most important factor for glued in rods and engineers should choose a reputable firm for installation of these connectors. M Stepinac stated that technical guidelines would be needed. A Frangi further discussed the importance of quality control and assurance and stated that one might be giving an illusion with a codified approach.

S Aicher stated that glued in rod performance depends on adhesive and quality control. M Stepinac stated clear design rules would also be needed along with good quality control; otherwise one would not be able to consider glued in rods for implementation at an international level and its use would be stuck at a national level only.

H Blass stated one needs technical approval and it should be a combination of technical approval and code provisions.

S Winter stated principal rules given in code and European technical approval would be the correct combination. Also the influence of common understanding of testing details, climate change influence (temperature and relative humidity) would be important issues of study.

S Aicher stated European work group on glued in rod and adhesive is available.

Comparison of design rules for glued-in rods and design rule proposal for implementation in European standards

Stepinac, Mislav
University of Zagreb, Faculty of Civil Engineering, Croatia

Hunger, Frank
Technische Universität München, Holzforschung München, Germany

Tomasi, Roberto
University of Trento, Italy

Serrano, Erik
Linnaeus University, Sweden

Rajcic, Vlatka
University of Zagreb, Faculty of Civil Engineering, Croatia

van de Kuilen, Jan-Willem
Technische Universität München, Holzforschung München, Germany

1 Introduction

Glued-in rods are often considered as "new, innovative and highly efficient" way to connect timber elements. However, they have been used for at least 30 years. Glued-in rods represent a versatile joint system with advantages such as high load transition, appropriate behaviour in case of fire, easy application combined with a high level of prefabrication for fast installation. In addition, the aesthetic appearance of the finished joint also plays an important role.

Despite many national and international research projects and many practical applications of glued-in rods in timber structures, there is still no universal standard covering the design thereof. Therefore, a project group within WG1 of COST Action FP1004 (dealing with enhancing mechanical properties of timber, engineered wood products and timber structures) focuses on this topic with the aim to prepare the way for the implementation of design rules for glued-in rods into European standards by defining common design procedure or technical guideline. The idea is to focus all research knowledge and experiences (GIROD, Licons, etc.) to point out key issues regarding glued-in rods that need to be resolved.

Different design methods are in use in a number of countries but there are some apparent contradictions between these models and the influence of parameters that they predict. This has been evaluated in various studies. A general-purpose European design procedure which is convenient and user-friendly would be helpful. Due to past disagreements, the design rules considering glued-in rods included in a previous version of the Eurocode 5 (EC5) [1] cannot be found in the current valid version. At recent CEN meetings, within TC 250 work programme for the next five years, glued-in rods have been highlighted as an important work item because they are widely used all over the world. Consequently, design rules are considered necessary in Eurocode 5. The benefits of this work item were stated as a harmonisation of the current state of the art. The output of design rules as a new clause in existing EN1995 [1] was suggested.

This paper gives an overview and presents known design models, technical approvals and regulations, national standards and guidance papers, comparing the different approaches. Although there are many proposals for calculation and design of glued-in rods, it is necessary to individuate a unique design method and guidance about safe design of glued-in rods.

In addition to the comparison of design rules an online survey on the usage, requirements for a design rule and scientific research was developed and sent to scientists, timber industrialists and structural designers all over Europe.

2 Methods

2.1 General

One outcome of the discussion within the COST Action FP 1004 was to gather relevant information from published articles and known design rules and try to find out what needs must be further researched and what hinders the introduction in EC5. After reviewing literature, information was compiled and a systematic procedure was established. A table was compiled that contained the parameters that were investigated and the test setup used, besides general and additional information provided in the article. Parameters are grouped as shown in Figure 1. This figure is only a methodical presentation of the full table which will be available online [4]. This table can assist in the development of further research because it is easy to identify where the lack of knowledge and research is.

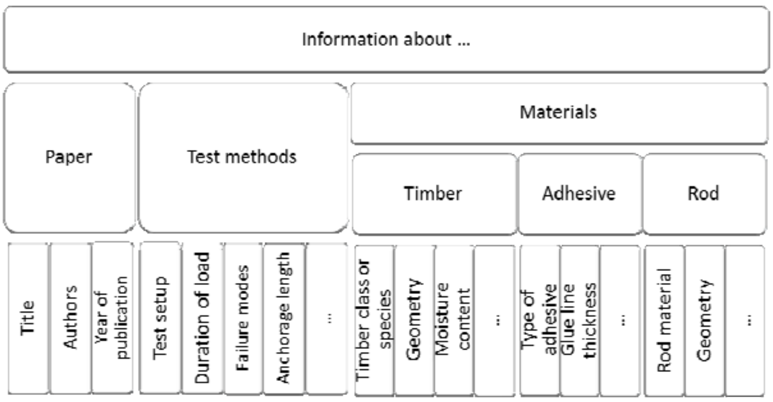

Figure 1: Overview of compiled information

Several studies were carried out to comprehend the influence of boundary conditions, loading modes and test setups. Different test setups have been used to obtain the capacity of a single glued in rod. The most common setups are pull-pull tests (see e.g. Bainbridge et al. (2000) [10]) where rods are glued-in on both sides of the specimen and pulled out axially (often in the longitudinal direction of the timber member). Others include pull-compression tests (Rajčić et al. 2006 [19]) which are carried out in a similar method to that outlined in EN 1382(1999) [3]. Tests carried out on the specimens in pull-compression setup do not correspond to the practical application (Tlustochowicz et al. 2011 [25]) but the test procedure is common and convenient for obtaining the capacity of a glued-in rod. By selecting the test setup and the anchorage length, different failure modes can be provoked or even excluded (Steiger et al. 2007 [24]). Typical failure modes are rod failure (preferably by yielding), shear failure in the adhesive or rupture of the timber around the bond and failure of the host timber member by splitting or tensile failure as shown in Figure 2.

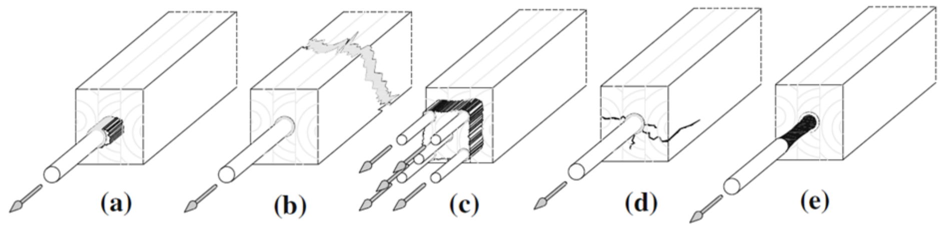

Figure 2: Failure modes for glued-in rods: (a) shear failure along the rod, (b) tensile failure, (c) group tear out, (d) splitting failure, (e) yielding of the rod (Tlustochowicz et al. 2011 [25])

A wide range in the tested timber quality can be noted because most of the tests are preformed to gain knowledge for a specific application (Kangas et al. 2001 [17]). The most typical timber quality was C24 or better. Glulam (Tomasi et al. 2009 [36]) or laminated veneer lumber made of softwood (Harvey et al. 2000 [15]) have also been used. This confirms the aspect to use glued-in rods for special and challenging applications. Steiger et al. (2004) [58] studied the interrelation of timber density and the pull-out strength. The study showed that the pull-out strength strongly depends on the timber density around the anchorage zone especially for glued-in rods parallel to the grain. Tests with hardwood are not so common and are rarely conducted (Otero et al. 2008 [18], Rajčić et al. 2006 [20]) but in practice glued-in rods are often used for retrofitting historical buildings of which the main structure is made of hardwood. Broughton et al. (2001a) [12] studied the influence of the moisture content at the time of bonding on the pull-out strength on hardwood. The generic types of adhesive most frequently studied were polyurethanes and epoxies. The experimental pull-out behaviour has been tested for different types of adhesives by Broughton et al. (2001b) [13] but nowadays technical approvals for both of the above mentioned adhesive types are available for use with softwoods. The fatigue performance of bonded-in rods was studied by Bainbridge et al. (2000) [10] for different types of adhesives but all in all the long-term behaviour is rarely considered because of the lack of standardized approval procedures and because the tests are time-consuming and expensive. This is a serious drawback since only standardized tests can deliver comparable test results that can be considered in the evaluation of the long-term behaviour in the design rules. Other parameters, subject of studies by Steiger et al. (2004) [58], concern the geometry of the tested samples including anchorage length, rod diameter and the slenderness ratio (the quotient of the anchorage length and the drill-hole diameter). While there is a negative relationship between anchorage length and the shear strength in the anchorage zone the shear strength increases with larger drill-hole and rod diameters. This causes a negative relationship between the shear strength and the slenderness ratio whilst the total pull-out force increases at higher slenderness values (Rossignon et al. 2008 [22]). This topic is important as it can dictate the failure mode. Feligioni et al. (2003) [14] found a good correlation between the pull-out strength of glued-in rods and the volume of the adhesive, which depended up on the anchorage length and the glue line thickness. It was concluded that the glue line thickness is an important parameter because it allows optimization of the stress transfer from timber to rod. Blass et al. (1999) [11] studied the influence of spacings between multiple rods and the edge distances at axially glued in rods. It was shown that the load-carrying capacity decreased if the edge distance was less than 2.5 times the rod diameter. The results of a study by Broughton et al. (2001a) [12] also confirmed this, demonstrating how multiple rods spaced too closely do not act individually but pull-out as one.

2.2 Introduction to the questionnaire

The main objective of the online survey was to gather overall knowledge and interest in glued-in rods. The questionnaire was divided into three parts: use of glued-in rods in practice, regulations and standards, and the extent of scientific research on the subject.

In the first part of the questionnaire the idea was to obtain information on the popularity of glued-in rods in practice, the usage of glued in rods instead of other similar applications and the main advantages and disadvantages of these applications. The second part of the survey was focused on standards and norms, in particular on the familiarity with regulations, standards and guidelines. Of special interest was to get knowledge about which standards are most widely used and why, as well as disadvantages of the standards and the parts that need improvement. The research part of the survey was aimed at gathering technical information about research methods, test conditions and common materials used in laboratory tests. All in all a total of 32 questions were asked in an online survey which can be found online [4].

2.3 Results of the questionnaire

The questionnaire was filled out by 56 respondents (from 15 European countries), including; scientists, timber industry representatives and designers (Figure 3). Of the total number of respondents only 2 knew very little about glued-in rods, 11 had only read articles, and 43 people indicated they were very familiar with the subject matter, whether as designers, researchers or people from the timber industry, filled out the survey.

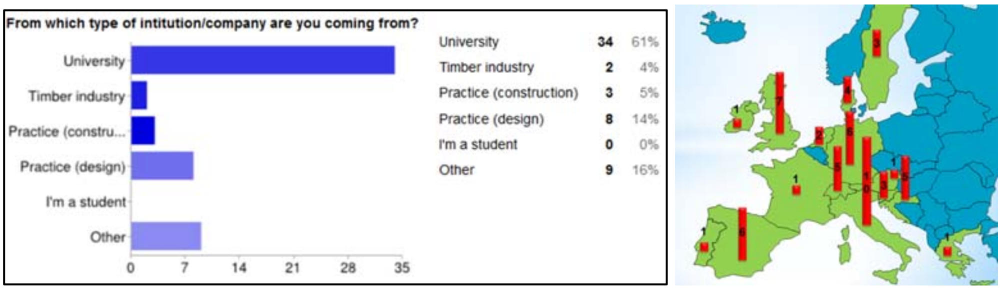

Figure 3: Left: Affiliation of respondents. Right: Distribution and number of respondents by country.

Glued-in rods were often recognized as systems which provided stiff joints, high load capacity, good fire resistance and which were aesthetically desirable at the same time. Yet given the large number of people indicating their familiarity with the matter, glued in rods were very seldom used in practice. Only 9% of respondents are using glued in rods frequently in practice, whilst 68% had never used them or used them in practice only a few times. The main reason for this was reported to be because of the lack of standards and regulations and consequently lack of adequate information about the design, quality control and installation methods. In new structures, e.g. timber bridges, residential houses, long-span buildings, glued-in rods are applied where they are desirable because they allow the execution of joints without external steel parts, and they can transfer significant moments from beams to columns. The embedded rods are protected against fire hazards, are more resistant to environmental conditions and they are easy to prefabricate. When talking about historic structures, they were very often applied in beams, trusses, joints and less in columns, timber plates and for anchoring in concrete. Glued-in rods are also often used as systems for replacing decayed parts and strengthening of critical parts in structures, where they allow the easy connection of the replacement material to the remaining timber structure on site. The connections in a traditionally jointed timber frame are one of the weakest spots and often suffer from decay in older structures. Glued in rods were reported to be very effective in attaching new sections to replace decayed timber. In some cases beams were undersized for structural changes of use or even for their original use. So it is possible to use glued-in steel rods or plates, the latter either set vertically in a slot cut in a beam or glued to the bottom side of a beam if it will be covered. This was a very effective way, causing minimal intrusion, to increase strength and stiffness of a beam. Figure 4 and show where and when are glued-in rods used when designing new and historical structures.

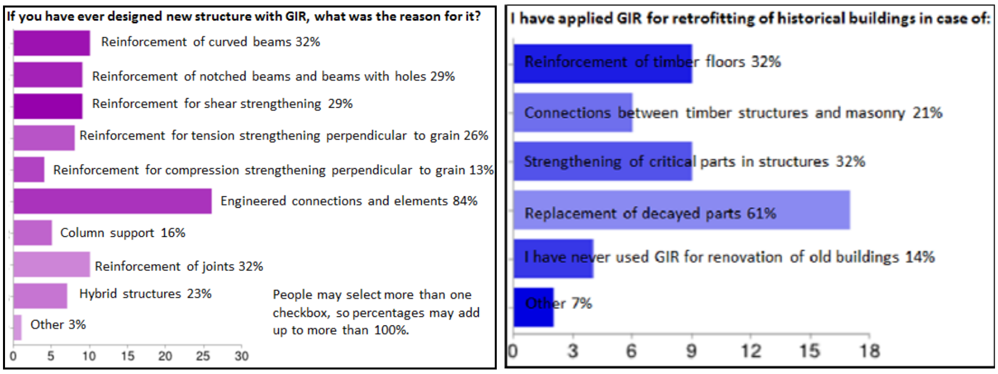

Figure 4: Left: Reasons for designing new structures. Right: Use of glued-in rods in retrofitting historical buildings.

Despite many advantages there were situations when glued-in rods were not desirable and caused lack of trust. One of the main reasons is uncertainty related to production and quality control. Qualified personnel is the prerequisite for good application because more expertise is needed compared to driving screws. The need for good workmanship in the preparation and cleaning of the rod and sealing holes in existing elements that, for example, allow the adhesive to leak out of the hole or the slot for the rod or the plate can be critical. It is also difficult to inspect and to assess glued-in rods once installed. The joints cannot be disassembled for repairing and if they are of poor workmanship this could lead to progressive failure in multiple rod connections because of the brittleness of the adhesive and/or the whole connection system. Applications performed directly on the building site (*in-situ*) require a system to connect them, but this can be expensive and may reduce the effectiveness of the connection due to very variable conditions such as temperature, skill of the personnel or dust. It was also difficult to certify that the joint is safe and functional. So, in conclusion, despite of the many advantages of glued-in rods they are not often used because there is little information about quality control, and a lack of standards and information about design (durability, detailing, stiffness, etc.).

When it comes to preferable materials for glued-in rods, the epoxy adhesive (EPX) with an maximum glueline thickness up to 2mm, threaded steel or Fibre-reinforced plastic bars (FRP), glulam or softwood were the ones mostly used. One of the reasons for using EPX (95% respondents are using EPX) with thickness up to 2mm was because EPX is one of the most mature structural adhesives for these types of applications and a thickness up to 2 mm is defined in the relevant technical approvals. If glued-in rods are compared to self tapping screws, the use of glued-in rods were, according to the answers from the respondents, preferable when using large diameter rods, whilst self tapping screws were preferred in the case of non-qualified personnel or for in-situ applications. Glued-in rods were thought to be a more complex and expensive system and extended quality control is necessary.

The second part of the questionnaire was oriented on present codes, standards and guidelines. Rules for design were characterized as unreliable and unsatisfying. As seen from Figure 5, almost 60% of respondents were not confident whilst 89% were not satisfied with present standards and regulations. It can be concluded that there is a general dissatisfaction with the present design rules and procedures.

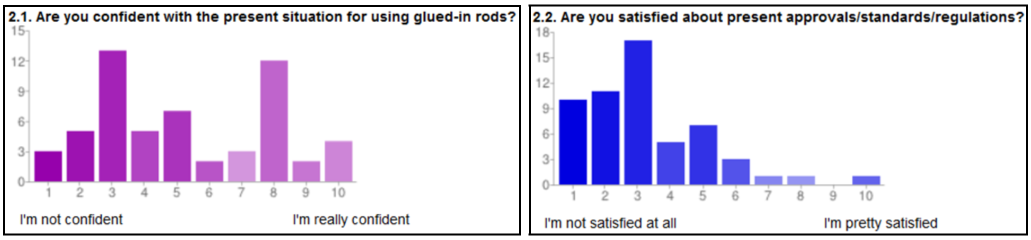

Figure 5: Confidence and satisfaction about present norms and design rules

It is evident that there is a large number of different design rules in usage, from EC5: Annex C [1], DIN:1052 [5], GIROD formulae [6] to the less known (Avis technique), and some as old as the Riberholt theory [21], some used manufacturer's datasheets, or simply referred to various published research papers, etc. Nevertheless, the most commonly applied were EC5: Annex C [1] and DIN:1052 Norm [5] as shown in Figure 6: Left.

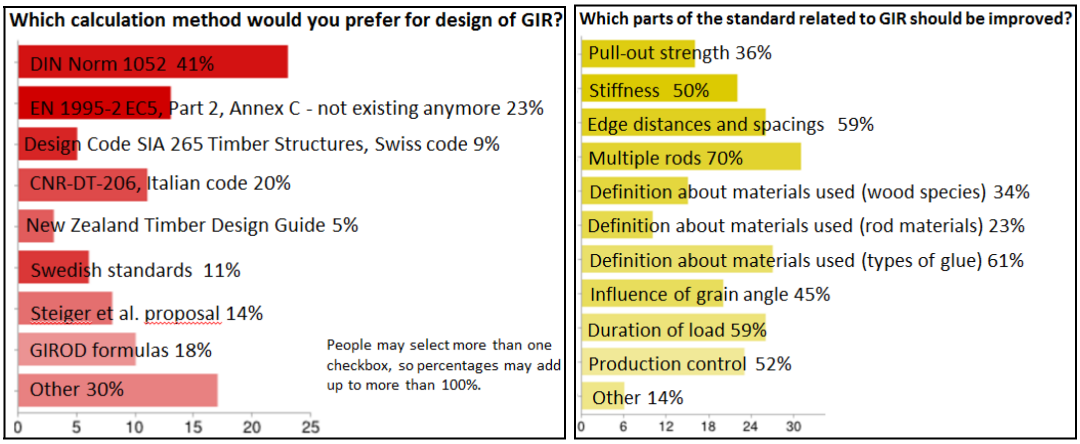

Figure 6: Left: Design rules, procedures and proposals in use. Right: Parts of standards which must be improved

As previously mentioned, there was significant dissatisfaction with standards and guidelines, to the point where most aspects need to be revisited. In particular, this applies to (Figure 6: Right): multiple rods, rod stiffness, timber density, adhesive type, duration of load and production control. The main application fields that can be drawn from Figure 4 should be the primary focus for optimization.

The key problems with design rules mentioned in the questionnaire were the following:

1. Unified EC5 design rules do not exist
2. Definition of rod spacing and edge distances were not reliable for rods under tension and shear load
3. Design rules were underestimating the load bearing capacity of the connection
4. The situation of combined bending and shear was not covered
5. Ductility should be treated as a key issue (e.g. ductility should be assigned to the steel rod and not to the adhesive)
6. There was no reliable rule for multiple rods (e.g. brittleness could lead to progressive failure in multiple rod connections)
7. Lack of understanding on duration of load, the interaction between axial load and transverse load, and the influence of grain angle
8. Non user-friendly formulae.

In the third section of the questionnaire, information about investigation methods, past laboratory tests and materials used in laboratory tests was collected. The most common loading configurations for testing were pull-pull and pull-compression methods (Figure 7: Left). However, it was generally regarded that tests conducted on specimens in a pull-compression setup did not correspond to the practical application of glued-in rods, and pull-out strengths were influenced by local excessive compression stresses in the area of the load transfer (Tlustochowicz et al. 2011 [25]), even though this method is often used. Results for load-bearing capacity vary significantly when the different methods are applied, thus the need for a standardized test method, which is easy to use, was identified.

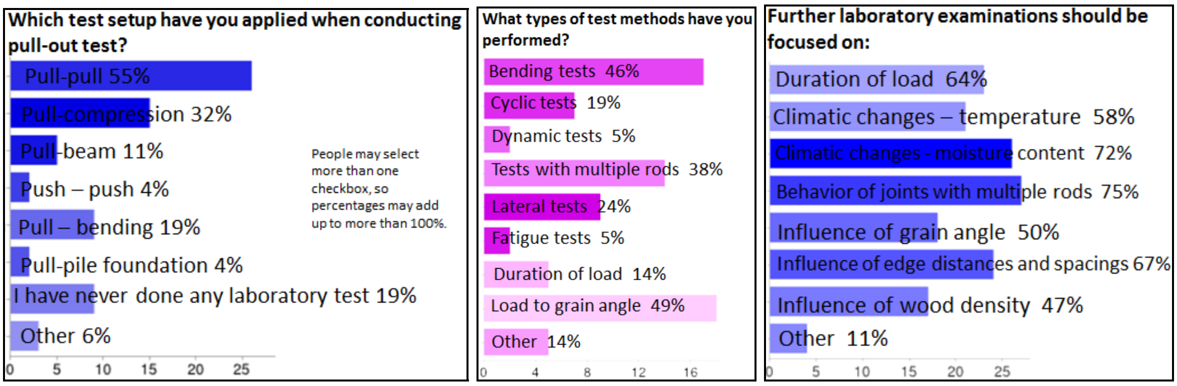

Figure 7: Left: Most common test methods. Middle: Distribution of performed tests. Right: Lack of information and proposals for further laboratory examinations

The results clearly show the lack of experimental investigation and the necessity to investigate problems such as duration of load, fatigue, and dynamic climatic tests. Many new experimental studies must be conducted in order to achieve load bearing capacities of such systems (Figure 7: Right) but for this standardized test-setups are necessary.

Other results from the online survey will be available online [4].

3 Introducing and comparing the design approaches

Over the past twenty five years, despite many national research projects, European projects, European Actions and constant practical application of glued-in rods there is still no universal standard for the design thereof. The main problems are due to the many different approaches available in the literature for defining the behaviour of the adhesive connections. The question is what kind of approach (strength analyses, linear elastic fracture mechanics, non-linear fracture mechanics) is the best and which parameters (anchorage length, diameter of rod, load-to-grain angle, density of timber, moisture content...) must be considered in the final design rules.

An early design proposal was published in 1988 by Riberholt [21], who proposed an equation for the calculation of axially loaded pull-out strength for a single glued-in rod.

In the 1990's a considerable amount of experimental work was done and different design methods were presented. Certain design methods were introduced into national design standards and in 1997 a proposal was implemented in a pre-version of the Eurocode 5: Part 2 [1]. When, in 1998, the European GIROD project started, the idea was to present a design method for glued-in rods. The project was divided into several tasks and working groups. It included studies on how the moisture content, duration of load, fatigue, effect of distances between the rods and edge distances, properties of the adhesives and other parameters affect the axial strength of the connection. A number of laboratory tests were conducted and guidelines for the manufacturing process and quality control of such joints were proposed. The main objective of this project was to establish design rules and the project result was a new calculation model based on the generalized Volkersen theory (GIROD Project Rapport 2002), [6]. This resulted in a proposal for implementation in a pre-version of the Eurocode 5 as Annex C in Part 2 [1]. At CEN/TC 250/SC 5 meeting in 2003 it was decided to discard the Annex C. Delegates supposed that the scientific research and the proposed text did not show all the necessary relationships to realize a design standard. After the GIROD project there were a number of other projects such as LICONS and COST Action E13 (Wood adhesion and glued products) [27] that dealt specifically with glued-in rods. Nevertheless, a final definition of the mechanics and a universal approach for designing still does not exist. In the last 3 years research in this area has been re-visited with a purpose to propose a design standard for replacing several national design standards by Eurocode 5. Some of the proposals and design rules during the years are shown in Figure 8.

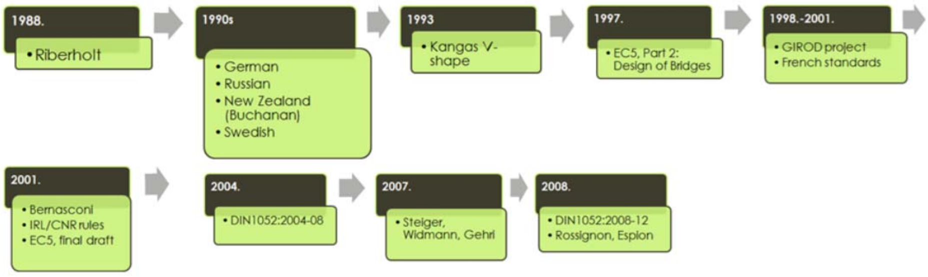

Figure 8: Design methods and proposals in last 25 years

A calculation model should take into account several parameters that are linked to different modelling approaches, influence of materials and geometrical parameters, type of load, and duration of load effects and boundary conditions. Also, three materials (steel, adhesive, timber) with distinct different mechanical properties are combined in such joints, thus representing a very complex system with a specific stress distribution. There are many parameters that influence and affect the resulting load-bearing capacity and creep of this system. Although there are numerous studies and calculation methods, and although an earlier version of Eurocode design methods exists, the basic problem is still which method to accept and implement in the European standard, but what is clear is that a lack of a common European design code is a serious hinder to the exploitation of this approach (Kallander 2004 [16]). For ten years many research efforts and research programs have contributed to the knowledge about glued-in rods and attempted to provide the information required to prepare standards (design approach, code models) that would allow an increased, more advanced and more reliable use of bonded-in rods in timber structures (Rossignon et al. 2008 [22]).

Design rules, methods, proposals and guidance notes for pull-out strength of single rod analyzed in this paper are as follows:

- Riberholt equation, 1998 [21]: $\mathbf{R_{ax,k} = f_{w1} \times \rho_c \times d \times l_g}$
- Buchanan & Townsend equation, 1990 [32]: $\mathbf{R_{ax,k} = 9{,}2 \times d \times l_g \times (r_d)^2 \times (r_e)^{0{,}5}}$
- Buchanan & Deng for EPX, 1990 [28]: $\mathbf{Q_k = 8.16\ k_b\ k_e\ k_m\ (l/d)^{0.86}\ (d/20)^{1.62}\ (h/d)^{0.5}\ (e/d)^{0.5}}$
- Swedish guidelines, 1992 [29]: $\mathbf{F_{t,k}=\pi \times d \times l \times f_{v3}}$
- Russian standards, 1990s [30]: $\mathbf{T=R_{sh} \times \pi \times (d+0{,}005) \times l \times k_1 \times k_2}$
- Eurocode 5, 1997 [2]: $\mathbf{R_{ax,k} = \pi \times d_{equ} \times l_a \times f_{v,k}}$
- French rules (according to Riberholt), 1999 [8]: $\mathbf{P_{f,k}= 85 f_{v,k} \times d \times (l_c)^{0.5}}$
- French rules (for EPX Mastafix), 1999 [8]: $\mathbf{P_{f,k}= 104 f_{v,k} \times d \times (l_c)^{0.45}}$
- Eurocode 5, 2001 [9]: $\mathbf{R_{ax,k} = \pi \times d_{equ} \times l_a \times f_{v,\alpha,k}}$

- Feligioni proposal, 2002 [14]: $\mathbf{R_{ax,k} = \pi \times l_g \times (f_{v,k} \times d_{equ} + k \times (d+e) \times e)}$
- Eurocode 5, 2003[1]: $\mathbf{R_{ax,k} = \pi \times d_{equ} \times l_a \times f_{ax,k} \times (\tan\omega)/\omega}$
- GIROD equation, 2003 [6]: $\mathbf{P_f = \tau_f \times \pi \times d \times l \times (\tan\omega/\omega)}$
- Steiger, Widmann, Gehri proposal, 2007 [24]: $\mathbf{F_{ax,mean} = f_{v,0,mean} \times \pi \times d_h \times l}$
- New Zealand Design Guide, 2007 [31]: $\mathbf{Q_k = 6.73\ k_b\ k_e\ k_m\ (l/d)^{0.86}\ (d/20)^{1.62}\ (h/d)^{0.5}\ (e/d)^{0.5}}$
- Rossignon, Espion proposal, 2008 [22]: $\mathbf{F_{ax,mean} = \pi \times d_h\ x\ l_a \times f_{v,0,mean}}$
- DIN standard, 2010 [34], CNR DT 206/2007 [35]: $\mathbf{R_{ax,d} = \pi \times d \times l_{ad} \times f_{k1,d}}$
- Yeboah, 2013 [26]: $\mathbf{P_{u,mean,k} = \pi \times d_h \times l_b \times f_{v,mean}}$

where:

- $R_{ax,k}/Q_k/\ F_{t,k}/\ T/\ P_{f,k}/\ P_f$ = characteristic axial resistance [N], [kN]
- $F_{ax,mean}/\ P_{u,mean,k}$ = mean axial resistance [N], [kN]
- $l,\ l_g/l_{ad}/l_a/l_b/l_c$ = glued-in length/effective anchorage length [mm]
- d = nominal diameter of rod [mm]
- d_h/h = diameter of drilled hole [mm]
- d_{equ} = equivalent diameter [mm]
- e = edge distance [mm]
- $k_b/k_m/k_e/k_1/k_2$ = bar type factor/moisture factor/epoxy factor/coeff. due to irregular stress distribution/reduction factor taking into account irregular force distribution among multiple rods
- ω = stiffness ratio of the joint
- τ_f = local bondline shear strength [N/mm^2]
- $f_{v3}/\ f_{v,k}/R_{sh}/\ f_{ax,k}/\ f_{k1,k}$ = strength parameter/ch. shear strength of the wood/ design shear strength of wood across the grain/ch. shear strength of the wood at the angle between the rod and grain direction/ ch. value of bond line strength [N/mm^2]
- $f_{v,0,mean}/\ f_{v,mean}$ = nominal shear strength of single axially loaded rod parallel to the grain [N/mm^2]

It can be concluded from past studies that pull-out capacity depends primarily on the interfacial layer and shear strength parameter which is influenced by mechanical and geometrical properties of three different materials. In general a simplified calculation model for axial loading could be summarized as:

$$R_{ax,k} = \pi \times d \times l \times f_{v,k}$$

where: $R_{ax,k}$ = characteristic pull-out capacity, l = anchorage length, d = diameter, $f_{v,k}$ = shear strength parameter.

However, the mechanics of glued-in rods are complex, so an accepted simplification of the equation might result in uneconomic connection designs. If we take a closer look at the simplified equation there are numerous unanswered questions such as which diameter (diameter of rod, diameter of hole or equivalent diameter) and anchorage length (length of bonded rod or equivalent anchorage length) to use, which parameters must be included in the shear strength parameter (timber density, MC content of timber, MOE of timber, rod and adhesive, rod surface, rod material, type of adhesive, slenderness ratio, geometrical factors, etc.). If we take a look at present standards and proposals (Figure 9: Left) it can be easily concluded that existing calculation models differ significantly.

From the consensus of expert discussions, and verified by the results of the questionnaire it can be concluded that most common design rules like EC5, the former DIN [5], and SIA [7] are on the "safe side" while equations proposed in various scientific papers deliver much higher values for the calculated pull-out capacity. Often designers are not satisfied about the

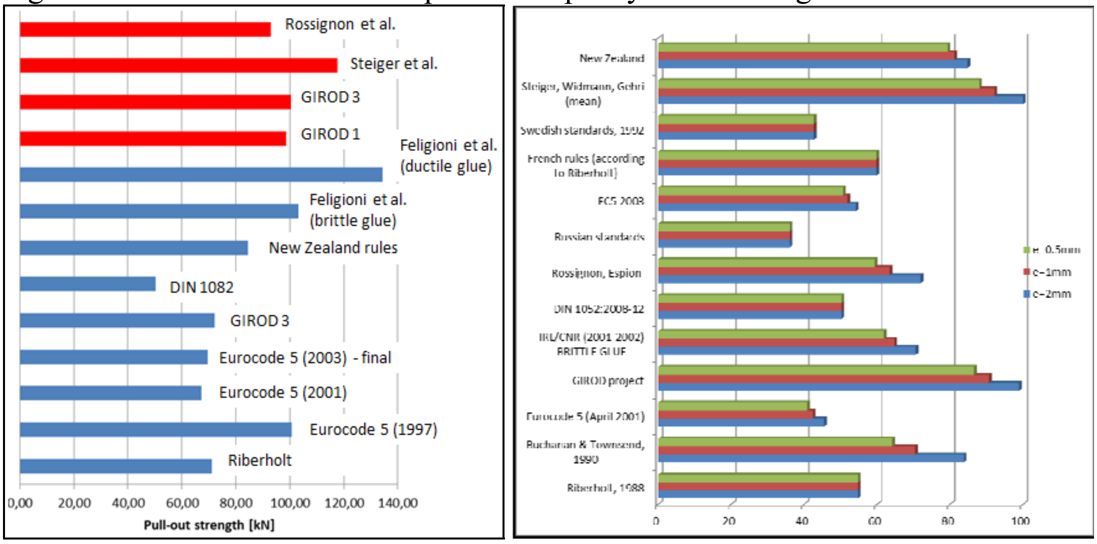

Figure 9: Left: Comparison of pull-out capacity [kN] between different design rules (EPX, l=200mm, ρ=370kg/m3, d=20mm, e=2mm). Blue lines represent characteristic values and red lines represent mean values. Right: Influence of glue-line thickness on capacity of rod

current state of the design standards because they were underestimating the possibility of a high load bearing capacity. On the other hand, some engineers were not confident with equations from scientific papers because effects like duration of load or influence of weather conditions were not taken into account. Figure 10 shows the characteristic pull-out capacity calculated on basis of different design rules whereby the diameter of rod and the anchorage length were varied. Problems occur when defining these two parameters in the equation. The diameter "d" is sometimes the diameter of rod (Riberholt [21], DIN [5]), the diameter of the drilled hole (Steiger et al. 2007 [24], Yeboah et al. 2013 [26]) or an equivalent diameter (EC5 [1], Feligioni et al. 2003 [14]). A similar problem applies for the definition of anchorage length.

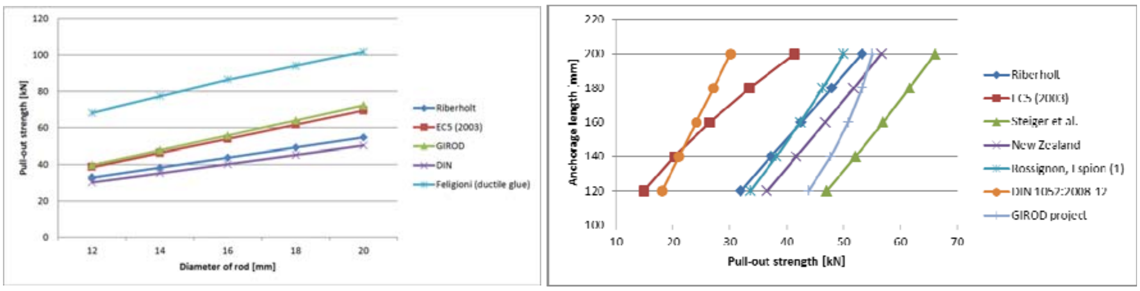

Figure 10: Comparison of pull-out strength [kN] between different design rules when varying diameter of the rod (EPX, l=200mm, ρ=370kg/m3, e=2mm) and anchorage length (EPX, d=12mm, e=2mm d=20mm).

The glue-line thickness is considered only in some formulas. Some standards propose a maximum value of 2mm [5, 7, 8] but do not provide answers for glue-line thickness which may be less than this value. Differences and the influence on the calculated load capacity are shown in Figure 9: Right.

The former EC5 [1] equation, which was based on the GIROD project findings, includes a number of influencing parameters including fracture mechanics parameters, which was often characterized as non-user-friendly for engineers in practice. Also, the influence of wood density, which possibly cannot be neglected, is not included in the equation. For example, some studies (Riberholt 1988 [21], Feligioni et al. 2003 [14]) define wood density as one of the main parameters and its influence on load bearing capacity is shown in Figure 11.

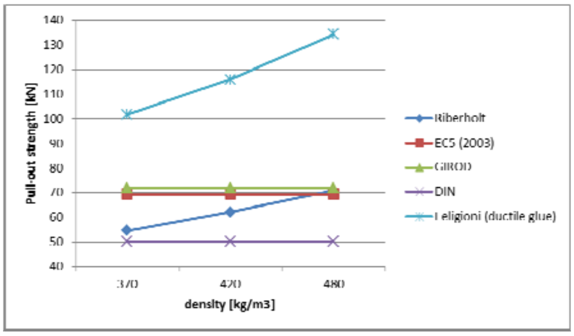

Figure 11: Comparison of pull-out capacity [kN] between different design rules when varying the timber density (EPX, l=200mm, e=2mm, d=20mm)

Edge distances are also a crucial factor for load bearing capacity because too small an edge distance may cause splitting of wood (Serrano 2001 [23]). However, there are some differences in the proposals; more than 2d (Riberholt 1988 [21]), more than 2.3d (Steiger et al. 2007 [24]) but values for edge distances more than 2.5d are present in most design equations.

4 Conclusion

Connections using glued-in rods have gained popularity as they provide solutions both for newly built structures and for strengthening existing structures. The aim of this paper was to analyse the present situation about the usage, the state of art in laboratory experiments and existing design methods or approaches. An online survey was employed to acquire an appreciation of the expert and user issues. The total number of 56 respondents appears sufficient to comprehend the present situation regarding glued-in rods, especially since 95% of the respondents confirmed they had a lot of experience with such applications. The performance of connections with glued-in rods is governed by very complex mechanisms and depends on a large number of geometrical, material and configuration parameters as well as their interaction. Previous standardization proposals, guidelines and other similar documents were compared and it can be concluded that there are unacceptable and possibly also unexplainable deviations and differences in the calculated values of the pull-out strength of single glued-in rods. However, despite a huge number of different design rules and approaches the basic principle is always similar. The calculation of the pull-out strength of single glued-in rod depends on several parameters, albeit with slight variations. These are the anchorage length, diameter of rod and a parameter that characterizes the shear strength of the rod/adhesive/timber interface. The problem is to define the shear strength parameter that should include the timber and the adhesive properties. There are still many outstanding questions regarding the load-carrying capacity of such applications. In addition to this, the issue is also the disagreement among the experts on the definition calculation equation. The implementation of a design rule in Eurocode 5 can only be achieved if some technical guideline is made before the implementation itself. Such a technical guideline must cover all applications and has to include all of the important parameters described in this paper, which will influence the load-carrying capacity. It is crucial that information is provided about production methods, production control, restrictions of use and recommendations of materials which can be used. There are many scientific papers published, experimental investigations performed and a number of experts involved in this topic already and there is probably no need for another comprehensive European project such as e.g. GIROD, unless some specific items are addressed such as complex load situations, duration of load, cyclic climatic conditions and fatigue. Having said this, there is indeed still some lack of experimental data and knowledge on general joint behaviour. The way forward towards a generally accepted design approach for glued-in rods should be a better cooperation among the scientists, designers and producers. COST Actions in which experts have the opportunity to cooperate and also host researchers are a good way to solve some of the problems. For now “The sad story about bonded-in bolts” (Larsen 2011 [33]) is still reality but lately a significant effort have been made to turn it into, if not a happy saga, at least a less sad story. COST Actions FP1004 and FP1101, among others, are dealing with glued-in rods and hopefully, by the end of the Actions, technical guidelines will be accessible to designers, industry and scientists.

Acknowledgement

The work described here was conducted in Holzforschung München (Germany) as a part of COST Action FP1004 "Enhance mechanical properties of timber, engineered wood products and timber structures". I would like to thank the representatives of COST office for their Short Term Scientific Mission grant, which contributed to a successful progress of this research. Also, I would like to thank the COST representatives from BIROD Core group (van de Kuilen, J-W, Serrano E., Broughton J., Widmann R., Harte A., Tomasi R., Hunger F.) for their professional assistance and representatives from both COST FP1004 and FP1101 Actions for a huge support.

REFERENCES

[1] European Committee for Standardization CEN (2003) prEN 1995-2 Eurocode 5-design of timber structures, Part 2: Bridges. Final Project Team draft (Stage 34). Document CEN/TC 250/SC 5: N 198. CEN, Brussels

[2] European Committee for Standardization CEN (1997) Eurocode 5-design of timber structures, Part 2: Bridges ENV 1995-2:1997. CEN, Brussels

[3] EN 1382-1999 Timber structures - Test methods - Withdrawal capacity of timber fasteners

[4] Online survey: https://docs.google.com/spreadsheet/viewform?formkey=dFBlSnpURldQMXc2NXZiQ2VWdm4yVlE6MQ#gid=0, results: https://sites.google.com/site/bondedinrods/

[5] Deutsches Institut für Normung e.V. DIN (2008) Norm 1052:2008-12 Entwurf, Berechnung und Bemessung von Holzbauwerken. DIN, Berlin

[6] GIROD - Glued in Rods for Timber Structures, SP Rapport 2002:26, Building Technology, Borås 2002

[7] Swiss Society of Engineers and Architects SIA (2003), Design Code SIA 265 Timber Structures. SIA, Zurich

[8] Faye C, Le Magorou L, Morlier P, Surleau J (2004) French data concerning glued-in rods. Paper 37-7-10. In: Proceedings of 37th conference of CIB-W18, Edinburgh, Scotland

[9] European Committee for Standardization CEN (2001) Eurocode 5-design of timber structures, Part 2: Bridges ENV 1995-2:2001. CEN, Brussels

[10] Bainbridge RJ, Mettem CJ, Harvey K, Ansell MP (2000) Fatigue performance of bonded-in rods in glulam, using three adhesive types. Paper 33-7-12. In: Proceedings of 33rd conference of CIB-W18, Delft, The Netherlands

[11] Blass HJ, Laskewitz B (1999) Effect of spacing and edge distance on the axial strength of glued-in rods. Paper 32-7-12. In: Proceedings of 32nd conference of CIB-W18, Graz, Austria

[12] Broughton JG, Hutchinson AR (2001a) Pull-out behaviour of steel rods bonded into timber. Mater Struct J 34(2): 100–109

[13] Broughton JG, Hutchinson AR (2001b) Adhesive systems for structural connections in timber. Int J Adhes Adhes 21(3):177–186

[14] Feligioni L, Lavisci P, Duchanois G, De Ciechi M, Spinelli P (2003) Influence of glue rheology and joints thickness on the strength of bonded-in rods. Holz als Roh un Werkstoff 61, P281-287

[15] Harvey K, Ansell MP (2000) Improved timber connections using bonded-in GFRP rods. Proceedings of the 6th WCTE, Whistler Resort, Canada

[16] Kallander B (2004) Glued in rods in load bearing timber structures—status regarding European standards for test procedures. Paper 37-7-9. In: Proceedings of 37th conference of CIB-W18, Edinburgh, Scotland

[17] Kangas J, Kevarinmaki A (2001) Quality control of connections based on V-shaped glued-in steel rods. Paper 34-7-4. In: Proceedings of 34th conference of CIB-W18, Venice, Italy
in timber engineering, Lahti, Finland

[18] Otero Chans D, Cimadevila JE, Gutierrez EM (2008) Glued joints in hardwood timber. Int J Adhes Adhes 28(8):457–463

[19] Rajčić V, Bjelanović A, Rak M (2006) Comparison of the pull-out strength of steel bars glued in glulam elements obtained experimentaly and numerically. Proceedings of the CIBW18

[20] Rajčić V, Bjelanović A, Rak M (2004) Experimental tests of the glued bolt using threaded steel bars, Proceeding of the WCTE 2004, Lahti page 317-320[21] Riberholt H (1988) Glued bolts in glulam—proposals for CIB code. Paper 21-7-2. In: Proceedings of the 21st conference of CIB-W18, Parksville, Canada

[22] Rossignon A, Espion B (2008) Experimental assessment of the pull-out strength of single rods bonded in glulam parallel to the grain. Holz als Roh- und Werkstoff 66(6): 419–432

[23] Serrano E (2001) Glued-in rods for timber structures—a 3D model and finite element parameter studies. Int J Adhes Adhes 21(2):115–127
[24] Steiger R, Gehri E, Widmann R (2007) Pull-out strength of axially loaded steel rods bonded in glulam parallel to the grain. Mater Struct J 40(1):69–78
[25] Tlustochowicz G, Serrano E, Steiger R (2011) State-of.the-art review on timber connections with glued-in steel rods. Material and Structures 44:997-1020
[26] Yeboah D, Taylor S, McPolin D, Gilfillan J (2013) Pull-out behaviour of axially loaded Basalt Fibre Reinforced Polymer (BFRP) rods bonded parallel to the grain of glulam elements. Construction and Building Materials, Volume 38, Pages 962–969
[27] COST Action E13 Wood Adhesion and Glued Products, Working Group 2: Glued Wood Products (2002) State of the Art – Report. Editors: Carl-Johan Johansson, Tony Pizzi, Marc Van Leemput
[28] Buchanon AH, Deng XJ (1996) Strength of steel rods in glulam timber. In: Proceedings of international wood engineering conference, New Orleans, LA, USA
[29] Carling O (1992) Dimensionering av trakonstruktioner. AB Svensk Byggtjanst och Tratek, Stockholm, Sweden
[30] Turkovsky SB (1989) Designing of wood glued structures joint on glued-in bars. Paper 22-7-13. In: Proceedings of the 22nd conference of CIB-W18, Berlin, German Democratic Republic
[31] New Zealand Design Guide (2007), Timber Industry Federation, NZW14085 SC
[32] Townsend PK (1990) Steel Dowels Epoxy Bonded in Glue Laminated Timber. Res. Report 90-11, Christchurch
[33] Larsen HJ (2011) The sad story of glued-in bolts in Eurocode 5. Essay 4.3, CIB-W18, A review of meeting 1-43
[34] DIN EN1995-1-1/NA:2010-12 (GERMAN NATIONAL ANNEX TO EC5)
[35] CNR-DT 206/2007, Istruzioni per la Protegattazione, l'Esecuzione ed il Controllo delle Strutture di Legno
[36] Tomasi R, Parisi MA, Piazza M (2009) Ductile design of glued-laminated timber beams. Practical Periodical and structural design and construction, ASCE, p:113-122

INTERNATIONAL COUNCIL FOR RESEARCH AND INNOVATION IN BUILDING AND CONSTRUCTION

WORKING COMMISSION W18 - TIMBER STRUCTURES

IN-SERVICE DYNAMIC STIFFNESS OF DOWEL-TYPE CONNECTIONS

T Reynolds

R Harris

Wen-Shao Chang

BRE Centre for Innovative Construction Materials

University of Bath

UNITED KINGDOM

Keywords: timber, connection, serviceability, vibration, dowel, Eurocode 5, analytical model

---

Presented by T Reynolds

A Leijten stated in European standard procedure there is a loop in the loading protocol and asked for clarification. T Reynolds answered that in the standard test method load goes up to 40% and down to 10% on a yield basis. The amplitude is too big compared to, for example, foot fall loading. With large amplitude of movement, too much nonlinearity would lead to lower dynamic stiffness.

J W van de Kuilen stated that the Eurocode 5 approach to estimate initial stiffness was incorrectly applied in this study. Apart from the load range, which was assumed between 0 % and 40 % of the maximum load instead of the correct range between 10 % and 40 %, recovery period between dowel loadings seemed not to be taken into consideration. T Reynolds stated that the frequency of loading is 1 Hz which is similar to wind induced frequency for tall building systems.

F Lam commented that half-hole and full-hole tests would yield different results as the dowel would be allowed to bend in the full hole tests.

A Frangi commented that the load path is different between the compressive and tension tests. T Reynolds stated that in terms of design method it would seem unreasonable to allow different stiffness in tension and compression. The approach taken in this study is pragmatic.

A Ceccotti received confirmation that the dynamic stiffness is five times the value calculated from Eurocode 5. T Reynolds further stated that the initial loading is dominated by the plastic loading of a small region. This was the reason that they believed the finding was significant.

M Fragiacomo asked whether different frequencies were considered. T Reynolds stated that different frequencies of loading were tried and the resulting difference was in the range of 10% to 15%. With large cycles, creep crushing of the contact surface contributed a lot to the initial stiffness.

E Serrano asked whether friction behaviour was included. T Reynolds responded that friction was considered for the distribution of load calculations but did not have strong effects on stiffness.

In-service dynamic stiffness of dowel-type connections

Thomas Reynolds

Richard Harris

Wen-Shao Chang

BRE Centre for Innovative Construction Materials, Department of Architecture and Civil Engineering, University of Bath, UK

1 Introduction

Checks in Serviceability Limit State are very significant in timber design - probably more so than for other materials. As taller buildings and longer spans are used, the ability to check for dynamic response becomes more important. This paper addresses the need for a simple expression to be derived, for inclusion in Eurocode 5 [1], to model dynamic stiffness of connections.

The effect of connection stiffness on the behaviour of frame structures is modelled by assuming semi-rigid connection behaviour. Eurocode 5 provides rules for calculating the slip modulus, which can be used to assess this connection stiffness for static load. The semi-rigid connection stiffness required for modelling and predicting the in-service dynamic behaviour of dowel-type connections is different to the stiffness appropriate to static loading.

Timber structures in service can be caused to vibrate by the dynamic loads imposed by, for example, footfall, turbulent wind load or vibrating machinery. In the majority of cases, these in-service loads impose one-sided vibration on connections. That is to say, the force in the connection oscillates without reversing, having a non-zero mean. Footfall, for example, imposes a small-amplitude dynamic load in comparison with the mean load applied by the self-weight and imposed loads on the structure. Similarly, the steady component of wind load applies a mean force, around which the turbulent component oscillates.

A process for prediction of the stiffness of connections in these conditions is required to allow effective design of timber structures to meet vibration serviceability criteria. A method is presented here which uses the experimental observation that this form of one-sided vibration exhibits a secant stiffness close to that predicted by elastic analysis of the dowel-timber interaction.

1.1 Current Guidance in Design Codes

Eurocode 5 [1] provides guidance for assessing the stiffness of a single-dowel connection with the implication that the guidance can be extended to allow for an arbitrary number of dowels and shear planes. Separate design guides [2] provide methods for the single-dowel stiffness calculated according to Eurocode 5 to be used to calculate the rotational stiffness of a moment connection. The stiffness K_{ser} given in Eurocode 5 allows for deformation of timber and connector in one empirical expression, and is independent of the geometry of the connection, relying only on the diameter of the connector and the density of the timber.

This literature review has not found details of the empirical derivation of the current Eurocode model for connection stiffness. The only reference which has been found is Ehlbeck and Larsen's statement [3] that it was derived by regression analysis of a large number of tests by various researchers. The nature of those tests has not been found, but it seems reasonable to suppose that the Eurocode method's omission of the foundation modulus is due to the difficulty in its measurement and calculation.

In contrast, Japanese design guidance [4], cited by Hwang and Komatsu [5], allows the stiffness of a connection to be calculated based on the empirically-derived foundation modulus for the timber surrounding the connector. The deformation of the connector and the geometry of the connection are then allowed for in a beam-on-elastic-foundation model.

The use of the foundation modulus in the stiffness calculation means that the geometry of the connection can be allowed for, in particular the length of the dowel and its consequent deformed shape. No analytical or numerical calculation method has so far been adopted for the foundation modulus. Its measurement by experiment is also difficult, since it is not possible to create a test in which the dowel passes through a hole in the timber and remains rigidly straight under load [6]. Measurements of the foundation modulus, therefore, need to be corrected for dowel deformation, and it may be this difficulty in predicting the foundation modulus which has led current design guidance to omit it from methods to predict stiffness, instead directly calculating the overall stiffness.

The main obstacle to the derivation of a model for the foundation modulus is the nonlinear behaviour observed under initial load. Even with a tight-fitting dowel, the connection stiffness is initially very low, and gradually rises as the load increases, going through a region of relatively constant stiffness until plastic behaviour begins to occur [7]. The unloading path has a much higher stiffness than the loading path, resulting in a residual displacement upon removal of the load. Dorn argues that this behaviour is a result of the contact behaviour between the face of the dowel and the timber, as the imperfections in the timber surface are crushed under the applied load.

2 Stress function model

It has been shown [8] that, after repeated cyclic loading, the embedment stiffness of a block of timber tended towards that predicted by elastic analysis. Using an analytical model for the elastic stiffness of a pin-loaded plate, with the geometry shown in Figure 1, equations can therefore be derived for the embedment stiffness of timber under cyclic load.

The mathematical form for such a model has been derived by several researchers [9-12] based on the underlying theory of orthotropic plates by Lekhnitskii [13], who showed that the general form of the stress functions for an infinite orthotropic plate with a hole is as given by (1) to (4). Finding the solution for a particular applied load relies on finding the coefficients a_n and b_n which correspond to the distribution of the load on the edge of the hole. ζ_n are transformed coordinates describing the point on the plate under consideration. The complex stress functions and ϕ_1 and ϕ_2 are defined so that the displacements u in the direction of the applied force are given by (5). i is the imaginary unit. These infinite-plate displacements u allow relative displacements to be calculated between points. This is done by superposition, as presented in Section 2.1.

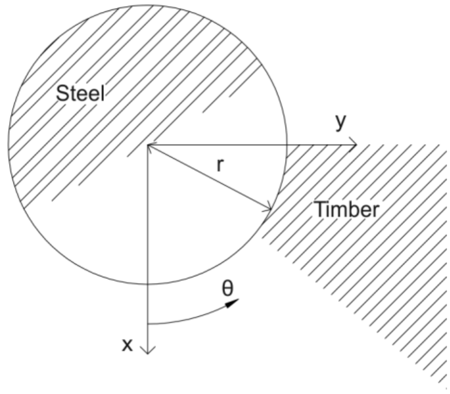

Figure 1 - Geometry and notation for stress function model

$$\Phi_1 = a_0 \ln\zeta_1 + \sum_{n=2}^{\infty} \frac{a_n}{\zeta_1^n} \quad (1)$$

$$\Phi_2 = b_0 \ln\zeta_2 + \sum_{n=2}^{\infty} \frac{b_n}{\zeta_2^n} \quad (2)$$

$$\zeta_1 = \frac{z_1 + \sqrt{z_1^2 - r^2(1+\mu_1^2)}}{r(1-i\mu_1)} \qquad z_1 = x + \mu_1 y \quad (3)$$

$$\zeta_2 = \frac{z_2 + \sqrt{z_2^2 - r^2(1+\mu_2^2)}}{r(1-i\mu_2)} \qquad z_2 = x + \mu_2 y \quad (4)$$

$$u = 2\mathrm{Re}(p_1\Phi_1 + p_2\Phi_2) + U \quad (5)$$

Re( ) denotes the real part of what is, in general, a complex number in the brackets. u is the displacement in the x direction relative to a particular fixed point, and so includes a constant of integration, U. μ_1, μ_2, p_1, p_2, q_1 and q_2 are derived from the material properties of the plate material, the timber, as in Equations (6) to (9), where E_1 is the elastic modulus of the plate material in the x direction, E_2 the elastic modulus in the y direction, G is the shear modulus, and v_1 the Poisson's ratio.

$$\mu_1 = \sqrt{\frac{(2\nu_1 - \frac{E_1}{G}) + \sqrt{(2\nu_1 - \frac{E_1}{G})^2 - 4\frac{E_1}{E_2}}}{2}} \qquad \mu_2 = \sqrt{\frac{(2\nu_1 - \frac{E_1}{G}) - \sqrt{(2\nu_1 - \frac{E_1}{G})^2 - 4\frac{E_1}{E_2}}}{2}} \quad (6)$$

$$p_1 = \frac{\mu_1^2}{E_1} - \frac{\nu_1}{E_1} \qquad p_2 = \frac{\mu_2^2}{E_1} - \frac{\nu_1}{E_1} \quad (7)$$

$$q_1 = \frac{1}{\mu_1 E_2} - \frac{\nu_1\mu_1}{E_1} \qquad q_2 = \frac{1}{\mu_2 E_2} - \frac{\nu_1\mu_2}{E_1} \quad (8)$$

$$a_0 = \frac{1}{\pi}\frac{i\mu_1\left(1+(\nu_1 E_2/E_1)(i\mu_2)^2\right)}{2((i\mu_2)^2-(i\mu_1)^2)} \qquad b_0 = \frac{1}{\pi}\frac{i\mu_2\left(1+(\nu_1 E_2/E_1)(i\mu_1)^2\right)}{2((i\mu_1)^2-(i\mu_2)^2)} \quad (9)$$

The general solution by Lekhnitskii [13] is a stress function for an infinite orthotropic plate in plane stress, with a hole loaded on its edge. Hyer and Klang [11] applied the general complex Fourier series to the plate, and related the values of the coefficients a_n and b_n in (1) and (2) to the Fourier coefficients by equating the forces at the hole edge. The boundary conditions at the hole edge and the derivation of the coefficients are described in Hyer and Klang's paper. The same approach was used in this study.

2.1 Using the stress function to calculate displacements

The solution can then be translated and superimposed to estimate the relative displacements between dowels. This method is appropriate when the free edges of the timber do not significantly affect the distribution of stress, an approximation which is reasonable for calculation of the rotational stiffness of a moment connection, where all the timber subject to significant stress is between the dowels forming the couple. The superposition for two dowels forming a couple is shown in Figure 2, as well as configurations for two closely-spaced dowels transmitting a compressive force, and a dowel supported by a rigid foundation.

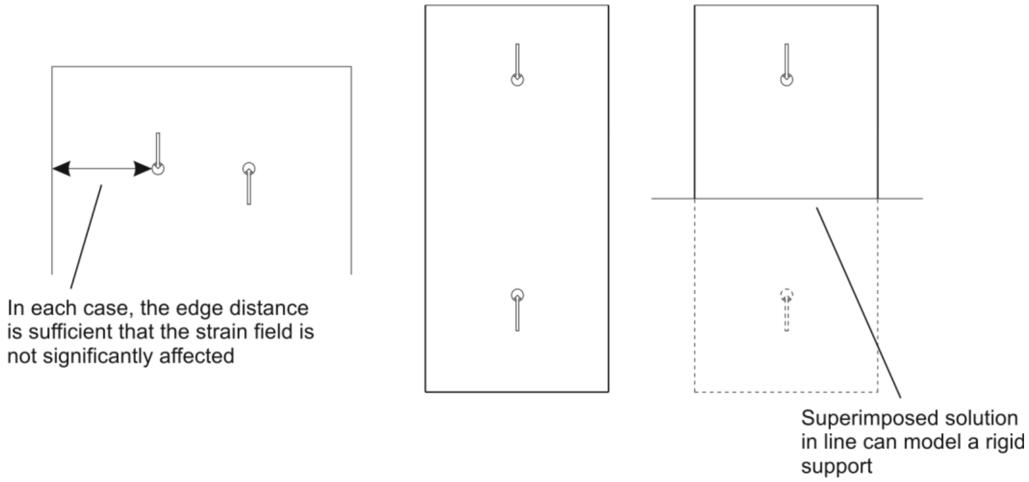

Figure 2 – Superimposing infinite-plate stress functions to model different orientations of connections

To allow for a non-zero far-field stress, Echavarría [12] added the stress function for a stretched plate to that for the pin-loaded plate. The general form of the stress function for a pin-loaded stretched plate, subject to a uniform tensile stress of $p/2$, is given by (10) and (11).

$$\phi_1 = Pa_0 \ln \zeta_1 + \frac{p}{2}\left(\frac{1}{\zeta_1}\left(\frac{-i}{\mu_1-\mu_2}\right) + \frac{z_1}{\mu_1^2-\mu_2^2}\right) + \sum_{n=1}^{\infty} \frac{a_n}{\zeta_1^n} \quad (10)$$

$$\phi_1 = Pb_0 \ln \zeta_2 + \frac{p}{2}\left(\frac{1}{\zeta_2}\left(\frac{-i}{\mu_2-\mu_1}\right) + \frac{z_2}{\mu_2^2-\mu_1^2}\right) + \sum_{n=1}^{\infty} \frac{b_n}{\zeta_2^n} \quad (11)$$

Each stress function in (10) and (11) can be broken down into three parts:

- the term in $\ln \zeta_{1,2}$ represents the net force applied to the hole edge, causing the movement of the hole, with unchanged size and shape, through the timber;
- the term in p represents the constant value towards which the stress in the member tends, far from the hole, stretching or compressing the plate; and
- the terms in $1/\zeta_{1,2}^n$ represent the change in shape of the hole itself, none of them applying a net force to the hole boundary, so that their effect is confined to the area immediately around the connector.

The three components are illustrated in Figure 2 for a single-dowel linear connection. The displacement field is formed by superimposing two infinite plate solutions, including the stretched-plate component, either side of the line of symmetry shown in the figure. The edge distances required in timber connections to prevent splitting ensure that edge effects do not significantly change the local stresses and strains around the hole described by the $1/\zeta_{1,2}^n$ terms, so they present a reasonable model of the deformed shape of the hole.

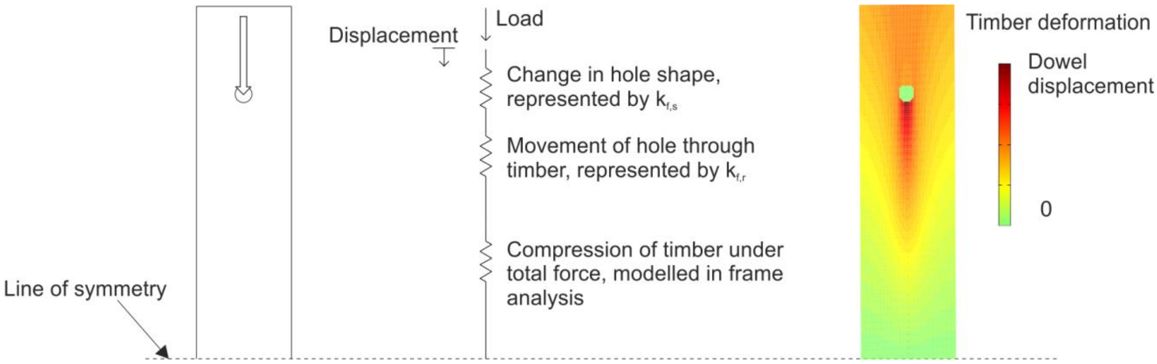

Figure 3 - Components of dowel movement in a linear connection, and the full displacement field given by the stress function

2.1.1 Simplification to form a design method

For simplification of the above equations into a method suitable for hand calculation, the division of the stress function solution into parts is convenient. The part of the stress function which represents the change in the shape of the hole is seen to dissipate quickly with distance from the hole: for the material properties of the Norway spruce used in these tests, loaded parallel-to-grain, it reduces to below 20% of its peak after 7 times the hole diameter in the loaded direction and 2 times the diameter perpendicular. The edge-distances and spacing required to prevent splitting therefore ensure that the edge of the timber and the presence of other dowel holes do not significantly effect this part of the stress function. As a result, it can be considered to be a property of the timber, in the same way as K_{ser} is in Eurocode 5. The calculation process can therefore be greatly simplified by tabulating this value for each timber grade.

The part of the stress function which represents the far-field stress is only necessary in cases where edge effects lead to the development of a constant stress in the distance between the dowels, such as in the translational movement of a connection to a beam or column. In that case, the effect of this constant stress is simply to produce a constant strain in the member, and this is considered in a normal frame analysis, independently of the connections. In calculating the semi-rigid connection stiffness for frame analysis, therefore, this component of deformation can be omitted.

If the component relating to the change in hole shape is tabulated, and the far-field stress omitted, then only one term remains in the equation for the stress function. It represents the movement of the circular hole relative to the timber around it, the 'rigid insert' displacement. The stress functions Φ_1 and Φ_2 for this term are given in (11), and is then used to find the displacement in the x-direction by (12) to (14), which can be simplified to (15). l is the distance between the connections as a multiple of the hole diameter.

$$\Phi_1 = a_0 \ln \zeta_1 \quad \Phi_2 = b_0 \ln \zeta_2 \tag{11}$$

$$\mathrm{u}_0 - \mathrm{u}_l = -2\mathrm{P}(\mathrm{p}_1 \mathrm{a}_0 \ln \frac{\zeta_{1,0}}{\zeta_{1,l}} + \mathrm{p}_2 b_0 \ln \frac{\zeta_{2,0}}{\zeta_{2,l}}) \tag{12}$$

$$\frac{\zeta_{1,0}}{\zeta_{1,l}} = \frac{1+\mathrm{i}\mu_1}{2l+\sqrt{4l^2-1+(\mathrm{i}\mu_1)^2}} \tag{13}$$

$$\frac{\zeta_{2,0}}{\zeta_{2,l}} = \frac{1+\mathrm{i}\mu_2}{2l+\sqrt{4l^2-1+(\mathrm{i}\mu_2)^2}} \tag{14}$$

$$\mathrm{u}_0 - \mathrm{u}_l = -2\mathrm{P}(\mathrm{p}_1 \mathrm{a}_0 \ln \frac{1+i\mu_1}{4l} + \mathrm{p}_2 b_0 \ln \frac{1+i\mu_2}{4l}) \tag{15}$$

Since μ_1 and μ_2 are purely imaginary quantities, $p_1 a_0$, $p_2 b_0$, $i\mu_1$ and $i\mu_2$ are four real-valued material properties which describe the orthotropic elastic behaviour of the timber, and can be calculated from the four independent elastic properties of the timber: the two elastic moduli, the shear modulus and the Poisson's ratio. Relabeling $p_1 a_0 = \beta_1$, $p_2 b_0 = \beta_2$, $i\mu_1 = \alpha_1$ and $i\mu_2 = \alpha_2$, the four properties are given by (16) and (17).

$$\alpha_1 = \sqrt{\frac{\frac{E_1}{G} - 2\nu_1 + \sqrt{(2\nu_1 - \frac{E_1}{G})^2 - 4\frac{E_1}{E_2}}}{2}} \qquad \alpha_2 = \sqrt{\frac{\frac{E_1}{G} - 2\nu_1 - \sqrt{(2\nu_1 - \frac{E_1}{G})^2 - 4\frac{E_1}{E_2}}}{2}} \qquad (16)$$

$$\beta_1 = \frac{1}{\pi}\frac{\alpha_1\left(1+(\nu_1 E_2/E_1)(\alpha_2)^2\right)}{2((\alpha_1)^2-(\alpha_2)^2)}\left(\frac{\alpha_1^2}{E_1} + \frac{\nu_1}{E_1}\right) \qquad \beta_2 = \frac{1}{\pi}\frac{\alpha_2\left(1+(\nu_1 E_2/E_1)(\alpha_1)^2\right)}{2((\alpha_2)^2-(\alpha_1)^2)}\left(\frac{\alpha_2^2}{E_1} + \frac{\nu_1}{E_1}\right) \quad (17)$$

The rigid insert stiffness for a linear connection can then be represented as $k_{f,r}$ in (18), where l represents the linear distance between connections, i.e. the length of the member.

$$k_{f,r} = \frac{1}{2\left(\beta_1 \ln\frac{1+\alpha_1}{4l} + \beta_2 \ln\frac{1+\alpha_2}{4l}\right)} \qquad (18)$$

For a moment connection, the rigid insert stiffness can be obtained by a similar method, and is given by (19), where l is now the distance between the connector and the centroid of the connection as a multiple of the hole diameter.

$$k_{f,r} = \frac{1}{2\left(\beta_1 \ln\frac{1+\alpha_1}{2l\alpha_1} + \beta_2 \ln\frac{1+\alpha_2}{2l\alpha_2}\right)} \qquad (19)$$

The foundation modulus can then be calculated by combining the stiffness associated with the change in hole shape $k_{f,s}$, which could be derived from (10) and (11) and tabulated for a particular timber grade, with the rigid insert stiffness $k_{f,r}$, which depends on the geometry of the structure and connection, using (20). For the Norway spruce used in these tests, $k_{f,s}$ is 3536N/mm/mm parallel and 857N/mm/mm perpendicular to grain.

$$k_f = \left(\frac{1}{k_{f,r}} + \frac{1}{k_{f,s}}\right)^{-1} \qquad (20)$$

2.1.2 Beam on Elastic Foundation

The complex stress function model gives an estimate of the stiffness of the timber in embedment in each plane along the length of the dowel. This stiffness can then be used as the foundation modulus for a beam-on-elastic-foundation model of the complete dowel. The geometry of the dowel in both a connection with a central flitch plate, for example, could be simplified to be represented as a beam on elastic foundation with a central point load.

The deflection under a point load of an infinitely long circular beam on elastic foundation, at the point where the load is applied, is given by (21), where k_f is the foundation modulus determined from the embedment behaviour of the timber, d is the diameter of the connector and E_s is the elastic modulus of the connector material.

$$K_{dyn} = d\left(\pi k_f^3 E_s\right)^{\frac{1}{4}} \qquad (21)$$

2.1.3 Design Method

The design method for a single connector can therefore be summarized as:

- read tabulated values of $k_{f,s}$ for standard timber grades,
- calculate $k_{f,r}$ using (16), (17), (18) and (19) for the geometry in question,
- calculate the foundation modulus according to (20) and
- calculate the stiffness for a single connector according to (21).

The stiffness K_{dyn} can then be used along with conventional design methods to assess the translational and rotational stiffness of connections.

3 Verification by Physical Tests

The method was verified using test results from simple structures made from glulam connected by dowel-type connections: a linear connection, a moment connection, and a complete portal frame. Each connection is formed by a central steel flitch plate and plain steel dowels. The stiffness of each could be identified either by making it part of a structure with imposed mass and using modal analysis techniques to identify its natural frequencies, or by applying an equivalent cyclic force and measuring displacement.

For the test of the moment connection and the frame, a modal test was possible. A mass was placed on a cantilever supported by a two-dowel moment connection, to give a static load of 20% of the predicted yield moment, which was considered representative of a connection in normal service. For the linear stiffness test, a servo-hydraulic loading machine was used to apply an equivalent cyclic load, and the displacement measured using a ±1mm linear variable differential transformer. The specimens are shown in Figure 4.

In order to predict the stiffness of each connection, and therefore the natural frequency of the cantilever or frame, the principal elastic moduli were measured according to EN 408:2010 [14].

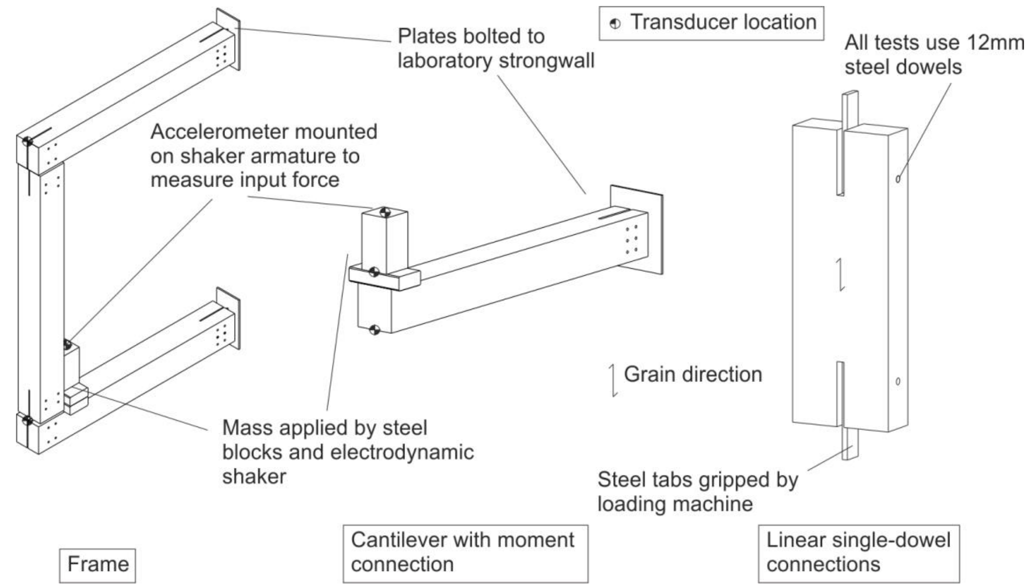

Figure 4 - Schematic test setup for tests on moment connections and frames

3.1 Results

3.1.1 Linear connection

The measured stiffness of the linear connection and its predicted stiffness based on the measured elastic moduli are shown in Figure 5. The results show a slight trend of increasing stiffness with the magnitude of the peak applied force. This is thought to be due to further compression of the contact surface between dowel and timber under higher loads, leading to a stiffness closer to that for a rigid contact surface.

The predicted stiffness was based on the mean elastic properties of specimens cut from the dynamic test pieces after testing. It represents a reasonable estimate of the stiffness under cyclic load. Under compressive load, the results at the higher peak applied force are slightly higher than the predicted value. This is thought to be due to the inaccuracies inherent in this simplified approach, particularly the assumption of a Winkler foundation.

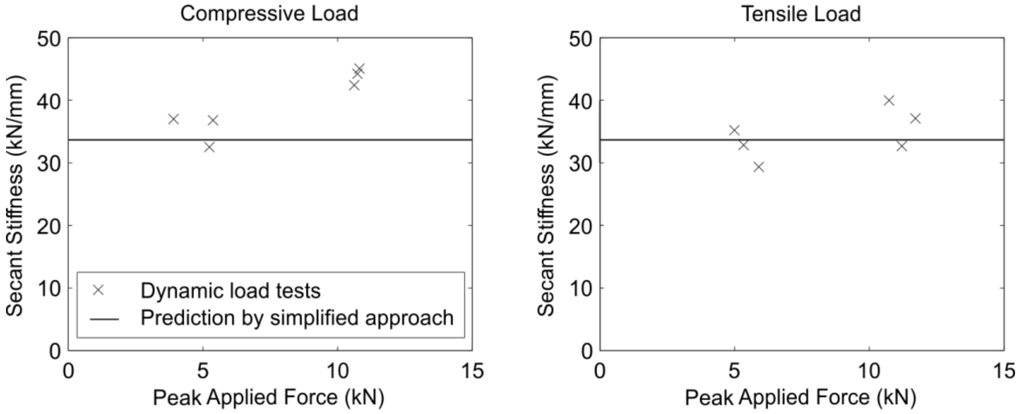

Figure 5 - Comparison of the results of the dynamic load tests on linear connections with the stiffness predictions by the simplified method

3.1.2 Moment connection

The linear connections tested were all single-dowel connections. A moment connection must have multiple dowels, but in its simplest form has just two. Figure 4 schematically shows the test setup used to test two- and six-dowel connections using an electrodynamic shaker.

Table 1 compares the measured natural frequencies with those predicted using the stress function model. It can be seen that, in the case of the two-dowel connection, the stress function model predicts the natural frequency with reasonable accuracy. In the six-dowel connection, the measured natural frequency is higher than the predicted value. It is thought that this is due to friction between the steel plate and the timber slot, since the steel plate was forced against one side of the slot by the installation of the dowels.

Table 1 - Test results for moment connections – measured frequency is the mean of two connections for the two-dowel tests and the result from a single connection for the six-dowel test

Number of dowels	Imposed mass	Predicted natural frequency	Measured natural frequency
2	37kg	8.86Hz	8.70Hz
6	67kg	7.67Hz	8.55Hz

3.1.3 Frame

In the frame tests, the natural frequency was measured using both a pseudo-random cyclic load from an electrodynamic shaker and an impulse from an instrumented hammer. The amplitude of the movement induced by the shaker at resonance was higher than that caused by the hammer: the root mean square value of acceleration due to the shaker was approximately 0.40g, while the peak acceleration caused by the impulse from the hammer had a mean value of 0.38g over the tests. The nonlinearity in the connection stiffness meant that these two excitations resulted in different resonant frequencies.

The impulse was applied at the shaker location, with the shaker in position to ensure that the mass distribution was the same with each form of excitation. The natural frequencies obtained from the impulse tests are shown in Table 2.

Table 2 - Test results for frames

Frame	Measured natural frequency (Impulse hammer)	Predicted natural frequency
Frame A	9.13Hz	10.6Hz
Frame B	9.88Hz	10.6Hz

Using the electrodynamic shaker, the amplitude of the applied force could be varied. The variation of the natural frequency with amplitude is shown in Figure 6, which shows how the receptance function changes as the root mean square value of the force applied by the shaker is increased. The peak value of the receptance, which approximately corresponds to the natural frequency, moves to a lower frequency for higher amplitude of applied force. It is notable, however, that the peak magnitude of receptance also decreases with amplitude of load, since the increase in damping outweighs the greater flexibility of the system. A design case using the stiffness and damping at the lower amplitude is therefore likely to be the most onerous case.

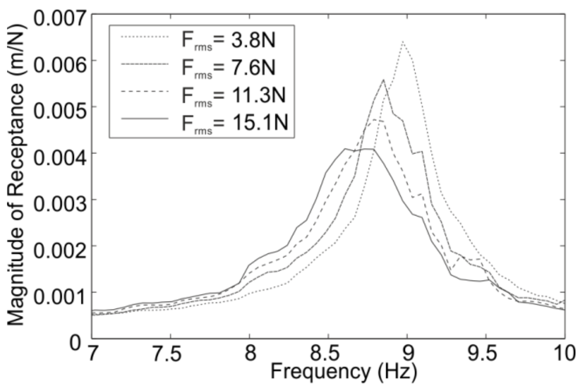

Figure 6 - Frequency response function for Frame A showing its variation with the magnitude of the applied force

Using the stress function model, the rotational and translational stiffness of each of the connections in the frame was predicted. A stiffness matrix model, incorporating the bending and shear deformation of the beams as well as the predicted connection stiffness, was then constructed to assess the dynamic properties of the frame. The eigenvalues of the stiffness matrix gave estimates of the natural frequency, which are shown in Table 2. It is thought that the measured natural frequency is slightly lower than the predicted natural frequency because of the low mean load on some of the connections in the frame. While the connections at the wall were loaded to approximately 20% of their predicted failure load, the connections between members were only loaded to around 10%. The single-dowel connection tests showed that a lower mean force, equivalent to a lower peak applied force in Figure 5, resulted in a lower stiffness, and this was considered to be due to the contact surface between dowel and timber not having reached its full stiffness at low loads. As a brief comparison, using the Eurocode 5 method would predict a natural frequency a little over 6Hz for this frame.

4 Conclusion

The methods for prediction of connection stiffness in current design codes are empirically based. This method allows stiffness calculation based on material properties, and can be applied, amongst other circumstances, to in-service vibration, such as that caused by footfall or turbulent wind load.

Previous work by the authors has shown that the embedment stiffness of a dowel in timber under the cyclic loads imposed by in-service vibration can be predicted using an elastic stress-function model, which can be expressed as a series of analytical equations. In this study, the model has been simplified into a set of equations amenable to calculation without specialist software, which have been tested for linear and moment connections in simple structures. The model has been shown to predict stiffness and natural frequency accurately in linear and moment connections. The experimental work presented here used small sample sizes, and a more thorough experimental validation will be required to prove the validity of the method in other configurations.

One of the potential advantages of this beam-on-foundation approach to connection stiffness is the ability to allow for the effect of the embedded length of the dowel. The simplified method presented here is just an approximation for a long dowel, but could be developed to allow for dowel length.

References

[1] BS EN 1995-1-1:2004+A1:2008, *Eurocode 5 Design of timber structures Part 1-1: General — Common rules and rules for buildings*, BSI, 2009.

[2] Porteous, J. & Kermani, A.: Structural Timber Design to Eurocode 5. Blackwell Oxford, 2007.

[3] Ehlbeck, J. & Larsen, H. J.: Eurocode 5-Design of timber structures: Joints. In: International workshop on wood connectors, Madison, USA. Forest Products Society, 9-23, 1991.

[4] *Wood structure design note (in Japanese)* Architectural Institute of Japan, 1995.

[5] Hwang, K. & Komatsu, K. Bearing properties of engineered wood products I: effects of dowel diameter and loading direction. *Journal of Wood Science,* 48(4): 295-301, 2002.

[6] Foschi, R. O., Yao, F. & Rogerson, D.: Determining Embedment Response Parameters from Connector Tests. In: World Conference on Timber engineering, Whistler, B.C., Canada. 2000.

[7] Dorn, M., De Borst, K. & Eberhardsteiner, J. Experiments on dowel-type timber connections. *Engineering Structures,* 47(0): 67-80, 2013.

[8] Reynolds, T. P. S., Harris, R. & Chang, W.-S. An analytical model for embedment stiffness of a dowel in timber under cyclic load. *European Journal of Wood and Wood Products*, 2013, 10.1007/s00107-013-0716-1.

[9] De Jong, T. Stresses around pin-loaded holes in elastically orthotropic or isotropic plates. *Journal of composite materials,* 11(3): 313, 1977.

[10] Zhang, K.-D. & Ueng, C. E. S. Stresses Around a Pin-loaded Hole in Orthotropic Plates. *Journal of composite materials,* 18(5): 432-446, 1984.

[11] Hyer, M. & Klang, E. Contact stresses in pin-loaded orthotropic plates. *International Journal of Solids and Structures*, 21(9): 957-975, 1985.

[12] Echavarría, C., Haller, P. & Salenikovich, A. Analytical study of a pin–loaded hole in elastic orthotropic plates. *Composite Structures,* 79(1): 107-112, 2007.

[13] Lekhnitskii, S. G.: Anisotropic Plates. Gordon and Breach New York, 1968.

[14] BS EN 408:2010, *Timber structures. Structural timber and glued laminated timber. Determination of some physical and mechanical properties* BSI, 2011.

INTERNATIONAL COUNCIL FOR RESEARCH AND INNOVATION IN BUILDING AND CONSTRUCTION

WORKING COMMISSION W18 - TIMBER STRUCTURES

DESIGN PROCEDURE TO DETERMINE THE CAPACITY OF TIMBER CONNECTIONS UNDER POTENTIAL BRITTLE, MIXED AND DUCTILE FAILURE MODES

P Zarnani

P Quenneville

The University of Auckland

NEW ZEALAND

Keywords: timber, connection, resistance, failure, brittle, ductile

---

Presented by P Quenneville

U Kuhlmann asked if the calculations were made based on a measured yield point of steel. She stated that the distinction between different modes of failures would depend on the real yield point of steel. After discussion it was clarified that the yield strength of the steel rivets were checked.

M Fragiacomo asked about the ductility value of the mixed failure mode and asked if some energy dissipation can be expected. P Quenneville answered that the mixed failure mode will be brittle with little energy dissipation.

BJ Yeh asked if one wants to avoid block tear out, could one install the rivets with the fasteners turned 90 degree, i.e., the major axis perpendicular to the wood grain. P Quenneville answered no, this is not recommended and one should use nails if one would want ductile failure mode.

C Sigrist asked about the purpose of the study since small penetration length of nails was considered. It would make more sense and be better to use longer nails. P Quenneville answered that we are researchers so the study was configured to force a particular mode of failure to check the prediction method. He agreed with C Sigrist's comments. The study checked the calculation method with nails even though it might not be the most optimal use of the fasteners.

H Blass commented the rivet yielding shape depicted in some of the figures (slide 17) was incorrect. P Quenneville agreed.

A Li asked and received clarification of how to evaluate the failure mode for different penetration depth of the fasteners.

Design Procedure to Determine the Capacity of Timber Connections under Potential Brittle, Mixed and Ductile Failure Modes

Pouyan Zarnani, Pierre Quenneville
University of Auckland, New Zealand

1 Motivations

Timber construction has experienced considerable progress in recent years. In such progress, apart from the implementation of new engineered timber products, the advancement of timber joints has played a significant role. Connections are often the most critical components of any type of timber structures. Different brittle, mixed and ductile failure modes of timber connections have long been observed by wood researchers. The wood engineering community has dedicated a significant amount of effort over the last decades to establish a reliable predictive model for the load-carrying capacity of timber connection under different failure modes, particularly, for wood failure mechanisms. Test results from various sources [2-12] demonstrate that for multi-fastener connections loaded either longitudinally or transversely, failure of wood can be the dominant mode. The design procedures for timber connections in most design codes are based mainly on the European Yield Model (EYM) originally proposed in 1949 by Johansen. While the EYM theory provides accurate predictions for connections that fail in ductile fashion, it does not take into account the failure of the connections due to the brittle rupture of wood.

In addition, in the majority of current codes, the definition of fastener resistance is based on the yielding point. The yielding capacity is defined by using the material property estimated at the 5% offset inserted in the EYM equations. While this can be an acceptable limit state when the design follows exactly an allowable stress approach (ASD), it might not be appropriate today when designers are following the Load and Resistance Factor Design (LRFD) method [13]. Using the LRFD philosophy, a designer can evaluate the reliability of a structure with regard to its ultimate behaviour under extreme loads (e.g., earthquake and wind) with significant displacements where knowledge about the connection capacity beyond the yielding load is crucial. In recognition of this fact, developing an accurate design procedure to be able to determine the wood and fastener capacities in different possible connection failure modes under ultimate design loads is necessary.

The design procedure presented is verified using tests conducted on riveted joints under longitudinal and transverse loadings on New Zealand Radiata Pine laminated veneer lumber (LVL) and glulam.

2 Proposed design procedure

2.1 Potential failure modes

The design of timber joints using dowel-type fasteners such as rivets, nails and screws is governed by either the brittle, mixed or ductile failure mode of the joint. The occurrence zone of these potential failure modes is illustrated on a typical load-deflection curve of a timber joint (Fig. 1). The block tear-out failure in parallel-to-grain loading and splitting in perpendicular-to-grain loading are the possible failure modes of the wood.

In the brittle zone, the fasteners deflection is in the elastic range, therefore, the effective wood thickness for the joint corresponds to the elastic deformation of the fasteners, $t_{ef,e}$ [14], as shown in Fig. 2a. In this failure zone, the wood capacity of the connection, $P_{w,tefe}$, is less than the fastener yielding resistance, $P_{r,yld}$. It should be noted that the $P_{r,yld}$ is not an ultimate failure but constitute a boundary. As the yield point is reached, the effective wood thickness reduces if the yield mode is not Mode I. This reduction in effective wood thickness, $t_{ef,y}$, leads to the generation of a new connection failure mode (Fig. 2b). If the wood capacity of the new connection, $P_{w,tefy}$, cannot resist the fastener yielding load ($P_{w,tefy} < P_{r,yld}$), a sudden failure with slight deflection on the fasteners which is called mixed failure mode occurs. Even if $P_{w,tefy} > P_{r,yld}$, the mixed failure mode can happen as the deflection of the connection progresses if $P_{w,tefy}$ is lower than the connection ultimate ductile strength, $P_{r,ult}$. If the wood strength based on $t_{ef,y}$ is greater than $P_{r,ult}$, the ductile failure governs and there is no wood rupture.

2.2 Design requirement

By following the described mechanism for the potential failure modes, the connection ultimate capacity, $P_{c,ult}$, can be predicted as follows;

$$P_{c,ult} = \begin{cases} P_{w,tefe} & \text{if } P_{w,tefe} < P_{r,yld} & \text{(Brittle mode)} \\ P_{r,yld} & \text{if } P_{w,tefy} < P_{r,yld} \leq P_{w,tefe} & \text{(Mixed mode)} \\ P_{w,tefy} & \text{if } P_{r,yld} \leq P_{w,tefy} \leq P_{r,ult} & \text{(Mixed mode)} \\ P_{r,ult} & \text{if } P_{r,ult} < P_{w,tefy} & \text{(Ductile mode)} \end{cases} \quad (1)$$

If a designer wants to rely only on the yield limit state as the connection maximum capacity, therefore, the above design procedure can be simplified to $P_{c,ult}$ = min ($P_{w,tefe}$, $P_{r,yld}$). However, this simplification could result in about 20% conservative design.

2.3 Rigid and stocky fasteners

For the case of rigid and stocky fasteners such as shear plates and split rings, the connection failure will be governed only by the wood characteristics (wood embedment in ductile mode I or shear and tension resistances in the brittle block tear-out and splitting). Therefore, the effective wood thickness, t_{ef}, is equal to the penetration depth of the fastener, L_p, and remains constant during the loading (Fig. 3). Thus, the connection ultimate capacity, $P_{c,ult}$, can be determined by;

$$P_{c,ult} = \begin{cases} P_{w,Lp} & \text{if } P_{w,Lp} < P_{r,yld} & \text{(Brittle mode)} \\ P_{w,Lp} & \text{if } P_{r,yld} \leq P_{w,Lp} \leq P_{r,ult} & \text{(Mixed mode)} \\ P_{r,ult} & \text{if } P_{r,ult} < P_{w,Lp} & \text{(Ductile mode)} \end{cases} \quad (2)$$

For the rigid fasteners, the mixed-mode region is function of the wood yielding only.

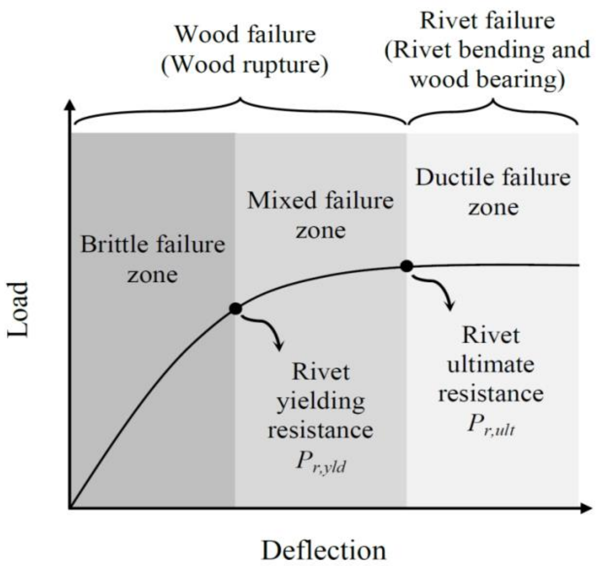

Fig. 1: Occurrence zone of potential failure modes of timber rivet joints

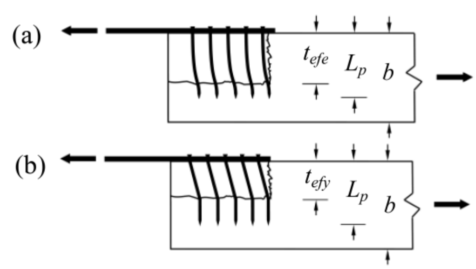

Fig. 2: Effective wood thickness:
(a) brittle failure corresponding to the rivet elastic deformation, (b) mixed failure corresponding to the rivet governing yielding mode

Fig. 3: Effective wood thickness for rigid and stocky fasteners

3 Load-carrying capacity of riveted joint

3.1 Wood block tear-out resistance parallel to grain

The wood block tear-out resistance under parallel-to-grain loading is predicted using the stiffness-based model proposed by Zarnani and Quenneville [10]. The proposed analysis for wood strength is best explained using the analogy of a linear elastic spring system in which the applied load transfers from the wood member to the failure planes in conformity with the relative stiffness ratio of each resisting adjacent volume to the individual failure plane (Fig. 4). By predicting these volumes stiffness, one can derive the portion of the connection load that is channelled to each resisting plane and from the resistance of each failure planes, one can determine which failure plane triggers the connection failure. The difference in the loads channelled to the tensile and shear planes is a function of the modulus of elasticity (E) and modulus of rigidity (G), the volume of wood surrounding each of the failure planes (bottom, end and edge distances - d_z, d_a and d_e) and also the connection geometry (Fig. 5). For details regarding the determination of stiffness of the resisting planes, refer to Zarnani and Quenneville [10].

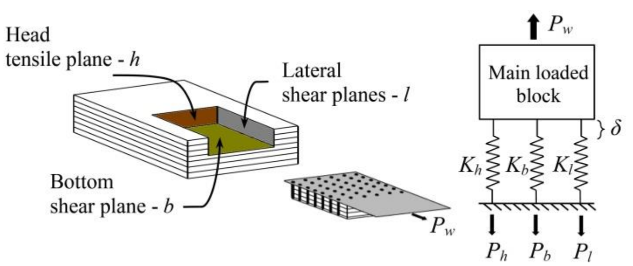

Fig. 4: Elastic spring model for wood block tear-out resistance – K_h, K_b and K_l are the stiffness of the wood blocks loading the head, bottom and lateral failure planes

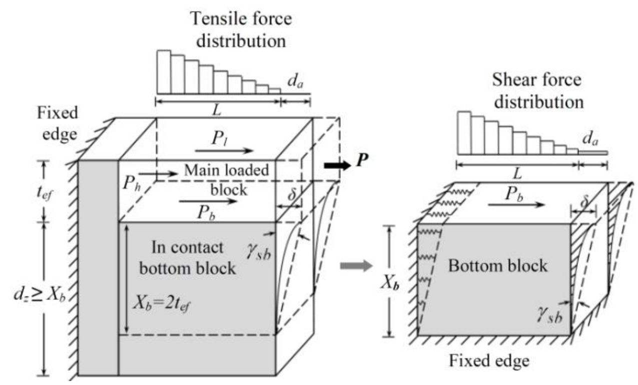

Fig. 5: Simplified analytical model

By predicting the stiffness of the wood surrounding each of the failure planes (K_h, K_b and K_l), one can predict the proportion of the total connection load applied to each plane, $R_i = K_i / \sum K$. By further establishing the resistance of each of the failure planes as a function of a strength criterion, one can verify which of the failure planes governs the resistance of the entire connection. It should be asserted that the strength of the shear planes cannot be higher than the tensile capacity of the adjacent wood volume where the load is channelled to these resisting planes (Fig. 6). If the attracted load by the resisting shear planes is larger than the tensile capacity of the associated wood volume, then the wood block torn out from the member would be as wide as or as deep as the member and corresponding to the wood failure mode (b) and (c) (Fig. 7).

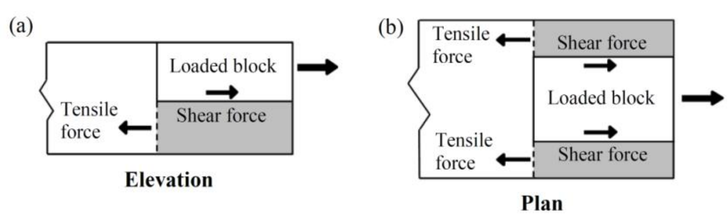

Fig. 6: Loads acting on the wood volume adjacent to the shear resisting planes: (a) bottom block, (b) lateral blocks

Thus, the wood load carrying capacity of the connection (Eq. 3) is the load which results in the earlier failure of one of the resisting planes due to being overloaded and equals to the minimum of P_{wh}, P_{wb}

and P_{wl}. It is important to note that the connection resistance given by Eq. (3) is a summation of the critical plane failure load plus the load carried by the other planes.

$$P_w = n_p.\min\begin{cases} P_{wh} = f_{t,m}A_{th}(1+\dfrac{K_b}{K_h}+\dfrac{K_l}{K_h}) & \text{, Mode (a)} \\ P_{wb} = (1+\dfrac{K_h}{K_b}+\dfrac{K_l}{K_b}).\min\begin{cases} f_{v,m}C_{ab}A_{sb} \\ f_{t,m}X_l d_z \end{cases} & \begin{matrix}\text{, Mode (a)} \\ \text{, Mode (c)}\end{matrix} \\ P_{wl} = (1+\dfrac{K_h}{K_l}+\dfrac{K_b}{K_l}).\min\begin{cases} f_{v,m}C_{al}A_{sl} \\ 2f_{t,m}t_{ef}d_e \end{cases} & \begin{matrix}\text{, Mode (a)} \\ \text{, Mode (b)}\end{matrix} \end{cases} \quad (3)$$

In Eq. (3), $f_{t,m}$ and $f_{v,m}$ are the wood mean strength in tension and in shear along the grain (MPa). A_{th}, A_{sb} and A_{sl} are the areas of the head, bottom and lateral resisting planes with respect to the wood effective thickness, t_{ef}, subjected to tension and shear stresses. Also, C_{ab} and C_{al} are the ratios of the average to maximum stresses on the bottom and lateral shear planes respectively [10]. X_l is the joint width and n_p is the number of the plates equal to 1 and 2 for one-sided and double-sided joints respectively.

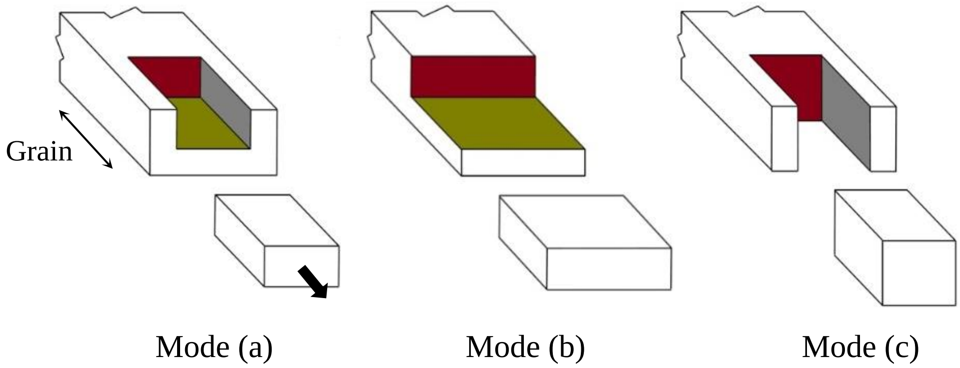

Fig. 7: Different possible failure modes of wood block tear-out

It should be noted that when one plane fails, then the entire connection load transfers to the remaining planes in accordance with their relative stiffness ratios. It could be possible that the occurrence of the first failure of one plane does not correspond with the maximum load of the connection. This is more susceptible in the case of either a small edge or bottom distance accompanying large shear resisting area which leads to a wood failure mode (b) and (c) respectively (Fig. 7). Therefore, Eq. (3) needs to be checked again for the remaining planes by defining no value for the terms related to the failed planes.

In the case of fasteners which are inserted into predrilled holes, the area corresponding to the cutting diameter is to be subtracted from the resisting plane surfaces. This affects the strength of the tensile and shear resisting planes and not their stiffnesses.

3.2 Wood splitting resistance perpendicular to grain

The wood splitting strength in perpendicular-to-grain loading is predicted using the model proposed by Zarnani and Quenneville [12]. The proposed approach is based on two different possible crack formations on the member cross-section: with partial splitting on each side of the member corresponding to the effective embedment depth, t_{ef} (Fig. 8b) or with full width splitting (Fig. 8a).

In fact, for connections with a large penetration depth in slender members, the governing failure mode will be the full width splitting, and as the ratio of member thickness to penetration depth increases, the conversion of wood failure mode from full to partial width splitting will occur (Fig. 9).

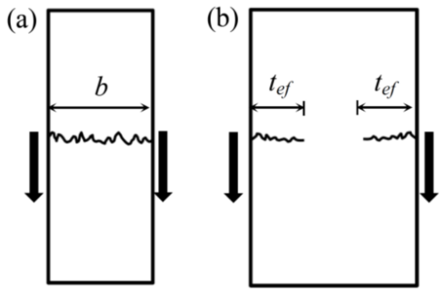

Fig. 8: Cross-section view of wood splitting perpendicular to grain: (a) full width failure mode, (b) partial width failure mode

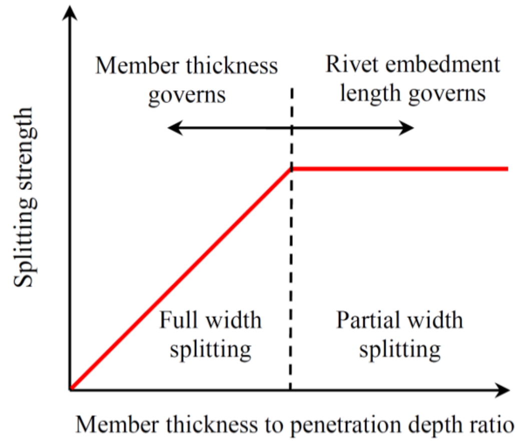

Fig. 9: Occurrence zone of possible failure modes of wood splitting

Therefore, the ultimate splitting resistance of the connection is determined as the minimum strength corresponding to these two failure modes and is given by (Eq. 4).

$$P_w = n_p \, . \, \min\,(P_{s,tef}, P_{s,b}) \tag{4}$$

The wood capacity for partial width splitting, $P_{s,tef}$, is predicted using a stress-based analysis (Eq. 5) and involves the perpendicular to grain tensile capacity of the splitting surface of the wood corresponding to the effective embedment depth, t_{ef} and the crack length that propagates along the member. The crack length along the member is considered as the summation of the joint net section width, w_{net}, and the symmetrical crack growth on the left and right sides of the joint as a factor of the effective depth, h_e. In Eq. (5), f_{tp} is the tensile strength perpendicular to grain; $a_{3c,L}$ and $a_{3c,R}$ are the unloaded end distance on the left and right side of the joint, respectively; C_t is a coefficient function of the unloaded edge distance and the connection length.

$$P_{s,tef} = C_t f_{tp} t_{ef}\,[w_{net}+\min(\beta h_e, a_{3c,L})+\min(\beta h_e, a_{3c,R})] \tag{5}$$

The predictive equation presented for wood splitting in the entire member cross-section, $P_{s,b}$ (Eq. 6) is adopted from the fracture mechanics based model developed by Van der Put and Leijten [8]. The significant difference is the application of the η factor which accounts for the effect of unloaded end distance and the connection width.

$$P_{s,b} = \eta b C_{fp}\sqrt{\frac{h_e}{1-\frac{h_e}{h}}} \tag{7}$$

, in which $\eta = \dfrac{\min(\gamma h_e, a_{3c,L}) + \min(\gamma h_e, a_{3c,R}) + w_{net}}{2\gamma h_e}$

and C_{fp} is the fracture parameter. For more details regarding the wood splitting model, refer to Zarnani and Quenneville [12].

3.3 Wood effective thickness

For brittle failure modes (Fig. 2a), the wood effective thickness, $t_{ef,e}$, is determined from the elastic deformation of the fastener modelled as a beam on a bilinear elastic foundation. The fastener is supported by springs with bilinear response that simulate the local nonlinear embedment behaviour of the timber surrounding it [14].

As there is a transition between a purely brittle wood failure and a purely ductile wood-fastener failure, there is a possibility that the failure observed is a mix of the two. In mixed failure mode (Fig. 2b), the wood fails following some deflection of the fasteners but before they reach complete yielding. In this failure mode, the effective wood depth, $t_{ef,y}$, is significantly smaller than the one associated with the brittle failure mode. In mixed failure modes, $t_{ef,y}$ is derived from the governing failure mode of the fastener. Since rivets are always used in single shear and the rivet head can be considered to be rotationally fixed as it is wedged into the steel plate's hole, only three yield modes need to be considered (Fig. 10). As reported in Zarnani and Quenneville [10,12], $t_{ef,y}$ can be predicted using Eq. (7) based on Johansen's yield theory [15] which is the foundation for the European Yield Model (EYM) prediction formulas in Eurocode 5 [16].

$$t_{ef,y} = \begin{cases} L_p & \text{, Mode I}_\text{m} \\ \sqrt{\dfrac{M_{r,y}}{f_{h,y}d} + \dfrac{L_p^2}{2}} & \text{, Mode III}_\text{m} \\ 2\sqrt{\dfrac{M_{r,y}}{f_{h,y}d}} & \text{, Mode IV} \end{cases} \tag{7}$$

In Eq. (7), d is the rivet cross-section dimension bearing on the wood, equal to 3.2 and 6.4 mm for the parallel and perpendicular to grain loadings, respectively; $f_{h,y}$ is the embedment strength estimated at 5% offset; and $M_{r,y}$ is the rivet yielding moment capacity.

3.4 Rivet resistance under ductile failure

The rivet ductile capacity under longitudinal and transverse loadings can be predicted by Johansen's yield theory [17]. Since rivets are always used in single shear and the rivet head can be considered to be rotationally fixed as it is wedged into the steel plate's hole, only three yield modes need to be considered [7] (Fig. 10). Using the Eurocode 5 [16] approach, the contribution of the fastener withdrawal resistance (f_{ax}) known as the rope effect is added to the rivet lateral strength for the failure modes III_m and IV (Eq. 8). The rivet connection resistance at the yielding ($P_{r,yld}$) and ultimate limit states ($P_{r,ult}$) are determined using the relevant wood embedment strength, f_h, and the rivet moment capacity, M_r (as recommended by AFPA [18]).

$$P_r = n_p.n_R.n_C.\min \begin{cases} f_h L_p d & \text{, Mode I}_\text{m} \\ f_h L_p d\left(\left(\sqrt{2+\dfrac{4M_r}{f_h d L_p^2}}\right)-1\right)+\dfrac{L_p f_w}{4} & \text{, Mode III}_\text{m} \\ 2\sqrt{M_r f_h d}+\dfrac{L_p f_w}{4} & \text{, Mode IV} \end{cases} \tag{8}$$

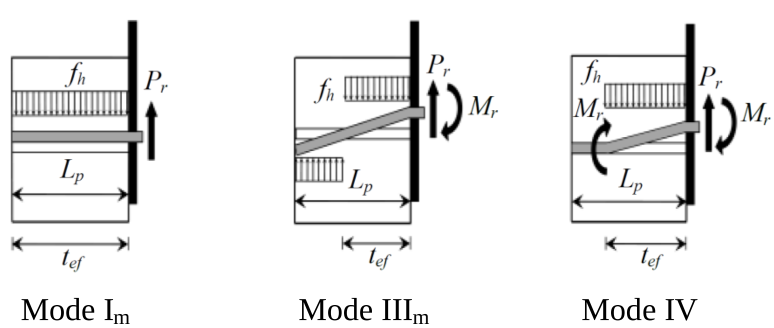

Fig. 10: Possible ductile failure modes of rivets

In Eq. (8), n_R and n_C are the number of rivet rows and columns; f_h and f_{ax} can be determined as a function of d and the density of the wood [17]. The rivet ultimate capacity is defined by using the ultimate embedment strength (corresponding to 2.1 mm deflection), $f_{h,u}$, in different loading directions and the rivet ultimate moment capacity, $M_{r,u}$, equal to 30,000 and 15,000 Nmm for the parallel and perpendicular to grain loadings, respectively [7]. For the rivet yielding capacity, the embedment strength estimated at yield point (5%-offset), $f_{h,y}$, and the rivet yielding moment capacity, $M_{r,y}$, equal to $0.83M_{r,u}$ were inserted in Eq. (8). The factor of 0.83 is the ratio between the fastener yield and ultimate bending strength, F_b, [18] averaged for the rivet cross-section dimensions.

4 Experimental program

Laboratory tests were set up to prompt wood failures and maximize the amount of observations on the brittle mechanism. Specimens were manufactured from New Zealand Radiata Pine LVL grade 11 and GL8 grade glulam. 3 replicates were tested for each group of specimens for LVL and 4 replicates for glulam. The specimens had riveted plates on both faces of timber, resulting in a symmetric connection. The steel side plates were 8.4 mm thick of 300 grade (F_y = 300 MPa) with predrilled 6.8 mm holes to ensure adequate fixity of the rivet head. The effect of geometry parameters such as connection width and length, fastener penetration depth, loaded and unloaded edge distances, end distance, and member thickness were evaluated. For more details regarding the connection configurations, refer to Zarnani and Quenneville [12,19].

The testing protocol outlined in ISO 6891 [20] was followed. The tension load was applied to the specimens using a displacement controlled MTS loading system. The deformation of the connection was measured continously with a pair of symmetrically placed LVDTs. The loading rate was adjusted to 1 mm/min and kept constant until the occurence of failure in both or either side of the riveted connections. A typical specimen in the testing frame is shown in Fig. 11.

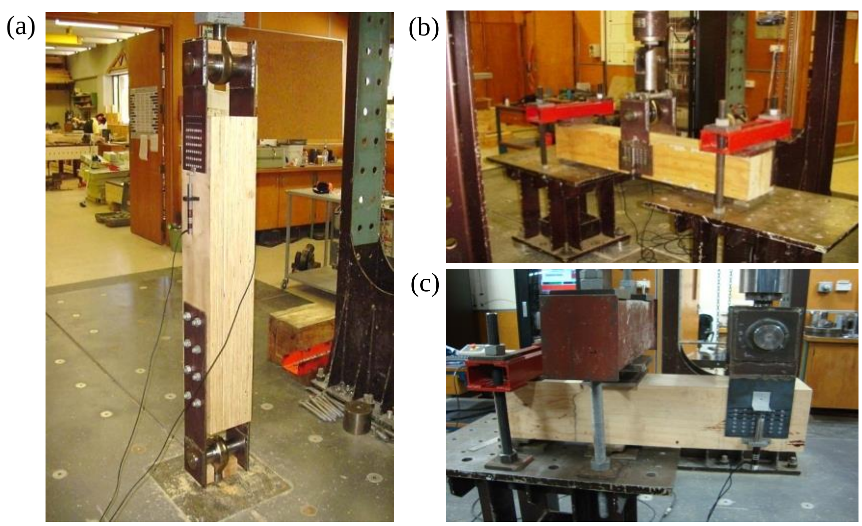

Fig. 11: Typical specimens in testing apparatus:
(a) longitudinal loading, (b) transverse loading - mid-span, (c) transverse loading - end of member

5 Material properties

All specimens were conditioned to 20°C and 65% relative humidity to attain a target 12% equilibrium moisture condition (EMC). The wood had an average density of 605 and 465 kg/m^3 for LVL and glulam members respectively. For the connection capacity parallel to grain, the average tensile and shear strengths evaluated were 34.3 MPa (COV=12%) and 6.8 MPa (COV=10%) for RP-LVL and 24.1 MPa (COV=24%) and 4.2 MPa (COV=15%) for RP-glulam (samples from inner laminations) respectively [19]. For the stiffness properties, based on data available in the literature, an average ratio of modulus of rigidity to modulus of elasticity (*G/E*) is considered equal to 0.045 and 0.069 for LVL and glulam respectively in order to make the planes' stiffness equations independent of *G* and *E* values. The fracture parameter value, C_{fp}, reported in Jensen et al. [3,20] and tensile strength perpendicular to grain values, f_{tp}, evaluated by Song [21] were used as inputs to the proposed splitting model. The average C_{fp} and f_{tp} were 22.7 N/mm$^{1.5}$ and 2.06 MPa (for the tangential direction with a COV=18%) for RP LVL and 18.4 N/mm$^{1.5}$ and 1.99 MPa (at 45° to the radial direction with a COV=24%) for RP glulam.

6 Test observations

As shown in Table 1 and 2, the ultimate load and the mode of failure were recorded for different test groups. BRG, MIG and DUG stand for tests series with brittle, mixed and ductile modes of failure correspondingly. Additionally, L stands for LVL and G for glulam. Test series with tightly spaced rivet pattern exhibited a brittle/mixed failure mode. For parallel to grain loading, a sudden failure happened where a block of wood bounded by the rivet group perimeter was pulled away from either one side or both sides of the specimens (Fig. 12a). As shown in Fig. 12b, in brittle failure mode, the failed block thickness, t_{block} corresponds to the elastic deformation of the rivets since no plastic deflection was observed. However, in the mixed failure mode (Fig. 12c), the t_{block} is significantly lower with observable small deformation of the rivets. In the mixed failure mode cases, the load-carrying capacity of the wood is based on the stiffness and strength of the tensile and shear planes corresponding to the effective depth of the wood, $t_{ef,y}$.

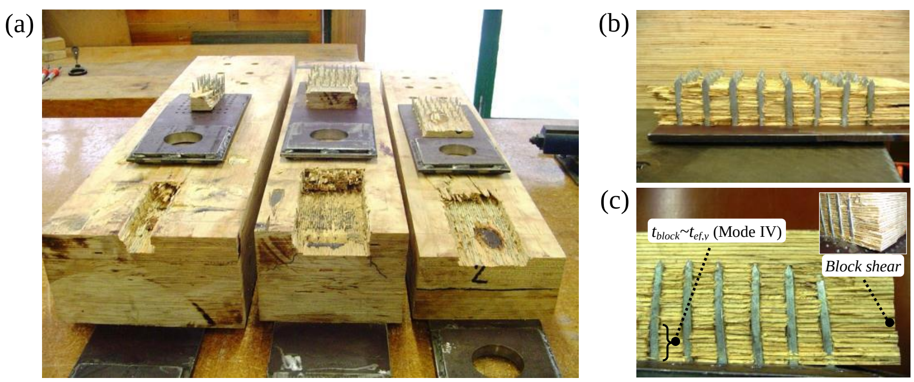

Fig. 12: Wood failure parallel to grain: (a) block tear-out bounded by the rivet cluster perimeter, (b) brittle failure - rivets within the elastic range, (c) mixed failure - rivets with small deformation

For the tests subjected to a perpendicular to grain loading, splitting of the wood occurred along the row of rivets next to the unloaded edge and propagated towards the timber member ends till reaching the unstable zone (Fig. 13a). The splitting crack formed either through the entire member width (for thin members with high penetration-to-thickness ratios), as shown in Fig. 13b or with a depth similar to the rivet effective embedment depth (for thick members with low penetration-to- thickness ratios), as shown in Fig. 13c.

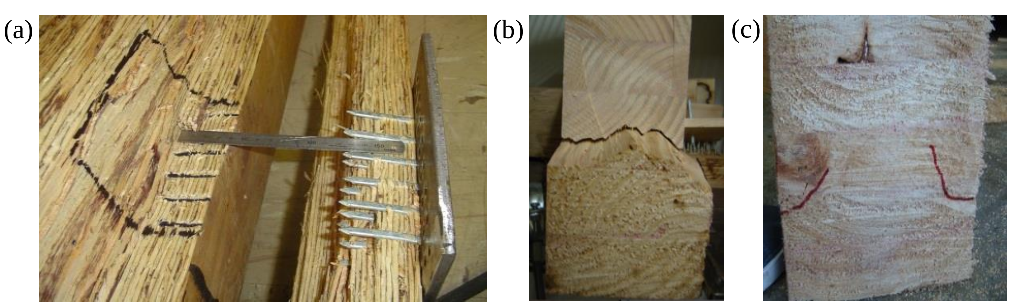

Fig. 13: Wood failure perpendicular to grain:
(a) crack propagation along the top row of rivets, (b) full width splitting, (c) partial width splitting

For large spaced rivet patterns, ductile failure of the rivet was observed with either one (Mode III_m) or two plastic hinge formations (Mode IV) accompanied by localized wood crushing. Fig. 14a and 14b show the possible ductile failure modes of the rivets tested under longitudinal and transverse loadings, respectively.

(a) (b)

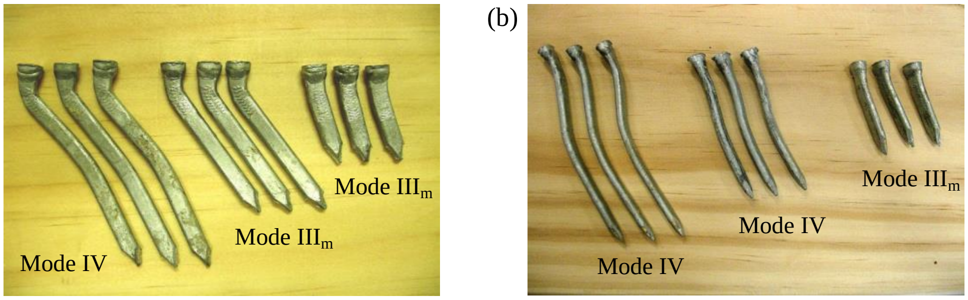

Fig. 14: Ductile failure modes of the rivets:
(a) parallel to grain loading, (b) perpendicular to grain loading

7 Verification of the proposed design approach

7.1 Riveted joint subjected to parallel-to-grain loading

The connection ultimate capacities were calculated using the proposed stiffness-based model and the algorithm presented to determine the connection failure mode. For the brittle failure mode, the elastic deformation of the rivet was considered to determine the $t_{ef,e}$. The estimated $t_{ef,e}$ was 27.1, 45.5 and 58.9 mm for a rivet penetration (L_p) equal to 28.5, 53.5 and 78.5 mm correspondingly. In the case of mixed failure, the $t_{ef,y}$ was predicted based on the bearing length corresponding to the governing yielding mode of the rivets equal to 28.4, 40.4 and 24.7 mm for the different penetration lengths. The $t_{ef,y}$ value for the longer rivet is lower compared to the other ones. This is due to the formation of the two plastic hinges (mode IV) for this length of rivet during the yielding failure, whereas the failure mode III_m governs for the smaller rivet sizes (Fig. 14a).

As shown in Table 1, for the BRG test groups, the estimated wood strength corresponding to the rivet elastic deformation, $P_{w,tefe}$, was lower than the rivet yielding resistance, $P_{r,yld}$, therefore the connection ultimate capacity was predicted as $P_{c,ult}=P_{w,tefe}$ with a brittle failure mode which was consistent with the observation. However, in the MIG test groups, the predicted wood strength for $t_{ef,e}$ was higher than the rivet yielding strength. The strength of the connection was thus checked for the possible mixed or ductile modes of failure. In these test series, a mixed mode failure occurred which can be explained by the wood strength corresponding to $t_{ef,y}$ being weaker than the rivets ultimate strength ($P_{w,tefy} < P_{r,ult}$). In the MIG22 and MIG23 test groups, since $P_{w,tefy}$ was greater than $P_{r,yld}$ thus, the connection ultimate capacity was determined as $P_{c,ult}=P_{w,tefy}$. However, for the MIG5, MIG20 and MIG21 test series where $P_{w,tefy} < P_{r,yld}$, $P_{c,ult}$ was predicted as $P_{r,yld}$. In the case of DUG test groups, the wood strength based on $t_{ef,y}$ was greater than the connection ultimate ductile strength, $P_{r,ult}$, therefore, the ductile failure governed ($P_{c,ult}=P_{r,ult}$) and there was no wood rupture.

There is very good conformity between the predictions and observations for the governing failure mode and the strength of the connection, as shown in Table 1. Fig. 15a shows the strength predictions of the experimental groups compared to the tests results. One can note that the proposed analysis results in precise predictions with a correlation coefficient (r^2) of 0.89, a mean absolute error (MAE) of 7.8% and a standard deviation (STDEV) of 10.3%.

Table 1: Prediction of the connection ultimate strength parallel to grain using the proposed design approach compared to experimental results on LVL and glulam

Test groups	Wood strength corresponding to rivet elastic deformation $P_{w,tefe}$ (kN)	Rivet yielding strength $P_{r,yld}$ (kN)	Wood strength corresponding to rivet yielding mode $P_{w,tefy}$ (kN)*	Rivet ultimate strength $P_{r,ult}$ (kN)*	Connection ultimate strength (predicted/observed (COV%))		
					$P_{c,ult}$ (kN)†	Failure mode‡	Ratio of predicted to observed
BRG1-L	314	410	N/A	N/A	314/358 (8%)	BRT/BRT	0.88
BRG2-L	362	410	N/A	N/A	362/370 (9%)	BRT/BRT	0.98
BRG3-L	380	410	N/A	N/A	380/375 (8%)	BRT/BRT	1.01
BRG4-L	376	410	N/A	N/A	376/391 (7%)	BRT/BRT	0.96
BRG5-L	381	410	N/A	N/A	381/402 (5%)	BRT/BRT	0.95
BRG6-L	378	410	N/A	N/A	378/410 (5%)	BRT/BRT	0.92
BRG7-L	391	410	N/A	N/A	391/435 (6%)	BRT/BRT	0.90
BRG8-L	419	595	N/A	N/A	419/463 (6%)	BRT/BRT	0.91
BRG9-L	392	446	N/A	N/A	392/384 (8%)	BRT/BRT	1.02
BRG10-L	423	446	N/A	N/A	423/419 (8%)	BRT/BRT	1.01
BRG11-L	432	446	N/A	N/A	432/427 (4%)	BRT/BRT	1.01
BRG12-L	432	446	N/A	N/A	432/398 (8%)	BRT/BRT	1.09
BRG13-L	436	446	N/A	N/A	436/456 (7%)	BRT/BRT	0.96
BRG14-L	440	446	N/A	N/A	440/468 (6%)	BRT/BRT	0.94
BRG15-L	427	446	N/A	N/A	427/437 (6%)	BRT/BRT	0.98
BRG16-L	434	446	N/A	N/A	434/445 (8%)	BRT/BRT	0.97
BRG17-L	392	297	362	339	339/290 (9%)	DUC/BRT	1.17
BRG18-L	237	230	229	N/A	230/247 (6%)	MIX/BRT	0.93
BRG19-L	330	334	N/A	N/A	330/315 (8%)	BRT/BRT	1.05
MIG20-L	436	345	233	N/A	345/285 (9%)	MIX/MIX	1.21
MIG21-L	338	230	176	N/A	230/207 (5%)	MIX/MIX	1.11
MIG22-L	255	223	234	255	234/214 (9%)	MIX/MIX	1.09
MIG23-L	178	154	166	183	166/159 (9%)	MIX/MIX	1.04
DUG24-L	505	307	498	365	365/345 (3%)	DUC/DUC	1.06
DUG25-L	515	334	479	382	382/388 (2%)	DUC/DUC	0.98
DUG26-L	419	154	213	179	179/185 (4%)	DUC/DUC	0.97
BRG1-G	340	448	N/A	N/A	340/335 (12%)	BRT/BRT	1.01
BRG2-G	328	336	N/A	N/A	328/301 (11%)	BRT/BRT	1.09
BRG3-G	188	250	N/A	N/A	188/224 (17%)	BRT/BRT	0.84
BRG4-G	226	224	N/A	N/A	226/315 (11%)	BRT/BRT	0.72
MIG5-G	222	192	127	N/A	192/160 (12%)	MIX/MIX	1.20
DUG6-G	397	252	379	317	317/298 (8%)	DUC/DUC	1.06

* Not applicable (N/A) for all the test groups based on the presented design algorithm. For instance, in MIG5-G test group, $P_{w,tefy}$ is calculated due to $P_{r,yld} < P_{w,tefe}$, however, there is no need to estimate $P_{r,ult}$ since $P_{w,tefy} < P_{r,yld}$.

† Coefficient of variation (COV%) calculated over 3 specimens for LVL and over 4 specimens for glulam members.

‡ BRT, MIX and DUC stand for brittle, mixed and ductile failure modes, correspondingly.

7.2 Riveted joint subjected to perpendicular-to-grain loading

There was a considerable difference between the predicted wood splitting strength and the rivet yielding resistance for the tested joints, therefore, the splitting failure was predicted to occur in a brittle fashion corresponding to the rivet elastic deformation. The estimated $t_{ef,e}$ was 24.2, 40.1 and 51.0 mm for the L_p equal to 28.5, 53.5 and 78.5 mm respectively. Following the presented design algorithm, for the BRG test groups (Table 2), the estimated wood splitting resistance corresponding to the rivet elastic deformation, $P_{w,tefe}$, was lower than the rivet yielding resistance perpendicular to grain, $P_{r,yld}$, therefore the connection ultimate capacity was predicted as $P_{c,ult}=P_{w,tefe}$ with a brittle failure mode which was in line with the observations. The DUG11, 12 and 13 tests groups were conducted on small specimens (n_R=2; n_C=3) using 40, 65 and 90 mm long rivets respectively under compression with no possibility of wood failure. The proposed design approach leads to a relatively good agreement between the predictions and the test results with a correlation coefficient (r^2) of 0.78, a mean absolute error (MAE) of 17.2% and a standard deviation (STDEV) of 17.2% (Fig. 15b).

Table 2: Prediction of connection ultimate strength perpendicular to grain using the proposed design approach compared to experimental results on LVL and glulam

Test groups	Wood strength corresponding to rivet elastic deformation $P_{w,tefe}$ (kN)	Rivet yielding strength $P_{r,yld}$ (kN)	Wood strength corresponding to rivet yielding mode $P_{w,tefy}$ (kN)†	Rivet ultimate strength $P_{r,ult}$ (kN)†	Connection ultimate strength (predicted/observed (COV%))		
					$P_{c,ult}$ (kN)‡	Failure mode	Ratio of predicted to observed
BRG1-L	168	274	N/A	N/A	168/173 (8%)	BRT/BRT	0.97
BRG2-L	132	274	N/A	N/A	132/158 (6%)	BRT/BRT	0.84
BRG3-L	120	274	N/A	N/A	120/144 (4%)	BRT/BRT	0.83
BRG4-L	168	274	N/A	N/A	168/167 (4%)	BRT/BRT	1.01
BRG5-L	156	274	N/A	N/A	156/205 (5%)	BRT/BRT	0.76
BRG6-L	102	230	N/A	N/A	102/115 (7%)	BRT/BRT	0.89
BRG7-L	132	154	N/A	N/A	132/134 (4%)	BRT/BRT	0.99
BRG8-L	174	274	N/A	N/A	174/147 (7%)	BRT/BRT	1.18
BRG9-L	170	302	N/A	N/A	170/198 (2%)	BRT/BRT	0.86
BRG10-L	120	243	N/A	N/A	120/160 (7%)	BRT/BRT	0.75
BRG11-L	74	274	N/A	N/A	74/117 (8%)	BRT/BRT	0.63
DUG12-L	N/A	N/A	N/A	N/A	44/49 (4%)	DUC/DUC	0.90
DUG13-L	N/A	N/A	N/A	N/A	53/62 (3%)	DUC/DUC	0.85
DUG14-L	N/A	N/A	N/A	N/A	58/65 (4%)	DUC/DUC	0.89
BRG1-G	114	209	N/A	N/A	114/141 (12%)	BRT/BRT	0.81
BRG2-G	90	209	N/A	N/A	90/115 (15%)	BRT/BRT	0.78
BRG3-G	110	209	N/A	N/A	110/116 (8%)	BRT/BRT	0.95
BRG4-G	114	209	N/A	N/A	114/133 (6%)	BRT/BRT	0.86
BRG5-G	186	209	N/A	N/A	186/161 (6%)	BRT/BRT	1.16
BRG6-G	70	151	N/A	N/A	70/107 (12%)	BRT/BRT	0.65
BRG7-G	54	76	N/A	N/A	54/85 (9%)	BRT/BRT	0.64
BRG8-G	104	105	N/A	N/A	104/108 (7%)	BRT/BRT	0.96
BRG9-G	146	223	N/A	N/A	146/166 (6%)	BRT/BRT	0.88
BRG10-G	82	139	N/A	N/A	82/139 (9%)	BRT/BRT	0.60

† Not applicable (N/A) for all the test groups based on the presented design algorithm.
‡ Coefficient of variation (COV%) calculated over 3 specimens for LVL and over 4 specimens for glulam members.

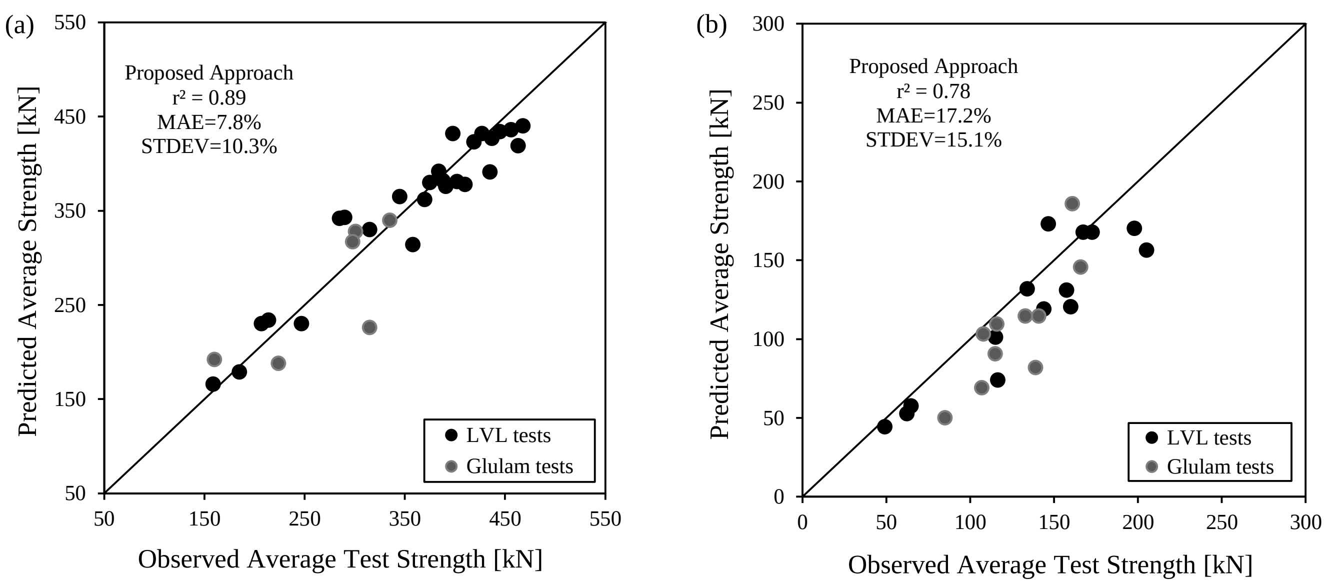

Fig. 15: Predictions vs. observations for the joint ultimate load-carrying capacity: (a) parallel to grain loading; (b) perpendicular to grain loading

8 Conclusions

The design procedures for timber connections in most design codes are based mainly on the European Yield Model. For multi-fastener connections either loaded parallel or perpendicular to grain, failure of the wood can be the dominant mode. A design procedure is proposed to identify the wood and fastener capacities under possible brittle, mixed and ductile failure modes of timber connections. For the wood capacity, the effective wood thickness is taken into account at each potential failure zone. The fastener resistance for yielding and ultimate limit states are determined using the relevant wood embedment strength and the fastener moment capacity. The proposed design procedure is verified using tests conducted on riveted joints under longitudinal and transverse loadings on New Zealand Radiata Pine LVL and glulam. The proposed design approach can be extended to other small dowel type fasteners such as nails and screws for connection design improvement and failure modes prediction.

Acknowledgements

The authors wish to thank the Structural Timber Innovation Company (STIC) for funding this research work. The authors wish also to express their gratitude to The University of Auckland undergraduate students Samuel Wong and Shuai Ma, who did the experimental work related to glulam splitting as part of their final year project.

References

[1] Smith I, Foliente G. Load and resistance factor design of timber joints: International practice and future direction. J Struct Eng ASCE 2002; 128:48-59.

[2] Foschi RO, Longworth J. Analysis and design of griplam nailed connections. J Struct Div ASCE 1975; 101:2537-2555.

[3] Jensen JL, Quenneville P, Girhammar UA, Källsner B. Splitting of timber beams loaded perpendicular to grain by connections - Combined effect of edge and end distance. Construction and Building Materials 2012; 35:289-293.

[4] Johnsson H. Plug shear failure in nailed timber connections. Doctoral dissertation, Department of Civil and Environmental Engineering, Lulea University of Technology, Sweden; 2004.

[5] Quenneville P, Mohammad M. On the failure modes and strength of steel-wood-steel bolted timber connections loaded parallel-to-grain. Can J Civ Eng 2000; 27:761-773.

[6] Quenneville P, Mohammad M. Design method for bolted connections loaded perpendicular to grain. Can J Civ Eng 2001; 28:949-959.

[7] Stahl DC, Wolfe RW, Begel M. Improved analysis of timber rivet connections. J Struct Eng ASCE 2004; 130:1272-1279.

[8] Van der Put TACM, Leijten AJM. Evaluation of perpendicular to grain failure of beams caused by concentrated loads of joints. Proc, CIB-W18, The Netherlands; 2000. paper 33-7-7.

[9] Yasumura M, Murota T, Sakai T. Ultimate properties of bolted joints in glued-laminated timber. Proc, International Council for Research and Innovation in Building and Construction, CIB-W18, Dublin, Ireland; 1987. paper 20-7-3.

[10] Zarnani P, Quenneville P. Wood block tear-out resistance and failure modes of timber rivet connections – A Stiffness-based approach. J Struct Eng ASCE; 2013a (in press).

[11] Zarnani P, Quenneville P. Wood load-carrying capacity of timber connections - An extended application for nails and screws. Proc, RILEM Conference, Materials and Joints in Timber Structures, Stuttgart; 2013b.

[12] Zarnani P, Quenneville, P. Wood splitting capacity in timber connections loaded transversely: Riveted joint strength for full and partial width failure modes. Proc, International Council for Research and Innovation in Building and Construction, CIB-W18, Vancouver; 2013c.

[13] Begel M, Wolfe RW, Stahl DC. Timber rivet connections in US domestic species. Research Paper FPL-RP-619, US Department of Agriculture Forest Products Laboratory, Madison, Wis; 2004.

[14] Zarnani P, Quenneville P. Wood effective thickness in brittle and mixed failure modes of timber rivet connections. Proc, 12th World Conference on Timber Eng, Auckland, New Zealand; 2012c.

[15] Johansen KW. Theory of timber connections. Publications of International Association for Bridge and Structural Engineering 1949; 9:249-262.

[16] European Committee for Standardization (CEN). Eurocode 5-Design of timber structures. EN 1995-1-1:2004, Brussels, Belgium; 2004.

[17] Zarnani P, Quenneville P. Reliable yield model for strength prediction of timber rivet connection under ductile failure. Proc, 12th World Conference on Timber Eng, Auckland, New Zealand; 2012b.

[18] American Forest and Paper Association (AFPA). General dowel equations for calculating lateral connection values. Technical Rep 12, Washington, DC; 1999.

[19] Zarnani P, Quenneville P. Predictive analytical model for wood capacity of rivet connections in glulam and LVL. Proc, 12th World Conference on Timber Eng, Auckland, New Zealand; 2012a.

[20] Jensen JL, Girhammar UA, Quenneville P, Källsner, B. Splitting of beams loaded perpendicular to grain by connections - Simple fracture mechanics models. Proc., 12th WCTE, Auckland, NZ.

[21] Song Y K. Investigation of tension strength perpendicular to grain of New Zealand Radiata Pine. Final Year Research Project Report, Depart of Civil and Environmental Eng, The University of Auckland, Auckland, New Zealand; 2010.

INTERNATIONAL COUNCIL FOR RESEARCH AND INNOVATION IN BUILDING AND CONSTRUCTION

WORKING COMMISSION W18 - TIMBER STRUCTURES

WITHDRAWAL STRENGTH OF SELF-TAPPING SCREWS IN HARDWOODS

U Hübner

Association of the Austrian Wood Industries

AUSTRIA

Keywords: connection, screw, withdrawal strength, hardwood, beech, ash, Black Locust

Presented by U Hübner

A Frangi commented about the load duration behaviour and different COV as a function of diameter and asked if there were any physical reasons. U Hübner responded that with larger diameter screws reinforcing specimens against splitting perpendicular to grain was needed and that this was a very complicated failure mechanism with mixture of failure modes. Also it was very difficult to distinguish what governed at which angle. Also tests from Graz and Karlsruhe with screws installed parallel to grain and loaded at 70% of the short-term failure load indicated failure within 1 week. More research is needed.

F Lam commented that installation at less than 30 degree parallel to grain can be risky especially in cyclic moisture conditions.

J Munch Andersen commented that in terms of comparison with code equations it would be better to compare with softwood.

J W van de Kuilen commented that the density of hardwood can range from 100 kg/m³ to 1200 kg/m³ and received clarification of the density of wood studied as 550 kg/m³ to 900 kg/m³ as medium density hardwood from central Europe.

H Blass received confirmation that these screws would be intended for reinforcing hardwood and predrilling diameter would not be larger than the core screw diameter. H Blass stated that high insertion moment/torque can develop in the longer screws.

J W van de Kuilen received confirmation that the density dependency model was used for different wood species. He questioned whether the density model worked for only one species, for example, beech. U Hübner responded that calculation model was developed for European Ash first and adding another species increased COV a little and there was not too much difference between species.

J Munch Andersen received confirmation that the graphs were based on mean values.

Withdrawal strength of self-tapping screws in hardwoods

Ulrich Hübner[a]

Abstract The axial withdrawal resistance of self-tapping screws of the diameters 6 mm (Z-9.1-435, 2009), 8 mm (Z-9.1-656, 2007), 10 and 12 mm (Z-9.1-519, 2011) was tested according to ON EN 1382 (1999) in glue laminated timer (GLT) made of European ash (*Fraxinus excelsior* L., $n = 2\,657$) with angles α between the fiber direction and the screw axis of $0°, 15°, \ldots, 90°$. Screws with 4 mm diameter (Z-9.1-435, 2009) and threaded bars ⌀ 20 mm (Z-9.1-777, 2010) according to DIN 7998 (1975) were pulled out parallel and perpendicular to the grain to determine the influence of the diameter over a large range. The influence of the screw tip and the screw embedment length were analyzed. Self-tapping screws of diameters 8, 10 and 12 mm were also pulled out of European beech (*Fagus sylvatica* L., $n = 371$) and Black locust (*Robinia pseudoacacia* L., $n = 300$) parallelly and perpendicularly to the grain.
If the moisture content rises 1 % the withdrawal resistance of screws decrease 2.7 % parallel to the grain and 2.4 % perpendicular to the grain direction. The lower withdrawal resistance of the tip should be considered with $l_{\text{ef}} = l_{\text{nom}} - 1.1\,d$, where l_{nom} is the inserted nominal length of the screw. The characteristic withdrawal resistance of self-tapping screws in European hardwoods should be calculated for the regular thread with a bilinear design model with a constant resistance from 30° to 90° according to $R_{\text{ax,k}} = f_{\text{ax,k}}\,\pi\,d\,l_{\text{ef}}$ with $f_{\text{ax,k}} = 7 \cdot 10^{-4} \cdot \rho_{\text{k}}^{1.6} \cdot d^{-0.34}$ and a linear reduction of 30 % to $\alpha = 0°$. Additionally the thread of partial-threaded screws should be embedded at least $2\,d$ under the surface of the timber for $0° \leq \alpha \leq 30°$. If the summation of characteristic withdrawal resistances was calculated according the new design model for angels of $30°, 45°, \ldots, 90°$, the diameters 6, 8, 10 and 12 mm, the effective lengths of $4\,d$, $5\,d$, $6\,d$ and the characteristic density 672 kg/m^3 the result exceeds the solution according to ON EN 1995-1-1 (2009) by a factor of 1.79

1 Introduction

GLT made of birch (Griesser, 2012), chestnut (MPA Stuttgart, 2012), European beech (Z-9.1-679, 2011), European ash (Bogusch, 2011) and oak (Z-9.1-704, 2012) but also laminated veneer lumber (LVL) made of European beech (Pollmeier, 2012) was developed. Effective connections should use the impressive performance of these materials.

The design of withdrawal resistance of self-tapping screws according to ON EN 1995-1-1 (2009) is based on tests with spruce. Eckelman (1975), Jablonkay (1999) and Schneider (1999) gave an indication of the capacity of screws in hardwoods but they used old fashioned screws, only one diameter and species respectivelly. Thus it was necessary to analyses a wide range of screw diameters, angles between screw axis and fiber direction with one species (ring porous European ash) and to compare the results with two other species representing different wood anatomies and densities (diffuse porous European beech, ring porous Black locust) in order to create a reliable data base for a new design model.

[a] Association of the Austrian Wood Industries
huebner@holzbauindustrie.at
T +43 (0)1 712 26 01 23

Table 2.1: Ratio of the core diameter and the pitch to the outer diameter for self-tapping screws with a German technical approval (see DIBt, 2012)

	core to outer diameter [−]				pitch to outer diameter [−]				characteristic tension strength $4\,R_{\mathrm{t,u,k}}/\left(\pi d_2^2\right)$ $\left[\mathrm{N/mm^2}\right]$			
diameter	6	8	10	12	6	8	10	12	6	8	10	12
# of approvals	35	41	29	14	35	41	29	14	35	40	29	16
Minimum	0.60	0.63	0.60	0.57	0.37	0.42	0.39	0.36	588	554	567	623
Mean	0.64	0.65	0.63	0.60	0.58	0.62	0.57	0.49	878	862	816	763
Maximum	0.72	0.68	0.69	0.71	0.82	0.81	0.75	0.55	1 110	1 477	1 027	977

2 Method

The beech and ash logs were harvested in the Austrian region *Bucklige Welt* in the growth area *Östliche Randalpen*. The logs of Black locust came from Zalaegerzeg/Hungary. The ash and Black locust boards (27 mm) were glued with MUF Kauramin 683 and hardener Kauramin 688 to form the GLT. The ash specimens for $15° \leq \alpha \leq 75°$ were sawn from six GLT. The beech scantlings had a section of 60 mm × 120 mm. All specimens were predrilled with diameters equal to the root diameters round down to 0.5 mm. In general the specimens were stored in a climate chamber with (20±2) °C and (65 ± 5) % relative humidity. The influence of moisture contents from 5 to 24 % on the withdrawal strength was investigated parallelly and perpendicularly to the grain direction.

The geometry of the regular thread of the used screws of 4 mm, 6 mm, 8 mm, 10 and 12 mm are repesentative for most of the screws with a German technical approval. The Table 2.1 shows the mean but also minimum and maximum ratios of the core diameter and the pitch of the outer diameter.

The regular spacing and edge distance was $5\,d$. The thickness of the specimens was limited by the tension resistance of the screws and rods. For the diameters 4 to 10 mm the thickness of the specimen was $l_{\mathrm{ef}}6\,d$. Screws with ⌀ 12 mm were tested with $l_{\mathrm{ef}}4\,d$ and the rods with $l_{\mathrm{ef}}8\,d$ The minimum width of specimen for the rods (⌀ 20 mm) was 140 mm. Pilot tests showed the need for reinforcement normal to the rod axis with four or eight screws ⌀ 8/160 mm to prevent splitting (see Figure 3.5)). The density and the moisture content of the hardwood around the screw axis were determined on cuboids $4\,d \times 4\,d \times$ *specimen thickness* to minimize the influence of density variations within the specimens. The moisture content of the specimens was analyzed according to ON EN 13 183-1 (2004).

The withdrawal resistance was tested according to ON EN 1382 (1999) with the diameter of the free surface around the screw of $4\,d$ The influence of radial or tangential screw axis to the annual growth rings was neglected following Cockrell (1933).

The influence of the screw tip and the embedded length were also analyzed. The samples contained in general 60 specimens and for the comparison of mean values 40. The density of the samples were representative for the basic population corresponding to the third method proposed by Leijten, Köhler and Jorissen (2006, p. 9).

3 Analysis of the test results

3.1 Moisture content and density

The values for the moisture content are listed in Table 3.1. The mean moisture content of the regular specimens is equal to the mois-

Table 3.1: Moisture content of the regular samples

Species	n [–]	min. [%]	mean [%]	max. [%]	*CoV* [%]
Ash	2 657	8.20	10.75	14.80	3.33
Beech	371	10.30	11.02	11.80	1.93
Black locust	300	10.00	10.85	14.90	4.33
All	3 328	8.20	10.80	14.90	3.41

Table 3.2: Density ρ_{12} $\left[\mathrm{kg/m^3}\right]$ of the samples

Species	n [–]	min.	mean	max.	*CoV* [%]
Ash	2 620	555	746	918	6.11
Beech	371	582	719	851	6.09
Black locust	300	609	750	884	6.84
All	3 291	555	744	918	6.29

ture content of ash in a climate of $(20 \pm 1)\,°\mathrm{C}$ and (65 ± 5) % relative humidity and desorption of moisture. Adsorption would lead to $u_{\mathrm{mean}} = 13.9\,\%$ as tested with 43 specimens.

Two samples ($n_{\shortparallel} = 37$, $n_{\perp} = 40$) made of ash were conditioned to a mean moisture content ($u_{\mathrm{mean},\shortparallel} = 31\,\%$, $u_{\mathrm{mean},\perp} = 27\,\%$) under the fiber saturation point of 33 % according to Popper and Niemz (2009) to analyses the influence of the moisture content on the withdrawal strength parallel and perpendicular to the grain direction. The two paired samples had a mean moisture content of 11 %. The equations (1) and (2) represent the regression lines for the withdrawal resistance versus the moisture content. If the moisture content rises 1 % the withdrawal resistance of screws parallel to the grain direction decreases 2.7 % and perpendicular to the grain 2.4 % relative to the withdrawal resistance at the reference moisture content of $u_{\mathrm{ref}} = 12\,\%$. This relationship was also used to adjust the withdrawal resistance of European beech and Black locust to u_{ref}.

$$R_{\mathrm{ax,mean},0} = -0.453\,u + 22.2 \tag{1}$$

$$R_{\mathrm{ax,mean},90} = -0.438\,u + 23.8 \tag{2}$$

The density was adjusted to u_{ref} according to ON EN 384 (2010, p. 13) and Table 3.2 gives an overview.

3.2 Influence of the screw tip

It is obvious that the withdrawal strength of the screw tip is lower than that of the regular thread. Specimens of the same thickness were tested with the tip flush to the surface and outside the specimen. The sample references in Table 3.3 show *ES* for European ash, the screw diameter, the angle between screw axis and grain direction and the thickness of the specimen.

Table 3.3: Samples with screw tip outside or inside the specimens

tip outside	tip inside	x_i
ES08_00_48	ES08_00_48S	1.28
ES08_90_32	ES08_90_32S	*2.02*
ES08_90_48	ES08_90_48S	0.98
ES08_90_64	ES08_90_64S	*0.76*
ES10_00_60	ES10_00_60S	1.29
ES10_90_60	ES10_90_60S	0.98
ES12_00_60	ES12_00_60S	1.00
ES12_90_60	ES12_90_60S	1.10
Mean $\bar{x}$		1.11

The mean value $\bar{x} = 1.11$ results if the outliers 2.02 and 0.76 in Table 3.3 are excluded and equation (3) was derived to calculate the effective embedment length l_{ef} based on the nominal embedment length l_{nom}.

$$l_{\mathrm{ef}} = l_{\mathrm{nom}} - 1.11\,d \tag{3}$$

Equation (3) corresponds to the regulation $l_{\mathrm{ef}} = l_{\mathrm{nom}} - d$ in SIA 265 (2003, p. 66), ON EN 1995-1-1 (2006, p. 83), Pirnbacher and Schickhofer (2009, p. 35), Eckelman (1975, p. 35) the rule to subtract the tip length according to Newlin and Gahagan (1938, p. 6). CEN TC124 decided after a discussion over several years with the statement: "For screws it is clearly defined that the point length is included in the threaded length, both in EN 1995-1 and EN 14592. It is decided to have the same rules for calculation of the withdrawal capacity of screws and nails by using the profiled length" (Ravasse, 2011, p. 7). "...all scientists agrees that the truth is that the tip should be disregarded" (Munch-Andersen, 2013). The challenge is a coherent system of test and design standard with logical rules for all dowel-type connectors.

The withdrawal test according to ON EN 1382 (2012) should use specimens with a thickness relative to the diameter of the dowel type fastener because of the influence of the transverse strain near the surface, which can be seen as a systematic error. The penetration depth l_d should only include the regular thread and not the whole profiled part including the tip and eventually the special threads of a reamer shaft.

3.3 Influence of the diameter

Screws with diameters of 4, 6, 8, 10 and 12 mm and rods with a thread of ⌀ 20 mm according to DIN 7998 (1975) were pulled out parallelly and perpendicularly to the grain to determine the influence of the diameter on the withdrawal strength of European ash over a large range. Self-tapping screws of diameters 8, 10 and 12 mm with the same technical approvals were also pulled out of European beech and Black locust parallelly and perpendicularly to the grain.

Figure 3.1 shows the normalized (ρ_mean, u_ref) mean values of the withdrawal strength parallel and perpendicular to the grain for all diameters and wood species. Two different models were used for the regression analysis of the values for ash. The gray curves represent the equations (4) and (5) and the black curves the equations (6) and (7). Power functions are often used to express size effects, but the logarithmic functions leads to more realistic limiting values.

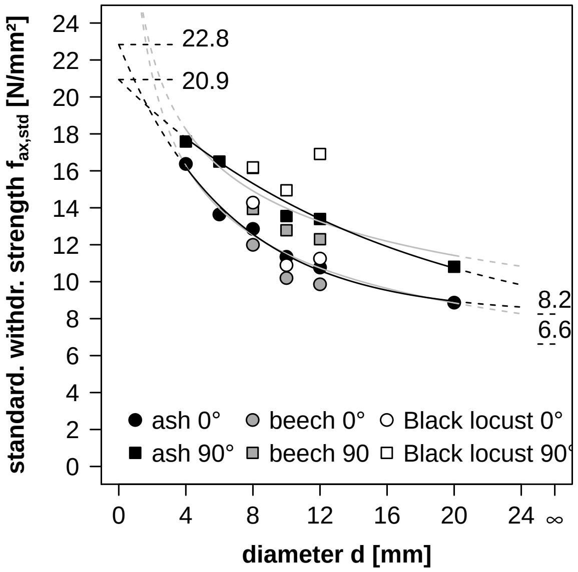

Figure 3.1: Standardized withdrawal strength versus diameter

$$f_\mathrm{ax,0,mean} = 27.5\,d^{-0.378} \tag{4}$$
$$f_\mathrm{ax,90,mean} = 27.3\,d^{-0.291} \tag{5}$$
$$f_\mathrm{ax,0,mean} = 8.25 + 14.6\,e^{-0.152\,d} \tag{6}$$
$$f_\mathrm{ax,90,mean} = 6.63 + 14.3\,e^{-0.0624\,d} \tag{7}$$

Büeler (2011, p. 22) published $f_\mathrm{v,mean} = 6.7\,\mathrm{N/mm^2}$ ($CoV = 16.7\,\%$) for five tests with glulam beams made of European ash (W 140 mm, H 480 or 600 mm, L 1 380 to 2 420 mm). The rupture area due to withdrawal tests parallel to the grain have to be around the screw and not necessarily at the weakest area of the section. This could be the explanation for $\lim_{d\to\infty} f_\mathrm{ax,0,nrm} = 8.2\,\mathrm{N/mm^2} > 6.7\,\mathrm{N/mm^2}$. The gray and white filled circles for the other two species follow the curves for ash. The exception ROB12_90_60 proves the rule.

Finally the regression curve (8) based on a power function was calculated for the 5th percentiles of the withdrawal strength of all samples for $\alpha = 0°$ and $\alpha = 90°$.

$$f_{\mathrm{ax,05}} = 23.3\, d^{-0.340} \tag{8}$$

This exponent of $1 - 0.340 = 0.660$ describes the influence of the screw diameter on the withdrawal resistance. Frese and Blaß (2009, p. 10) published the exponent $1 - 0.3423 = 0.656$ for self-tapping screws in spruce and Rajak and Eckelman (1993, p. 29) $1 - 0.355 = 0.645$ for MDF-panels. Thus the influence of the diameter of $d^{0.66}$ on the withdrawal resistance is reliable for MDF, soft- and hardwoods. The design model for the withdrawal resistance in ON EN 1995-1-1 (2009) emanates from $d^{0.5}$, published in the fundamental work of Bejtka (2005, p. 21) for screws with diameters from 6 to 12 mm. The wider range of diameters from 4 to 20 mm allows a more precise regression analysis.

3.4 Withdrawal resistance

Figure 3.2 on p. 6 shows the boxplots of the withdrawal strength at u_{ref} of all regular samples with European ash. The withdrawal strength decreases with increasing diameter as described in Section 3.3. The black bars of the medians for screws parallel are always lower than for screws perpendicular to the grain direction. The inter quartile range for $\alpha = 90°$ is in general wider than for $30° \leq \alpha \leq 75°$. Table 3.4 indicates the coefficients of variation for all samples including extreme values.

Table 3.4: Coefficients of variation for all samples of withdrawal strength $f_{\mathrm{ax,12}}$ for European ash

diameter	angle screw axis/fiber direction 0°	15°	30°	45°	60°	75°	90°
4	13.8	–	–	–	–	–	14.7
6	13.0	13.9	10.7	9.2	9.4	10.1	11.8
8	19.4	16.3	9.8	11.0	9.8	8.1	14.3
10	18.5	15.6	11.1	10.9	9.2	7.7	12.2
12	17.1	17.1	12.6	13.3	8.7	8.4	14.6
20	15.2	–	–	–	–	–	8.8

3.5 From regression analysis to design model

The first regression analysis was based on the design model of ON EN 1995-1-1 (2009) for the withdrawal resistance and equation (9) shows the logarithmized version. This was necessary to obtain normal distributed residues with the same variation over the whole diameter range.

$$\ln R_{\mathrm{ax,mean}} = \ln A + B \ln l_{\mathrm{ef}} + C \ln \rho_{12} + \ldots$$
$$\ldots D \ln d - \ln\left(\sin^2\alpha + E\cos^2\alpha\right) \tag{9}$$

$$\ln R_{\mathrm{ax,mean}} = \ln A + B \ln l_{\mathrm{ef}} + C \ln \rho_{12} + \ldots$$
$$D \ln d - \begin{cases} \ln\left(1 - E\,(30° - \alpha)\right) & 0° \leq \alpha < 30° \\ 0 & 30° \leq \alpha \leq 90° \end{cases} \tag{10}$$

The standardization of the withdrawal strength of European beech, European ash and Black locust was calculated for the reference values is $\rho_{\mathrm{mean}} = 744\,\mathrm{kg/m^3}$, $d_{\mathrm{std}} = 10\,\mathrm{mm}$ and $l_{\mathrm{ef}} = 60\,\mathrm{mm}$ with the coefficients $B = 0.972$, $C = 1.604$ and $D = 0.666$ of equation (9).

Table 3.5: Parameters for equation (10)

parameter	estimate	standard error
A	−12.9	0.230
B	1.08	0.020 8
C	1.58	0.034 6
D	0.568	0.021 8
E	0.00576	0.000 136

The boxplot for the normalized withdrawal strength of all tested ash samples are shown in Figure 3.3 for different angles between screw axis and grain direction. The white squares indicate the 5th percentiles and the dotted curve connects the 5th percentiles for $\alpha = 0°$ and $\alpha = 90°$ with a Hankinson-function. The white squares for $15° \leq \alpha \leq 75°$ are always above the dotted line on the (very) safe side.

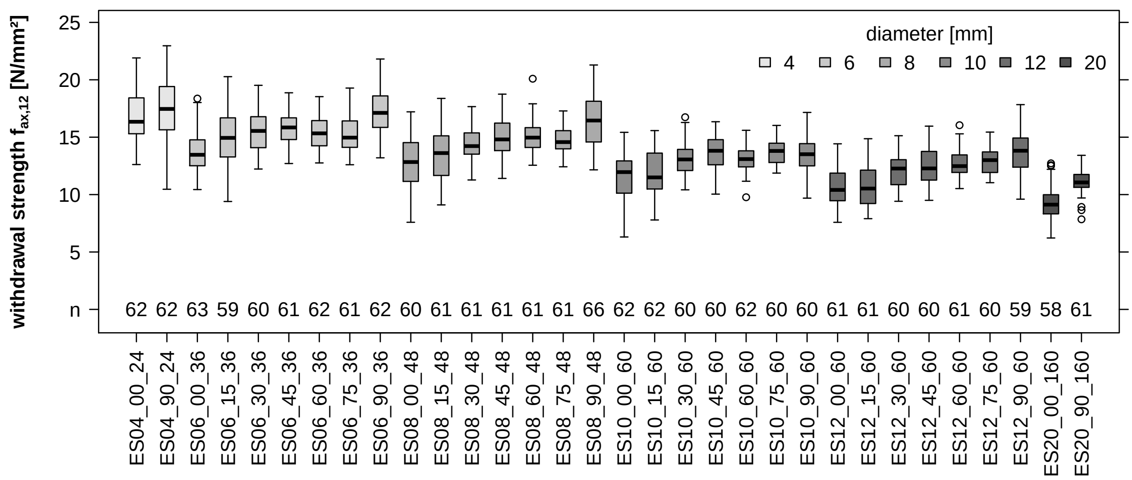

Figure 3.2: Boxplots of the withdrawal strength for ash

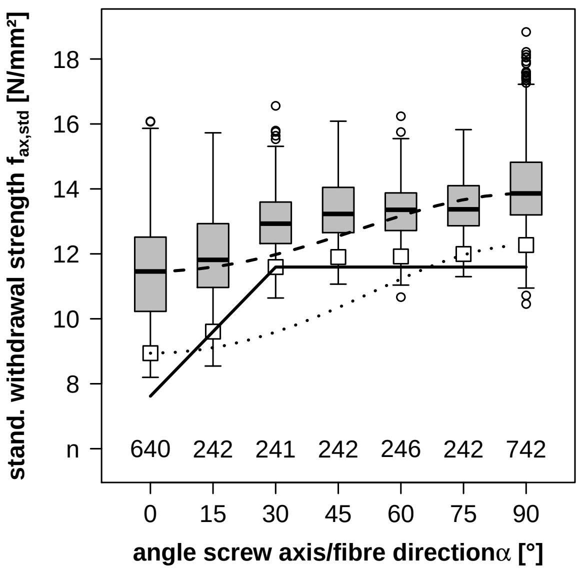

Figure 3.3: Boxplots of standardised withdrawal strength

The break of slope for the bilinear curve is always the 5$^{\text{th}}$ percentile for $\alpha = 30°$. The slope of the left part results from the tangent to the 5$^{\text{th}}$ percentile for $\alpha = 15°$. The sum of the differences between the 5$^{\text{th}}$ percentiles and the bilinear curve is smaller than between the bilinear curve and the dotted line. The following regression analysis was thus based on the bilinear equation (10).

$$\tilde{\epsilon} - 5.2\,\text{med}\left(|\hat{\epsilon}_i - \tilde{\epsilon}|\right) \leq \hat{\epsilon}_i \leq \tilde{\epsilon} + 5.2\,\text{med}\left(|\hat{\epsilon}_i - \tilde{\epsilon}|\right) \tag{11}$$

Equation (11) was choosen due to its robustness according to Hampel (1985, p. 98) to eliminate 24 outliers of 2 621 datasets based on the residues $\hat{\epsilon}_i$ and the mean residue $\tilde{\epsilon}$.

$$R_{\text{ax,mean}} = 2.39 \cdot 10^{-3}\, l_{\text{ef}}\, \rho_{\text{mean}}^{1.6}\, d^{0.66} \ldots$$
$$\ldots \begin{cases} 1 - 0.006\,(30° - \alpha) & 0° \leq \alpha < 30° \\ 1 & 30° \leq \alpha \leq 90° \end{cases} \tag{12}$$

$$R_{\text{ax,05}} = 2.2 \cdot 10^{-3}\, l_{\text{ef}}\, \rho_{05}^{1.6}\, d^{0.66} \ldots$$
$$\ldots \begin{cases} 1 - 0.006\,(30° - \alpha) & 0° \leq \alpha < 30° \\ 1 & 30° \leq \alpha \leq 90° \end{cases} \tag{13}$$

The estimates and their standard errors of the parameters in equation (10) are listed in Table 3.5. For practical reasons the parameter B was set to 1.0 and the other parameters were calculated again. Then C was rounded to 1.6. The regression analysis was repeated until all parameters were rounded and fixed. $R_{\text{ax,mean},i}$ according to equation (12) and the test results are plotted in Figure 3.4 and form an ideal type scatter band. The orange circles for Black locust and the red circles for beech fit to the circles for ash. The different wood anatomies can be sufficiently represented by the densities.

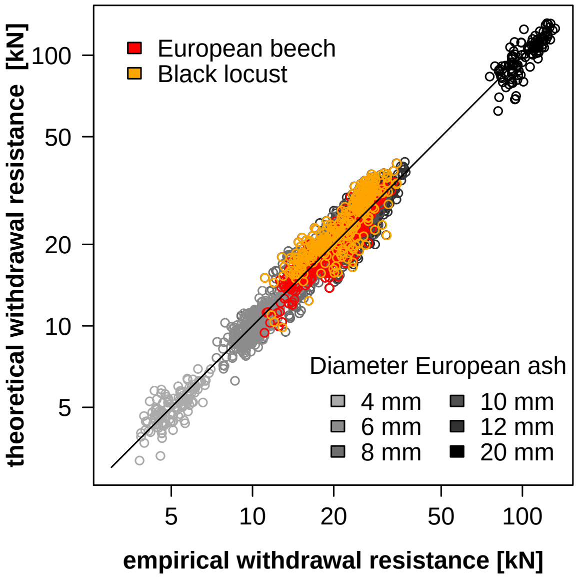

Figure 3.4: Tested versus theoretical withdrawal resstance according to equation (12)

The adjusted coefficient of determination was $r^2_{\text{adj}} = 0.966$. The normal distributed residues had an estimated standard deviation of $\hat{\sigma} = 0.1073$. Thus the expected value for the withdrawal resistance has a coefficient of variation of 10.77 %. The relation of the 5th percentile to the mean of the expected withdrawal resistance is constant for all parameter combinations according to the design model and equal to 0.823. The 5th percentile of the density of the dataset is $672\,\text{kg/m}^3$ and the mean value $743\,\text{kg/m}^3$. If the characteristic density is introduced in equation (12) a reduction to 90.5 % follows. The parameter $\exp(A)$ has to be multiplied with $1-(0.905-0.823) = 0.917$ to get the necessary 82.2 % of the expected withdrawal resistance equal to the estimated 5th percentile of equation (13).

The 5th percentile of the density of each species was calculated and introduced in equation (13) to calculate with each dataset of $l_{\text{ef},i}$ and α_i the estimated 5th percentile of the withdrawal resistance. These theoretical values were compared to all the measured values and for 32 of 44 samples all test values including the extreme values exceed the estimates. In nine samples 98 % passed, in two sampels 97 % and in one sample the limit of 95 % was reached. Only 16 out of 2 621 vaues or 0.6 % were on the unsafe side.

Pirnbacher and Schickhofer (2012, p. 132) stated concerning the long term behavior of screws parallel to the grain: "when the applied load does not exceed a threshold at about 73 % of the ultimate strength their behavior is covered by the application of k_{mod} as currently present in the EC5". SIA 265 (2012, p. 71) requires a minimum effective thread length of 100 mm or $8\,d$ respectively for screws parallel to the grain direction. A similar rule was formulated in SIA 265 (2003). Uibel and Blaß (2013, p. 132) reported about long term tests in spruce with screws axially loaded with 70 % of the design resistance. 19 of the 48 screws (40 %) failed during the test of almost five years. Equation (13) is valid for short term loads with a load duration of (300 ± 120) s. Pirnbacher (2011, p. 81) reported a positive effect of the embedment of the thread of partially-threaded screws on the long term behavior. Summarizing these publications it is necessary to reduce the withdrawal resistance for screws parallel to grain with the factor 0.01 instead of 0.006 in equation (13) and additionally use an embedment length of $l_{\text{emb}} = 2\,d$.

$$R_{\text{ax,k}} = 2.2 \cdot 10^{-3}\, l_{\text{ef}}\, \rho_{\text{k}}^{1.6}\, d^{0.66} \ldots$$
$$\ldots \begin{cases} 1 - 0.01\,(30° - \alpha) & 0° \le \alpha < 30° \cap l_{\text{emb}} = 2\,d \\ 1 & 30° \le \alpha \le 90° \end{cases} \tag{14}$$

If all the characteristic withdrawal resistances are calculated according to equation (14) for angles of $30°, 45°, \ldots, 90°$, the diameters 6, 8, 10 and 12 mm, the effective lengths of $4\,d$, $5\,d$, $6\,d$ and the characteristic density $672\,\text{kg/m}^3$ the results exceed the solution according to ON EN 1995-1-1 (2009) by the factor 1.79. A second advantage is that the new model covers a wider range of diameters from 4 to 20 mm and angles between screw axis and grain direction from 0° to 90°.

Engineers like mechanically logical design models where the parameters with their corresponding units give reasonable results. In equation (15) $f_{\mathrm{ax,k}}$ is the withdrawal *strength* in $\mathrm{N/mm^2}$ not the withdrawal *parameter* according to ON EN 1995-1-1 (2009).

$$R_{\mathrm{ax,k}} = f_{\mathrm{ax,k}}\, \pi\, d\, l_{\mathrm{ef}} \tag{15}$$

The description of $f_{\mathrm{ax,k}}$ should cover complete different rupture mechanisms. The withdrawal strength parallel to the grain is the shear strength around the outer diameter of the screw with an influence of the screw tip and the transverse strain near the surface of the timber. The withdrawal resistance perpendicular to grain is much more complicated to describe. The rupture is a mix of shear cracks parallel to grain due to the bending of the fibers, rolling shear, compression and tension perpendicular to grain (see Figure 3.5). Additional size effects have to be considered. The equation (14) summarizes the different parameters and effects. The alternative is to combine equations (15) and (16).

$$f_{\mathrm{ax,k}} = 7 \cdot 10^{-4} \cdot \rho_{\mathrm{k}}^{1.6} \cdot d^{-0.34} \ldots$$
$$\ldots \begin{cases} 1 - 0.01\,(30° - \alpha) & 0° \leq \alpha < 30° \cap l_{\mathrm{emb}} = 2\,d \\ 1 & 30° \leq \alpha \leq 90° \end{cases} \tag{16}$$

4 Comparison with other design models

Schneider (1999) published a design model for the withdrawal resistance of self-tapping screws (anchor for window frames ⌀ 7.5 mm) in European beech. The orange curve and circle in Figure 4.1 a and 4.2 a respectivelly represent this model. Equation (14) was plotted as the black curve and the design model

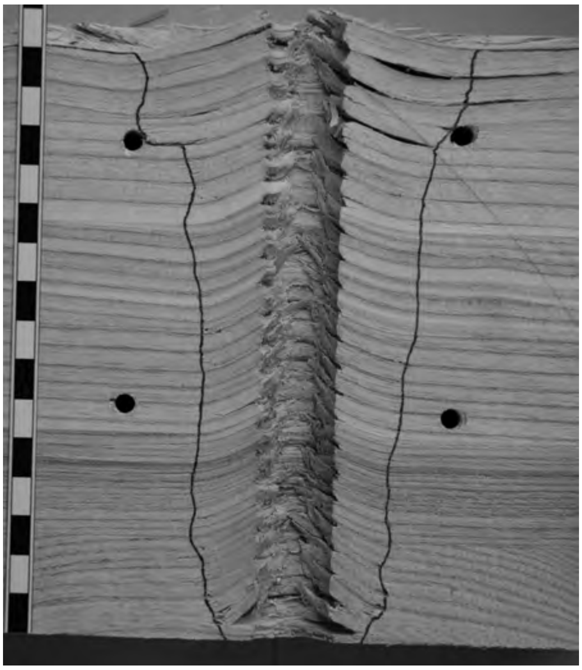

Figure 3.5: Cut in half specimen after withdrawal test (ES20_90_160_54, ⌀ 20 mm, $\alpha = 90°$)

for European ash according to Hübner, Rasser and Schickhofer (2010) as the black dashed curve. The blue curve was plotted according to ON EN 1995-1-1 (2009). The slope of the blue curve in Figure 4.1 is flat due to the $\rho_{\mathrm{k}}^{0.5}$ for softwoods. The design model of SIA 265 (2003) is no longer valid but the red curve was plotted to show the former performance compared to ON EN 1995-1-1 (2009). DIN 1052 (2008) was replaced by the Eurocode. The light green horizontal lines limitation according to DIN 1052 (2008) are the result of the restriction to $\rho_{\mathrm{k}} = 500\,\mathrm{kg/m^3}$ for softwoods for the three load bearing classes for screws. The steep slope due to ρ_{k}^2 in the former design model is remarkable. The German technical approval Z-9.1-519 (2012) was the first which allowed the application of modern screws in hardwoods. The dark green curves are the closest to the black curve for equation (14). Figure 4.1 shows that the design models for soft- and hardwoods should consider the different influences of the density. The influence of the diameter is the same for soft- and hard-

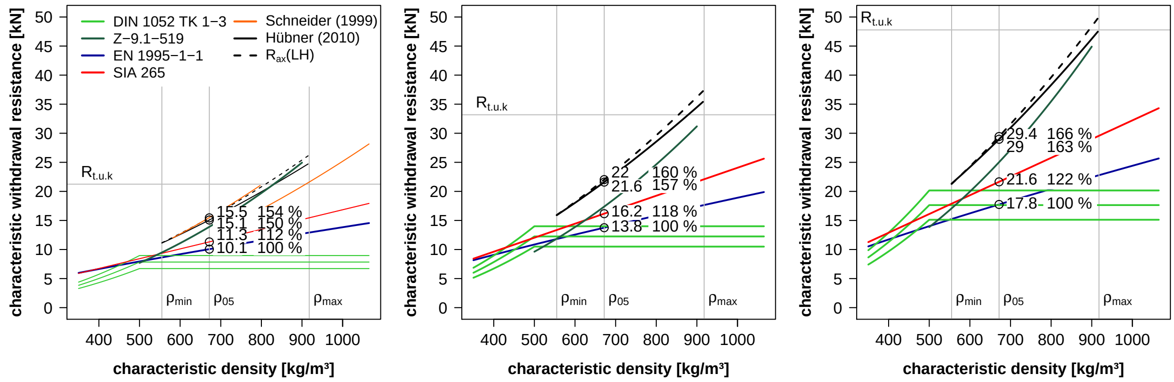

(a) diameter 8 mm (b) diameter 10 mm (c) diameter 12 mm

Figure 4.1: Withdrawal resistance for screw diameters ($l_{\mathrm{ef}} = 7\,d$, $\alpha = 90°$)

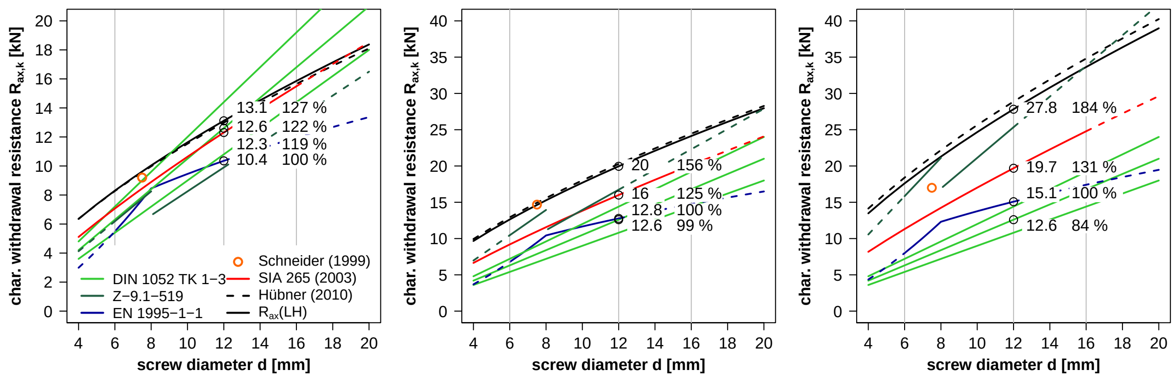

(a) characteristic density $500\,\mathrm{kg/m^3}$ (b) charact. density $650\,\mathrm{kg/m^3}$ (c) characteristic density $800\,\mathrm{kg/m^3}$

Figure 4.2: Withdrawal resistance for different characteristic densities ($l_{\mathrm{ef}} = 60\,\mathrm{mm}$, $\alpha = 90°$)

woods. The curves in Figure 4.2 are more parallel with the exception of the blue curve for ON EN 1995-1-1 (2009). The slope for diameters $d \geq 8\,\mathrm{mm}$ is too flat but for $d < 8\,\mathrm{mm}$ it is too steep.

5 Further research

The new design model allows reaching the tensile resistance of the screws with shorter effective lengths. The question is how to increase the transferable load. One answer could be screws with a greater ratio of core to outer diameter. Another answer are optimized minimum spacings's and edge/end distances. In technical approvals for screws the spacing perpendicular to the grain direction can be reduced to $a_2 = 2.5\,d$ if $a_1 \cdot a_2 = 25\,d^2$.

Plieschounig (2010) recommends $a_1 \geq 7\,d$ and $a_2 \geq 3{,}5\,d$ with $a_1 \cdot a_2 = 24.5\,d^2$ for screws perpendicular to the grain. Parallel to the grain direction a quadratic grid with $a = 5\,d$ and for $\alpha = 45°$ seam $a_1 \geq 6\,d$ and $a_2 \geq 4\,d$ with $a_1 \cdot a_2 = 24\,d^2$ logically. For the time being these are theoretical considerations and more research like published by Mahlknecht (2011) has to be carried out.

6 Acknowledgment

This research work Was part of the COMET-K-project *1.2.3_hardwood_ connections* of the competence centre holz.bau forschungs gmbh and was carried out in collaboration with the Institute for Timber Engineering and Wood Technology at the Graz University of Technology and industrial partners *HAAS Fertigbau GmbH & Co.KG* and *SPAX International GmbH & Co. KG.* The withdrawal tests were executed with the aid of Bernd Heissenberger, Markus Kummer, Manuel Lögl and Mathias Rasser. The research work was financed through the Austrian State Ministry of Economic Affairs and Employment, the Ministry of Transport, Innovation and Technology as well as by the *Steirischen Wirtschaftsförderungsgesellschaft mbH* and the federal state Steiermark.

References

[Bejtka 2005] Bejtka, Ireneusz: *Karlsruher Berichte zum Ingenieurholzbau.* vol. 2: *Verstärkungen von Bauteilen aus Holz mit Vollgewindeschrauben.* Karlsruhe : Universitätsverlag Karlsruhe, Januar 2005. – URL `http://digbib.ubka.uni-karlsruhe.de/volltexte/1000003354`. – date of access: 12. Juli 2010. – ISBN 3-937300-54-6

[Büeler 2011] Büeler, Michael: *Schubverhalten von Brettschichtholzträgern aus Buche und Esche.* Zürich, Institut für Baustatik und Konstruktion – Stahl-, Holz- und Verbundbau, ETH Zürich, Masterarbeit, 4. Juli 2011

[Bogusch 2011] Bogusch, Walter: Eschenholz im Tragwerkbau. In: *Newsletter Forum Holzbau* 51 (2011), März

[Cockrell 1933] Cockrell, Robert A.: A study of the screw-holding properties of wood / New York State College of Forestry. Syracuse, New York, 1933. – Technical Publication No. 44

[DIBt 2012] DIBt: Verzeichnis der allgemeinen bauaufsichtlichen Zulassungen – Zulassungsbereich: Holzbau und Holzwerkstoffe. Berlin : Deutsche Institut für Bautechnik (DIBt), 22. Februar 2012. – research report

[DIN 1052 2008] DIN 1052: *Entwurf, Berechnung und Bemessung von Holzbauwerken – Allgemeine Bemessungsregeln und Bemessungsregeln für den Hochbau.* Dezember 2008

[DIN 7998 1975] DIN 7998: *Gewinde und Schraubenenden für Holzschrauben.* Februar 1975

[Eckelman 1975] Eckelman, Carl A.: Screwholding performance in hardwoods and particleboard. In: *Forest Products Journal* 25 (1975), No. 6, p. 30–35

[Frese and Blaß 2009] Frese, Matthias ; Blass, Hans Joachim: Models for the calculation of the withdrawal capacity of self-tapping screws. In: *Proceedings of CIB-W18.* Dübendorf, Schweiz, August 2009. – Paper 42-7-3

[Griesser 2012] Griesser, Doris: Fichte und Birke als tragende Elemente. In: *Der Standard* (2012), 7. März, p. 17

[Hampel 1985] Hampel, Frank R.: The breakdown points of the mean combined with some rejection rules. In: *Technometrics* 27 (1985), No. 2, p. 95–107

[Hübner et al. 2010] Hübner, Ulrich ; Rasser, Mathias ; Schickhofer, Gerhard: Withdrawal resistance of screws in common ash (*Fraxinus Excelsior* L.). In: *Proceedings of 11^{th} World Conference on Timber Engineering (WCTE)* vol. 1. Riva del Garde, Italy, 21. Juni 2010. – Paper 481

[Jablonkay 1999] Jablonkay, Peter: *Schrauben auf Ausziehen*, ETH Zürich, Forstwissenschaften, Abteilung VI, diploma thesis, 1999

[Leijten et al. 2006] Leijten, Ad J. M. ; Köhler, Jochen ; Jorissen, André J. M.: Timber density restrictions for timber connection tests according to EN 28 970/ISO 8970. In: *Proceedings of CIB W18.* Florence, Italy, August 2006. – Paper 39-21-1

[Mahlknecht 2011] Mahlknecht, Ursula: *Untersuchung von rechtwinklig zur Faser eingebrachten, axial beanspruchten Schraubengruppen im Vollholz und Brettsperrholz*, Institut für Holzbau und Holztechnologie der TU Graz, diploma thesis, 2011

[MPA Stuttgart 2012] MPA Stuttgart: *EC-Certificate of Conformity 0672 for GLT made of sweet chestnut.* Sierolam S. A., Los Cuentos s/n Argüelles, 33188 Siero, Spain. 31. August 2012. – certificate number 0672-CPD-114.21.53

[Munch-Andersen 2013] Munch-Andersen, Jørgen: *Re: AW: Effective length l_ ef for screws.* E-Mail. 14. Juni 2013

[Newlin and Gahagan 1938] Newlin, J. A. ; Gahagan, J. M.: Lag-screw joints: Their behavior and design / United States Departement of Agriculture. Washington, D. C., Januar 1938. – Technical bulletin No. 597

[ON EN 13 183-1 2004] ON EN 13 183-1: *Feuchtegehalt eines Stückes Schnittholz – Teil 1: Bestimmung durch Darrverfahren.* 1. Februar 2004

[ON EN 1382 1999] ON EN 1382: *Holzbauwerke – Prüfverfahren – Ausziehtragfähigkeit von Holzverbindungsmitteln.* 1. November 1999

[ON EN 1382 2012] ON EN 1382: *Timber Structures – Test methods – Withdrawal capacity of timber fasteners.* Mai 2012

[ON EN 1995-1-1 2006] ON EN 1995-1-1: *Eurocode 5: Bemessung und Konstruktion von Holzbauten – Teil 1-1: Allgemeines – Allgemeine Regeln und Regeln für den Hochbau.* November 2006

[ON EN 1995-1-1 2009] ON EN 1995-1-1: *Eurocode 5: Bemessung und Konstruktion von Holzbauten – Teil 1-1: Allgemeines – Allgemeine Regeln und Regeln für den Hochbau.* 1. Juli 2009

[ON EN 384 2010] ON EN 384: *Structural timber – Determination of characteristic values of mechanical properties and density.* 15. Mai 2010

[Pirnbacher 2011] Pirnbacher, Gernot: Screws_Long_Time: Zeitabhängige Entwicklung der Traglast und Kriechverhalten von selbstbohrenden Holzschrauben / holz.bau forschungs gmbh. Graz, Oktober 2011. – Vorläufiger interner Forschungsbericht

[Pirnbacher and Schickhofer 2009] Pirnbacher, Gernot ; Schickhofer, Gerhard: Base parameters of self-tapping screws. In: *Proceedings of CIB-W18.* Dübendorf, Schweiz, August 2009. – Paper 42-7-1

[Pirnbacher and Schickhofer 2012] Pirnbacher, Gernot ; Schickhofer, Gerhard: Zeitabhängige Entwicklung der Traglast und des Kriechverhaltens von axial beanspruchten, selbstbohrenden Holzschrauben / holz.bau forschung gmbh. 2012. – research report

[Plieschounig 2010] Plieschounig, Stefan: *Ausziehverhalten axial beanspruchter Schraubengruppen.* Graz, Institut für Holzbau und Holztechnologie der TU Graz, diploma thesis, November 2010

[Pollmeier 2012] Pollmeier Massivholz GmbH & Co. KG: Furnierschichtholz aus Buche: Datenblatt/Statische Kennwerte. Creuzburg, 21. Dezember 2012. – research report

[Popper and Niemz 2009] Popper, Rudolf ; Niemz, Peter: Wasserdampfsorptionsverhalten ausgewählter heimischer und überseeischer Holzarten. In: *Bauphysik* 31 (2009), No. 2, p. 117–121

[Rajak and Eckelman 1993] Rajak, Zaini Ithnin Bin Haji Abdul ; Eckelman, Carl A.: Edge and face withdrawal strength of large screws in particleboard and medium density fiberboard. In: *Forest Products Journal* 43 (1993), No. 4, p. 25–30

[Ravasse 2011] Ravasse, François: *Minutes meeting Paris REV 2011 on April 19 and 20.* 27. Juli 2011. – N 1079

[Schneider 1999] Schneider, Patric: Auszugsfestigkeit von EJOT-Rahmenschrauben / Eidgenössische Technische Hochschule. Zürich, 29. Oktober 1999. – research report

[SIA 265 2003] SIA 265: *Holzbau.* 1. März 2003

[SIA 265 2012] SIA 265: *Holzbau.* 1. Januar 2012

[Uibel and Blaß 2013] Uibel, Thomas ; Blass, Hans J.: Joints with dowel type fasteners in CLT structures. In: Harris, R. (eds.): *Focus Solid Timber Solutions - European Conference on Cross Laminated Timber (CLT).* Graz : TU Graz, 21./22. Mai 2013, p. 119–134. – ISBN 1-85790-181-9

[Z-9.1-435 2009] Schmid Schrauben Hainfeld GmbH: Holzbauschrauben Star Drive, Rapid, Rapid Perfekt und Schmid SP als Holzverbindungsmittel. Berlin : Deutsches Institut für Bautechnik, 16. Dezember 2009. – Allgemeine bauaufsichtliche Zulassung Z-9.1-435

[Z-9.1-519 2011] SPAX International GmbH & Co. KG: Spax-S Schrauben mit Vollgewinde als Holz-Verbindungsmittel. Berlin : Deutsches Institut für Bautechnik, 11. März 2011. – Allgemeine bauaufsichtliche Zulassung Z-9.1-519

[Z-9.1-519 2012] SPAX International GmbH & Co. KG: Spax-S Schrauben mit Vollgewinde als Holz-Verbindungsmittel. Berlin : Deutsches Institut für Bautechnik, 31. Januar 2012. – Allgemeine bauaufsichtliche Zulassung Z-9.1-519

[Z-9.1-656 2007] Schmid Schrauben Hainfeld GmbH: Holzbauschrauben Star Drive Vollgewinde und Star Drive 2 Gewinde als Holzverbindungsmittel. Berlin : Deutsches Institut für Bautechnik, 25. Juni 2007. – Allgemeine bauaufsichtliche Zulassung Z-9.1-656

[Z-9.1-679 2011] Studiengemeinschaft Holzleimbau e. V.: BS-Holz aus Buche und BS-Holz Buche-Hybridträger. Berlin : Deutsches Institut für Bautechnik, 7. Juni 2011. – Allgemeine bauaufsichtliche Zulassung Z-9.1-679

Z-9.1-704 2012] ELABORADOS Y FABRICADOS GÁMIZ S. A.: VIGAM Brettschichtholz aus Eiche. Berlin : Deutsches Institut für Bautechnik, 04. Mai 2012. – Allgemeine bauaufsichtliche Zulassung Z-9.1-704

Z-9.1-777 2010] SFS INTEC GMBH: Gewindestangen mit Holzgewinde als Holzverbindungsmittel. Berlin : Deutsches Institut für Bautechnik, 30. November 2010. – Allgemeine bauaufsichtliche Zulassung Z-9.1-777

**INTERNATIONAL COUNCIL FOR RESEARCH AND INNOVATION
IN BUILDING AND CONSTRUCTION**

WORKING COMMISSION W18 - TIMBER STRUCTURES

WOOD SPLITTING CAPACITY IN TIMBER CONNECTIONS LOADED TRANSVERSELY: RIVETED JOINT STRENGTH FOR FULL AND PARTIAL WIDTH FAILURE MODES

P Zarnani

P Quenneville

The University of Auckland

NEW ZEALAND

Keywords: timber, connection, resistance, failure, splitting, perpendicular

Presented by P Quenneville

A Leijten commented that on slide 11 about the test set up the force was high and the span to beam depth was small. He questioned whether some of the applied force could go directly into the supports. P Quenneville clarified about the span and stated that one would need to verify that some of the forces did not go directly into the supports.

JW van de Kuilen received clarification that the LVL was not cross banded and splitting would not happen in cross banded LVL.

F Lam received clarification that the sample size for LVL and glulam was 3 and 5, respectively and COV information was in the paper.

Wood Splitting Capacity in Timber Connections Loaded Transversely: Riveted Joint Strength for Full and Partial Width Failure Modes

Pouyan Zarnani, Pierre Quenneville
University of Auckland, New Zealand

1 Objectives and scope

Connections are an extremely important part of a structure. Evaluation of timber buildings damaged after extreme wind and earthquake events have shown that weak connections are one of the major causes of problem [1]. Design techniques and procedures for dowel-type connections loaded perpendicular-to-grain are well understood for ductile behaviour. However, research into brittle splitting failures is still at the progressing stage [2,3]. The existing models for the prediction of the splitting failure of large dowel-type connections loaded perpendicular to grain are determined generally based on an assumption of the crack growth through the entire member cross-section (Fig. 1a). These models can be appropriate for stocky or rigid fasteners extending through the full thickness of the wood member. However, for slender dowel-type fasteners such as timber rivets or nails, particularly when the penetration depth of the fastener does not cover the whole member thickness, the crack formation is different (Fig. 1b). The observations from the current riveted joint tests in thick members show that the crack growth across the grain occurs corresponding to the effective embedment depth of the fastener, t_{ef}, and propagates along the grain until reaching the unstable condition.

Rivets are part of the U.S. and Canadian structural wood design standards. However, in the current standards, there is no closed form solution for the wood splitting strength prediction of this type of connection and the standards restrict the use of rivets to specific configurations and for glulam and sawn timber of some limited species. In addition, the important connection configuration variables (Fig. 2) such as loaded edge distance, a_{4t}, unloaded end distance, a_{3c}, and member thickness, b, are not respected in these standards. A simple closed form analytical method to determine the load-carrying capacity of wood under perpendicular-to-grain loading in rivet connection for various timber products is thus desirable. The proposed design method takes into account the different possible failure modes of wood splitting (Fig. 1) and covers the shortcomings of existing models (Table 1).

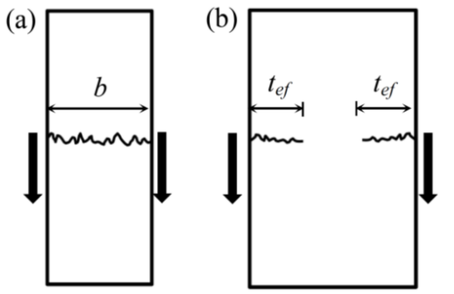

Fig. 1: Different failure modes of wood splitting: (a) crack growth in full member thickness; (b) crack growth corresponding to t_{ef} on each side

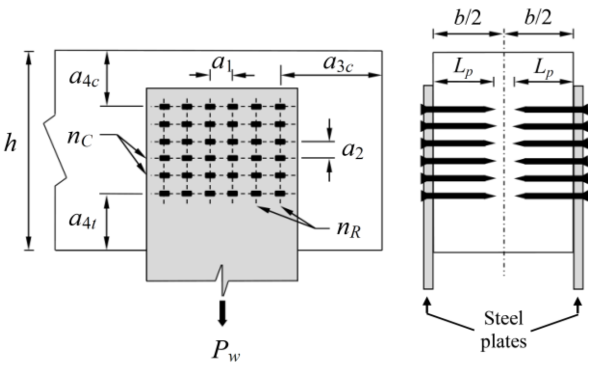

Fig. 2: Definition of connection geometry variables

Results of tests on New Zealand Radiata Pine LVL and glulam and test data available from literature confirm the validity of this new method and show that it can be used as a design provision for timber riveted connections loaded transversely.

2 Background research

The most significant work on timber rivets is that of Foschi and Longworth [4] which forms the basis for the timber rivet design procedures in the U.S. NDS [5] and the Canadian O86-09 [6] codes. The authors proposed a prediction model (Eq. 1) based on a finite element analysis for calculating the wood splitting strength, P_w, of a rivet connection loaded perpendicular-to-grain. Splitting failure was considered as the formation of cracks along the timber fibres just above the top row of rivets near the unloaded edge. In their predictive model, the brittle failure involves the tensile capacity of the splitting surface of the wood corresponding to penetration depth L_p and the cluster width of the rivets. The authors provided tables of values for numerically derived factors (K_t, β_t and β_D) which are related to the connection geometry.

$$P_w = \frac{f_{tp} L_p a_1 (n_R - 1)}{K_t \beta_t \beta_D} \tag{1}$$

In another study of rivet connections, Stahl et al. [7] presented a simplified analysis to determine the wood splitting strength. In their proposed equation (Eq. 2), failure was considered as the formation of a crack with a depth equal to the rivet penetration and extending laterally from the edge of the rivet group for a distance h_e equivalent to the distance between the top of the rivet group to the loaded edge, h-a_{4c}. This means that the strength of wood in a brittle failure improves as the connection is placed higher away from the loaded edge.

$$P_w = 0.4\, f_{tp}\, L_p[a_1(n_R\text{-}1)+2\min(h_e, a_{3c})] \tag{2}$$

In 2012, Jensen et al. [3] proposed an analytical model (Eq. 3) to predict the splitting potential of timber beams loaded perpendicular-to-grain using dowel-type connections. The authors assumed that the fastener is sufficiently stiff to ensure that the crack propagates along the grain simultaneously through the entire width of the beam. The model was based on fracture mechanics (FM) where the criterion for the initiation of crack propagation is defined as the loss of potential energy due to cracking being equal to the critical fracture energy, G_c [8]. The generalized model proposed by the authors can be applied to small end distances as well which is an advantage to the FM-based model developed by Van der Put and Leijten [9], which is currently used as the basis for calculation of the splitting capacity (Eq. 4) in the Eurocode 5 [10].

$$P_w = P_0 \,.\, \min \begin{cases} \dfrac{1}{2\sqrt{2\lambda+1}} + \dfrac{b f_{tp} a_{3c}}{P_0} \\ \dfrac{\sqrt{2\lambda+1}}{\lambda+1} \end{cases} \quad (3) \qquad \text{, and} \quad P_0 = 2bC_{fp}\sqrt{\frac{h_e}{1-\frac{h_e}{h}}} \quad (4)$$

in which, $C_{fp} = \sqrt{\frac{5}{3} G G_c}$ and $\lambda = \frac{C_{fp}}{f_{tp}} \sqrt{\frac{10G}{h_e E}}$.

Here, G and E are the modulus of rigidity and elasticity, respectively and C_{fp} is the fracture parameter.
Using numerical test series and advanced non-linear fracture mechanics methods, Franke and Quenneville [2] developed an empirical design approach (Eq. 5) for the splitting failure of dowel-type connections loaded perpendicular to grain. Their approach is based on a quadratic failure criterion in which the fracture Mode I and II for tension and shear is considered. One needs to note that the critical energy release rate for Mode II is difficult to determine experimentally because the fracture in this mode is inherently instable and it is hard to prevent unstable crack propagation occurring [11].

$$P_w = \frac{b.10^3}{\left(\frac{G_{Inorm}}{G_{Ic}} + \frac{G_{IInorm}}{G_{IIc}}\right)}.k_r \quad (5)$$

where G_{Ic} and G_{IIc} are the critical material fracture energies. G_{Inorm} and G_{IInorm} are the so-called normalized fracture energies depending on the member depth, h, the connection width, $a_1(n_R\text{-}1)$ and the effective depth, h_e. The k_r factor takes into account the effect of the number of columns.

Table 1: Connection geometry variables considered in the existing predictive models

Parameters\Prediction models	Foschi & Longworth	Stahl's method	Jensen's model	Franke & Quenneville	Proposed analysis
Loaded edge distance, a_{4t}	x	✓	✓	✓	✓
Unloaded edge distance, a_{4c}	✓	x	✓	✓	✓
Connection width, $a_1(n_R\text{-}1)$	✓	✓	x	✓	✓
Connection length, $a_2(n_C\text{-}1)$	✓	x	x	x	✓
Fastener penetration depth, L_p	✓	✓	x	x	✓
End distance, a_{3c}	x	✓	✓	x	✓
Member thickness, b	x	x	✓	✓	✓

3 Proposed approach for wood splitting strength

The proposed approach for the splitting strength of wood is based on two different possible crack formations on the member cross-section: with partial splitting on each side of the member corresponding to the effective embedment depth, t_{ef} (Fig. 1b) or with full width splitting (Fig. 1a). In fact, for connections with large penetration depth in slender members, the governing failure mode will be the full width splitting, and as the ratio of member thickness to penetration depth increases, the conversion of wood failure mode from full to partial width splitting will occur (Fig. 3). Therefore, the ultimate splitting resistance of the connection is determined as the minimum strength corresponding to these two failure modes and is given by (Eq. 6)

$$P_w = n_p \, . \, \min\,(P_{s,tef}, P_{s,b}) \quad (6)$$

where n_p is the number of plates which equals to one for one-sided joint and two for double-sided one.

3.1 Partial splitting corresponding to effective embedment depth

The stress-based analysis developed (Eq. 7) involves the perpendicular to grain tensile capacity of the splitting surface of the wood corresponding to the effective embedment depth, t_{ef} and the crack length that propagates along the member. The crack length along the member is considered as the summation of the joint net section width, $w_{net} = a_1\,(n_R\text{-}1)–6.4n_R$, and the symmetrical crack growth on the left and right sides of the joint as a factor of the effective depth, h_e (Fig. 4). It can be asserted that this model is a comprehensive version of Stahl's approach.

$$P_{s,tef} = C_t f_{tp} t_{ef}\,[w_{net}+\min(\beta h_e,a_{3c,L})+\min(\beta h_e,a_{3c,R})] \quad (7)$$

where,

$$C_t = \begin{cases} 1.264\,\zeta^{-0.37} & \text{, If } \zeta < 1.9 \\ 1 & \text{, If } \zeta \geq 1.9 \end{cases} \quad \text{, and } \zeta = \frac{a_{4c}}{a_2(n_C-1)}$$

Here, β is the effective crack length coefficient for partial width splitting calibrated based on the current tests and data from the literature [4,12] and equals to 2.4 for LVL and 1.6 for glulam. The ratio between the values of effective crack length coefficients for LVL and glulam is associated with the different stiffness properties in these two wood products. Based on the literature, an average ratio of modulus of rigidity to modulus of elasticity (G/E) can be considered equal to 0.045 and 0.069 for LVL and glulam respectively. The ratio between these two values for LVL and glulam is also comparable to the ratio between the values of effective crack length coefficients derived based on the test data for the LVL and glulam. $a_{3c,L}$ and $a_{3c,R}$ are the unloaded end distance on the left and right side of the joint, respectively. The C_t coefficient, which is function of the unloaded edge distance, a_{4c} and the connection length, $a_2(n_C\text{-}1)$, is the inverse of the β_D factor derived by [4].

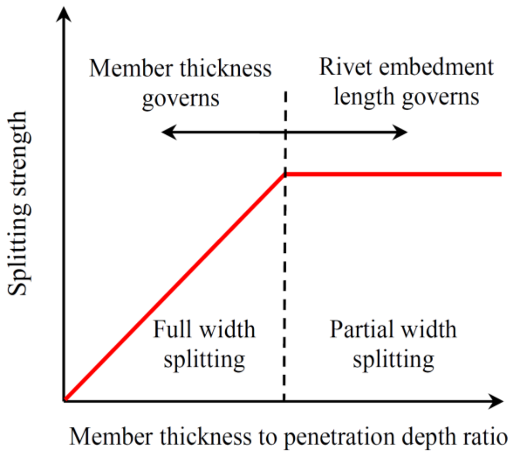

Fig. 3: Occurrence zone of possible failure modes of wood splitting

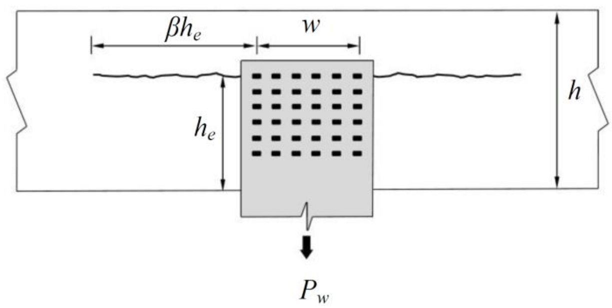

Fig. 4: Effective crack length on either side of the joint

3.2 Full width splitting

The predictive equation presented for wood splitting in the entire member cross-section (Eq. 8) is adopted from the FM-based model developed by Van der Put and Leijten [9]. The significant difference is the application of the η factor which accounts for the effect of unloaded end distance and the connection width. The Van der Put and Leijten model is derived based on a point load acting on the middle of a beam. Therefore, the η factor is needed and is effective while the joint is close to the beam end or if the load is transferred to the member through more than one row of fasteners and not as a point load. Franke and Quenneville [2] have shown that the joint width influences the wood splitting load. This is intuitive since the splitting capacity of a member loaded transversely by multiple rows of fasteners through the whole member length cannot be estimated by ignoring the effect of connection width. The effect of connection width is not included in Jensen's model [3] either.

$$P_{s,b} = \eta b C_{fp}\sqrt{\frac{h_e}{1-\frac{h_e}{h}}} \qquad (8) \qquad \text{, in which} \quad \eta = \frac{\min(\gamma h_e, a_{3c,L}) + \min(\gamma h_e, a_{3c,R}) + w_{net}}{2\gamma h_e}$$

in which γ is the effective crack length coefficient for full width splitting. The value of η equals to 1 when the unloaded end distance is greater than the effective crack length on either side of the joint, $a_{3c}>\gamma h_e$ and the load is applied using one row of fasteners, w_{net}=0. The results from the tests conducted by Jensen et al. [3] on Radiata Pine LVL show that the wood splitting resistance increases by moving the joint from the beam end towards the mid span which represents larger unloaded end distance. Observations have shown that this increase in wood splitting strength resulting from the mobilization of a larger area diminishes as the ratio of unloaded end distance to the effective depth (a_{3c}/h_e) approaches a value of about 4. Their observation is applied when considering the effective crack length, γh_e. Therefore, the effective crack length coefficient, γ, for full width splitting in LVL is set as 4. In the case of glulam members, this coefficient is estimated by using the ratio of β factor of glulam to LVL for partial width splitting. Thus, the γ coefficient for full width splitting in glulam is given as 2.7.

If there is enough end distance on either sides of the joint, then the location of the joint on the beam does not have any effect on the splitting strength. This is in agreement with the tests conducted by Jensen et al. [12] on beams loaded at mid-span and quarter-span which resulted in similar strengths. Their observations refute the predictions by Eurocode 5 which is based on the maximum shear force on either side of a joint and therefore leads to the splitting strength of a joint at beam mid-span being 50% higher than the one at quarter-span.

As it can be deduced from Eq. (8), the increasing rate of wood splitting resistance when there is more than one row of fasteners is estimated as $w_{net}/2\gamma h_e$. As shown in Table 2, except for the smallest widths, there is relatively a good agreement between the predicted strength increment due to increasing of the joint width and the observed test results by Kasim and Quenneville [13].

Table 2: Effect of connection width on wood splitting strength [13]

h_e (mm)	n_R	w_{net} (mm)	Test result (kN)	Increase of strength: Observed	Increase of strength: Predicted
204	2	399	100.4	+47%	+36%
204	2	301	83.2	+22%	+27%
204	2	206	83.8	+23%	+19%
204	2	58	66.6	-2%	+5%
204	1	0	68.2	-	-
134	2	301	63.2	+54%	+42%
134	2	206	58.7	+43%	+28%
134	2	136	41.5	+1%	+19%
134	2	58	32.6	-21%	+8%
134	1	0	41.1	-	-

3.3 Effective embedment depth

For brittle failure modes, the effective embedment depth, $t_{ef,e}$ (Eq. 9) is determined from the elastic deformation of the rivet modelled as a beam on a bilinear elastic foundation as reported in Zarnani and Quenneville [14]. The rivet is supported by springs with bilinear response that simulate the local nonlinear embedment behaviour of the timber surrounding it [15].

As there is a transition between a purely brittle wood splitting failure and a purely ductile wood-fastener failure, there is a possibility that the failure observed is a mix of the two. If the wood splitting strength corresponding to $t_{ef,e}$ is greater than the rivet yielding strength, P_r, then the effective embedment depth needs to be determined based on mixed failure mode [16]. In mixed failure modes, the effective embedment depth, $t_{ef,y}$ is derived from the governing failure mode of the rivets. Since rivets are always used in single shear and the rivet head can be considered to be rotationally fixed as it is wedged into the steel plate's hole, only three yield modes need to be considered [7]. $t_{ef,y}$ can be derived using Eq. (10) based on Johansen's yield theory [17] which is the foundation for the EYM prediction formulas in Eurocode 5 [10]. In Eq. (10), d_p is the rivet cross-section dimension bearing on the wood perpendicular-to-grain, (equal to 6.4 mm); $f_{h,90}$ is the embedment strength of the wood which can be determined as a function of d_p and the density of the wood [15]; and $M_{r,p}$ is the perpendicular-to-grain moment capacity of the rivet, equal to 15,000 Nmm [7].

$$t_{ef,e} = \begin{cases} 0.85L_p & \text{, for } L_p \text{ equals to 28.5 mm} \\ 0.75L_p & \text{, for } L_p \text{ equals to 53.5 mm} \\ 0.65L_p & \text{, for } L_p \text{ equals to 78.5 mm} \end{cases} \qquad (9)$$

$$t_{ef,y} = \begin{cases} L_p & \text{, Mode I}_m \\ \sqrt{\dfrac{M_{r,p}}{f_{h,90}d_p} + \dfrac{L_p^{\,2}}{2}} & \text{, Mode III}_m \\ 2\sqrt{\dfrac{M_{r,p}}{f_{h,90}d_p}} & \text{, Mode IV} \end{cases} \qquad (10)$$

4 Experimental program

4.1 Specimens

Laboratory tests were set up to prompt wood splitting failures and maximize the amount of observations on the brittle mechanism. To achieve this, connection configurations were set so that the total rivet yielding strength of each test group was higher that the predicted wood strength corresponding to $t_{ef,e}$ for that group. The rivet capacity on LVL specimens were estimated based on conducted yielding tests and for glulam by using the values reported by Buchanan and Lai [18]. Specimens were manufactured from New Zealand Radiata Pine LVL grade 11 and GL8 grade glulam with average density of 625 and 450 kg/m^3, respectively. The tests series were divided into 11 groups for LVL and 10 groups for glulam (Table 3). 3 replicates were tested for each group of specimens for LVL and 4 replicates for glulam. In Table 3, L and G stands for LVL and glulam respectively. The parameters for connection geometries such as connection width and length, fastener penetration depth, loaded and unloaded edge distances, end distance, and member thickness were evaluated. The specimens had riveted plates on both faces of the timber, resulting in a symmetric connection.

Radiata Pine LVL and glulam fracture parameters, C_{fp}, reported in Jensen et al. [3,11] based on the plate specimen test method developed by Yasumura [19] and tensile strength perpendicular to grain values, f_{tp}, evaluated by Song [20] based on the ASTM D143-09 test method were used as inputs to the proposed model. The average C_{fp} and f_{tp} were 22.7 N/mm$^{1.5}$ and 2.06 MPa (at tangential direction with a COV=18%) for RP LVL and 18.4 N/mm$^{1.5}$ and 1.99 MPa (at 45° to radial direction with a COV=24%) for RP glulam respectively.

Table 3: Configuration of the tested connections on LVL and glulam

Test groups	No. of rows by columns n_R*n_C	Spacing of rows by columns a_1/a_2 (mm)	Rivet penetration L_p (mm)	Member thickness b (mm)	Effective embedment depth $t_{ef,e}$ (mm)	Distance of loaded edge by unloaded one a_{4t}/a_{4c} (mm)	Unloaded end distance on joint left side by right one $a_{3c,L}/a_{3c,R}$ (mm)
G1-L	6*6	25/15	53.5	180	40.1	72.5/72.5	538/538
G2-L	6*6	25/15	53.5	180	40.1	72.5/152.5	538/538
G3-L	6*6	25/15	53.5	126	40.1	72.5/72.5	538/538
G4-L	6*6	25/15	53.5	225	40.1	72.5/72.5	538/538
G5-L	6*6	25/15	53.5	180	40.1	202.5/72.5	538/538
G6-L	6*6	25/15	28.5	180	24.2	72.5/72.5	538/538
G7-L	6*6	25/15	28.5	180	24.2	122.5/72.5	538/538
G8-L	3*8	25/15	53.5	180	40.1	42.5/72.5	575/575
G9-L	6*6	25/15	78.5	180	51.0	72.5/72.5	538/538
G10-L*	2*8	25/15	53.5	180	40.1	42.5/72.5	538/38
G11-L†	6*6	25/15	53.5	180	40.1	72.5/72.5	345/75
G1-G	6*6	25/15	53.5	180	40.1	75/75	538/538
G2-G	6*6	25/15	53.5	180	40.1	75/165	538/538
G3-G	6*6	25/15	53.5	126	40.1	75/75	538/538
G4-G	6*6	25/15	53.5	225	40.1	75/75	538/538
G5-G	6*6	25/15	53.5	180	40.1	210/75	538/538
G6-G	6*6	25/15	28.5	180	24.2	75/75	538/538
G7-G	6*3	25/15	28.5	180	24.2	120/75	538/538
G8-G	3*6	25/15	53.5	180	40.1	75/75	575/575
G9-G	6*6	25/15	78.5	180	51.0	75/75	538/538
G10-G*	2*6	25/15	53.5	180	40.1	75/75	538/38

* Two identical joints acting perpendicular to grain with a clear distance of 76 mm.
† Joint located at the end of a cantilever beam.

4.2 Test setup

The testing procedure outlined in ISO 6891 was followed. The load was applied to the specimens using a displacement controlled MTS loading system. The deformation of the connection was measured continously with a pair of symmetrically placed LVDTs. The specimens were simply supported at each ends and were loaded in tension perpendicular-to-grain at mid-span except for one test group which was set up as a cantilever beam. Typical specimens in the testing frame are shown in Fig. 5. The loading rate was adjusted to 1 mm/min and kept constant until the occurence of failure in both or either side of the riveted connections.

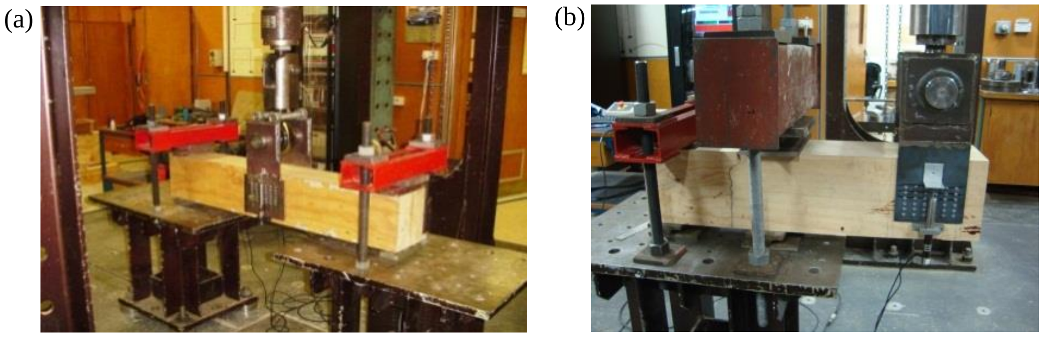

Fig. 5: Typical specimens in testing apparatus: (a) simply supported beam; (b) cantilever beam

5 Results and discussion

5.1 Test observation

The load-slip curve of each group was plotted (Fig. 6). The modes of splitting failure (Fig. 1) and the highest load reached at displacement up to 4.8 mm were recorded. This common measure of ultimate load on a rivet group [7,18,21] is based on a maximum deflection equal to the average of the rivet's cross section dimensions; 6.4 by 3.2 mm.

Brittle splitting of wood was observed in all specimens. Failure occurred along the row of rivets next to the unloaded edge and propagated towards the timber member ends till reaching the unstable zone (Fig. 7).

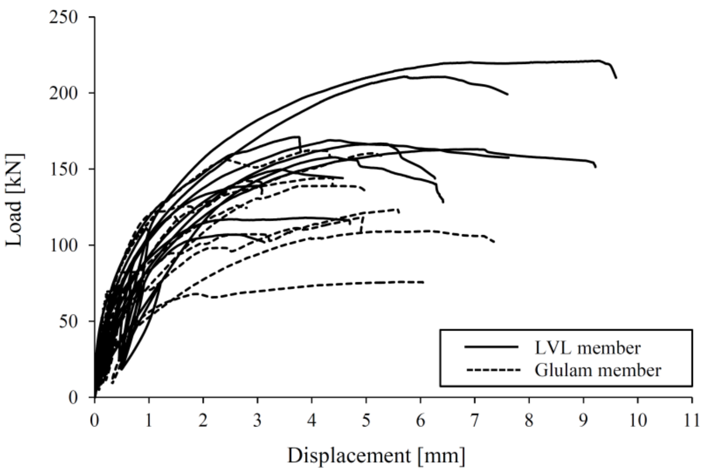

Fig. 6: Typical load-slip plots for joint tensile tests loaded perpendicular to grain

Fig. 7: Specimen exhibiting the brittle mode of wood splitting failure

Test results show two types of failure mode for wood splitting (Fig. 8). The crack formed either through the entire member width (for thinner members) or with a depth similar to the rivet effective embedment depth (for thicker members).

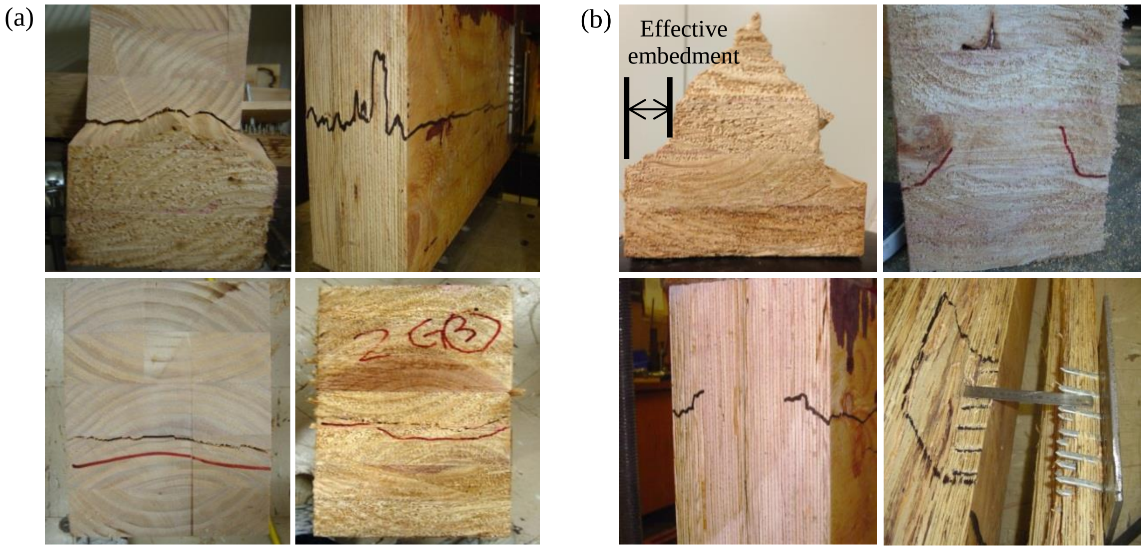

Fig. 8: Wood splitting failure modes in LVL and glulam:
(a) full width splitting; (b) partial width splitting

5.2 Validation of proposed analysis and comparison with other models

Strength predictions of the current tests and of tests reported on splitting resistance of riveted joints in the literature were made using the proposed method to compare it with other predictive models. Predictions made using the Foschi and Longworth [4], Stahl et al. [7], Franke and Quenneville [2], and the prediction model proposed by Jensen et al. [3] were used in the comparison. One should note that both the U.S. NDS standard and the Canadian O86-09 are based on the Foschi and Longworth model.

5.2.1 Effect of connection configuration parameters

Results for the LVL and glulam groups with different connection geometries are listed in Table 4. Along with the results, connection splitting capacities have been calculated using the proposed analysis and four previously outlined models. For the predictions by the Franke and Quenneville model, the value of fracture energy Mode I (G_{Ic} = 0.23 N/mm) given in Franke and Quenneville [2] was used for glulam and three times the G_{Ic} value was considered to estimate the fracture energy Mode II (G_{IIc} = 0.69 N/mm), as recommended in Jensen et al. [11]. 1.47 times the fracture energies of glulam were used for LVL. The factor of 1.47 was determined by comparing the values of the mixed mode fracture energies (G_c) for Radiata Pine LVL and glulam reported in Jensen et al. [3,11]. In the proposed analysis, the estimated wood splitting capacity for the G10-L test group was reduced by 30% to take into account the effect of interaction between joints. This strength reduction is derived by comparing the test results on wood splitting failure of single and double bolted joints conducted by Schoenmakers [22].

The tests series G1-L, G3-L and G4-L in LVL and G1-G, G3-G and G4-G in glulam were targeted to identify the effect of member thickness. The results in Table 4 indicate that the wood strength increases as the member thickness gets larger and then remains approximately constant after a certain thickness. As shown in Fig. (12a) and (12b), neither Foschi and Longworth model nor Stahl's method consider the member thickness effect. The Jensen and Franke and Quenneville models assume the splitting across the entire thickness and therefore show a continuous increasing of wood strength. In the proposed analysis, the member thickness is taken into account up to a certain limit with full width splitting and beyond that rivet embedment depth governs with partial splitting (as seen in Fig. 3). Therefore, it is the only approach that follows the exact trend and considers two possible modes of splitting failure as observed.

Table 4: Splitting strength predictions using the proposed analysis and the other models compared to experimental results on LVL and glulam

Test groups	Test results		Predicted splitting strength (kN)						
	Mean strength (COV%)* (kN)	Failure mode†	Jensen's model	Stahl's method	Franke & Quenneville	Foschi & Longworth	Proposed analysis		
							Full width splitting ($P_{s,b}$)	Partial width splitting ($P_{s,tef}$)	Ultimate strength n_p.min ($P_{s,b}$, $P_{s,tef}$)
G1-L	173 (8%)	*P*	160	85	244	83	85	84	168
G2-L	158 (6%)	*F*	129	85	172	55	69	66	132
G3-L	144 (4%)	*F*	112	85	171	83	60	84	120
G4-L	167 (4%)	*P*	200	85	305	83	106	84	168
G5-L	205 (5%)	*F*	285	143	281	83	78	123	156
G6-L	115 (7%)	*P*	160	45	244	50	85	51	102
G7-L	134 (4%)	*P*	208	57	266	50	81	66	132
G8-L	147 (7%)	*F*	160	74	202	109	87	88	174
G9-L	198 (2%)	*F*	160	125	244	113	85	107	170
G10-L	160 (7%)	*F*	144	30	249	208	60	67	120
G11-L	117 (8%)	*F*	86	41	244	83	37	54	74
G1-G	141 (12%)	*P*	130	53	164	79	78	57	114
G2-G	115 (15%)	*F*	104	53	112	50	62	45	90
G3-G	116 (8%)	*F*	91	53	114	79	55	57	110
G4-G	133 (6%)	*P*	163	53	205	79	98	57	114
G5-G	161 (6%)	*P*	234	87	189	79	93	101	186
G6-G	107 (12%)	*P*	130	28	164	48	78	35	70
G7-G	85 (9%)	*P*	130	28	153	25	78	27	54
G8-G	108 (7%)	*P*	130	44	134	71	73	52	104
G9-G	166 (6%)	*F*	130	78	164	107	78	73	146
G10-G	139 (9%)	*P*	121	25	165	133	55	41	82

* Coefficient of variation (COV%) calculated over 3 specimens for LVL and over 4 specimens for glulam.
† F and P stand for full width and partial width splitting correspondingly.

In the case of increasing the rivet embedment depth (Fig. 9c and 9d), the results for the test series G1-L, G6-L and G9-L in LVL and G1-G, G6-G and G9-G in glulam show the increase in wood splitting strength. The Jensen and Franke and Quenneville models, since they do not consider the effect of the embedment depth, provide constant predictions for wood strength. As shown in Fig. (12c), after a certain limit of penetration depth, the increasing rate of wood strength decreases. This can be explained by the fact that if the member thickness is constant, the increment of the penetration depth leads to a change of the wood failure mode from partial width splitting to full width splitting. Therefore, when the full width splitting governs, the penetration depth effect diminishes. This deterioration of penetration effect and transformation of wood failure modes is not included in Foschi and Longworth model and Stahl's method either.

Test results demonstrate that the wood splitting strength increases (Fig. 9e) as the connection gets wider (G1-G and G8-G). Jensen's model is the only one that does not take the connection width into consideration, since the model is derived based on a point load acting on a beam. As shown in Fig. 9f, the observed trend indicates that the wood strength increases as the connection length increases (G6-G and G7-G). Jensen's model and Stahl's method do not consider the connection length effect and therefore the predicted strength for these approaches remain constant. Though Franke and Quenneville model does not consider the effect of spacing between the columns, however, it takes into account the effect of increasing the number of columns, n_C, which leads to less localized stresses on the wood and thus higher splitting strength.

In terms of other connection parameters, as shown in Table 4, decreasing the unloaded edge distance (e.g., G1-L and G2-L), increasing the loaded edge distance (e.g., G6-L and G7-L), and increasing the end distance (G1-L and G11-L), all resulted in raising the connection wood capacity as was predicted in the proposed analysis. Whereas, the predictions using Franke and Quenneville approach and also Foschi and Longworth model are constant for the variation of the end distance.

Furthermore, in Foschi and Longworth model and Stahl's method the effect of loaded edge distance (Fig. 9g) and the unloaded edge distance (Fig. 9h) is not respected correspondingly, hence, no change on the predictions can be observed.

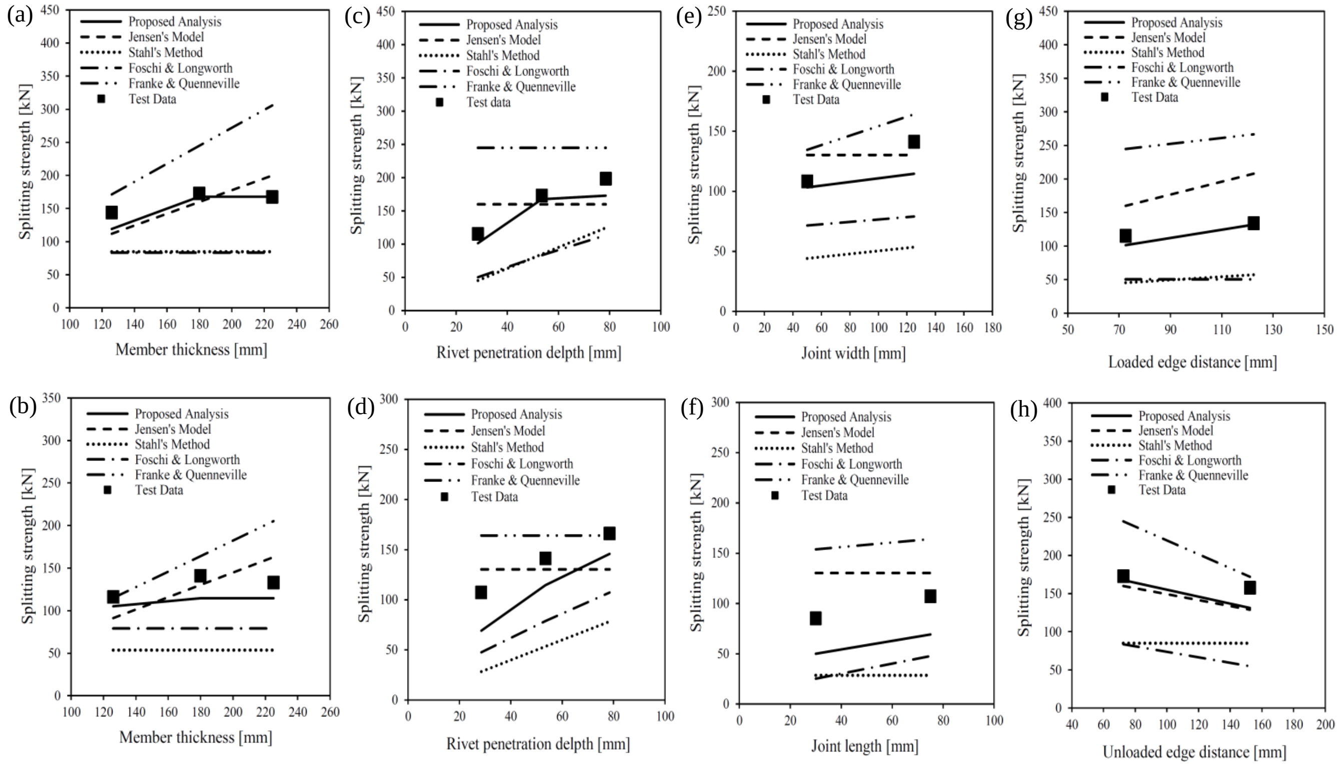

Fig. 9: Connection geometry effect on splitting strength: (a) member thickness-LVL sample; (b) member thickness-glulam sample; (c) rivet penetration depth-LVL sample; (d) rivet penetration depth-glulam sample; (e) joint width; (f) joint length; (g) loaded edge distance; (h) unloaded edge distance

As shown in Table 4, there is good agreement between the predictions and observations for the governing splitting failure mode and the strength of the connection. Fig. 10a and 10b show the strength predictions of the experimental groups using the proposed analysis and the predictions from other predictive models. The proposed analysis results in better predictions with a correlation coefficient (r^2) of 0.68 and a mean absolute error (MAE) of 17.4% and a standard deviation (STDEV) of 16.1% (Fig. 10a). The connections strength predicted by Jensen's model are overestimated for about half of the test groups (Fig. 10b), in particular, for the shortest rivet penetrations in which this overprediction can reach up to 55%. This is due to Jensen's model assumption of crack forming through the entire timber width, which did not occur for all the test configurations, especially in the thicker members. Thus, the necessity for predicting the connection strength under the partial width splitting mode of failure is required. Using the Franke and Quenneville model leads to overestimated values particularly for LVL beams (up to 100%) though the values used for the critical fracture energies are considerably lower than what were found in Jensen et al. [3,11]. A portion of such overestimation is related to the assumption of the crack propagation across the entire member. The predictions by Foschi and Longworth model and Stahl's method also show underestimated values (Fig. 10b). The underestimation of Stahl's method becomes considerable in the case of small end distances. This is due to the assumption of symmetric crack propagation in Stahl's method.

5.2.2 Existing test data from literature

A similar comparison was made using results available in the literature and current ones (Fig. 10c to 13f). Two sets of results were considered from the literature on the wood splitting of rivet connections: tests performed by Foschi [23] on Douglas Fir-Larch glulam, and Begel et al. [12] on Southern Pine glulam. In the prediction calculations, material properties reported in Jensen et al.

[3,11] and Song [20] and values available in the literature were used. By comparing the various model predictions, it can be deduced that there is more conformity between the predictions using the proposed analysis and the available test data. The predictions from the proposed method (Fig. 10c) results in a higher correlation coefficient (0.75) and a lower STDEV (17.1%) and MAE (16.9%).

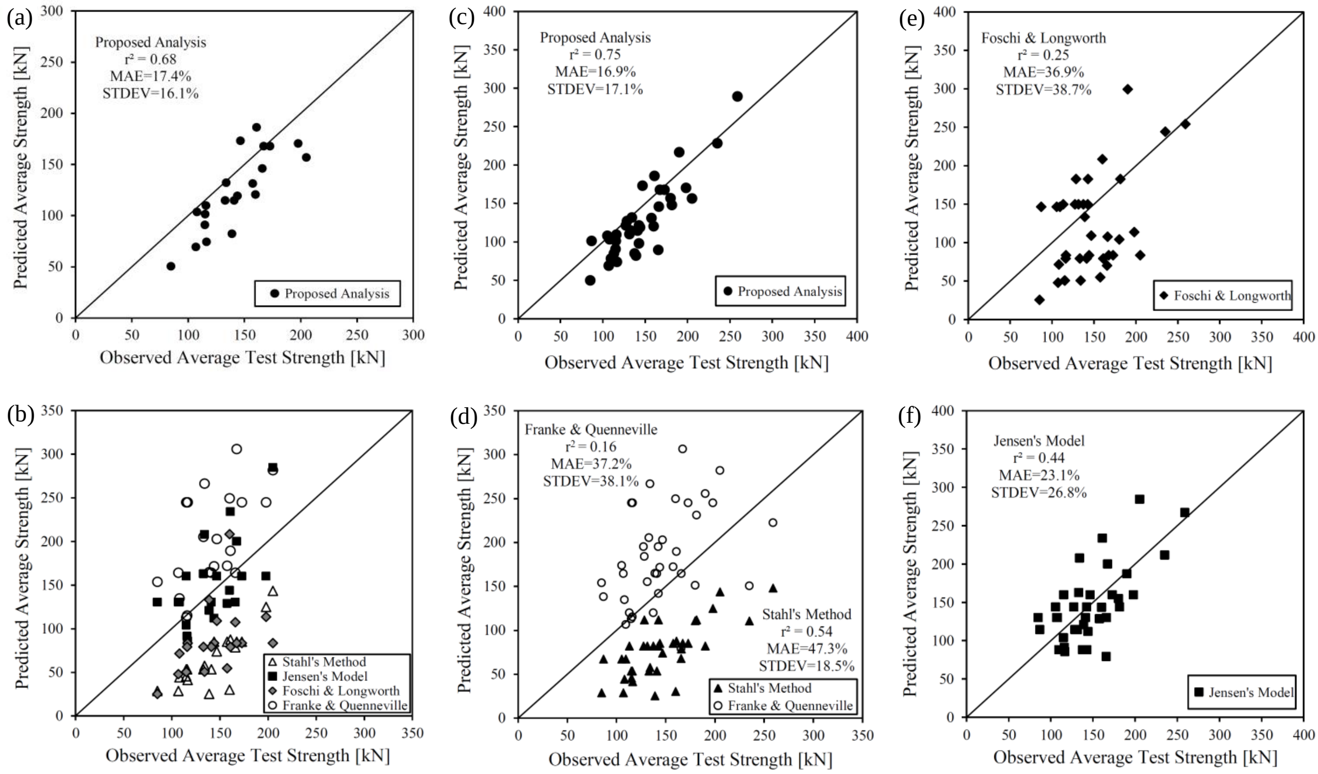

Fig. 10: Comparison of analyses and test data: (a) proposed analysis-current tests; (b) other models-current tests; (c) proposed analysis-all data; (d) Stahl's method and Franke & Quenneville-all data; (e) Foschi & Longworth-all data; (f) Jensen's model-all data

The predictions using Stahl's method and Jensen's model are better than the ones using the other models. The predictions by the Franke and Quenneville model (Fig. 10d) shows lower correlation compared to the test results. One reason can be related to the geometry-dependant equations developed for the normalized fracture energies which cannot be generalized for all the timber species and products. As shown in Fig. (13e), it can be noted that for a group of test data, the predictions by Foschi and Longworth are overestimated. This is due to the small end distances for those connection tests and the absence of this parameter in their model. There is strength over prediction for connections with partial width splitting using the Franke and Quenneville and Jensen's models (Fig. 10d and 10f). This supports the theory developed in this study which states that in thicker members, the load carrying capacity of the connection does not increase correspondingly to an increase in wood member thickness since partial width splitting is then observed. As Stahl's method takes into account the effect of penetration depth, thus, the predictions by his model leads to slightly better correlation compared to the ones using the Jensen and Franke and Quenneville models, however they are too conservative (Fig. 10d).

6 Conclusions

An analytical model developed to determine the wood splitting resistance of riveted connections under perpendicular to grain loading in timber products is proposed. The design method takes into account the different possible failure modes of wood; with partial or full width splitting. The proposed model is found to be the most comprehensive model according to the test observations on the effect of different connection configuration parameters. Results of current tests and from tests available in the literature confirm that this closed form analytical method results in more precise predictions for timber riveted connections. The proposed method could be extended to other small dowel type fasteners; e.g. nails and screws where the occurrence of partial width splitting of wood is more susceptible.

Acknowledgements

The authors wish to thank the New Zealand Structural Timber Innovation Company (STIC) for funding this research work. Likewise the authors would like to express their gratitude to The University of Auckland undergraduate students Samuel Wong and Shuai Ma, who did the experimental work related to glulam as part of their final year project.

References

[1] Smith, I., and Foliente, G. (2002). “Load and resistance factor design of timber joints: International practice and future direction.” *J. Struct. Eng. ASCE,* 128(1), 48-59.

[2] Franke, B., and Quenneville, P. (2012). “Prediction of the load capacity of dowel-type connections loaded perpendicular to grain for solid wood and wood products.” *Proc., 12th WCTE,* Auckland, New Zealand.

[3] Jensen, J. L., Quenneville, P., Girhammar, U. A., and Källsner, B. (2012). “Splitting of timber beams loaded perpendicular to grain by connections - Combined effect of edge and end distance.” *Construction and Building Materials,* 35, 289-293.

[4] Foschi, R. O., and Longworth, J. (1975). “Analysis and design of griplam nailed connections.” *J. Struct. Div. ASCE,* 101(12), 2537-2555.

[5] National design specification (NDS). (2012). “National design specification for wood construction.” *Standard ANSI/AWC NDS-2012,* American Wood Council, Washington, DC.

[6] Canadian Standards Association (CSA). (2009). “Engineering design in wood (limit states design).” *CAN/CSA-O86.09,* Mississauga, Ontario.

[7] Stahl, D. C., Wolfe, R. W., and Begel, M. (2004). “Improved analysis of timber rivet connections.” *J. Struct. Eng. ASCE,* 130(8), 1272-1279.

[8] Schniewind, A. P., and Pozniak, R. A. (1971). “On the fracture toughness of Douglas fir wood.” *Engineering Fracture Mechanics,* 2(3), 223-233.

[9] Van der Put, T. A. C. M., and Leijten, A. J. M. (2000). “Evaluation of perpendicular to grain failure of beams caused by concentrated loads of joints.” *Proc., CIB-W18,* The Netherlands, paper 33-7-7.

[10] European Committee for Standardization (CEN). (2004). “Eurocode 5-Design of timber structures.” *EN 1995-1-1:2004,* Brussels, Belgium.

[11] Jensen, J. L., Girhammar, U. A., Quenneville, P., and Källsner, B. (2012). “Splitting of beams loaded perpendicular to grain by connections - Simple fracture mechanics models.” *Proc., 12th WCTE,* Auckland, NZ.

[12] Begel, M., Wolfe, R. W., and Stahl, D. C. (2004). “Timber rivet connections in US domestic species.” *Research Paper FPL-RP-619,* U.S. Department of Agriculture, Forest Products Laboratory, Madison, Wis.

[13] Kasim, M., and Quenneville, P. (2002). “Effect of row spacing on the capacity of perpendicular to grain loaded timber joints with multiple timber connections.” *Proc., International council for research and innovation in building and construction, CIB-W18,* Kyoto, paper 35-7-6.

[14] Zarnani, P., and Quenneville, P. (2012b). “Wood effective thickness in brittle and mixed failure modes of timber rivet connections.” *Proc., 12th WCTE,* Auckland, New Zealand.

[15] Zarnani, P., and Quenneville, P. (2012a). “Reliable yield model for strength prediction of timber rivet connection under ductile failure.” *Proc., 12th WCTE,* Auckland, New Zealand.

[16] Zarnani, P., and Quenneville, P. (2013). “Wood block tear-out resistance and failure modes of timber rivet connections - A stiffness-based approach.” *Journal of Structural Engineering, ASCE* (in press).

[17] Johansen, K. W. (1949). “Theory of timber connections.” *Publications of International Association for Bridge and Structural Engineering,* 9, 249-262.

[18] Buchanan, A. H., and Lai, J. C. (1994). “Glulam rivets in Radiata Pine.” *Can. J. Civ. Eng.,* 21(2), 340-350.

[19] Yasumura, M. (2002). “Determination of fracture parameter for dowel-type joints loaded perpendicular to wooden grain and its application.” *Proc., CIB-W18,* Japan, paper 35-7-9.

[20] Song, Y. K. (2010). “Investigation of tension strength perpendicular to grain of New Zealand Radiata Pine.” *Final Year Research Project Report, Depart. of Civil and Environmental Eng., University of Auckland,* Auckland, NZ.

[21] Karacabeyli, E., Fraser, H., and Deacon, W. (1998). “Lateral and withdrawal load resistance of glulam rivet connections made with sawn timber.” *Can. J. Civ. Eng.,* 25(1), 128-138.

[22] Schoenmakers, J. C. M. (2010). “Fracture and failure mechanisms in timber loaded perpendicular to the grain by mechanical connections.” *Doctoral dissertation, Structural Design and Construction Technology, Eindhoven University of Technology,* Eindhoven, The Netherlands.

[23] Foschi, R. O. (1973). “Stress analysis and design of glulam rivet connections for perpendicular-to-grain loading of wood.” *Information Report VP-X-117,* Department of the Environment, Canadian Forestry Service, Vancouver, British Columbia.

**INTERNATIONAL COUNCIL FOR RESEARCH AND INNOVATION
IN BUILDING AND CONSTRUCTION**

WORKING COMMISSION W18 - TIMBER STRUCTURES

DESIGN APPROACH FOR THE SPLITTING FAILURE OF DOWEL-TYPE CONNECTIONS LOADED PERPENDICULAR TO GRAIN

Bettina Franke
The University of Auckland, New Zealand
Bern University of Applied Sciences
SWITZERLAND

P Quenneville
The University of Auckland
NEW ZEALAND

Keywords: timber, connection, resistance, splitting, perpendicular, numerical, model

Presented by P Quenneville

C Sigrist asked for clarification of how the loads in the dowels were monitored. P Quenneville stated the Plexiglas plate was strain gauged and calibrated, and even though the method was not precise, it gave a good indication. C Sigrist further asked whether optical method could be used. P Quenneville stated yes although the method was considered outdated.

S Aicher commented that the numerical solution depended on fracture energy normalized to available tested material. He asked to what extent these numerical models could be extended to other material. P Quenneville agreed with the comments and was not sure if the models could be extended to other material.

A Leijten commented that in slide 15 two cracks existed. With reference to the test results at Delft he questioned whether it was possible that gaps between the bolt and the bolt hole existed might have an influence on the results. He further questioned the validity of the unit of Ge' being N/mm^2. P Quenneville did not believe the units were wrong but will check and could provide example calculations. S Aicher confirmed the correctness of the units in the paper. A Leijten further commented that the spacing of dowels was increased for scientific interest but in practice one would want to have minimal spacing. P Quenneville responded that the spacing was kept the same in the study and the information was used for model.

A Frangi discussed existing rules for loaded edge distance and in European technical approval database splitting was observed even though the rules were followed. P Quenneville stated that if you have very big bolts one should check carefully as mixed mode of failure could happen.

A Frangi asked if one could have a ductile failure, would the Johansen approach be still correct for this type of connection given the stress variation between bolts. P Quenneville stated that the Johansen approach would be valid as there is redistribution of loads once plasticity was reached in one of the bolts.

C Sigrist discussed the choice of slenderness of dowel which was chosen to check splitting failure mode. He commented that it would not be possible to check the issue of ductile behaviour raised by A Frangi.

Design approach for the splitting failure of dowel-type connections loaded perpendicular to grain

Bettina Franke[1,2], Pierre Quenneville[1]

[1]The University of Auckland, New Zealand

[2]Bern University of Applied Sciences, Switzerland

1 Introduction

For the prediction of the splitting failure of dowel-type connections loaded perpendicular to grain (as shown in Figure 1), different design equations are available in publication or various international standards. Depending on the size, layout as well as the loading situation, the connection behaves in brittle or ductile failure. The ductile failure depends on the embedment strength of the wood and the bending capacity of the dowel. For the prediction of the ductile failure, the established European Yield Model (EYM) is used in international standards. The brittle failure of connections occurs due to the exceeding of tension or shear stress in the wood member. Based on the anisotropy of wood, the tension stress perpendicular to grain leads to very brittle failure behaviour and it is the most critical case for the failure of connections.

For the splitting failure of double shear connections loaded perpendicular, the design standards can be mainly distinguished between a strength criterion which was introduced by Ehlbeck, Görlacher & Werner (1989) and a fracture mechanic model introduced by v. d. Put & Leijten (1990). Current research results and publications show that there are disagreements between the experimental results and the design values, which result in uncertain predictions or in conservative values, Ballerini (2004), Jensen (2005), Schoenmakers (2010), and Franke & Quenneville (2010).

The splitting failure behaviour of double shear dowel-type connections loaded perpendicular to grain were investigated in experimental test series and using a numerical model. The failure behaviour was analyzed by fracture mechanic methods. The fracture mechanic is a recent design method compared to the established strength criteria which provides the assessment of the stress singularities like in connection, notches or holes.

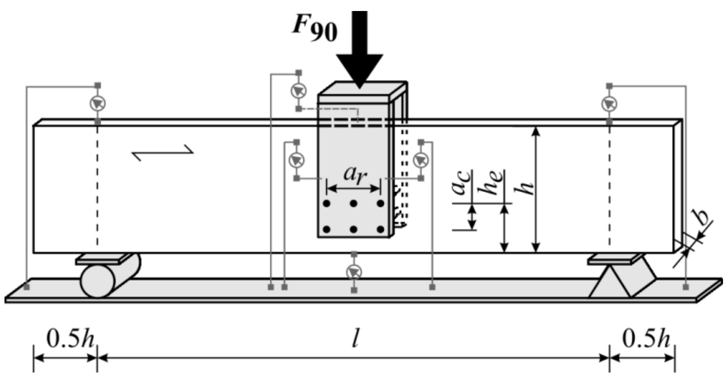

Figure 1: Test setup and connection layout defined

2 Material and Method

2.1 Test program

Experimental and numerical test series are used for the analyses of the failure behaviour. The experimental test series with multiple dowel-type connections and different loaded edged distances were conducted in Laminated Veneer Lumber of Radiata Pine (LVL). The test specimens were in large scale format to provide comparable results to practical construction details. Parallel to the load displacement curves in the test series, the distribution of the load over the number of dowels at the connection and the crack initiation as well as crack propagation were measured, as described in Franke et al. (2012) and shown in Figure 1 and Figure 2.

In addition, various numerical test series with single or multiple dowel-type connections with different loaded edge distances, positions, different number of dowels per row or column as well as different spacing within the connection are simulated. The numerical model used is defined as a 2-dimensional model based on the purpose to especially investigate the splitting of the wood and is presented in Franke & Quenneville (2011b). The numerical model simulates the splitting failure of wood under tension perpendicular to grain and shear as well as the ductile failure of wood due to compression. However, since the focus is to investigate the brittle failure mechanism, the bending of the dowel is not included in the numerical model and the influence is neglected. This is acceptable if the dowel slenderness ratio is small and ductile behaviour due to dowel bending is minimized. The capabilities of the numerical model were verified on comprehensive experimental test series done in Canadian spruce glulam and also with the experimental test series done in LVL. The correlation reached is shown in Figure 3.

The complete experimental and numerical test programme is summarized in Table 1. In each test series, the dowel diameter *d* was 20 mm.

Table 1: Experimental and numerical test program

				Connection Layout		
Material	**Test setup**	**Sizes *b* / *h* / *l* [mm]**	**Dowel *m* x *n***	**Loaded edge distance h_e/h**	**Connection width a_r**	**Connection height a_c**
LVL	exp.	63/400/1600	3x1	0.2/ 0.4/ 0.6	8*d*	-
LVL	exp.	63/600/2400	3x1	0.13/ 0.4/ 0.6	8*d*	-
LVL	exp.	63/400/1600	3x2	0.4/ 0.6	8*d*	4*d*
LVL	exp.	63/400/2400	3x2	0.4/ 0.6	8*d*	4*d*
LVL	exp.	63/400/2400	3x2	0.4/ 0.6	8*d*	4*d*
LVL	exp.	63/400/2400	3x2	0.4	8*d*	4*d*
LVL	exp.	63/600/2400	5x2	0.4	16*d*	4*d*
LVL	num.	63/(200, 400, 600)/4*h*	2x2	0.2/ 0.4/ 0.6/ 0.8	3*d*/ 6*d*/ 10*d*/15*d*/20*d*/25*d*	-
GL	num.	80/(190, 300, 400, 600, 800)/610	1x1	0.2/ 0.3/ 0.4/ 0.5/ 0.6/ 0.7/ 0.8	-	-
GL	num.	80/190/4*h*+*ar*	2x1	0.2/ 0.3/ 0.4/ 0.5/ 0.6/ 0.7/ 0.8	3*d*/ 4*d*/ 6*d*/ 8*d*/ 10*d*/ 15*d*/ 20*d*/ 25*d*	-
GL	num.	80/(300, 400, 600, 800)/(4*h*+*ar*)	2x1	0.3/ 0.5/ 0.7	3*d*/ 6*d*/ 8*d*/ 10*d*/ 20*d*	-
GL	num.	80/190/610	1-6x1	0.4/ 0.6	(*n* - 1) 3*d*	-
GL	num.	80/304/1320	1-4x1-3	0.44/ 0.7	16.8*d*	(*m*-1) 3*d*
GL	num.	80/304/1320	2-3x2	0.44/ 0.7	16.8*d*	3*d*, 4.5*d*, 6*d*

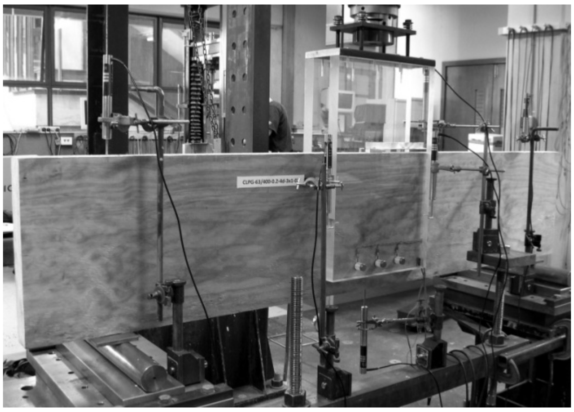

Figure 2: Test setup of LVL test series

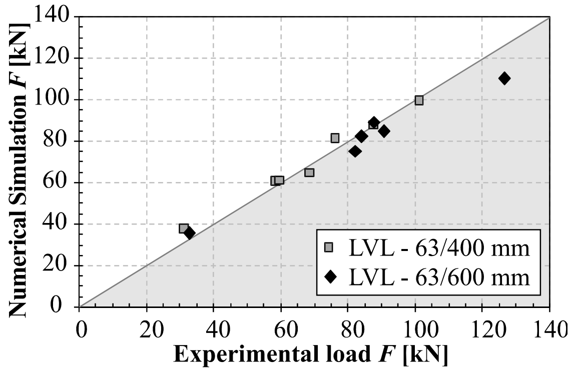

Figure 3: Correlation of the numerical model to test results in LVL

2.2 Splitting failure behaviour

For the characterization of the brittle failure behaviour of double shear connections investigated, the energy balance method together with crack resistance curves were used as one of the fracture mechanic methods. The crack resistance curves evaluated for double shear connections show a nonlinear material behaviour. The crack grows stable as long as the crack resistance increases more than the crack extension force under a constant load during crack propagation. If the crack resistance exceeds the critical value, the crack will grow in an unstable manner and the system fails. The fracture energies determined were split into the fracture mode I and mode II using the method of Ishikawa et al. (1979). The critical fracture energies determined are not comparable with the fracture energies known for different materials for the pure fracture modes I or II because they are caused by a stress situation related to one connection layout and do not relate to test setups for the investigation of a single fracture mode. Therefore, in this paper, the fracture energies determined for dowel-type connections are called specific critical fracture energies, $\mathcal{G}^{I,II}_{spec,c}$.

The splitting failure of the double shear dowel-type connections is classified by the fracture mode I (transverse tension) and mode II (in plane shear). The fracture values reached show that the connection layout and the depth of the beam influence the ratio between these two fracture modes. Figure 4 shows as an example the numerical solution for a 3 by 2 dowel type connection and Figure 5 the corresponding crack resistance curve for the dowel at the edge with the largest loaded edge distance. In the case shown, the failure load is 60 kN.

The analysis of the single crack resistance curves of each dowel of a connection shows that the outside dowels with the largest loaded edge distances of the connection trigger the

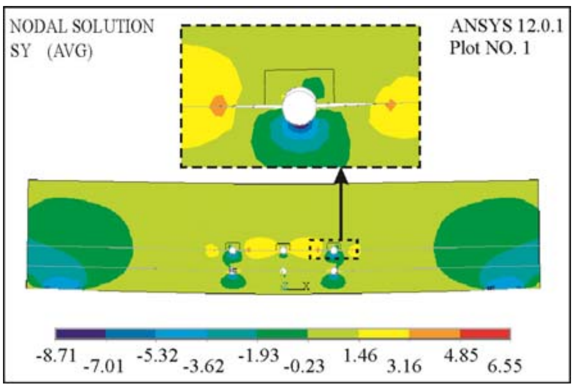

Figure 4: Numerical solution - transverse stress for 3 x 2 dowel type connection

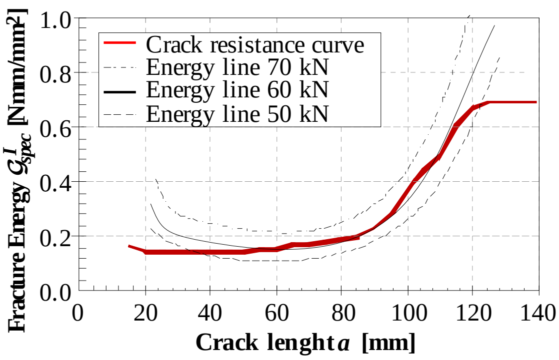

Figure 5: Crack resistance curve for mode I with energy lines for the outside side of the dowel marked in Figure 4

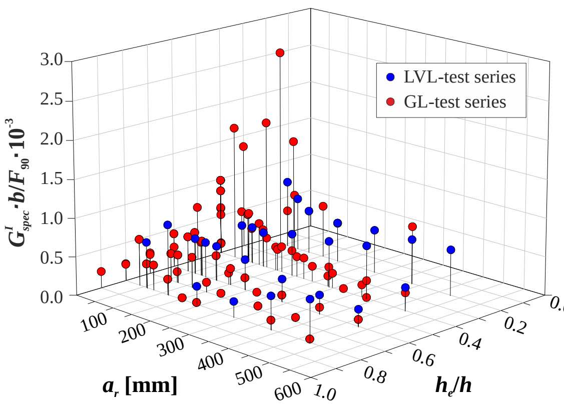

Figure 6: Distribution of fracture energies for mode I for Glulam and LVL

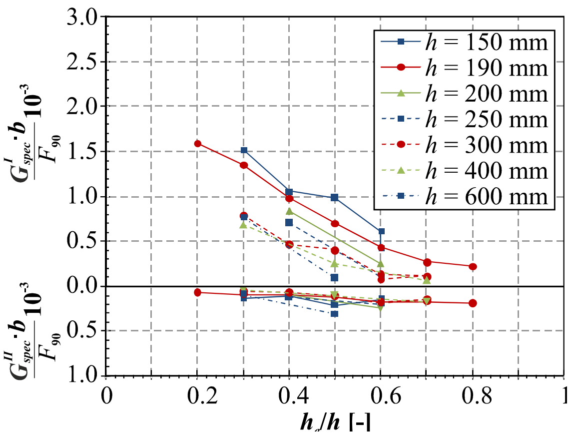

Figure 7: Dependency of fracture energies on depth of the member for Glulam

unstable failure of the connection, Franke & Quenneville (2011a). The cracks between the outer dowels (inner part of the connection) become also unstable and the wood between these dowels is then completely separated.

For each dowel of every connection layout investigated, the crack resistance curves as well as the critical specific fracture energies were determined, as described above. The distribution of these fracture energies of the outside dowel with largest edge distance shows a dependency on the loaded edge distance h_e/h, the connection width parallel to grain a_r and the depth of the member h, as shown in Figure 6 and Figure 7. In general, the normalized fracture energies for solid wood, including glulam, show a different behaviour than LVL. Due to the multi-layered cross section of the engineered wood product LVL being more homogeneous, the brittle failure behaviour is different from the solid wood one.

The distribution of the specific critical fracture energies in relation to the member depth shows an influence on the fracture mode I but not on mode II, as shown as example for single dowel-type connections in Figure 7. The test programme considers member depths from 150 mm up to 600 mm. The increase of the member depth results in a decreasing of the normalized specific critical fracture energy for fracture mode I. Whereas the values respectively the corresponding curves are all close together for the fracture mode II.

2.3 Failure criteria

The splitting failure of dowel-type connections can be summarized using a common failure criteria. The failure criteria describes the interaction between the fracture modes I and II. The distribution of the numerical test series investigated are compared with the linear-, quadratic- and Wu-failure criterion (1967), as shown in Figure 8. The assessment of the distribution of the specific critical fracture energies for the test programme shows that the quadratic failure criterion mostly encloses all failure cases for Glulam and LVL test series. The quadratic failure criterion will be used for the prediction of the splitting failure behaviour of dowel-type connections. The quadratic failure criterion takes into account the important parameters of the connection layout of single and multiple dowel type connections as well as the ratio between the fracture modes I and II.

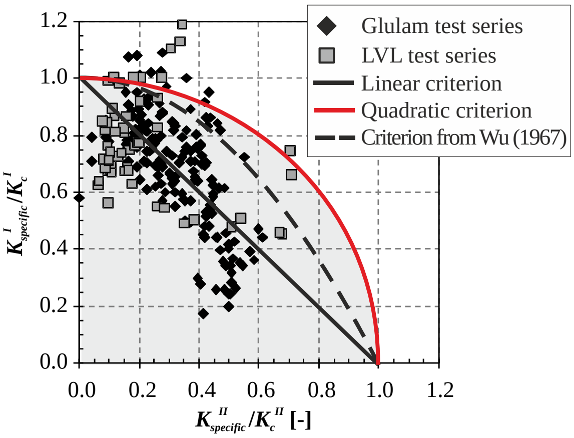

Figure 8: Failure criteria for dowel-type connections loaded perpendicular to grain for Glulam and LVL test series

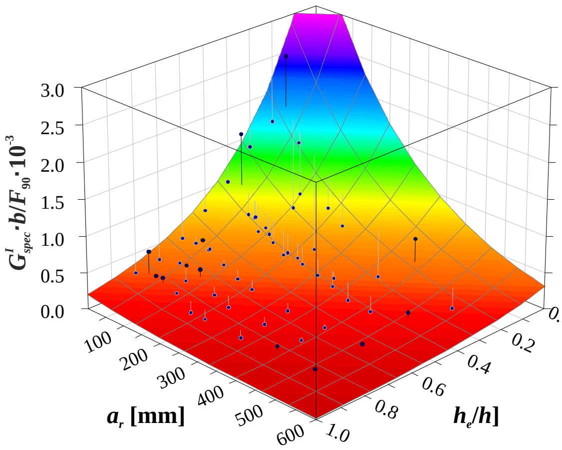

Figure 9: 3-dim. curve of the normalized fracture energies for mode I compared to the individual test results for solid wood/glulam

3 Design approach

Depending on the connection layout and its position over the member depth, double shear dowel type connections fail either in a ductile manner such as bending of the dowel or the embedment failure of the wood or in splitting of the wood. Therefore the design for double shear connections loaded perpendicular to grain has to be used in combination with the European Yield Model (EYM) for the prediction of the ductile failure behaviour as given in Eq. (1).

$$F_{connection} = \min \begin{cases} F_{ductile}\left(\mathrm{EYM}\right) \\ F_{splitting} = F_{90} \end{cases} \tag{1}$$

For the design proposal for predicting the splitting failure, the quadratic failure criterion will be used to consider the interaction between the transverse tension and shear failure. Substituting the individual critical specific fracture energies with the distribution of the normalized fracture energies $\mathcal{G}^{I,II}_{norm}$, the splitting load F_{90} for dowel-type connections in timber becomes:

$$F_{90} = \frac{b}{\left(\dfrac{\mathcal{G}^{I}_{norm}\left(h_e/h, a_r, h\right)}{\mathcal{G}^{I}_{c}} + \dfrac{\mathcal{G}^{II}_{norm}\left(h_e/h, a_r, h\right)}{\mathcal{G}^{II}_{c}}\right)} k_r \tag{2}$$

Where F_{90} in [N] is the load capacity depending on the splitting failure of the wood. $\mathcal{G}^{I}_{c}$ and $\mathcal{G}^{II}_{c}$ [Nmm/mm²] are the critical material fracture energies for the fracture mode I or II and b [mm] is the width of the member. The normalized fracture energies $\mathcal{G}^{I,II}_{norm}$ enclose all individual critical specific fracture energies of the various connection layouts considered. Therefore, the critical specific fracture energy of each connection layout investigated was normalized with the specimen width b and the splitting load F_{90}, see Eq. (3).

$$\mathcal{G}^{I,II}_{norm} = \frac{\mathcal{G}^{I,II}_{spec} \cdot b}{F_{90}} \tag{3}$$

The distribution of all values for solid wood and glulam test series were expressed with a 3-dimensional group of curves, which depends on the loaded edge distance ratio h_e/h, the connection width a_r [mm] and the member depth h, as shown in Eq. (4) and Eq. (6) and for LVL as in Eq. (5) and Eq. (6). Figure 9 shows as example the 3-dimensional curve for the member depth $h = 190$ mm compared to the individual values of the test series. The empirically determined Eq. (4), Eq. (5) and Eq. (6) are based on more than 200 different connection layouts investigated in solid wood, glulam or LVL.

$$\mathcal{G}^{I}_{norm} = e^{\left(h^{-1}\left(200-10h_e\cdot h^{-0.25}-a_r\right)\right)} \text{ for solid wood and glulam} \tag{4}$$

$$\mathcal{G}^{I}_{norm} = e^{\left(0.8-1.6h_e h^{-1}-1\cdot 10^{-3}a_r\right)} \text{ for LVL} \tag{5}$$

$$\mathcal{G}^{II}_{norm} = \left(0.05+0.12\frac{h_e}{h}+1\cdot 10^{-3}a_r\right) \text{ for solid wood, glulam and LVL} \tag{6}$$

The approach given in Eq. (2) considers the dependency on the geometry parameters of single and multiple dowel-type connections as well as on the member's cross section. The influence on the position of the connection along the span of the beam could not be observed and is therefore not considered in the design approach, Franke & Quenneville (2010).

The analysis of the test results shows that the load capacity as well as the stress situation beside the outside dowel with the largest loaded edge distance increases with increasing the number of rows and becomes constant for a higher number of rows, as shown in Figure 10, Franke & Quenneville (2012). This behaviour could be summarized using the quadratic interaction of the areas of the tension stress perpendicular to grain and the shear stress besides the dowels at the corner of the top row, Franke & Quenneville (2011a). The effect of the number of rows n is described with the following factor k_r:

$$k_r = \begin{cases} 1 & \text{for} \quad n = 1 \\ 0.1+\left(\arctan(n)\right)^{0.6} & \text{for} \quad n > 1 \end{cases} \tag{7}$$

It was observed that the load capacity does not increase for connections with constant loaded edged distance but different spacing between the rows, Franke & Quenneville (2011a). Therefore a dependency on the spacing between the rows is not included in the factor k_r.

For wider connections with more than two columns, e.g. nail plate connections, as shown in Figure 8, the splitting load has to be determined as either for the whole connection with the complete connection width a_r or as for single connections with the individual connection widths $a_{r,i}$. The minimum of the load capacities of Eq. (8) is the governing splitting load capacity of the connection.

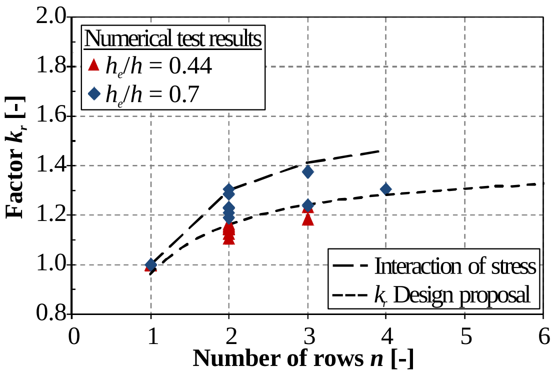

Figure 10: Factor k_r, depending on the numerical load capacities and stress situations determined

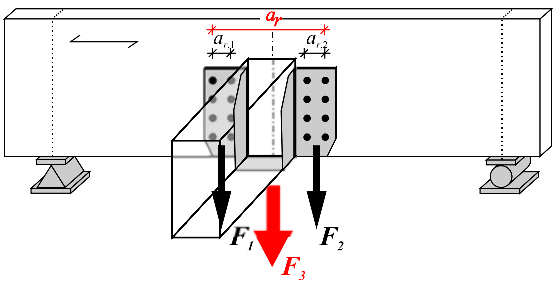

Figure 11: Design characteristics for nail plates or double dowel-type connections

$$F_{90} = \min \begin{cases} F_1\left(a_{r,1}\right) + F_2\left(a_{r,2}\right) \\ F_3\left(a_r\right) \end{cases} \tag{8}$$

4 Discussion

The design proposal is compared with experimental test series in solid wood, glulam and LVL. Figure 12 includes the correlation with the experimental test series in Canadian spruce glulam done by Reshke (1999), Kasim (2002) & Lehoux (2004). The test series cover single and multiple dowel-type connections. Furthermore, the design proposal are also compared with the experimental test series from: Ballerini (2004, 2003, 1999) who investigated mainly different depths of the member and different loaded edge distances; Möhler & Lautenschläger (1989) who observed different numbers of rows, connection widths and loaded edge distances; Ehlbeck & Görlacher (1989) who did tests with nailed steel-to-wood connections; and Schoenmaker (2010) where test series encloses various double-shear connections in European spruce. The comparisons are always related to Eq. (1), because for all cases of the experimental test results published, the differentiation between the ultimate or splitting load capacities is not given.The material values used for Canadian spruce glulam and European spruce are $\mathcal{G}_c^I = 0.225\,\text{Nmm/mm}^2$ and $\mathcal{G}_c^{II} = 0.650\,\text{Nmm/mm}^2$, as referenced in Vasic (2000) and Larsen & Gustafsson (1990). Figure 12 always shows a close correlation in the comparison of the experimental test series and the design proposal.

Figure 13 shows the comparison of the splitting load capacity and the design load F_{90} for the experimental and numerical test series in LVL. In this case the splitting load is known and the direct correlation to the new design approach can be shown. The material values used for LVL are $\mathcal{G}_c^I = 1.0$ Nmm/mm^2 and $\mathcal{G}_c^{II} = 6.0$ Nmm/mm^2, as referenced in Franke & Quenneville (2012), Ardalany et al. (2012). The design approach for LVL also shows a very good correlation to the experimental results.

For the comparison of the design proposal with the current two main international design standards, the same experimental and numerical test series were used. For the comparisons with solid wood and glulam, the 5% percentile values of the material parameters, as given in CSA O86-09, DIN 1052:2008, EN 1995-1-1:2004 and experimental results are used. In the experimental test series, where the values are unknown, the average values were reduced by about 15%. For the comparison with the average values of the test series in LVL, the tension strength of 1.4 N/mm² was used for the DIN 1052:2008 equations and the value C_1 = 22.9 N/mm$^{1.5}$ found by Jensen & Quenneville (2011) for LVL was used for the EN 1955-1-1:2004 equations instead of C_1 = 14 N/mm$^{1.5}$.

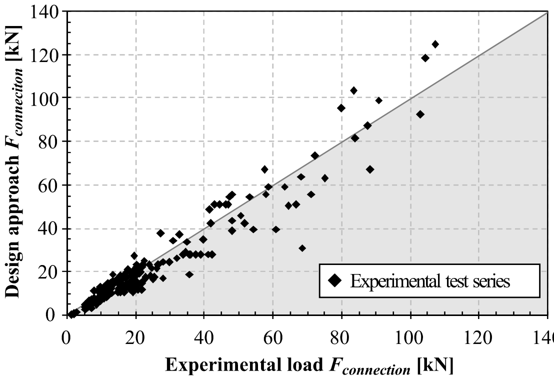

Figure 12: Comparison of design proposal and experimental test series published for European spruce or Canadian spruce

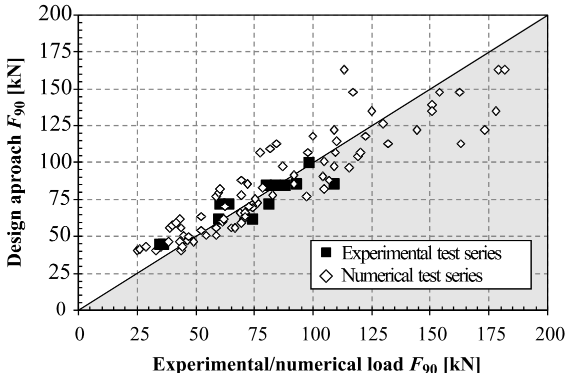

Figure 13: Comparison of design proposal and experimental as well as numerical test series for LVL

From Figures 14, 15, 16 and 17, one can observe that both the DIN 1052:2008 and the EN 1955-1-1:2004 design equations result in more inconsistent predictions of the failure strength and show also generally a wider variation. Whereas the predictions using the DIN 1052:2008 equations for solid wood show mostly conservative results, they are mostly unconservative for LVL. The opposite can be seen for the predictions using the EN 1995-1-1:2004 equations. Many predictions for solid wood are overestimated whereas almost all predictions for LVL are underestimated. The differences clearly reflect the nonconsideration of the effect of important connection configuration parameters.

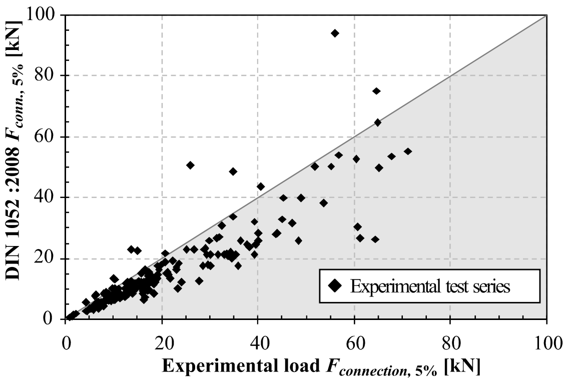

Figure 14: Comparison of DIN 1052:2008 and experimental test series published for European spruce or Canadian spruce

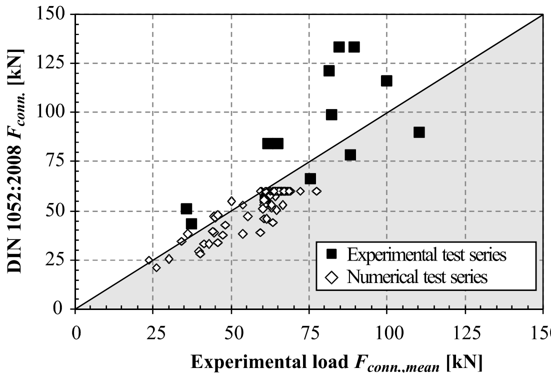

Figure 15: Comparison of DIN 1052:2008 and experimental as well as numerical test series for LVL

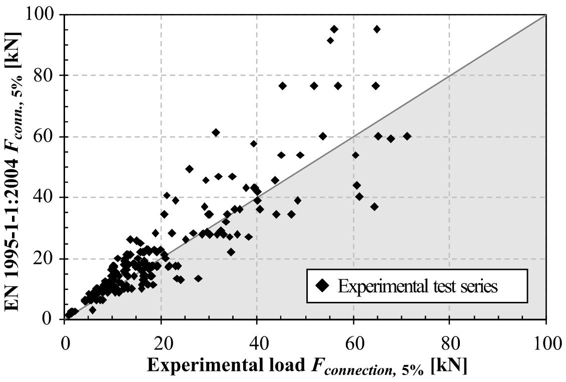

Figure 16: Comparison of EN 1995-1-1:2004 and experimental test series published for European spruce or Canadian spruce

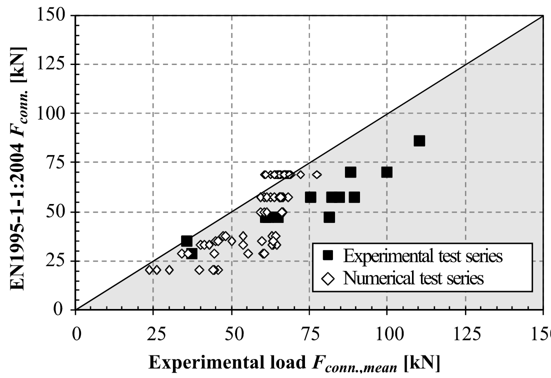

Figure 17: Comparison of EN 1995-1-1:2004 and experimental as well as numerical test series for LVL

5 Conclusion and view

A new design proposal is presented for double shear connections in solid wood, glulam and also LVL which allows one to predict the splitting failure of the wood due to connections loaded perpendicular to grain. The design approach is based on fracture mechanic methods including the important parameters which influence the load capacity of the connection. The comparison of the design results with comprehensive experimental test series done in Canadian and European spruce confirms the procedure of the design proposal. The good agreement is based on over 200 different experimental test configurations and 600 numerical test results.

The correlation between the new design proposal for double shear dowel-type connections loaded perpendicular to grain and the experimental test results confirms the methods used and the failure criteria determined, as shown in Figure 13. The new design approach, based on fracture mechanics methods, encloses the important parameters which influence the load capacity of the connection and would improve the current international design approaches. The comprehensive design approach presented for LVL as well as for solid wood previously published (Franke & Quenneville 2011a) could further be modified to a more simplified design equation for the practical design engineers and a code proposal but it can also already be used in its current state.

6 Acknowledgement

The research work was generously supported by the Structural Timber Innovation Company (STIC) from New Zealand.

References

Ardalany M, Deam B, Fragiacomo M (2012) Experimental results of fracture energy and fracture toughness of Radiata Pine laminated veneer lumber (LVL) in mode I (opening). Materials and Structures 45: 1189-1205

Ballerini M (2004): A new prediction formula for the splitting strength of beams loaded by dowel-type connections. In: CIB-W18, paper 37-7-5, United Kingdom.

Ballerini M (2003) Beams transversally loaded by dowel-type joints: Influence on splitting strength of beam thickness and dowel size. In: CIB-W18, paper 36-7-8, USA, 2003

Ballerini M (1999) A new set of experimental tests on beams loaded perpendicular to grain by dowel-type joints. In: CIB-W18, paper 32-7-2, Austria, 1999

Canadian Standards Association (2009) O86-09 Engineering design in wood, Canada.

Deutsches Institut für Normung e. V. (2008) DIN 1052:2008 Entwurf, Berechnung und Bemessung von Holzbauwerken – Allgemeine Bemessungsregeln und Bemessungsregeln für den Hochbau,Berlin, Germany.

Ehlbeck J, Görlacher R, Werner H (1989): Determination of perpendicular to grain tensile stresses in joints with dowel-type fasteners. In: CIB-W18, paper 22-7-2, Germany.

European Committee for Standardization (CEN) (2004) EN 1995-1-1:2004 Design of Timber Structures. Brussels, Belgium.

Franke B, Quenneville P (2012): Investigation of the splitting behaviour of Radiata pine and LVL under tension and shear. In: Proceedings of 12th World Conference on Timber Engineering, New Zealand.

Franke S, Franke B, Quenneville P (2012): Analysis of the failure behaviour of multiple dowel-type connections loaded perpendicular to grain in LVL. In: Proceedings of 12th World Conference on Timber Engineering, New Zealand, 2011.

Franke B, Quenneville P (2011a): Design approach for the splitting failure of dowel-type connections loaded perpendicular to grain. In: CIB-W18, paper 44-7-5, Italy.

Franke B, Quenneville P (2011b): Numerical modeling of the failure behavior of dowel connections in wood. ASCE, Journal of Engineering Mechanics 137, 186, 155-226.

Franke B, Quenneville P (2010): Analyses of the failure behaviour of transversly loaded dowel type connections in wood. In: Proceedings of 11th World Conference on Timber Engineering, Italy.

Ishikawa H, Kitagawa H, Okamura H (1979): J Integral of a mixed mode crack and its application. In: Volume3, ICM 3, Cambridge, England

Jensen, JL (2005): Splitting strength of beams loaded perpendicular to grain by dowel joints, In: Journal of Wood Science 51, p. 480-485.

Jensen JL, Quenneville P (2011): Splitting of beams loaded perpendicular to grain by connections - some issues with EC5. In: CIB-W18, notes, Italy.

Kasim MH (2002): Bolted timber connections loaded perpendicular-to-grain - Effect of row spacing on resistance. Royal Military College of Canada, Kingston, Canada

Larsen HJ, Gustafsson PJ (1990): The fracture energy of wood in tension perpendicular to grain – results from a joint testing project. In: CIB-W18, paper 23-19-2, Portugal

Lehoux MCG (2004): Bolted timber connections loaded perpendicular to grain. A proposed design approach. Royal Military College of Canada, Kingston, Canada

Reshke R (1999): Bolted timber connections loaded perpendicular-to-grain - Influence of joint configuration parameters on strength. Royal Military College of Canada, Kingston, Canada

Schoenmakers JCM (2010): Fracture and failure mechanisms in timber loaded perpendicular to the grain by mechanical connections. Doctoral thesis, University of Technology Eindhoven, Netherlands.

Van der Put TACM, Leijten AJM (2000): Evaluation of perpendicular to grain failure of beams caused by concentrated loads of joints. In: CIB-W18, paper 33-7-7, Netherlands.

Vasic S (2000): Applications of fracture mechanics to wood. Doctoral dissertation, University of New-Brunswick, Canada

Wu EM (1967): Application of fracture mechanics to anisotropic plates. Journal of Applied Mechanics, Series E, 34(4):967-974

INTERNATIONAL COUNCIL FOR RESEARCH AND INNOVATION IN BUILDING AND CONSTRUCTION

WORKING COMMISSION W18 - TIMBER STRUCTURES

BEAMS LOADED PERPENDICULAR TO GRAIN BY CONNECTIONS

J C M Schoenmakers

A J M Leijten

A J M Jorissen

Eindhoven University of Technology

THE NETHERLANDS

Keywords: timber, beams, connections, splitting, failure, perpendicular to grain,

---

Presented by A Leijten

H Blass asked how would one define a double or triple connection and asked why not every column considered as a connection. He further commented that if spacing was taken as minimum would they not be considered as individual connection. He stated the reason for the question was that one needed to give limit to the results so that they can be applied. A Leijten discussed the capacity would be influenced by distance and they did not do tests by varying spacing. In standards if the spacing is more than 2 times the depth, they can be considered as individual connection.

J W van de Kuilen asked what kind of moisture adjustment factor would one apply? A Leijten stated the same as Eurocode 5. He discussed that as the number of connections increased, the results showed that it was not proportional.

W Seim asked if a minimum height could be used to avoid such an effect. A Leijten stated that higher than 70% of the depth one should see bending failures.

J W van de Kuilen questioned about the influence of growth rings. A Leijten stated that no significant influence was found.

Beams loaded perpendicular to grain by connections

J.C.M. Schoenmakers, A.J.M. Leijten, A.J.M Jorissen
Eindhoven University of Technology, the Netherlands

1 Introduction

This contribution addresses the following issues regarding splitting:

- Is the splitting strength dependent on the connection width along the grain when laterally loaded dowel-type fasteners are applied?
- Is the Eurocode 5 model valid for axially loaded screws?
- Is the Eurocode 5 model safe for multiple connections along the span?

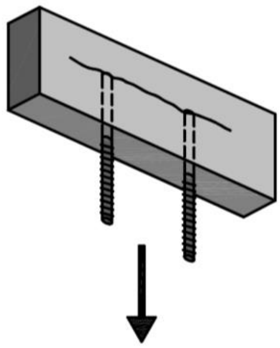

1 The influence of fastener spacing and number fasteners

In EN1995-1-1 (Eurocode 5) a linear elastic fracture model is implemented based on a model by Van der Put and Leijten (2000) that does not consider how the load is applied, nor the type and spacing of and number of fasteners but only what the conditions are for unstable crack growth outside the connection area. Other empirical or semi-empirical models Ehlbeck et al. (1989), Franke et al. (2012), among others, take into account the influence of the number of rows, columns and the spacing of the fasteners (nails, dowels).

A systematic and comprehensive study into the influence of rows and columns with mid span connections with 4 mm and 6mm nails was carried out by Schoenmakers (2010), Figure 1. The test results apply to mid span connections. The wood species was Spruce (C24) with a mean density of 450 kg/m^{3}and 12.7% m.c. The cross-sectional dimensions of the beams were 45x220mm and span 1600mm. Single shear (SS) nails and double shear (DS) nails fitted in predrilled holes. The holes in the steel side members matched the nail diameter as to prevent any clearance. The steel side plates were 15mm thick. For every connection five replicates were tested with two loaded edge distances, h_e. The load-slip curves were reported in Schoenmakers (2010). The failure mode of some tests are shown in Figure 2 were n = the number nails. It will be clear that with 5 nails plastic hinges in the nails appear.

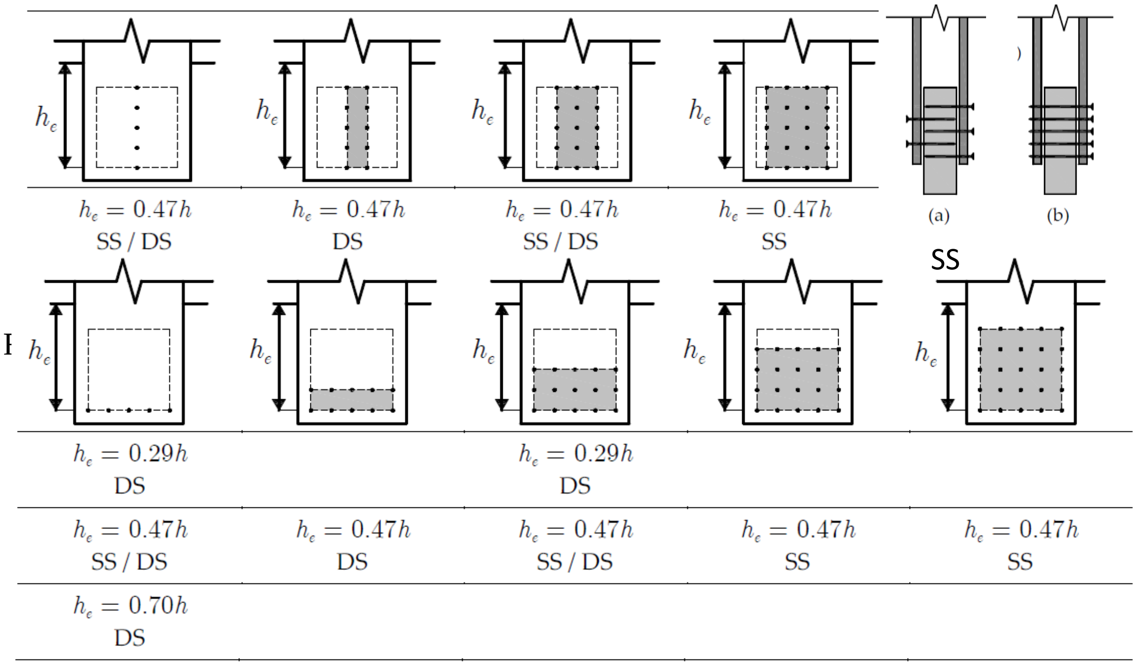

Figure 1: Connections with 4mm nails loaded in single shear (SS) and double shear (DS).

For higher numbers of nails splitting occurs when the embedment stresses are still low and no plastic hinges appear.

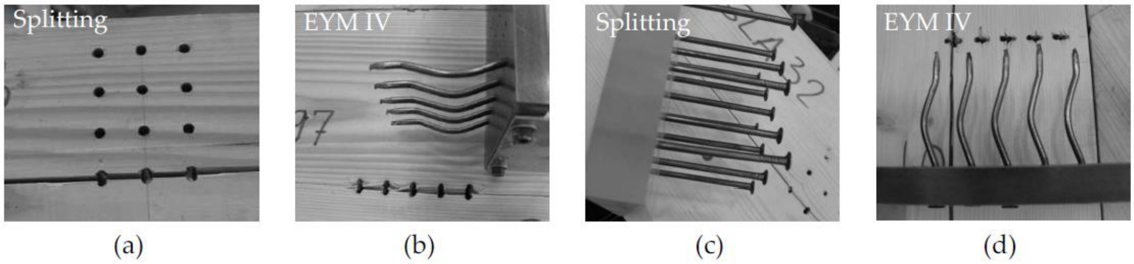

Figure 2; Typical failure modes (a) splitting n=12 (b) plastic hinges, n=5 (c) splitting n=20 (d) plastic hinges n=5; with n= number of fasteners.

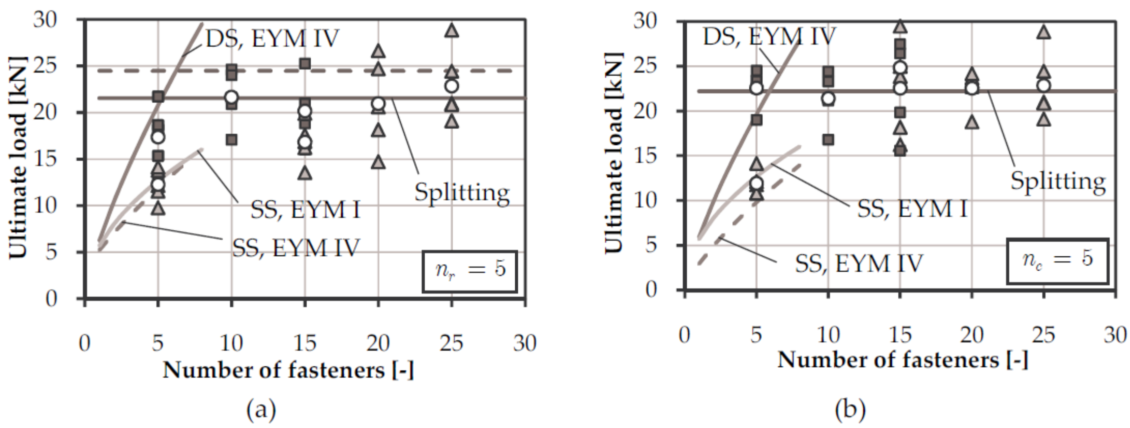

Figure 3: Results with 4mm nails: (a) top pattern Figure 1, (b) bottom pattern Figure 1.

In Figure 3 the open dots represent the mean value of each test series while the lines drawn show the predictions based on the EYM (including a number I to IV representing the governing failure modes) and the calibrated EN1995-1-1 model for splitting. It follows that when more than 10 nails are used the maximum load becomes independent of the nail pattern for both single (SS) and double shear (DS) loaded nails. The test results with connections with 6mm nails gave similar results. Schoenmakers (2010) also reports test with high density tropical hardwoods.

In the light of these results punched metal plates (PMP) connections which can be regarded as close spaced nailed connections show comparible results. In addition to Reffold et al. (1999) Schoenmakers (2010) performed a comprehensive test program in which he varied the plate orientation as well as the loading angle (inclined load introduction).

It is concluded that for more nails than a critical number splitting goverens independent of the number of fasteners as predicetd by Van der Put and Leijten (2000).

3 Mid span connections with axial loaded screws

The semi-empirical models by Ehlbeck et al. (1989) and Ballerini and Rizzi (2007) do not consider connections with axial loaded screws although the same splitting phenomenon occurs. For this type of load introduction a fracture mechanical model might be applicable as this type of model does not consider how the load is introduced. To verify this point Schoenmakers (2010) carried out test using SPAX-S screws with a diameter *d* of 8 and 12 mm and 200 mm length, inserted in the bottom of the beam. Two basic configurations were tested: one row of 3 screws and two rows of 3 screws, respectively, Figure 4. To examine the influence of the number of screws, spacing along the grain (s=4*d* and 8*d*) and insertion depth (0.3 and 0.5 beam depth) were varied. To satisfy the edge requirements for screws the timber beams thickness was adjusted without changing the beam depth 240 and span of 1600mm. The tests comprised 16 test series of 5 replicates each.

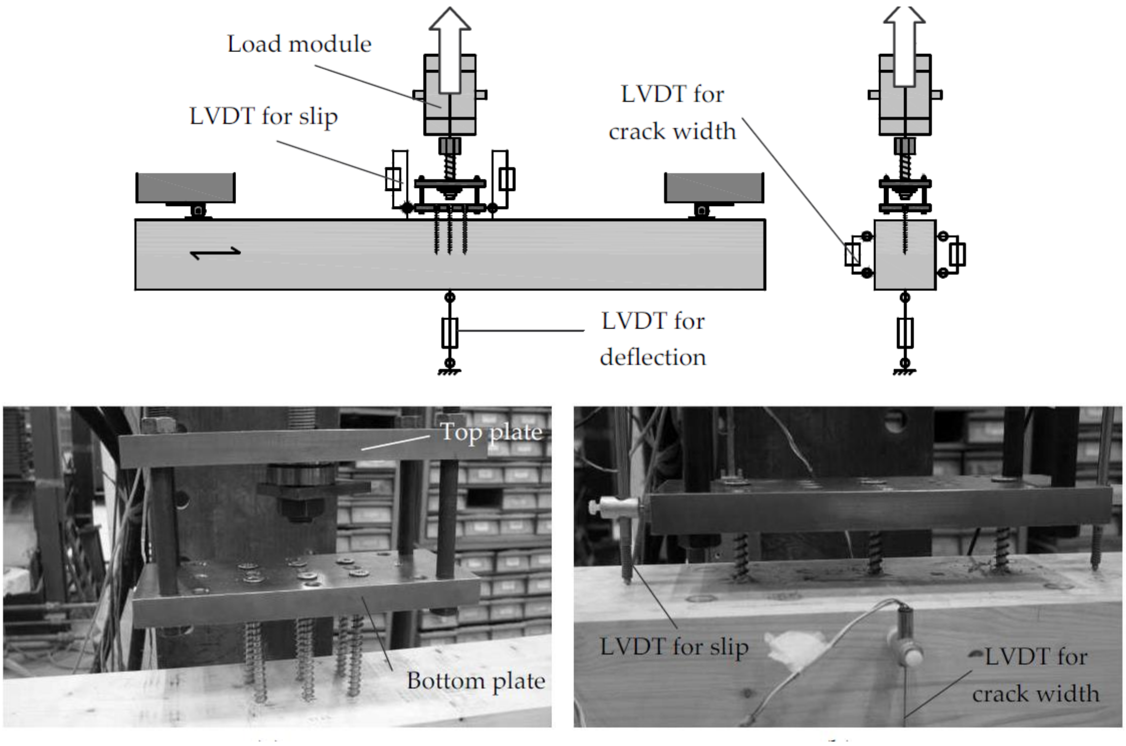

Figure 4: Test setup for bottom inserted self-tapping screws; (left) two rows of three screws; (right) one row of three screws.

Glued laminated beams of Spruce with an average density of 458 kg/m^3 at 12.2% m.c. were used. Only in the series with three 12mm screws 8d along the grain withdrawal was governing while in all other cases splitting occurred. The crack planes at the screwed section of the beam are schematically drawn in Figure 5. The observed crack plane varied at random over the test series and was either horizontal or inclined $\pm 30^0$ although more inclined cracks appeared for the 12 mm diameter screws than for the 8mm screws. In all cases the crack initiated approximately at the insertion depth minus 10 mm.

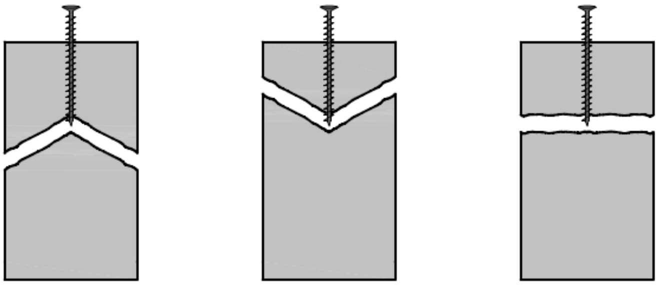

Figure 5: Crack orientation at the screwed section of the beam.

When the fracture parameter $(GG_c)^{0.5}$ of Eq. (3), see 4.1, was calibrated for each screw diameter, for 8mm screws the mean was $(GG_c)^{0.5}$ = 17.4 N/mm$^{1.5}$ for 12mm screws $(GG_c)^{0.5}$ = 12.6 N/mm$^{1.5}$. The predictions by Eq.(3) resulted in Figure 6(a). Schoenmakers also evaluated the test results using only one mean value of $(GG_c)^{0.5}$=14.9 N/mm$^{1.5}$ based on all his tests with glued laminated beams and dowel-type fasteners, Figure 6(b). This results in a conservative prediction for connections with d=8mm screws and slightly less conservative predictions for the 12mm screws. The influence of screw diameter was left unexplained.

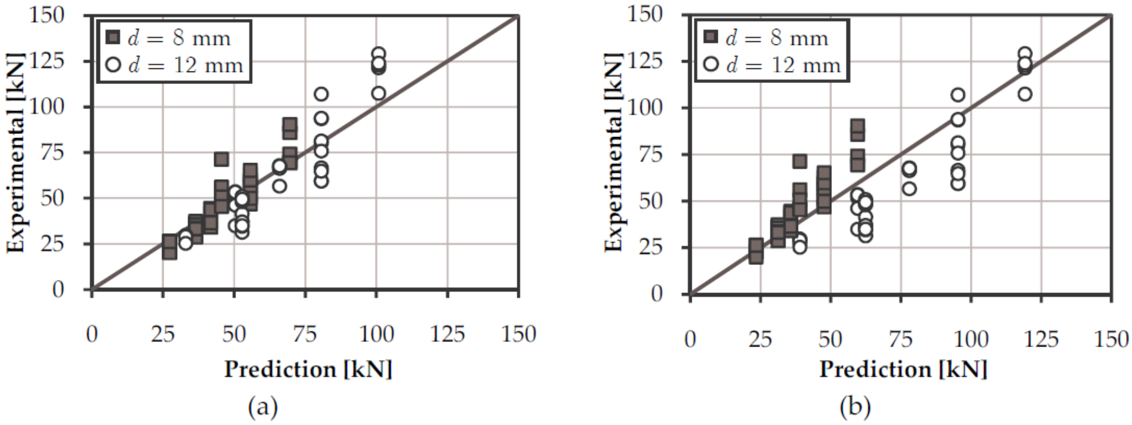

Figure 6: Eq.(3) predictions (a) calibrated per screw diameter (b) using an average calibration value.

In conclusion the fracture mechanical model of EN1995-1-1 is well able to predict the splitting capacity for axially loaded self-tapping screwed connections.

4 Multiple connections along the span

The overall majority of test so far reported in literature focus on a test configuration with a single connection at mid span. There are models that assume that when enough spaced, for instance twice the beam depth, multiple connections can be considered as individual connections and no interaction will affect the load carrying capacity. Kasim and Quenneville (2002) however, claimed that if the spacing between two connections increases the total load carrying capacity does not exceed 1.4 the single connection failure load, Figure 7. This phenomenon was left unexplained by the authors.

Jensen (2003) tried to explain this phenomenon using a beam-on-elastic-foundation-model with somewhat more success. The same compliance method as Van der Put and Leijten

(2000) was used but now for two connections symmetrically positioned along the beam span assuming symmetrical crack development, Figure 8. Main assumption in Jensen's model was crack propagation on either side of the connections at an equal rate (i.e. both cracks initiated at a connection extending equally). However, his model was unable to explain the two connection phenomenon just mentioned. Applying the same method Schoenmakers (2010) derived a different solution. The beam was modelled as shown in Figure 8 accounting for the situation where crack growth might be not symmetrical on either side of the connection. In his model crack lengths were denoted by λ, and the indices 3 and 4 indicate the beam segment the crack is attributed to (left-hand or right-hand side).

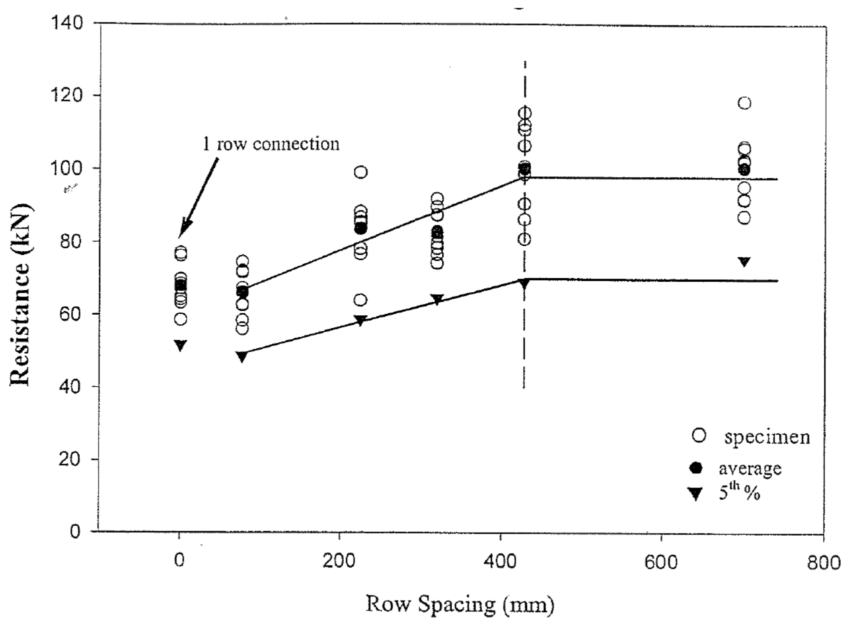

Figure 7: Result of increasing spacing between two connections (with two dowels), Kasim and Quenneville (2002).

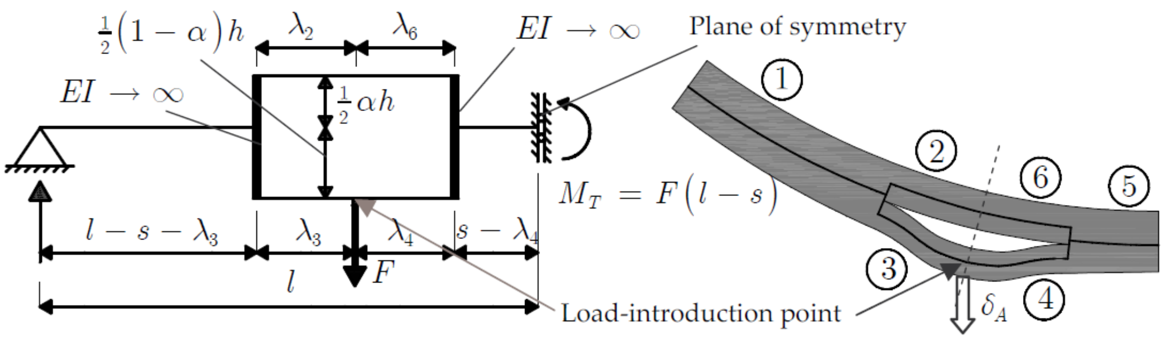

Figure 8: Modelling the symmetrical half of the beam by using only the centre lines of the deformed cracked beam (right), Schoenmakers (2010).

The compliance, $C = \delta_A/F$ in Eq. (1), contains the contribution of every (beam) element and the type of internal strain involved (normal, shear or bending) using the energy method and Mohr's Integral on each beam segment analytically as function of λ. In eq. (1), λ_3 and λ_4 correspond to both mutually independent cracks. Expressions for the internal bending moment en normal force (sectional method) used to satisfy compatibility conditions at the interface between beam segment 2 and 6, resp. were derived. The critical load per connection is obtained using the standard procedure determining the compliance change Eq. (2). Maple software was used to derive an analytical expression for the derivatives.

$$\frac{\delta_A}{F} = \frac{6}{5}\frac{1}{GA}\left(l - s - \lambda_3 + \frac{(1-\xi\gamma)\lambda_3}{\alpha}\right) + \frac{1}{3EI}\left((l-s-\lambda_3)^3 + 3(l-s)^2(s-\lambda_4)\right) + \frac{\lambda_3^2}{6E\alpha^3 I}\left((1-\xi\gamma)(3(l-s)-\lambda_3)\right) + \frac{\left(-\frac{M_Q}{F} + \left(\xi\gamma\left(\frac{1}{2}\lambda_3 + \frac{1}{2}\lambda_4\right) + l - s - \lambda_3\right) + \frac{1}{2}\frac{N_Q}{F}h\right)}{E\alpha^3 I}\left((l-s)(\lambda_3+\lambda_4) - \frac{\lambda_3^2}{2}\right) + \frac{(l-s)\lambda_3\lambda_4}{E\alpha^3 I}\left(1 - \xi\gamma\left(1 + \frac{\lambda_4}{2\lambda_3}\right)\right) \tag{1}$$

$$F_{ult} = 2F_{crit} = 2\sqrt{\frac{2\mathcal{G}_c t}{\frac{\partial C}{\partial \lambda_3}d\lambda_3 + \frac{\partial C}{\partial \lambda_4}d\lambda_4}}\sqrt{d\lambda_3 + d\lambda_4} \tag{2}$$

Details can be found in Schoenmakers (2010). The results of the analysis are interesting because the conditions on either side of the connection might not be the same and crack growth either. In Figure 9 a summary of the model results is provided.

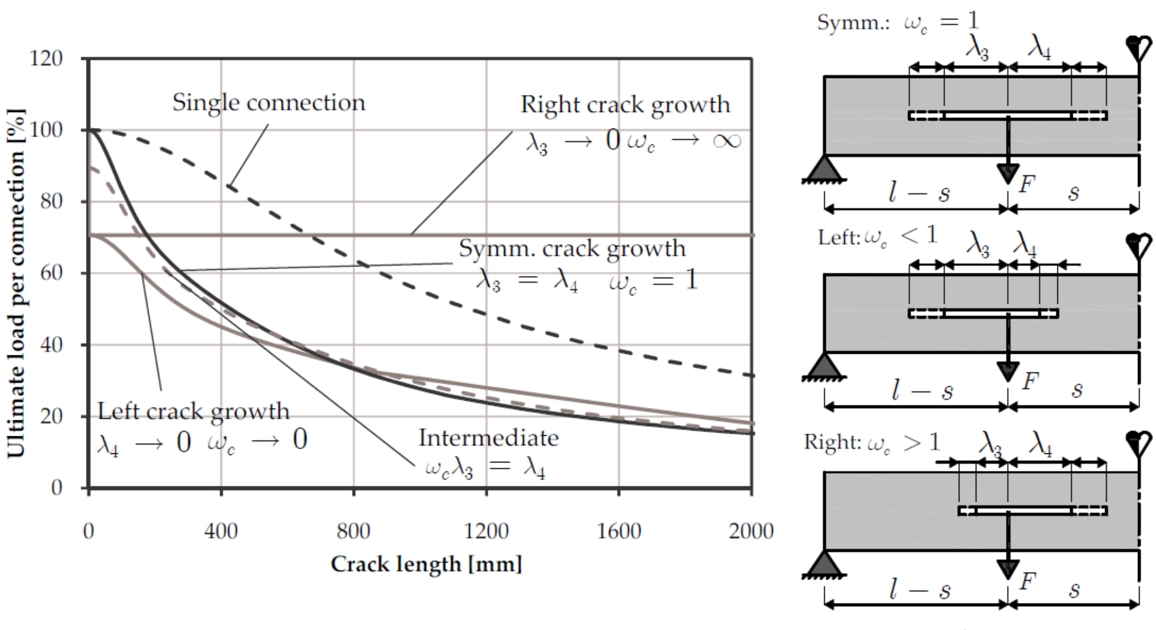

Figure 9: Critical load per connection as function of the crack length. (a) Comparison to the critical load corresponding to the beam with a single mid span connection. (b) Three cases of dominant crack propagation direction.

When a (dominant) crack grows usually other cracks also grow simultaneously but may be at a different rate. Plausible situations were investigated and evaluated. The critical failure load of one mid span connection is taken as a reference (100%), top curve in Figure 9. This curve goes down with increasing symmetrical crack growth. To consider different crack growths on either side of the connection ω_c is introduced. This parameter represents the ratio of the length of two growing cracks, for instance $\omega_c = \lambda_4/\lambda_3$ including the increments,

Figure 9b. In case of symmetrical crack growth, $\lambda_4 = \lambda_3$ and so ω_c=1, the splitting strength of two connections is double the single connection; agrees with Jensen's (2003) model. However, the lowest curve associated with a dominant crack growth towards the support while the crack growth towards mid span is very small, the critical load per connection will become $0.5(2)^{0.5}$=0.71 times the single mid span critical load. This explains the results of Kasim and Quenneville (2002). However, if the crack growth is neither symmetrical nor dominating towards the support an intermediate situation occurs with a critical load per connection between 0.71 and 1.0 time the critical load of a single mid span connection.

4.1 Experimental verification

Apart from the theoretical model development Schoenmakers (2010) performed many tests some of which were conducted to verify his two connection model. Later tests by Leijten, used three equally spaced connections along the span, Figure 10. The latter tests were carried out in 2013 and used the timber from the same batch of Spruce beams as Schoenmakers, strength class C24.

A)

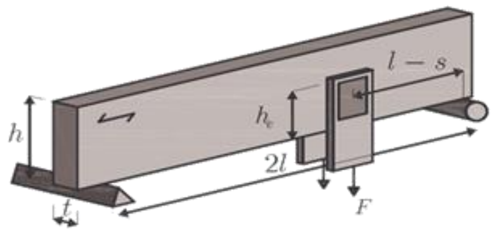

B)

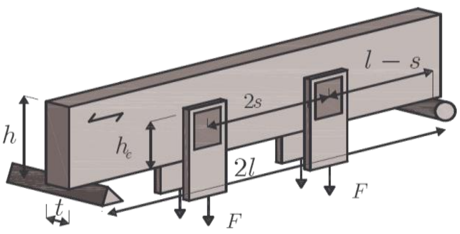

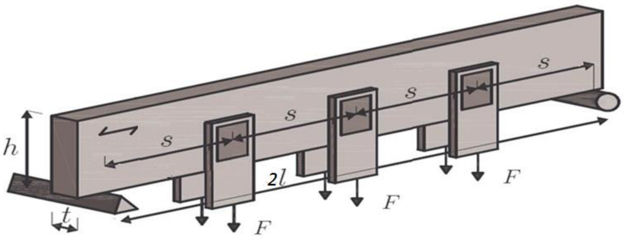

C)

Figure 10: Overview of Table 1 test series
A) Test Series 1 to 8. B) Series 9&10 and 14&15. C) Series 16 and 17.

In Table 1 the test series are grouped according to the type of fasteners, the dimensions of the beams and other parameters are indicated in column (2) to (9). The glued laminated beams used had a mean density of 450 kg/m^3 and moisture content of 12.7%. Nailed connections had 5 rows of 5 nails= 25 nails in a square pattern. For the other tests sawn timber beams was used with a mean density of 455 kg/m^3 and 12.9% m.c. For the sawn wood beams four close spaced (4*d*) 12mm diameter dowels were used set in a square pattern. All beams failed brittle by splitting. In addition Schoenmakers (2010) also tested cantilevered beams with connections at the end and half way the cantilever length but left out here. Series 16 and 17 beams comprised of three connections equally spaced at two times the beam depth, 2*h* along the span. All three connections were loaded by separate hydraulic actuators each having a load cell to check for any differences, which were insignificant. Crack initiation and growth direction were studied with special LVDT's mounted at close distance on either side of each connection. In addition a high speed camera was used to observe the crack growth visually. In 70% of the tests the crack initiation started at the connections near the support. A dominant crack growth direction was difficult to determine. In 30% of tests a symmetric crack growth could be determined. In 50% of the cases a leading crack direction could not be established.

The number of connections along the span is given in column (5), Table 1. The critical load, F_{crit} is the load per connection, column (10). To allow comparison between test series using different cross-sections, distance from the support, number and type of fasteners the mean apparent fracture parameter $(GG_c)^{0.5}$ was calculated per test series with Eq.(3).

$$F_{ult} = 2F_{crit} = 2t\sqrt{\frac{GG_c h\alpha}{\frac{3}{5}(1-\alpha)}} \tag{3}$$

(1)	(2)	(3)	(4)	(5)	(6)	(7)	(8)	(9)	(10)	(11)	(12)
Test	cross	no	span	num	distance	num	loaded	diam,	mean max	adjusted	
series	section	of		of	from	of	edge		load per	calibration	
		test		con	support	fast	distance		connection	(GGc)^0,5	
no	bxh	n	2l			n	he/h	d	Fcrit	mean	mean
	[mm2]	-	[mm]		[mm]	-	[%]	[mm]	[kN]	[N/mm1,5]	
1	45x300	5	2600	1	650	25	47	4	27,78	13,19	
2	45x300	5	2600	1	900	25	47	4	29,41	13,97	
3	45x220	5	1600	1	800	25	47	4	22,79	14,04	
4	45x220	5	1600	1	800	20	47	4	22,54	13,89	
5*	45x220	5	1600	1	800	20	47	4	22,52	13,88	13,35
6	45x220	5	1400	1	700	15	47	4	21,82	13,45	
7	45x220	5	1200	1	600	15	47	4	20,11	12,39	
8	45x220	5	1000	1	500	15	47	4	19,43	11,97	
9	45x300	5	2600	2	900	25	47	4	19,68	9,35	9,38
10	45x300	5	2600	2	650	25	47	4	19,83	9,42	
11	45x220	3	1400	1	700	4	44	12	17,91	11,72	
12	45x220	5	1200	1	600	4	44	12	18,76	12,28	11,97
13	45x220	5	1000	1	500	4	44	12	18,17	11,90	
14	45x220	5	1600	2	400	4	44	12	16,68	10,92	11,21
15	45x220	5	1600	2	200	4	44	12	17,56	11,50	
16	45x220	10	2000	3	440	4	46	12	11,68	7,34	7,71
17	40x220	10	2000	3	440	4	33	12	8,68	8,07	
)* one extreem low left out											

Table 1: Test results of beam with multiple connections.

This fracture parameter was adjusted for the following reasons:

- From evaluation of his total data base Schoenmakers (2010) found a 10% higher value with glued laminated beams. This takes 10% off for test series 1, 2 and 9 & 10.

- When two or three connections are tested simultaneously the weakest will always fail first and distorts comparison of the mean between series. Therefore the average values of the fracture parameter of these test series were adjusted using established statistical procedures, Douwen et al. (1982). It assumes that the results are normally distributed which results in a rise of the mean fracture parameter of approximately 10%.

Having taken these factors into account the corrected apparent fracture parameter is given column (11). Column (12) shows the mean of the test series grouped by fastener type and number of connections.

For the nailed connections there is a distinct difference in strength between tests with one and two connections. The strength ratio 9.38/13.35=0.70 which is close to Schoenmakers (2010) lower bound prediction of 0.71. For connections with dowels the situation is different because no significant difference is found between the corrected fracture parameter of one and two connections, i.e. 11.97 and 11.21 respectively. However, three connections apparently have a very significant effect, with a drop in strength to 7.71/11.97=0.64 per connection. No model is yet able to explain this behaviour. However, Schoenmakers model might be a good candidate when extended to three connections.

The consequences of these test results are considerable if one understands that in a number of semi-empirical and empirical models connections are considered as separate connections when spaced more than twice the beam depth. In Figure 11 the total load on the beam is presented as ratio of the single connection strength. The two dots for beams with two connections represent the connections with nails and the other one for dowels. The predictions by EN1995-1-1 are indicated as well as the lower bound prediction by Schoenmakers for two connections. As shown the EN1995-1-1 prediction is conservative.

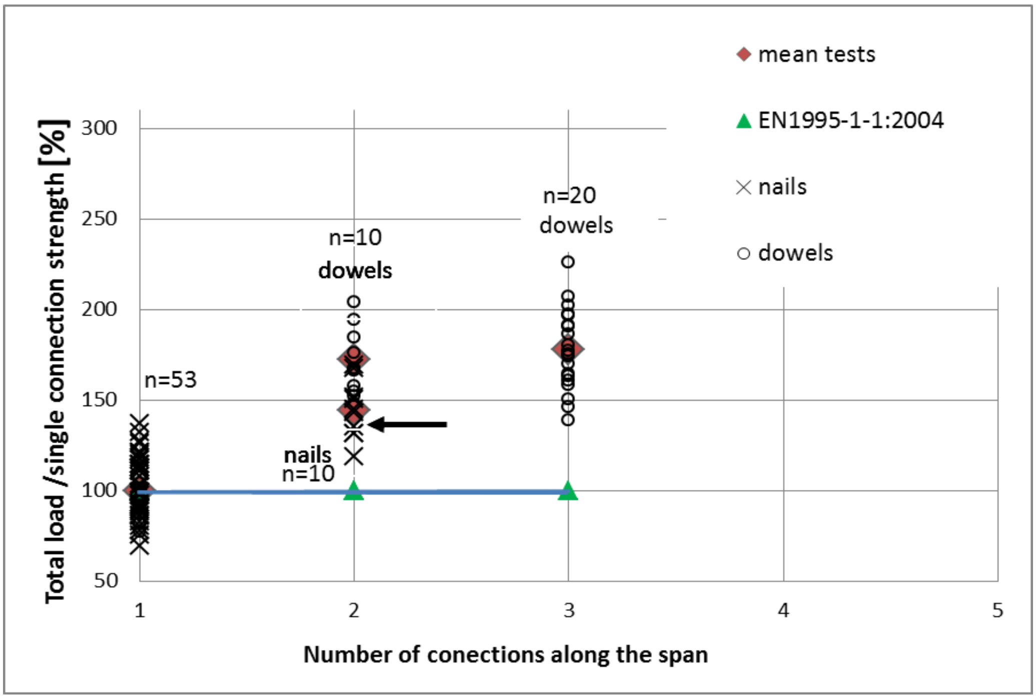

Figure 11: Code predictions and test results: ← = mean lower boundary by Schoenmakers (2010) for two connection.

5 Proposed revision for Eurocode 5:2004 (EN1995-1-1)

Test results with multiple connections show Eurocode 5 provisions to be conservative. This is caused by the shear force criterion. Because the effect of multiple connections is not yet fully understood and theoretical models are lacking the proposal is not to change the shear force criterion for beams with multiple connections. For one connection placed anywhere along the span however, this shear strength criterion is too restrictive and be deleted or exchanged by a more appropriate criterion, Jensen et al. (2013). The tentative suggestion for beams with connections at the end face is to regard them as notched beams.

6 Conclusions

- splitting as governing failure mode is independent of the number of fasteners when a certain critical number is exceeded.

- models based on fracture mechanics have the ability to predict splitting of beams loaded by axial loaded screwed connections.

- multiple connections spaced along the span of a simply supported beam significantly affect the total load bearing capacity. The fracture model by Schoenmakers (2012) for two connections is able to predict a lower boundary. This model is a good candidate to be extended to more than two connections. Current Eurocode 5 splitting provisions are conservative and therefore safe.

7 Acknowledgment

The Dutch Research Council (STW) is gratefully acknowledged for its financial support

8 References

Schoenmakers J.C.M. (2010), Fracture and failure mechanisms in timber loaded perpendicular to the grain by mechanical connections, PhD-thesis, Eindhoven University of Technology, The Netherlands, ISBN 978-90-386-2223-1.

Van der Put T.A.C.M. and Leijten A.J.M.(2000) Evaluation of perpendicular to grain failure of beams caused by concentrated loads of joints, Proc. of CIB-W18/paper 33-7-7, Delft, the Netherlands.

Ehlbeck J. Görlacher R. Werner H. (1989), Determination of perpendicular-to-grain tensile stresses in joints with dowel-type-fasteners, Proc. of CIB-W18/paper 22-7-2, Berlin, Germany.

Frank S. Franke B. Quenneville P. (2012), Analysis of the failure behaviour of multiple dowel-type connections loaded perpendicular to grain in LVL, Proc. of World Conference on Timber Engineering, 15-19 July, Auckland, New Zealand.

Jensen (2003) Splitting strength of beams loaded by connections, Proc. CIB-W18/paper 36-7-8, Colorado, USA.

EN 1995-1-1:2004, European Committee for Standardization (CEN): Design of Timber structures. Brussels, Belgium, 2004.

Reffold A. Reynolds T.N. and Choo B.S. (1999) An investigation into tension strength of nail plate timber joints loaded perpendicular to grain, Journal of the Institute of Wood Science, 85:19-27.

Ballerini M. and Rizzi M. (2007) Numerical analyses for the prediction of the splitting strength of beams loaded perpendicular-to-grain by dowel-type connections, Materials and Structures, 40: 139-149.

Kasim M. Quenneville P (2002) Effect of row spacing on the capacity of bolted timber connections loaded perpendicular-to-grain, Proc. Of CIB-W18/ paper 35-7-6, Kyoto, Japan.

Douwen A.A. Kuipers J. Loof H.W. (1982) Corrections to the mean value and the standard deviation from test series with symmetrical test specimens, Stevin report 4-82-9/ oe-5, May TU-Delft.

Jensen JL, Quenneville P, Girhammar UA, Källsner B (2012) Splitting of timber beams loaded perpendicular to grain by connections – Combined effect of edge and end distance. Construction and Building Materials, 35, 289–293.

CIB-W18/46-7-8

INTERNATIONAL COUNCIL FOR RESEARCH AND INNOVATION IN BUILDING AND CONSTRUCTION

WORKING COMMISSION W18 - TIMBER STRUCTURES

INFLUENCE OF FASTENERS IN THE COMPRESSION AREA OF TIMBER MEMBERS

M Enders-Comberg

H J Blaß

Karlsruhe Institute of Technology

GERMANY

Keywords: net cross-section, compression test, compressive strength, fasteners, mechanical connections

---

Presented by M Enders-Comberg

P Quenneville asked about the smallest diameter. M Enders-Comberg stated self-tapping screws had 6.5 mm inner thread diameter. P Quenneville asked what would be the case if 2 to 3 mm diameter nails were used. M Enders-Comberg stated they do not know.

S Winter received confirmation that smooth surface normal dowel was used. M Enders-Comberg and S Winter further discussed that glue in rod did not show any influence as stresses can be transferred by the glue and glue can be regarded as local reinforcement. S Winter received clarification that the glue used was epoxy. S Winter asked what would happen if screws were included in service class 2. M Enders-Comberg stated that there would be less reduction.

G Schickhofer received confirmation about the screw inner thread diameter.

C Sigrist stated that he was not 100% convinced as the study only dealt with defect free wood and standard quality wood would not see this level of reduction. M Enders-Comberg and H Blass showed pictures where the wood considered was a normal standard quality timber.

T Reynolds commented on the issue that a perfectly fitted connection was not possible. M Enders-Comberg stated that contact element was used in the model and its surface was studied.

E Serrano received clarification of local reduction for glued-in threaded rod connection.

K Ranasinghe questioned about the closeness of the fasteners. M Enders-Comberg stated that spacing rules were followed.

J W van de Kuilen received clarification that moisture content influence was done with glulam.

W Seim received an example that this connection can be used in a truss chord. W Seim commented that one should apply this specific example in Eurocode 5. H Blass commented that in practice this has not surfaced as a problem in service class 1 as there is a large buffer in service class 1 for compressive strength. This is not the same for service class 2.

S Aicher made an analogy to reinforced concrete and matrix basis.

A Frangi asked if the same result would be obtained if one considers it as a wood steel wood connection. M Enders-Comberg stated that it was not applicable.

A Buchanan asked if there were also results for tension loaded specimens. M Enders-Comberg stated that yes it was done in Karlsruhe Institute of Technology.

INFLUENCE OF FASTENERS IN THE COMPRESSION AREA OF TIMBER MEMBERS

MARKUS ENDERS-COMBERG, HANS JOACHIM BLAß

Karlsruher Institut für Technologie, Holzbau und Baukonstruktionen, Germany

1 Introduction

At present, the European timber design code comprises a rule relating to the design of net cross-sections in timber members. EN 1995-1-1 (2010) [1], but also DIN 1052 (2008) [2] and DIN 1052 (1969) [3] prescribe that "reductions in the cross-sectional area shall be taken into account in the member strength verification". However, "the reductions in the cross-sectional area may be ignored for the following cases: […] holes in the compression area of members, if the holes are filled with a material of higher stiffness than the wood".

This paper presents the results of a research project [4] dealing with timber truss connections. The influence of fastener holes in the compression area of timber and glulam members with regard to their load-carrying capacity under compression parallel to the grain was studied. Two test set-ups were considered: an experimental study of the global influence of reductions in the cross-sectional area in glulam connections and a study of the local behaviour around a fastener with experimental and numerical analyses.

2 Materials and Methods

2.1 General

The compression tests parallel to the grain were carried out in two groups of specimens with glulam (global influence) and clear wood (local influence). In addition to the non-weakened reference specimens, different weakened specimens were tested. Table 1 gives an overview of the test programme with specimen notations.

Table 1: Test programme and specimen notation

	Reference specimen	Specimen with holes and/or fasteners	Material
Global reduction	Type A	Types B - E	Glulam
Local reduction	Type a	Types b - f	Clear wood

2.2 Global Reduction

2.2.1 Material

In general, the glulam material used nominally belongs to strength class GL24h. The material's apparent density, referring to the entire specimen volume of 80 x 200 x 480 mm³, includes knots with higher local density. The material properties of the glulam used (5 laminations) are shown in Table 2. The following specimen types were investigated:

- Type A: Non-weakened cross-section
- Type B: 45° inclined threaded rod (∅ 20 mm) in a 16 mm pre-drilled hole
- Type C: Steel-to-timber dowel connection (7 mm saw-cut for a 6 mm steel plate and 3 x 4 dowels ∅ 10 mm in 10 mm pre-drilled holes)
- Type D: 2 x 5 self-tapping screws (SPAX T-STAR ∅ 10 mm with cut point) without pre-drilling
- Type E: Glued-in rod (∅ 16 mm metric thread in ∅ 20 mm pre-drilled hole)

The five specimen types are shown in Figure 1. The tests covered an average of 50 specimens of each type. The specimens were loaded with inserted fasteners and steel plate. Only specimen type D was not pre-drilled before inserting the fasteners.

The gross density and the moisture content of the glulam members were determined before inserting the different fasteners. Afterwards, the glulam pieces were ranked according to their density and were assigned to the specimen types. This assignment ensured a similar density distribution of the weakened and the non-weakened specimens. Altogether three batches were considered. Batch 1 was used for the tests of specimen types A1, B and C, batch 2 for specimen types A2 and D and batch 3 for specimen types A3 and E. The relevant material properties (density and moisture content) and the reduction of the cross-section are given in Table 2.

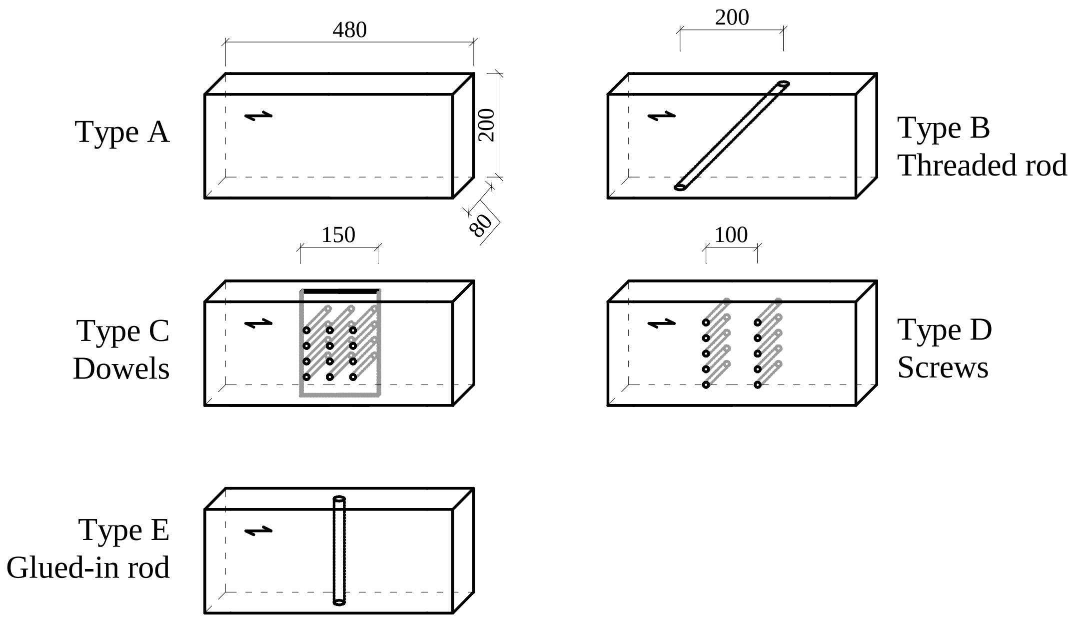

Figure 1: Specimen types, dimensions in mm

Table 2: Material properties of glulam (GL24h) in service class 1

	Batch	u_{mean} in %	Quantity	$\rho^{1)}$ in kg/m³			$\frac{A_{net}}{A_{gross}}$
				$\bar{x}$	s	$x_{0.05}$	
Type A1	1	10.2	51	457	21	417	1.0
Type B			50	458	21	418	0.8
Type C			49	459	20	419	0.71
Type A2	2	11.5	51	473	29	423	1.0
Type D			50	473	29	425	$0.85^{2)}$
Type A3	3	13.0	49	476	23	435	1.0
Type E			52	477	22	435	$0.75^{3)}$

$\bar{x}$ Mean, s Standard deviation, $x_{0.05}$ 5th Percentile
1) Density for moisture content u_{mean}
2) Based on inner thread diameter (∅ 6.1 mm)
3) Based on drilled hole diameter (∅ 20 mm)

2.2.2 Method

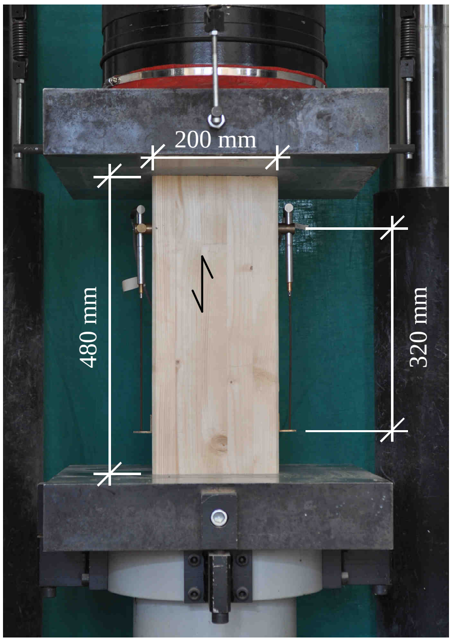

Figure 2: Test set-up

About 350 compression tests with glulam specimens were conducted within the research project. These tests were used to analyse the influence of fastener holes in the compression area of glulam members on their load-carrying capacity under compression parallel to the grain.

The test configuration corresponded to the standard EN 408 [5]. Figure 2 shows the test set-up and the dimensions of the specimen and the gauge length of 320 mm. The displacements were measured with two displacement transducers which were arranged on both narrow sides of the specimens. The upper three-dimensional hinge allowed inclinations of the steel plate around two axes. The lower bearing, however, was fixed. The load was applied monotonously until failure with a constant rate of piston displacement of 0.6 mm/min.

2.3 Local Reduction

2.3.1 Material and Method

The parallel-to-grain compression strength of clear wood was tested using specimens with and without fasteners as shown in Figure 4. Six specimen types (a-f) were used for the investigation of the local reduction. Ten boards (around 720 mm long) were cut in six pieces of clear wood with similar structural properties and therefore similar density, growth ring thickness and mechanical properties, as shown in Figure 3. This way of proceeding warrants the comparability among the different tests.

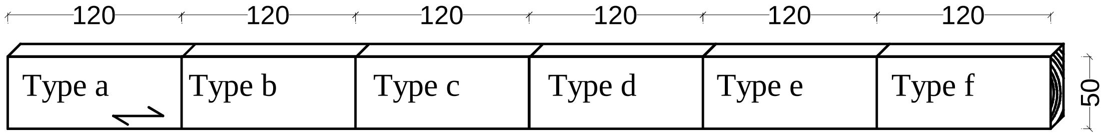

Figure 3: Pre-cut board and cross-section grouping; dimensions in mm

The following specimen types were investigated:

- Type a: Non-weakened cross-section
- Type b: 10 mm pre-drilled hole without a fastener
- Type c: Dowel (∅ 10 mm) with a smooth surface in a 10 mm pre-drilled hole
- Type d: Dowel (∅ 10 mm) with a rough surface in a 10 mm pre-drilled hole
- Type e: Self-tapping screw (SPAX T-STAR ∅ 10 mm with cut point) without pre-drilling
- Type f: Glued-in dowel (∅ 10 mm) with a smooth surface in a 10 mm pre-drilled hole

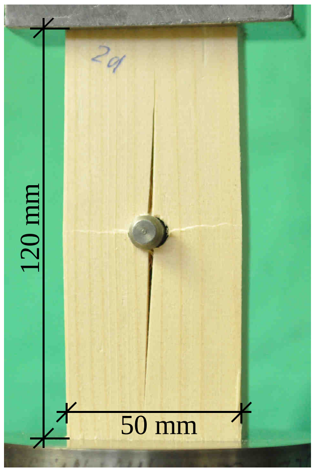

Figure 4: Specimen in the testing machine; Type d

The specimen size was w = 50 mm, h = 30 mm and ℓ = 120 mm. The hole diameter of 10 mm caused a reduction of the cross-section of 20 %. The mean values and the standard deviations of the relevant material properties (density and moisture content) and the net cross-section are given in Table 3. The compression load parallel to the grain was increased (0.5 mm/min) until specimen failure.

Table 3: Material properties of clear wood (Picea abies)

	u_{mean} in %	Quantity	ρ in kg/m³		$\frac{A_{net}}{A_{gross}}$
			$\bar{x}$	s	
Type a	8.5	10	412	27	1.0
Type b		10	413	29	0.8
Type c		10	416	27	0.8
Type d		10	415	26	0.8
Type e		10	423	22	0.88*
Type f		10	424	21	0.8

$\bar{x}$ Mean, s Standard deviation

* Based on inner thread diameter (∅ 6.1 mm)

2.4 Service Class 2

Analogously to the experimental series under 2.2 “Global reduction”, 150 tests were conducted to analyse the influence of fasteners in service class 2. Three different series were investigated:

- Type A-SC1: Non-weakened cross-section (service class 1)
- Type A-SC2: Non-weakened cross-section (service class 2)
- Type D-SC2: 2 x 5 self-tapping screws (SPAX T-STAR ∅ 10 mm with cut point) without pre-drilling (service class 2)

The inner thread diameter of the self-tapping screws (∅ 6.1 mm) causes a theoretical reduction of 15 %. The values of the material properties are given in Table 4.

Table 4: Material properties of glulam (GL24h) in service class 1 and 2

	Service class	Batch	u_{mean} in %	Quantity	$\rho_{oven\text{-}dry}$ in kg/m³			$\frac{A_{net}}{A_{gross}}$
					$\overline{x}$	s	$x_{0.05}$	
Type A-SC1	1		9.5	50	441	19	415	1.0
Type A-SC2	2	3	16.0	50	441	20	414	1.0
Type D-SC2	2		16.0	50	442	19	415	0.85

$\overline{x}$ Mean, s Standard deviation, $x_{0.05}$ 5th Percentile

3 Results

3.1 Global Reduction

Figure 5 shows typical failure patterns of the specimens after the compression tests. It is obvious that the zones in immediate proximity to the fasteners are the weakest cross-sections of the glulam members and exhibit the typical compression wrinkles. In some cases, a crack parallel to the grain can be observed. It is assumed that this failure starts in the area of contact between the wood and the fastener. The compression test results with glulam carried out according to EN 408 [5] are given in Table 5. The compression MOE $E_{c,0}$ and the strain ε_0 were established over the gauge length of 320 mm. Table 5 also shows the mean compressive strength, the standard deviation and the 5th percentile of the gross and the net cross-section. A comparison between the relative compression strength $f_{c,gross,Type\ X}$/ $f_{c,gross,Type\ A}$ and the net cross-section relating to the gross cross-section A_{net}/A_{gross} is summarized in the last two columns.

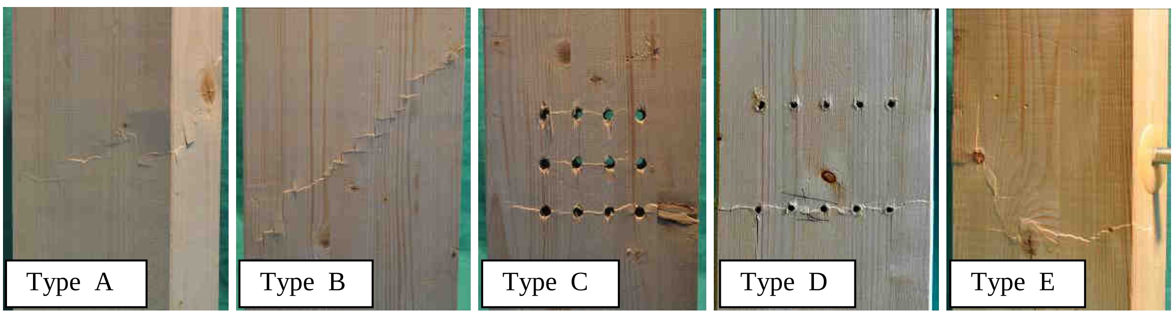

Figure 5: Failure patterns

Table 5: Results of compression tests with glulam (GL24h)

		$E_{c,o}$ MPa	$f_{c,gross}$ MPa	$f_{c,net}$ MPa	ε_0 %	$\frac{f_{c,gross,Type\ X}}{f_{c,gross,Type\ A}}$	$\frac{A_{net}}{A_{gross}}$
Type A1	$\overline{x}$	13,000	42.1		0.40		
Batch 1	s	1,400	3.3		0.05	1.0	1.0
N = 51	$x_{0.05}$	10,700	36.4		0.31		
Type B	$\overline{x}$	12,300	33.3	41.8	0.34		
Batch 1	s	1,400	2.0	2.5	0.04	0.79	0.8
N = 50	$x_{0.05}$	10,000	30.0	37.4	0.29		
Type C	$\overline{x}$	10,800	31.1	43.7	0.41		
Batch 1	s	1,000	1.8	2.6	0.05	0.74	0.71
N = 49	$x_{0.05}$	9,200	28.0	39.2	0.35		
Type A2	$\overline{x}$	12,900	39.8		0.40		
Batch 2	s	1,200	2.6		0.05	1.0	1.0
N = 51	$x_{0.05}$	10,800	35.4		0.32		
Type D	$\overline{x}$	12,500	35.8	42.3	0.41		
Batch 2	s	1,200	2.5	3.0	0.05	0.9	0.85
N = 50	$x_{0.05}$	10,400	31.5	37.2	0.32		
Type A3	$\overline{x}$	12,100	34.7		0.39		
Batch 3	s	1,000	1.9		0.04	1.0	1.0
N = 49	$x_{0.05}$	10,400	31.4		-		
Type E	$\overline{x}$	11,900	34.7	46.3	0.41		
Batch 3	s	1,200	1.9	2.5	0.06	1.0	0.75
N = 52	$x_{0.05}$	9,900	31.4	41.9	-		

N Quantity, $\overline{x}$ Mean, s Standard deviation, $x_{0.05}$ 5th Percentile

3.2 Local Reduction

The results of the compression tests with clear wood and specimens with a reduction in the cross-sectional area are given in Table 6. The values are similar, because of the similar structural properties. The failure patterns (cf. Figure 4) are similar to those which resulted from the tests with glulam members. The relative compression strength $f_{c,gross,Type\ x}$/ $f_{c,gross,Type\ a}$ and the net cross-section relating to the gross cross-section A_{net}/A_{gross} are given in the Table 6. The compressive strength of the specimens with glued-in dowels (type f) with $f_{c,net,Type\ f}$ = 50.1 MPa is higher than the mean value $f_{c,net} \approx 45$ MPa of the other types. Apart from that, the cross-section of specimen types b to f is weakened and hence the load-carrying capacity of clear wood ($f_{c,gross,Type\ a}$ = 45.9 MPa) decreases due to the presence of mechanical fasteners, e. g. $f_{c,gross,Type\ c}$ = 36.1 MPa.

Table 6: Results of compression tests with clear wood (Picea abies)

		$E_{c,o}$ MPa	$f_{c,gross}$ MPa	$f_{c,net}$ MPa	$\frac{f_{c,gross,Type\ x}}{f_{c,gross,Type\ a}}$	$\frac{A_{net}}{A_{gross}}$
Type a	$\bar{x}$	13,100	45.9	45.9	1.0	1.0
N = 10	*s*	3,200	4.8			
Type b	$\bar{x}$	11,900	34.7	43.4	0.76	0.8
N = 10	*s*	3,000	3.5			
Type c	$\bar{x}$	12,800	36.1	45.1	0.79	0.8
N = 10	*s*	2,900	2.9			
Type d	$\bar{x}$	12,700	37.2	46.4	0.81	0.8
N = 10	*s*	2,700	3.6			
Type e	$\bar{x}$	12,800	40.3	45.9	0.88	0.88
N = 10	*s*	2,500	3.0			
Type f	$\bar{x}$	12,800	40.1	50.1	0.87	0.8
N = 10	*s*	2,300	3.7			

N Quantity, $\bar{x}$ Mean, *s* Standard deviation

3.3 Service Class 2

Table 7 shows an extract from the results of the compression tests in order to compare the load-carrying capacity of glulam with a full cross-section in service class 1 (type A-SC1) to the load-carrying capacity in service class 2 (type A-SC2 and D-SC2). In addition to this, it shows the compression strength of specimens with inserted screws in service class 2.

Table 7: Results of compression tests with glulam (GL24h) in service class 1 and 2

		$f_{c,gross}$ MPa	u %	$\frac{f_{c,gross,Type\ D-SC2}}{f_{c,gross,Type\ A-SC2}}$	$\frac{A_{net}}{A_{gross}}$
Type A-SC1	$\bar{x}$	45.7	9.5	-	1.0
N = 50	*s*	3.1			
	$x_{0.05}$	40.4			
Type A-SC2	$\bar{x}$	31.8	16.0	-	1.0
N = 50	*s*	2.1			
	$x_{0.05}$	28.2			
Type D-SC2	$\bar{x}$	29.1	16.0	0.92	0.85
N = 50	*s*	1.8			
	$x_{0.05}$	25.9			

N Quantity, $\bar{x}$ Mean, *s* Standard deviation, $x_{0.05}$ 5th Percentile

3.4 Discussion

One can clearly notice a decrease of the load-carrying capacity under compression parallel to the grain, caused by the reduction of the cross-sectional area of glulam and clear wood. Even when the holes were filled with mechanical fasteners of higher stiffness than the wood and similar wood materials were used, different maximum compressive stresses in the gross cross-section were observed. The comparison of the relative loading capacity $R_{mean,weakened}/R_{mean,non\text{-}weakened}$ and A_{net}/A_{gross} of glulam is shown in Figure 6. The mean maximum compressive stress of the specimens with a steel-to-timber dowel connection (type c) is 26 % lower than the value of the non-weakened specimens. The theoretical reduction of the cross-sectional area amounts to 29 %. Even self-tapping screws without pre-drilling cause a decrease (approximately 10 %) of the load-carrying capacity which is not negligible. The results show that the present assumption, which is that reductions in the cross-sectional area may be ignored if the holes are filled with a material of higher stiffness than the wood, does not reflect reality. The failure patterns support this conclusion and identify stress peaks in the vicinity of the fasteners (cf. Figure 5). This shows that the reductions in the cross-sectional area have to be taken into account in the member strength verification. Exceptions are rods that are glued in, because they cause no obvious decrease of the load-carrying capacity in spite of a 25 % calculated reduction of the cross-sectional area.

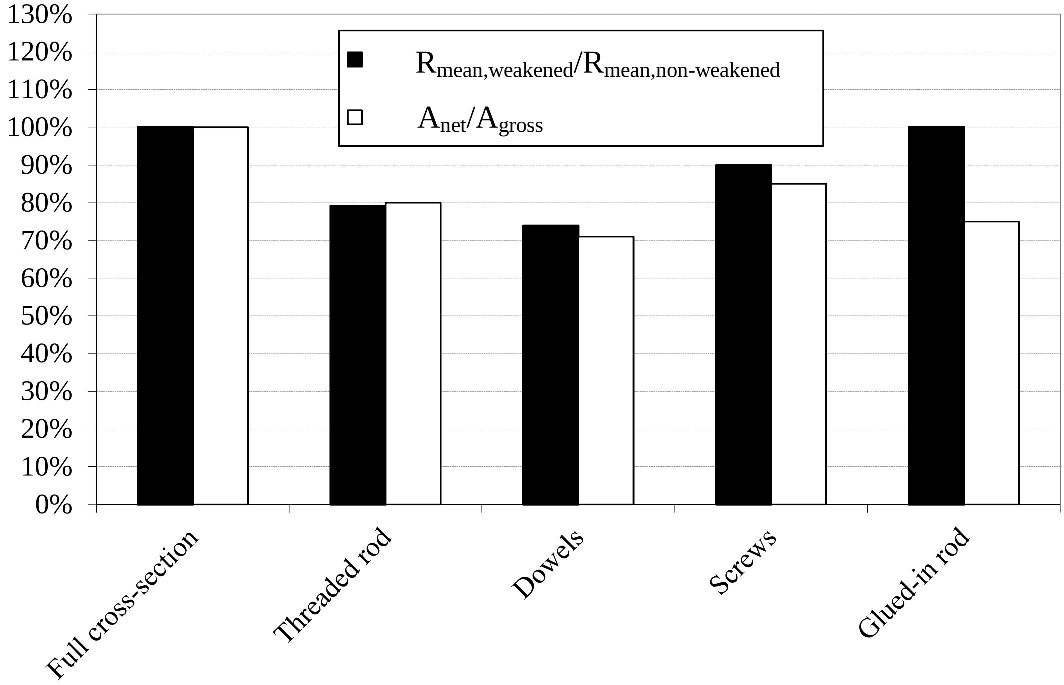

Figure 6: Load-carrying capacity and cross-sectional area of glulam specimen types related to the gross cross-section

The results of the compression tests (Table 6) and the failure patterns (e. g. Figure 4) of clear wood also show a reduction of the load-carrying capacity caused by inserting mechanical fasteners. Even inserting dowels with a rough surface, glued-in dowels with a smooth surface and self-tapping screws without pre-drilling cause significant stress peaks and compression failure in the vicinity of the mechanical fasteners. The mean capacities of the weakened specimens are 12 % to 24 % lower than the non-weakened specimens.

Based on theoretical and experimental investigations ([6] and [7]), it is established that the embedment strength of dowels with a rough surface increases in comparison to the embedment strength of dowels with a smooth surface and hence the load-carrying capacity of steel-to-timber dowel connections also rises. This effect is also observable for the load-carrying capacity under compression parallel to the grain. A rough surface has a beneficial effect on the load-carrying capacity. However, its influence is insignificant (cf. type c and d).

The tests of glulam members with low (9.5 %) and high (16 %) moisture content confirm the assumption (e. g. [8]) of a significant correlation between moisture content and compressive strength (cf. Figure 7). The results also show the influence of self-tapping screws in the compression area of glulam in service class 2. The mean load-carrying capacity of the specimen type D-SC2 is approx. 8-9 % lower than the load-carrying capacity of members without fasteners (type A-SC2).

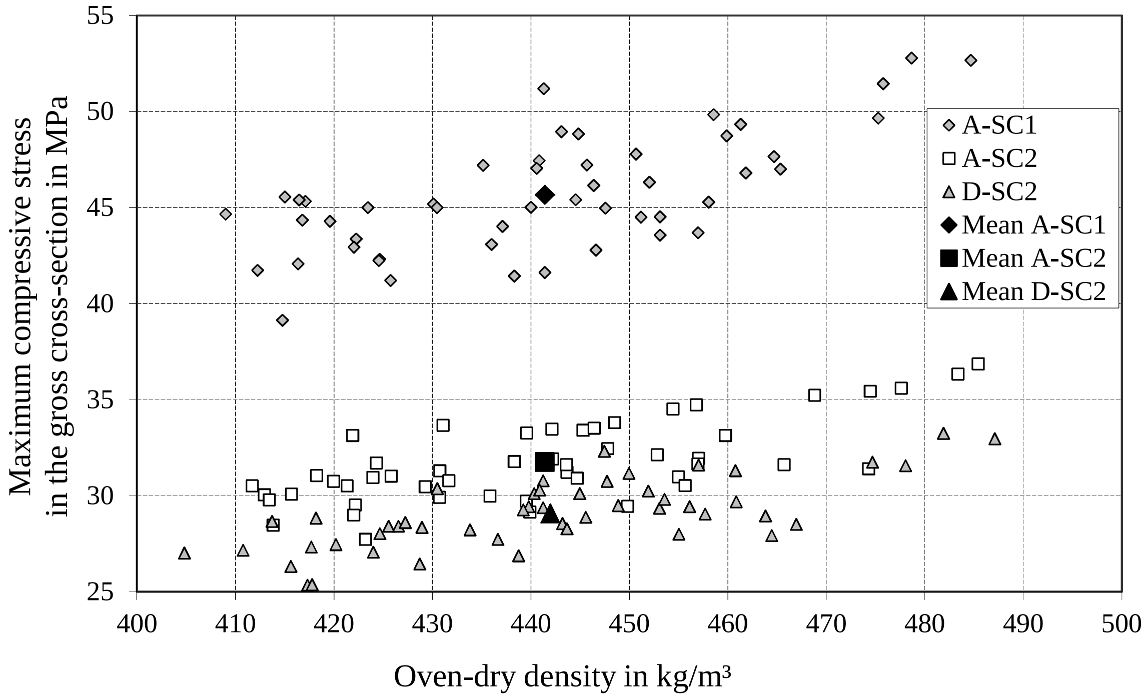

Figure 7: Maximum compressive stress in the gross cross-section depending on the mean specimen oven-dry density. Moisture content 9.5 % (type A-SC1) and 16 % (type A-SC2 and D-SC1)

4 Simulation of the Compression Area

The following part shows simulation results of a compression specimen with rough surface fasteners and its qualitative stress distribution. Two details were specifically examined:

- Stresses parallel to the grain in the vicinity of fasteners
- Stresses perpendicular to the grain below and above a mechanical fastener

A two-dimensional finite element model is used for the simulation of the compression tests using the ANSYS software. The size of the simulated specimen follows the dimensions of glulam members in chapter 2.2. The positions of the ten fasteners modelled in cylinder shape are identical to the positions of screws in the specimens type D. The state of stress is plane stress and the model is based on plane183-elements (6-node structural solid elements). In order to simplify the calculation, the homogeneous material, which is used, is assumed to be ideal-elastic-plastic (cf. [9]). This assumption deviates from reality; however, it is adequate enough for this study. A compression load was applied as a displacement of the upper edge of the specimen. Contact and target elements are used for modelling the contact between the mechanical fasteners and the wood. A friction coefficient is attributed to the contact elements enabling to consider the influence of fastener surface roughness.

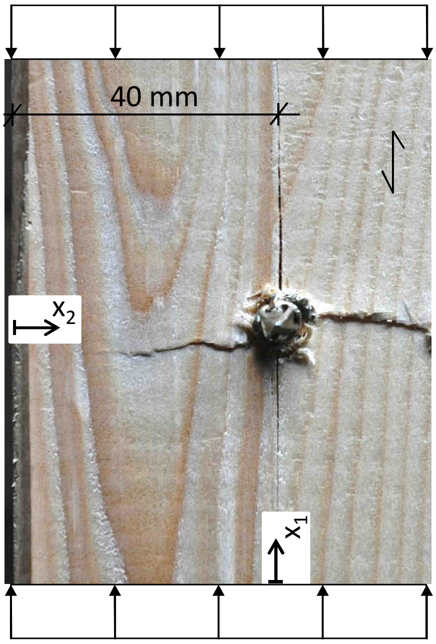

Analogous to the studies of dowel embedment strength from Rodd [6] and Sjödin et al. [7], the influence of friction on the stress peaks was considered. The difference between a rough and a smooth surface on the stress distribution of compression tests parallel to the grain was shown in an earlier contribution [10]. However, its influence on the compressive strength is insignificant.

The finite element model of a connection with a 10 mm diameter dowel and a coefficient of friction $\mu = 0.4$ was generated. Figure 9 shows the stresses perpendicular and parallel to the grain in the vicinity of the fastener in the leftmost position in consideration of five load steps until a strain $\varepsilon_0 = 0.31$ % in the direction of fibre. It is obvious that the results of a simulated doweled connection are transferable to the typical compression failure mode of a member with self-tapping screws (cf. Figure 8).

Figure 8: Typical failure mode of type D and definition of way x_1 and x_2

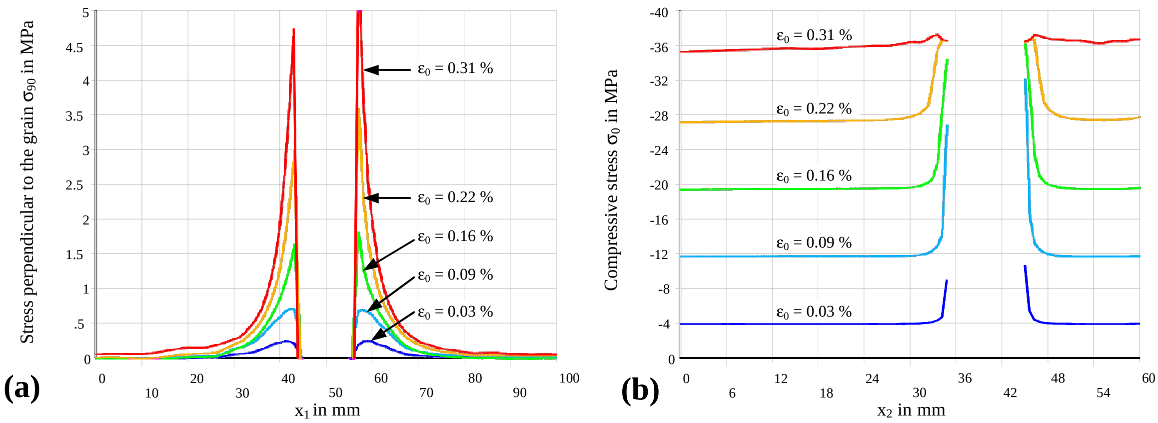

Figure 9: Stress distributions in the area of a dowel with a rough surface in the leftmost position plotted over way x_1 and x_2

The stress curves (cf. Figure 9 (a)) show the danger of splitting due to the stresses perpendicular to the grain. The result of these stresses is a crack parallel to the grain, shown in Figure 8. The stress curves of the compressive stress parallel to the grain are shown in Figure 9 (b). The stress peaks in the area of a mechanical fastener are evident in this numerical model even if a low strain ε_0 is put on the specimen.

5 Summary

The most important conclusion from this study is that mechanical fasteners weaken the cross-section significantly and hence the load-carrying capacity of the member in the connection area decreases. The traditional assumption ([1], [2], [3], [11] and [12]), that reductions in the cross-sectional area may be ignored if holes are filled with a material of higher stiffness than the wood, turns out to be wrong. The numerical simulation model supports this conclusion and shows stress peaks in the vicinity of the fasteners which coincide with the failure patterns of the compression tests. It is suggested to generally take into account reductions in the cross-sectional area in the member strength verification at least for service classes 1 and 2. Only glued-in rods do not reduce the load-carrying capacity in the compression area of wooden members.

The characteristic compressive strength parallel to the grain of an non-weakened cross-section in spruce glulam with a moisture content in the range of 9 to 13 % is higher (cf. [9] and [13]) than the corresponding nominal values in current product standards ([14] and [15]). Frese et al. [16] suggested a separation of the compressive strength for glulam with a maximum moisture content of 12 %, which corresponds to service class 1, and the compressive strength for glulam with a maximum moisture content of 20 % for service class 2. In this way, significantly higher strength values could be used for compression members in service class 1. However, it is still necessary to consider the holes in the compression area of members, even if the holes are filled with a material of higher stiffness than the wood.

6 References

[1] EN 1995-1-1 (2010) Design of timber structures – Part 1-1: General – Common rules and rules for buildings. European Committee for Standardization, Brussels

[2] DIN 1052 (2008) Entwurf, Berechnung und Bemessung von Holzbauwerken – Allgemeine Bemessungsregeln und Bemessungsregeln für den Hochbau. DIN Deutsches Institut für Normung e. V., Berlin

[3] DIN 1052 (1969) Holzbauwerke – Berechnung und Ausführung. DIN Deutsches Institut für Normung e. V., Berlin

[4] Blaß HJ, Enders-Comberg M (2012) Fachwerkträger für den industriellen Holzbau. Karlsruher Berichte zum Ingenieurholzbau, Band 22, Karlsruhe, KIT Scientific Publishing. ISBN 978-3-86644-854-4

[5] DIN EN 408 (2010) Holzbauwerke – Bauholz für tragende Zwecke und Brettschichtholz – Bestimmung einiger physikalischer und mechanischer Eigenschaften

[6] Rodd P (1973) The analysis of timber joints made with circular dowel connectors. Dissertation, University of Sussex, England

[7] Sjödin J, Serrano E, Enquist B (2008) An experimental and numerical study of the effect of friction in single dowel joints. Holz Roh-Werkstoff 66:363–372

[8] Neuhaus H (2011) Ingenieurholzbau Grundlagen – Bemessung – Nachweise – Beispiele. 3. Auflage, Vieweg + Teubner, Wiesbaden

[9] Frese M, Enders-Comberg M, Blaß HJ, Glos P (2011) Strength of spruce glulam subjected to longitudinal compression. Alghero, Italy. CIB-W18, Paper 44-12-2, ISSN 1864-1784

[10] Enders-Comberg M, Blaß HJ (2013) Querschnittsschwächung bei Druckbeanspruchung parallel zur Faser. Eur J Wood Prod 71:309-317, DOI 10.1007/s00107-013-0672-9

[11] Kollmann F (1951) Technologie des Holzes und der Holzwerkstoffe. Zweite Auflage, Band 1, Springer-Verlag, Berlin, Göttingen, Heidelberg

[12] Blaß HJ, Ehlbeck J, Kreuzinger H, Steck G (2005) Erläuterungen zu DIN 1052: 2004-08 Entwurf, Berechnung und Bemessung von Holzbauwerken. München, Bruderverlag

[13] Glos P (1978) Zur Bestimmung des Festigkeitsverhaltens von Brettschichtholz bei Druckbeanspruchung aus Werkstoff- und Einwirkungskenngrößen. Berichte zur Zuverlässigkeitstheorie der Bauwerke, Heft 35/78, Laboratorium für den konstruktiven Ingenieurbau, TU München

[14] prEN 14080 (2011) Timber structures – Glued laminated timber and glued solid timber – Requirements. DIN Deutsches Institut für Normung e.V., Berlin

[15] EN 1194 (1999) Timber structures – Glued laminated timber – Strength classes and determination of characteristic values. European Committee for Standardization, Brussels

[16] Frese M, Enders-Comberg M, Blaß HJ, Glos P (2012) Compressive strength of spruce glulam. Eur J Wood Prod, DOI 10.1007/s00107-012-0623-x

INTERNATIONAL COUNCIL FOR RESEARCH AND INNOVATION IN BUILDING AND CONSTRUCTION

WORKING COMMISSION W18 - TIMBER STRUCTURES

DESIGN OF SHEAR REINFORCEMENT FOR TIMBER BEAMS

P Dietsch

H Kreuzinger

S Winter

Lehrstuhl für Holzbau und Baukonstruktion

Technische Universität München

GERMANY

Keywords: glued laminated timber, shear, reinforcement, threaded rod, screw, composite section, structural anisotropy, semi-rigid composite, shear analogy

---

Pesented by P Dietsch

P Dietsch discussed the question whether the thesis covered cases where shear cracks followed a step pattern and did not follow a horizontal line. P Dietsch stated the model could consider such cases however friction could come into play in a step pattern which would not be considered.

M Fragiacomo stated it would be a good idea to pre-stress. P Dietsch stated that pre-stressing could be lost due to creep. M Fragiacomo suggested using a spring to maintain pre-stressing. P Dietsch stated this might not be the best idea.

A Frangi questioned whether minimum stiffness of the screw can be given. P Dietsch stated that a general method was presented without presenting a minimum value. He further discussed results from TU Munich and Karlsruhe Institute of Technology where different connectors were considered and large glued in rods achieved higher stiffness compared to self-tapping wood screws. H Blass commented that stiffness per unit length should be considered. P Dietsch commented that 45 degree inclined screw angle made the best option for shear reinforcement.

F Lam asked about availability of information for stiffness as a function of inclined angle. P Dietsch responded that not much information is available although the Karlsruhe data indicated a trend that the stiffness increased as the angle decreased.

U Kuhlmann stated that rehabilitation of existing structures could be an interesting field of study. P Dietsch agreed and stated there are many practical examples for such applications.

M Fragiacomo asked whether one can achieve full capacity using screws to reinforce a fully cracked beam. P Dietsch stated very close screw spacing would be needed to achieve full capacity.

Design of shear reinforcement for timber beams

P. Dietsch, H. Kreuzinger, S. Winter

Lehrstuhl für Holzbau und Baukonstruktion

Technische Universität München, Germany

1 Introduction and objective

The use of glulam beams with changing depth offers the possibility to adapt the section modulus to the bending moment. In the case of single-span beams under uniformly distributed load, however, a change in beam depth will lead to a contrary effect for the shear stresses, see Figure 1. Curved and pitched cambered beams feature not only high utilization rates in bending but also areas of high tension stresses perpendicular to the grain and shear parallel to the grain stresses, two stress components for which timber features only small capacities as well as brittle failure modes. Out of 245 cases of damaged or failed large-span timber structures, evaluated in [1], several failures document the possibility of a shear fracture (full separation) developing in grain direction from the curved part towards the supports, partly followed by a failure of the beam in flexural tension due to a change in stress distribution resulting from the change in section modulus. Reinforcements against tension stresses perpendicular to the grain in form of fully threaded screws or threaded rods can be considered state of the art [2], [3]. With respect to their application as shear reinforcement, not many research results are yet available [4], [5], resulting in a lack of experimentally validated design approaches.

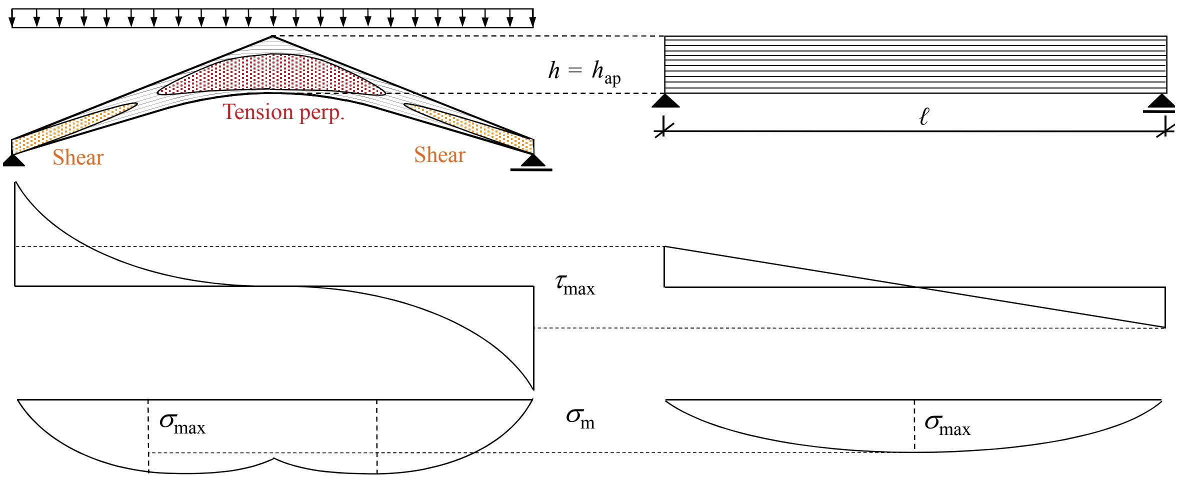

Figure 1: Schematic illustration of the distribution of shear stresses and bending stresses in straight beam and pitched cambered beam

Most approaches to design reinforcement against tension stresses perpendicular to the grain assume that the stresses are entirely carried by the reinforcement [2], [3]. However, with respect to an economic use of reinforcing elements it is of interest, whether a proportionate distribution of shear stresses between the timber beam and the shear reinforcement can be achieved in the unfractured state. This is particularly relevant, if a high number of reinforcing elements is necessary to achieve the full design capacity of the timber beam. For timber, the shear strength is in the range of five times the magnitude of tension perpendicular to the grain strength.

Within this paper, approaches to design shear reinforcement for glulam beams in the unfractured and the fractured state are presented, validated and discussed. The moment of failure, i.e. the transition from the unfractured to the fractured state is characterized by dynamic effects. This situation is not covered in this paper. A possible approach is given in [1]. The same applies to the subject of moisture induced stresses, resulting from the reinforcement restricting the free shrinkage or swelling of the glulam beam.

2 Design of shear reinforcement for the unfractured state

2.1 Analytical approach

In the following, an analytical approach is presented which allows calculating the effectivity of shear reinforcement in the unfractured state (see also [6]). Using matrix format, the approach is based on common theoretical concepts and constitutive equations for material properties. It considers the structural anisotropy of the cross-sections with shear reinforcement and enables to incorporate the semi-rigid composite action between the reinforcement and the wood material. The stresses caused by the shear forces are used to determine the shear strains which are in turn used to determine the stresses in the reinforcement and in the timber beam.

The approach is applicable to structural members featuring uniaxial load transfer and - within segments of the member - a uniform arrangement of reinforcing elements and uniform shear stress. The latter is given for beams under concentrated loads and correspondingly segment-wise constant shear stress. In the case of beams under uniform load, featuring common length to depth ratios, an adequate approximation can be assumed. For areas close to the supports ($0 \leq x \leq h$ from the support), separate investigations have to be carried out, if necessary. In the case of direct supports, the area close to the supports is subjected to compression stresses perpendicular to the grain, resulting in an increased shear capacity of the timber beam in this area [7].

The approach is based on the theory for composite materials. In [8] (and on the basis of [9] and [10]), anisotropic material properties of composite materials were derived for the example of laminated timber elements under in-plane loading and in bending. The orientation of the different layers of boards is accounted for; the effect of the composite action is described. In [11], these material properties were used in combination with the theory of composite materials to conduct numerical calculations on walls made of cross-laminated timber. The derivation of stiffness coefficients for individual layers with different orientation to enable a calculation of the overall stiffness of the system under consideration [8] can be transferred to reinforcement in timber elements.

According to the law of elasticity, the stress-strain-relationship of an element under in-plane loading in the *x*-*z*-plane (see Figure 2) is: $\varepsilon = S \cdot \sigma$. Inverting the matrix *S* leads to the stiffness matrix *C*, enabling to determine the resulting stresses due to known strains:

$$\begin{vmatrix} \sigma_x \\ \sigma_z \\ \tau_{xz} \end{vmatrix} = \begin{vmatrix} C_{11} & C_{12} & C_{13} \\ C_{21} & C_{22} & C_{23} \\ C_{31} & C_{32} & C_{33} \end{vmatrix} \cdot \begin{vmatrix} \varepsilon_x \\ \varepsilon_z \\ \gamma_{xz} \end{vmatrix} \quad \text{resp.} \quad \sigma = C \cdot \varepsilon = S^{-1} \cdot \varepsilon \tag{1}$$

Regarding a composite section, featuring two or more layers of structural elements with different orientations, the stiffness matrices of the individual layers have to be transformed into a global coordinate system. Using the global stiffness matrix, loads can be applied on the composite section. Based on this, the resulting strains are determined, which are in turn used to determine the stresses in the individual layers of structural elements. The procedure is shown schematically in Figure 2. Since the local coordinate system of layer 1 coincides with the global coordinate system, neither a transformation of its stiffness matrix (C_1), nor of the strains determined for the global system (ε_0) is required. Therefore, for the calculation of the global stiffness matrix, only the stiffness matrix of layer 2 (C_2) has to be transformed into the global system. According to the law of elasticity, the strains (ε_0) of the composite section can be determined by a multiplication of the inverse global stiffness matrix (C_0^{-1}) with a load vector (n_0). To determine the stresses in layer 2 (n_2), the strains in the global system have to be rotated into the local coordinate system of layer 2.

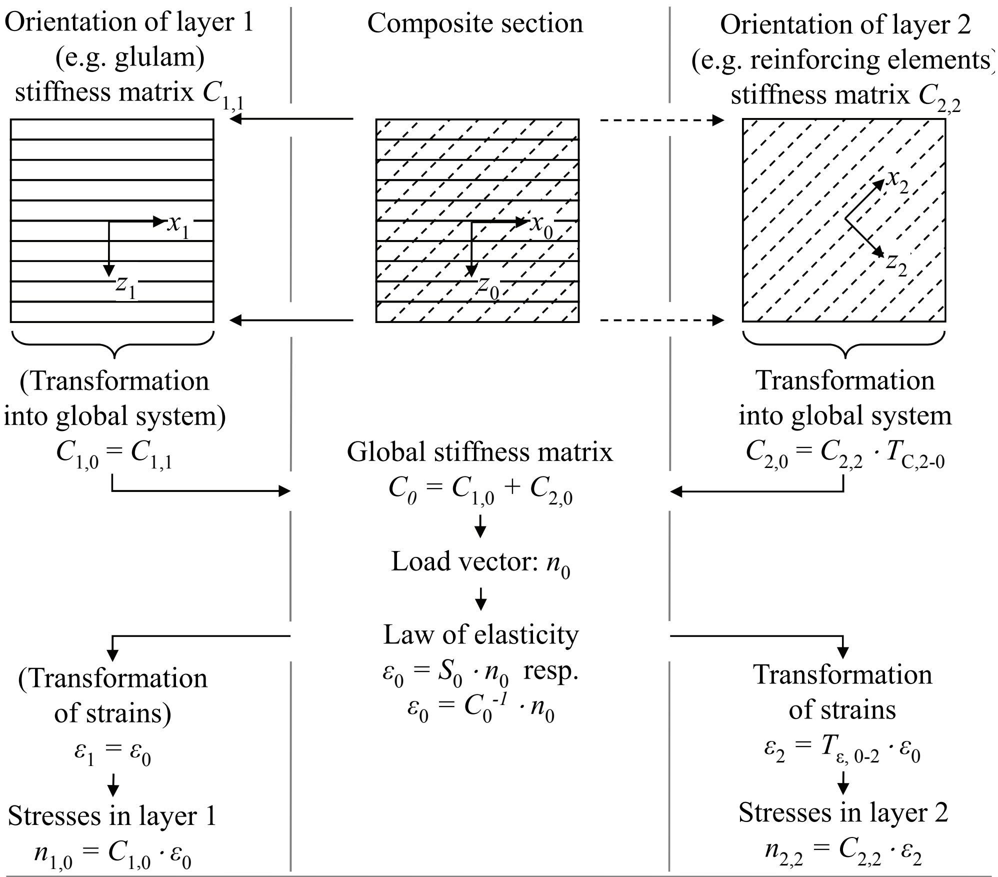

$C_{i,j}$ Stiffness matrix of layer *i* relating to coordinate system *j*
$T_{C,i\text{-}j}$ Matrix to transform the stiffness matrix from coordinate system *i* to *j*
$T_{\varepsilon,i\text{-}j}$ Matrix to transform the strains from coordinate system *i* to *j*
$n_{i,j}$ Stresses in layer *i* relating to coordinate system *j*

Figure 2: Calculation procedure based on the structural anisotropy

2.2 Application to shear reinforcement

The before explained method can also be applied to glulam elements (and cross-laminated timber (CLT) elements) featuring shear reinforcement, see [6]). For simplification, the global coordinate system should be matched with the local coordinate system of the timber section, see Figure 3.

Considering the coordinates and angular relationships defined in Figure 3, the stiffness coefficients of the reinforcing elements can be transformed into the global system, following common mechanical rules (see e.g. Equation 3 and [6]). The same is valid for the strains in the reinforcing elements which are determined by transforming the strains in the global system into the local coordinate system (see e.g. Equation 9 and [6]).

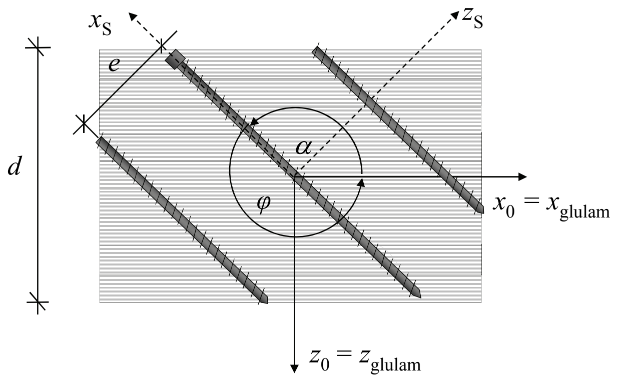

x_0, z_0	global coordinates (= local coordinates of glulam element)
x_S, z_S	local coordinates of reinforcing elements
φ, α	Angles for transformation
e	Distance of reinforcing elements perpendicular to longitudinal axis
d	Element depth
b	Element width (perpendicular to plane of representation)

Figure 3: Denomination of coordinates and angles for the transformation of stiffness parameters within the structural anisotropy

2.2.1 Determination of stiffness parameters in the global system

When determining the global stiffness, the cross-sectional layup of the structural element to be reinforced has to be considered. In the case of glulam elements, constant material properties are assumed in direction of the global coordinates, meaning that the stiffness matrix of the glulam element, $C_{GL,0}$, is a result of the material parameters in the respective directions. Due to the lack of precise data for wood and for purposes of simplification, the Poisson's ratio μ is set to zero.

$$C_{GL,0} = \begin{vmatrix} E_0 & 0 & 0 \\ 0 & E_{90} & 0 \\ 0 & 0 & G \end{vmatrix} \tag{2}$$

Assuming that the shear reinforcement in the form of threaded rods or fully threaded screws is primarily loaded in axial direction, the axial stiffness EA_S of the reinforcement is essential with respect to the load bearing behavior. The bending stiffness has a minor effect and is therefore neglected for reasons of simplification. By means of the transformation matrix, the stiffness matrix of the reinforcement with respect to the global system, $C_{S,0}$, can be determined as follows:

$$C_{S,0} = \left(\frac{n_s}{b} \cdot \frac{EA_S}{e}\right) \cdot T_{C,S-0} = \left(\frac{n_s}{b} \cdot \frac{EA_S}{e}\right) \cdot \begin{vmatrix} \cos^4\varphi & \sin^2\varphi \cdot \cos^2\varphi & -\sin\varphi \cdot \cos^3\varphi \\ \sin^2\varphi \cdot \cos^2\varphi & \sin^4\varphi & -\sin^3\varphi \cdot \cos\varphi \\ -\sin\varphi \cdot \cos^3\varphi & -\sin^3\varphi \cdot \cos\varphi & \sin^2\varphi \cdot \cos^2\varphi \end{vmatrix} \tag{3}$$

with:

EA_S	Axial stiffness of the reinforcing elements
n_S	number of rows of reinforcing elements perpendicular to loaded plane

The total stiffness of the composite section in the global system, C_0, is determined by adding the stiffness matrices of the glulam element, $C_{GL,0}$, and the reinforcement, $C_{S,0}$.

$$C_0 = C_{GL,0} + C_{S,0} \tag{4}$$

2.2.2 Determination of stresses

The load on a reinforced timber element can be introduced by means of the vector n_0. The vector contains the stresses σ_{x0} and σ_{z0} in the main axes of the global system as well as the shear stresses τ_{xz0} in the x-z-plane. The stresses applied by the vector n_0 are constant in the segment under consideration. The strains resulting from the given stresses are determined by multiplying the vector n_0 with the inverse stiffness matrix C_0^{-1}:

$$\varepsilon_0 = C_0^{-1} \cdot n_0 \tag{5}$$

Due to the differently oriented local coordinate systems, the strains determined for the global system are used to separately determine the stresses in the glulam element and the shear reinforcement.

Glulam element:

Since the local coordinates of the glulam element coincide with the global coordinates, no transformation of the strains is necessary when determining the stresses.

$$n_{GL} = C_{GL,0} \cdot \varepsilon_{GL} = C_{GL,0} \cdot \varepsilon_0 \tag{6}$$

A comparison between the shear stresses in the global system τ_{xz0} and the resulting shear stresses in the glulam element $\tau_{GL,xz0}$ delivers the degree of strengthening η_τ, which describes the reduction in shear stress due to the reinforcement.

$$\eta_\tau = \frac{\tau_{xz_0}}{\tau_{GL,xz_0}} \tag{7}$$

In addition, Equation (6) delivers the normal stress component $\sigma_{GL,z0}$. If the arrangement is chosen so that the shear reinforcement is loaded in axial tension, the resulting stresses in the glulam element are in compression perpendicular to the grain. Several experimental investigations, e.g. [12], [13], [14] have shown, that compression stresses perpendicular to the grain have a positive effect on the shear capacity. This means that the shear reinforcement leads not only to a reduction of shear stresses in the timber but, in the case of appropriate arrangement, to a stress interaction which has a positive effect on the shear capacity of the glulam element. In [4], based on the results given in [12], the following equation is proposed:

$$\tau = 4.75\ N/mm^2 - 1.15 \cdot \sigma_\perp - 0.13 \cdot \sigma_\perp^2 \qquad [N/mm^2] \tag{8}$$

Shear reinforcement:

The stresses in the shear reinforcement are determined by transforming the strains in the global coordinate system into the local coordinate system of the shear reinforcement. Since only the axial stiffness EAs of the shear reinforcement is considered, it is sufficient to calculate the strain parallel to the axis of load transfer of the reinforcement.

$$\varepsilon_S = \varepsilon_0 \cdot T_{\varepsilon,0-S} \quad \text{here:} \quad \varepsilon_{x_S} = \begin{vmatrix} \varepsilon_{x_0} \\ \varepsilon_{z_0} \\ \gamma_{xz_0} \end{vmatrix} \cdot \begin{vmatrix} \cos^2\alpha & \sin^2\alpha & \sin\alpha \cdot \cos\alpha \end{vmatrix} \tag{9}$$

The stresses in the axis of the reinforcement σ_S in each reinforcing element are:

$$\sigma_{S,x_S} = \varepsilon_{x_S} \cdot E_S \tag{10}$$

2.2.3 Incorporation of the semi-rigid composite action between the reinforcement and the wood material

In the determination of the global stiffness matrix C_0, see 2.2.1, a rigid bond between the shear reinforcement and the glulam element is assumed. This is approximately the case, if glued-in rods are applied, see e.g. [15]. Reinforcing with pre-drilled, screwed-in threaded rods or fully threaded screws leads to a semi-rigid composite action between the wood material and the thread of the reinforcement. It is therefore necessary to take into account that different strains occurr in the timber section and the reinforcement. The semi-rigid composite action can be incorporated by an embedment modulus (modulus of foundation). This can be determined from appropriate tests, see e.g. [16].

Alternatively it is possible to describe the semi-rigid composite action with the axial slip modulus $K_{ax,ser}$, which is usually included in the technical approvals of fully threaded screws or threaded rods. This is comparable to a spring stiffness and enables to determine the relative displacement between an axially loaded screw or rod and the wood surface.

The axial slip modulus $K_{ax,ser}$ is only of limited suitability for the method presented, since it does not provide information about the distribution of shear stresses in the embedding wood material and the resulting distribution of normal forces in the reinforcing element. However, it is possible to deduce an embedment modulus from the coefficient $K_{ax,ser}$. For this purpose, the load-bearing behavior of the reinforcement can be described by an equivalent mechanical system that consists of an elastically (in the direction of the reinforcement) supported beam, see Figure 4.

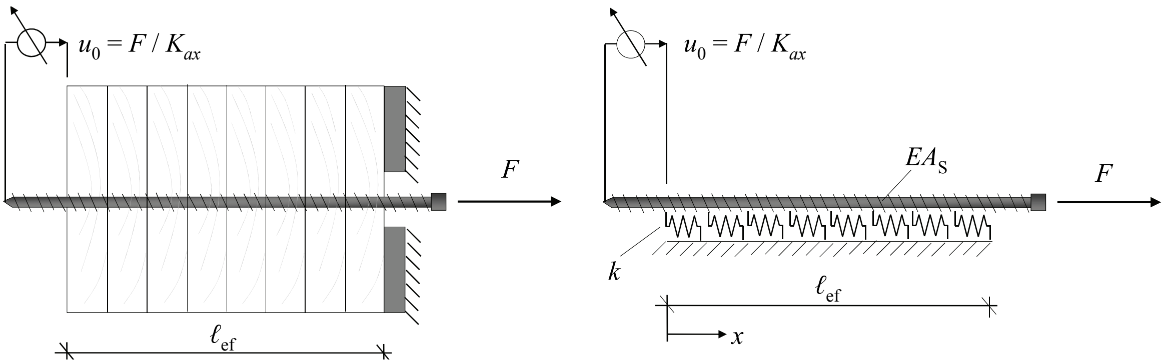

Figure 4: Experimental setup to determine K_{ax} [17] and equivalent mechanical system

The general approach for the homogeneous solution of the differential equation of the beam on horizontally elastic foundation is:

$$u_{(x)} = C_1 \cdot e^{\lambda \cdot x} + C_2 \cdot e^{-\lambda \cdot x} \qquad \text{with:} \quad \lambda = \sqrt{k / EA_S} \tag{11}$$

Taking into account the present boundary conditions, the following solution for the differential equation can be obtained:

$$\lambda \cdot \left(e^{\lambda \cdot l_{ef}} - e^{-\lambda \cdot l_{ef}} \right) = 2 \cdot K_{ax} / EA_S \tag{12}$$

The coefficient λ can be determined iteratively or by using appropriate software. Subsequently the embedment modulus *k,* can be calculated with Equation 13.

$$k = \lambda^2 \cdot EA_S \tag{13}$$

Values for the axial slip modulus $K_{ax,ser}$, given in literature or technical approvals, are generally valid for angles of 90° between the screw or rod axis and the grain direction (as shown in Figure 4. In the case of shear reinforcement, the typically applied angle is 45° (as shown in Figure 5). In [4], axial slip moduli were determined for screwed-in threaded rods of d = 16 mm and 20 mm, penetration lengths of 200 mm and 400 mm and angles between the rod axis and the grain direction of 45° and 90°. For angles of 45°, higher axial slip moduli are determined. In addition, a disproportionate (above-average) increase of the axial stiffness is determined when doubling the penetration length. When applying these values within the analytical method, it should be considered that the applicable length ℓ_{ef} corresponds to half the length of the reinforcing element, see Figure 5.

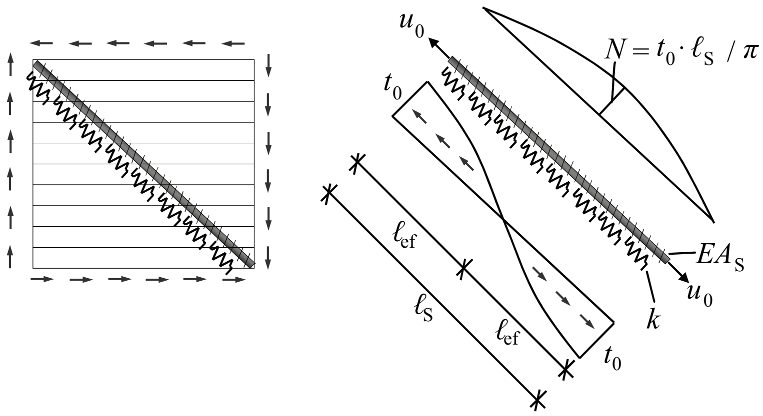

Figure 5: Semi-rigid composite between reinforcement and the wood material

Different methods exist to account for the semi-rigid composite action between two structural elements. One common approach in structural timber design is the γ-method [7]. This method is mostly applied to timber-concrete composite elements or mechanically jointed beams, however it can be extended in order to utilize it for the semi-rigid composite action of shear reinforcements. In this case, the relationships given in Figure 5 apply.

Assuming that the shear deformation of the glulam element will approximately result in a sinusoidal distribution of axial force in the reinforcement, the distribution of shear flow in the embedment has to follow cosinusoidal form. The deformation u_0 is a combination of the deformations in the composite and in the reinforcement under normal force.

$$u_0 = \frac{t_0}{k} + t_0 \cdot \frac{(2 \cdot l_{ef})^2}{\pi^2} \cdot \frac{1}{EA_S} \tag{14}$$

The deformation of a reinforcing element with an effective axial stiffness $efEA_S$ under given load, and without consideration of the elastic foundation, is calculated as follows:

$$u_0 = t_0 \cdot \frac{(2 \cdot l_{ef})^2}{\pi^2} \cdot \frac{1}{efEA_S} \tag{15}$$

Combining Equations (14) and (15), the effective axial stiffness $efEA_S$ is obtained:

$$efEA_S = EA_S \cdot \frac{1}{1 + \dfrac{\pi^2 \cdot EA_S}{(2 \cdot l_{ef})^2 \cdot k}} = EA_S \cdot \gamma \tag{16}$$

In analogy to the γ-method, the axial stiffness of the reinforcing element can be reduced by the factor γ to account for the semi-rigid composite action. For the stiffness matrix of the reinforcement with respect to the global system, the following applies:

$$C_{S,0} = \left(\frac{n_s}{b} \cdot \frac{efEA_S}{e} \right) \cdot T_{C,S-0} = \left(\frac{n_s}{b} \cdot \frac{\gamma \cdot EA_S}{e} \right) \cdot T_{C,S-0} \tag{17}$$

The semi-rigid composite action leads to the following equation to determine the axial stresses $\sigma_{S,xs}$ in each reinforcing element:

$$\sigma_{S,x_S} = \varepsilon_{x_S} \cdot \gamma \cdot E_S \tag{18}$$

$$N_{S,x_S} = \varepsilon_{x_S} \cdot \gamma \cdot EA_S \tag{19}$$

with: factor γ according to Equation (16)

2.3 Comparison with experimental tests

To validate the design method for shear reinforcement in the unfractured state, experiments on glulam beams, shear reinforced with fully threaded screws were performed. First, non-destructive tests, according to EN 408 [18], were performed in the linear-elastic range to determine the effective shear stiffness of the reinforced glulam beams. The same specimen was tested several times, while its properties (reinforcement) were changed between the experiments. Cracks were introduced in half of the twelve glulam specimens, to study a potential increase in the effect of the reinforcement in cracked members. After assessing the pros and cons of introducing cracks through drying processes or mechanically (in which the wood fibers are cut locally), latter option was chosen since only in this case, the depth of the crack and remaining cross-section can clearly be defined. After testing all specimens without shear reinforcement, two configurations of shear reinforcement (at a distance of 160 mm and 80 mm) were applied and tested, see Figure 6. For this, fully threaded screws, featuring a diameter $d = 8$ mm and a length $\ell_S = 280$ mm were used [19].

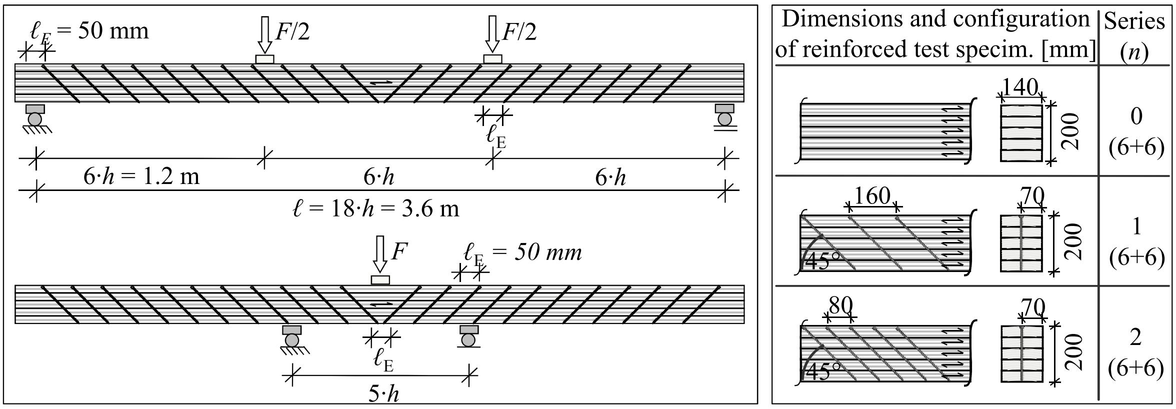

Figure 6: Experimental tests to determine the effective shear modulus G of glulam elements with fully threaded screws as shear reinforcement - experimental setup and geometry

Based on the data obtained from the unreinforced elements, the expected effective shear modulus G was determined for the reinforced elements by means of the analytical method. The embedment modulus k of the reinforcement was derived from test results for fully threaded screws in glulam, given in [4] and [20]. The increase of the effective shear modulus G, determined from tests and analytical calculations, was for all configurations in the single digit percentage range. The results of the analytical calculations and the experimental results are compared in Figure 7. The compression perpendicular to the grain stresses induced into the glulam element by the reinforcement were too small to have a positive influence in terms of the stress interaction between shear and compression perpendicular to the grain.

The test results confirm the small effect of the reinforcing elements on the shear stiffness (see also [5]) and hence the low transfer of shear from the glulam beams to the shear reinforcement in the unfractured state. The reduction of shear stiffness due to the cracks could clearly be seen. For the second level of reinforcement, no further increase of the effective shear modulus could be observed. Comparative experiments to study a potential reduction of the axial slip modulus $K_{ax,ser}$ in the case of repeated loading could not confirm this possibility. On the contrary, an improvement of stiffness of the composite between reinforcement and the wood material was found in the case of repeated loading [1]. A possible explanation can be concluded from the known sensitivity of the shear modulus G to the apparent modulus of elasticity $E_{app,}$ see [21], which has to be determined at small span $\ell = 5 \cdot h$ (see Figure 6 lower part) and hence small deformations w and high loads F.

A comparison with two other methods to determine the shear modulus (dynamic response, shear field) showed that the applied bending method returned the most acceptable accuracy.

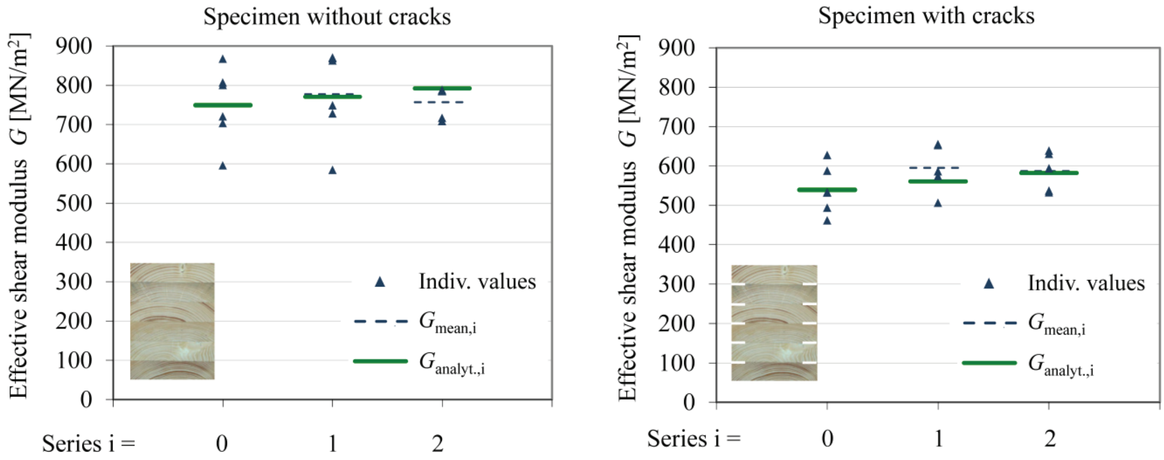

Series	i=0	i=1	i=2
$G_{mean,i}$ [MN/m²]	749,3	777,3	757,0
$G_{Analyt,i}$ [MN/m²]		770,8	792,2
$G_{Analyt,i}$ / $G_{mean,i}$		99%	105%

Series	i=0	i=1	i=2
$G_{mean,i}$ [MN/m²]	539,4	595,1	586,8
$G_{Analyt,i}$ [MN/m²]		560,9	582,3
$G_{Analyt,i}$ / $G_{mean,i}$		94%	99%

Figure 7: Effective shear modulus G of glulam beams with and without cracks at different levels of shear reinforcement – comparison of analytical approach with experimental results

After the non-destructive tests in the linear-elastic range had been completed, the beams were cut into smaller segments. By removing some of the screws, three different configurations of reinforcement could be realized with at least ten specimens for each configuration, see Figure 8. The destructive tests to determine the shear strength of each series were carried out again on the basis of EN 408 [18], see Figure 8.

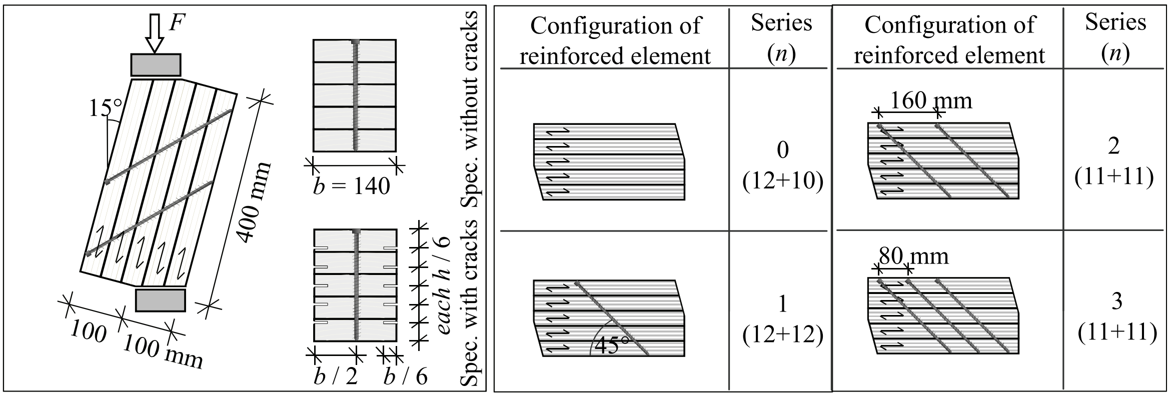

Figure 8: Experimental tests to determine the shear strength f_v of glulam elements with self-tapping screws as shear reinforcement – experimental setup and geometry

The experimental and analytical results were in accordance with abovementioned finding. Again, the increase in shear strength was only in the single digit percentage range, see Figure 9. Here, the influence of compression stresses perpendicular to the grain on the shear capacity was taken into account using the abovementioned proposal. The increase in shear strength determined in the tests correlates well with the tensile load-carrying capacity of the screws in direction of the shear plane [4]. For the specimens featuring more reinforcing elements (series 2 and 3), a resumption of load-carrying capacity could be observed at lower load-level after the shear fracture. Here, after fracture, the load was carried by the screws. The activation of friction led to an additional load-carrying capacity. The shear strength of specimens with cracks was on average 14% lower than that for the specimens without cracks. The reason is believed the local weakening of the cross-section due to the local cutting of the wood fibers when introducing the cracks mechanically.

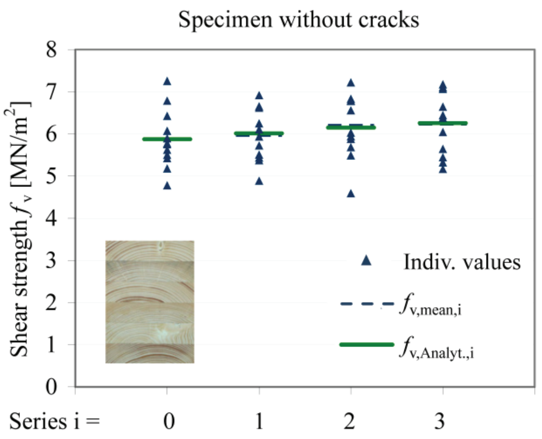

Series	i=0	i=1	i=2	i=3
$f_{v,mean,i}$ [MN/m^2]	5,87	5,96	6,21	6,22
$f_{v,Analyt,i}$ [MN/m^2]		6,01	6,15	6,26
$f_{v,Analyt,i} / f_{v,mean,i}$		101%	99%	101%

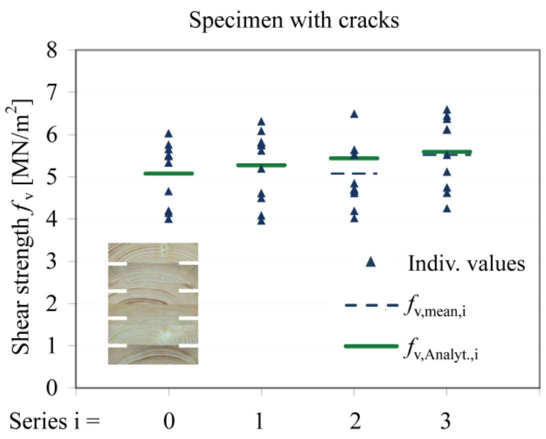

Series	i=0	i=1	i=2	i=3
$f_{v,mean,i}$ [MN/m^2]	5,08	5,29	5,08	5,52
$f_{v,Analyt,i}$ [MN/m$^{2]}$		5,27	5,44	5,59
$f_{v,Analyt,i} / f_{v,mean,i}$		100%	107%	101%

Figure 9: Shear strength f_v of glulam elements with and without cracks at different levels of shear reinforcement – comparison of analytical approach with experimental results.

For the purpose of further validation, previous experiments carried out by [4] with glulam beams featuring shear reinforcement in form of fully threaded screws or screwed-in threaded rods, were calculated using the analytical method. For this comparison, all test series were utilized which complied with the prerequisites for the application of the analytical method (i.e. consistent positioning of the reinforcing elements). Furthermore, the axial slip moduli $K_{ax,ser}$, determined by the same authors [4] were applied. In the experiments, considerable increases of the shear capacity (max. 38 %) were recorded, due to the partly very high extent of reinforcement. The differences between the experimentally obtained shear capacity and the analytical results were on average below 4%. Also, the negative influence of tension stresses perpendicular to the grain on the shear strength, occurring in the case of reinforcing elements under compression, was approximated well.

3 Design of shear reinforcement for the fractured state

The analytical approach presented in chapter 2 to calculate the effectiveness of shear reinforcement, ends with the shear fracture of the timber beam. During the destructive tests it was found, that after shear fracture of the glulam element, the reinforcing elements were mostly still intact and able to carry loads, resulting in the activation of frictional resistance in the fracture plane. This finding can be considered positive with respect to the robustness of the reinforced beam: reinforcement can be designed to carry the full shear stresses parallel to the grain or tension stresses perpendicular to grain in the damaged state, preventing a full separation of the upper and lower parts of the beam in the case of a fracture. Thereby the reinforcement introduces internal redundancy since it provides a second barrier against brittle failure mechanisms, see Figure 10 and [22].

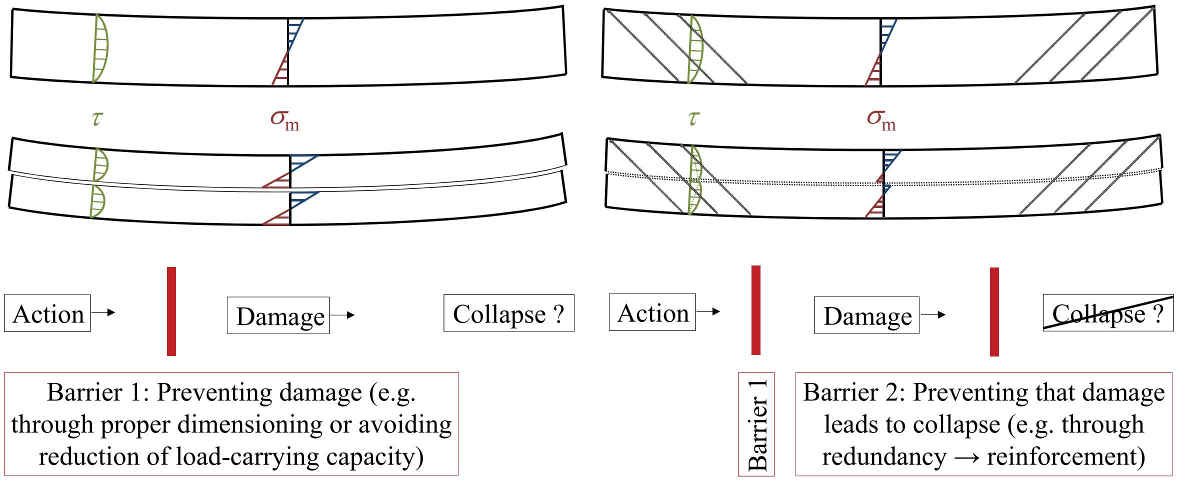

Figure 10: Barrier model in terms of robustness considerations

A method to calculate the load-carrying capacity of the two parts of the beam, mechanically jointed by reinforcing elements, is given by the shear analogy developed by Kreuzinger (e.g. [23], [24], [25] and [3]). Here, the composite section is transformed into an imaginary two-point section, featuring two levels A and B which are only coupled in terms of deflections. Level A represents the proportion of the unconnected layers to the bending rigidity of the complete section. Accordingly, the sum of bending stiffness of the individual parts is assigned to level A. The shear stiffness of level A is infinite. Level B describes the interaction of the individual parts of the cross-section due to the composite effect, i.e. the influence of shear deformation in or between the layers. Accordingly, an equivalent shear stiffness is assigned to level B which is derived from the stiffness of the fasteners/reinforcement and their distance or the shear stiffness of the layers. In addition, the bending rigidity assuming a rigid bond between the layers (parallel axis theorem) is assigned to level B. After determining the internal forces in the imaginary system, the real stresses in the individual parts of the composite section are calculated by reverse transformation. Figure 11 contains a schematic representation of the procedure.

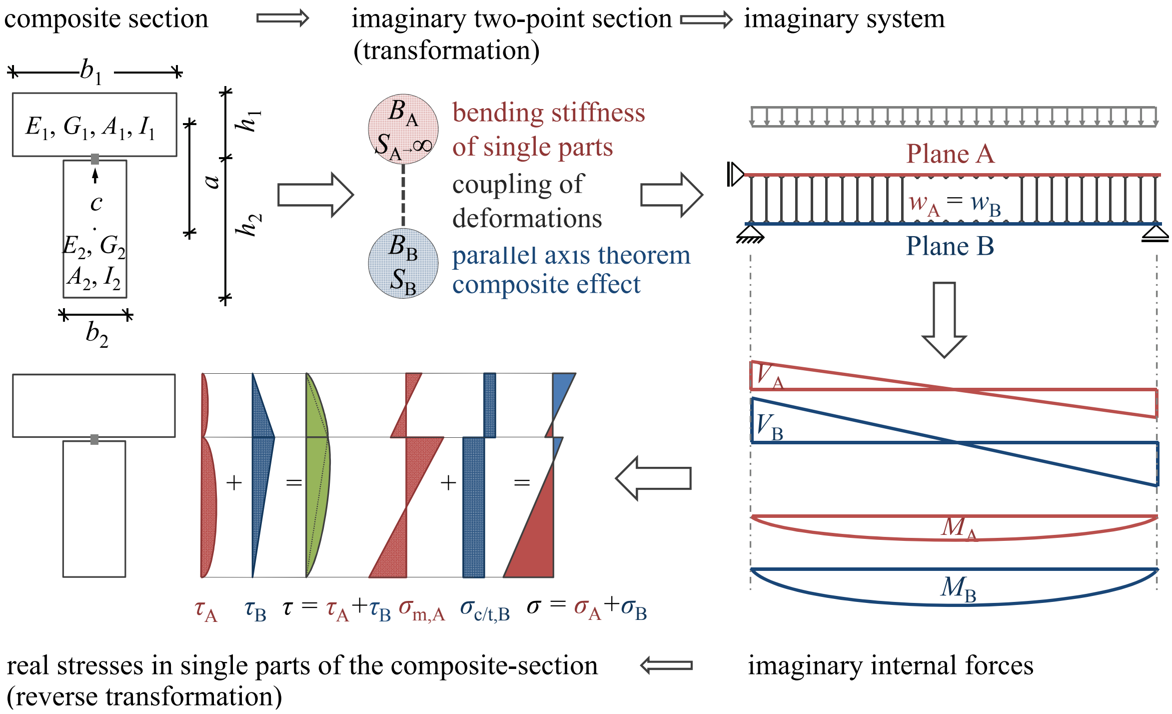

Figure 11: Schematic representation of the procedure applied in the shear analogy

The shear analogy is suitable for a computer-based implementation by means of structural analysis software. This software, e.g. 2-D frame programs, has to be able to account for shear deformation. Computer-based implementation creates the possibility of a segment-wise definition of the section properties and stiffness values. This enables the calculation of beams with varying depth and segment-wise variable stiffness of the joint between the cross-sections.

Using this method, a parametric study on curved and pitched cambered beams was performed, featuring geometries which are 1) relevant for building practice and 2) feature a high utilization rate in bending, shear and tension perpendicular to the grain. To determine the relevant geometries, all boundary conditions associated with curved and pitched cambered beams were varied in equal step sizes, whereby all relevant stress verifications were performed [1]. With predefined lower bounds (economical limit) and upper bounds (stress limits), a relevant subset was determined for each stress verification. By superimposing these subsets, the intersecting set of geometries which are relevant with regard to abovementioned objectives was determined. From this set, ten samples were selected for each beam shape (curved and pitched cambered beams). These samples covered the entire intersecting set of highly stressed geometries. For these geometries, a minimum reinforcement was determined to carry the shear flow and tension perpendicular to the grain stresses, occurring after fracture of the timber beam. Here, the approach was that the load-carrying capacity of the reinforcing elements just covered the occurring stresses, i.e. the reinforcing elements are fully utilized and placed at maximum possible distances. Due to the correlation between joint stiffness and resulting shear flow, this process is iterative. To cover the worst case in terms of bending stresses, the fracture plane was assumed to occurr at half the beam depth. A possible frictional resistance in the fracture plane was neglected. The axial slip moduli $K_{\mathrm{ax,ser}}$ of the pre-drilled and screwed-in threaded rods were taken from [4]. Characteristic values for the load-carrying capacity of threaded rods, $F_{\mathrm{ax,Rk}}$ and $F_{\mathrm{v,Rk}}$, are given for example in [26]. With regard to the slip moduli K_{ser} and the necessary number of reinforcing elements to carry the occurring stresses in tension perpedicular to the grain, a standardized procedure was applied [2]. The length segment featuring reinforcements was varied between 10 % and 20 % of the total beam length, starting at the supports, so that in extreme cases the total beam length featured reinforcements (including reinforcement against tension stresses perpendicular to the grain in the curved part).

In the case of the smallest chosen length segment featuring shear reinforcement, the maximum increase of bending stresses, compared to the intact (unfractured) state, reached 33 %, see Figure 12. This can be explained by the high axial slip moduli of the threaded rods and the resulting high joint stiffness. This in turn results in high shear flows and thus - taking into account the axial load-carrying capacity of the threaded rods - in rather small distances of the reinforcing elements. At a given level of joint stiffness, an increase of the joint stiffness will only result in a highly under-proportional increase of shear flow and thus in only marginal changes of bending stresses. Between the different forms of beams, only minor differences of utilization factors could be determined. With increasing ratio $\ell/(h_{\mathrm{ap}}$ or $h_1)$, the utilization rate slightly increased.

An increasing length of the segment featuring shear reinforcement resulted in a significantly lower increase of bending stresses in the case of fracture. Furthermore, with an increasing length of shear reinforced area, a significant change in magnitude of shear flow but only a marginal change in the sum of shear flow to be transferred was determined. Accordingly, the sum of necessary reinforcing elements increases only marginally with increasing length of the shear reinforced segment, meaning that the maximum possible distances between the reinforcing elements increase in a nearly linear manner.

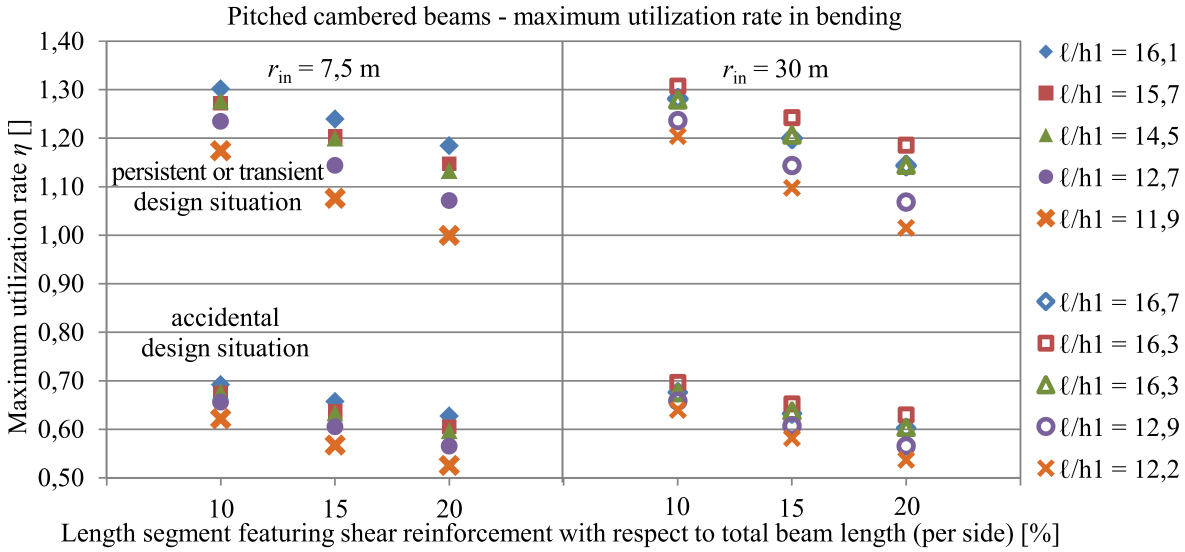

Figure 12: Exemplary results (pitched cambered beam) of the parametric study on the increase of bending stresses in the case of fracture of the glulam beam – variation of geometry and arrangement of shear reinforcement

To validate the results presented above, selected forms of curved and pitched cambered beams were calculated using the finite element method [27]. The calculations were performed using two different models, 1) a model with plane elements and spring elements to model the stiffness of the reinforcing elements and 2) a model with plane elements in which the reinforcing elements were completely modelled by beam elements, see [1] and [28] for further information. The results obtained with both models were almost identical. The beam geometries were chosen to differ greatly from the form of a straight beam, i.e. the variation of depth as well as the curvature were distinctive. The comparison was made based on the bending stresses on the top and bottom edge along the length of the beam. A comparison with the results obtained with the shear analogy showed good agreement for the areas of the beam with varying depth. In the apex area (within ca. $\pm 2 \cdot h_{ap}$) however, the differences were not negligible. They were more pronounced in the case of short lengths of shear reinforced area in comparision to longer lengths featuring shear reinforcement. The reason for the differences is mainly described by the fact that the shear analogy is derived from the beam theory, while the non-linear stress-distribution in the apex area of curved or pitched cambered beams has to be approximated by plate theory [29]. Accordingly, a significantly better fit could be achieved when the coefficients given in [29] are applied to account for the non-linear stress distribution However it should be noted that these coefficients were not derived for the given case of the fractured, mechnically jointed cross-section. In all cases, the shear analogy method provided slightly higher absolute values of maximum bending stresses, i.e. delivered results on the safe side.

4 Conclusions

An analytical approach is proposed to determine the load-carrying capacity of timber beams in the intact (unfractured) state, featuring shear reinforcement in form of threaded rods or fully threaded screws. A comparison was conducted with results from laboratory tests with reinforced glulam beams as well as with experimental data from other research institutions. This showed good agreement between the experimental shear stiffness and analytically determined stiffness as well as experimental failure load and analytically determined load-carrying capacity. The best agreement is found if the increase in shear capacity due to the interaction between shear and compression stresses perpendicular to the grain is taken into account, in addition to the proportional load uptake of the reinforcement. The quality of the results depends on the accuracy of the input parameters (e.g. the axial slip modulus of the fully threaded screws or threaded rods) and the principles describing the effect of stress interaction on shear capacity.

Considering the intact (unfractured) state, comparative calculations of glulam elements which are reinforced by threaded rods indicate that, under realistic constructive conditions (dimensions and configuration), an increase in shear capacity of up to 20% is feasible. These calculations include a potential reduction of shear capacity of the glulam beam due to e.g. shrinkage cracks as well as the influence of relaxation effects. Preliminary investigations with respect to a further increase in shear capacity by using threaded rods show, that an examination of pre-stressed threaded rods, anchored in disc springs with degressive spring characteristics (load-deformation curves) could prove adequate. In existing structures, the upper portion of the threaded rod could be screwed or glued into the timber beam and the remaining part of the threaded rod would remain without bond. The anchorage of the lower part of the threaded rod in the disc springs could be realized by means of nuts, which could simultaneously be used for applying the pretensioning force.

With respect to internal redundancy of the reinforced beam against brittle failure mechanisms such as shear or tension perpendicular to the grain it is possible to design the reinforcing elements such that they prevent the complete separation of the upper and lower parts in the event of fracture of the beam along the grain. For the fractured beam, which is mechanically jointed by the reinforcing elements, an applicable approximation method is given by the shear analogy. This method is also applicable to curved and pitched-cambered beams in which the maximum bending stresses occur outside the apex zone. In these cases, the shear analogy method provides slightly higher absolute values of maximum bending stresses, i.e. delivers results on the safe side. Extensive comparative calculations of highly stressed shapes of glulam beams, featuring the minimum required reinforcement to carry the released stresses after fracture, show that the maximum increase in bending stresses between the intact state and the fractured state is in the range of one third. When the accidental design situation is applied for this case, it translates into a maximum utilization rate of 70%. Due to the resulting high level of joint stiffness, a change of joint stiffness will only have a minor influence on the magnitude of bending stresses. A reduction of the distance of the reinforcing elements or the use of glued-in instead of pre-drilled, screwed-in threaded rods would not lead to any noteworthy improvement of stress levels in the fractured state. However, an increasing length of the segment featuring shear reinforcement leads to significantly lower increase in bending stresses in the case of fracture of the beam along the grain. The sum of shear flow to be transferred increases only marginally. It is therefore desirable to choose an arrangement of the shear reinforcement over longer segments of the beam length since this also implicates clear benefits for construction practice due to larger possible distances between the reinforcing elements.

Literature

[1] Dietsch, P., Einsatz und Berechnung von Schubverstärkungen für Brettschichtholzbauteile, Dissertation, Technische Universität München, 2012.

[2] DIN 1052:2008-12, Entwurf, Berechnung und Bemessung von Holzbauwerken. Allgemeine Bemessungsregeln und Bemessungsregeln für den Hochbau, DIN, Berlin, 2008.

[3] DIN EN 1995-1-1/NA:2010-12, Nationaler Anhang – National festgelegte Parameter – Eurocode 5: Bemessung und Konstruktion von Holzbauten – Teil 1-1: Allgemeines – Allgemeine Regeln und Regeln für den Hochbau, DIN, Berlin, 2010

[4] Blaß, H.-J., Krüger, O., Schubverstärkung von Holz mit Holzschrauben und Gewindestangen, Karlsruher Berichte zum Ingenieurholzbau, Band 15, Universitätsverlag Karlsruhe, 2010.

[5] Trautz, M., Koj, C., Mit Schrauben Bewehren – Neue Ergebnisse, Bautechnik, Vol. 86, No. 4, 2009, pp. 228-238.

[6] Dietsch, P., Mestek, P., Winter, S., Analytischer Ansatz zur Erfassung von Tragfähigkeitssteigerungen infolge von Schubverstärkungen in Bauteilen aus Brettschichtholz und Brettsperrholz, Bautechnik, Vol. 89, No. 6, 2012, pp. 402-414.

[7] EN 1995-1-1:2004, Eurocode 5: Design of timber structures – Part 1-1: General – Common rules and rules for buildings, CEN, Brussels, 2004.

[8] Lischke, N., Zur Anisotropie von Verbundwerkstoffen am Beispiel von Brettlagenholz, Fortschritts-Bericht VDI, Reihe 5, Nr. 98, VDI-Verlag, Düsseldorf, 1985.

[9] Klöppel, K., Schardt, R., Systematische Ableitung der Differentialgleichungen für ebene anisotrope Flächentragwerke, Stahlbau, Vol. 29, No. 2, 1960, pp. 33-43.

[10] Lekhnitskii, S., G., Anisotropic Plates (translated from Russian by Tsai, S.,W., Cheron, T.,G.), Gordon and Breach Science Publishers, New York London Paris, 1968.

[11] Bosl, R., Zum Nachweis des Trag- und Verformungsverhaltens von Wandscheiben aus Brettlagenholz, Dissertation, Universität der Bundeswehr, München, 2002.

[12] Spengler, R., Festigkeitsverhalten von Brettschichtholz unter zweiachsiger Beanspruchung, Teil 1 - Ermittlung des Festigkeitsverhaltens von Brettelementen aus Fichte durch Versuche, Berichte zur Zuverlässigkeitstheorie der Bauwerke, Heft 62, LKI der TU München, 1982.

[13] Hemmer, K., Versagensarten des Holzes der Weißtanne (Abies Alba) unter mehrachsiger Beanspruchung, Dissertation, TH Karlsruhe, 1984.

[14] Steiger, R., Gehri, E., Interaction of shear stresses and stresses perpendicular to the grain, CIB-W18 / 44-6-2, Proceedings of the international council for research and innovation in building and construction, Working commission W18 - timber structures, Meeting 44, Alghero, Italy, 2011.

[15] abZ. Nr. Z-9.1-705 vom 26. Januar 2009, 2K-EP-Klebstoff WEVO-Spezialharz EP 32 S mit WEVO-Wärter B 22 TS zum Einkleben von Stahlstäben in Holzbaustoffe, DIBt, Berlin, 2009.

[16] Mestek, P., Punktgestützte Flächentragwerke aus Brettsperrholz (BSP) - Schubbemessung unter Berücksichtigung von Schubverstärkungen, Dissertation, Technische Universität München, 2011.

[17] Blaß, H.J., Bejtka, I., Uibel, T., Tragfähigkeit von Verbindungen mit selbstbohrenden Holzschrauben mit Vollgewinde, Karlsruher Berichte zum Ingenieurholzbau, Band 4, Universitätsverlag Karlsruhe, 2006.

[18] EN 408:2003, Timber structures - Structural timber and glued laminated timber - Determination of some physical and mechanical properties, CEN, Brussels, 2003.

[19] abZ. Nr. Z-9.1-519 vom 07. Mai 2007, SPAX-S Schrauben mit Vollgewinde als Holzverbindungsmittel - ABC Verbindungstechnik GmbH & Co. KG, Ennepetal, DIBt, Berlin, 2007

[20] Mestek, P., Winter, S., Konzentrierte Lasteinleitung in Brettsperrholzkonstruktionen – Verstärkungsmaßnahmen, Schlussbericht zum AiF-Forschungsvorhaben Nr. 15892, Lehrstuhl für Holzbau und Baukonstruktion, Technische Universität München 2011.

[21] Divos, F., Tanaka, T., Nagao, H., Kato, H., Determination of shear modulus on construction size timber, Wood Science and Technology, Vol. 32, No. 6, 1998, pp. 393-402.

[22] Dietsch, P., Robustness of large-span timber roof structures - Structural aspects, Engineering Structures, Vol. 33, No. 11, 2011, pp. 3106–3112.

[23] Kreuzinger, H., Platten, Scheiben und Schalen – ein Berechnungsmodell für gängige Statikprogramme, Bauen mit Holz, Vol. 101, No. 1, 1999, pp. 34-39.

[24] Kreuzinger, H., Verbundkonstruktionen, in: Holzbaukalender 2002, Bruderverlag, Karlsruhe, 2001, pp. 598-621.

[25] Kreuzinger, H., Mechanically Jointed Beams: Possibilities of Analysis and some special Problems, CIB-W18 / 34-12-7, Proceedings of the international council for research and innovation in building and construction, Working commission W18 - timber structures, Meeting 34, Venice, Italy, 2001.

[26] abZ. Nr. Z-9.1-777 vom 30. November 2010, Gewindestangen mit Holzgewinde als Holz-verbindungsmittel – SFS Intec GmbH, Oberursel, DIBt, Berlin, 2010.

[27] ANSYS, Release 12.0, ANSYS Inc., Canonsburg/PA, 2010

[28] Danzer, M., Verstärkte Brettschichtholzträger veränderlichen Querschnitts, Master Thesis, Lehrstuhl für Holzbau und Baukonstruktion, Technische Universität München 2011.

[29] Blumer, H., Spannungsberechnungen an anisotropen Kreisbogenscheiben und Satteltr];gern konstanter Dicke, Lehrstuhl für Ingenieurholzbau und Baukonstruktionen, Universität Karlsruhe, 1972/1979.

INTERNATIONAL COUNCIL FOR RESEARCH AND INNOVATION IN BUILDING AND CONSTRUCTION

WORKING COMMISSION W18 - TIMBER STRUCTURES

MODELLING THE BENDING STRENGTH OF GLUED LAMINATED TIMBER - CONSIDERING THE NATURAL GROWTH CHARACTERISTICS OF TIMBER

G Fink

A Frangi

ETH Zurich, Institute of Structural Engineering, Zurich

SWITZERLAND

J Kohler

NTNU, Department of Structural Engineering, Trondheim

NORWAY

Keywords: glued laminated timber, natural growth characteristics, modelling GLT, hierarchical model, censored regression

---

Presented by G Fink

M Li asked about the basis for justifying the assumption on tension strength of finger joints. G Fink stated the finger joint was considered as 0.2 KAR. Finger joint strength would be dependent on the strength of the wood as well as the manufacturing process.

E Serrano received clarification that the resolution of FEM was 50 mm and transverse direction was taken as an element. They tried more elements but not much effect.

R Görlacher clarified that in the research performed at Karlsruhe Institute of Technology knot clusters were never divided into two (corrected by the author in the published paper).

R Foschi stated he likes the approach of using model to predict performance since a verified model can be used to study size effect and quality control techniques. In UBC he worked with industry to develop similar models. He asked for clarification how failures were defined and when failed elements were removed to continue the analysis. The majority of failure was defined as first failure.

F Lam commented that since finger joint failure dominated the failure mode it would make sense to obtain experimental data on finger joint strength rather than relying on assumptions.

JW van de Kuilen commented that the laminate E seemed to have low variability. G Fink stated that it seemed to be consistent with other studies.

H Blass stated that model can be used to consider timber from different regions to expand the variability of the resource.

R Harris commented that the model considered only tension failure and did not consider cases where compression failure initiated the failure. G Fink stated that the influence from model of such effect would be small.

A Buchanan agreed the usefulness of the approach but commented that with other species this work would need to start again. G Fink agreed.

Modelling the bending strength of glued laminated timber - considering the natural growth characteristics of timber

Gerhard Fink[1)], Andrea Frangi[1)], Jochen Kohler[2)]
[1)] ETH Zurich, Institute of Structural Engineering, Zurich, Switzerland
[2)] NTNU, Department of Structural Engineering, Trondheim, Norway

1 Introduction

Timber is a natural grown material. Thus, compared to other building materials, timber properties demonstrate higher variability. The variability is pronounced between different structural elements (e.g. through different growth conditions) and within single elements (through knots and knot clusters). In Nordic spruce timber specimens knot clusters are distributed over the length of a board with rather regular longitudinal distances. Within glued laminated timber (GLT) the variability is slightly reduced through the homogenisation effect. However, because of the relatively regular distance between knot clusters the joint appearance of knot clusters from different lamellas in the same cross section is quite frequent.

The load bearing capacity of GLT, or rather the characteristic value of the bending strength $f_{\mathrm{m,g,k}}$ is investigated since more than 20 years within numerous different studies [1]. The outcome of the majority of these studies is an empirical equation to predict $f_{\mathrm{m,g,k}}$ based on the properties of the source material; e.g. $f_{\mathrm{t,0,l,k}}$ and $f_{\mathrm{m,j,k}}$. From an scientific perspective those equations are often unreproducible. One example therefore is the equation given in the current pre-version of the EN 14080 [2], that contains altogether 7 empirical values; c.f. Eq. (1). However, the basis for these models are in general test results or model simulations. Regarding the huge number of influencing parameters the latter has to be established as the more efficient within the last decades. Examples are the *Model of Foschi and Barrett* [3], the *Prolam model* [4, 5] or more recently the *Karlsruher Rechenmodel* [6, 7, 8].Until now, none of the existing models have ever been validated on GLT with well-known local material properties; i.e. the exact position of each particular knot cluster and each particular finger joint connection.

$$f_{\mathrm{m,g,k}} = -2.2 + 2.5 f_{\mathrm{t,0,l,k}}^{0.75} + 1.5(f_{\mathrm{m,j,k}}/1,4 - f_{\mathrm{t,0,l,k}} + 6)^{0.65} \tag{1}$$

In the present research project, a model for the probabilistic representation of the material properties of GLT is developed that considers the natural growth characteristic of timber. Further, 24 GLT beams with well-known local material properties are produced and tested in order to validate the model.

2 Experimental investigation

Within this project a total amount of 24 GLT beams with well-known local material properties are investigated under 4-point bending. The beams are produced out of $2 \cdot 200$ lamellas of two strength grades L25 and L40 (Norway spruce); the grading of the lamellas is performed by the GoldenEye 706 grading device [9]. Lamellas of this grade classes fulfil the requirements for the production of GL24h and GL36h, respectively [10, 11, 12]. At this point it has to be mentioned that the strength grade GL36h is no longer existing within the current pre-version of the EN 14080 [2]. However, the new version was not published when the project started and the former code is still valid.

In a first step of the experimental investigation the material properties of the lamellas, which are used for the GLT fabrication, are investigated non-destructively. From all lamellas the dimensions and the position of each knot with a diameter larger than 10mm is assessed and recorded. Additional, several indicators to predict the mean stiffness (Eigenfrequency, ultrasonic runtime and density) and the moisture content are measured. On half of the specimens non-destructive tensile tests are performed to estimate the tensile stiffness within the lamellas by using an infrared camera device. Prior to the experiment every board is subdivided into two types of sections: Knot sections (KS) and clear wood sections (CWS); KS representing sections containing knot clusters or single major knots and CWS representing sections between the KS. From all these sections the stiffness properties are measured (Fig. 1). The tensile tests are conducted on the lamellas, that are indented to be used in the tensile loaded area of the GLT.

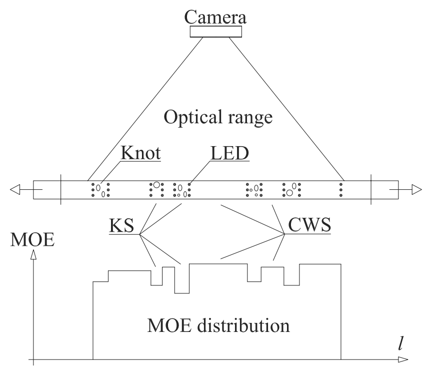

Fig. 1: Illustration of the test setup

Out of the investigated lamellas GLT beams are produced. Hereby the position of each lamella and each finger joint connection (denoted FJ) is defined, previously. Thus, beams are produced where the exact position and the strength properties of each particular lamella within the beams is well-known; i.e. (1) the position of each FJ, (2) the position of each knot with a diameter larger then 10mm, (3) the estimated mean stiffness of each lamella and (4) the stiffness properties of each KS and CWS located in the tensile loaded area of the beams are known. In Fig. 3 the material properties within one GLT beam are illustrated: (a) total knot area ratio - tKAR, (b) dynamic MOE based on Eigenfrequency measurement E_F and (c) measured tensile stiffness E_{t}. The black lines show the position of FJ. In the following 4-point bending tests are conducted to estimated the bending capacity $f_{\mathrm{m,g}}$ and the bending stiffness $E_{\mathrm{m,g}}$. Further the type of failure (KS, CWS, FJ) is investigated for all specimens (Fig. 2). A detailed description of all conducted experiments including test results is presented in [13, 14].

3 GLT - Model

In this research project a model for the probabilistic representation of the material properties of GLT is developed that considers the natural growth characteristic of timber. The principle idea of the developed model is comparable to existing models; i.e. GLT beams having a specific beam set-up are simulated and their bending capacity will be estimated. The approach presented here is illustrated in Fig. 4 and will be explained in more detail in the following.

3.1 Simulation of timber boards

Based on the results of the experimental investigations a model is developed, that describe the growth characteristic of timber boards (strength grades L25, L40). That includes a representation of the geometrical setup as well as a hierarchical representation of strength and stiffness related indicators (tKAR, E_F).

Fig. 2: Failed GLT member

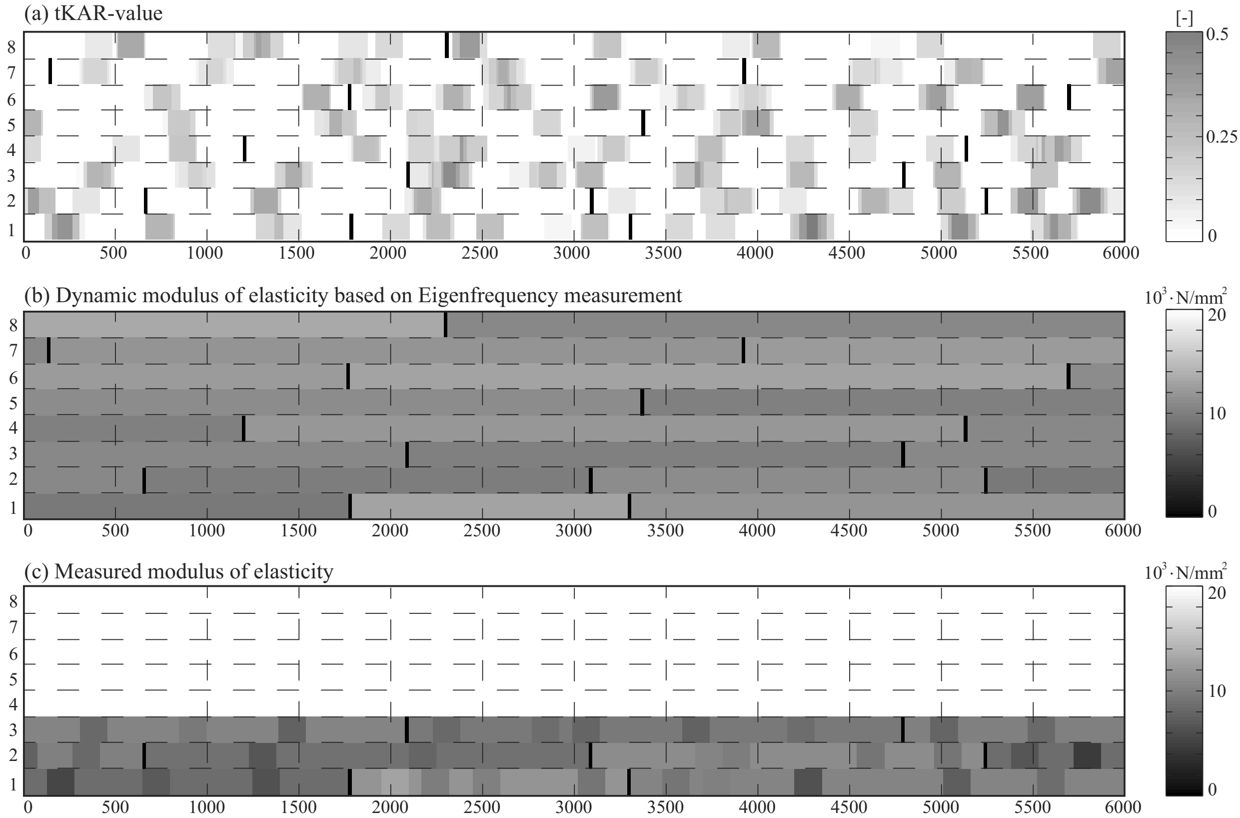

Fig. 3: Material properties within GLT

The geometrical setup of timber boards is described with the distance d between weak sections (denoted WS). A WS is defined as a knot cluster with tKAR $\geq$ 0.1, having a constant length $l_{\text{WS}} = 150$mm. d is defined as the distance between the mid-points of two adjacent WS. In a growing tree the appearance of knot clusters in the longitudinal direction of the stem might be represented by a Poisson process and therefore the distances between knot clusters would be exponential distributed. When sawing out timber boards from a tree not every knot cluster might appear in every particular board. The distance between knot clusters that appear in the boards might be best represented by the gamma distribution, which corresponds to the distribution of the distance between the i^{th} and $i + k^{th}$ occurrence of a Poisson process. The distribution is generalized when k is not an integer. According to definition, a WS has a constant length ($l_{\text{WS}} = 150$mm). Thus the minimal distance between two adjacent WS is $d_{\min} \geq 150$mm. Accordingly a shifted gamma distribution is used to describe d; Eq. (2). Between the two strength grades only marginal differences are identified, that correspond to the findings presented in Colling [15]. Consequently d is identified for all specimens, independent of the strength grade. The estimated parameters are summarized in Tab. 1. The parameters correspond to $\text{E}(d) = 529$mm and $\sigma(d) = 246$mm. Compared to former studies here the expected value is relatively large; e.g. Isaksson [16]: $\text{E}(d) = 494$mm,

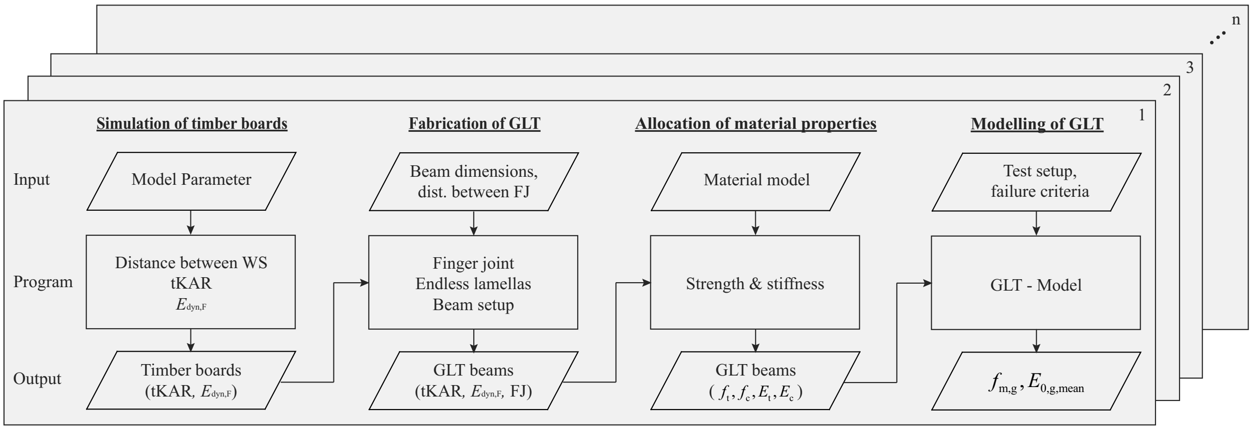

Fig. 4: Framework for modelling GLT

Colling [15]: $\mathrm{E}(d) = 450 - 500$mm. The difference is a result of the definition of WS. Here a WS is defined as a section with tKAR ≥ 0.1. Choosing a lower tKAR-value more WS will be detected and thus d would decrease; e.g. tKAR $= 0.05 \rightarrow \mathrm{E}(d) = 485$mm, $\sigma(d) = 215$mm.

As mentioned above the appearance of the knot clusters within one particular tree is relatively regular. Thus it seems likely to model d hierarchically; i.e. with a mean d of a timber board and a variability of d within the board. However the investigation shows that this approach is not efficient. This might be a result of the sawing process combined with the definition of a WS - not every knot cluster within the tree might appear as a WS in every particular timber board. Further explanation might be the limited amount of data.

$$f(d) = \frac{\nu(\nu(d - l_{\mathrm{WS}}))^{k-1}}{\Gamma(k)} e^{-\nu(d - l_{\mathrm{WS}})} + l_{\mathrm{WS}} \quad \text{for} \quad l_{\mathrm{WS}} \leq d \leq \infty \tag{2}$$

Both strength and stiffness related indicators are described using a log-normal distribution; Eq. (3-4). The first parameter E_F is essential to model the mean material properties within a timber board. Whereas the other one, the tKAR-value will be used to model the local strength and stiffness reduction through knots. For modelling the tKAR-value the distribution has to be truncated in the upper part. According to definition, the tKAR-value of every board section has to be within the interval $[0, 1]$. Through to grading process an upper limit $\mathrm{tKAR}_{\mathrm{limit}}$ could be introduced. It is obvious that $\mathrm{tKAR}_{\mathrm{limit}}$ decrease with an increase of the strength grade. However it has to be considered that in reality the grading process is not perfect; i.e. there is a certain probability that the tKAR-value of WS exceed the defined threshold. Thus in the present study no upper limit through the grading process is introduced.

Assuming the truncated lognormal distribution with ($\mathrm{tKAR}_{\mathrm{max}} = 1$) the expected values of tKAR of the two documented strength grades are 0.240 and 0.192, respectively. Compared to former studies here the mean tKAR is relatively high; e.g. Colling and Dinort [15] measured a mean tKAR of $0.15 - 0.20$ (considering only sections with tKAR ≥ 0.1). The reason for the increase might be the different grading criteria of the two studies. Further it should be considered that the time between the studies is more than 25 years and thus the requirements of the forest and the sawmill industry have changed.

The tKAR-value of the WS is described by a hierarchical model having two hierarchical levels (Kersken-Bradley and Rackwitz [17], Köhler [18]): Meso scale and micro scale. The tKAR-value of the WS j in a board i (tKAR_{ij}) is represented as a truncated lognormal random variable. μ is the logarithm mean tKAR of all WS within a sample of boards, considered to be deterministic. The meso scale $\tau_i \sim N(0, \sigma_\tau)$ describes the variability of a single board within a sample of boards. The micro scale $\varepsilon_{ij} \sim N(0, \sigma_\varepsilon)$ describes the variability within one board.

$$E_F = \exp(\mu + \tau_i) \tag{3}$$

$$\text{tKAR}_{ij} = \exp(\mu + \tau_i + \varepsilon_{ij}) \quad \text{with} \quad \tau_i + \varepsilon_{ij} \leq \text{tKAR}_{\max} - ln(\mu) \tag{4}$$

The estimated model parameter are summarized in Tab. 1. In addition the correlations between the parameter are investigated. Thereby it is particularly focused on the correlations between timber boards; i.e. the correlations between E_F, mean tKAR-value and mean d within one timber boards. For both strength grades only marginal correlation ($\rho \leq \pm 0.25$) could be identified. Following the correlations are not considered.

Tab. 1: Estimated parameter

Strength grade	Distance d k	ν	tKAR-value μ	σ_τ	σ_ε	E_F μ	σ_τ
L25	2.37	$6.3 \cdot 10^{-3}$	-1.50	0.184	0.335	9.35	0.124
L40			-1.70	0.171	0.281	9.68	0.0877

3.2 Fabrication of GLT

Afterwards the simulated timber boards are virtually finger jointed and glued together to GLT beams. Thereby in principle every kind of fabrication procedure can be simulated. In the present study the timber boards are simulated in accordance to the investigations of Larsen [19][1] and Ehlbeck & Colling [21][1]; i.e. shorted boards $\sim N(2.15, 0.50)$, non-shorted boards $\sim N(4.3, 0.71)$. Further a minimal and a maximal board length is introduced $l = [1, 6]$. The distance from the board edges to the outmost located WS is $d - 100$mm, to simulate the fabrication process most realistically. The simulated boards are finger jointed to endless lamellas, cut to the specific beam length and glued together. After this part of the simulation process GLT beams are virtually produced where the exact position of each WS and FJ as well as the E_F of each timber board is well-known.

3.3 Allocation of material properties

In a next step the strength and stiffness properties of each part of the GLT beam are calculated, based on information about the E_F, tKAR and FJ. It is well established that $f_{\text{m,g}}$ is highly related to the tensile strength of its weak zones; that are knot clusters and FJ. Therefore it is of particular importance that the material model shows a large accurancy within those zones. For an optimal reproducibility linear regression models are developed.

$$ln(Y) = \beta_0 + \beta_1 E_F + \beta_2 \text{tKAR} + \varepsilon \tag{5}$$

The model for the prediction of the tensile strength and tensile stiffness of WS ($E_{\text{t,WS}}$, $f_{\text{t,WS}}$) is developed on full scale tensile tests on 4 meter long timber boards. As described above $E_{\text{t,WS}}$ is measured using an optical measurement device; the tensile stiffness is measured

[1]citated in Wiegand [20]

on 864 WS. For the strength model altogether 450 destructive tensile tests are performed. When performing tensile tests the tensile capacity of the timber board and thus the tensile strength of the weakest section within each board are known. Further it is known that the tensile strength of all other WS is at least the tensile capacity of the corresponding board. To consider both the equality and the inequality information the censored regression analysis [22, 23] is used. For the strength model the tKAR-value of altogether 2577 WS is considered. Both the strength and the stiffness model are described in detail in [24]. Using the models to predict the tensile stiffness of clear wood (with tKAR = 0) those will be slightly underestimated (about 3%).

Compared to other strength and stiffness models the approach presented here shows a significant larger influence of knots on the strength and stiffness reduction. This might be the result of several reasons such as: (1) the natural growth characteristics are taken into account, (2) the testing length, (3) the test setup or (4) the chosen method (censored regression analysis).

Using the presented model it is also possible to estimate the tensile strength and stiffness of FJ. Therefore the corresponding literature has to be taken into account. The stiffness properties of FJ are analysed in Samson [25], Heimeshoff & Glos [26] for bending and Ehlbeck et. al [7] for tension. All studies identified no significant difference to the stiffness properties of CWS. Thus $E_{\mathrm{t,j}}$ is assumed to be the mean of the two adjacent CWS; Eq. (6).

To model the tensile strength of finger joints $f_{\mathrm{t,j}}$, which is one of the most important parameter for modelling the mechanical performance GLT a very simple and comprehensible approach is chosen: It is assumed that $f_{\mathrm{t,j}}$ is equal to $f_{\mathrm{t,WS}}$ having a specific tKAR-value. This approach is already mentioned in other studies; e.g. Pellicane et. al [27] and Colling [8]. Based on the mentioned literature and our experimental experience $0.2 \leq \mathrm{tKAR} \leq 0.3$ seems to be realistic.

$$E_{\mathrm{t,j}} = \frac{1}{2}\sum_{i=1}^{2} E_{\mathrm{t,CWS},i} \qquad f_{\mathrm{t,j}} = \min_{i=1,2}\{f_{\mathrm{t,WS},i}|\mathrm{tKAR}\} \tag{6}$$

For the estimation of the compression stiffness, models from the literature are taken into account [7, 26, 6, 28]. The analysis shows that WS under compression load are slightly stiffer (~5%) than under tensile load, whereas CWS are slightly weaker (~4%), for typical strength grades. Only for FJ significant reduced stiffness properties are identified. However in the approach described here a tensile failure is assumed, thus the compression stiffness is of minor importance. Following, for the modelling of the stiffness properties it is not distinguished between tension and compression.

It is obvious that the prediction of material properties is associated to model uncertainties. The model uncertainties, expressed through the error term ε, are identified for the strength and stiffness model of WS. However using censored regression analysis for the parameter estimation the model uncertainty is underestimated. To compensate that, a slightly higher value is assumed $\sigma_\varepsilon = 0.2$. To consider the correlation of the material properties within each particular member, ε is separated in two parts: One part for the uncertainty of the mean material properties (constant within one timber board) and one part for the uncertainty of the strength/stiffness reduction of each particular WS. A ratio between those two parts of 2:1 is chosen in accordance to the investigations of Colling [8]. Furthermore a correlation between strength and stiffness $\rho = 0.8$ is assumed. For modelling $f_{\mathrm{t,j}}$ the same model uncertainties are assumed as for WS. All model parameters and their correlations are summarized in Tab. 2.

Tab. 2: Parameter for the model to predict (left) E_{WS} and (right) $f_{t,WS}$ [MPa]

	Expected value	Correlation
β_0	8.41	$\rho(\beta_0, \beta_1) = -0.922$
β_1	$7.69 \cdot 10^{-5}$	$\rho(\beta_0, \beta_2) = -0.564$
β_2	$-9.02 \cdot 10^{-1}$	$\rho(\beta_1, \beta_2) = 0.234$
σ_ε	$1.00 \cdot 10^{-1}$	$\rho(\beta_i, \sigma_\varepsilon) \approx 0$

	Expected value	Correlation
β_0	2.96	$\rho(\beta_0, \beta_1) = -0.922$
β_1	$8.50 \cdot 10^{-5}$	$\rho(\beta_0, \beta_2) = -0.596$
β_2	-2.22	$\rho(\beta_1, \beta_2) = 0.274$
σ_ε	$2.00 \cdot 10^{-1}$	$\rho(\beta_i, \sigma_\varepsilon) \approx 0$

After this part of the simulation process GLT beams with well-known material properties are virtually produced. Through the hierarchical model of the parameter E_F and tKAR, the within member correlation is automatically considered; i.e. the correlation of sections within the same timber board. Further the correlation between strength and stiffness properties is considered as a result that both material parameter are calculated with the same E_F and tKAR-value.

3.4 Modelling of GLT

From the simulated beams the bending capacity $f_{\mathrm{m,g}}$ and the bending stiffness $E_{\mathrm{m,g}}$ has to be estimated. Therefore a numerical, strain based model is developed where the local material properties of the entire beams are taken into account. Constant strength and stiffness properties are assumed, within the entire lamella cross section over a length of 50mm. Using a simplified numerical model (iso-parametric 4-node elements; isotroph, linear elastic material properties) the deformation of the GLT beams under a unit load $F = 1\mathrm{kN}$ is calculated. Following mean axial stresses $\sigma_{\mathrm{t},i}$ of each lamella-section i are calculated based on the mean axial strains ε_i of the particular section. Through a comparison between $\sigma_{\mathrm{t},i}$ and the corresponding tensile strength $f_{\mathrm{t},i}$, the load until the first section would fail under tension can be estimated $\rightarrow f_{\mathrm{m,g,1}}$, $E_{\mathrm{m,g,1}}$. After failure the stiffness of the specific section is assumed to be zero $E_{\mathrm{t},i} = 0$ and the calculation will be repeated $\rightarrow f_{\mathrm{m,g,2}}$, $E_{\mathrm{m,g,2}}$. This iteration is repeated up to a significant stiffness reduction (here a reduction of 1% is assumed as the threshold). Finally the following material properties are assumed:

$$f_{\mathrm{m,g}} = \max_j\{f_{\mathrm{m,g},j}\} \qquad\qquad E_{\mathrm{m,g}} = E_{\mathrm{m,g,1}} \tag{7}$$

Often a significant reduction of the stiffness properties occur after the first iteration. Thus their bending capacity corresponds to the bending capacity of the first iteration respective to the tensile capacity of the most utilised lamella-section. However the introduced failure criteria is important to cover low realisations of the $f_{\mathrm{t},i}$ located in the middle of the beam. This is getting more important for longer and higher beams.

In addition to the material properties $f_{\mathrm{m,g}}$ and $E_{\mathrm{m,g}}$ the type of failure (WS, CWS, FJ) can be estimated. The model is valid on the 24 tested GLT beams. The results are illustrated and described in Section 4.

At this point it has to be mentioned that the numerical model presented here is clearly simplified. Theoretically it can be exchanged through a more advanced model that considers anisotropy, plasticity, shear and so on. However the basic idea behind this research project is the investigation of the natural growth characteristic, thus the emphasis is lying on the simulation of the beam setup.

3.5 Simulation model

Using the simulation process described in Section 3.1 to 3.4 the material properties of a simulated GLT-beam can be estimated. Based on a sufficient amount of simulations the distribution function of $f_{\mathrm{m,g}}$ and $E_{\mathrm{m,g}}$ can be estimated. Following the interrelation between the source material (e.g. $f_{\mathrm{t,l}}$) and code related parameter such as $f_{\mathrm{m,g,k}}$ or $E_{\mathrm{m,g}}$ can be investigated.

According to the authors it is of particular importance to focus on the relation between the distribution functions of the source material and the distribution functions of the GLT beams and not only on the relation between characteristic values. Those might help for a better understanding of the influence of the individual parameter.

3.6 Results

In the following the results of a few selected investigations are illustrated and described. All simulated GLT beams have a height of $h = 600$mm and a span of $l = 18 \cdot h = 10'800$mm, to garanty an optimal comparability to the values given in the codes. GLT of both strength grades (GL24h, GL36h) are simulated, one time with shorted boards $\sim N(2.15, 0.50)$ and one time with non-shorted boards $\sim N(4.3, 0.71)$. For all calculation it is assumed that $f_{\mathrm{t,j}} = f_{\mathrm{t,WS}}|\mathrm{tKAR}{=}0.2$. For all kind of beams $n = 10^4$ simulations are conducted to estimate the material properties. The results are illustrated in Tab. 3. Further in Fig. 5 the results of all simulations and the fitted log-normal distribution for GL24h (shorted boards) are illustrated.

The results show a small underestimation for both strength grades, compared to the values given in EN 1194 [12]. In both strength classes, the beams fabricated out of longer boards have a slightly higher load bearing capacity. This might be a result of the lower number of FJ. In addition to the absolute values, also their variability seem quite realistic, JCSS [29] recommend COV=0.15 for $f_{\mathrm{m,g}}$.

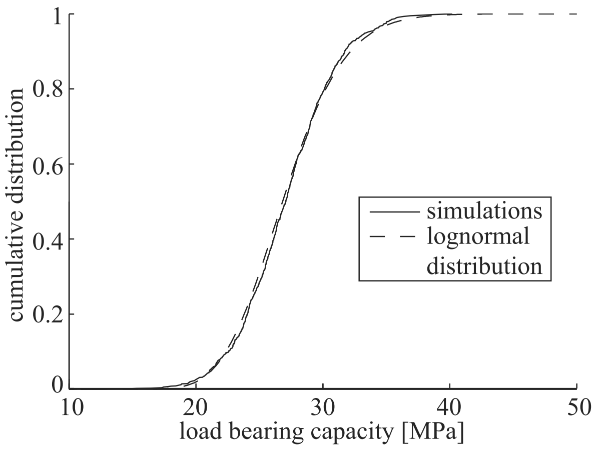

Fig. 5: Estimated bending capacity of GL24h - shorted timber boards.

It is obvious that the amount of FJ failure increases with increasing strength grade and/or decreasing board length. In average the amount of FJ failure is about 20% for the lower and 35% for the upper strength class. This corresponds to different studies presented in the literature: In the study of Johansson [30][2] 31% failed through FJ. Blaß et al. [6] presented the failure within the lowest lamella of altogether 50 beams, of the strength classes GL32c and GL36c. 6 failed FJ, 37 timber failure (WS and CW) and 7 combined failure (FJ and timber) are documented. Thus 13 of the GLT beams failed related to FJ, that are about 26%. Conspicuous is that within the lower strength grade significantly more FJ (9) failed than in the upper strength glass (4), which is contradictory. Schickhofer [32] investigated 115 GLT beams. The investigation shows that the amount of failures related to FJ is increasing with increasing timber quality. GLT fabricated out of timber boards MS10 failed in 5-9% trough FJ, MS13 in 11% and MS17 in

[2]citated in Thelandersson [31]

Tab. 3: Estimated material properties [MPa] and type of failure [%]

Strength class	Board length	f_m			E_m		Failure lowest lamella		
		$\bar{f}_m$	$f_{m,k}$	COV	$\bar{E}_m$	COV	FJ	WS	CW
GL24h	shorted	27.1	21.1	0.14	10'700	0.03	26	62	12
	non-shorted	27.7	21.4	0.15	10'600	0.04	14	78	8
GL36h	shorted	42.2	33.9	0.13	15'200	0.03	43	48	9
	non-shorted	44.6	35.0	0.13	15'100	0.04	26	66	8

24-39%. The only exception is the investigation of Colling [8]. He analysed the influence of FJ on a compilation of numerous studies; altogether the compilation consists 1767 GLT beams. The investigation shows that about 79% of the investigated GLT beam, having a FJ located in the lowest lamella within the area of the maximal bending moment failed through FJ.

At this point it has to mentioned that the model is sensible to the chosen parameters; e.g. assuming $f_{t,j} = f_{t,WS}|\text{tKAR}{=}0.25$ the load bearing capacity would decrease: $f_{m,g,k} = 21.4\text{MPa} \rightarrow f_{m,g,k} = 20.5\text{MPa}$ and $f_{m,g,k} = 35.0\text{MPa} \rightarrow f_{m,g,k} = 33.4\text{MPa}$. That is a result of the higher amount of FJ failure (GL24h: 21%, GL36h: 30%).

3.7 Further developments

The approach presented here is based on two parameter measured in the laboratory; E_F and tKAR-value. Both are relatively time consuming and thus not really efficient for practical application. However, as mentioned above all the investigated timber boards are machine graded using the Goldeneye 706 grading device. Following from all boards a stiffness estimation E^m as well as a machine measured knot parameter K^m are known. Within the next steps of the project the laboratory measured data should be exchanged through the data from the grading device (E^m, K^m).

The advantage would be that such machine measured parameters are identified for each particular timber board, that is graded by a x-ray based grading device (e.g. Goldeneye 706). As a result a large database for the parameter estimation would exist. Thus the presented parameter can be predicted more precisely. Furthermore the model can be easily adapted to timber boards having different strength grades.

In principle the approach presented here could be also applied in the GLT fabrication process. Through a combination of the grading process and the GLT fabrication, GLT beams having well-known material properties could be produced. From those boards it might be relatively easy to estimate the load bearing capacity as described in Section 4. Thus would lead to an significant increase of the reliability of GLT.

4 Validation of the model

The approach presented here contains altogether 4 different, independent models. Models 1 and 3 one are developed based on experimental investigations, model 2 is developed based on common practice and model 4 is developed based on a idealised tensile failure criteria within an entire lamella cross section. In particular the models 3 and 4 have to be validated to guaranty their efficiency. Within this study 24 GLT beams with well-known local material properties (E_F of each timber board, position of each FJ, position and tKAR-value of each knot clusters) are produced and tested. Based on the results the models 3 and 4 can be validated.

Primary the strength and stiffness properties have to be allocated to the beams. Therefore the material model introduced in Section 3.3 will be used. For the calculation it is assumed that $f_{\mathrm{t,j}} = f_{\mathrm{t,WS}}|\mathrm{tKAR}{=}0.2$. As mentioned, the material model has model uncertainties, expressed through ε. As a result different realisations of the beams are possible. In this study 100 possible realisations of each beam are simulated and their material properties are estimated. It is obvious that different realisations lead to different strength and stiffness properties. In Fig. 6 the estimated bending capacities of all 100 realisations of one beam (strength class GL36h) are illustrated. The majority of the realisation are located near by the measured bending capacity. However there are also realisations significantly above and below the test result. For this particular beam the uncertainty of the estimated load bearing capacity is COV = 0.11. The other beams show similar results.

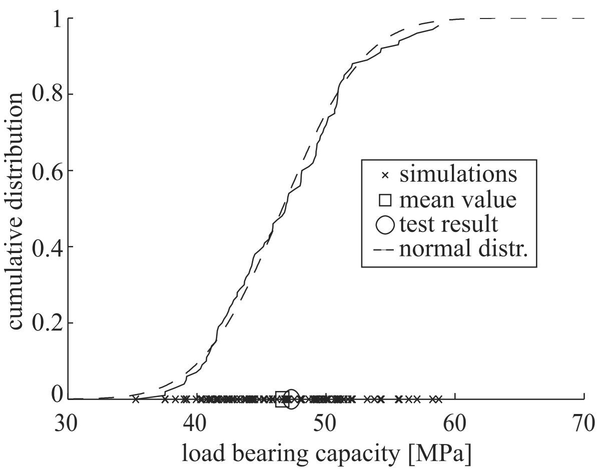

Fig. 6: Estimated bending capacity of one beam - GL36h, 100 realisations.

Taking into account all the 100 realisations an expected value of the bending capacity and the bending stiffness can be estimated. In Fig. 7 the measured and the estimated values of all 24 GLT beams are illustrated. Overall a very good agreement between the measured and the estimated material properties could be identified. Only the stiffness properties for the lower strength class are slightly underestimated (~5%). Especially the estimation of the upper strength class seems to be quite accurate.

In average the load bearing capacity $f_{\mathrm{m,g}}$ is slightly underestimated 2.5MPa (~6%). The maximal underestimation is 10.0MPa and the maximal overestimation is 7.3MPa. For the bending stiffness $E_{\mathrm{m,g}}$ the mean underestimation is 120MPa (~1%), the maximal underestimation is 980MPa and maximal overestimation is 980MPa. As a result of the very good agreement between the measured and the estimated material properties it seems possible to estimate accurately $f_{\mathrm{m,g}}$ and $E_{\mathrm{m,g}}$ of beams having well-known information about E_F, tKAR-value and FJ.

In addition to the material properties also the type of failure is investigated. Only within 5 beams (GL24h: 0, GL36h: 5) a FJ failure within the lowest lamella is observed within the experimental investigation. The numerical analysis shows a comparable result: here in altogether 10 beams (GL24h: 2, GL36h: 8) a FJ failure was identified. All 5 'real' FJ failure are detected. Following the tensile strength of FJ might be slightly underestimated.

5 Conclusion & Outlook

In the present study, a model for the probabilistic representation of the material properties of GLT is developed. The major difference to existing models is that the natural growth characteristic of timber is considered; i.e. the position of knot clusters and finger joint connections are modelled as much as possible close to reality. The advantage of this method

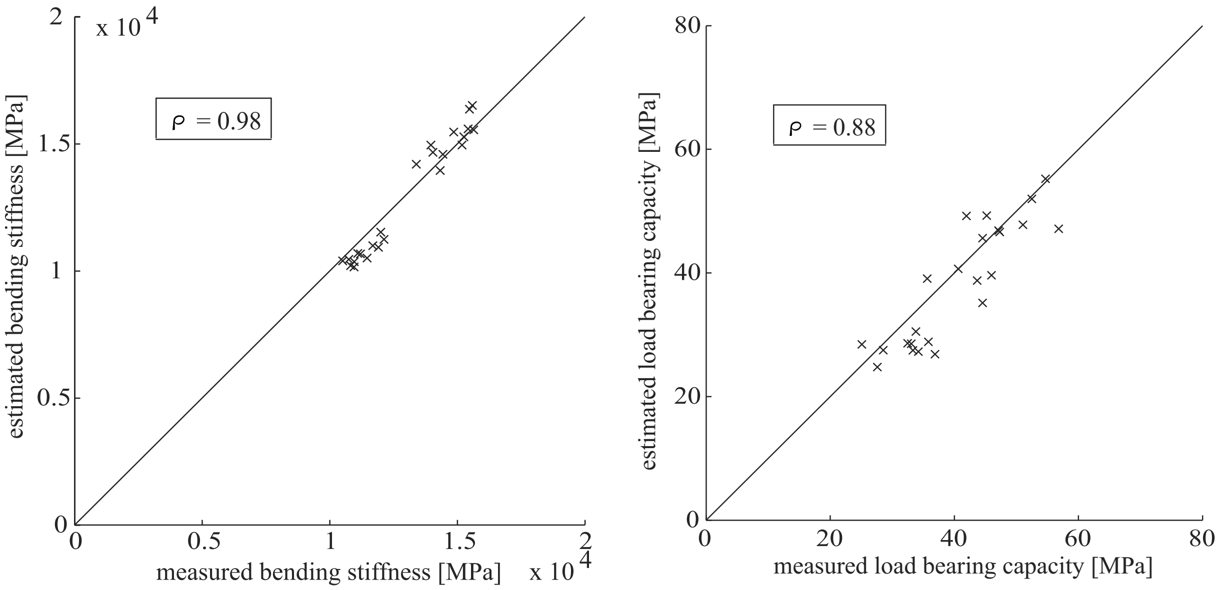

Fig. 7: Estimated bending capacity and bending stiffness of all 24 GLT beam.

is that the probability of inappropriate configurations, such as knot clusters above each other, can be considered.

In a first part the natural growth characteristic of timber is investigated and described in a probabilistic manner. The strength and stiffness related indicators (E_F, tKAR) are modelled hierarchically to consider the within and between member variability of timber boards. The analysis shows that for the estimation of the tKAR-value distribution, the natural growth characteristic has to be considered. Otherwise the tKAR-value will be significantly underestimated.

To model the relation between the strength and stiffness related indicators (E_F, tKAR) and the material properties (f_{t}, E_{t}), destructive and non-destructive tensile tests are performed. The major difference to existing investigations is that all material properties are measured on 4 meter long timber boards on full scale tensile tests. The local stiffness properties are measured according to the natural growth characteristic using an optical measurement device. For the estimation of the tensile strength model the censored regression analysis is chosen; a method where both equality and inequality information are considered. Compared to other strength and stiffness models the approach presented here shows a significant larger influence of knots on the strength and stiffness reduction.

For validation altogether 24 GLT beams with well-known local material properties are produced and tested. The analysis shows a very good agreement between the measured and the estimated material properties. Thus it seems likely that the presented model can be used to estimate accurately the load bearing capacity and the bending stiffness of GLT having well-known information about E_F, tKAR-value and FJ. However the model has to extended to timber boards of different strength grades. Furthermore the model could further be validated on more test results or well documented experimental investigations from the literature.

The outcome of this research project facilitates the reliable prediction of the bending capacity of GLT based on the material properties of the source material and may be used in the future as the basis for a simplified representation of $f_{\mathrm{m,g,k}}$ in the corresponding material codes.

References

[1] R. Brandner and G. Schickhofer. Glued laminated timber in bending: new aspects concerning modelling. *Wood Science and Technology*, 42(5):401–425, 2008.

[2] DIN. prEN 14080 - Timber structures - Glued laminated timber and glued laminated solid timber - Requirements; German version, 2011.

[3] R.O. Foschi and J.D. Barrett. Glued-laminated beam strength: a model. *Journal of the Structural Division, American Society of Civil Engineers*, 106(ST8):1735–1754, 1980.

[4] R. Hernandez, D.A. Bender, B.A. Richburg, and K.S. Kline. Probabilistic modeling of glued-laminated timber beams. *Wood and fiber science*, 24(3):294–306, 1992.

[5] D.A. Bender, F.E. Woeste, and E.L. Schafler. *Reliability formulation for the strength and fire endurance of glued-laminated beams.* US Department of Agriculture, Forest Service, Forest Products Laboratory, 1985.

[6] H.J. Blaß, M. Frese, P. Glos, J.K. Denzler, P. Linenmann, and A. Ranta-Maunus. *Zuverlässigkeit von Fichten-Brettschichtholz mit modifiziertem Aufbau*, volume 11. KIT Scientific Publishing, 2008.

[7] J. Ehlbeck, F. Colling, and R. Görlacher. Einfluß keilgezinkter Lamellen auf die Biegefestigkeit von Brettschichtholzträgern. *European Journal of Wood and Wood Products*, 43(8):333–337, 369–373, 493–442, 1985.

[8] F. Colling. *Tragfähigkeit von Biegeträgern aus Brettschichtholz in Abhängigkeit von den festigkeitsrelevanten Einflussgrößen.* Versuchsanst. für Stahl, Holz und Steine, 1990.

[9] F. Giudiceandrea. Stress grading lumber by a combination of vibration stress waves and x-ray scanning. In *Proceedings of the 11th International Conference on Scanning Technology and Process optimization in the wood Industry (ScanTech 2005).*, Las Veagas, 2005.

[10] DIN. EN 14081-4 - Timber structures - Strength graded structural timber with rectangular crosssection - Part 4: Machine grading - Grading machine settings for machine controlled systems; German version, 2009.

[11] DIN. prEN 14080 - Timber structures - Glued laminated timber and glued laminated solid timber - Requirements; German version, 2009.

[12] DIN. EN 1194 Brettschichtholz - Festigkeitsklassen und Bestimmung charakteristischer Werte, 1999.

[13] G. Fink and J. Kohler. *Zerstörungsfreie Versuche zur Ermittlung des Elastizitätsmodules von Holzbrettern.* IBK Report No. 339. ETH Zurich, Zurich, 2012.

[14] G. Fink, J. Kohler, and A. Frangi. *Bending tests on glued laminated timber beams with well-known material properties.* IBK Report. ETH Zurich, Zurich, in press.

[15] F. Colling and R. Dinort. Die Ästigkeit des in den Leimbaubetrieben verwendeten Schmittholzes. *Holz als Roh-und Werkstoff*, 45(1):23–26, 1987.

[16] T. Isaksson. *Modelling the Variability of Bending Strength in Structural Timber.* PhD thesis, Lund Institute of Technology, 1999.

[17] M. Kersken Bradley and R. Rackwitz. *Stochastic modelling of material properties and quality control, JCSS Working Document.* IABSE-publication, 1991.

[18] J. Köhler. *Reliability of Timber Structures.* Phd, ETH Zurich, 2006. Reliability/Probability Theory.

[19] H.J. Larsen. *Strength of Glued Laminated Beams, Part 2 (Properties of Glulam Laminations).* Institute of Buildung Technology and Structural Engineering, Aalborg University, Aalborg, Dänemark, 1980.

[20] T. Wiegand. Entwicklung eines Rechenverfahrens für keilgezinkte Rahmen-ecken und Biegeträger ohne oder mit Zwischenstück aus Brett-schichtholz oder Holzwerkstoffplatten. 2003.

[21] J. Ehlbeck and F. Colling. *Biegefestigkeit von Brettschichtholz in Abhängigkeit von Rohdichte, Elastizitätsmodul, Ästigkeit und Keilzinkungen der Lamellen, der Lage der Keilzinkungen sowie von der Trägerhöhe.* Forschungsbericht der Versuchsanstalt für Stahl, Holz und Steine, Abt. Ingenieurholzbau, Universität Karlsruhe, 1987.

[22] J. Buckley and I. James. Linear regression with censored data. *Biometrika*, 66:429–36, 1979.

[23] S. Chatterjee and D. L. McLeich. Fitting linear regression models to censored data by least squares and the method of maximum likelihood. Technical report, Department of statistics - Standford University, 1981.

[24] G. Fink and J. Kohler. Model for the prediction of the tensile strength and tensile stiffness of knot clusters within structural timber. *submitted to European Journal of Wood and Wood Products.*

[25] M. Samson. Potential of finger-jointed lumber for machine stress-rated lumber grades. *Forest Products Journal*, 35, 1985.

[26] B. Heimeshoff and P. Glos. Zugfestigkeit und Biege-E-Modul von Fichten-Brettlamellen. *European Journal of Wood and Wood Products*, 38(2):51–59, 1980.

[27] P.J. Pellicane, K. Stanfill-McMillan, and R.J. Tichy. Effects of knots near the fingers of finger-jointed dimension lumber. *Forest products journal*, 37, 1987.
[28] J. Sell. *Eigenschaften und Kenngrößen von Holzarten.* Baufachverlag Zürich, 1997.
[29] JCSS. Probabilistic Model Code Part III - Resistance Models (3.05 Timber), 2006.
[30] C.J. Johansson. Strength and stiffness of glulam with laminations of machine stress graded timber. SP RAPPORT 1990:22. Technical report, Swedish National Testing and Research Institute, Boras, Sweden (in Swedish), 1990.
[31] S. Thelandersson, H.J. Larsen, et al. *Timber engineering.* Wiley West Sussex, England, 2003.
[32] G. Schickhofer. Development of efficient glued laminated timber. In *Proceedings of the 29th Meeting, International Council for Research and Innovation in Building and Construction, Working Commission W18 - Timber Structures, Bordeaux, France, CIB-W18, Paper No. 29-12-1*, 1996.

INTERNATIONAL COUNCIL FOR RESEARCH AND INNOVATION IN BUILDING AND CONSTRUCTION

WORKING COMMISSION W18 - TIMBER STRUCTURES

IN PLANE SHEAR STRENGTH OF CROSS LAMINATED TIMBER (CLT): TEST CONFIGURATION, QUANTIFICATION AND INFLUENCING PARAMETERS

R Brandner

Graz University of Technology

Competence Centre holz.bau forschungs gmbh

T Bogensperger

Competence Centre holz.bau forschungs gmbh

G Schickhofer

Graz University of Technology

AUSTRIA

Keywords: shear in plane, net-shear, cross laminated timber, shear mechanisms, shear strength, single node, test configuration

---

Presented by G Schickhofer

H Blass commented that the interaction of shear and compression perpendicular to grain should be interaction of shear and compression parallel to grain.

BJ Yeh asked how to relate the test results of the inclined test and whether one could use this for beams and header applications. G Schickhofer stated that it was very difficult to get shear failure (in-plane) for CLT. The in-plane shear strength of 5.5 MPa was conservative based on a referenced shear element. BJ Yeh asked if there was volume effect in shear and how one could relate the information to beam results. G Schickhofer stated that this study was very different from the beam situation where other stresses would be present.

C Sigrist asked whether this method could be used for quality control. G Schickhofer stated no and perhaps it could be considered as a later option. The current study was intended to get basic information.

M Fragiacomo and G Schickhofer discussed the existence of different failure modes within the specimens and the results might depend on which mode governed more. Glue area failure happened first and there could be thickness effect.

J Schmid asked about the process of standardization of laminate thickness to 20, 30 and 40 mm. G Schickhofer stated that it would be important for the industry to have standardised laminate thickness. U Hübner added that this ongoing process would take time to arrive at an agreement. It would not be possible to arrive at a change over a very short time.

In plane Shear Strength of Cross Laminated Timber (CLT): Test Configuration, Quantification and influencing Parameters

R Brandner [1) 2)]; T Bogensperger [2)]; G Schickhofer [1)]

Graz University of Technology, Institute of Timber Engineering and Wood Technology [1)]

Competence Centre holz.bau forschungs gmbh [2)]

1 Abstract

Cross laminated timber (CLT) has become a well-known and widely applied two-dimensional, engineered timber product worldwide. It constitutes a rigid composite of an odd number of orthogonal and glued layers. Focusing on a single glued node loaded in plane in shear and composed of two crossed board segments and the adhesive layer in-between, in principle three types of shear mechanisms can be distinguished: mechanism I "net-shear" (shearing perpendicular to grain), mechanism II "torsion" and mechanism III "gross-shear" (shearing parallel to grain). In fact, while having generally accepted values for the resistance against mechanism II and good estimates for mechanism III the resistance against "net-shear" (mechanism I) is still in discussion. In spite of numerous investigations on nodes and on whole CLT elements in the past, a common sense concerning the test procedure, the consideration and handling of distinct influencing parameters and the quantification of the shear strength are open.

We focus on the in plane shear resistance of single nodes according to mechanism I. We (i) propose a test configuration for reliable determination of the shear strength, (ii) determine the shear resistance in case of shear loads perpendicular to grain, (iii) discuss influences of some parameters on the shear strength of single nodes, and (iv) give a brief outlook concerning the resistance of CLT elements against shear loads in plane.

2 Introduction

Cross laminated timber (CLT) constitutes a solid, laminar engineered timber product with high resistances against loads in and out of plane. Common CLT is a rigid composite of an odd number of orthogonal and face bonded layers. Each single layer consists of side-by-side aligned (finger jointed) boards with or without edge bonding. In CLT without edge bonding gaps between the boards, more or less regular in width, are evident. Common gap widths allowed by technical approvals for CLT are 2 (3) mm in the top and 4 (6) mm in the core layers (Brandner 2013).

We focus on the mechanical properties of CLT loaded in plane. In particular, the resistance in plane in shear of CLT made of Norway spruce (*Picea abies*) is addressed. Three principle shear mechanisms are distinguished: mechanism I "net-shear", mechanism II "torsion" and mechanism III "gross-shear" (see e.g. Bogensperger et al. 2007 & 2010, Blaß and Flaig 2012). Mechanism I "net-shear" corresponds to shearing perpendicular to grain of the net cross sections in the controlling plane. Mechanism III "gross-shear" is associated with shearing parallel to grain of the whole CLT element. For clarification of these mechanisms, at first some simplifications for the mechanical treatment are made according to Bogensperger et al. (2010).

2.1 Some general Comments on the Shear Mechanisms

Following Bogensperger et al. (2010) a representative volume element (RVE) is introduced, which is in thickness equal to a CLT element and in width and depth equal to the width of one board plus the half of the width of gaps between adjacent boards. Focusing on shear in a CLT element with constant layer thicknesses ($t_{l,i} \equiv t_l$, $i = 1, \ldots, N$) and an infinite number of layers $N \to \infty$ (neglecting boundary conditions) the RVE can be further simplified to a representative volume sub-element (RVSE). This RVSE is in width and depth equal to the RVE but in thickness equal to t_l, composed of both half thicknesses of two orthogonal boards in one node and the face bonding in-between (see Fig. 1).

As consequence of $N \to \infty$ a proportional shear force $n_{xy,\text{RVSE}}$ instead of the overall shear force n_{xy} is defined. The nominal shear stress τ_0 is given as (see Bogensperger et al. 2010)

$$\tau_0 = \frac{n_{xy,\text{RVSE}}}{a \cdot t_l}, \tag{1}$$

with a as width and depth, and t_l as thickness of the RVSE, respectively. This more theoretical shear stress corresponds to **mechanism III** "gross-shear" (see Fig. 1). Thereby a constant shear stress distribution over the cross section is assumed, which may lead to shear failures parallel to grain in all layers. Therefore, an intact edge bonding between the boards within one layer and the absence of checks is required. Missing or insufficient connection between the boards at the edges disables the transfer of shear stresses in that direction. For the resistance against mechanism III Blaß and Flaig (2012) recommend a characteristic (5 %-quantile) shear strength of $f_{v,\text{gross,k}} = 3.5$ N/mm². In view of EN 338 and with $k_{\text{cr}} = 1.00$ (factor which considers the influence of cracks on the shear strength) a value of $f_{v,\text{gross,k}} = 4.0$ N/mm² for CLT composed of boards of strength class C24 according to EN 338 (the common material used for CLT in Europe) is proposed (Flaig and Blaß 2013). In case of stress relieves adaptation of $f_{v,\text{gross}}$ seems to be necessary.

Of course, in CLT composed of layers without edge bonding, shear force can only be transferred via the cross sections of boards and via the gluing interface of the face bonding. Comparable conditions are expected in edge bonded CLT exposed to common climate variations. Moisture induced stresses caused by these climate variations lead to checks, which again restrict the possibilities for shear transfer. Consequently, mechanism I and II become active and their verification mandatory in the design process, even in cases of gap widths $t_{\text{gap}} \to 0$.

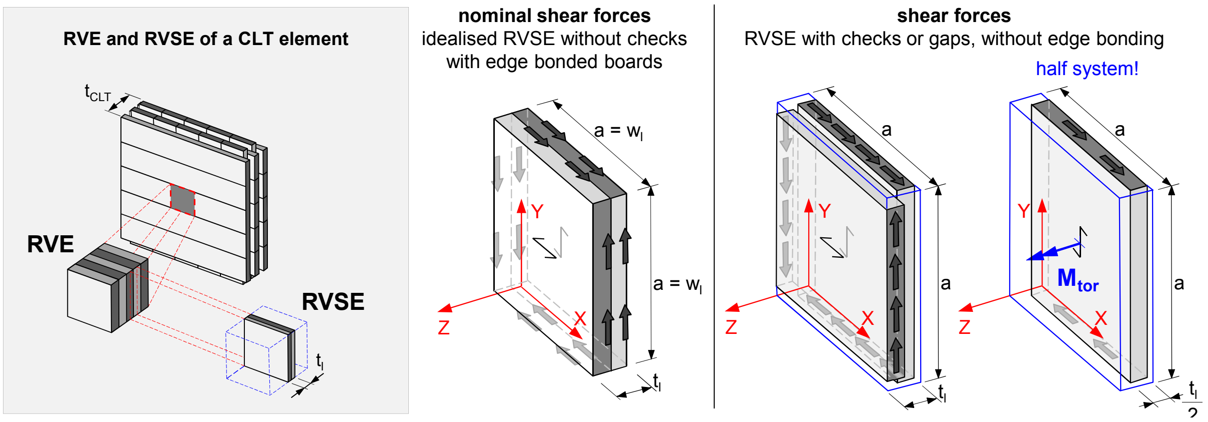

Fig. 1: (block left) RVE and RVSE of a CLT element; (block right) shear stresses in a RVSE: nominal shear stress τ_0 (left), real shear stress τ_{net} (middle; superposing left & right), torsional stress τ_{tor} on the gluing interface (right) (Bogensperger et al. 2010; adapted)

Mechanism I considers the transfer of shear forces via the cross sections of boards within a RVSE. Consequently, the shear stress is given as

$$\tau_{\text{net}} = 2 \cdot \tau_0, \tag{2}$$

with τ_{net} as the shear stress dedicated to the net cross section (see Fig. 1). For calculation of stresses caused by n_{xy} in a real CLT element, considering e.g. boundary conditions caused by finite N and variations in layer thickness, a procedure is provided e.g. in Bogensperger et al. (2010).

Shear strain in the RVSE, in case of insufficient or missing connection between the board edges, causes also torsional strain in the surface bond layer. This may cause failure in the gluing interface, which is dedicated to **mechanism II** "torsion" (see Fig. 1). Assuming polar torsion, the torsional shear stresses τ_{tor} are given as

$$\tau_{\text{tor}} = \frac{M_{\text{tor}}}{I_p} \cdot \frac{a}{2} = 3 \cdot \tau_0 \cdot \frac{t_l}{a}, \tag{3}$$

with M_{tor} as torsional moment and I_p as polar moment of inertia. Consequently, τ_{tor} depends on the geometric parameter ratio t_l / a. Thus, in a real CLT element with varying layer thicknesses the thickest layer governs the design (Bogensperger et al. 2010). Concerning the resistance of a RVSE against torsion, numerous investigations were made in the past, e.g. Blaß and Görlacher (2002), Jeitler (2004) and Jöbstl et al. (2004). A possible redistribution of torsional stresses from zones exposed to rolling shear to zones exposed to shear is mentioned. Despite some influences of parameters (i) annual ring pattern, and (ii) surface area under torsion (see e.g. Jeitler 2004, Jöbstl et al. 2004) there is common sense to use $f_{\text{tor,k}}$ = 2.5 N/mm² as characteristic (5 %-quantile) torsional shear strength.

To conclude, in a real CLT element at common use the occurrence of checks due to climate variations or gaps due to missing edge bonding, in the design process both shear mechanisms, mechanism I "net-shear" and mechanism II "torsion", need verification. As there is common sense on the resistance against torsion in the gluing interface this contribution concentrates on the determination and quantification of the resistance against shear according to mechanism I.

2.2 Shear Mechanism I "net-shear": State-of-the-Art

In general, investigations on the shear strength of CLT in plane by testing can be classified in (i) investigations performed on whole CLT elements (e.g. Bosl 2002, Bogensperger et al. 2007, Andreolli et al. 2012), and (ii) investigations performed on single nodes (in dimension corresponding to a double or multiple RVSE; e.g. Wallner 2004, Jöbstl et al. 2008, Hirschmann 2011).

2.2.1 Investigations on CLT Elements

Bosl (2002) report on tests conducted on five-layer CLT elements with dimension 1,200 x 1,200 x 85 (5 x 17 mm) mm³. The elements were freely placed in a squared, diagonally in tension loaded four-hinged steel-frame (see Fig. 2, left). Consequently, the CLT was stressed in shear and compression. In all four specimens with orthogonal layers, the ultimate load was limited by buckling of single boards in the top-layers as consequence of delaminated layers. An insufficient surface bonding can be concluded. A significant damage of the elements at zones of load introduction was not observed. The mean ultimate load was $F_{\text{max,mean}}$ = 325 kN, which corresponds to shear stresses of $\tau_{\text{gross,mean}} \equiv \tau_{0\text{,mean}} \approx$ 2.3 N/mm² and $\tau_{\text{net,mean}} \approx$ 5.6 N/mm².

Later, Traetta et al. (2006) and Bogensperger et al. (2007) made tests on three-layer CLT elements of dimension 560 x 560 x 120 (30 + 60 + 30 mm) mm³, with gaps between the boards of 5 mm. A steel frame with two squared test fields, equal in size and hinged at all corners, was used for the three-point bending tests. The load on the steel frame was applied in compression. For a continuous load transfer the CLT elements were continuously bonded to the steel frame and at the boarders reinforced by hardwood lamellas (see Fig. 3, left). However, the observed failures were not in shear but locally in compression. Nevertheless, considering the inner shear field of 5 x 5 boards per layer and all five tests a maximum shear stress of at least $\tau_{\text{net,mean}} \approx$ 6.0 N/mm² (F_{max} = 78.1 to 134.0 kN) can be calculated.

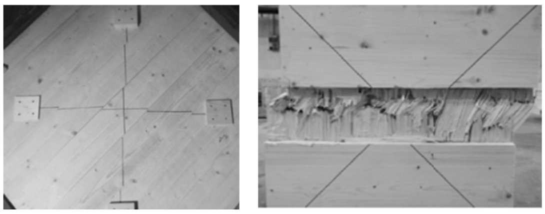

Fig. 2: Tests on CLT elements: Bosl (2002; left), Andreolli et al. (2012; right)

Andreolli et al. (2012) mention tests on three and five layer CLT elements loaded (i) edgewise in four-point bending as well as (ii) diagonally in compression by means of short steel angles. In test group (ii) two of four tests failed in torsion (one with edge bonding but cracks, the other without edge bonding), one delaminated in the lateral surfaces (three layer specimen with edge bonding), and the forth failed in shear perpendicular to grain, allocable to mechanism I (Fig. 2, right). This last test provided $f_{v\text{,net}}$ = 12.7 N/mm² as maximum value of shear stress. The stress calculation was carried out dividing the maximum load by the net cross section multiplied by a correction factor, taking into account the real stress distribution in diagonal compression test, which is not pure shear stress but an interaction between shear and compression in the central area of the panel (Andreolli et al. 2012). A test procedure for CLT columns with nodes stressed in 45° angle can also be found in Kreuzinger and Sieder (2013). Although a successful verification of the proposed procedure by tests is mentioned, the data is not presented.

CUAP (2005) provides a test configuration for determination of shear strength for European Technical Approvals (ETAs) based on the four-point bending test according to EN 408. A gap between the longitudinal boards enforces transfer of shear forces via the cross layers and the gluing interfaces. However, Jöbstl et al. (2008) and other report that in almost all cases not the intended failure in shear perpendicular to grain according to mechanism I, but rather bending failures occur. Jöbstl et al. (2008) mention eight test series of three and five layer CLT elements (in total 90 specimens) tested according to the CUAP procedure. None of these specimens failed in shear perpendicular to grain; nearly 100 % failed in bending between the loading points. Some exceptions failed in rolling shear or in shear parallel to grain, whereby both failure mechanisms are not conform to the failure scheduled for shear verification. According to CUAP this has to be done on the net cross section. The observed mean shear stresses $\tau_{net,mean}$ at bending failure are in the range of 5.4 to 11.5 N/mm², with an overall weighted mean of 8.4 N/mm².

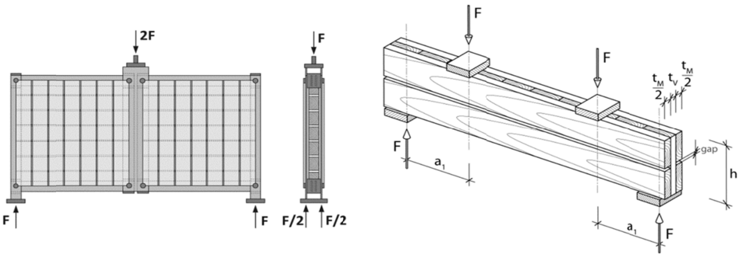

Fig. 3: Test configurations CLT elements: Traetta et al. (2006; left), CUAP (2006, right)

To summarise: until now test data regarding pure shear failures in CLT elements according to mechanism I are missing. The only reported single test, which failed in shear perpendicular to grain, is the one of Andreolli et al. (2012). Other investigations lead to failures others than in “net-shear”. In fact, stress levels of τ_{net} at maximum test loads are in the range of 6.0 to 11.5 N/mm² on average. This indicates that the resistance of CLT against shear perpendicular to grain is even higher. Of course, the experiences made outline also the challenge in generating failures according to mechanism I in CLT elements.

In view of the motivation to establish bearing models, which base on strength and stiffness properties of the elements “boards” composing the system CLT, it is the aim to define reliable strength values for all three, in principle possible shear mechanisms. Based on them it is intended to provide bearing models, at least for representative CLT diaphragms, e.g. of 4 x 4 nodes, five layers and boards with w_l = 150 mm and t_l = 30 mm as reference.

2.2.2 Investigations on Nodes

Wallner (2004) investigated rolling shear strength and stiffness of nodes, in particular of the gluing interface, on three layer CLT of Norway spruce. The setup was a symmetrical three-point bending test with a loading in compression (see Fig. 4, left). Beside primary failures in rolling shear at the gluing interface, also shear failures parallel to grain in the horizontal board were observed. In that cases the mean shear stresses $\tau_{v,net,mean}$ at failures of several test series are in the range of 5.9 to 7.0 N/mm².

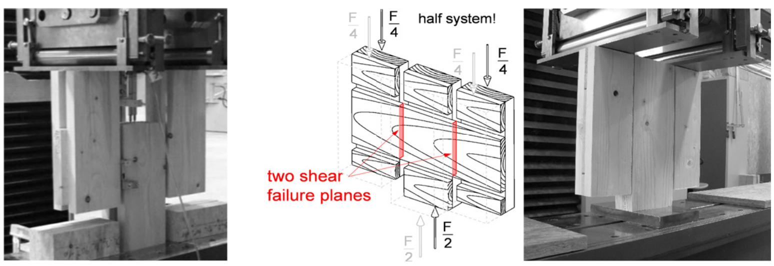

Fig. 4: Test configurations: Wallner (2004; left), Jöbstl et al. (2008; middle & right)

Based on Wallner (2004) and CUAP (2005) an adapted test configuration was developed for determining the bearing capacity of single nodes (Jöbstl et al. 2008; Fig. 4). The setup provides two possible failure planes of the cross section with w_l x t_l = 200 x 10 mm² at the vertical gaps with t_{gap} = 5 mm. As the weaker of both planes determines the ultimate load the test results are right censored. Jöbstl et al. (2008) did 20 tests with flat grain board material (Norway spruce) which all successfully failed at the cross sections. The main statistics gained from tests are $f_{v,\text{net,mean}} = 12.8$ N/mm², coefficient of variation $CV[f_{v,\text{net}}] = 11.3$ % and the empirical 5 %-quantile $f_{v,\text{net,05}} = 11.1$ N/mm². Applying maximum likelihood estimation (MLE) for right censored data, assuming a lognormal distribution with $f_{v,\text{net}} \sim$ 2pLND, the adapted statistics are $f_{v,\text{net,mean,MLE}} = 13.9$ N/mm², $CV[f_{v,\text{net,MLE}}] = 13.5$ % and $f_{v,\text{net,05,MLE}} = 11.0$ N/mm².

In view of current design procedures, which verify the shear resistance on a single node (see Bogensperger et al. 2010) it is mandatory to define a test procedure for mechanism I which allows to quantify the relevant resistance reliable. In fact, interaction of mechanism I and II cannot be avoided. However, the interaction relationship has not been quantified until now. The test procedure has to allow for variation of test parameters in a range at least relevant for the practical use of CLT, e.g. in respect to the thickness and width of commonly used boards and the annual ring pattern, e.g. the differentiation between flat and rift grain boards. Based on a comprehensive comparison of current technical approvals of CLT available in Europe the common ranges in thickness t_l and width w_l of single lamellas are (12) 20 to 40 (45) mm and (40) 100 to 240 (300) mm, respectively (Brandner 2013).

3 Development and Verification of a Test Configuration

3.1 Principal Considerations

Based on the successfully proved test setup of Jöbstl et al. (2008) further developments were made in the frame of the Master thesis of Hirschmann (2011). Considering the test configuration for in plane shear strength of engineered wood products in EN 789 and the shear configuration for solid timber in EN 408 advancements of the setup of Jöbstl et al. (2008) were made, see Fig. 5. In brief: resultant forces of loading and support are in-line. The test specimen is rotated 14°, equal to the recommendations in EN 408. In contrast to the setup of Jöbstl et al. (2008) only one failure plane for shear loads perpendicular to grain is provided. This allows direct use of test results without further data processing, e.g. by means of MLE for right censored data. Another advantage is the possibility to gain the specimen directly from full-size CLT elements. A general disadvantage is the interaction of shear and compression perpendicular to grain in the cross layer. Consequently, the bearing capacity in shear is somehow overestimated. However, because of the small angle of 14° only a small influence is expected.

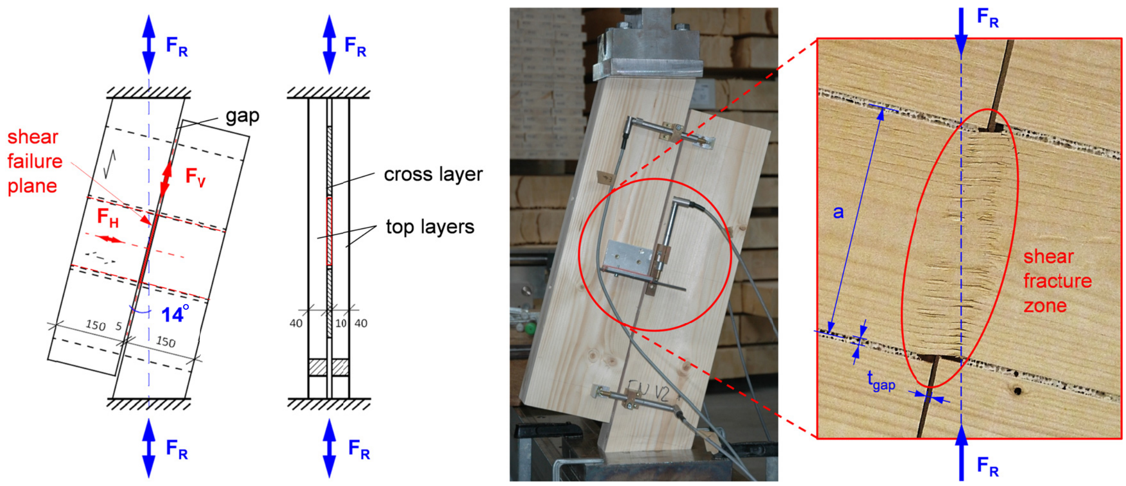

Fig. 5: Configuration and geometric parameters for testing shear perpendicular to grain on single CLT nodes by loading in tension or compression (left); test loaded in compression, including measurement of deformation and fractured cross section (right) (Hirschmann 2011; adapted)

Clarifying the possible influence of loading in tension or compression on the shear capacity two series of three specimen each were tested with core layers w_l x t_l = 150 x 10 mm². The mean shear strengths for loading in compression and tension are 9.6 N/mm² ($\rho_{12,\text{mean}} = 427$ kg/m³) and 9.8 N/mm² ($\rho_{12,\text{mean}} = 423$ kg/m³), respectively. The hypothesis of equal medians cannot be rejected (Mann-

Whitney test; $p = 0.7$). For convenience in test preparation and execution, the main series were tested in compression.

The aims of Hirschmann (2008) were (i) to investigate the applicability of the setup, (ii) to compare the results with that gained from the setup of Jöbstl et al. (2008), and (iii) to analyse the influences of selected geometric and material parameters on the shear perpendicular to grain resistance.

For clarification, the test series according to the setup of Jöbstl et al. (2008) are further given as “CIB” and that according to Hirschmann (2011) as “EN”.

3.2 Material and Methods

The test material was Norway spruce (*Picea abies*) of nominal strength class C24 according to EN 408. All material was classified according to the density. Thus, “matched samples” for series “CIB” and “EN” were created. The material was conditioned at 20 °C and 65 % relative humidity to reach an expected average moisture content of $u = 12$ %. Ten tests per series were executed. In the reference test series “C” the core boards were flat grained (fgB) of $w_l \times t_l = 150 \times 20$ mm² and with gaps of $t_{gap} = 5$ mm. In all tests, top layers with 40 mm thickness were used. Following variations of parameters were made (see also Tab. 1):

- width w_l: 150, 200 mm;
- thickness t_l: 10, 20, 30 mm;
- annual ring orientation (AR): flat grain boards (fgB), rift grain boards (rgB) and heart boards (hB);
- gap width t_{gap}: 1.5, 5.0, 25.0 mm.

As no rift grain boards were available, “pseudo rift grain boards” were produced by trimming out the heart of heart boards and edge gluing of the residual parts.

The geometry of the test setups “CIB” and “EN” was planned to resist (i) compression at loading and support, (ii) torsion in the gluing interface, and (iii) rolling shear in the gluing interface until failing in shear perpendicular to grain in the net cross section of the core layer. A compilation can be found in Hirschmann (2011). The test segments in the core were taken consecutively from 4 m long boards with the aim to assure regions free of growth characteristics like knots, checks and reaction wood in the expected failure zone of the specimen. Consequently, in tested series one to five specimens are from the same board.

The tests were executed way controlled. The velocity was adapted to ensure an average time until ultimate load of 300 ± 120 s.

3.3 Test Results

A summary of tested parameters and of main statistics is provided in Tab. 1. All executed tests in series “CIB” and “EN” failed in the expected plane due to shear perpendicular to grain. Classification according to density was successful comparing the series with equal parameters of “CIB” and “EN”. However, series “G”, “H” and “I” of both setups show significant higher densities. For the test results of “CIB” a MLE for right censored data, as in chapter 2.2.2, was executed.

Although mean and median shear strengths at equal parameter settings in series “CIB” are always higher than in series “EN” (on average + 0.5 N/mm²), the hypothesis of equal medians cannot be rejected in five of seven paired groups (Mann-Whitney test, $p > 0.05$), beside of series “C” and “I”. The reasons for systematically higher shear strengths in “CIB” are seen in the load path. Whereas setup “EN” provides resulting forces of loading and support in-line, in “CIB” the cross layer is additionally stressed in bending. Furthermore, it can be assumed that the load path in “CIB” in proportion to the shear stress leads to higher compression perpendicular to grain stresses. However, due to the moment also an interaction of tension perpendicular to grain and shear is given. Following the work of Spengler (1982) the higher compression stresses in “CIB” in comparison to “EN” are seen as reason for the roughly 5 % higher shear strengths in “CIB”. A possible stiffening of the compression zone attracts additional loads. It is concluded that both configurations provide comparable test values. As the uncertainty in statistical inference in series “CIB” is higher and the load path more complex, the test setup "EN" is preferred. Hirschmann (2011) also shows that in comparison to "CIB" the setup "EN" allows testing of a wider range in examined parameters.

Although the material quality and parameter settings are comparable, the mean and dispersion of $f_{v,\mathrm{net}}$ in series "CIB_A" are significantly lower than in Jöbstl et al. (2008). In fact, in all series of Hirschmann (2011) an unexpected low coefficient of variation is observed. One reason is caused by the test preparation, whereby more than one specimen per series origin from the same board. Considering the hierarchical material structure of timber, in case of a second order hierarchical model with differentiation in variation within and between board properties, it is concluded that the results are somehow biased. As the assignment of test specimen to former boards is possible, estimates for coefficients of variation of $f_{v,\mathrm{net}}$ within and between boards are 3.0 % and 3.6 %, respectively. Following Källsner et al. (1997) an equicorrelation coefficient, as measure for the correlation of $f_{v,\mathrm{net}}$ within boards, can be estimated as $\rho_{\mathrm{equi}} \approx 0.59$. This equicorrelation is higher than found on average for other strength properties (Brandner 2012). This is argued by the restriction of test material regarding growth characteristics and by a strict classification in density. The coefficient of variation of density $CV[\rho_{12}]$ is in the range of 2 % to 8 % (on average 4 %). However, the expected mean range is 6 % to 8 %; thus, the test material is very homogeneous. For material commonly used in timber engineering a higher variation in shear strength than the herein observed range in "EN" test series of $CV[f_{v,\mathrm{net}}]$ = (5 to 10) % is expected. In view of the experiences reported in Jöbstl et al. (2008) a range of $CV[f_{v,\mathrm{net}}]$ = (12 to 15) % and a lower equicorrelation appears reasonable.

Tab. 1: Test parameters and main statistics of density and shear strength at 12 % moisture content according to Hirschmann (2011); results partly adapted and reassessed

		EN								CIB						
		A	B	C	D	F	G	H	I	A	B	C	F	G	H	I
base p. [-]	w_l [mm]	200	150							200	150					
	t_l [mm]	10		20	30	20				10		20				
	AR [-] [1]	fgB				rgB	hB	fgB		fgB			rgB	hB	fgB	
	t_{gap} [mm]	5.0						1.5	25.0	5.0					1.5	25.0
ρ_{12} [kg/m³]	quantity [-]	à 10								à 10						
	mean	396	401	399	395	397	443	413	419	405	400	397	398	435	424	439
	median	396	404	400	400	395	444	413	416	405	396	407	397	432	427	453
	CV [%]	1.8	4.4	2.6	3.7	3.3	1.9	8.4	7.0	3.0	4.2	5.6	6.9	2.4	1.8	7.0
$f_{v,\mathrm{net},12}$ [N/mm²]	min	10.0	10.2	8.4	6.4	6.3	8.2	8.5	7.1	–	–	–	–	–	–	–
	mean	**10.8**	**11.2**	**8.9**	**7.5**	**7.2**	**8.8**	**9.5**	**8.0**	**11.1** [2]	**11.7** [2]	**9.4** [2]	**8.0** [2]	**9.2** [2]	**9.8** [2]	**8.8** [2]
	median	**10.8**	**11.2**	**8.7**	**7.4**	**7.4**	**8.9**	**9.3**	**8.1**	**11.0** [2]	**11.7** [2]	**9.4** [2]	**7.9** [2]	**9.2** [2]	**9.8** [2]	**8.7** [2]
	max	12.1	12.4	9.6	8.4	8.0	9.4	10.6	8.6	–	–	–	–	–	–	–
	CV [%]	6.0	6.3	4.9	9.3	10.1	4.2	8.5	5.6	7.4 [2]	6.9 [2]	7.4 [2]	15.1 [2]	7.4 [2]	5.2 [2]	7.9 [2]
	5 %-qu.	10.1 [3]	10.3 [3]	8.5 [3]	6.7 [3]	6.3 [3]	8.3 [3]	8.5 [3]	7.2 [3]	9.8 [2]	10.4 [2]	8.3 [2]	6.2 [2]	8.2 [2]	9.0 [2]	7.7 [2]

1) AR … annual ring orientation | fgB … flat grain boards | rgB … "pseudo" rift grain boards | hB … heart boards

2) statistics estimated by means of Maximum Likelihood Estimation (MLE) for right censored data, assuming $f_{v,\mathrm{net}} \sim$ 2pLND

3) empirical 5 %-quantile, gained from rank statistics

3.4 Shear Perpendicular to Grain: Load-Displacement and Failure Behaviour

Both setups, "EN" and "CIB", show similar characteristic load-displacement behaviour, see Fig. 6 (left). The load-displacement curve can be divided in two main parts: the first part showing a roughly linear course until the ultimate load $F_{\max}$ is reached, and the second part a clear softening property, where failure due to a new shear mechanism can be observed (see also Fig. 5, right).

In the first part, after some hardening until approximately 20 % of $F_{\max}$, a linear elastic material behaviour within approximately $0.2 \cdot F_{\max}$ to $0.8 \cdot F_{\max}$ is given, followed by a regressive non-linear relationship until $F_{\max}$. At this point, a combined failure of shear mechanisms I "net-shear" and II "torsion" takes place, initiated by local exceeded resistance in opposite corners of the failure plane, at the zones of interacting shear and tension perpendicular to grain. In the second part after the peak load, softening is characterised by reaching a steady state at about 40 % to 50 % of $F_{\max}$, enabling large deformations. These deformations increase shearing parallel to grain, mainly in the transition zone of early- and latewood. It follows a successive dissolution of the material by separation of annual rings. This leads to a flexible composite of fixed-end beams, active in bending and tension parallel to grain (see also Jöbstl et al. 2008).

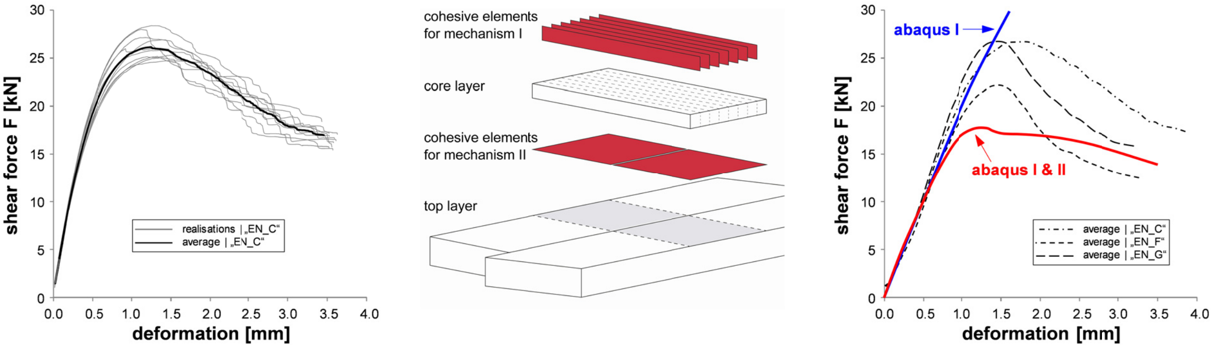

Fig. 6: Typical load-displacement behavior exemplarily for series “EN_C”: single and average curves (left); placement of cohesive elements in the numerical model (middle); comparison of average load-displacement curves with the numerical results on characteristic (5 %-quantile) level (right)

The complexity of the failure behaviour motivated a numerical model with the aim to mirror the load-displacement curve in a satisfying manner. Therefore, a FE-model with cohesive elements was implemented in ABAQUS. These elements allow fracturing in the observed failure planes by following the Dugdale-Barenblatt model of elastic-plastic fracture mechanics. Separation in fracture mode I and shear sliding in mode II and III according to this theory occur after a critical stress value has been achieved. Thus, characteristic (5 %-quantile) strength values and fracture energies are input parameters of the numerical model, see Feichter (2013).

To account for both shear mechanisms, mechanism I “net-shear” and II “torsion”, cohesive elements must be implemented in both failure regions, see Fig. 6 (middle). The outcome of the numerical model is shown in Fig. 6 (right) together with the average load-displacement curves from series “EN_C” (fgB), “EN_G” (hB) and “EN_F” (rgB). Numerical results are shown for (i) cohesive elements only for mechanism I (abaqus I), and (ii) cohesive elements for mechanism I and II (abaqus I & II). The annual ring orientation was not considered in the numerical model. However, the results of the numerical study clearly outline, that at F_{max} both mechanisms, I and II, take place and consequence also the non-linear load-displacement behaviour before F_{max}, and the softening afterwards.

The sequence in the fracturing process can also be explained by means of a simple engineering model, see Fig. 7. Thereby and under the circumstance of a supposed lateral support by orthogonal boards, a simple planar model of slender fixed-end beams is considered in the shear area. For simplicity, this fixed-end beam is replaced by a fixed cantilever beam with half in length from left support to the middle, where an asymmetric boundary condition acts and shear force can be introduced. Following assumptions are made:

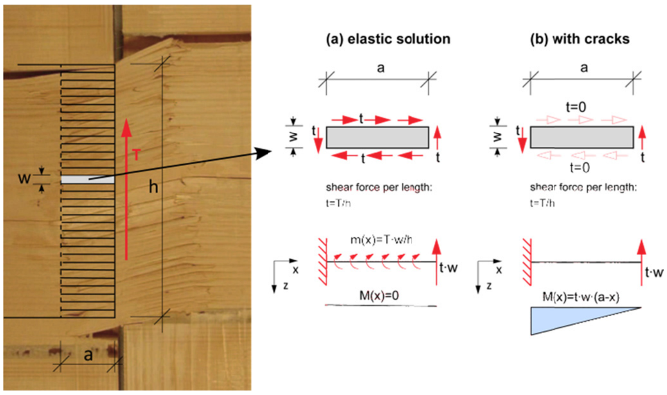

Fig. 7: Simple engineering model

- T is the total shear force to be transmitted;
- the elastic behaviour dominates at beginning (a); after fracture the loading changes to (b).

It can be easily shown that the elastic solution (a) transmits shear forces as a pure shear field without bending. After cracking shear forces can only be transferred via the cross sections of the cantilever (b). In that case a linear increasing bending moment develops and consequences a successive failure of the cantilever in bending and tension.

In brief: failure at F_{max} due to shear forces perpendicular to grain is caused by exceeding the local resistance of interacting mechanism I and II. The numerical model verifies this. Further a softening to a steady state at approximately 40 % to 50 % of F_{max} is given. A successive dissolution of the shear fracture zone, by increasing shearing parallel to grain at the transition zone of early- and latewood and separation of the annual rings, occurs. A flexible composite of fixed-end beams becomes active in tension and bending. This is the cause for the high residual forces. A simple engineering model demonstrated this sequence of fracturing. However, there is no doubt that the shear forces applied perpendicular to grain lead to shearing parallel to grain. Consequently, the shear capacities and the shear behaviour parallel to grain, in reference to a relatively small shear area and volume, indicate the shear resistance perpendicular to grain.

3.5 Main influencing Parameters

In the following the investigated parameters (i) annual ring orientation, (ii) layer width, (iii) layer thickness, and (iv) gap width are discussed individually regarding a possible influence on the shear capacity perpendicular to grain. For statistical inference the Mann-Whitney test was used for testing the hypothesis of pairwise equal medians. This was done although a symmetric distribution is not realised in all series. Box-plots of all results of setup “EN” together with median values of setup “CIB” are provided in Fig. 8.

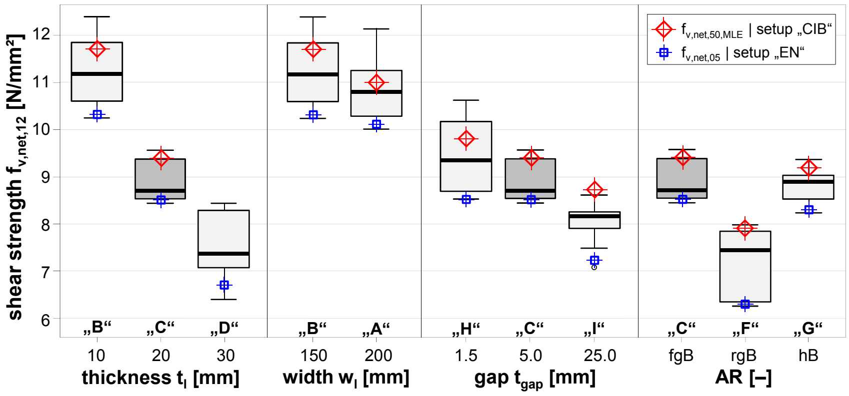

Fig. 8: Box-plot of shear strength $f_{v,\mathrm{net},12}$ of setup “EN” vs. parameter variations; median values of setup “CIB” included

3.5.1 Annual Ring Orientation

Investigating the influence of AR, the following series were tested: series “C” comprising flat grain boards (fgB), series “F” with “pseudo” rift grain boards (rgB) and series “G” with heart boards (hB). The parameters width $w_l = 150$ mm, thickness $t_l = 20$ mm and gap width $t_{gap} = 5$ mm were kept constant. The average densities of “fgb” and “rgB” are well comparable whereas both series “EN_G” and “CIB_G” (hB) show significantly higher densities (mean difference 30 to 40 kg/m³). The results are presented in Fig. 8.

As shear loads perpendicular to grain lead to failures in shear parallel to grain (see chapter 3.4) there is evidence for influences caused by the parameter “annual ring orientation”. Keenan et al. (1985), Denzler and Glos (2007), Dahl and Malo (2009) and Brandner et al. (2012) found significant higher shear strength (on average 6 % to 40 %) in RL (radial-longitudinal) in comparison to TL direction (tangential-longitudinal), Müller et al. (2004) not. In TL shearing occurs in the transition zone of early- und latewood. In RL, shearing requires fracturing of early- and latewood. Consequently, a higher resistance and a positive dependency of $f_{v,\mathrm{RL}}$ on specimen’s global density are expected. Thus, flat grain boards, in comparison to rift grain and heart boards, have commonly a higher resistance in shear. The annual ring orientation in heart boards may comprise both, shearing in RL in the core and in TL at the edges. In dependency of the width of the core lamella a resistance in-between flat and rift grain boards is expected.

Statistical inference confirms the expectations regarding significant lower shear strengths in rift grain boards in comparison to flat grain boards ($p < 0.01$). Also between series “rgB” and “hB” significant differences in the medians are observed ($p < 0.01$). Some impact of the significant higher density in series "hB" cannot be excluded. As flat grain boards are commonly used in CLT production, relatively high shear resistances can be realised. However, in both setups, "EN" and "CIB", an interaction of shear and compression perpendicular to grain occurs. Keenan (1973, 1974) observed that $f_{v,\mathrm{RL}}$ is much more influenced in case of interaction with $\sigma_{c,90}$ than $f_{v,\mathrm{TL}}$.

3.5.2 Layer Width

A comparison is made between w_l = 150 mm (series "A") and 200 mm (series "B") wide boards. This corresponds to a ratio of 1 : 1.33. The parameters t_l = 10 mm, t_{gap} = 5 mm and AR = "fgB" were kept constant. The average densities of all series are in-line. Comparison shows that the hypothesis of equal medians cannot be rejected ($p > 0.05$). This is also obvious considering the comparable ranges of realisations in series "A" and "B", see Fig. 8. However, as the range in commonly used board widths (100 mm $\leq w_l \leq$ 240 mm) is much larger than tested some relevant influence on the shear resistance cannot be excluded, in particular in wide boards were shearing at the edges more and more occurs in TL, known to realise lower shear resistances (see chapter 3.5.1).

3.5.3 Layer Thickness

Test series "B" (t_l = 10 mm), "C" (t_l = 20 mm) and "D" (t_l = 30 mm) were conducted for examining the influence of layer thickness. The parameters w_l = 150 mm, t_{gap} = 5 mm and AR = "fgB" were kept constant. The average densities of all series are in-line. The results are visualised in Fig. 8. In both test setups "EN" and "CIB" and in all pairwise comparisons the hypothesis of equal medians was rejected ($p < 0.01$). Two main reasons are identified: at first, the impact of size on shear strength parallel to grain is well known and documented, e.g. in Brandner et al. (2012). They report on a regressive course of shear strength with increasing shear area A_s. Secondly, load transfer from top layers to the core layer via the gluing interfaces causes a locking effect. This locking effect, which restrains the shear action, is at highest in the gluing interface and declines until the centre of the core lamella.

Fig. 9 contains a comparison of the size effect on shear strength parallel to grain for construction timber, based on a literature survey and tests reported in Brandner et al. (2012), some additional data sets for clear wood and the results found for setup "EN". The plot shows the shear strength versus the shear area A_s. Deviating from the definition of A_s in Brandner et al. (2012), for the herein presented test setup and results A_s is defined by the cross section of the core lamella, with $A_s = w_l \cdot t_l$. Overall, good congruence is found. The steeper regressive course in $f_{v,\mathrm{net,mean}}$ vs. the shear area A_s is dedicated to the locking effect. In view of the tendency to standard lamella thicknesses t_l = 20, 30, 40 mm an extrapolation for 40 mm thick lamellas is required.

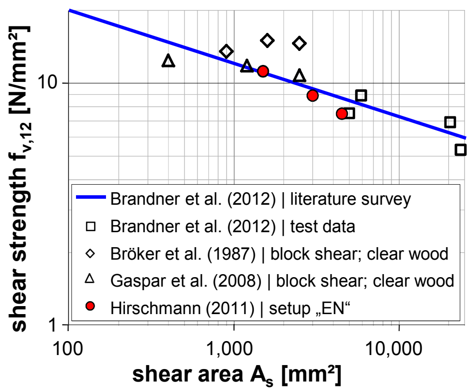

Fig. 9: Size effect on mean shear strength

3.5.4 Gap Width

The influence of gap width on shear strength was analysed for t_{gap} = 1.5 mm (series "H"), 5.0 mm (series "C") and 25.0 mm (series "I"). The parameters w_l = 150 mm, t_l = 20 mm and AR = "fgB" were kept constant. The average densities of series "H" and "I" are well comparable whereas both series "EN_C" and "CIB_C" (t_{gap} = 5.0 mm) show significantly lower densities (mean differences of 15 to 20 kg/m³ in "EN" and 25 to 40 kg/m³ in "CIB"). Because of the dependency of $f_{v,\mathrm{RL}}$ on the density in softwood, an influence on $f_{v,\mathrm{net}}$ cannot be excluded. The results are shown in Fig. 8.

As a quantitative correction of the differences in density is not available statistical inference is made on observed pairwise median shear strengths. Significant differences in medians are found between t_{gap} = 1.5 mm and 5.0 mm and 5.0 mm and 25.0 mm in setup "CIB" ($p < 0.05$). High significant differences ($p < 0.01$) are identified between t_{gap} = 1.5 mm and 25.0 mm in both setups "EN" and "CIB" and between t_{gap} = 5.0 mm and 25.0 mm in "EN". However, the hypothesis of equal medians cannot be rejected comparing series with t_{gap} = 1.5 mm and 5.0 mm in setup "EN" ($p = 0.10$).

In general, a decrease in the resistance with increasing gap width is expected. This is because of a reduced influence of the locking effect as well as by increasing bending stresses in the gap. Thus, a regressive course of shear strength versus gap width is expected.

4 Resistance in Shear Loads perpendicular to Grain: Proposal

In chapter 3 the resistance against shear loads perpendicular to grain was demonstrated and relevant influencing parameters identified. The interaction of shear and compression perpendicular to grain, which leads to some overestimation of the real shear resistance, was mentioned. However, at the ultimate load interaction of shear mechanisms I "net-shear" and II "torsion" may counteract the shear-compression interaction. In view of the material commonly used for CLT in Europe, flat grain boards with cross section w_l x t_l = 150 x 30 mm² and a gap width of t_{gap} = 5 mm (as upper boundary) are defined as reference. Furthermore, a lognormal distribution ($f_{v,\text{net}} \sim$ 2pLND) and a coefficient of variation $CV[f_{v,\text{net}}]$ = 15 % are assumed. Based on $f_{v,\text{net},12,\text{mean}}$ = 7.5 N/mm² in series "EN_D" the characteristic (5 %-quantile) shear strength is $f_{v,\text{net},05}$ = 5.8 N/mm². In case of lamellas with t_l = 40 mm, as the upper boundary of commonly used raw material, a value of $f_{v,\text{net},05}$ = 5.3 N/mm² is found by extrapolating the power regression model, based on mean values of series "EN_B", "EN_C" and "EN_D". However, these strength values are gained from examinations made on single nodes of a three layer CLT element. The question remains if the verification of shear in plane, currently done on single nodes and RVSEs, is representative for a whole CLT diaphragm. As demonstrated in chapter 2 this question cannot be answered yet, but an engineering judgement can be made.

In view of the bearing model for CLT in bending out of plane, we define a reference CLT diaphragm of 4 x 4 nodes and of five layers, each composed of board material in reference dimension. Assuming a shear load, homogeneously applied on the cross sections of this diaphragm, in total two times the tested node in thickness direction are found to act in parallel. Due to allocated shear stresses, a failure of the diaphragm in plane according to "net-shear" can only take place in cases where all nodes in x-direction (direction of the top layers) fail. Again, a parallel system action, active in y-direction (direction of the cross layers) of the diaphragm, can be identified. Of course, in a 4 x 4 element this kind of shearing can occur on three planes, whereby the weakest plane governs the ultimate load. This confirms to a serial system action, active in x-direction of the diaphragm. Considering the load-displacement curve of shear perpendicular to grain, a non-linear behaviour, already before reaching the ultimate load, and the ability to withstand large deformations on a moderate load level after softening is found. Taking into account the remarkable possibility to transfer loads between the parallel active nodes, there is evidence that the mean resistance of the diaphragm in shear will not be remarkable different from the mean shear resistance of single nodes. However, because of the parallel system action of 2 x 4 nodes a significant reduction in dispersion of $f_{v,\text{net}}$ is expected. On the one hand this circumstance reduces the influence of serial system action between the shear planes, and on the other hand it offers the possibility of rising $f_{v,\text{net},05}$.

Although a theoretical and practical verification is not available yet the current procedure of verifying in plane shear resistance on single nodes (see e.g. Bogensperger et al. 2010) is judged as reliable and proposed in the meantime until further progress is made. For simplicity a characteristic (5 %-quantile) shear strength of **$f_{v,\text{net}}$ = 5.5 N/mm²** is proposed for all lamella thicknesses $t_l \leq$ 40 mm.

5 Conclusions and Outlook

We presented a test configuration, which allows determining the resistance in shear perpendicular to grain on single CLT nodes. Relevant parameters were investigated and their influence on shear strength $f_{v,\text{net}}$ quantified. Thereby, the parameters (i) thickness of the core lamella t_l, (ii) the annual ring orientation AR, and (iii) the gap width t_{gap} were found to affect the shear strength significantly.

Additional to testing, the load-displacement behaviour and in particular the failure process were studied by means of a numerical and a simple engineering model. The interaction of both shear mechanisms, mechanism I "net-shear" and II "torsion", the fracturing in shear parallel to grain and successive dissolution of the material was verified. Analogies to shear resistance parallel to grain of structural timber were identified, in particular regarding the size effect.

Based on engineering judgement the shear resistance according to mechanism I was discussed for a whole CLT diaphragm. In conclusion, a characteristic (5 %-quantile) value of $f_{v,net,05}$ = 5.5 N/mm² for common flat grain board material of Norway spruce with $t_l \leq 40$ mm and $t_{gap} \leq 5$ mm, and the verification of shear in plane on single nodes or RVSEs, including both, the verification of mechanism I and II, is proposed.

Current investigations are made on a hardening property after softening and on the shear resistance at $t_{gap} = 0$. Fig. 10 illustrates first results of flat and rift grain boards at $t_{gap} = 5$ and 0 mm. Although and not to the full extend relevant for the shear behaviour of a whole CLT diaphragm, a tremendous ability to large deformations at a steady state on a relatively high load level, followed by a hardening which exceeds mostly the first, currently evaluated peak level, is observed. Further tests and investigations on whole CLT elements are scheduled.

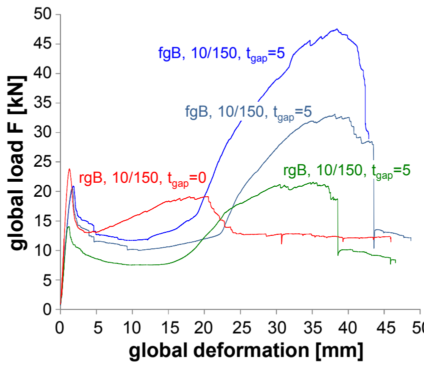

Fig. 10: Single test results on specific parameter settings

6 Acknowledgement

The work and progress made by Hirschmann (2011) and Feichter (2013), as part of their Master theses, is thankfully acknowledged. Thanks also to Prof. Roberto Tomasi from University of Trento / Italy for discussing several aspects concerning the tests published in Andreolli et al. (2012).

7 References

Andreolli M, Tomasi R, Polastri A (2012) **Experimental investigation on in-plane behaviour of cross-laminated-timber elements**. Paper and Presentation, CIB-W18/45-12-4, Växjö, Sweden

Blaß H J, Görlacher R (2002) **Zum Trag- und Verformungsverhalten von Brettsperrholz-Elementen bei Beanspruchung in Plattenebene**. *Bauen mit Holz*, 11:34–41; 12:30–34 (in German)

Blaß H J, Flaig M (2012) **Stabförmige Bauteile aus Brettsperrholz**. Karlsruher Berichte zum Ingenieurholzbau, No. 24, Karslruher Institut für Technologie (KIT), Lehrstuhl für Ingenieurholzbau und Baukonstruktionen, ISBN 978-3-86644-922-0 (in German)

Bogensperger T, Moosbrugger T, Schickhofer G (2007) **New test configuration for CLT-wall-elements under shear load**. CIB-W18/40-21-2, Bled, Slovenia

Bogensperger T, Moosbrugger T, Silly G (2010) **Verification of CLT-plates under loads in plane**. WCTE'2010, Riva del Garda, Italy

Bosl R (2002) **Zum Nachweis des Trag- und Verformungsverhaltens von Wandscheiben aus Brettlagenholz**. Dissertation, Universität der Bundeswehr München, Fakultät für Bauingenieur- und Vermessungswesen (in German)

Brandner R (2012) **Stochastic system actions and effects in engineered timber products and structures**. Dissertation, Institute of Timber Engineering and Wood Technology, Graz University of Technology

Brandner R, Gatternig W, Schickhofer G (2012) **Determination of Shear Strength of Structural and Glued Laminated Timber**. CIB-W18/45-12-2, Växjö, Sweden

Brandner R (2013) **Production and Technology of Cross Laminated Timber (CLT): A state-of-the-art Report**. In: Harris R, Ringhofer A, Schickhofer (ed.) Focus Solid Timber Solutions – European Conference on Cross Laminated Timber (CLT), 21st–22nd May 2013, Graz, Austria

Bröker F W, Meierhofer U A, Radović B (1987) **Einfluss der Probengröße auf die Druckscherfestigkeiten würfelförmiger Fichtenholzproben**. *Holz als Roh- und Werkstoff*, 45:445–448 (in German)

CUAP Common Understanding of Assessment Procedure (2005) **Solid wood slab element to be used as a structural element in buildings**. ETA request No 03.04/06, Österreichisches Institut für Bautechnik (OIB), Vienna, Austria

Dahl K B, Malo K A (2009) **Linear shear properties of spruce softwood**. *Wood Science and Technology*, 43:499–525

Denzler J K, Glos P (2007) **Determination of shear strength values according to EN 408**. *Materials and Structures*, 40:79–86

EN 338:2009-10 **Structural timber – Strength classes**. European Standard, European Committee for standardization

EN 408:2012-07 **Timber structures – Structural timber and glued laminated timber – Determination of some physical and mechanical properties**. European Standard, European Committee for standardization

EN 789:2004-10 **Timber structures – Test methods – Determination of mechanical properties of wood based panels**. European Standard, European Committee for standardization

Feichter I (2013) **Spannungs- und Traglastberechnungen an ausgewählten Problemen der Holz-Massivbauweise in Brettsperrholz**. Master thesis, Institute of Timber Engineering and Wood Technology, Graz University of Technology (in German)

Flaig M, Blaß H J (2013) **Shear strength and shear stiffness of CLT-beams loaded in plane**. CIB-W18/46-12-3, Vancouver, Canada

Gaspar F, Cruz H, Gomes A (2008) **Evaluation of glued laminated timber structures – core extraction and shear testing**. World Conference on Timber Engineering (10th WCTE), Miyazaki, Japan

Hirschmann B (2011) **Ein Beitrag zur Bestimmung der Scheibenschubfestigkeit von Brettsperrholz**. Master thesis, Institute of Timber Engineering and Wood Technology, Graz University of Technology (in German)

Jeitler G (2004) **Versuchstechnische Ermittlung der Verdrehungskenngrößen von orthogonal verklebten Brettlamellen**. Diploma thesis, Institute of Steel, Timber and Shell Structures, Graz University of Technology (in German)

Jöbstl R A, Bogensperger T, Schickhofer G, Jeitler G (2004) **Mechanical Behaviour of Two Orthogonally Glued Boards**. WCTE'2004, Lahti, Finland

Jöbstl R A, Bogensperger T, Schickhofer G (2008) **In-plane shear strength of cross laminated timber**. CIB-W18/41-12-3, St. Andrews, Canada

Källsner B, Ditlevsen O, Salmela K (1997) **Experimental verification of a weak zone model for timber in bending**. IUFRO S 5.02 – Timber Engineering, Copenhagen, Denmark

Keenan F J (1973) **The shear strength of glued-laminated timber**. University of Toronto, Department of Civil Engineering

Keenan F J (1974) **Shear strength of wood beams**. *Forest Products Journal*, 24(9):63–70

Keenan F J, Kryla J, Kykong B (1985) **Shear strength of spruce glued-laminated timber beams**. *Canadian Journal of Civil Engineering*, 12:661–672

Kreuzinger H, Sieder M (2013) **Einfaches Prüfverfahren zur Bewertung der Schubfestigkeit von Kreuzlagenholz / Brettsperrholz**. *Bautechnik*, 90(5):314–316 (in German)

Müller K, Sretenovic A, Gindl W, Grabner M, Wimmer R, Teischinger A (2004) **Effects on macro- and micro-structural variability on the shear behaviour of softwood**. *IAWA Journal*, 25(2):231–243

Spengler R (1982) **Festigkeitsverhalten von Brettschichtholz unter zweiachsiger Beanspruchung, Teil 1 – Ermittlung des Festigkeitsverhaltens von Brettelementen aus Fichte durch Versuche**. Berichte zur Zuverlässigkeitstheorie der Bauwerke, Heft 62, Laboratorium für den konstruktiven Ingenieurbau, Technische Universität München (in German)

Traetta G, Bogensperger T, Moosbrugger T, Schickhofer G (2006) **Verformungsverhalten von Brettsperrholzplatten unter Schubbeanspruchung in der Ebene**. In: Moosbrugger M, Schickhofer G, Unterwieser H, Krenn H (ed.) Brettsperrholz – Ein Blick auf Forschung und Entwicklung. 5. Grazer Holzbau-Fachtagung (5.GraHFT'06), 29th Sept. 2006, Graz, Austria (in German)

Wallner G (2004) **Versuchstechnische Ermittlung der Verschiebungskenngrößen von orthogonal verklebten Brettlamellen**. Diploma thesis, Institute of Steel, Timber and Shell Structures, Graz University of Technology (in German)

INTERNATIONAL COUNCIL FOR RESEARCH AND INNOVATION
IN BUILDING AND CONSTRUCTION

WORKING COMMISSION W18 - TIMBER STRUCTURES

SHEAR STRENGTH AND SHEAR STIFFNESS OF CLT-BEAMS LOADED IN PLANE

M Flaig
H J Blaß

Karlsruhe Institute of Technology

GERMANY

Keywords: cross laminated timber, CLT, beam, in plane, shear strength, shear stiffness

Presented by M Flaig

M Fragiacomo asked in which application shear deformation would be important. M Flaig stated that in glulam the shear deformation might be in the range of 3 to 6 %, but in CLT as a beam the shear deformation might be in the range of 10%; therefore, shear component would be more important for CLT used as a beam.

G Schickhofer asked and received clarification about the failure mode of CLT elements. Typical elements were discussed in relationship to the realistic failure modes.

A Buchanan asked about the rolling shear failure and whether it was indeed rolling shear failure. M Flaig stated that torsion shear strength would be higher than that of rolling shear strength and discussed the small area of thickness near the glue interface and stated it was indeed rolling shear failure.

F Lam asked about past work of using CLT as beam by I Bejtka. M Flaig stated that they are aware of the work.

S Aicher received clarification about the low shear modulus slip value in equation 13.

BJ Yeh asked about the influence of gaps, laminate thickness etc. on shear strength and stiffness. M Flaig stated single basic strength value was used in the model without consideration of the gaps and laminate thickness.

M Popovski stated that the FPinnovations results showed that shear strength of beams varied from 2 to 6 MPa. Method was needed to account for the large variations and the method presented could explain the varying test results.

A Aicher asked if edge glued material was used and what k value would one use. M Flaig responded k would be assumed as ∞ resulting in $G_{eff,bsp}$=G_{lam}; therefore no torsion in between.

Shear strength and shear stiffness of CLT-beams loaded in plane

M. Flaig, H. J. Blaß
Holzbau und Baukonstruktionen
Karlsruhe Institute of Technology, Germany

1 General

Beams made of cross laminated timber (CLT) offer several advantages over solid or glued laminated timber beams due to their typical layup of orthogonally bonded layers. One major benefit of CLT is the high tensile strength perpendicular to the beam axis making CLT-beams less susceptible to cracks. Therefore, the use of CLT for the production of beams with tensile stresses perpendicular to the beam axis provides a considerably improved robustness.

In Europe, the requirements for the production and design of CLT-products are currently governed by technical approvals. However, a draft European standard specifying the performance requirements of cross laminated timber products has already been published in 2011. Although most of today's CLT-products are very similar in their structure and also efforts are made to develop standardised methods for design and verification of CLT, there is, so far, no general approach for the shear design of CLT-members loaded in plane. In fact, the strength properties and also the design methods given in different technical approvals for the verification of in plane shear stresses vary significantly and, moreover, for most products no information on the shear stiffness in plane direction is given at all. One main reason for the disparities seems to be the more complex calculation of shear stresses and deformations in CLT-members compared to traditional timber materials and therefore, in many cases, vastly simplified methods are used.

The intention of the present paper is to contribute to the development of standardised methods for the shear design of CLT-members loaded in plane. Therefore, at first, analytical solutions for the calculation of shear stresses and shear deformations in CLT-beams loaded in plane are presented. The equations are then validated by test results.

2 Shear strength of CLT-beams loaded in plane

2.1 Failure modes

In CLT-beams, like in solid materials, transversal forces acting in plane direction will cause shear stresses. The shear stress distribution can be assumed to be constant over the element thickness. In CLT-beams where adjacent lamellae within individual layers are not glued to each other at their edges, however, the thickness is not constant throughout the beam. In sections that coincide with unglued joints between neighboured lamellae shear forces can hence only be transferred by lamellae arranged perpendicular to the joints. The shear stresses in these net cross sections will consequently be greater than in the gross cross sections in-between unglued joints. The transfer of shear forces between longitudinal and transversal layers also causes shear stresses in the crossing areas of orthogonally bonded lamellae. Considering both shear stresses in the lamellae and the crossing areas three different failure modes can be distinguished in CLT-beams subjected to shear stresses as shown in Figure 1.

Failure mode I is characterised by shear failure parallel to the grain in the gross cross section of a beam. The failure occurs in sections between unglued joints with equal shear stresses in longitudinal layers and transversal layers.

Failure mode II is characterised by shear failure perpendicular to the grain in the net cross section of a beam. The failure occurs in sections coinciding with unglued joints with shear stresses only in lamellae perpendicular to the joints.

Failure mode III is characterised by shear failure within the crossing-areas between orthogonally bonded lamellae. The failure is caused by torsional and unidirectional shear stresses resulting from the transfer of shear forces between adjacent layers.

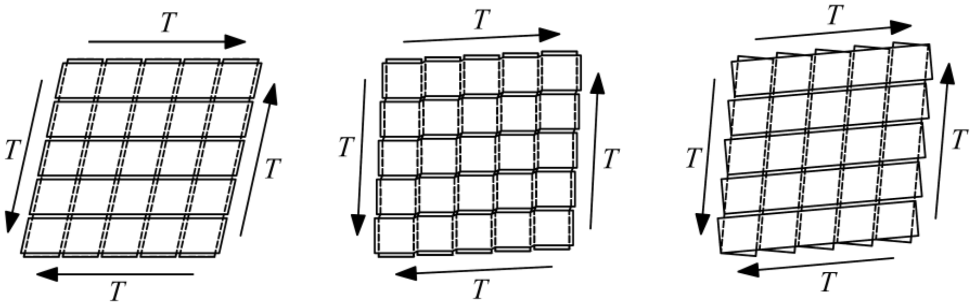

Figure 1: Failure modes I, II and III in CLT-beams subjected to transversal forces in plane direction (from left to right)

2.2 Calculation of shear stresses

For design and verification of CLT beams the shear stresses, corresponding to each of the three failure modes need to be calculated. In failure modes I and II shear stresses in the gross and the net cross section, respectively, need to be evaluated. In failure mode III three different components of shear stresses can be distinguished. The calculation of the five different shear stress components is described in the following sections.

2.2.1 Shear stresses in the lamellae

In CLT-beams the bonding between adjacent longitudinal lamellae, although connected only indirectly via transversal layers, is strong enough to ensure the layers to act as solid units. Shear stresses τ_{xz} in the lamellae causing failure parallel and perpendicular to the grain in failure modes I and II, respectively, can therefore be calculated according to Bernoulli-Euler Beam Theory by taking into account the appropriate thickness of the cross section considered.

$$\tau_{\text{xz,gros}} = \frac{V_{\text{z}} \cdot S_{\text{y,gross}}}{I_{\text{y,gross}} \cdot t_{\text{gross}}}$$ Shear stress in the gross cross section (Failure Mode I) Eq. 1

$$\tau_{\text{xz,net}} = \frac{V_{\text{z}} \cdot S_{\text{y,net}}}{I_{\text{y,net}} \cdot t_{\text{net}}}$$ Shear stress in the net cross section (Failure Mode I) Eq. 2

where t_{gross} is the total thickness of the element
and t_{net} is the smaller of the sum of the thickness of longitudinal or transversal layers

The parabolic functions in Eq. 1 and Eq. 2 describe curves that envelope the actual shear stresses in the net and the gross cross section. In CLT-beams normally the proportion of transversal layers will be kept as small as possible. Therefore, in most cases the net cross section of transversal layers is decisive for the calculation of shear stresses $\tau_{xz,net}$. Starting from the upper and lower edge of a cross section, at first shear stresses both in longitudinal and transversal layers follow the parabolic function calculated with the gross cross section. In unglued joints between adjacent lamellae, however, shear stresses must be zero. In horizontal sections through unglued joints between longitudinal lamellae the shear stresses acting in transversal layers consequently can be found on a parabola calculated with the net cross section of transversal layers. As an example the distribution of shear stresses in the gross and the net cross section of a three layered CLT-beam is shown in Figure 2. The width of grooves and peaks in the curves of shear stresses depend on the stiffness of crossing areas and the stiffness ratios within a beam and is depicted only in a general manner in the graphs.

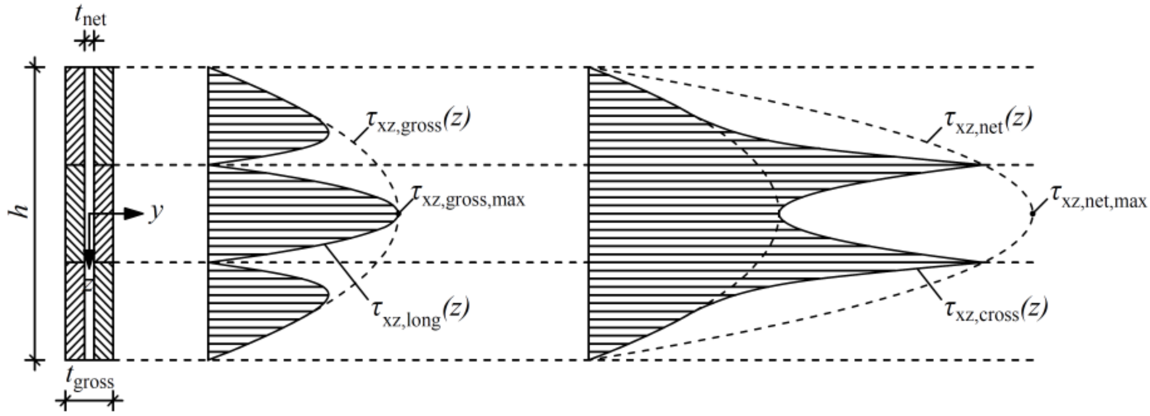

Figure 2: Distribution of shear stresses in the lamellae of a three-layered CLT-beam in cross sections within transversal lamellae: shear stresses $\tau_{xz,long}$ in longitudinal lamellae (left) and shear stresses $\tau_{xz,cross}$ in transversal lamella (right)

A conservative estimate of the actual maximum shear stress in longitudinal and transversal layers can be made by calculating the peak values of the parabolic functions according to Eq. 3 and Eq. 4.

$$\tau_{xz,gross,max} = \frac{3 \cdot V_z}{2 \cdot h \cdot t_{gross}}$$ Theoretical maximum shear stress in longitudinal layers — Eq. 3

$$\tau_{xz,net,max} = \frac{3 \cdot V_z}{2 \cdot h \cdot t_{net}}$$ Theoretical maximum shear stress in transversal layers — Eq. 4

For beams with an even number of lamellae in longitudinal layers Eq. 3 overestimates the maximum shear stress in the gross cross section whereas in beams with an odd number of lamellae in longitudinal layers too large shear stresses in the net cross section result from Eq. 4. For the cross section depicted in Figure 2 the difference between the theoretical and the actual maximum shear stress in the transversal layer amounts to 11%. However, the error decreases rapidly with an increasing number m of lamellae in longitudinal layers.

Table 1: Error in shear stresses calculated according to the expressions given in Eq. 3 and Eq. 4

number m of lamellae in longitudinal layers	2	3	4	5	6	7	8	9	10	11	12
error in the gross cross section in %	25	-	6.3	-	2.8	-	1.6	-	1.0	-	0.7
error in the net cross section in %	-	11	-	4.0	-	2.0	-	1.2	-	0.8	-

2.2.2 Shear stresses in the crossing areas

In failure mode III three different components of shear stresses occurring in the crossing areas have to be considered:

Shear stresses parallel to the beams axis which are caused by the change of the bending moment and the balancing of the resulting differential normal stresses in longitudinal lamellae,

Torsional shear stresses which arise due to the eccentricity between the centre lines of adjacent lamellae and

Shear stresses perpendicular to the beam axis occurring in the crossing areas at supports and concentrated load application points and in beams with variable cross section, such as notched beams, beams with holes and tapered beams.

The first two shear stress components can be derived from the model of a composite beam, where the longitudinal lamellae represent the individual parts of the beam. The third component corresponds to transverse tensile or compressive stresses occurring in glulam beams and can be calculated accordingly.

a) Shear stresses parallel to the beam axis

Since adjacent lamellae within longitudinal layers are not bonded at their edges differential normal forces dN_i caused by the change of the bending moment along the axis of a CLT-beam need to be transferred via the crossing areas between longitudinal and transversal layers. The normal forces N_i and the corresponding differentials dN_i acting in longitudinal lamellae can be calculated using the model of a composite beam shown in Figure 3. The resulting unidirectional shear stresses τ_{yx} in the crossing areas are obtained by dividing the differential normal force in a section of a longitudinal lamella through the crossing areas of the specific lamella within the considered section. As a result the distribution of shear stresses τ_{yx} within the element thickness depends on the ratio between the axial stiffness of longitudinal lamellae and the stiffness of the connections between longitudinal and transversal layers, i.e. the stiffness of crossing areas.

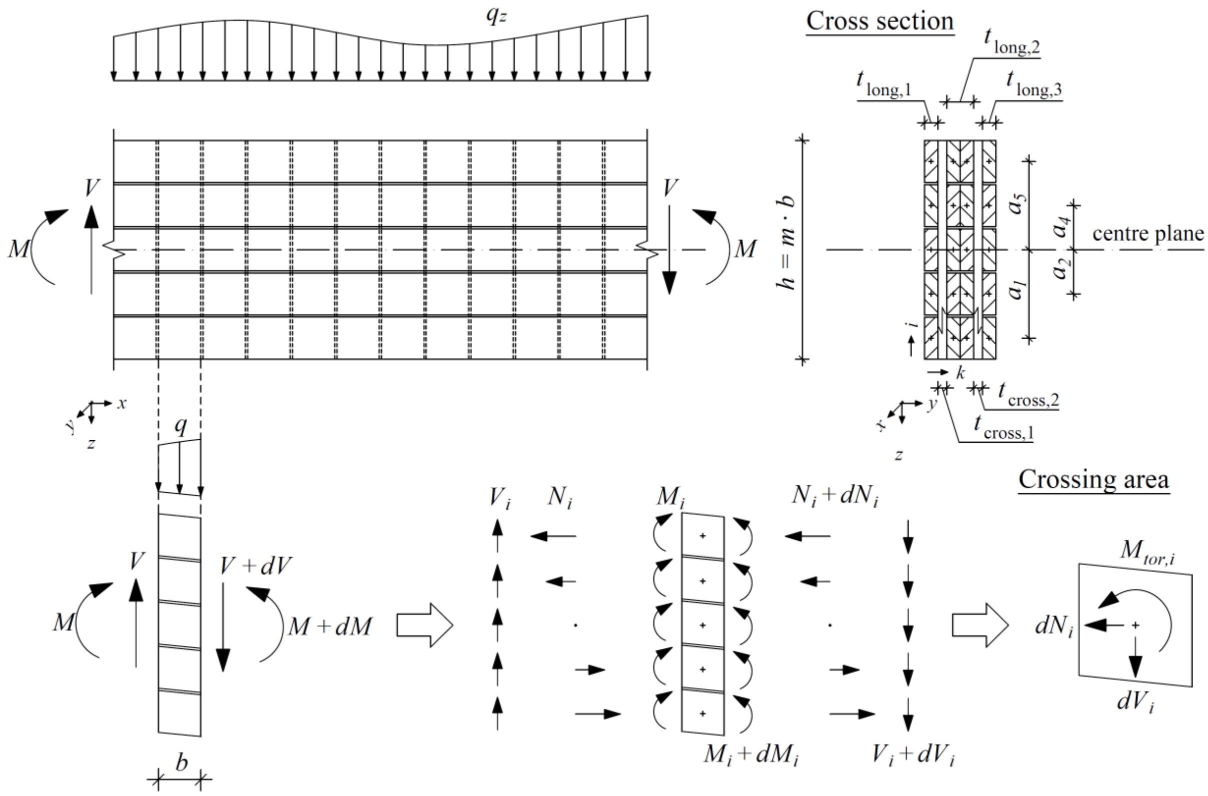

Figure 3: Side view and cross section of a four-layered CLT-beam loaded in plane (top) and internal forces in the beam, in individual lamellae and in the crossing areas (bottom, from left to right)

$$\tau_{yx} = \frac{dN_{i,max}}{n_{CA} \cdot b^2} \qquad \text{Eq. 5}$$

where $dN_{i,max} = \dfrac{dM}{I_{y,net,long}} \cdot a_{i,max} \cdot t_{net,long} \cdot b$ with $dM = V \cdot dx = V \cdot b$

$$I_{y,net,long} = \frac{m^3 \cdot b^3 \cdot t_{net,long}}{12} \quad \text{and} \quad a_{i,max} = \frac{m-1}{2} \cdot b$$

Substituting the given expressions for dN_i, $I_{net,long}$ and $a_{i,max}$ into Eq. 5 yields

$$\tau_{yx} = \frac{6 \cdot V}{b^2 \cdot n_{CA}} \cdot \left(\frac{1}{m^2} - \frac{1}{m^3} \right) \qquad \text{Eq. 6}$$

As can be seen, shear stresses τ_{yx} are linearly dependent on the reciprocal values of the squared width of lamellae b and the number of crossing areas n_{CA} within the element thickness. The last term in brackets describes the influence of the number of lamellae m within longitudinal layers. Eq. 5 and Eq. 6 provide accurate results for CLT-beams with a constant ratio of $t_{long,k}/n_{CA,k}$ between the thickness of an individual longitudinal layer and the number of glue lines the respective layer shares with adjacent transversal layers. In such beams shear stresses τ_{yx} in the crossing areas are constant within the element thickness since the ratio between the axial stiffness and the stiffness of adjacent crossing areas is equal for all longitudinal lamellae. In contrast to this, shear stresses τ_{yx} vary within the thickness of CLT-beams where the ratio of $t_{long,k}/n_{CA,k}$ is not equal for all longitudinal layers. However, within the range of layups that are used in practice the variation of shear stresses τ_{yx} within the element thickness is small, especially in CLT-beams made of softwood, with a modulus of elasticity of lamellae of about 11,000 N/mm² and a slip modulus of crossing areas of about 5 N/mm³ (see 3.2). Therefore Eq. 5 and Eq. 6 provide good approximations for the shear stresses τ_{yx} in such beams.

b) Torsional shear stresses

Due to the eccentricity of the normal forces N_i acting in the centre lines of adjacent longitudinal lamellae the differential normal forces dN_i transferred via the crossing areas not only induce shear stresses parallel to the beam axis, but also torsional shear stresses within the crossing areas. Like shear stresses τ_{yx} acting in the direction of the beam axis, torsional shear stresses τ_{tor} can be derived from the model of a composite beam shown in Figure 3. Assuming that torsional shear stresses are, like shear stresses τ_{yx}, constant within the beam thickness and in addition also uniformly distributed within the beam height, which is given on the condition that the lamellae in transversal layers stay straight in the deformed beam, torsional shear stresses in the crossing areas can be calculated according to Eq. 7. In Eq. 7 τ_{tor} is the stress vector acting parallel to the shorter edges of a crossing area causing rolling shear stresses in the narrower of the two bonded lamellae and b is the width of the broader lamellae.

$$\tau_{tor} = \frac{\sum_{i=1}^{m} M_{tor,i}}{n_{CA} \cdot \sum_{i=1}^{m} I_{p,CA}} \cdot \frac{b}{2} \qquad \text{Eq. 7}$$

where $\sum_{i=1}^{m} M_{tor,i} = \sum_{i=1}^{m} dN_i(x) \cdot a_i = \dfrac{dM(x)}{I_{y,net,long}} \cdot t_{net,long} \cdot b \cdot \sum_{i=1}^{m} a_i^2$,

$$\sum_{i=1}^{m} a_i^2 = b^2 \cdot \sum_{i=1}^{m} \left(\frac{m+1}{2} - i \right)^2 = b^2 \cdot \frac{(m^3 - m)}{12} \quad \text{and} \quad \sum_{i=1}^{m} I_{p,CA} = m \cdot \frac{b^4}{6}$$

The assumption of a constant width b of lamellae in all longitudinal and transversal layers and the substitution of the expressions above into Eq. 7 yields the closed-form solution given in Eq. 8. A closed-form solution for beams with lamellae of different widths in longitudinal and transversal layers can be found in Blaß and Flaig (2012).

$$\tau_{\text{tor}} = \frac{3 \cdot V}{b^2 \cdot n_{\text{CA}}} \cdot \left(\frac{1}{m} - \frac{1}{m^3} \right). \qquad \text{Eq. 8}$$

The torsional shear stresses τ_{tor} are, like shear stresses τ_{yx}, linearly dependent on the reciprocal values of the squared width of lamellae b and the number of crossing areas n_{CA} within the element thickness. The term in brackets describes again the influence of the number of lamellae m within longitudinal layers. In beams with a large number m of lamellae within longitudinal layers the third order term $1/m^3$ becomes very small and therefore may be neglected. This simplifies Eq. 8 to

$$\tau_{\text{tor}} = \frac{3 \cdot V}{b^2 \cdot n_{\text{CA}} \cdot m} = \frac{V \cdot b}{\Sigma I_{\text{p,CA}}} \cdot \frac{b}{2}. \qquad \text{Eq. 9}$$

The expression on the right side can also be found in many technical approvals, where it is given for the calculation of torsional shear stresses in shear walls and diaphragms.

c) Shear stress components perpendicular to the beam axis

Shear stresses τ_{yz} in the crossing areas of CLT-beams may result from both external forces, e.g. support reactions and loads, and internal forces arising from changes in the cross section or the direction of the beam axis. Equations for the calculation of shear stress components τ_{yz} in the crossing areas of CLT-beams with holes and notches as well as for tapered CLT-beams and CLT-beams with dowel type connections loaded perpendicular to the beam axis are specified in Blaß and Flaig (2012).

For beams subjected to external forces acting in plane and on the surface, shear stresses τ_{yz} can be calculated according to Eq. 10, provided that the loads are transferred by contact via the end grain surfaces of transversal layers only and on the assumption that shear stresses τ_{yz} are uniformly distributed within the beam height.

$$\tau_{\text{yz}} = \frac{q_{\text{z}}}{m \cdot b} \qquad \text{Eq. 10}$$

2.3 Strength properties and verification of shear stresses

In the design of CLT-beams each of the above-described shear stresses must be verified with the corresponding shear strengths related to the relevant shear failure mode. In the crossing areas also the interaction of simultaneously acting shear stress components has to be taken into consideration.

2.3.1 Failure Mode I

Since failure mode I is characterised by shear failure parallel to the grain within the lamellae, the shear strength specified in EN 338 is used for the verification of shear stresses. Since, in general, the cross sections of the individual lamellae are rather small and moreover the development of large, individual cracks is impeded by transversal layers, the influence of cracks on the shear strength of the lamellae is low. Therefore, a factor k_{cr} = 1,0 can be assumed, which is also specified in Germany's National Annex to Eurocode 5.

2.3.2 Failure Mode II

In failure mode II shear failure occurs in the net cross section within the joints between non edge bonded lamellae. Jöbstl et al. (2008) determined a mean value of the corresponding shear strength $f_{v,lam,90}$ perpendicular to the grain of 12.8 N/mm² and a characteristic value of 10.3 N/mm² by tests with single boards subjected to shear forces perpendicular to the grain. Considerably higher shear stresses perpendicular to the grain were evaluated from tests with beams with holes (Blaß and Flaig, 2012), however, none of the tested beams failed within the net cross section.

2.3.3 Failure Mode III

In CLT-beams subjected to transversal forces in plane direction failure in the crossing areas is caused by the interaction of at least two shear stress components, since both torsional shear stresses and shear stresses in direction of the beam axis always occur simultaneously. In addition shear stresses perpendicular to the beam axis may arise from external or internal forces. In the verification of shear stresses in failure mode III the interaction of the different shear stress components has to be considered.

In recent years the shear strength of crossing areas against both shear forces and torsional moments, has been determined in several test series. An overview of the shear strengths evaluated from tests with small specimens comprising one or two crossing areas is given in Table 2, lines 2 - 5.

Table 2: Torsional shear strength and rolling shear strength of crossing areas determined by tests with small specimens and with CLT-beams

Author	description of test setup	n	$f_{v,tor,mean}$ in N/mm²	$f_{v,tor,k}$ in N/mm²	$f_{R,mean}$ in N/mm²	$f_{R,k}$ in N/mm²
Blaß/Görlacher (2002)	single crossing areas	57	3.59	2.82	-	-
Jöbstl (2004)	single crossing areas	81	3.46	2.71	-	-
Wallner (2004)	two symmetric crossing areas	122	-	-	1.51	1.18
Blaß/Flaig (Figure 4)	two symmetric crossing areas	6	-	-	1.43	1.18
Blaß/Flaig (2012)	notched beams (bending tests)	13	3,98	2,76	1,71	1.19
Blaß/Flaig (2012)	beams with holes (bending tests)	13	3,69	2.79	1.58	1.20
Blaß/Flaig (2010)	CUAP (see Table 3)	12	4.67	2,68	1.99	1.15

From the different test series that were performed with small specimens it can be concluded that the shear strength of crossing areas against unidirectional shear stresses is equal to the rolling shear strength of timber. The torsional shear strength in contrast exceeds this value considerably, although the failure is also governed by rolling shear stresses. The torsional shear strengths found by Blaß and Görlacher and Jöbstl et al., respectively, are very similar, both mean and characteristic values, although the size of the tested crossing areas varied considerably (Blaß/Görlacher 40 x 40 mm, 40 x 64 mm, 62 x 95 mm, 62 x 75 mm, 64 x 64 mm, 64 x 100 mm; Jöbstl et al. 100 x 145 mm, 150 x 145 mm, 200 x 145 mm). The results within either test series also showed no significant influence of the crossing area size on the shear strength. The same applies to the shear strength against unidirectional shear stresses where the tested crossing areas had dimensions of 100 x 150 mm, 150 x 150 mm, 200 x 150 mm (Wallner) and 75 x 150 mm (Blaß/Flaig, Figure 4). Both rolling shear strength and torsional shear strength of crossing areas seem therefore to be size independent within the sizes tested and occurring in practice.

To identify a suitable criterion for the verification of shear stresses in the crossing areas – considering the interaction of unidirectional and torsional shear stress components – the results of bending tests where failure occurred due to shear stresses in the crossing areas were evaluated using equations Eq. 6, Eq. 8 and Eq. 10. The considered tests were performed with prismatic beams (see Table 3), notched beams and beams with holes (Blaß and Flaig, 2012).Tests with prismatic beams were performed according to CUAP 03.04/06 involving a kerf that was sawn into the longitudinal layers in the middle of the beam height. The tested CLT-beams with notches and holes were three- and six-layered with heights of 300 mm and 600 mm. The span of all tested beams was within the range of 7.5 to 10 times the beam height.

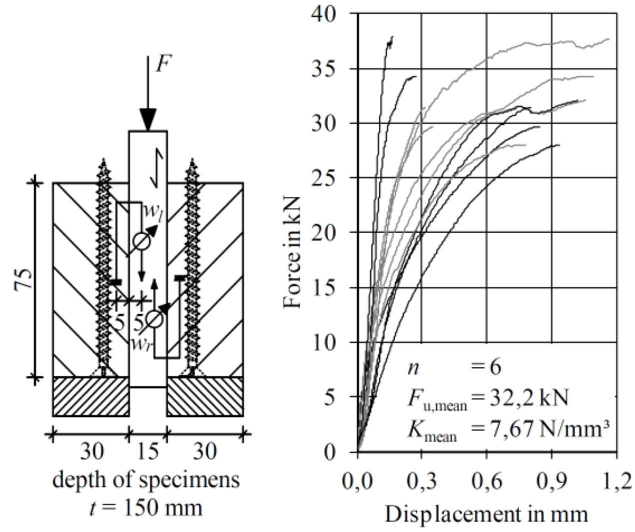

Figure 4: Compressive shear tests to determine the shear strength and the slip modulus of crossing areas subjected to unidirectional shear stresses

Table 3: Torsional shear strength and rolling shear strength of crossing areas evaluated from bending tests according to CUAP 03.04/06

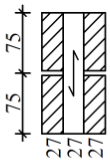	series 27-27-27						
	$f_{v,tor}$ in N/mm²	3.68	4.43	3.72	3.72	3.51	3.61
	f_R in N/mm²	1.58	1.90	1.59	1.59	1.50	1.55
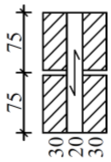	series 30-20-30						
	$f_{v,tor}$ in N/mm²	4.64	6.49	6.05	3.66	6.26	6.33
	f_R in N/mm²	1.99	2.78	2.59	1.57	2.68	2.71

To evaluate the strength properties of crossing areas from beam tests a total of six different failure criterions were investigated (Flaig, 2013). The best agreement between the shear properties evaluated from beam tests and the respective values obtained from tests with small specimens was found for the failure criterion given in Eq. 11, which takes into account the interaction of torsional and unidirectional shear stresses, but no interaction of unidirectional shear stresses in direction of and perpendicular to the beam axis.

$$\frac{\tau_{tor,d}}{f_{v,tor,d}} + \frac{\tau_{yx,d}}{f_{R,d}} \leq 1 \quad \text{and} \quad \frac{\tau_{tor,d}}{f_{v,tor,d}} + \frac{\tau_{yz,d}}{f_{R,d}} \leq 1 \qquad \text{Eq. 11}$$

To evaluate both strength properties, a constant ratio between torsional and rolling shear strength of 2.33 was assumed that was derived from the results of tests performed with small specimens given in Table 2. In beams with holes and notches also stress peaks near holes and notches were considered (Blaß and Flaig, 2012). In Table 2, lines 6, 7 and 8 the rolling shear strength and the torsional shear strength evaluated from test series with CLT-beams are given.

2.3.4 Effective shear strength of prismatic CLT-beams

Depending on the width of lamellae and on the thickness and the arrangement of longitudinal and transversal layers within the beam the shear resistance of a CLT-beam is governed by either of the three failure modes. The effective shear strength $f_{v,CLT}$ related to the gross cross section of CLT-beams can be calculated as the minimum value resulting from the three expressions given in Eq. 12, each representing one of the three failure modes.

$$f_{v,CLT} = \min \begin{cases} f_{v,lam} \\ f_{v,lam,90} \cdot \dfrac{t_{net}}{t_{gross}} \\ \dfrac{b \cdot n_{CA}}{2 \cdot t_{gross}} \cdot \dfrac{1}{\dfrac{1}{f_{v,tor}} \cdot \left(1 - \dfrac{1}{m^2}\right) + \dfrac{2}{f_R} \cdot \left(\dfrac{1}{m} - \dfrac{1}{m^2}\right)} \end{cases} \qquad \text{Eq. 12}$$

In Figure 5 characteristic shear strengths of CLT-beams determined from Eq. 12 are given in graphical form.

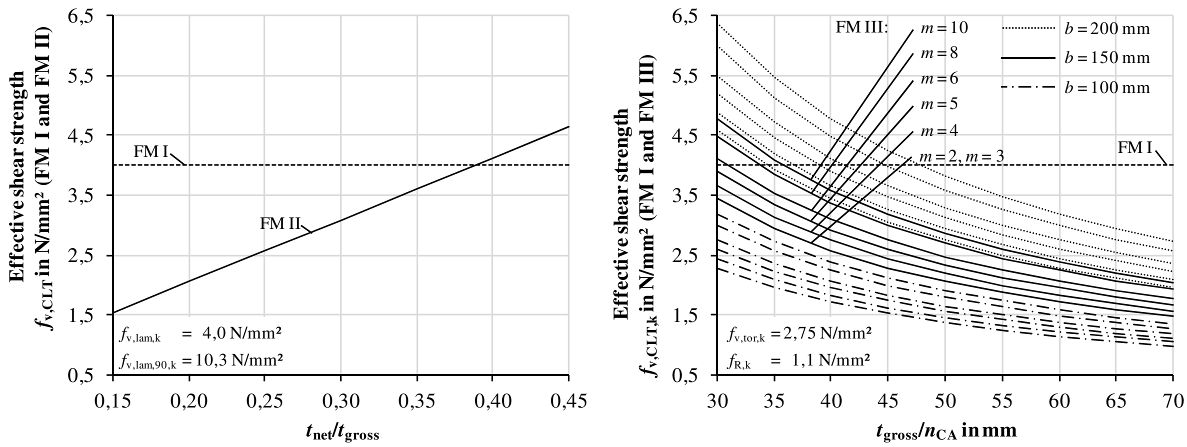

Figure 5: Effective shear strength $f_{v,CLT}$ of CLT-beams resulting from failure modes I and II (left) and failure modes I and III (right)

In the diagram on the left side the shear strength calculated from the second expression in Eq. 12, corresponding to failure mode II (FM II), is plotted against the ratio t_{net}/t_{gross}, which in CLT-beams normally equals the proportion of transversal layers. The shear strength calculated from the third expression in Eq. 12, representing failure mode III (FM III), is plotted in the diagram on the right side. Here, the beam layup is given on the abscissa in form of the ratio t_{gross}/n_{CA}, where t_{gross} is the total thickness of the beam and n_{CA} is the number of glue lines between longitudinal and transversal layers within the total thickness. The three different sets of curves demonstrate the influence of the width b of lamellae in failure mode III whereas the influence of the number m of lamellae within longitudinal layers is represented by the curves within each set.

The graphs were calculated assuming a characteristic value of the shear strength perpendicular to the grain of 10.3 N/mm² and characteristic torsional and rolling shear strength of 2.75 N/mm² and 1.1 N/mm², respectively. In both diagrams the effective shear strength resulting from failure mode I (FM I) is given, too. The characteristic value was determined with the shear strength of strength class C24 given in EN 338 and a crack reduction factor of 1.0.

3 Shear stiffness of CLT-beams loaded in plane

3.1 Analytical approach

In CLT-beams subjected to in plane transversal forces, shear stresses acting within the crossing areas will entail mutual displacements between the bonded lamellae. Therefore, the shear deformation of CLT-beams originates not only from shear strain within the lamellae but also from rotational and translational displacements in the crossing areas. Using the definitions given in Figure 6 the shear strain components γ_{yx} and γ_{tor} resulting from the displacements within the crossing areas can be calculated according Eq. 13 and Eq. 14, where K is the slip modulus of the crossing areas in N/mm³.

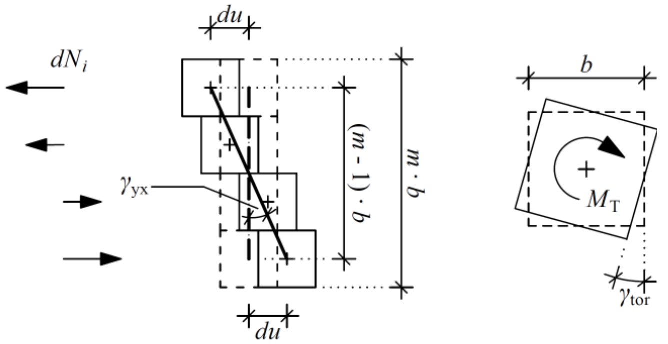

Figure 6: Shear strain components γ_{tor} and γ_{yx} resulting from shear stresses in the crossing areas of CLT-beams

$$\gamma_{\mathrm{yx}} = \frac{2 \cdot du}{b \cdot (m-1)} = \frac{2 \cdot t_{\mathrm{yx}}}{K \cdot b \cdot (m-1)} \qquad \text{Eq. 13}$$

$$\gamma_{\mathrm{tor}} = \frac{2 \cdot t_{\mathrm{tor}}}{K \cdot b} \qquad \text{Eq. 14}$$

By substituting the shear stresses τ_{yx} and τ_{tor} given in Eq. 6 and Eq. 8 into the expressions given in Eq. 13 and Eq. 14, respectively, the relations given in Eq. 15 and Eq. 16 are obtained.

$$\gamma_{\mathrm{tor}} = \frac{6 \cdot V}{b^3 \cdot K} \cdot \left(\frac{1}{m} - \frac{1}{m^3} \right) \cdot \frac{1}{n_{\mathrm{CA}}} \qquad \text{Eq. 15}$$

$$\gamma_{\mathrm{yx}} = \frac{12 \cdot V}{b^3 \cdot K \cdot} \cdot \frac{1}{m^3} \cdot \frac{1}{n_{\mathrm{CA}}} \qquad \text{Eq. 16}$$

Using the constitutive equation $\tau = \gamma \cdot G$ an effective shear modulus $G_{eff,CA}$ representing the shear deformation in the crossing areas can be calculated. For CLT-beams with rectangular cross section the shear modulus $G_{eff,CA}$ related to the gross cross section can be obtained from the expression given in Eq. 17.

$$G_{\mathrm{eff,CA}} = \frac{6 \cdot V}{5 \cdot A_{\mathrm{gross}} \cdot \left(\gamma_{\mathrm{tor}} + \gamma_{\mathrm{yx}} \right)} = \frac{K \cdot b^2}{5} \cdot \frac{n_{\mathrm{CA}}}{t_{\mathrm{gross}}} \cdot \frac{m^2}{\left(m^2 + 1 \right)} \qquad \text{Eq. 17}$$

The superposition of shear deformations in the lamellae and in the crossing areas yields the effective shear modulus $G_{eff,CLT}$ of CLT-beams given in Eq. 18, which again is related to the gross cross section.

$$G_{\mathrm{eff,CLT}} = \left(\frac{1}{G_{\mathrm{lam}}} + \frac{1}{G_{\mathrm{eff,CA}}} \right)^{-1} \qquad \text{Eq. 18}$$

In Figure 7 the effective shear modulus of CLT-beams calculated from Eq. 18 is given as a function of the ratio t_{gross}/n_{CA} between the element thickness and the number of glue lines within the element thickness and for different widths b and numbers m of lamellae in longitudinal layers The graphs plotted in the diagram apply to a shear modulus of the lamellae of 690 N/mm² and a slip modulus of the crossing areas of 5 N/mm³. The large distances between the sets of curves demonstrate the influence of the size of crossing areas – expressed through the width of lamellae b – on the shear stiffness of CLT-beams. The ratio of t_{gross}/n_{CA} also significantly affects the shear stiffness, whereas the number of lamellae within longitudinal layers has rather small influence, especially if m is greater than 2.

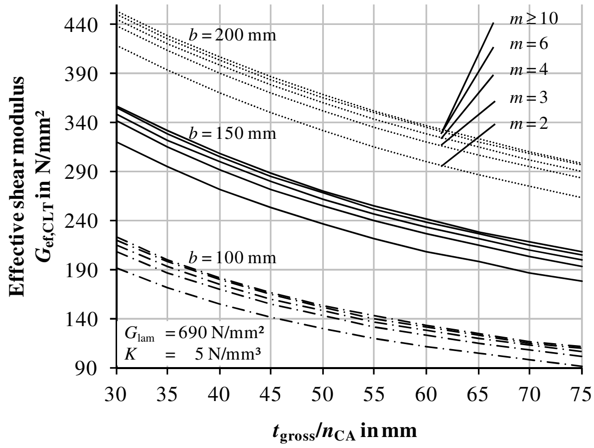

Figure 7: Effective shear modulus of CLT-beams

3.2 Test results

Until today only few test have been performed to determine the shear stiffness of CLT loaded in plane (Bosl, 2002; Traetta et al., 2006) but various tests have been performed to determine the stiffness of crossing areas of orthogonally bonded boards, both with torsional and unidirectional shear stresses. In Table 4 the results from tests with small specimens comprising one or two crossing areas are given. Tests to determine the torsional slip modulus of crossing areas have been performed by Blaß and Görlacher (2002) and by Jöbstl et al. (2004). The obtained values differ quite significantly but the disparity most likely originates from shear deformations within the bonded boards, which are, at least partly, included in the results presented by Jöbstl et al. but not contained in the values given by Blaß and Görlacher. However, the values presented by Blaß and Görlacher still include deformations due to compressive stresses perpendicular to the grain since the torsional moment was transferred to the specimens through contact by means of a clamping. From tests with crossing areas subjected to shear forces similar slip moduli have been determined by (Wallner 2004). However, these test results again comprise parts of the shear deformation within the boards. Considering the influence of the different test setups used to determine the slip moduli of crossing areas the disparity between the obtained values becomes much less pronounced.

Table 4: Slip modulus K of orthogonally bonded lamellae determined by tests performed with specimens with one or two crossing areas

Author	description of test setup	shear stress in crossing area	n	K_{mean} in N/mm³
Blaß/Görlacher (2002)	single crossing areas	torsion	30	4.87
Jöbstl (2004)	single crossing areas	torsion	81	3.45
Wallner (2004)	two symmetric crossing areas	unidirectional	122	4.26

From the difference between local and global modulus of elasticity of CLT-beams, measured in four-point bending tests, a distinctly higher slip modulus with an average of 7.58 N/mm³ was evaluated (Blaß and Flaig, 2012). The results of the performed tests are summarised in Table 5. The effective shear moduli and the slip moduli of crossing areas given in the table have been evaluated using Eq. 17 and Eq. 18, assuming a constant shear modulus of the lamellae of 690 N/mm².

The slip moduli evaluated from the bending tests are distinctly higher than the values obtained from tests with single crossing area whereas the agreement with the value of 7.67 N/mm² evaluated from the tests described in Figure 4 is very good.

Table 5: Local and global modulus of elasticity and effective shear modulus of CLT-beams and slip modulus of crossing areas evaluated from four-point-bending tests with CLT-beams

series 2-2	$E_{lok,gross}$	$E_{glob,gross}$ in N/mm²	$G_{eff,CLT}$	K in N/mm³	series 3-2	$E_{lok,gross}$	$E_{glob,gross}$ in N/mm²	$G_{eff,CLT}$	K in N/mm³
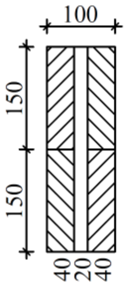	12160	10880	300	7.35	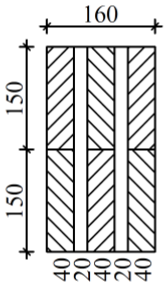	9255	8685	409	11.1
	13024	11528	291	6.99		9240	8558	336	7.27
	13752	11744	233	4.89		10568	9495	271	4.96
	10400	9376	276	6.39		9165	8573	384	9.64
	10952	9416	195	3.76		9983	9353	430	12.6
	7680	7216	346	9.64		7433	6893	275	5.08
	8120	7424	251	5.47		7613	7163	351	7.95
	7872	7016	187	3.56		6983	6630	381	9.43
	8048	7560	361	10.5		7200	6863	424	12.2
	8184	7448	240	5.11		6975	6930	-	-
mean			268	6.36				362	8.92

4 Summary and conclusions

In shear design of CLT-beams three different failure modes are distinguished considering shear stresses acting parallel and perpendicular to the grain within the lamellae and shear stresses within the crossing areas of orthogonally bonded lamellae, respectively. For the calculation of shear stresses occurring in the lamellae and the crossing areas of CLT-beams subjected to transversal loads acting in plane direction an analytical approach is presented. On the basis of experimental data, published by other researchers and obtained by own tests, strength properties and criteria for the verification of shear stresses corresponding to the different failure modes were specified. From the equations for the calculation of shear stresses and the respective failure criteria an expression for the calculation of the effective shear strength related to the gross cross section of CLT-beams was derived to simplify the verification of shear stresses and it was shown that the effective shear strength of CLT-beams is strongly dependent on cross sectional arrangement and thickness ratio of longitudinal and transversal layers and on the width of lamellae. The equations for the calculation of shear stresses were also used to derive solutions for the calculation of shear strain components resulting from mutual displacements in the crossing areas of CLT-beams. By the superposition of strain components resulting from shear stresses in the crossing areas and in the lamellae a closed-form expression for the calculation of an effective shear modulus of CLT-beams was obtained. The expression shows that the effective shear stiffness of CLT-beams, like the effective shear strength, strongly depends on the width of lamellae and their cross sectional arrangement. The presented analytical approach was used to evaluate strength and stiffness properties of crossing areas from tests performed with different types of CLT-beams comprising prismatic beams, notched beams and beams with holes. The obtained values were compared to strength and stiffness properties determined by tests with small specimens and good agreement was found.

Due to its simplicity and the good agreement with experimental results the presented approach represents a suitable and effective tool for the shear design of CLT-beams including both the calculation of shear stresses and shear deformations and it provides conservative results if strength and stiffness properties determined by tests with small specimens are used.

5 Symbols

a_i	distance between the centre line of an individual longitudinal lamella and the xy-centre plane of the gross cross section
$a_{i,max}$	distance between the centre line of the uppermost/lowermost longitudinal lamella and the xy-centre plane of the gross cross section
b	width of lamellae (here constant within all layers)
$dN_{i,k}$	differential normal force within an individual longitudinal lamella *i,k*
dM	differential bending moment within the gross cross section
$f_{v,lam}$	shear strength of the lamellae according to EN 338
$f_{v,90,lam}$	shear strength perpendicular to the grain in joints between non edge bonded lamellae
$f_{v,tor}$	torsional shear strength of crossing areas of orthogonally bonded lamellae
f_R	rolling shear strength
G_{CA}	shear modulus of a CLT-beam resulting from the joint slip in crossing areas
$G_{eff,CLT}$	effective shear modulus of a CLT-beam
G_{lam}	shear modulus of lamellae
h	beam height
$I_{y,net,long}$	second moment of area of longitudinal layers about y-axis
$I_{p,CA}$	polar moment of inertia of a single crossing area
K	slip modulus of crossing areas in N/mm per mm²
m	number of longitudinal lamellae within the beam height
n_{CA}	number of glue lines between longitudinal and transversal layers within the element thickness
S_y	static moment about y-axis
t_{gross}	overall thickness of the CLT-element
t_{net}	smaller of the sum of the thickness of longitudinal and transversal layers; in CLT-beams usually the sum of the thickness of transversal layers
$t_{net,cross}$	sum of the thickness of transversal layers
$t_{net,long}$	sum of the thickness of longitudinal layers
V	transversal force
q_y	external load
τ_{eff}	shear stress according to the beam theory calculated with the gross cross section
τ_{tor}	torsional shear stress acting in crossing areas
$\tau_{xz,gross}$	shear stress calculated with the gross cross section
$\tau_{xz,net}$	shear stress calculated with the net cross section
τ_{yx}	unidirectional shear stress parallel to the beam axis acting in crossing areas
τ_{yz}	unidirectional shear stress perpendicular to the beam axis acting in crossing areas

6 References

Bejtka, I.: Cross (CLT) and diagonal (DLT) laminated timber as innovative material for beam elements. Karlsruher Berichte zum Ingenieurholzbau, Bd. 17, KIT Scientific Publishing, 2011

Blaß, HJ; Flaig, M.: Stabförmige Bauteile aus Brettsperrholz. Karlsruher Berichte zum Ingenieurholzbau, Bd. 24, KIT Scientific Publishing, 2012

Blaß, H J; Görlacher, R: Zum Trag- und Verformungsverhalten von Brettsperrholzelementen bei Beanspruchung in Plattenebene. In: Bauen mit Holz 104, 2002, H. 11 S. 34-41, H. 12 S. 30-34.

Bogensperger, T; Moosbrugger, T; Silly, G: Verification of CLT-plates under loads in plane. In: Proceedings. 11th World Conference on Timber Engineering, Riva del Garda, Italy, 2010

Bogensperger, T; Moosbrugger, T; Schickhofer, G: New Test Configuration for CLT-Wall Elements under Shear Load. In: Proceedings. CIB-W18 Meeting 40, Bled, Slovenia, 2007, Paper 40-12-3

Bosl, R: Zum Nachweis des Trag- und Verformungsverhaltens von Wandscheiben aus Brettsperrholz. Dissertation, Universität der Bundeswehr, München, Germany, 2002

CUAP 03.04/06: Solid wood slab element to be used as a structural element in buildings. Version June 2005

EN 338, 2009. Structural timber - Strength classes. European Committee for Standardization (CEN), Brussels, Belgium.

EN 1995-1-1, 2004. Eurocode 5. Design of timber structures - Part 1-1: General - Common rules and rules for buildings. European Committee for Standardization (CEN), Brussels, Belgium.

Flaig, M: Biegeträger aus Brettsperrholz bei Beanspruchung in Plattenebene. Dissertation, Karlsruher Berichte zum Ingenieurholzbau, Bd. 26, KIT Scientific Publishing, 2013

Jöbstl, RA; Bogensperger, T; Schickhofer, G: In-Plane Shear Strength of Cross Laminated Timber. In: Proceedings. CIB-W18 Meeting 41, St. Andrews, Canada, 2008, Paper 41-12-3

Jöbstl, RA; Bogensperger, T; Schickhofer, G: Mechanical Behaviour of Two Orthogonally Glued Boards. In: Proceedings. 8th World Conference on Timber Engineering, Lahti, Finland, 2004

Moosbrugger, T; Guggenberger, W; Bogensperger, T: Cross Laminated Timber Wall Segments under homogeneous Shear — with and without Openings. In: Proceedings. 9th World Conference on Timber Engineering, Portland, Oregon, USA, 2006

Schickhofer et al. BSPhandbuch - Holz-Massivbauweise in Brettsperrholz". Technische Universität Graz, holz.bau forschungs gmbh, Karlsruher Institut für Technologie, Technische Universität München, Eidgenössische Technische Hochschule Zürich, 2009

Traetta, G, Bogensperger, Th, Schickhofer, G: Verformungsverhalten von Brettsperrholzplatten unter Schubbeanspruchung in der Ebene. In: 5. Grazer Holzbau-Fachtagung, September 2006

Wallner, G: Versuchstechnische Ermittlung der Verschiebungskenngrößen von orthogonal verklebten Brettlamellen, Diplomarbeit, Institut für Stahlbau, Holzbau und Flächentragwerke, TU Graz, 2004

INTERNATIONAL COUNCIL FOR RESEARCH AND INNOVATION IN BUILDING AND CONSTRUCTION

WORKING COMMISSION W18 - TIMBER STRUCTURES

STIFFNESS OF SCREW-REINFORCED LVL IN COMPRESSION PERPENDICULAR TO THE GRAIN

C P Watson

W van Beerschoten

T Smith

S Pampanin

A H Buchanan

University of Canterbury

NEW ZEALAND

Keywords: laminated veneer lumber, screws, reinforcing, compression perpendicular to grain, post-tensioning, timber.

Presented by A Buchanan

H Blass commented that when they studied this issue, buckling of the screws and push in failure of the screws were observed. Also there were compression perpendicular to grain failures at the tip of the screws. He asked whether the compression failures were observed in this study. A Buchanan responded that this study was about stiffness and did not look into this aspect.

F Lam received confirmation that the tests were under load control.

H Blass asked about the compression perpendicular to strength of LVL. A Buchanan responded ~5 MPa typically. If stress spreading was included, ~ 12 MPa and 8 MPa in blocks.

G Schickhofer received clarification that the material was cross banded. They were 36 mm thick with 12 veneers out of which 2 were in the orthogonal direction. Five pieces were glued together to form the test specimens.

K Ranasinghe asked why three different lengths of screws considered. A Buchanan stated that long screws could hit each other if they were driven in from other sides. Also predrilling up to 300 mm was performed because of splitting issues.

C Sigrist asked if this solution was cheaper than other options. A Buchanan stated that there is no right or wrong answers but this was introduced as one option. When working with steel there could be tolerance issues even though screws are not cheap. In general screws could be commonly available and therefore economical. S Winter stated in Germany for a practical design solution if one could avoid steel and use screw, the solution would be typically 50% cheaper.

E Serrano received confirmation that typical loading until 8 MPa. In some cases higher loading was used.

R Harris commented that this would be an intuitive way to carry loads across to the joint. Reinforcement of surface allowed the load to spread through the timber but creep might be important. A Buchanan agreed and they will look into the creep issue.

Stiffness of Screw-Reinforced LVL in Compression Perpendicular to the Grain

C.P. Watson[1], W. van Beerschoten[1], T. Smith[1], S. Pampanin[1], A.H. Buchanan[1]

[1] University of Canterbury, New Zealand

ABSTRACT

This paper gives design guidance for the stiffness of Laminated Veneer Lumber (LVL) reinforced with fully-threaded screws, when loaded in compression perpendicular to grain. The paper describes an experimental study using LVL made from Radiata pine grown in New Zealand, to evaluate the influence of different numbers and lengths of screws, as well as the effects of stress spreading on the compressive stiffness of LVL when loaded perpendicular to grain. Comparisons of the new experimental data have been made against existing equations and simplified design equations have been developed to determine the stiffness of screw reinforced LVL in compression perpendicular to the grain.

Keywords: *Perpendicular to the grain, screw reinforcing, Laminated Veneer Lumber (LVL), Pres-Lam, stiffness*

1 INTRODUCTION

It is well known that wood is significantly stronger and stiffer when loaded in compression parallel to grain compared with perpendicular to grain loading. Despite this there are numerous design scenarios where loading wood perpendicular to grain cannot be avoided, i.e. beam supports, platform building construction, stress-laminated bridge decks and post-tensioned timber structures. Screw reinforcement has been identified as an efficient method of improving the perpendicular to grain performance of wood under large compressive forces (Bejtka & Blass, 2006). Several screw manufacturers have published detailed design information to calculate the *strength* of screw reinforced timber; however the *stiffness* is usually not specified.

Pres-Lam (pre-stressed laminated) multi-storey timber buildings are under development at the University of Canterbury (Palermo *et al.*, 2005, Buchanan *et al.*, 2011) in collaboration with the international research consortium Structural Timber Innovation Company (STIC). The Pres-Lam system uses prefabricated post-tensioned Laminated Veneer Lumber (LVL) or glulam in structural frames and walls adapted from similar systems developed for precast concrete (Pampanin, 2005, Priestley *et al.*, 1999).

One of the main issues associated with horizontally post-tensioned timber frames, is local column deformation concentrated at the beam-column joints, as shown in Figure 1. This deformation is due to high local compressive stresses, and the low strength and stiffness of LVL in compression perpendicular to the grain. Under ultimate limit-state seismic loading or gravity loading, a gap opens between the beam and the column face, and the post-tensioning force is transferred into the column over a small area, resulting in high perpendicular to grain compression stresses. The strength perpendicular to grain is limiting the amount of post-tensioning that can be applied, and the stiffness of the interface in compression reduces connection stiffness, leading to increased deflections. Under ULS seismic loading, the low perpendicular to the grain stiffness of LVL in the columns reduces the lateral stiffness of the frame, causing excessive non-structural damage (due to larger inter-storey drifts) and delaying the activation of energy dissipaters (Newcombe, 2011).

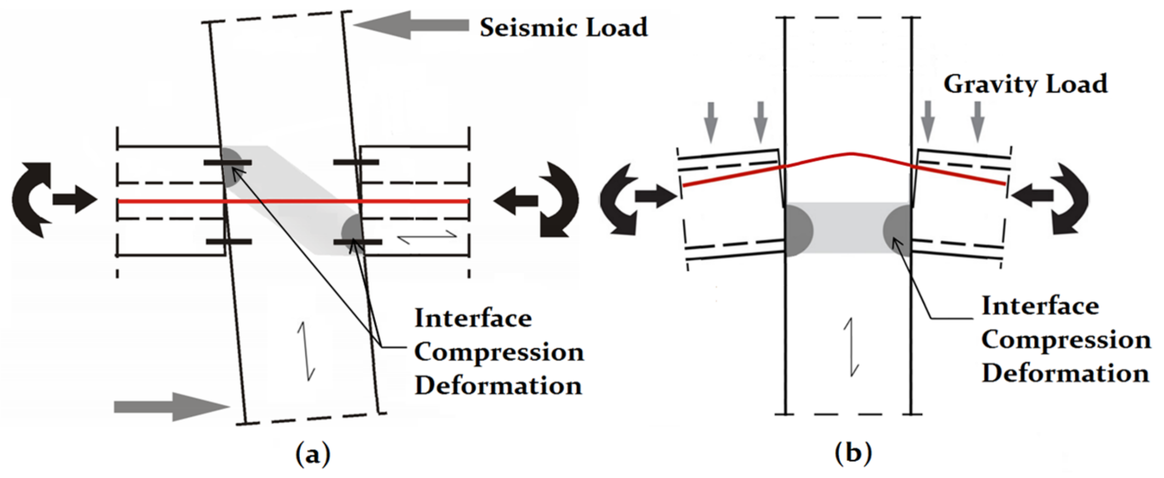

Figure 1: Typical concentration of perpendicular to grain compression forces in post-tensioned timber (a) seismic frames (adopted from Smith *et al*., 2012) and (b) gravity frames (adapted from van Beerschoten *et al*., 2011)

In recent Pres-Lam buildings constructed in New Zealand, the effects of the low stiffness of LVL in compression perpendicular to the grain have been reduced by providing internal or external structural steel reinforcing. One example of external reinforcing is shown in Figure 2(a). Figure 2(b) shows a column being reinforced locally with a 2.5% screw density (reinforcing ratio) of long screws in a laboratory experiment related to the research described in this paper.

(a)

(b)

Figure 2: Examples of (a) external structural steel reinforcing for beam-column joints in a Pres-Lam building and (b) a column being locally reinforced with long screws (2.5% reinforcing ratio)

Screw reinforcing has been shown to provide an increase in ultimate strength and initial stiffness when compared to unreinforced timber members loaded in compression perpendicular to the grain (Blass & Bejtka, 2004; Bejtka & Blass, 2006; Crocetti & Kliger, 2010). While the increase in strength provided by screw reinforcing is relatively well documented in the literature, the increase in stiffness provided is sparsely known.

When a specimen reinforced with screws is loaded in compression perpendicular to the grain, three failure modes have been shown to occur (Blass & Bejtka 2004); pushing of screws into the timber, buckling of screws, and wood failure in a plane formed at the tip of the screws. Design equations for the compression strength perpendicular to the grain using fully-threaded self-tapping screws were developed, and have been adopted into the design guidelines of several screw-manufacturers. Furthermore, testing has showed that screw reinforcement can increase the stiffness by up to three times (Bejtka & Blass, 2006). Design equations were provided for the calculation of the stiffness perpendicular to grain based on the spacing and type of screws, the compressive stiffness of wood and screws, load distribution, and elastic embedment stiffness of the screws into wood.

Crocetti & Kliger (2010) used screw reinforcing to increase the capacity and long-term performance of post-tensioning anchorages in a timber stress-laminated bridge deck. Their research showed a significant increase in compressive strength perpendicular to grain, but a negligible increase in stiffness. Murakami et al. (2012) performed experimental testing of screw reinforced beams subjected to both axial loading and a rotational moment, resulting in triangular loading perpendicular to grain. A two fold increase in stiffness was observed, but only two screws were placed in the wood and not all tests were performed with fully threaded screws.

The contradicting results described above show the need for further research on the stiffness of screw-reinforced timber. The formula proposed by Bejtka & Blass (2006) will be compared with new experimental data and simplified design equations and charts will be proposed for determining the compressive stiffness of screw reinforced LVL, based on the testing regime presented below.

2 EXPERIMENTAL TESTING

An experimental campaign was carried out in order to define the elastic stiffness of screw-reinforced LVL members in compression perpendicular to the grain. Parameters considered in the investigation include the screw length as a ratio of the LVL depth, the screw reinforcing ratio and the grade of LVL material.

2.1 TEST SPECIMENS

An overview of the LVL specimens and the configuration for each test is presented in Table 1. In total, 64 individual tests were carried out on 13 LVL column specimens, with 3 different types of LVL material, 4 different screw reinforcing ratio (reinforcing ratio = nominal steel area divided by gross timber area) and 3 different screw length ratios (screw length divided by specimen depth). While different materials were considered for the testing, the primary objective of the testing was to experimentally determine the stiffness of screw-reinforced LVL with different length and densities of screw reinforcing. The listed screw diameters in Table 1 are the nominal diameters from the manufacturers' literature. In general the listed diameter is the outside diameter of the screw thread.

The LVL specimens used for testing were cut out of full scale LVL columns, rotated 90° for vertical testing in compression perpendicular to the grain. Two sizes of column cross-section were used; 500x300mm and a 600x200mm. Three types of LVL were tested; 10.7GPa Nelson Pine LVL (LVL11), 13.2GPa Carter Holt Harvey LVL (LVL 13.2) and Nelson Pine cross-banded LVL (CB LVL). Specimen length (about 1.5m) was chosen such that stress spreading (at an assumed angle of 45°) was allowed to occur without reaching the ends of the test specimen. Two to four separate compression tests were carried out at different locations along each test specimen.

Tests were carried out on unreinforced LVL and on specimens reinforced with short ($l_s/h_c = 0.24$), medium ($l_s/h_c = 0.48$) and long ($l_s/h_c = 0.89$) fully threaded screws with a range of varying screw densities (l_s is the fully threaded length of the screw and h_c is the depth of the column). All tests had a 25mm thick steel bearing plate sitting directly on the screw heads which were flush with the wood surface. The width of the steel bearing plate was the full width of the columns (200mm or 300mm) and the length of the steel bearing plate was 150mm or 200mm for the 500 and 600mm deep columns, respectively, to ensure uniform contact with the heads of the screws.

When preparing the test specimens, it was found that pre-drilling was necessary when placing the screws. If no holes were pre-drilled, it became impossible to place all the screws to full depth because of the very high torque needed in the screwing machine, resulting in a number of screws shearing off with failures near the screw head or at the wood surface. Best results were achieved when holes were drilled for the full length of the screws, with the hole diameter being the same as the core diameter of the screws (~60% of the outside thread diameter).

Table 1: Overview of screw reinforced LVL testing

Specimen Code	LVL	Test	Screw Reinforcing	Specimen Code	LVL	Test	Screw Reinforcing
LVL11-1A	LVL 11	1	No screws	LVL11-3B	LVL11	1	10 – φ10 x 240mm screws
		2	No screws			2	10 – φ10 x 240mm screws
		3	No screws			3	12 – φ10 x 240mm Screw
		4	No screws			4	12 – φ10 x 240mm Screw
LVL11-1B	LVL 11	1	6 – φ10 x 450mm screws	CB11-A	CB LVL	1	No screws
		2	6 – φ10 x 450mm screws			2	No screws
		3	12 – φ10 x 450mm screws			3	No screws
		4	12 – φ10 x 450mm screws	CB11-A	CB LVL	1	No screws
LVL11-2A	LVL 11	1	6 – φ10 x 120mm screws			2	6 – φ10 x 240mm screws
		2	6 – φ10 x 120mm screws			3	12 – φ10 x 240mm screws
		3	8 – φ10 x 120mm screws	LVL13-1A	LVL13.2	1	No screws
		4	8 – φ10 x 120mm screws			2	No screws
LVL11-2B	LVL 11	1	10 – φ10 x 120mm screws	LVL13-2A	LVL13.2	1	6 – φ10 x 530mm screws
		2	10 – φ10 x 120mm screws			2	6 – φ10 x 530mm screws
		3	12 – φ10 x 120mm screws	LVL13-2B	LVL13.2	1	8 – φ10 x 530mm screws
		4	12 – φ10 x 120mm screws			2	8 – φ10 x 530mm screws
LVL11-3A	LVL 11	1	6 – φ10 x 240mm screws	LVL13-3A	LVL13.2	1	10 – φ10 x 530mm screws
		2	6 – φ10 x 240mm screws			2	10 – φ10 x 530mm screws
		3	8 – φ10 x 240mm screws	LVL13-3B	LVL13.2	1	12 – φ10 x 530mm screws
		4	8 – φ10 x 240mm screws			2	12 – φ10 x 530mm screws

2.2 TEST SETUP

Testing was carried out using a DARTEC universal testing machine, shown schematically in Figure 3. The LVL specimens were placed in the testing machine with an additional steel plate at the top and bottom of the specimen to ensure that the load was uniformly applied over the steel bearing plate. Temporary supports were provided at each end of the specimen to provide vertical stability. The specimens were tested in compression perpendicular to the grain as per the loading protocol specified in EN 408:2010 (CEN, 2010). This testing standard was used as a guide, but it was not followed directly because the standard is focused on carrying out a large number of small scale tests, while the experimental tests carried out here were focused a small number of full scale beam-column test specimens.

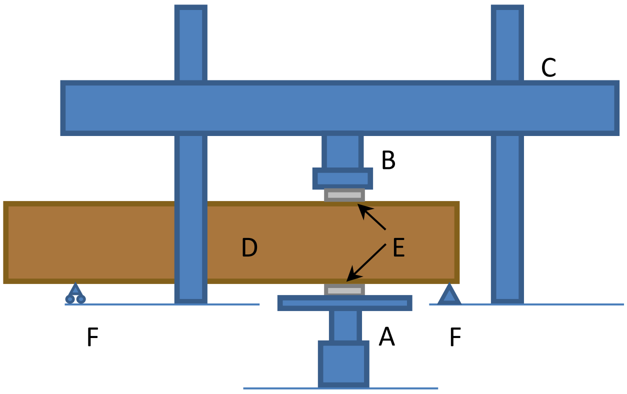

A – DARTEC actuator

B – 1000kN load cell

C – DARTEC reaction frame

D – LVL column specimen

E – 25mm thick steel bearing plate

F – Temporary supports

Figure 3: Diagrammatic illustration of test setup

The published characteristic strength of LVL in compression perpendicular to the grain is 12MPa for both Nelson Pine LVL11 (NPI, 2010) and Carter Holt Harvey LVL13.2 (CHH, 2008), based on small scale rail tests which include stress spreading (van Beerschoten *et al*. 2013). The maximum elastic strength based on block testing according to EN 408:2010 (CEN, 2010) is 8MPa. Therefore this value was selected as the maximum contact stress for testing. Most test specimens were loaded in the elastic range with only a limited number of specimens being tested to failure.

The key measurement from testing was the total displacement of the LVL specimen in compression perpendicular to the grain. This was measured using linear potentiometers fixed between the top and bottom steel plates. Measurements were taken over the full height of the specimen, h_c (100%H) the standard gauge length of $0.6h_c$ (60%H, as per EN 408:2010), and an intermediate length, $0.8h_c$ (80%H). The measurements were all taken on both sides of the test specimen, along the centre-line of the loading point. A 1000kN load cell was used to record the load. A photo of the instrumentation layout and test setup is given in Figure 4.

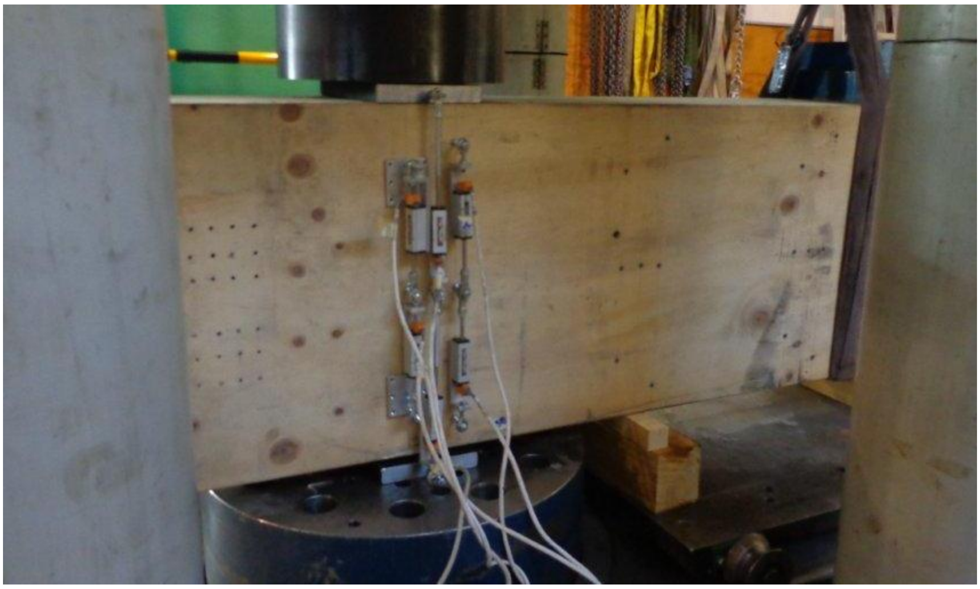

Figure 4: Photo of test setup for perpendicular to the grain compression tests

Deformation of the LVL specimens were also recorded using high definition photography. High resolution (18MegaPixel) RAW images were taken with a DSLR camera for use with image analysis software. Approximately 50-60 photos of the loading cycle were taken for each test.

3 TEST RESULTS

3.1 DEFORMATION AND STIFFNESS

A set of typical test results is shown in Figure 5 for the ULS perpendicular to the grain compression testing of the LVL13.2 specimens with increasing screw reinforcing.

The behaviour of the screw reinforced LVL can be qualitatively observed from the series of graphs shown in Figure 5. As the amount of screw reinforcement is increased, there is a corresponding increase in initial stiffness, as well as an increase in the ultimate capacity of the member in compression perpendicular to the grain.

The initial stiffness of the LVL should be analysed for each test over a range of approximately 10-40% of the maximum timber strength, as per EN408:2010. As testing was mainly carried out within the elastic range, the maximum timber strength of each test was generally undefined. For each group of tests a compression load of 15MPa was applied in order to provide an estimation of the timber strength required for analysis of the results. For each individual test, the loading stiffness was calculated over the total height of the column specimen (100% H), for both sides of the column section. In general there were approximately 4-6 individual tests carried out for each type of screw reinforcing and reinforcing ratio. An average stiffness for each group of tests was found by taking the mean of the results. The average stiffness was normalised by the average stiffness of the unreinforced specimens. By normalising the results, a factor (k_{scr}) for the increase in stiffness due to screw reinforcing was found.

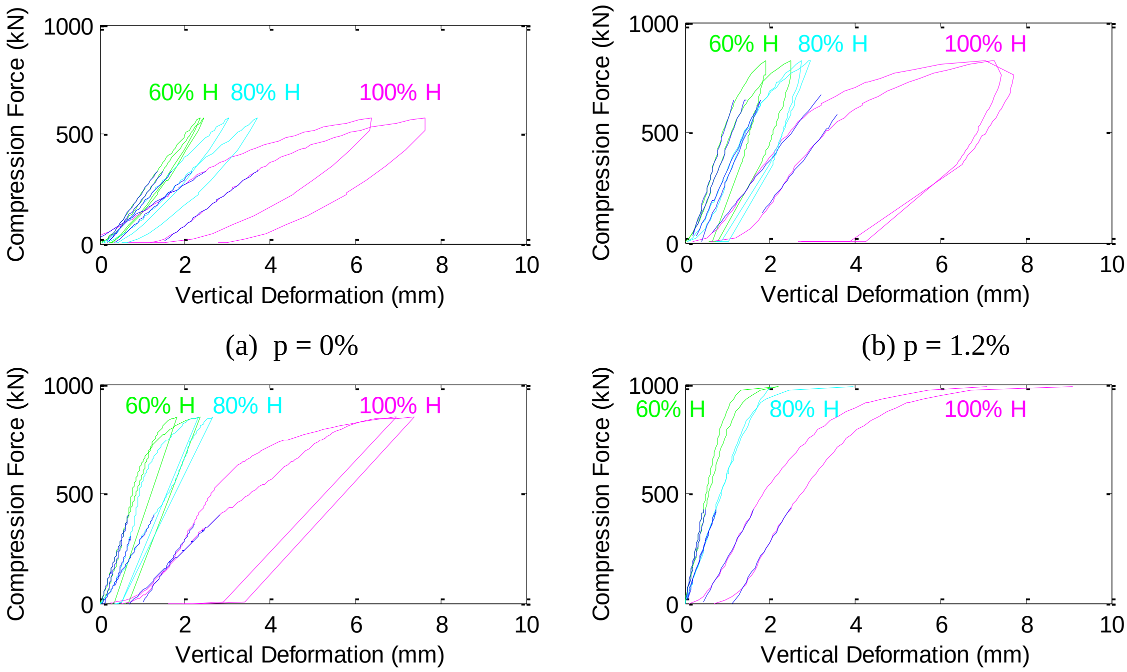

(a) p = 0% (b) p = 1.2%

(c) p = 2.1% (d) p = 2.5%

Figure 5: Force-deformation behaviour of LVL13.2 column specimens with long fully threaded screws (l_s/h_c=0.89) for a range of reinforcing ratios (p). Percentages %H indicates gauge length of instrumentation.

A summary of the normalised results for all of the tests, excluding the cross-banded LVL, is given in Figure 6. A line of best fit, passing through k_{scr} = 1 for no screws, has been fitted to the averaged experimental data (shown as solid markers). From the figure it can be seen that the largest increase in stiffness is provided by screws with a long length (relative to the beam depth) and a high screw reinforcing ratio. A twofold increase in stiffness was found for long screws with a reinforcement ratio larger than 2%, while conversely only a very small increase was found with short screws for any reinforcement ratio.

Figure 6 shows that, in general terms, the stiffness over the whole cross section can be doubled by reinforcing the LVL with long screws occupying 2% of the stressed wood area. At a lower level, a 50% increase in stiffness can be achieved with about half the volume of screws, being either the same density of half-length screws or half the density of full length screws.

An interesting effect that was observed during testing was the apparent ‘ductility’ of the timber at failure. The failure of an unreinforced member was a relatively ductile, as a large amount of crushing was allowed to occur without a reduction in strength. For the specimen with a 2.5% screw reinforcing ratio, the ultimate limit state capacity was almost double that of the unreinforced specimen, however the failure appeared to be more ‘brittle’ in nature with buckling of the screws in compression, causing some glue lines and veneers to be forced apart.

3.2 CROSS-BANDED LVL

The tests with cross-banded LVL were carried out on timber columns manufactured from several layers of 36mm LVL, each with 10 parallel veneers and two perpendicular veneers giving a percentage of $2/12 \approx 17\%$ cross banding. The results showed that this modest amount of cross-banding resulted in a three times stiffer specimen than unreinforced Nelson Pine LVL11. This is in line with small scale testing results of cross-banded LVL (van Beerschoten *et al.*, 2013) which showed a two times increase in stiffness for rail tests, whereas block testing showed a five times increase in stiffness. This increase in stiffness of the timber cross layers, was larger than the maximum increase in stiffness provided by long screws. A limited number of tests with medium length screw reinforcing were carried out; however no noticeable increase in stiffness was measured compared to the non-reinforced specimens.

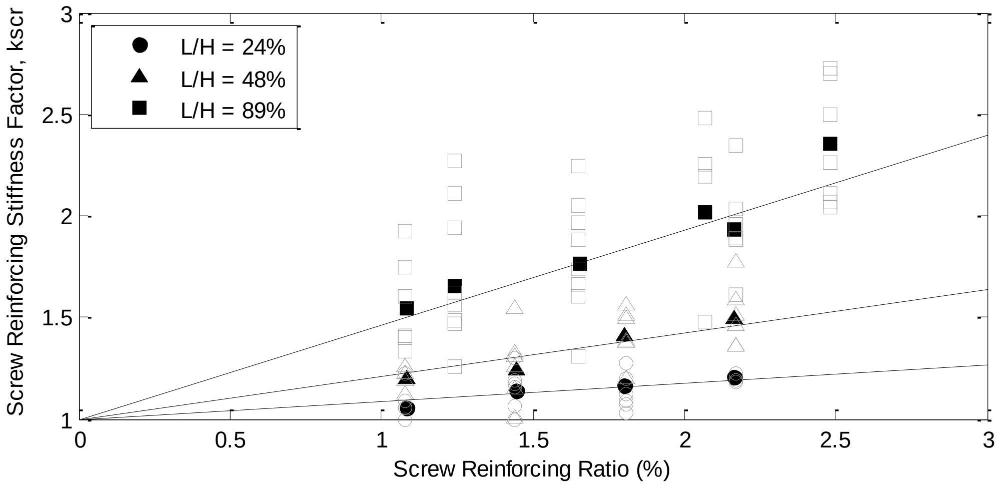

Figure 6: Increase in perpendicular to the grain column stiffness due to screw reinforcement. Open icons show testing result and solid icons indicate average results for a given screw length and reinforcing ratio.

3.3 DIGITAL IMAGE CORRELATION

Image analysis software was used to track the displacement of a large number of virtual markers on every test specimen. Each virtual marker represented a group of 50 x 50 pixels. Seventeen columns each with 28 markers were used and the strain in each of the columns was calculated, resulting in 27 strain values along the depth of the column. An average strain of all columns was calculated at a load of 8MPa and 15MPa. The resulting strain plots for the Nelson Pine LVL 11 specimens with 12 screws (p=2.2%) are shown in Figure 7. Also shown in Figure 7 (a) is the strain distribution based on a linear-elastic 2D finite element model (FEM).

From Figure 7(a) it can be seen that the measured strain without screw reinforcing matches very well with results from FEM. The strains with short screws are slightly lower at the top and bottom of the section, but very similar in the middle section. The strains with medium and long screws are clearly much less compared to no screw reinforcement, showing the benefit of screws at a medium load level. An even clearer difference in strains between unreinforced and reinforced specimens can be seen at 15MPa loading. The unreinforced specimen shows large plastic strains (>6%), whereas strains for medium and long reinforced specimens are less than 1%.

A second analysis has been performed for four extreme cases, without screws and with maximum screw reinforcement for LVL11 and cross-banded LVL. Full displacement fields of these specimens under the maximum load of 15MPa were generated based on a grid of markers as shown in Figure 8(a). The vertical deformation of each marker relative to the centreline of the specimen was calculated. An example of this deformation for LVL11 with maximum screw reinforcement is shown in Figure 8(b), where the horizontal axis is the distance from the centreline of load application. The thick black lines indicate the loading plates and the grey area is the timber directly between the loading plates, which has been used for analysis of the strain profiles in Figure 7.

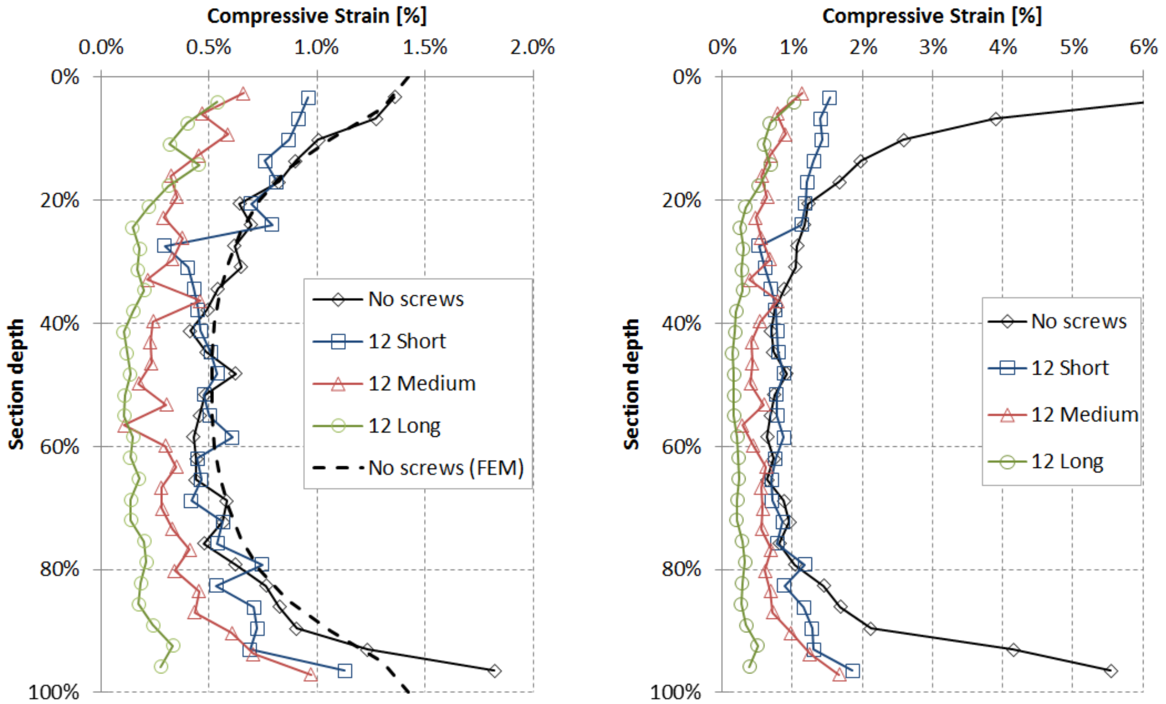

(a) (b)

Figure 7: Strain profiles along depth of LVL 11 specimens (p=2.2%); (a) 8MPa load, (b) 15MPa load. (No screws = 11-1A-3, short screws = 11-2B-4, medium screws = 11-4B-3, long screws = 11-1B-3)

The deformation of the specimen at several locations relative to the maximum deformation under the loading plates has been evaluated. These percentages are plotted in Figure 9, for top and bottom of the four analysed specimens. From this figure it can be seen that cross-banded LVL has much less deformation on either side of the loading area than LVL11. This leads to the conclusion that cross-banded LVL exhibits less stress spreading than LVL11. Furthermore, specimens with screw reinforcement show about the same deformation profile as specimens without screw reinforcement, leading to the conclusion that screw reinforcement does not influence stress spreading.

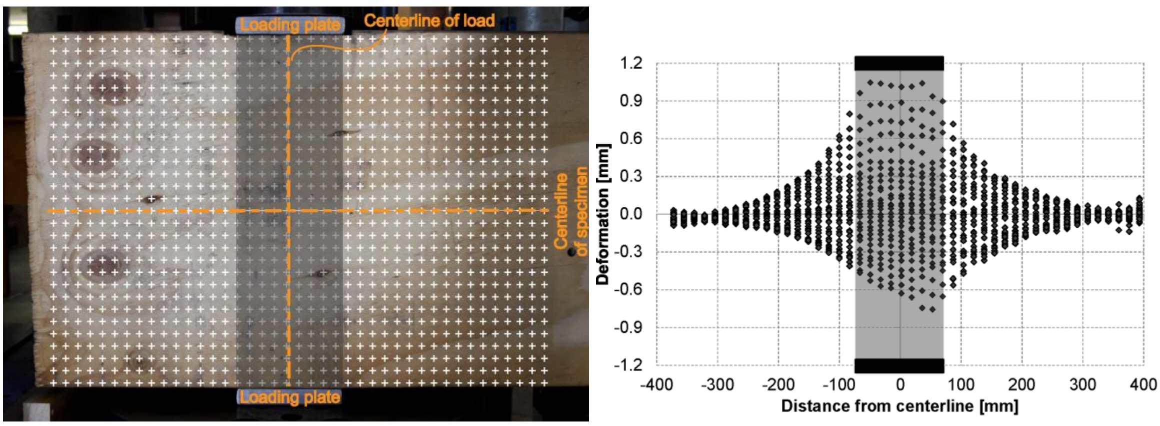

(a) (b)

Figure 8: Full displacement fields at 15MPa (a) specimen without screws, (b) specimen with 12 long screws.

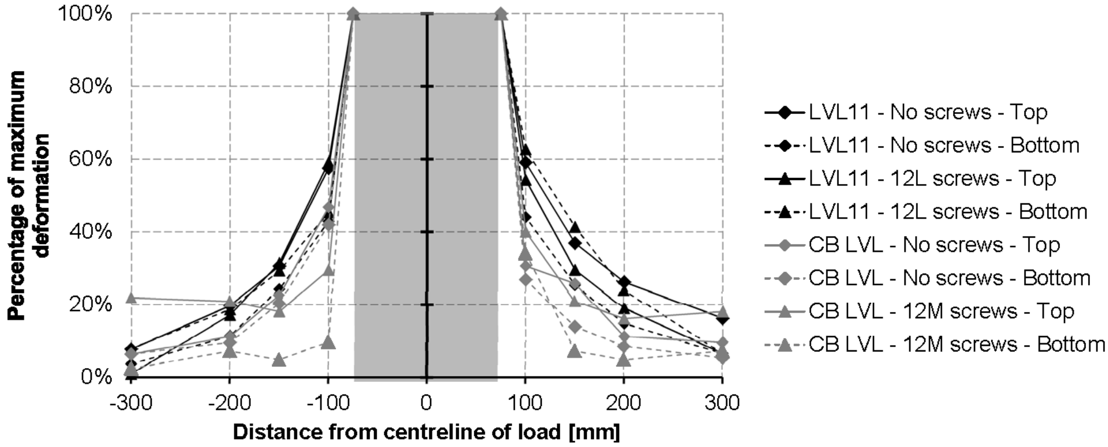

Figure 9: Comparison of displacements in LVL11 and Cross-banded LVL with and without screws

4 STIFFNESS OF SCREW REINFORCED LVL

A simplified procedure is required to describe the perpendicular to grain deformation of LVL in order to improve analytical models describing the joint behaviour of Pres-Lam post-tensioned frame systems. A very simplified model is to assume that the deformation occurs over an isolated block of timber with a uniform compressive stress as shown in Figure 10.

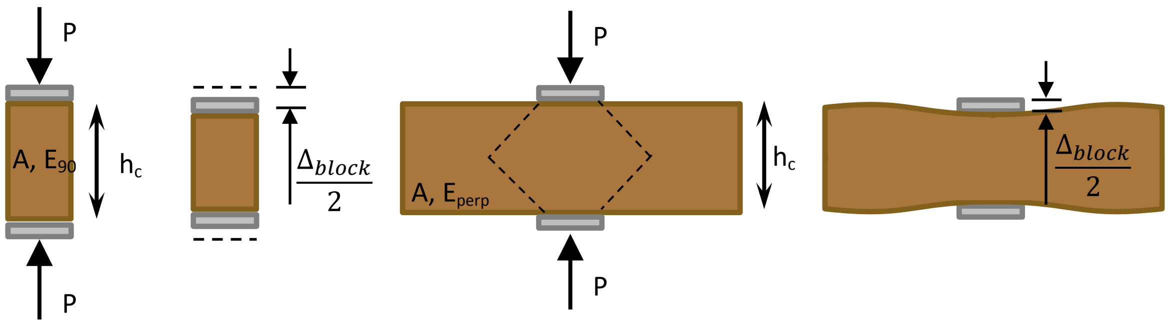

Figure 10: Deformation of a timber block under perpendicular to the grain compression without and with stress spreading

The deformation of the block without stress spreading can be expressed as:

$$\Delta_{block} = \frac{Ph_c}{AE_{90}}$$

In this equation P is the compression load, h_c is depth of the column section, A is the area of perpendicular to the grain timber in compression and E_{90} is the elastic modulus of the LVL in compression perpendicular to the grain.

In reality the compression force in a beam-column joint (and in the specimens tested) are applied over a section of the column rather than a discrete block, resulting in stress spreading (**Error! Reference source not found.**). The transverse stresses in the column reduce with depth to the centreline of the column. It is assumed that the stresses spread at an angle of 45°. The perpendicular to grain stiffness of the column, including elastic stress spreading can be expressed as:

$$E_{perp} = k_{ss}E_{90} \qquad \text{\& hence} \qquad \Delta_{block} = \frac{Ph_c}{AE_{perp}}$$

In this equation k_{ss} is the increase in stiffness due to stress spreading and E_{perp} is the perpendicular to the grain stiffness of the column section. From previous research by Blass & Görlacher (2004) an analytical solution to elastic stress spreading in timber beams was derived, where b_L is the width of the applied compression load:

$$k_{ss} = \frac{h_c}{b_L \ln\left(\frac{h_c}{b_L} + 1\right)}$$

Digital image correlation of the experimental testing has shown that an additional increase in compression stiffness is provided by screws (k_{scr}), which does not influence stress spreading:

$$E_{perp} = k_{scr} k_{ss} E_{90}$$

A design chart for values of the screw reinforcing stiffness factor, k_{scr}, over a range of screw depth and reinforcing ratios is given in Figure 11. The solid lines are based on the averaged experimental results and the dashed lines provide interpolated results using the following empirical equation:

$$k_{scr} = 1 + 54 \frac{A_{scr}}{A_t} \left(\frac{l_s}{h_c}\right)^{1.26}$$

Where l_s is the full threaded length of the screw, h_c is the depth of the column, A_{scr} is area of the screw reinforcing and A_t is area of timber loaded in compression perpendicular to the grain.

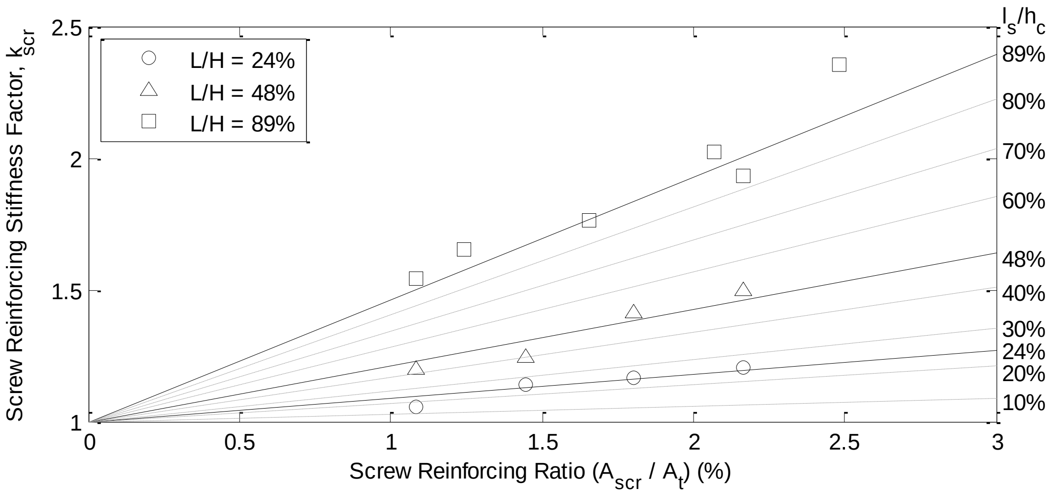

Figure 11: Preliminary design chart for screw reinforcing stiffness factor (k_{scr}), based on screw reinforcement ratios for a range of screw length over section depth (l_s/h_c)

The design chart provides screw reinforcing stiffness factors for reinforcing ratios up to 3%, as it is difficult to achieve screw reinforcing ratios over 3% if the design is to remain within the screw spacing requirements set out by most manufacturers. These spacing requirements are around '5d' spacing parallel to grain and '3d' perpendicular to grain, resulting in a timber area of $15d^2$ for one screw. The steel area for one screw is $0.25\pi d^2$ so the equivalent screw reinforcement ratio for this minimum spacing is $0.25\pi d^2/15d^2 \approx$ 5%. Edge distance and end distance requirements do not normally allow this percentage to be reached. For long screws installed from both sides, an additional tolerance is required to ensure that adjacent screws do not touch each other. Note that when long screws are installed from both sides of the column at 2% density, the total area of both groups of screws is approximately 4% of the wood volume in the overlapping area.

Because screw reinforcing ratios below 1% were not investigated, the preliminary values provided by the design chart are unverified and it may be more conservative to assume that there is no increase in stiffness for screw reinforcing ratios less than 1%.

The test results were also compared to the formula derived by Bejtka & Blass (2006):

$$E_{tot} = \frac{E_{90}\, f_{LD}\, n\, l_s \left(\frac{\psi}{n} + 1\right) \omega \sinh(\omega\, l_s)}{\varphi - \psi + n\left(\frac{\psi}{n} + 1\right) \cosh(\omega\, l_s) + 0.7\, f_{LD}\, l_s\, \varphi\, \omega \sinh(\omega\, l_s)}$$

A comparison of the experimental results against the effective stiffness values predicted by the formula show that the formula (Figure 12) over-predicts the actual stiffness of the screw reinforced LVL for all of the cases tested and that a calibration of the formula for screw-reinforced LVL may be required.

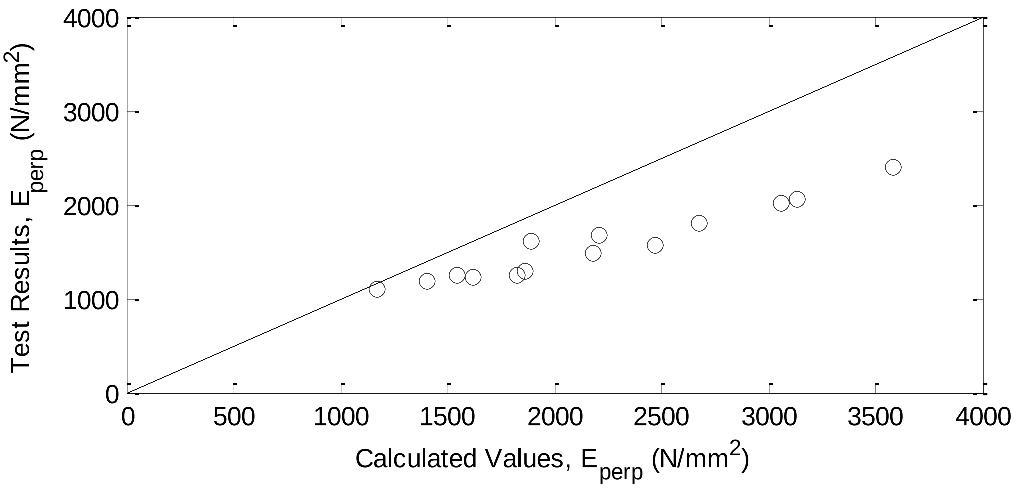

Figure 12: Comparison of calculated effective stiffness with the test results

5 CONCLUSIONS

The results from experimental testing show that screw reinforcing is an excellent way of increasing the perpendicular to grain stiffness of LVL. A design chart and empirical design equation for the increase in stiffness are presented. In general terms, the stiffness over the whole cross section can be doubled (k_{scr} = 2) by reinforcing the LVL with long screws (almost full-length) with the screw density occupying 2% of the stressed wood area on each surface. At a lower level, a 50% increase in stiffness (k_{scr} = 1.5) can be achieved with about half the volume of screws, being either the same density of half-length screws or half the density of full length screws.

For cross-banded LVL it was generally found that additional screw reinforcing provided almost no increase in stiffness compared to unreinforced cross-banded LVL, however the unreinforced cross-banded LVL was three times stiffer than unreinforced LVL.

Digital image processing showed that strains were significantly lower for screw-reinforced LVL than for unreinforced LVL at 8MPa and at 15MPa load levels. Furthermore, screw reinforcing did not influence stress spreading. Stress spreading was found to be less effective in cross-banded LVL. For a conservative design the assumption can be made that no stress spreading occurs in cross-banded LVL, so k_{ss} = 1.0.

By comparing the new experimental data against an existing analytical equation (Bejtka & Blass, 2006) it was found that the equation over-predicts the increase of stiffness provided by screw reinforcing for LVL in compression perpendicular to the grain. A design graph and an empirical design equation have been provided to quantify the increase in stiffness provided by screw reinforcing when Radiata pine LVL is loaded in compression perpendicular to the grain.

5.1 FUTURE RESEARCH

Further tests should be carried out to more comprehensively define the stiffness of screw reinforced LVL over a wider range of screw length to column heights and screw reinforcing ratios. Screw reinforcement has the potential to reduce long-term creep perpendicular to grain. Further tests are being planned at the University of Canterbury to quantify this effect. Work is on-going to incorporate the results presented in this paper into design procedures for post-tensioned timber frames.

ACKNOWLEDGEMENTS

The authors wish to acknowledge STIC for their financial support. The screws were kindly provided by Würth New Zealand Limited and SPAX Pacific Australia & New Zealand Limited. Testing was performed with the help of John Maley, Russell McConchie & Gavin Keats in the structures laboratory of the University of Canterbury. Development of DIC Matlab software by C. Eberl and his team from Karlsruhe Institute of Technology has been vital to this publication, their work and the free online access to this software has been much appreciated.

REFERENCES

Bejtka, I., & Blass, H. J. (2006). *Self-Tapping Screws as Reinforcements in Beam Supports.* 39-7-2. CIB W18 Workshop on Timber Structures, Florence, Italy.

Blass, H. J., & Bejtka, I. (2004). *Reinforcements Perpendicular to the Grain using Self-Tapping Screws*. 8th World Conference on Timber Engineering, Lahti, Finland

Blass, H. J. & Görlacher, R. (2004). *Compression Perpendicular to the Grain*. 8th World Conference on Timber Engineering, Lahti, Finland

Buchanan, A., Palermo, A., Carradine, D. and Pampanin, S. (2011). *Post-Tensioned Timber Frame Buildings*. The Structural Engineer 89 (17).

Carter Holt Harvey (2008) Engineering Bulletin No. 1 - *Strength Limit States Design Capacity Tables for CHH LVL sections.* CHH Woodproducts New Zealand

CEN (2010). *EN 408:2010 Timber structures - Structural timber and glue laminated timber - Determination of characteristic values of mechanical properties and density*. CEN, Brussels, Belgium

Crocetti, R., & Kliger, R. (2010). *Anchorage Systems to Reduce the Loss of Prestress in Stress Laminated Bridges*. International Conference on Timber Bridges, Lillehammer, Norway.

Murakami, S., Kitamori, A., Jung, K., Chang, W. & Komatsu, K. (2012). *Prediction of Reinforcement Effect by Screw on Triangular Embedment Perpendicular to the Grain with Variation of Screw Locations*. Open Journal of Civil Engineering, 2, p167-173.

Nelson Pine Industries (2010) Nelson Pine LVL11. Nelson Pine Industries Limited, Nelson, New Zealand

Newcombe, M. P. (2011). *Lateral Force Design of Post-Tensioned Timber Frame and Wall Buildings.* PhD Thesis, University of Canterbury, Christchurch, New Zealand.

Palermo, A., Pampanin, S., Buchanan, A., & Newcombe, M. (2005). *Seismic Design of Multi-Storey Building using Laminated Veneer Lumber*. New Zealand Society Earthquake Engineering Conference, Wairakei, New Zealand.

Pampanin, S. (2005). *Emerging Solutions for High Seismic Performance of Precast/Prestressed Concrete Buildings*. Journal of Advanced Concrete Technology, 3(2), 207-223.

Priestley, M. J. N., Sritharan, S., Conley, J. R., & Pampanin, S. (1999). *Preliminary Results and Conclusions from the PRESSS Five-Storey Precast Concrete-Test Building*. PCI Journal, 44(6), 42-67.

Smith, T., Ponzo, F. C., Di Cesare, A., Auletta, G., Pampanin, S., Carradine, D., Palermo, A. & Nigro, D. (2012). *Seismic Performance of a Post-Tensioned Glue Laminated Beam to Column Joint: Experimental and Numerical Results.* 12th World Conference on Timber Engineering. Auckland, New Zealand

van Beerschoten, W. A., Smith, T., Palermo, A., Pampanin, S., Ponzo, F.C. (2011). *The Stiffness of Beam to Column Connections in Post-Tensioned Timber Frames*. 44-7-4. CIB W18 Workshop on Timber Structures, Alghero, Italy.

van Beerschoten, W.A., Carradine, D.M. & Palermo, A. (2013). Compressive strength and stiffness of Radiata Pine Laminated Veneer Lumber. European Journal of Wood and Wood Products (under publication).

INTERNATIONAL COUNCIL FOR RESEARCH AND INNOVATION
IN BUILDING AND CONSTRUCTION

WORKING COMMISSION W18 - TIMBER STRUCTURES

EXPERIMENTAL INVESTIGATIONS ON SEISMIC BEHAVIOUR OF CONVENTIONAL TIMBER FRAME WALL WITH OSB SHEATHING PROPOSAL OF BEHAVIOUR FACTOR

C Faye

L Le Magorou

P Garcia

J-C Duccini

Technological Institute for Forestry, Cellulose, Timber Construction and Furniture (FCBA)

FRANCE

Keywords: seismic design, behavior factor q, shaking table tests, light frame timber wall, OSB sheathing

---

Presented by C Faye

M Fragiacomo stated that q of 3 seemed to be very conservative for timber walls and if one moves from wall components to system, higher values of q would be expected. C Faye responded that the results showed OSB has similar q as plywood even though it might be conservative. She agreed that consideration of other building components could lead to higher q.

W Seim stated the results would be helpful. He received clarification that three different typical earthquakes were considered with No. 1 and No. 2 from French zone and No. 3 simulated. He commented that the earthquakes from the French zone might need to be scaled to consider higher level of acceleration. Discussions were taken about comparing results from different earthquakes.

A Ceccotti commented that the study seemed to rely on experiments to estimate q and did not perform analytical work. C Faye stated that FEM models are being developed. A Ceccotti asked how one would reach the PGA near collapse. C Faye stated that FEM models would be needed.

F Lam commented that the statement of no damage was inaccurate as there was permanent deformation. He commented that coupling with model is important for establishing q but the database of shake table test results is very valuable especially for model verification. D Moroder stated that the statement should be no visible damage rather than no damage.

M Li asked whether nail connection tests were performed. C Faye stated that connection tests were performed only on 12 mm OSB.

Experimental investigations on seismic behaviour of conventional Timber Frame Wall with OSB sheathing Proposal of behaviour factor

Carole Faye
Laurent Le Magorou
Patrice Garcia
Jean-Charles Duccini

Technological Institute for Forestry, Cellulose, Timber Construction and Furniture (FCBA), France

1 Context and objectives

According to Eurocode 8 [1], timber buildings shall be designed using one of the following concepts:

(1) low dissipative structural behaviour. In this case, behaviour factor q may be taken as 1.5;

(2) dissipative structural behaviour. In this case, structures shall belong to medium or high capacity classes to dissipate seismic energy.

Concerning shear walls, following requirements for plywood, particleboard and fibreboard sheathing for density and minimum thickness must be fulfilled to satisfy concept (2) without the need of further studies:

a) particle board panels have a density of at least 650 kg/m^3;
b) plywood sheathing is a least 9 mm thick;
c) particle board and fibreboard sheathing are at least 13 mm thick.

In these cases and with additional requirements for fasteners (nail diameter d not exceeding 3.1 mm and sheathing panel thickness of 4×d minimum), wall panels with nailed diaphragms, connected by nails or bolts can be assigned to high ductility class with a value of the behaviour factor q taken as up to 5. It should be noticed that there are no specific requirements or provisions for OSB.

In France, the behaviour factor is limited to a value of q= 3 even for buildings that comply with high ductility class.

Concerning OSB sheathing panels, q =3 is accepted if they comply with the requirements for particleboard which implies a minimum thickness of 13 mm. As a consequence, for 12 mm thick OSB sheathing panel, q is limited to 1.5 due to the lack of specific background as mentioned in the French National Annex. This leads to the use of 15 mm thick OSB sheathing. This situation is very penalizing because OSB sheathing represent up to 80% of timber shear walls on the French market and most of the current structures don't need such thickness.

Then, this paper presents an experimental study on walls with 12 mm thick OSB sheathing panel. For comparison purposes, walls made with particle board and plywood sheathing were also tested. The objective is to assess experimentally a seismic behaviour factor q for 12 mm thick OSB sheathing.

2 Walls configurations

Tests were performed on walls of 2,4 m height by 2,4m long with the three following types of sheathing panels:

- **(config. CP10)** 10 mm thick plywood complying with EN 636-3,
- **(config. P16)** 16 mm thick particleboard complying with EN 312/P5,
- **(config. OSB12)** 12 mm thick OSB/3 complying with EN 300.

These three configurations correspond to the minimum configurations used in seismic zones in France.

Except for the sheathing panels, shear walls for tests have identical characteristics:

- sheathing panels are fixed using threaded nails of 2.5 mm diameter and 50 mm length complying with EN 14 592,
- the spacing of the nails is 150 mm and 300 mm respectively on panel edges and panel center,
- the span of studs is 600 mm. Studs and horizontal members are connected by 4 threaded nails.

In these conditions, according to Eurocode 8, configurations **(CP10)** and **(P16)** can be assigned to the high ductility class. A wall description is presented in Figure 1.

3 Cyclic load tests

The objective of the cyclic load tests was to determine a displacement limit at the top of the wall which will be used as the near-collapse criterion for dynamic tests. The displacement limit ($V_{90\%}$) was chosen as the displacement at the top of the wall corresponding to the reduction of the maximum force by 10%.

3.1 Test Methods

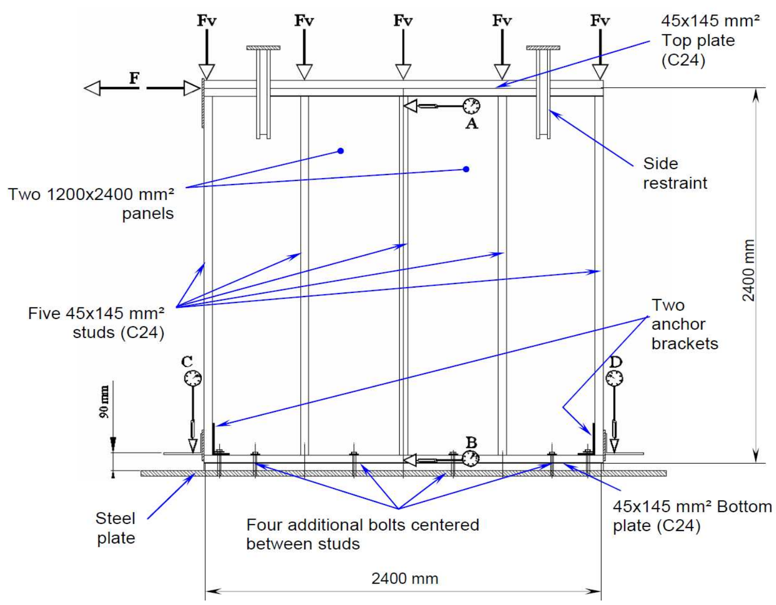

Figure 1 : Shear wall dimensions and loading for cyclic test.

For each configuration, two cyclic tests were performed with realistic boundary conditions (wall is anchored by available stiff commercial anchor brackets and a total vertical dead load of 15 kN is applied) according to the standard ISO 21581:2010 [2] based on [3]. Test assembly and shear wall dimensions are presented in Figure 1. The rate of displacement was chosen to achieve ultimate displacement within 1 minute. The ultimate displacements, measured previously with the static monotonic test, were respectively 124 mm, 116 mm and 100 mm for plywood, particle board and OSB configurations.

3.2 Cyclic tests on plywood, particle board and OSB configurations

Cyclic tests on plywood, particle board and OSB configurations are presented, respectively, in Figure 2, Figure 3 and Figure 4.

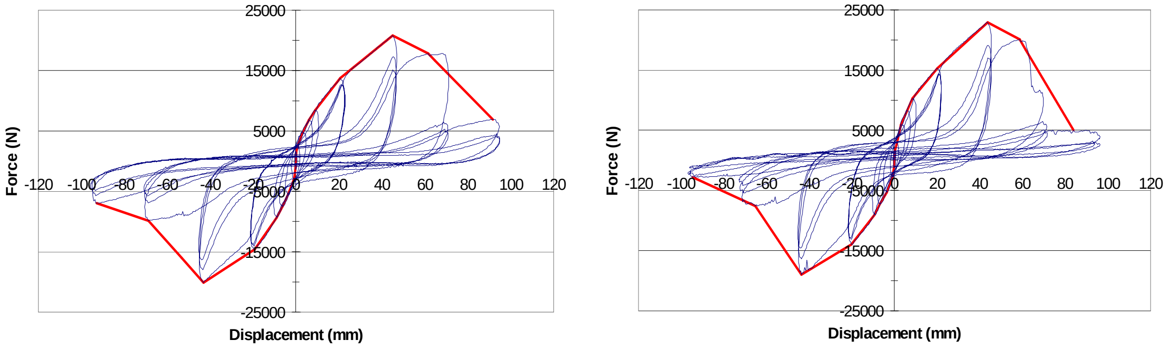

Figure 2 : load-displacement and envelope curves for cyclic tests at the top of the wall with 10 mm thick plywood sheathing (CP10) (left: test n°1 / right: test n° 2).

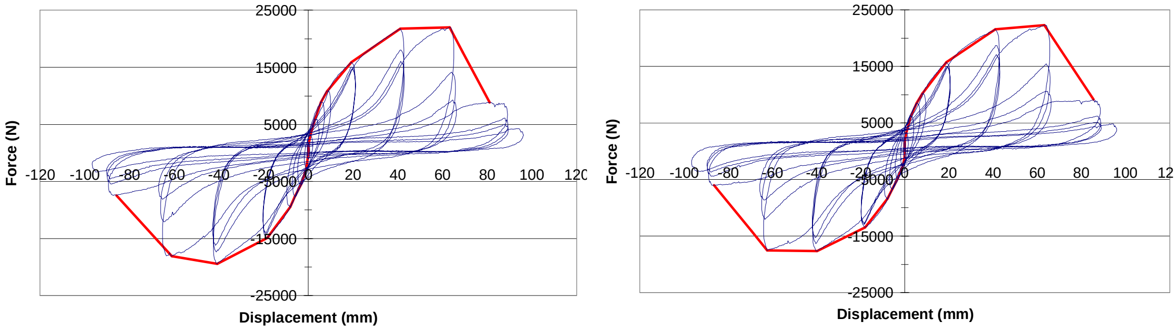

Figure 3 : load-displacement and envelope curves for cyclic tests at the top of the wall with 16 mm thick particle board sheathing (P16) (left: test n° 1 / right: test n°2).

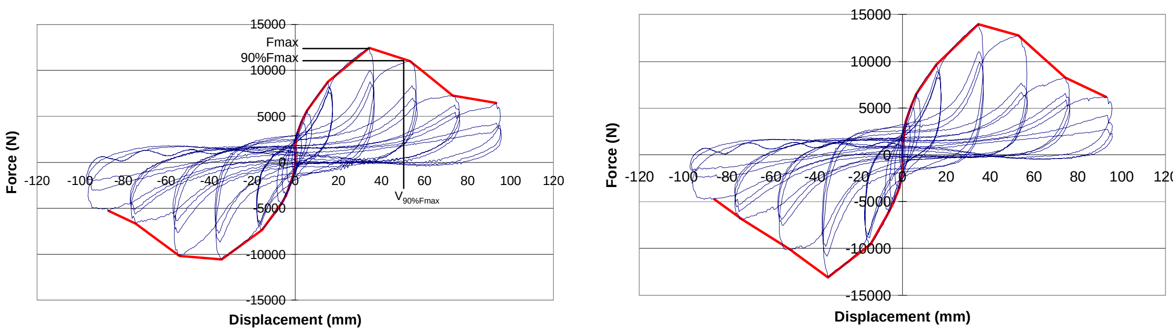

Figure 4 : load-displacement and envelope curves for cyclic tests at the top of the wall with 12 mm thick OSB sheathing (OSB12) (left: test n°1 : right : test n°2).

The following were observed:

- shear failure mode of the fasteners of the panels,
- hardening of the nails,
- damage to the particle boards around the nails,
- the anchorage brackets were undamaged.

3.3 Near-collapse criterion for dynamic tests

In Table 1, for each cyclic test, are given:

- the maximum force F_{max} (see figure 4, left),
- the following displacements V_{Fmax}, $V_{90\%Fmax}$, $V_{80\%Fmax}$ corresponding respectively to the displacements at the forces F_{max}, 90% F_{max},and 80% F_{max},
- and the displacement limit chosen as the near collapse criterion.

	F_{max} (kN)	V_{Fmax} (mm)	$V_{90\%Fmax}$ (mm)	$V_{80\%Fmax}$ (mm)	Limit displacement (mm) for dynamic test
CP10 /1,5T/ ISO 21581	20,8	45	54	64	54
CP10 /1,5T / ISO 21581	22,2	44	56	62	
P16 /1,5T/ ISO 21581	22,0	63	66	69	60(*)
P16 /1,5T / ISO 21581	22,2	63	67	71	
OSB12 /1,5T/ ISO 21581	12,4	34	51	59	51
OSB12 /1,5T / ISO 21581	14	34	54	62	

Table 1 : Maximum force and displacements corresponding to F_{max}, $90\%F_{max}$, $80\%F_{max}$, determined from the envelope curve of cyclic tests. (*) To avoid any geometrical instability of the structure, displacement on the top the wall is limited to 60 mm.

4 Dynamic tests

4.1 Test Methods

The same wall configurations were then tested on a shaking table with the following conditions:

- a total dead load of 15 kN or 20 kN is applied on the top of the wall,
- wall is anchored by stiff fasteners in accordance with the provisions of Eurocode 5 and Eurocode 8,
- the direction of shaking test is parallel to the wall plane.

The horizontal displacement is measured at the top of the wall.

Figure 5: shear wall and dead load for dynamic test.

The test method for each wall is the following :

Step a) vibration test with white noise is performed at a low level to determine its natural frequency f_0;

Step b) a seismic test is performed with the earthquake signal at its original Peack Ground Acceleration to determine the displacement at the top of the wall; this step is not systematically made;

Step c) a seismic test is performed with the same earthquake at an increased PGA, named $PGA_{near\ collapse,\ test}$, calibrated in order to reach a displacement at the top of the wall as close as possible to the near collapse criterion (see column 6 of Table 1), without over passing it.

Step d) a seismic test, identical to the step (b), is performed to verify shear wall load bearing capacity after the seismic events.

Thus, for each shear wall tested, we can calculate the experimental value of the behaviour factor q_{test} according to:

$$q_{test} = PGA_{near\ collapse,\ test} / PGA_{design\ EC8,\ q=1} \quad (1)$$

where $PGA_{design\ EC8,\ q=1}$, is the ground acceleration corresponding to the maximum allowable PGA for the tested wall if designed according to linear lateral force method of analysis of Eurocode 8, with q=1. The relation (1) was used by [4] and [5] in a hybrid approach coupling finite elements modeling and experimentation.

These values of q are presented in tables 2, 3 and 4 (column 10) respectively for configurations CP10, P16 and OS12 for each wall tested.

The total number of shear walls tests that were performed is 16: 8 seismic tests for OSB12, 4 seismic tests for particleboard P16 and 4 seismic tests for plywood CP10.

4.2 Choice of earthquakes

Three different earthquake signals were applied for each configuration test.

Two of them were selected from a database of 40 earthquakes representative of medium (PGA=1.6g) and high (PGA=3g) seismic zones in France (where g=9.81 m/s^2). Both earthquakes were chosen with the following criteria:

- to be the most destructive to the walls. To achieve this, the power spectral density and other general seismic indicators (Arias intensity, cumulative absolute velocity …) were determined for each earthquake normalized at PGA=1g;

- to be compatible with the limitations (allowed displacement and acceleration) of the shaking table.

Finally, both selected earthquakes (hereafter named earthquake 1 and earthquake 2) were among the five most destructive on our dtabase. More details are given in [6].

Additionally, a third earthquake, named Aquila (occurred in Italy in 2009, named earthquake 3), was also used for seismic tests.

Figures 6, 7 and 8 represent respectively the acceleration vs time curve for earthquakes 1, 2 and 3.

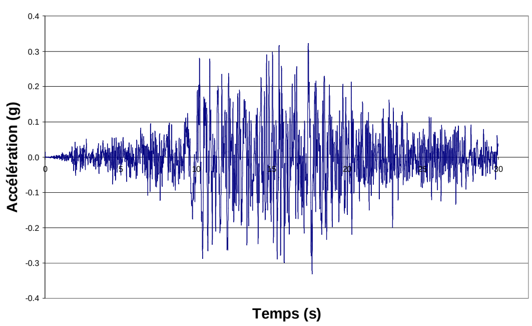

Figure 6: earthquake 1 (PGA=0.33g)

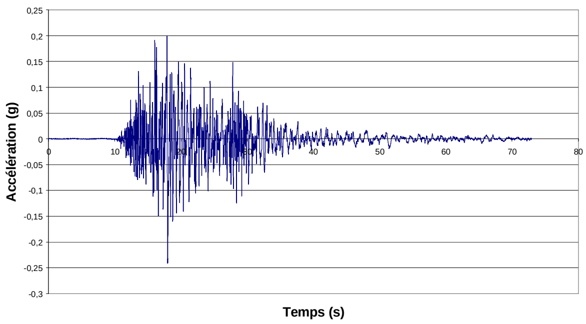

Figure 7: earthquake 2 (PGA=0.24g)

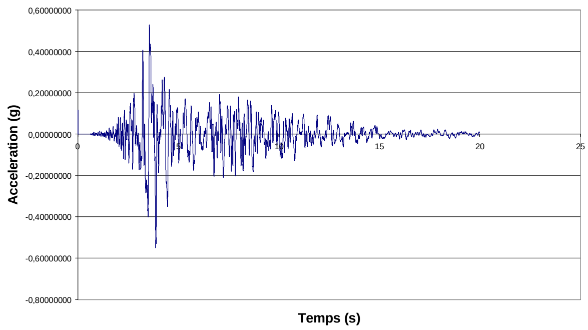

•

Figure 8: earthquake 3 (PGA=0.56g)

4.3 Results of the CP10 configuration

Four walls CP10 were tested on the shaking table with the three earthquakes. The results are presented in Table 2.

The displacement at the top of the wall vs time curves of dynamic tests of CP10 walls n°9 and n°21 (compared with OSB12 wall n° 7 and n°18) are presented in Figure 10 and 9 in section 4.5.

				results concerning only seismic test performed with $PGA_{near\text{-}collapse}$ (see section 4.1, step c)					
Wall N°	**f_0 (Hz)**	**dead load (kN)**	**earthquake signal**	**Max. displ. (mm) and associated input $PGA_{near\text{-}collapse}$**	**damage**	**permanent displ. (mm)**	**actual $PGA_{near\text{-}collapse}$ (A)**	**$PGA_{designEC8,q=1}$ (B)**	**q_{test} = (A)/(B)**
9	5.8	15	1	**42 mm** at 1.19g	shear failure on 3 nails	0.1	1.1 g	0.32 g	**3.4**
19	5	20	2	**50 mm** at 0.88g	shear failure on 5 nails	5	1.1 g	0.24 g	**4.5**
21	7	20	2	**45 mm** at 0.73g	none	3.5	0.9 g	0.24 g	**3.7**
20	5.4	20	3	**49 mm** at 1.3g	shear failure on 5 nails	5	1.4 g	0.24 g	**5.8**

Table 2 : results of dynamic tests for CP10 walls: column 2 indicates the natural frequency of the wall determined before the first seismic test (see section 4.1, step a); column 7 indicates the permanent displacement at the top of the wall after the seismic test made with $PGA_{near\text{-}collapse}$; column 8 indicates the actual value of $PGA_{near\text{-}collapse,\ test}$ which can be different from the input PGA; column 10 indicates the q_{test} value for each wall, calculated as mentioned in section 4.1. (g = 9.81 m/s^2)

The main observations are the following:

- concerning all CP10 walls, the only visible damage (see column 8 of Table 2) due to earthquake at $PGA_{near\text{-}collapse,test}$ (see § 4.1 step c) is shear failure of the nails without damage of the panel ;
- all walls having suffered the earthquake at $PGA_{near\text{-}collapse,test}$, are able to withstand an earthquake at its regular PGA, without collapsing;
- the maximum displacement of wall n°9 (42 mm) for seismic at $PGA_{near\text{-}collapse,test}$ level (see step c of section 4.1) is well below the criterion of 54 mm. So, the value of 3.4 for q, calculated for the earthquake1 is very conservative. Tests performed on walls n° 19 and n° 20, with earthquakes 2 and 3, led to higher conservative values for q: respectively 4.5 and 5.8.

4.4 Results of the P16 configuration

Four walls P16 were tested on the shaking table using two of the three earthquakes. The results are presented in Table 3.

The displacement at the top of the wall vs time curve of dynamic test of P16 walls n°16 (compared with OSB12 wall n° 15) is presented in Figure 11 in section 4.5.

The main observations are the following:

- concerning wall n°17, damage of the panel around only 3 nails was observed;
- all walls having suffered the earthquake at $PGA_{near\text{-}collapse,test}$, are able to withstand an earthquake at its regular PGA, without collapsing;
- the maximum displacement of walls n°10 and n°17 at $PGA_{near\text{-}collapse,test}$ are below the criterion of 60 mm. So, the values of 4.5 and 8 for q, are conservative respectively for the earthquakes 1 and 3.

				results concerning only seismic test performed with $PGA_{near\text{-}collapse}$ (see section 4.1, step c)					
Wall N°	**f_0 (Hz)**	**dead load (kN)**	**earthquake signal**	**Max. displ. (mm) and associated input $PGA_{near\text{-}collapse}$**	**damage**	**permanent displ. (mm)**	**actual $PGA_{near\text{-}collapse}$ (A)**	**$PGA_{design\ EC8,q=1}$ (B)**	**q_{test} = (A)/(B)**
5	7.4	15	1	**39 mm** at 1.25g	shear failure on 2 nails	0.1	1.15 g	0.35 g	**3.3**
10	6.2	20	1	**54 mm** at 1.25g	10 nailed withdrawals / panel without damage	1.5	1.17 g	0.26 g	**4.5**
16	7	15	3	**41 mm** at 1.8g	none	0.2	2.07 g	0.35 g	**6.0**
17	5	20	3	**51 mm** at 1.8g	damage of the panel around 3 nails	10	2.09 g	0.26 g	**8.0**

Table 3 : results of dynamic tests for P16 walls. For explanations, see Table 2.

4.5 Results of the OSB12 configuration and proposal for the behaviour factor for OSB12

Height walls OSB12 were tested on the shaking table using the three earthquakes. The results are presented in Table 4.

The main observations are the following:

- concerning all OSB12 walls (except wall n°13 which over-passed the displacement limit of 51mm), there was no damage induced by seismic tests;
- all walls having suffered the earthquake at $PGA_{near\text{-}collapse,test}$, are able to withstand an earthquake at its regular PGA, without collapsing;
- concerning earthquake 1, four identical tests were performed (on walls n° 7, 8, 11 and 12). The variation (around 9%) of the experimental values of the maximum displacement at the top is explained by the higher stiffness of the walls n°7, 11 and 12 in comparison with wall n°8.

The following values for behaviour factor of OSB12 were calculated:

- a conservative value of 3.2 for earthquake 1 (walls n° 7, 8, 11, 12)
- a conservative value of 3.8 for earthquake 2 (wall n° 18)
- a conservative value of 4.5 for earthquake 3 (wall n° 15).

Furthermore, comparison of experimental displacements curves of OSB12 and CP10 measured for identical (or very close) seismic tests are presented in Figure 9 and Figure 10. We can observe that dynamic behaviour of OSB12 and CP10 walls are very similar.

In the opposite, comparison between OSB12 and P16, presented in Figure 11, shows that P16 walls can suffer significantly higher seismic event than OSB12 wall with similar displacements.

				results concerning only seismic test performed with $PGA_{near\text{-}collapse}$ (see section 4.1, step c)					
Wall N°	f_0 (Hz)	dead load (kN)	earthquake signal	Max. displ. (mm) and associated input $PGA_{near\text{-}collapse}$	damage	permanent displ. (mm)	actual $PGA_{near\text{-}collapse}$ (A)	$PGA_{design\ EC8,q=1}$ (B)	q_{test} = (A)/(B)
7	6.8	15	1	**39 mm** at 1.06g	none	7	1 g	0.31 g	**3.2**
8	5.8	15	1	**45 mm** at 1,06g	none	10	0.98 g	0.31 g	**3.1**
11	7.2	15	1	**36 mm** at 1,06g	none	4	1 g	0.31 g	**3.2**
12	7	15	1	**38 mm** at 1,06g	none	2	1 g	0.31 g	**3.2**
13	5.6	20	1	**57 mm** at 1,06g	1 nail withdrawal	7	1 g	0.24 g	**/***
14	6.5	15	2	**42 mm** at 0,88g	none	1	1.1 g	0.31 g	**3.5**
18	5.5	20	2	**46 mm** at 0,73g	none	3	0.9 g	0.24 g	**3.8**
15	6	15	3	**40 mm** at 1,3g	none	6	1.4 g	0.31 g	**4.5**

Table 4 : results of dynamic tests for OSB12 walls. For explanations, see Table 2. * Concerning wall n° 13, q_{test} is not calculated because the near collapse criterion is over-passed.

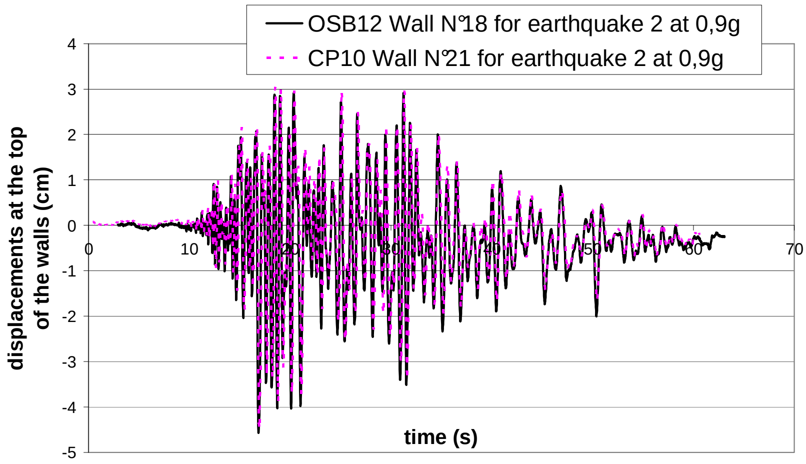

Figure 9 : experimental displacements vs time curves for wall n°18 (OSB12) and wall n° 21 (CP10) when submitted to same seismic test (earthquake 2 at 0,9g).

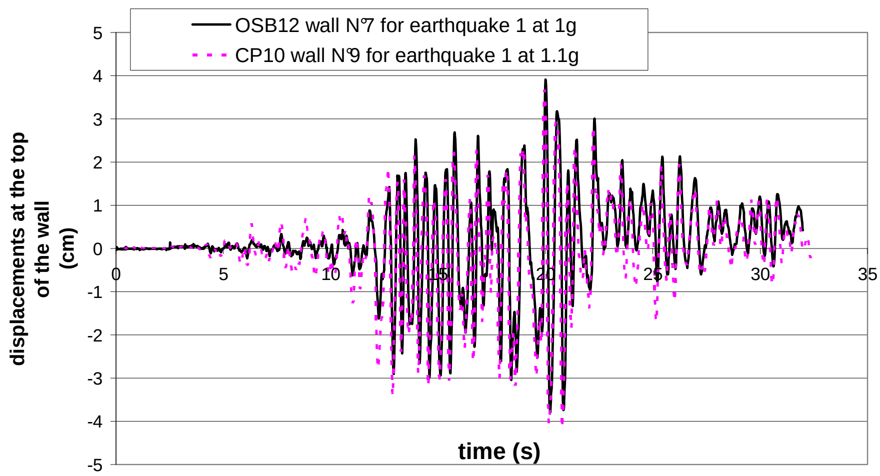

Figure 10 : experimental displacements vs time curves for wall n°7 (OSB12) and wall n° 9 (CP10) when submitted to quasi-same seismic test (earthquake 1 at 1g).

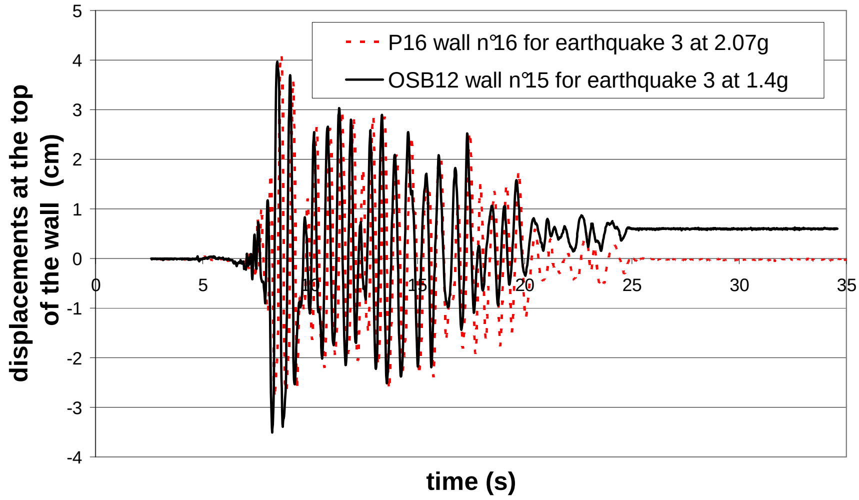

Figure 11 : experimental displacements curves vs time for wall n°15 (OSB12) and wall n° 16 (P16) when submitted to earthquake 3, first one at 1.4g, second one at 2.07g.

5 Conclusions

This experimental study concerned dynamic tests carried out on three different light frame walls having racking resistances designed according to the capacity design principles and supporting a dead load up to 850 kg/m.

The dynamic tests showed that failure modes are due to the yield moment of the fasteners connecting the sheathing panels to the wooden frame.

For earthquake 1, which is among the five most destructive of our database on 40 representative earthquakes of seismic French zones, a conservative value q of 3.2 was calculated for OSB12 walls.

Moreover, the dynamic behaviour of walls with OSB (12 mm) and plywood (10 mm) sheathing panels are very similar:

- their near-collapse criterion displacement are very close,
- during dynamic tests performed with identical earthquakes, their experimental dynamic displacement curves are very similar.

Thus, it is proposed that a conservative behaviour factor q for OSB sheathing panel with a thickness of 12 mm should be q = 3, as is the value allowed for CP10 complying requirements for high ductility class in France.

6 Acknowledgments

This research project was supported by CODIFAB (French Federation of Wood Industry) and DHUP (French Ministry of Lodging).

7 References

[1] EN 1998-1: Design of structures for earthquake resistance- Part 1: General rules, seismic actions and rules for buildings.

[2] ISO 21581:2010 : Timber structures- Static and cyclic lateral load test metrhods for shear walls.

[3] Yasumura M., Karacabeyli E.: *International test standard development for lateral load test for shear walls,* Proceedings of CIB-W18, paper 40-15-5, 2007, Slovenia.

[4] Ceccotti A., Sandhaas C., *A proposal for a standard procedure to establish the seismic behaviour factor q of timber buildings***,** WCTE, World Conference on Timber Engineering, 2010, Italy.

[5] Schädle P., Blass HJ., *Influence of different standards on the determination of earthquake properties of timbre shear wall systems,* Proceedings of CIB-18, paper 43-15-2, 2010, New-Zealand.

[6] Research report, FCBA, *comportement parasismique des murs à ossature bois*, 2012.

INTERNATIONAL COUNCIL FOR RESEARCH AND INNOVATION IN BUILDING AND CONSTRUCTION

WORKING COMMISSION W18 - TIMBER STRUCTURES

CAPACITY SEISMIC DESIGN OF X-LAM WALL SYSTEMS BASED ON CONNECTION MECHANICAL PROPERTIES

I Gavric

M Fragiacomo

Department of Architecture, Design and Urban Planning, University of Sassari

Alghero

Ario Ceccotti

CNR IVALSA Trees and Timber Institute, S. Michele all'Adige

ITALY

Keywords: capacity based design, seismic resistance, CLT walls, X-Lam connections, overstrength, rocking behaviour, cross-laminated timber, ductility

Presented by I Gavric

A Buchanan commented that the principal concern with the approach was that the location where ductility is to take place needs to be identified. He asked whether there was any thought on how to regain strength and stiffness after an earthquake, especially a large earthquake. I Gavric responded that installation of additional energy dissipation elements would be possible and there should not be huge effort to replace elements if damaged.

F Sarti discussed about the rocking mechanism and self centering mechanism of CLT buildings. M Fragiacomo stated that shake table tests of CLT buildings showed no severe damage was concentrated in a few points.

A Buchanan further commented that coupled wall and properly designed joints including corner joints are critical. He received confirmation that in the corner of a building, connections in perpendicular walls could cause uplift of the perpendicular walls.

D Moroder stated that overstrength factor of 1.6 might be too conservative and that there were so many overstrength factors which could result in non-economical designs.

Capacity seismic design of X-LAM wall systems based on connection mechanical properties

Igor Gavric
Department of Architecture, Design and Urban Planning, University of Sassari
Alghero, Italy

Massimo Fragiacomo
Department of Architecture, Design and Urban Planning, University of Sassari
Alghero, Italy

Ario Ceccotti
CNR IVALSA Trees and Timber Institute, S. Michele all'Adige, Italy

1 Introduction

This paper presents some results of a research carried out as a continuation of the SOFIE project, the aim of which was to develop seismic resistant multi-storey timber buildings using prefabricated cross-laminated panels. An extensive experimental research programme was conducted: cyclic tests on typical X-Lam connections [1, 2], cyclic tests on single and coupled walls [3, 4], pseudo-dynamic tests on a 1-story building [5], shake table test on a 3-story building with ground acceleration in one direction [6], and finally a shake table test on a 7-story building with ground accelerations in all three directions [7].

Further research in this field is still needed in order to better understand the seismic behaviour of typical X-Lam connections (1-D models), the behaviour of single wall panels or series of adjacent wall panels (2-D models) and the behaviour of entire X-Lam buildings (3-D models). Analytical [1] and numerical models [8, 9] were developed to investigate the behaviour of X-Lam wall systems and to understand how to obtain the desired response of this construction system under earthquake excitation. The comparisons among analytical methods, numerical models and experimental tests have confirmed that the layout and design of the joints is critical for the overall behaviour of the X-Lam structural system.

The next step in the SOFIE research project is the development of a design procedure for this type of buildings, with the goal of a safe and economic construction that should be easy to repair after a major seismic event. This result can be achieved when the lateral load resisting system has a complete load path properly designed for seismic forces. By knowing the mechanical properties of each single connector, fastener, wooden panel and their interaction, the designer can decide how the building will perform in terms of stiffness, strength, energy dissipation and ductility and ensure the objectives of the design stated above. Through proper dimensioning and detailing of the structural elements it is possible to achieve an overall ductile behavior of X-Lam buildings.

The aim of a modern seismic design is to dimension buildings which will respond in a ductile way during the earthquake, preventing any possibility for brittle failures. The structure should have an adequate capacity to deform beyond its elastic limit without substantial reduction in the overall resistance against horizontal and vertical loads. Even more, with proper detailing and design, almost all damage during earthquakes can be concentrated in specific parts of building designed for this aim, thus reducing financial costs associated with the downtime and repair of the buildings after major seismic events. To achieve this result, capacity based design should be applied, in order to ensure that ductile modes of failure should precede brittle modes of failure with sufficient reliability.

2 Behaviour of X-Lam connections under cyclic loads

An extended experimental programme on typical X-Lam connections was performed at IVALSA Trees and Timber Institute. Shear and pull-out monotonic and cyclic tests according to EN12512 standard [10] were carried out on hold-downs and steel angle brackets used to anchor the wall panels to foundation and to connect walls to floor panels in upper stories. In-plane shear tests were also performed on mechanical screwed connections between adjacent X-Lam panels, using different types of vertical joints [1]. In addition, cyclic tests were carried out on orthogonally connected panels (wall-wall and wall-floor) subjected to shear and withdrawal load [2].

Although in most cases a very good mechanical response of connectors was obtained, some undesired failure modes and undesired behaviour were also observed. More specifically, brittle failure modes occurred when the metal connector itself did not have sufficient stiffness and strength to carry the forces from the fasteners (nails) to the foundation or to the floor panel. For example, when too many nails were used in the hold-down HTT22, a brittle failure in the net section area of the steel part occurred before the nails could start to plasticize (Figure 1a) and develop the ductile failure mode. Steel angle brackets BMF90x116x48x3 mm with 11 annual ringed nails 4x60 mm anchoring X-Lam wall panel to the foundation failed in tension due to bolt pull-through the steel part of angle bracket (Figure 1b). Again, brittle failure occurred before nails could start to plasticize. A third case of undesired connection response was found the in case of tension test of angle bracket type BMF105 when connecting X-Lam wall panel with X-Lam floor slab. A combination of yielding of the steel part of the bracket and withdrawal of anchoring nails occurred before the shear plastic mechanism of nails in the wall panel could develop (Figure 1c).

(a) (b) (c)

Fig. 1 Undesired (brittle) failures modes of X-Lam connections: (a) failure of steel part of hold-down; (b) pull-through of the bolt in the steel part of angle bracket; (c) yielding of steel part of angle bracket with nails withdrawal

In several other research projects some undesired failure modes of typical X-Lam connections were observed as well: bolt withdrawals from concrete foundation while testing angle brackets in tension [11], and shear plug failure of X-Lam panel during BMF105 angle bracket test (10 nails 4x40 mm) in tension [12].

These types of failure modes demonstrate that capacity based design should not only be implemented at the building level (for example ensuring that brittle failure modes of X-Lam panels are avoided), but also at the connection level (namely, avoiding the brittle failure of one part of the connection system – for example, the failure in tension of the metal part of the hold-down) and, even more, at the fastener level (i.e. by ensuring a ductile failure characterized by formation of either one or two plastic hinges in the fastener and avoiding brittle failure mechanisms such as splitting in the timber). Principles of capacity design will be discussed more in detail in Section 4.

Some proposals for a better mechanical performance of metal connectors (hold-downs and angle brackets) are listed herein after:

- using screws with larger diameter in the lower part of the angle brackets in wall to floor connections instead of using slender nails (due to the higher withdrawal capacity of screws) so as to avoid brittle failure for withdrawal of nails;
- re-designing the steel connectors by using larger sections (increased thicknesses) and better detailing to provide higher moment yielding capacity so as to avoid connector plasticization in the metal part;
- choosing the number and diameter of holes for fasteners to ensure brittle failure for fracture in tension of the metal connection will always follow the failure of the nailed connection between the metal connector and the X-Lam panel;
- using slender nails or screws to ensure plasticization of the fastener and achieve the ductile connection between the steel connector and the X-Lam panel;
- using longer nails for a better ductility performance of X-Lam wall panels and decreasing the risk for brittle shear plug failure.

Overall, some of the metal connectors currently manufactured do not comply with these requirements: they could be improved by following the capacity based design recommendations provided above to avoid the undesired brittle failures.

3 Behaviour of X-Lam wall systems under cyclic loads

Cyclic tests were carried out also on full-scale single and coupled cross-lam wall panels with different geometrical properties and layouts of mechanical connectors subjected to lateral force. The experimental data was processed with special attention to energy dissipation properties and damping capacity of X-Lam timber panels [1, 4, 13]. A new analytical method for seismic design of X-Lam wall systems was developed [1]. It takes into account all the stiffness and strength components of hold-downs and angle brackets, also in the weaker direction. Analyses showed that most deformations occurred due to rocking and sliding of wall panels, while the contribution of shear and bending deformation of the wall panels itself was negligible. Basically the deformed shape of a X-Lam panel can be obtained with acceptable approximation by assuming the panel as in-plane rigid and concentrating all the deformations into the connectors (hold-downs, angle brackets). The only exceptions are X-Lam walls with large openings where panel deformations during lateral loading cannot be neglected. The contribution of angle brackets in vertical (uplift) direction was found to be significant, as it is responsible for up to 50% of the overall wall overturning resistance (Figure 2b) [1]. If the load carrying capacity of angle brackets in vertical direction is not taken into account (Figure 2a), the stiffness of X-Lam building is markedly underestimated. This results in calculating higher natural vibration periods which (for higher buildings) results in underestimating the seismic effects as these buildings fall in the descending part of the response spectrum.

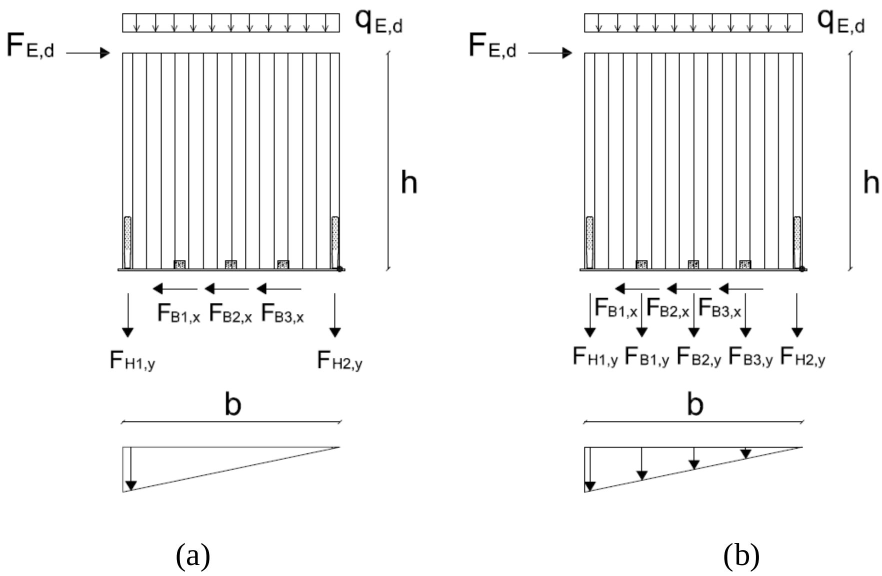

Fig. 2 Distribution of forces in X-Lam walls when exposed to lateral loads: (a) simplified design model, with hold-downs resisting uplift forces, and brackets resisting shear forces; (b) more accurate design model, with hold-downs resisting uplift forces, and brackets resisting both uplifting and shear forces

A comparative study among experimental results of 49 X-Lam wall panel cyclic tests conducted in research projects at CNR-IVALSA [3, 4] and FPInnovations research institute [14] showed some typical behaviour properties of X-Lam wall systems in terms of predominant types of deformations and interaction of panels during cycling loading [13]. The influence on seismic performance of various parameters, including geometry of panels, vertical loads, connection configuration, number and type of metal connectors, type of fasteners and type of vertical joint between adjacent panels was studied. An investigation was performed on how these elements and behaviour types affect X-Lam wall system properties such as strength and stiffness capacity, displacement (drift) capacity, ductility ratios, energy dissipation capacity and hysteretic damping values, which are all important in seismic design of X-Lam systems. In addition, observations of failure modes of the connections provided an insight on how a proper design of typical X-Lam connections should be carried out.

3.1 Predominant types of deformations of X-Lam wall systems during cyclic loading

Based on the results of numerous X-Lam wall cyclic tests, the following classification in terms of predominant deformations of X-Lam wall systems can be proposed: (i) rocking behaviour; (ii) combined rocking-sliding behaviour; (iii) sliding behaviour [13].

Experimental tests showed that walls with predominant sliding mechanism at collapse have lower ductility and ultimate displacement with respect to walls with predominant rocking mechanism. Consequently that leads to lower q factors in the former case. In addition, energy dissipation capacity of walls with sliding mechanism is lower than the ones with rocking mechanism or combined rocking-sliding mechanism [4]. Last but not least, full scale building tests at FPInnovations [15] showed that sliding of walls results in a withdrawal of fasteners in walls perpendicular to them. That causes a reduction in strength and stiffness of the wall system in the opposite direction, thus reducing the overall strength and stiffness capacity of the entire building.

When the sliding failure mechanism precedes the rocking failure mechanism, X-Lam wall tends to slide almost without any rocking. All horizontal displacement of the wall comes from shear deformation of angle brackets (plasticization of nails), whereas the hold-downs do not contribute to the wall stiffness nor to the wall strength as the steel part of the hold-down rotates as the wall slides and consequently the nails in the hold-downs do not work in shear direction. This means that hold-downs in walls with predominant sliding mechanism do not meet the design intention as they are not contributing to the wall resistance under lateral loads.

To increase the ductility and the ultimate displacement capacity, lateral resisting X-Lam walls should be designed to first develop rocking mechanism, which then transforms into a combination of rocking and sliding until the desired ultimate displacement is reached. Rocking behaviour precedes the sliding behaviour when the resistance of walls to shear forces is higher than their overturning resistance [1]. As the aforementioned experimental tests and analytical analyses showed, both hold-downs and angle brackets resist uplift forces due to overturning moments while only angle brackets resist shear forces due to the lateral loading of the panel. Angle brackets are always loaded in two directions at the same time, shear and uplift. Combined forces (two-direction loading) result in reduced strength capacity, described with the following interaction inequality from ETA-07/0055, Annex B [16]:

$$\left(\frac{F_{Bi,Ed,x}}{F_{Bi,Rd,x}}\right)^2 + \left(\frac{F_{Bi,Ed,y}}{F_{Bi,Rd,y}}\right)^2 \leq 1 \qquad (1)$$

where $F_{Bi,Ed,x}$ *and* $F_{Bi,Ed,y}$ denote the shear and uplift design forces on the brackets, while $F_{Bi,Rd,x}$ and $F_{Bi,Rd,y}$ signify the design resistances of brackets in shear and uplift direction.

As soon as the brackets start to uplift, their shear capacity starts to reduce due to the interaction of forces. Consequently, rocking of the wall transforms to a combination of rocking and sliding, when in most cases leads X-Lam walls to reach their ultimate limit state [13]. After the ultimate displacement, defined as the displacement at 80% of the peak force in the descending part of the backbone curve [10], has been attained X-Lam panels continue to deform with increasing percentage of sliding deformation, until the panel reaches complete failure in shear direction.

Understanding the behaviour of X-Lam panels at ultimate state is important to assess whether there is any risk of losing global stability of X-Lam buildings in cases of seismic events stronger than the ones that the building was designed for. Theoretically, if only hold-downs were taken into account for resisting the uplifting forces caused by overturning moments, there would not be anything else to prevent the wall panel from overturning after the failure of the hold-downs, which is considered as an undesirable failure mechanism. In the reality, the rotations of X-Lam panels, even the ones with predominant rocking behaviour, due to horizontal loads, are too small to cause any threat of global overturning. Even more, when the panel starts to fail due to exceeded overturning moment, the resistance of the panel in shear direction also decreases, leading to a failure mechanism for combined rocking and sliding of the panel. Thus, even after major seismic events, there is no risk of global instability of X-Lam wall systems.

In addition, the self-weight of the panel with its center of gravity far away from the rotation point, and the additional gravity loads transmitted by the wall and floor panels above, enable the re-centering of the panel back to the initial position after the seismic event. The only residual deformation would be horizontal (shear) displacement, which does not pose any threat for global instability nor for human life. Furthermore, residual horizontal displacements due to sliding in predominant rocking behaviour are only a relatively small percentage of the total inter-story drift [13] due to the design seismic actions. That basically means that even for high level of damages in the connectors, which have dissipated energy during an earthquake, the X-Lam building can snap back to the initial position. The only residual damage will be localized in the nailed connections between the steel brackets/hold-downs and the X-Lam panel, where some timber crushing at the X-Lam panel-fastener connection will occur together with the plasticization of some fasteners. However, there will be little or no permanent deformation of the building, as the full-scale shaking table tests have clearly demonstrated [6,7]. This can significantly reduce financial costs and time needed for the repair of X-Lam buildings after major seismic events.

Thus, design of the X-Lam wall systems as lateral load resisting system should be done in such a way that their predominant deformation mechanism will be rocking. To achieve that, capacity design principles at the wall level are required.

3.2 X-Lam wall panels interaction during cyclic loading

Theoretically, there are three possible scenarios of the behaviour of adjacent X-Lam wall panels subjected to cyclic lateral loads: (i) coupled wall behaviour, where the panels behave as independent, individual panels; (ii) combined single-coupled wall behaviour, where the panels behave as partly fixed with semi-rigid screw connection; (iii) single wall behaviour, where the panels behave as a single wall panel with rigid screw connection.

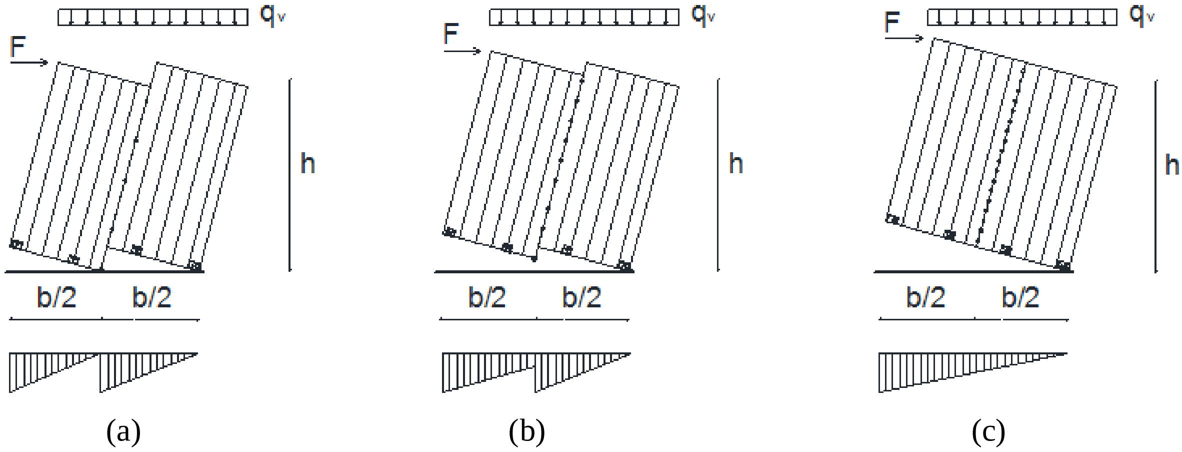

Fig. 3 Types of behaviour of adjacent wall panels: (a) coupled wall behaviour; (b) combined single-coupled wall behaviour; (c) single wall behaviour

In the first case, the vertical joint between wall panels is relatively weak in comparison with the anchoring connections, thus providing low level of shear stiffness between individual wall panels. While being loaded with lateral forces, connected panels behave as individual panels, rocking around each individual lower corner (Figure 3a). Conversely, if the vertical connection between coupled wall panels is very stiff, the behaviour of coupled walls is the same as the behaviour of a single wall panel, as shown in Figure 3c. In this case, the vertical connection has higher resistance than the shear forces between wall panels, and is very stiff. The third possibility is an intermediate, combined behaviour between individual wall behaviour and fully connected walls behaviour. As vertical connections between coupled wall panels are semi-rigid, slight deformations (slip) of the vertical connection can take place (Figure 3b).

Different types of global panel behaviour resulted in different mechanical properties and energy dissipation capacities. X-Lam wall panels with single wall panel behaviour performed better than walls with coupled wall behaviour in terms of total dissipated energy until a certain level of interstory drift, and had higher strength and stiffness capacity. On the other hand, panels with coupled wall behaviour exhibited lower elastic stiffness but attained larger ultimate displacements, which are also very important in earthquake design. Hence, the type of behaviour of wall subassemblies should be always decided a priori and then implemented into a proper design of the vertical joints.

Thus, special attention in coupled walls design should be given to the vertical connection between adjacent panels. Over-sizing the vertical connection may result in a completely different behaviour of the coupled wall panels.

4 Capacity based design

Capacity based design aims to ensure that ductile modes of failure precede brittle modes of failure with sufficient reliability. In addition, the formation of a soft story mechanism must be avoided, and certain parts of the structure will have to remain elastic during an earthquake if it is so chosen in design. The structure should have an adequate capacity to deform beyond its elastic limit without substantial reduction in the overall resistance against horizontal and vertical loads. Global instabilities must also be prevented before the development of a full plastic failure mechanism of the structure. With proper detailing and design, almost all damage during an earthquake can be concentrated in specific parts of the building designed for this aim, thus reducing financial costs associated with the downtime and repair of the buildings after major seismic events.

This result can be achieved when the lateral load resisting system has an effective load path for seismic forces. With clever use of different types of metal connectors and their layout, type and number of fasteners, and geometry of wall panels it is possible to control the seismic behavior of X-Lam building and ensure the objectives of the design stated above. By knowing the mechanical properties of each single connector, fastener, wooden panel and their interaction, the designer can decide how the building will perform in terms of stiffness, strength, energy dissipation and ductility. Through proper dimensioning and detailing of the structural elements it is possible to achieve an overall ductile behavior of X-Lam buildings.

Thus, capacity based design should be applied, in order to ensure that plasticization of dissipative elements, and therefore energy dissipation during a seismic event, is not prevented by anticipated brittle failures. Brittle members in timber structures must be designed for the overstrength of the ductile connections to ensure the ductile failure mechanism will take place before the failure of the brittle members with sufficient reliability. It should also be ensured that the actual plastic capacity of ductile elements does not exceed the design plastic capacity, otherwise the dissipative zones will resist forces larger than designed, thus redistributing deformations and damages somewhere else in the structure.

To design structures with ductile behaviour, the hierarchy of strengths of the various structural components must be ensured. In X-Lam building systems, capacity based design should be applied at different levels: (i) connectors (angle brackets, hold-downs, vertical screwed connections between adjacent panels); (ii) wall systems; and (iii) the entire building. In the following sections, capacity design principles for X-Lam construction system will be presented and possible implementations into Eurocode 8 [17] will be discussed.

4.1 Connector level

Capacity based design provisions at the connector level in X-Lam buildings aim to ensure ductile failure mechanism of simple fasteners (nails, screws) in hold-downs, angle brackets and vertical screwed joints in coupled walls. Undesired brittle failures should be avoided to ensure ductile response of connections and, therefore, ductile behaviour of the wall systems and of the entire building. The basic principle of the capacity based design at the connection level is that nail plasticization should be always ensured, whereas the steel parts of the connector should be overdesigned to prevent any plasticization. In this way all energy dissipation is concentrated in the nailed X-Lam wall panel-metal bracket/hold-down connections, and even more, the same metal connector can be reused after undergoing a major seismic event. A plasticization of the steel connector would have significant disadvantages: (i) the ductility of the connector metal part is in general lower than the ductility of the nailed steel-timber connection; (ii) failure of an hold-down or angle-bracket in its metal part is likely to cause significant increases in stresses in the other connectors, leading to a potential failure for loss of equilibrium; and (iii) the development of plastic strains in the metal part of the connector is likely to prevent the re-centring of the X-Lam structure, which is an important feature to reduce downtime and repair costs.

Thus, according to the EC5 [18], (b), (d) or (e) yielding modes of failure of fasteners in steel-timber connection, corresponding to either one or two plastic hinge formations, have to be ensured with a proper design and detailing [19] (Figure 4a). Similar provisions also apply to timber-timber connection (failure modes (d), (e) and (f) according to EC5), as shown in Figure 4b.

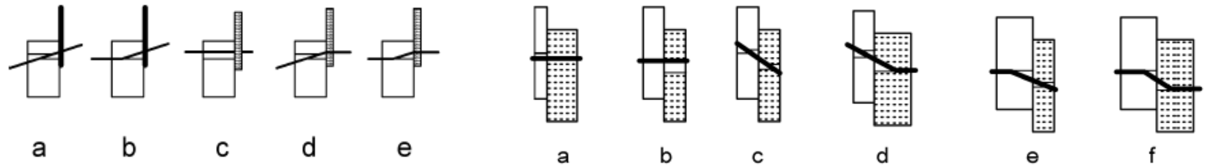

(a) (b)

Fig. 4 (a) Failure modes for steel-to-timber connections according to the EC5; (b) Failure modes for timber-to-timber connections according to the EC5 [18]

To ensure that the desired ductile failure mode of the fastener will always precede the undesired brittle failure modes characterized by no plastic hinge formation, the following design condition should be satisfied:

$$F_{Rd,ductie}\gamma_{Rd} \leq F_{Rd,brittle} \qquad (2)$$

where $F_{Rd,ductile}$ represents the connection design resistance associated with the ductile failure mode, and $F_{Rd,brittle}$ signifies the connection design resistance related to the brittle failure mode. As an example, for a steel-timber connection, $F_{Rd,ductile}$ is the lowest design shear resistance associated with the ductile failure modes (modes (b), (d) and (e) in Figure 4a), whilst $F_{Rd,brittle}$ is the lowest design resistance associated with the brittle failure modes (modes (a) and (c) in Figure 4a) according to EC5. The coefficient γ_{Rd} can be regarded as the overstrength factor of the ductile failure modes, and accounts for the scatter of the experimental results. The first proposal for this coefficient is 1.3 for nailed steel-timber connections, and 1.6 for screwed timber-timber connections. The latter value is higher due to larger scatter of the experimental results [1,2].

Each metal connector (hold-down, angle bracket) shall be properly anchored to the foundation or to the floor panel underneath, and this anchoring detail shall be designed for the overstrength of the other ductile connection. Also the steel part of the connector shall be overdesigned in comparison with the strength capacity of the ductile connection with the X-Lam panel to avoid brittle failure of the steel part. For example, the net section of the hold-down in the uplift direction has to be stronger than the nailed connection by the overstrength factor γ_{Rd}. Brittle failure modes such as shear plug, splitting of timber, tension of wood, and tear out [21] must also be avoided. Equations (3) and (4) present capacity based design provision for X-Lam metal connectors in shear direction (x) and uplift direction (y):

$$F_{Rd,x} = n_{nail} F_{Rd,nail,x} \gamma_{Rd} \leq \begin{cases} F_{Rd,steel,net} & \text{Design shear resistance of net steel part of connector} \\ F^{*}_{Rd,bolt,s} & \text{Design shear resistance of bolt} \\ F^{*}_{Rd,steel,oval} & \text{Design resistance of connector due to ovalization of the bolt hole} \\ F^{**}_{Rd,fast,s} & \text{Design shear resistance of fasteners in the lower part of the connector} \\ F_{Rd,wood} & \text{Design shear resistance of wood due to brittle failure modes} \end{cases} \tag{3}$$

$$F_{Rd,y} = n_{nail} F_{Rd,nail,y} \gamma_{Rd} \leq \begin{cases} F_{Rd,steel,bend} & \text{Design bending resistance of connector} \\ F_{Rd,steel,net} & \text{Design tensile resistance of net steel part of connector} \\ F^{*}_{Rd,bolt,pull} & \text{Design pull-through resistance of bolt} \\ F^{*}_{Rd,bolt,t} & \text{Design tension resistance of bolt} \\ F^{**}_{Rd,fast,w} & \text{Design withdrawal resistance of fasteners in the lower part of connector} \\ F_{Rd,wood} & \text{Design shear resistance of wood due to brittle failure modes} \end{cases} \tag{4}$$

where: $F_{Rd,wood}$ is a minimum design resistance due to brittle failure of the wooden panel (shear plug, splitting, tension failure, group tear out); $F_{Rd,x}$ and $F_{Rd,y}$ signify the design resistances of metal connectors in shear direction and axial direction respectively; n_{nail} is the number of nails in each metal connector; $F_{Rd,nail}$ represents the design shear resistance of one nail, and γ_{Rd} is ovestrength factor of the ductile connection [12, 19]. The terms with * applies only to wall-foundation connections, whilst the terms with ** applies only to wall-floor connections. For wood-wood screwed connections in vertical joints between adjacent wall panels, the following equation applies:

$$n_{sc} F_{Rd,s} \gamma_{Rd} \leq F_{Rd,wood} \tag{5}$$

where n_{sc} is number of screws, $F_{Rd,s}$ signifies the design shear resistance of one screw in the vertical joint, and $F_{Rd,wood}$ denotes the design resistance of the timber panel due to splitting.

4.1.1 Overstrength factors

Brittle members in timber structures must be designed for the overstrength related to the strength of the ductile connections to ensure the ductile failure mechanism will take place before the failure of the brittle members. The ovestrength ratio γ_{Rd} is defined as the ratio between the 95th percentile of the connection strength distribution and the design connection strength F_d [12]. Based on the statistical analysis of the 6 cyclic tests performed on each connection configuration [1,2,4] the design strength capacity F_d was calculated by dividing the characteristic experimental strength $F_{0.05}$ by the strength partial factor γ_M, assumed equal to one according to the Eurocode 8 [17] for dissipative timber structures.

The overstrength factor values for hold-downs in tension range from 1.2 to 1.3. For angle brackets in shear direction the overstrength factors range from 1.1 to 1.3. This results are consistent with the values of 1.26 in shear and 1.18 in axial direction proposed by Fragiacomo et al. [12] for angle bracket BMF105 with ten 60 mm nails, and Flatscher & Schickhofer [11], where the overstrength values for angle brackets were found to be below the value of 1.3 for both directions, shear and uplift. In comparison with hold-downs and angle brackets, test results of strength capacity in shear parallel to the joint line of in-plane screwed joints were more scattered, which resulted in higher coefficients of variation (8-13%) and consequently in higher values of the overstrength factor, suggesting a conservative value 1.6.

The overstrength ratio values should be implemented in the new generation of the Section 8 (Timber structures) of Eurocode 8 [17] as currently there is no value suggested for timber structures, although the need for capacity based design is clearly stated. A conservative proposal would be to use an overstrength factor of 1.3 for angle brackets and hold-downs in shear and axial direction, whilst a value of 1.6 could be recommended for screwed connections between X-Lam panels. It should be also pointed out that these values of the overstrength factors should be used only for connections that were experimentally tested and for which the characteristic value of the strength is provided by the producers. For connections that were not experimentally tested, higher values of the overstrength factors shall be used to allow for the difference between the predictions using the analytical formulas of the EC5 [18], and the actual experimental values.

4.2 Wall system level

In Section 3 of this paper different types of X-Lam walls behaviour types were presented and discussed. The design of the connections used in X-Lam wall systems dictates the wall behaviour and their seismic performance. Therefore, capacity design rules at the wall system level should be applied in order to ensure the desired behaviour of X-Lam walls as a lateral load resisting system.

The lateral design resistance of a X-Lam wall panel (F_{Rd}) is the minimum value of design resistance due to horizontal forces ($F_{Rd,H}$) and design resistance due to the overturning moment ($F_{Rd,M}$):

$$F_{Rd} = \min(F_{Rd,M}, F_{Rd,H}) \tag{6}$$

A suggestion is given that at the wall level, plasticization should preferably occur in the hold-downs and angle brackets loaded in tension, whereas the angle bracket should ideally remain elastic in shear so that there is no residual slip in the wall at the end of the seismic event. The gravity load applied on the walls act as a stabilizing load and can re-centre the structure at the end of a seismic event. The sum of the design values of the shear resistance of angle brackets should be larger than γ_{Rd} =1.3 times the design values of the uplift resistance of hold-downs and angle brackets (triangular distribution of forces, see Figure 2b):

$$F_{Rd,M}\gamma_{Rd} \leq F_{Rd,H} \tag{7}$$

A practical design rule is that all brackets in each individual wall panel should be placed symmetrically with respect to both panel edges. This provides symmetrical wall behaviour in both directions, which is needed as horizontal earthquake and wind loads alternate their direction.

In the design of coupled walls (Figure 3a) care must be taken to ensure the design shear capacity of the vertical screwed connection is significantly lower than the shear demand in the case of an only one single panel without any vertical connection or, two panels with rigid vertical connection (Figure 3c) divided by the overstrength factor (γ_{Rd} = 1.6) of the screwed connection. This is to ensure the flexibility of the vertical joint and enable the “coupled wall behaviour” kinematic mechanism (Figure 3a). If adjacent wall panels designed for the “single wall behaviour” (Figure 3c), the vertical screwed connection should be fully rigid and its design resistance should be greater than or equal to the shear force demand between the two panels.

Walls with large openings should be designed in such a way that possible brittle failures due to concentration of forces in the corners of the wall openings are avoided. Therefore, the resistance of the panel ($F_{Rd,wood}$) should be γ_{Rd} = 1.3 times higher than the wall resistance due to the overturning moment ($F_{Rd,M}$):

$$F_{Rd,M}\gamma_{Rd} \leq F_{Rd,wood} \tag{8}$$

4.3 Building level

As discussed before, X-Lam wall systems act as a lateral load resisting system in X-Lam buildings, which exhibit a typical box-type behaviour. For efficient transfer of horizontal forces induced by seismic event or wind to the foundations, the load path has to be properly chosen. For uniform distribution of lateral forces from the slabs of the building to the walls below, the floor panels should act as non-dissipative rigid diaphragms.

Similarly, floor panel-wall panel connections should be over-designed, as no deformation or energy dissipation should be allowed there for an efficient transmission of forces from floor panels to lateral load resisting walls underneath. In the case of perpendicular wall-wall connections, over-design factor should be applied as well (allowing corner walls to resist large forces), as perpendicular walls can also contribute to resist lateral forces in the opposite direction of loading (box effect). In all aforementioned cases, an overstrenght factor γ_{Rd} = 1.3 shall be chosen (see Section 4.1.1).

Therefore, the dissipative zones in X-Lam buildings are located in:

- metal connectors, which anchor wall panels to foundations (ground level of the building) and wall panels to floor panels underneath (upper levels of the building);
- vertical joints between adjacent wall panels

Each floor should be designed for the corresponding seismic force so that the plasticization of the dissipative zones at different levels can occur simultaneously. Thus, the upper stories should be designed for lower seismic forces, according to the seismic demand [20].

5 Conclusions

In this paper, a new capacity design approach for designing X-Lam structures was presented. Based on the results of an extended experimental test program on typical X-Lam connections, X-Lam wall panels and full-scale X-Lam buildings, analytical and numerical studies were performed and behaviour properties of X-Lam structures subjected to horizontal loads were determined. Different classifications of the global behaviour of X-Lam wall systems were introduced. Typical failure mechanisms of connections and wall systems used in X-Lam system were presented and provisions for a proper X-Lam seismic design were given. Also, the influences of different types of X-Lam walls behaviour on mechanical properties and energy dissipation of the X-Lam wall systems were introduced and critically discussed. The axial stiffness and resistance of angle brackets are important and should not be neglected in the equilibrium of the wall under lateral forces. Rocking behaviour of wall systems should precede sliding behaviour to achieve higher ductility, energy dissipation capacity and easier repair after seismic events. Special attention should be given to the design of vertical joints between adjacent wall panels, as the global behaviour of wall panels can change dramatically and, consequently, the wall performance in terms of mechanical properties, energy dissipation capacity and displacement capacity can significantly differ.

Overstrength values and capacity design principles were investigated and proposed. For metal connectors an overstrength factor 1.3 proved to be sufficient for both directions (tension and shear). For screwed connections, the scatter of strength was higher, thus also the overstrength factors resulted in higher values (1.6).

Both, overstrength factors and capacity-based design principles, could be implemented in the new generation of the Section 8 (Timber structures) of Eurocode 8 as currently there is no value suggested for the overstrength factors for timber structures, although the need for capacity based design is clearly stated.

6 References

[1] Gavric I., Ceccotti A., Fragiacomo M. Experimental cyclic tests on cross-laminated timber panels and typical connections. Proceedings of the 14th ANIDIS Conference, Bari (Italy), September 2011.

[2] Gavric I., Fragiacomo M, Ceccotti A. Strength and deformation characteristics of typical X-Lam connections. Proceedings of the 12th World conference on timber engineering, Auckland (New Zealand), July 2012.

[3] Ceccotti A., Lauriola M., Pinna M., Sandhaas C. SOFIE project - cyclic tests on cross-laminated wooden panels. Proceedings of the 9th World conference on timber engineering, Portland, Oregon (USA), August 2006.

[4] Gavric I. Seismic behaviour of cross-laminated timber buildings. Ph.D. Thesis, University of Trieste (Italy), 2013. http://hdl.handle.net/10077/8638.

[5] Lauriola M.P., Sandhaas C. Quasi-static and pseudo-dynamic tests on XLAM walls and buildings. Cost E29 International Workshop on Earthquake Engineering on Timber Structures, pages 119-133, Coimbra (Portugal), 2006.

[6] Ceccotti A. New technologies for construction of medium-rise buildings in seismic regions: The XLAM case. Journal of the International Association for Bridge and Structural Engineering, 2-2008, 156-165.

[7] Ceccotti A., Sandhaas C., Okabe M., Yasumura M., Minowa C., Kawai N. SOFIE project – 3D shaking table test on a seven-storey full-scale cross-laminated building. Earthquake Engineering & Structural Dynamics, 2013. Published online: DOI: 10.1002/eqe.2309.

[8] Rinaldin G., Amadio C., and Fragiacomo M. A Component approach for the hysteretic behaviour of connections in cross-laminated wooden structures. Earthquake Engineering & Structural Dynamics, 2013. Published online: DOI: 10.1002/eqe.2310.

[9] Gavric I., Rinaldin G., Fragiacomo M., Ceccotti A., Amadio C. Experimental-numerical analyses of the seismic behavior of cross-laminated wall systems. Proceedings of the 15th World Conference on Earthquake Engineering, Lisboa (Portugal), September 2012.

[10] EN12512 (2001). Timber structures – Test methods – Cyclic testing of joints made with mechanical fasteners. CEN, Brussels, Belgium, 2001.

[11] Flatscher G., Schickhofer G. Verbindungstechnik in BSP bei monotone und zyklischer Beanspruchung – Statusbericht TU Graz. 9. Grazer Holzbau-Fachtagung, Graz (Austria), September 2011.

[12] Fragiacomo M., Dujic B., Sustersic I. Elastic and ductile design of multi-storey crosslam massive wooden buildings under seismic actions, Engineering structures, 2011, 33(11):3043-3053.

[13] Gavric I., Fragiacomo M., Popovski M., Ceccotti A. Behaviour of cross-laminated timber panels under cyclic loads. RILEM Conference: Materials and Joints in Timber Structures – Recent Advancement of Technology, Stuttgart (Germany), October 2013, accepted.

[14] Popovski M., Schneider J., Schweinsteiger M. Lateral load resistance of cross-laminated wood panels. Proceedings of the 11th World conference on timber engineering, Riva del Garda (Italy), June 2010.

[15] Popovski M. Personal communication, May 2013.

[16] ETA-07/0055. European technical approval. European organisation for technical approvals, Charlottenlund, Denmark, 2009.

[17] European Committee for Standardization (CEN), Eurocode 8 – Design of structures for earthquake resistance, Part 1: General rules, seismic actions and rules for buildings, Brussels, Belgium, 2004.

[18] European Committee for Standardization (CEN), Eurocode 5 – Design of timber structures – Part 1-1: General rules and rules for buildings, Brussels, Belgium, 2004.

[19] Fragiacomo M. Seismic behaviour of cross-laminated timber buildings: numerical modelling and design provisions. Proceedings of the COST Action FP1004 Conference, Graz (Austria), May 2013.

[20] Follesa M., Fragiacomo M., and Lauriola M.P. A proposal for revision of the current timber part (Section 8) of Eurocode 8 Part 1. Proceedings of the 44th CIB-W18 Meeting, Paper 44-15-1, Alghero (Italy), August 2011.

[21] Quenneville, J.H.P., and Mohammad, M. On the failure modes and strength of steel-wood-steel bolted timber connections loaded parallel-to-grain. Canadian Journal of Civil Engineering, 2000, Vol. 27, pp. 761-773.

**INTERNATIONAL COUNCIL FOR RESEARCH AND INNOVATION
IN BUILDING AND CONSTRUCTION**

WORKING COMMISSION W18 - TIMBER STRUCTURES

AN APPROACH TO DERIVE SYSTEM SEISMIC FORCE MODIFICATION FACTOR FOR BUILDINGS CONTAINING DIFFERENT LLRS'S

Z Chen
Ying-Hei Chui
University of New Brunswick

Chun Ni
M Mohammad
FPInnovations

G Doudak
University of Ottawa

CANADA

Keywords: multi-storey buildings; hybrid structures; lateral load resisting elements; seismic response; finite element method; seismic force modification factor

---

Presented by Z Chen

F Lam commented that he was confused by the presentation and asked for clarification of the spring analogy used in the analysis. Z Chen stated that a spring represented hybrid walls which were assumed to undergo the same lateral movements due to rigid diaphragm assumptions. F Lam questioned the generality of the assumption.

A Ceccotti asked for clarification and 3D sketches of the Vancouver buildings studied. They were not available as they were not real buildings but design of buildings that could be used in Vancouver.

C Moroder commented that for frame and wall large forces could be present in diaphragm therefore modeling of the deformability of the diaphragm would be important.

An Approach to Derive System Seismic Force Modification Factor for Buildings Containing Different LLRS's

Zhiyong Chen
University of New Brunswick, Canada
Chun Ni
FPInnovations, Canada
Ying-Hei Chui
University of New Brunswick, Canada
Ghasan Doudak
University of Ottawa, Canada
Mohammad Mohammad
FPInnovations, Canada

1 Introduction

In seismic design of buildings, a common approach is to specify force modification factors to reflect the energy absorption and ductility characteristics of the lateral load resisting system (LLRS) of the building. For instance, Eurocode 8 (CEN 2013) uses the '*q*' factor while the National Building Code of Canada (NBCC) (NRC 2010) specifies two factors, a ductility-related (R_d) and an over-strength related force modification factor (R_o).

In the NBCC, values for R_o and R_d factors are provided according to structural types for each LLRS (NRC 2010). For a hybrid structure consisting of more than one type of LLRS, NBCC specifies that the lowest R_dR_o value of all the LLRS's is used. Although the over-strength related force modification factor R_o factor can be expressed explicitly (NRC 2010), all the parameters in the equation were derived statistically. In addition, the variation of R_o factors between different LLRS's is small with the maximum difference of 0.7 compared with that of R_d factors with the maximum difference of 4.0. As a result it is proposed that the lowest value for R_o factor among the LLRS's for the hybrid building system is used. As for the R_d factor NBCC does allow for the use of a more liberal seismic force modification factor if it can be supported by an appropriate analysis. A suitable analysis is to conduct non-linear time history analysis of a building designed with different R_d values (Lee and Foutch 2006; Pei et al. 2012). This process is time consuming and the results are specific to the particular building under investigation.

Hence, a balanced approach that is more user friendly, while less conservative than the method proposed in NBCC for estimating R_d factor for hybrid structures is desirable. The purpose of this paper is to present a method of estimating an overall seismic modification force factor for multi-storey hybrid buildings consisting of different types of LLRS based on the relevant mechanical characteristics of the individual LLRS's, such as ductility, stiffness and strength.

2 Derivation of Method for Estimating R_d of Hybrid Building Systems

Newmark and Hall (1982) derived a relationship between the ductility ratio, μ, and the ductility-related force modification factor, R_d, according to the period (T) of a structure, Eq. (1).

T > 0.5 s $$R_d = \mu \tag{1a}$$

0.1 < T < 0.4 s $$R_d = \sqrt{2\mu - 1} \tag{1b}$$

T < 0.03 s $$R_d = 1 \tag{1c}$$

where μ is the measured ductility expressed as the ratio of the displacement at failure to that at yield, determined using the Equivalent Energy Elastic-Plastic (EEEP) approach (ASTM 2005). In NBCC (NRC 2010), the same R_d factor is assigned to the buildings containing the same type of LLRS for any natural periods. As the building period will likely be greater than 0.03s, the Eq. (1b) is used for estimating R_d in this study. Though a more conservative R_d would be obtained for building period greater than 0.5s, this approach is consistent with the approach in NBCC.

From a structural mechanics perspective, the system R_d factor can be interpreted as a function of $R_{d,i}$ factors, the relative strength and stiffness of the individual LLRS's. Therefore an initial attempt was made to develop a model that expresses the system R_d factor in terms of these properties.

2.1 A macro model of lateral load resisting element (LLRE)

To conduct the finite element analysis (FEA) in this study, a suitable model for the LLRE is needed. For wood shear wall, the pinched, strength and stiffness degrading hysteretic load-deformation response can be characterized using a numerical model presented by Xu and Dolan (2009). The model (Fig. 1a) is composed of three boundary framing members and two diagonal hysteretic springs. The predictive capability of the macro element model has been demonstrated by comparing its predictions with the results of shake table tests performed on a two-storey single-family house (Xu and Dolan 2009). This validation has provided confidence that the developed macro model can be used to reasonably predict system response. This is considered adequate for the purpose of this paper, which is intended to present a potential method of evaluating the ductility-related force modification factor for a hybrid building system.

The macro element model was employed here with some further modifications to make the load-transferring path simple as well as to reduce the computation time. It was simplified into a model including three boundary framing members and one diagonal modified hysteretic spring, as shown in Fig. 1b. Eqs. (3) and (4) of Xu and Dolan (2009) were changed to Eqs. (2) and (3), correspondingly.

$$K'(t) = \frac{K(t)}{|\cos(\theta)|} \tag{2}$$

$$r'(t) = \frac{r(t)}{|\cos(\theta)|} \tag{3}$$

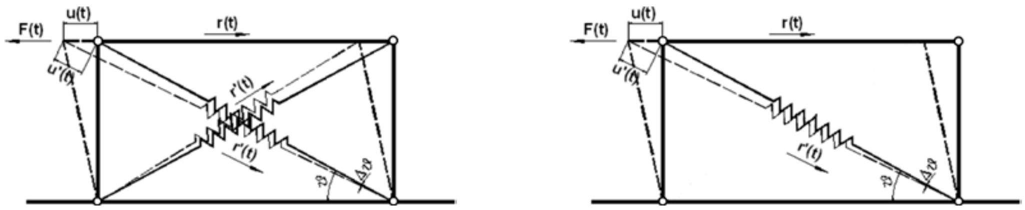

(a) Two-spring model (b) One-spring model

Fig. 1. Macro models for LLRE

2.2 Numerical Models (2-D)

Two types of hybrid building systems with various combinations of two LLRS's were modelled and analysed using the finite element software, ABAQUS (2011), under a concentrated cyclic load, *P*, as shown in Fig. 2. One type was a 1-storey building with five LLRE's aligned horizontally and the other one was a 5-storey building represented by five LLRE's aligned vertically.

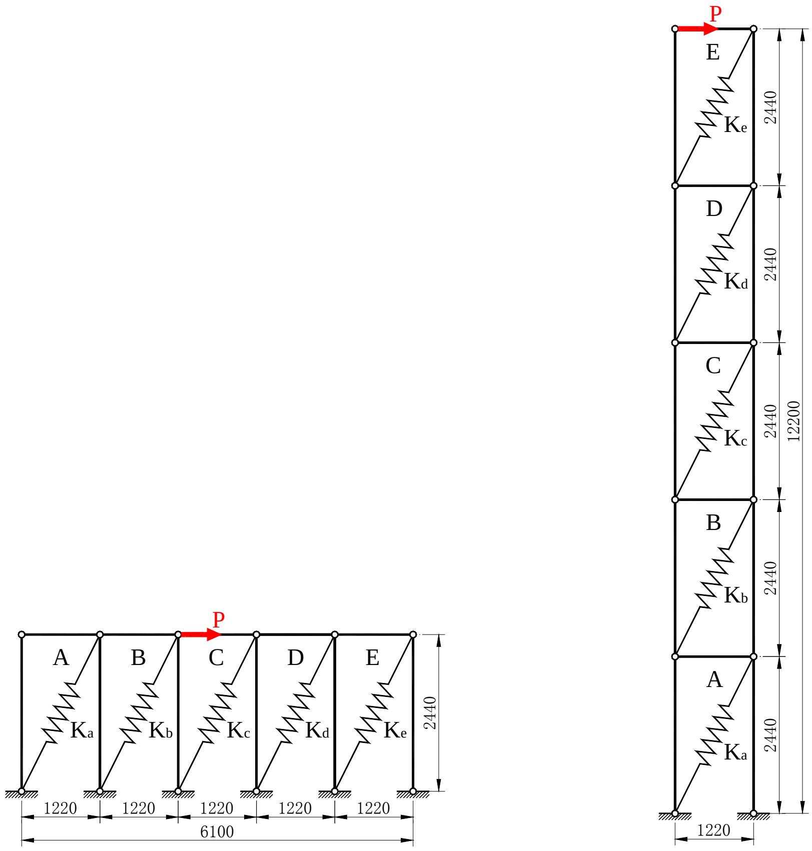

(a) 1-storey (b) 5-storey

Fig. 2. Hybrid building models

Two types of LLRE's were considered in this study. One was a low strength (LS) element, the properties of which were represented by the traditional wood shear wall (Rainer and

Karacabeyli 2000). The other is a high strength (HS) element, with its properties represented by those of a wood portal frame (Simpson Strong-Tie 2009). As given in Table 1, 20 (1-storey) and 32 (5-storey) combination cases of LS and HS elements were analysed to investigate the effect of strength ratio, α, of HS element relative to the total strength of LLRS and the location of HS element on the system R_d factor. Additionally, three types of HS element with varying ductility properties were employed to investigate their influences on the system R_d factor.

Table 1. Design matrix of hybrid building with varying ratio between LS and HS elements

α'	0.0			0.2						0.4										0.6								0.8			1.0
Case No. (1-storey)	1	2	3	4			5	6	7	8	9	10					11	12	13	14	15	16					17	18	19			20
Case No. (5-storey)	1	2	3	4	5	6	7	8	9	10	11	12	13	14	15	16	17	18	19	20	21	22	23	24	25	26	27	28	29	30	31	32
A	LS	LS	LS	LS	LS	HS	LS	LS	LS	LS	HS	LS	LS	HS	HS	HS	LS	LS	LS	HS	HS	HS	HS	LS	HS	HS	LS	HS	HS	HS	HS	HS
B	LS	LS	LS	LS	HS	LS	LS	LS	LS	HS	LS	HS	HS	HS	LS	LS	LS	HS	HS	LS	LS	LS	HS	HS	HS	HS	HS	LS	HS	HS	HS	HS
C	LS	LS	LS	HS	LS	LS	LS	HS	HS	LS	LS	LS	HS	LS	LS	HS	HS	HS	LS	LS	HS	HS	HS	HS	LS	LS	HS	HS	LS	HS	HS	HS
D	LS	LS	HS	LS	LS	LS	HS	HS	LS	LS	LS	HS	LS	LS	HS	LS	HS	HS	HS	HS	HS	LS	LS	LS	LS	HS	HS	HS	HS	HS	LS	HS
E	LS	HS	LS	LS	LS	LS	HS	LS	HS	HS	HS	LS	LS	LS	LS	LS	HS	LS	HS	HS	LS	HS	LS	HS	HS	LS	HS	HS	HS	LS	HS	HS

Note: α' - the nominal strength ratio between HS element and total LLRE's in either horizontal or vertical direction, was simply the ratio of number of HS element over 5; A to E represents the location of the five LLRE's, as shown in Fig. 2.

This system-level modelling approach simulated the three-dimensional response of 1- and 5-storey hybrid buildings through a degenerated two-dimensional planar analysis, as shown in Fig. 2. Both LS (shear wall) and HS (portal frame) elements were simulated by the modified macro model of LLRE within the ABAQUS finite element software (ABAQUS 2011). This macro model (Fig. 1b) is composed of three truss elements (T3D2) with large sectional properties to represent member rigidity, and a user element (UEL) of the hysteretic spring. Fig. 3 shows the hysteresis loops for the LS and HS elements used in this study. Fig. 3a shows the response of LS element which was a 1220 × 2440 mm wood shear wall evaluated by Salenikovich (2000). Fig. 3b shows the hysteresis loops of the HS element, which was the reinforced portal frame specimen PF-11 tested by Ni and Mohammad (2011) but with its strength magnified by 50% as proposed by Mamun et al. (2012). These were chosen because of the availability of the load-deformation hysteresis loop response from Salenikovich (2000) and Ni and Mohammad (2011), respectively. The corresponding strength, stiffness, ductility and R_d values are shown in the figures. Essentially, as can be observed from Fig. 3, the HS element has considerably higher strength and stiffness values but is less ductile. In order to evaluate the influence of individual element ductility on the resulting system ductility ratio, three artificial hysteresis loops of the HS elements (Fig. 4) with different stiffness, maximum resistance and R_d factor (1.5, 2.0, and 2.5) were derived by modifying the hysteresis loop of HS element.

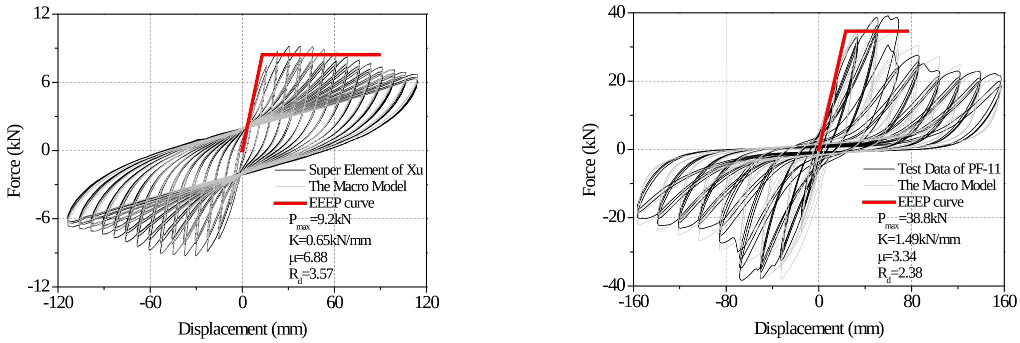

(a) LS element (wood shear wall)   (b) HS element (wood portal frame)

Fig. 3. Hysteresis loops of LS and HS LLRE's

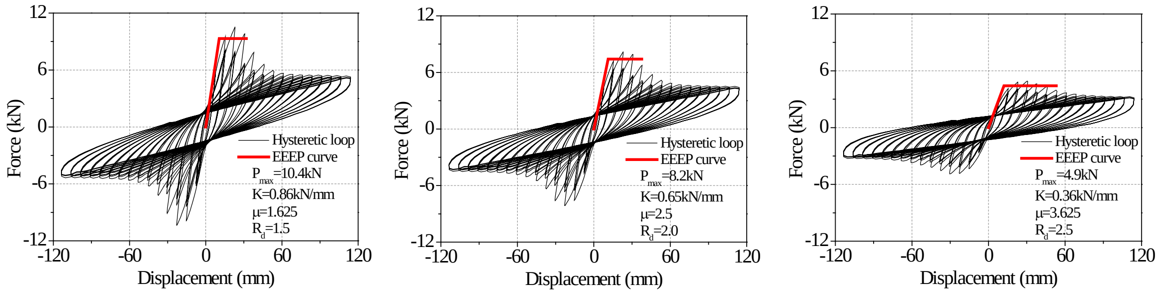

(a) HS_I (b) HS_II (c) HS_III

Fig. 4. Hysteresis loops of HS elements with different mechanical properties

Based on the structural behaviour of these building models, an approach to estimate the system R_d factor of a hybrid building incorporating two LLRS's which exhibit different ductility characteristics was proposed.

2.3 System R_d of hybrid buildings

In the non-linear static stress/displacement analysis using the automatic incrementation method (ABAQUS 2011), the hybrid buildings were subjected to a reversed cyclic load of P, as shown in Fig. 2. The system ductility ratio μ was determined using the EEEP approach (ASTM 2005), and the ductility-related force modification factor, R_d, of hybrid building was calculated from Eq. (1b), based on the average skeleton curve derived from the hysteresis loop.

It was found that the location of HS element did not affect the system R_d factor. The hybrid buildings with the same strength ratio but different locations of HS element had nearly the same R_d factors. Hence, the average R_d of hybrid buildings with the same strength ratio is presented. The ductility-related force modification factor, R_d, of 1- and 5-storey hybrid buildings with different α and $R_{d,HS}$ of HS element are shown in Fig. 5.

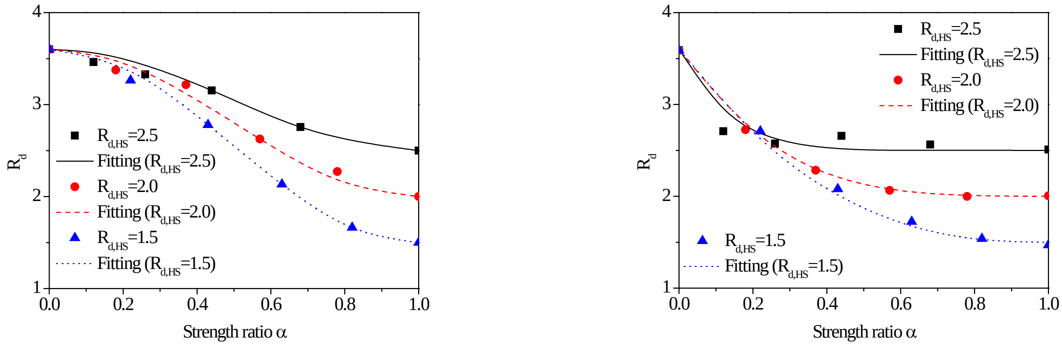

(a) 1-storey (b) 5-storey

Fig. 5. System R_d of hybrid buildings with different strength ratios

The R_d, as shown in Fig. 5, of 1- and 5-storey hybrid building decreases with increasing strength ratio of the HS element to the LLRS. By fitting the FEA results using the least square method, Eqs. (4) and (5) were obtained to estimate the system R_d of 1- and 5-storey hybrid buildings, respectively.

1-storey
$$R_d = R_{d,HS} \sin^2\left(\alpha \frac{\pi}{2}\right) + R_{d,LS} \cos^2\left(\alpha \frac{\pi}{2}\right) \tag{4}$$

5-storey
$$R_d = \left(R_{d,LS} - R_{d,HS}\right)\left(1-\alpha\right)^t + R_{d,HS} \tag{5}$$

where $R_{d,HS}$ and $R_{d,LS}$ are the ductility-related force modification factors of HS and LS elements, and the exponent t is a function of the stiffness of HS element, K_{HS}, and LS, K_{LS}, and can be calculated by Eq. (6).

$$t = -5.9\frac{K_{HS}}{K_{LS}} + 10.2 \tag{6}$$

As shown in Eqs. (4) and (5), only R_d factors of the LS and HS elements and the strength ratio of HS element affect R_d of single-storey hybrid buildings, whereas the stiffness of LLRE's also influences the R_d of multi-storey hybrid buildings. The preliminary results shown here point to the feasibility of relating the system R_d to sub-system $R_{d,i}$, the stiffness and strength ratios.

2.4 Approach to Estimate the System R_d factor of hybrid buildings

In practice, for a multi-storey hybrid building the ductility-related force modification factor, R_d, would likely vary from storey to storey. It would be more complicated to estimate the R_d of the real buildings than the situation of the 5-storey building analysed above. There are two possible methods to address this:

(a) Assuming that $R_{d,\max}$ for any storey with only the element having the larger ductility factor and $R_{d,\min}$ for storey containing different types of LLRE, where $R_{d,\min}$ is the minimum storey R_d determined from Eq. (4), the system R_d of the hybrid building can be estimated from Eq. (7);

Multi-storey $$R_d = \left(R_{d,\max} - R_{d,\min}\right)\left(1-\alpha\right)^t + R_{d,\min} \tag{7}$$

where the exponent t is a function of the stiffness of $K_{R_d,\max}$ and $K_{R_d,\min}$, which are the stiffness of the storey with the maximum and minimum R_d factor respectively, and can be calculated by Eq. (8).

$$t = -5.9\frac{K_{R_d,\min}}{K_{R_d,\max}} + 10.2 \tag{8}$$

(b) The lowest storey R_d derived from Eq. (4) is taken as the system R_d of the hybrid building. Compare to method (a), this approach is simpler but more conservative.

The validity of this assumption and the proposed approach is subject to further investigation as discussed below.

3 Validation of Proposed Approach

3.1 Structural design

In order to investigate the structural behaviour of hybrid buildings under earthquakes and to assess the proposed approach for estimating system R_d factor, four buildings (Table 2) with different layouts (Fig. 6) and number of storeys were designed. The building site was assumed to be located in Vancouver, British Columbia, which has a PGA of 0.46g (City Hall: $S_a(0.2)$=0.94, $S_a(0.5)$=0.44, $S_a(1.0)$=0.33, $S_a(2.0)$=0.17), and have a stiff soil condition (Site Class D). Six- and four-storey buildings were analysed, since six and four are the storey limits for some provincial building codes and the NBCC (NRC 2010). Two reference buildings, 4 and 6 storeys high, with only one type of LLRE of LS, plus two hybrid buildings also of 4 and 6 storeys high were included. The storey height of these buildings is 2.44m, and the dimensions of the floor and roof diaphragms are 12.2m × 12.2 m (40 ft × 40 ft), as shown in Fig. 6. The seismic weight of the floor and roof was 1.8 and 1.36 kPa, respectively.

Table 2. Structural design matrix of reference and hybrid buildings

Building	Storey	Reference case				Hybrid case			
		Nail spacing (mm)*	HS/LS☆	R_d Storey	R_d System	Nail spacing (mm)*	HS/LS☆	R_d Storey	R_d System
6-storey	6th	150	LS	3.57	3.57	150	HS & LS	3.43	3.43
	5th	150	LS	3.57		150	HS & LS	3.43	
	4th	100	LS	3.57		100	HS & LS	3.49	
	3rd	100	LS	3.57		100	HS & LS	3.49	
	2nd	75	LS	3.57		75	HS & LS	3.52	
	1st	75	LS	3.57		75	HS & LS	3.52	
4-storey	4th	150	LS	3.57	3.57	150	HS & LS	3.43	3.43
	3rd	150	LS	3.57		150	HS & LS	3.43	
	2nd	100	LS	3.57		100	HS & LS	3.49	
	1st	100	LS	3.57		100	HS & LS	3.49	

Note: * - One OSB with thickness of 12.0 mm was used in shear wall. ☆ - ‘HS’ indicates a portal frame in the corresponding storey, while ‘LS’ indicates that shear wall was used rather than the portal frame in the corresponding storey with the layout of reference.

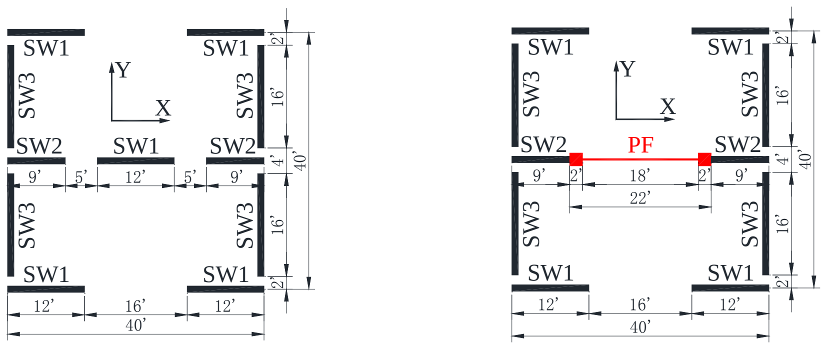

(a) Reference case

(b) Hybrid case

Fig. 6. Layouts of multi-storey buildings

Note: ‘SW’ and ‘PF’ indicate LS (shear wall) and HS (portal frame) elements, respectively.

In the reference case (Table 2), the buildings were constructed with LS element (shear wall) only, with R_d = 3.57 which was calculated using Eq. (1b). In the hybrid buildings, HS (portal frame) and LS (shear wall) elements are combined in the same system. Based on the R_d of LS (3.57) and HS (2.38) elements, shown in Fig. 3, and the strength ratio, the storey R_d factors were calculated using Eq. (4) and are given in Table 2. According to the proposed scheme, the lowest storey R_d factor was taken as the system R_d factor for the multi-storey hybrid building (Table 2).

The natural period used for designing the base shear calculation was assumed to be twice the period (Table 3) determined in accordance with Clause 4.1.8.11.(3)(c) of NBCC (NRC 2010), since the calculated periods of all buildings using the APEGBC (2009) equation were greater than twice the empirically calculated periods. The design demand for each storey of the reference and hybrid buildings was determined using the equivalent static force procedure according to NBCC. The lateral forces were distributed to each wall based on tributary area. The LS elements (Table 2) were designed based on the shear resistance design values in CSA O86 (CSA 2009). The HS element was assumed to have a shear resistance of 26.25 kN, which was determined in accordance with AC130 (ICC-ES 2009) based on test data. The maximum inter-storey drift at any storey was limited to 2.5% (1/40) of storey height in the drift check.

Table 3. Fundamental natural periods (seconds) of building models

Building	APEGBC (2009) equation	NBCC (2010) equation	Reference			Hybrid		
			RD	SD	FD	RD	SD	FD
6-Storey	1.093	0.415×2=0.830	0.935	0.949	1.348	0.969	0.985	1.420
4-Storey	0.773	0.306×2=0.612	0.703	0.722	1.175	0.723	0.743	1.236

Note: RD - Rigid diaphragm; SD - Semi-rigid diaphragm; and FD - Flexible diaphragm.

3.2 Numerical models (3-D)

Four three-dimensional finite element (FE) models were developed using ABAQUS. In these models, the diaphragm acted elastically; the LS and HS elements were connected to the diaphragm through the horizontal framing member of the modified macro model (Fig. 1b), and the slip between the lateral resistant element and diaphragm was neglected. The mass was uniformly distributed in the floor and roof diaphragms. Fig. 7 shows the 6-storey FE models of the reference and hybrid buildings.

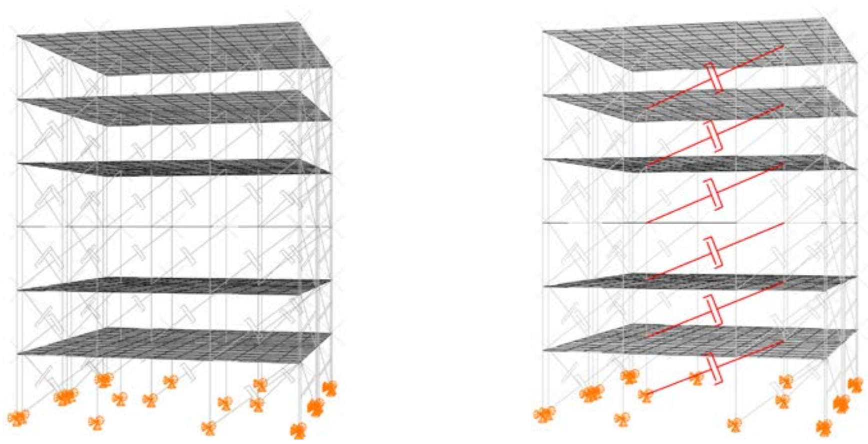

(a) Reference (b) Hybrid

Fig. 7. FE models of 6-storey LWFBs

Note: The highlighted dashpots belong to the HL elements.

Similar to the 2D FE models of hybrid buildings for investigating the system R_d factor, LS and HS elements were simulated by the macro model of LLRE respectively (Fig. 1b). The hysteresis loops of LS elements in the design buildings were obtained by scaling the load value of the hysteresis loops of the 1220 × 2440 mm shear wall (Fig. 3a) based on the ratio of shear wall design values given in CSA O86 (CSA 2009) to that of the reference shear wall. The loops given in Fig. 3b were used for the HS element. A dash pot element (DASHPOTA), as shown in Fig. 7, with a damping ratio of 1% (Xu and Dolan 2009) was placed in each LLRE to account for the elastic damping effect.

The horizontal diaphragm was modelled using the shell element (S4R) with a thickness of 235 mm. In accordance with ASCE 41-06 (ASCE, 2006), 0.001 ($10^{-3.0}$), 0.0398 ($10^{-1.4}$) and 10.0 ($10^{1.0}$) GPa were taken as the in-plane modulus of elasticity of the flexible, semi-rigid and rigid diaphragm, respectively. In total 12 FE models covering the three diaphragm flexibility cases were developed. The equivalent viscous damping ratio of the diaphragm of

8.3% tested by Fischer et al. (2001) was used. The Rayleigh damping was employed for the diaphragms of all the FE models.

3.3 Structural behaviour of hybrid buildings

3.3.1 Fundamental natural perod

The fundamental natural periods of the 12 undamped building models were obtained by conducting frequency analysis (ABAQUS, 2011) and the results are shown in Table 3. The fundamental period increases with building height and diaphragm flexibility. It agrees with the general understanding that a taller building and a building with a more flexible diaphragm, lead to a longer fundamental period. The reference and hybrid cases with the same storey number had almost identical fundamental natural period. This indicates that the replacement of LS element with HS element does not affect the dynamic characteristic of hybrid building designed with the R_d factor estimated using the proposed method.

3.3.2 Response under design earthquakes

The seismic behaviour of the 12 building models under the design hazard level was analysed with the implicit dynamic analysis method using direct integration (ABAQUS 2011). Nine "Far-Field" earthquake records in the fault normal (FN) direction (ATC 2009) were scaled at the corresponding fundamental period of each building model (Table 3) to match the spectral acceleration, S_a, of the Vancouver design spectrum, as shown in Fig. 8.

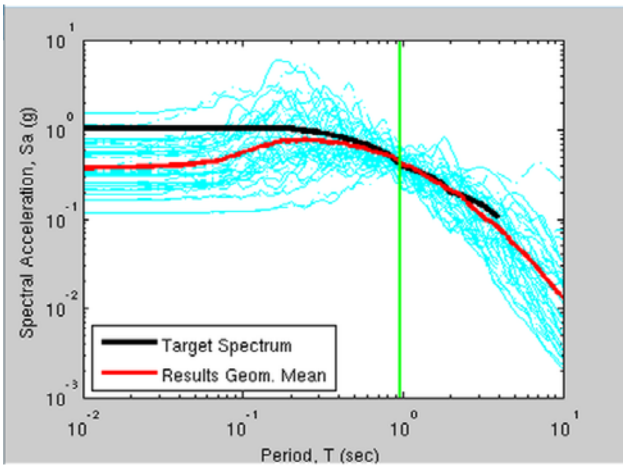

Fig. 8. Scaling earthquake records (T = 0.935 s)

In total 108 non-linear time history analyses were conducted, and the relationship between the cumulative distribution function (CDF) and the maximum drift ratio is shown in Fig. 9. All the maximum drift ratios of the 12 building models are less than the design criterion of 2.5%. It means that the design of the building models fulfilled the seismic design requirement of NBCC (NRC 2010). There was no distinguishable difference in drift ratios between reference and hybrid cases. This indicates that the seismic response of the hybrid buildings including LS and HS elements designed with the R_d estimated from the proposed approach is nearly the same as the reference building containing LS elements only. Hence, the approach for estimating the system R_d factor is appropriate.

With regards to the influence of diaphragm flexibility on the structural behaviour of hybrid buildings, from a structural perspective, larger diaphragm rigidity enhances the system

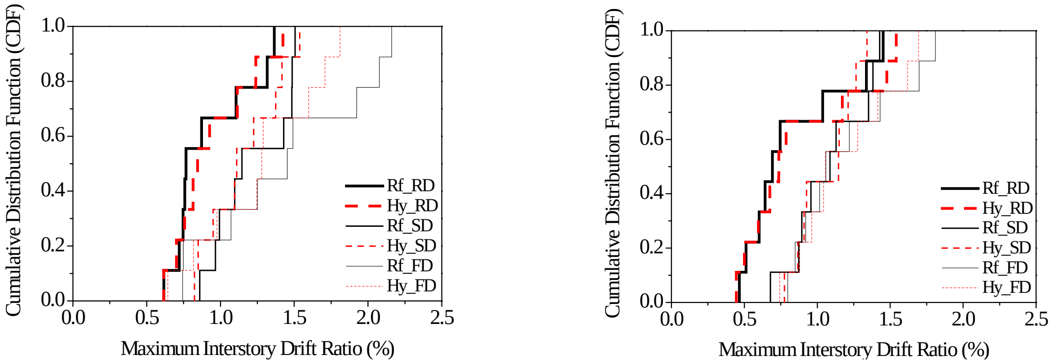

(a) 4-storey (b) 6-storey

Fig. 9. CDF's of maximum inter-storey drift ratio

Note: Rf and Hy indicate the Reference and Hybrid cases, respectively.

effect of the structure to resist lateral load, and a smaller drift can be expected. Similar responses were found in 4- and 6-storey cases.

3.3.3 Margin ratio

The margin ratio, *MR*, of inter-storey drift ratio limit, which is defined in this study as the ratio of the spectral acceleration of the ground motions, $\hat{S}_{CT}$, which induces a building to have a maximum inter-storey drift ratio of 2.5% under half of the number of "Far-Field" earthquake records, to the design ground motion, $S_a(T_o)$, with a 2% probability of exceedance in 50 years (NRC 2010), Eq.(9).

$$MR = \hat{S}_{CT} / S_a(T_o) \tag{9}$$

To derive the margin ratios of the building models with rigid diaphragm, 440 nonlinear dynamic analyses were conducted with 22 "Far-Field" earthquake records in the fault normal (FN) direction (ATC 2009). All the earthquake records were scaled at the corresponding fundamental period (T_o) of each building model to match *n* times (0.5, 1, 2, …) the S_a from the Vancouver design spectrum (Fig. 8) until the building model has a maximum inter-storey drift ratio of 2.5% under half of the 22 earthquake records. Fig. 10 shows the relationship between $S_a(T_o)$ and maximum inter-storey drift ratio, and the margin ratio, *MR*, of the four multi-storey buildings with rigid diaphragm.

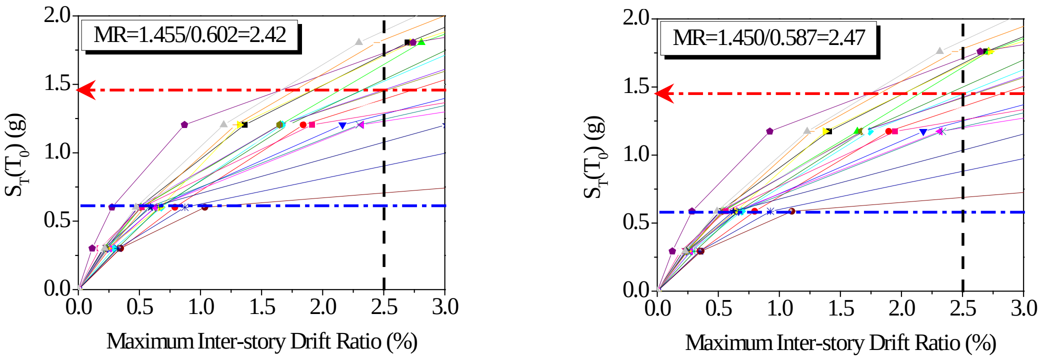

(a) 4-Storey Reference (b) 4-Storey Hybrid

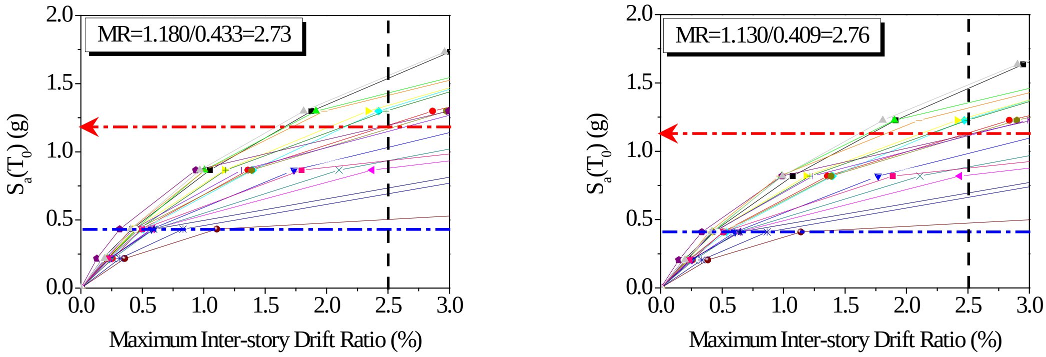

(c) 6-Storey Reference (d) 6-Storey Hybrid

Fig. 10. Margin ratios (*MRs*) of inter-storey drift ratio limit

Based on the definition of margin ratio, the more the excess load-carrying capacity the structure has, the larger the *MR* is. The margin ratios of all the building models are in the range 2.42 ~ 2.76. The *MR*s of hybrid buildings containing both LS (shear wall) and HS (portal frame) elements were nearly the same as the *MR*s of reference buildings with LS (shear wall) elements only. This indicates that the seismic performance of the hybrid building designed with the system R_d estimated from the proposed approach is similar to that of the reference building that contains one type of LLRE with a single R_d, thus providing confidence that the proposed method of estimating system force modification for hybrid building has the potential to be adopted for design use.

4 Conclusions

A method for estimating the ductility-related force modification factor, R_d, of multi-storey hybrid buildings is proposed, based on the structural performance of 1- and 5-storey hybrid buildings incorporating LS and HS elements. Empirical models relating the stiffness and strength ratios and ductility ratio of the individual LLRS are provided.

Four different mid-rise hybrid building models were designed using the proposed method and their seismic performance was evaluated using frequency analysis and non-linear time history response analysis. The frequency analyses and non-linear time history analyses were conducted using the finite element program, ABAQUS, with a macro model of the LLRE. According to the finite element analysis results: (1) the proposed method of estimating system R_d for a hybrid building leads to designs that provide comparable seismic performance of a similar building constructed with one material and designed according to current NBCC seismic design provisions. (2) Rigid diaphragms are more effective in resisting lateral load and produce smaller drift in hybrid buildings and smaller natural period than elastic diaphragms.

5 Acknowledgements

The authors greatly acknowledge the financial support provided by Natural Sciences and Engineering Research Council (NSERC) of Canada under the Strategic Research Network on Innovative Wood Products and Building Systems (NEWBuildS). Thanks are also extended to FPInnovations for providing test results of portal frames.

6 References

ABAQUS. (2011). *ABAQUS analysis user's manual (Version 6.11)*. Hibbitt, Karlsson, and Sorenson, Pawtucket, R.I.

APEGBC. (2009). *Structural, fire protection and building envelope professional engineering services for 5 and 6 storey wood frame residential building projects (mid-rise buildings)*. Professional Engineers and Geoscientists of BC (APEGBC) Technical and Practice Bulletin.

ASTM. (2005). *ASTM E2126 Standard test methods for cyclic (reversed) load test for shear resistance of framed walls for buildings*. American Society for Testing and Materials (ASTM), West Conshohocken, Pa.

ATC. (2009). *Quantification of building seismic performance factors – ATC-63/FEMA P–695 Project report.* Applied Technology Council (ATC), Redwood City, CA.

CEN. (2013). *EN 1998-1:2004/A1:2013 Eurocode 8: Design of structures for earthquake resistance – Part 1: General rules, seismic actions and rules for buildings*. European Committee for Standardization (CEN), Brussels, Belgium.

CSA. (2009). *CSA O86-09: Engineering design in wood,* Canadian Standards Association (CSA), Toronto, Canada.

ICC Evaluation Service (ICC-ES). (2009). *AC130: Acceptance criteria for prefabricated wood shear panels*. <www.icc-es.org/Criteria/pdf_files/ac130.pdf> (Apr. 20, 2012)

Lee, K., and Foutch, A. D. (2006). "Seismic evaluation of steel moment frame buildings designed using different R-values." *J. Struct. Eng.*, ASCE, 132(9): 1461-1472.

Mamun, A. A., Doudak, G., Ni, C., and Mohammad, M. (2012). "Portal frame bracing systems using fiber reinforced polymer (FRP) in light-wood frame buildings." *The 12th World Conference on Timber Engineering*, WCTE, Auckland, New Zealand, 418-423.

Newmark, N. M., and Hall, W. J. (1982). *Earthquake spectra and design*. Earthquake Engineering Research Institute, Berkeley, CA.

Ni, C. and Mohammad, M. (2011). "Evaluation of lateral load prescriptive details of small wood buildings." *Report prepared for Canadian Forest Service*, Natural Resources Canada, Ottawa, Canada.

NRC. (2010). *National building code of Canada*. Canadian Commission on Building and Fire Codes and National Research Council of Canada (NRC), Ottawa, Canada.

Pei, S., Popovski, M., and van de Lindt, J. W. (2012). "Force modification factors for cross laminated timber buildings." *Report prepared for Canadian Forest Service*, Natural Resources Canada, Ottawa, Canada.

Rainer, J. H., and Karacabeyli, E. (2000). *Ensuring good seismic performance with platform-frame wood housing, construction technology update, No. 45.* National Research Council of Canada (NRCC), Ottawa, Canada.

Salenikovich, A. J. (2000). *The racking performance of light-frame shear walls*. Ph.D. dissertation, Dept. of Wood Science and Forest Products, Virginia Polytechnic Institute and State Univ., Blacksburg, VA.

Simpson Strong-Tie. (2009). *Wood strong-wall: garage portal systems on concrete foundations.* Simpson Strong-Tie Company Inc., Pleasanton, CA.

Xu, J., and Dolan, J. D. (2009). "Development of a wood-frame shear wall model in ABAQUS." *J. Struct. Eng.*, ASCE, 135(8), 977-984.

INTERNATIONAL COUNCIL FOR RESEARCH AND INNOVATION IN BUILDING AND CONSTRUCTION

WORKING COMMISSION W18 - TIMBER STRUCTURES

CONNECTIONS AND ANCHORING FOR WALL AND SLAB ELEMENTS IN SEISMIC DESIGN

M Schick

T Vogt

W Seim

University of Kassel, Department of Structural Engineering

GERMANY

Keywords: seismic design, timber frame, overstrength, full scale testing

---

Presented by W Seim

M Fragiacomo asked which embedment strength was used in the equation. W Seim stated that experimental mean values were used. M Fragiacomo commented that using the predicted embedment strength might be better because the designers could find the information easier.

A Buchanan commented that a hierarchic failure process was needed to get the desirable failure and this was a rational approach.

I Gavric received clarification that the mean values for metal connections came from experiments.

T Reynolds asked how to define the expected probability of failure. W Seim responded that this would be similar to a safety consideration with the comparison of fractile of demand and resistance and introduction of safety factors.

J Munch Andersen commented that the factor of 1.15 in the Johansen-type equation should not be used for the mean strength. S Seim agreed.

Connections and anchoring for wall and slab elements in seismic design

Michael Schick

Tobias Vogt

Werner Seim

University of Kassel, Department of Structural Engineering, Chair for Building Rehabilitation and Timber Engineering, Kurt-Wolters-Straße 3, 34125 Kassel, Germany.

1 Introduction

This paper focus on the consideration of over-strength for connections and interconnections of light frame elements used for wall and slab structures.

If ductility and energy dissipation under cyclic loading are utilised in the case of earthquake design, it is indispensable to ensure that all the elements outside the ductile zone remain elastic. Figure 1.1a shows a typical situation of a timber-framed wall element. A square element with no vertical loading was chosen for simplification. While the wall element must reach its load-bearing capacity, the anchoring of the wall remains more or less elastic. Failure modes of the anchoring, such as stud failure (see Fig. 1.2a) or tie down rupture (see Fig. 1.2b), are typically brittle.

The engineer follows the load flow from the top to the foundation of the building by using force-based design methods. Consequently, the anchoring and the wall element itself are both designed for the same action E_d if there are no further reflections. The characteristic value for resistance R_k and – assuming an identical partial safety factor for resistance – the design values R_d are then both on the same level. The hidden reserves of the ductile element may now cause preliminary failure of the anchoring before any energy dissipation can be activated.

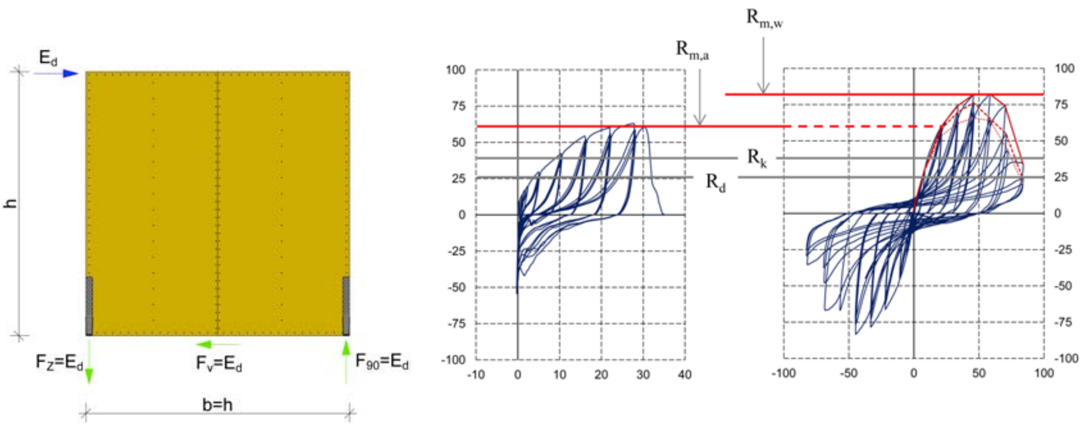

(a) (b) (c)

Figure 1.1: Test set-up of wall elements (a), hysteretic curves of anchoring (b) and wall element (c) from testing

(a) stud failure

(b) tie down rupture

Figure 1.2: Brittle failure modes

Figures 1.1b and 1.1c illustrate that the anchoring should always be designed for a sufficient over-strength to ensure that there is no brittle failure before the capacity of the wall element is reached. The specification of EC 8 [1] is “sufficient over-strength” for this case.

2 State-of-the-art

2.1 Design of light frame elements

The dimensioning of light framed timber walls and connections is based on the lower bound theorem of the theory of plasticity for the wall and on the upper bound theorem for the connections.

An application of the lower bound theorem within the theory of plasticity is the design method for light frame walls according to EC5 [2]. The deformation capacity is provided here by many single fasteners placed to connect the sheathing materials to the studs. The maximum load capacity is reached when the fasteners achieve their maximum load capacity. It is inherent to the application of the lower bound theorem that the maximum load lies above the load bearing resistance calculated.

The characteristic resistance of dowelled type connections could be described by a function in relation to the yielding moment M_y of the fastener and the embedding strength f_h of the connected parts.

$$R_k = R_k(M_{y,k}, f_{h,k}) \qquad (1)$$

Yielding moment and embedding strength which are given as characteristic values in EC 5 are based on experimental data. The appraisal of the characteristic values for the yielding moment for circular sections needs the diameter d of the fastener and the tensile strength $f_{u,k}$ of the steel. The pure mechanical approach was modified to consider the bending angle at a joint slip of 15 mm (see Blass et al. [3]).

$$M_{y,k} = 0.3 \cdot d^{2.6} \cdot f_{u,k} \qquad (2)$$

Embedding strength values f_h for solid timber in nailed connections are defined as

$$f_{h,k} = 0.082 \cdot d \cdot \rho_k^2 \tag{3}$$

where ρ_k is the density of the timber. The characteristic values of embedding strength for oriented strand board (OSB) can be calculated by

$$f_{h,k} = 0.65 \cdot d^{-0.7} \cdot t^{0.1} \tag{4}$$

where t is the thickness of the sheathing material. Values for gypsum fibre board (GFB) can be taken from product information or general approval as

$$f_{h,k} = 7 \cdot d^{-0.7} \cdot t^{0.9} . \tag{5}$$

The characteristic value for the load-bearing resistance of timber-framed wall elements is mainly defined by the connection between the sheathing board and the timber framing,

$$R_k = \frac{R_{c,k} \cdot b_i}{s} \tag{6}$$

where $R_{c,k}$ is the characteristic resistance of one single fastener, b_i is the length of the wall element and s is the spacing of the fasteners. Other failure modes, such as shear failure of the board, tensile and compression failure of the stud, failure in anchoring, or the transfer of compression forces, can be excluded by a balanced design and detailing.

2.2 Statistics

It is necessary to transfer mean values into characteristic values to ensure that a predefined safety level is achieved. This applies to material strength as well as to the load-bearing resistance of structural elements. Figure 2.1a shows the standard deviation of a basic population. The Gaussian distribution

$$f(x) = \frac{1}{\sigma_x \cdot \sqrt{2 \cdot \pi}} \cdot e^{\frac{-(x-\mu_x)^2}{2 \cdot \sigma_x}} \tag{7}$$

can be used to describe a symmetrical distribution of samples.

The standard deviation σ_x of the basic population is crucial for the form of the distribution; the smaller the standard deviation, the more slender the curves become. The mean value of the basic population is μ_x.

Statistics in engineering practice are mostly applied on sample testing. On the basis of the results of a number of n sample tests, the mean value $\overline{x}_n$ of the random sample is ascertained by

$$\overline{x}_n = \frac{1}{n} \sum_{i=1}^{n} x_i . \tag{8}$$

For simplification, statistical assessment in civil engineering assumes symmetrical distribution. The standard deviation again describes the form of the frequency distribution. The standard deviation S_x depending on sample tests is defined by

$$S_x = \sqrt{\frac{1}{n-1} \cdot \sum_{i=1}^{n} (x_i - \overline{x}_n)} . \tag{9}$$

Based on the definition of the confidence interval, EC 0 [4] defines characteristic values for load-bearing resistance $x_{0.05}$ as material properties by

$$x_k = \overline{x} \cdot (1 - k_n \cdot \frac{S_x}{\overline{x}}) \tag{10}$$

where k_n is a factor to determine the p-fractile of the deviation. The value of k_n depends on whether S_x is equal to σ_x or not and on the number n of the samples. k_n is 1.64 for an infinite number of test results. Figure 2.1b shows the approach to get characteristic out of mean values for an infinite series assuming a normal distribution.

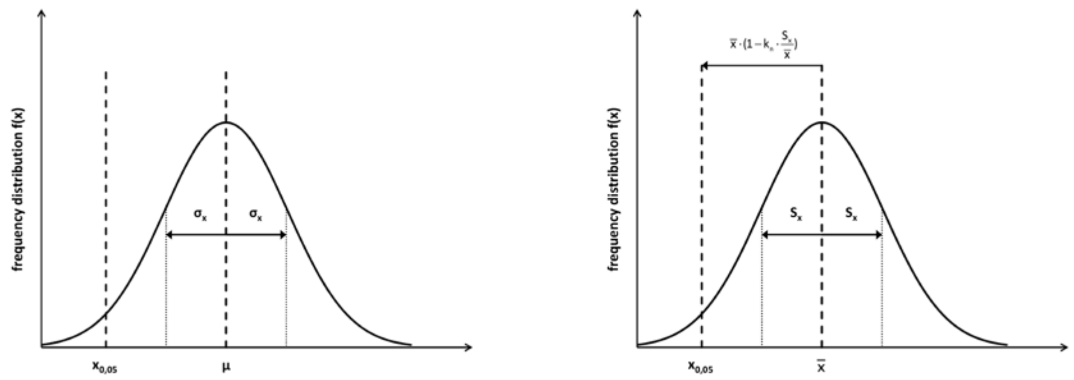

(a) (b)

Figure 2.1: Normal frequency distribution of a population (a) and a random sample (b)

2.3 Over-strength

The connections with nails or staples are the part of the light framed shear walls which is able to dissipate energy in case of an earthquake impact due to the plastic deformation behaviour of the steel. To reach the plastic behaviour of the shear wall, it is necessary to ensure that all the other parts do not exhibit preliminary failure.

If the load-bearing capacity of a wall element is taken as the action imposed on the anchoring and on the connection, then the definition is

$$R_{a,0.05} \geq R_{w,0.95} \tag{11}$$

with

$$R_{w,0.95} = \gamma_{Rd} \cdot R_{w,k} \tag{12}$$

according to Figure 1.1 with the over-strength factor γ_{Rd}. It is also obvious from Figure 1.1 that the calculation of γ_{Rd} must account for material and mechanical over-strength (“hidden reserves”) and statistics.

While the over-strength values for steel structures and structural concrete structures are specified between 1.1 and 1.35, there is no specific information about the over-strength factors for timber structures in EC 8.

The Canadian standard contains over-strength factors for structural timber construction as those documented and explained by Mitchell et al. [5]. Over-strength is defined there as a product of partial factors, considering statistics, hardening effects, and the level of simplification for the modelling and the load-bearing resistance. The over-strength factor is defined as 1.7 for nailed shear walls.

Jorissen and Fragiacomo [6] derive over-strength factors for dowelled type connections. The over-strength factor is defined as a product of partial factors considering the approximation of the analytical formulas used to predict the strength properties and the material safety factor.

Over-strength factors for different types of specimens are derived between 1.18 and 2.08. The average value of the over-strength factor is calculated as 1.6.

According to the approach suggested by Jorissen and Fragiacomo, Brühl and Kuhlman [7] proposed an over-strength factor for beams under bending stress with yielding links of 1.28.

Sustersic et al. [8] determined the same over-strength factors for typical steel connectors with nails and self-tapping screws as those used for the anchoring of cross laminated timber (CLT) wall elements. Over-strength is again defined there as a product of partial factors with values reaching from 1.182 to 2.119.

3 Experimental investigation

Comprehensive testing on connection units, wall elements and anchoring units was carried out at the University of Kassel. These experimental investigations were part of a project on the optimisation of wall and slab elements for multi-storey buildings (see www.optimberquake.eu).

3.1 Tests on connection units

Table 3.1 shows the testing programme and the material parameters of the connection units. Nails with diameters of 2.5 mm, 2.8 mm and 3.1 mm and staples with a diameter of 1.53 mm were used for the connections. OSB panels, respectively GFBs, with a thickness of 10 mm and 18 mm were connected to solid construction timber (SCT) of 110 mm x 75 mm.

Table 3.1: Connection units – testing programme and material parameter

number	specimen 1)	connectors		sheathing	$f_{h,k}$	$f_{h,k}$ 2)	$M_{y,k}$	$M_{y,m}$ 3)	$f_{ax,k}$	$f_{ax,m}$	ρ_k (sct)	ρ_m 3) (sct)
		type	Ø - length		N/mm²	N/mm²	Nmm	Nmm	N/mm²	N/mm²	kg/m³	kg/m³
1	na2.5-o18-m		2.5-60 mm		45.7	77.3	1949	2492				
3	na2.5-o18-c											
4	na2.8-o18-m	nails	2.8-65 mm	OSB 18 mm	42.2	71.4	2617	3146	2.45	3.96	350	413
3	na2.8-o18-c											
1	na3.1-o18-m		3.1-65 mm		39.3	66.5	3410	4213				
3	na3.1-o18-c											
5	na2.5-o10-m		2.5-60 mm		43.1	72.9	1949	2492				
1	na2.8-o10-m	nails	2.8-65 mm	OSB 10 mm	39.8	67.4	2617	3146	2.45	3.96	350	413
3	na2.8-o10-c											
5	na3.1-o10-m		3.1-65 mm		37.1	62.7	3410	4213				
5	na2.5-g18-m		2.5-60 mm		49.7	73.1	1949	2492				
1	na2.8-g18-m	nails	2.8-65 mm	GFB 18 mm	45.9	67.5	2617	3146	2.45	3.96	350	413
3	na2.8-g18-c											
5	na3.1-g18-m		3.1-65 mm		42.8	62.9	3410	4213				
1	st1.53-g18-m	staples	1.53-55 mm	GFB 18 mm	70.1	103.1	725	674	2.45	23.5	350	413
3	st1.53-g18-c											
1	st1.53-g10-m	staples		GFB 10 mm	41.3	60.8	725	674				
3	st1.53-g10-c											

1) m: monotonic, c: cyclic according to ISO 16670 [12]
2) mean values – for OSB according to [9], for GFB according to [10]
3) mean values from sample testing

The loading protocol of EN 26891 [11] with a rate of 0.2 mm/s was used for the monotonic tests. The cyclic tests were carried out according to ISO 16670 [12]. The yielding moment, pull-out resistance of the nails and staples and density of SCT was determined experimentally. The mean values for embedding strength are taken from internal reports. The material values are documented in Table 3.1. See Table 4.1 for the test results. Detailed information about the test series is documented in Deliverable 2A of the research project Optimberquake [13].

3.2 Full-scale tests

The wall elements for full-scale testing consist of studs with a cross-section of 140 mm x 60 mm and a distance of 625 mm between the studs and bottom and top rails with a cross-section of 140 mm x 85 mm. OSB panels and GFBs with thicknesses of 10 mm and 18 mm on one or both sides were used for the sheathing.

The OSB panels are connected with nails with a diameter of 2.8 mm and a distance between the fasteners of 75 mm. The GFBs are connected with staples with a diameter of 1.53 mm and a spacing of 75 mm. A vertical load of 10 kN/m was applied. The loading protocol from ISO 21581 [14] with a rate of 1.0 mm/s for the monotonic tests comes into play. The cyclic tests were carried out according to ISO 21581 and CUREE (basic loading history) [15]. The testing programme is shown in Table 3.2. The results of these tests are given in Table 4.2. Detailed information about the test series is documented in Deliverable 2B of the research project Optimberquake [16].

Table 3.2: Full-scale wall elements – testing programme

test series	specimen	loading	speed / rate	sheathing	connectors type	connectors Ø - length	spacing	type of anchoring
I	WL-1.1	monotonic	1.0 mm/s	2x OSB 18 mm	nails	2.8-65 mm	75 mm	centric, narrow side
	WL-1.2	cyclic (ISO)	0.2 mm/s					
	WL-1.3	cyclic (ISO)	1.0 mm/s					
	WL-1.4	cyclic (CUREE)	0.025 Hz					
II	WL-2.1	monotonic	1.0 mm/s	2x GFB 18 mm	staples	1.53-55 mm	75 mm	centric, narrow side
	WL-2.2	cyclic (ISO)	1.0 mm/s					
	WL-2.3	cyclic (ISO)	1.0 mm/s					
	WL-2.4	cyclic (CUREE)	0.025 Hz					
III	WL-3.1	cyclic (ISO)	1.0 mm/s	1x OSB 10 mm	nails	2.8-65 mm	75 mm	centric, narrow side
	WL-3.2	cyclic (CUREE)	0.025 Hz					
	WL-3.3	cyclic (ISO)	1.0 mm/s	1x OSB 18 mm				
	WL-3.4	cyclic (CUREE)	0.025 Hz					
IV	WL-4.1	cyclic (ISO)	1.0 mm/s	2x OSB 18 mm	nails	2.8-65 mm	75 mm	eccentric, on board
	WL-4.2	cyclic (ISO)	1.0 mm/s	2x GFB 18 mm	staples	1.53-55 mm		
	WL-4.3	cyclic (ISO)	1.0 mm/s	1x OSB 18 mm	nails	2.8-65 mm		
	WL-4.4	cyclic (ISO)	1.0 mm/s	1x GFB 18 mm	staples	1.53-55 mm		
V	WL-5.1	cyclic (ISO)	1.0 mm/s	1x GFB 10 mm	staples	1.53-55 mm	75 mm	centric, narrow side
	WL-5.2	cyclic (CUREE)	0.025 Hz					
	WL-5.3	cyclic (ISO)	1.0 mm/s	1x GFB 18 mm				
	WL-5.4	cyclic (CUREE)	0.025 Hz					

4 Statistical evaluation of test results

4.1 Relation of characteristic values and test results

Characteristic values calculated according to EC 5 are based on the assumption that 95% of the basic population will reach these characteristic values. This applies to structural elements as well as connections. On the other hand, there will be a distribution of test results with a mean value – in most cases – higher than expected and a form more or less slender compared to the distribution of calculated values (see Figure 4.1). Three steps are proposed to explain the difference between the characteristic values according to EC 5 and the mean values from testing. Firstly, the expected mean values of the connections have to be calculated according to EC 5 by using the material properties as mean values (see Table 3.1).

$$R^*_m = R^*_m(f_{h,m}, M_{y,m}) \tag{13}$$

The "hidden reserves" can then be specified as the difference between R^*_m from the calculation and $R_{exp,m}$ from the test results.

Finally, the quantile value can be calculated depending on the standard deviation and the number of test results.

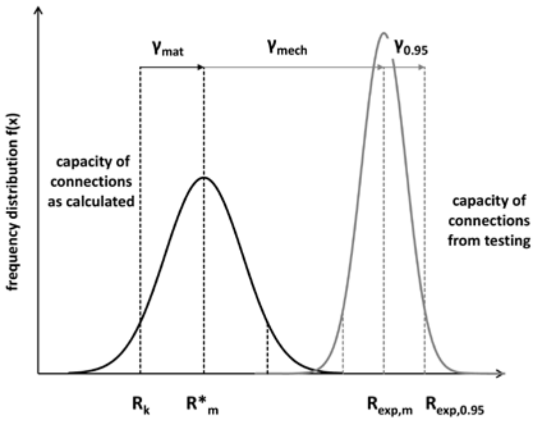

(a)

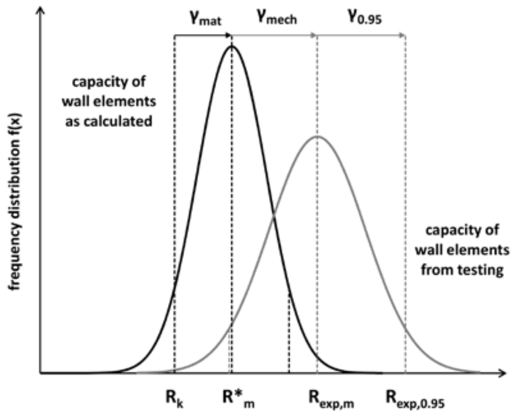

(b)

Figure 4.1: Capacity as calculated and from testing for connections (a) and wall elements (b)

Figure 4.1 shows the distribution of calculated values and the distribution of the experimental data with

R_k design value according to code provisions

R^*_m mean value of resistance by using the mean values of material properties

$R_{exp,m}$ mean value of capacity from testing

$R_{exp,0.95}$ 95% quantile from testing

In order to get the $R_{exp,0.95}$ values from characteristic values, according to the design codes, the over-strength factor γ_{Rd} is introduced:

$$\gamma_{Rd} = \gamma_{mat} \cdot \gamma_{mech} \cdot \gamma_{0.95} \tag{14}$$

where γ_{mat} considers the spread between the characteristic values according to design provisions and the calculated values using the material properties as mean values:

$$\gamma_{mat} = \frac{R^*_m}{R_k}. \tag{15}$$

The mechanical effects are considered by the factor γ_{mech}. Mechanical effects resulting in an increase of the load-bearing capacity are mainly due to friction and pull-out resistance of the fastener. Furthermore, the underestimation due to the application of the lower bound theorem is included within the mechanical effects.

$$\gamma_{mech} = \frac{R_{exp,m}}{R^*_m}. \tag{16}$$

In order to consider 95% quantile values, $\gamma_{0.95}$ is defined as

$$\gamma_{0.95} = 1 + k_n \cdot \frac{S_x}{R_{exp,m}} \tag{17}$$

resulting from

$$R_{exp,0.95} = R_{exp,m} \cdot (1 + k_n \cdot \frac{S_x}{R_{exp,m}}) \tag{18}$$

4.2 Connection units

Table 4.1 depicts the test results, characteristic values according to EC 5 and the mean values calculated based on the European yielding model by using the mean values of material properties. The over-strength factors are calculated according to section 4.1.

The $\gamma_{0.95}$ values are calculated based on the assumption that the standard deviation is known for the basic population.

Table 4.1: Test results and over-strength factors for connection units

number	specimen[1)]	R_k kN	R^*_m kN	$R_{exp,m}$ kN	S_x kN	k_n	γ_{mat}	γ_{mech}	$\gamma_{0.95}$
1 3	na2.5-o18-m na2.5-o18-c	0.69	0.90	0.89	0.07	1.83	1.31	0.99	1.14
4 3	na2.8-o18-m na2.8-o18-c	0.82	1.06	1.11	0.06	1.76	1.30	1.05	1.10
1 3	na3.1-o18-m na3.1-o18-c	0.92	1.25	1.47	0.18	1.83	1.36	1.18	1.22
5	na2.5-o10-m	0.55	0.78	1.15	0.13	1.80	1.42	1.48	1.20
1 3	na2.8-o10-m na2.8-o10-c	0.62	0.86	1.09	0.04	1.83	1.39	1.27	1.07
5	na3.1-o10-m	0.70	0.96	1.53	0.12	1.80	1.38	1.58	1.14
5	na2.5-g18-m	0.70	0.90	1.64	0.21	1.80	1.29	1.82	1.23
1 3	na2.8-g18-m na2.8-g18-c	0.83	1.05	1.61	0.08	1.83	1.27	1.54	1.09
5	na3.1-g18-m	0.96	1.24	2.27	0.41	1.80	1.29	1.83	1.32
1 3	st1.53-g18-m st1.53-g18-c	0.76	0.81	1.33	0.25	1.83	1.07	1.64	1.35
1 3	st1.53-g10-m st1.53-g10-c	0.62	0.76	1.00	0.17	1.83	1.23	1.32	1.31
						mean value	1.30		

4.3 Wall elements

The results of the testing series on wall elements are documented in Table 4.2. The capacity was calculated based on a plastic model (see section 2.1).

$$R^*_{m,w} = \frac{R^*_m \cdot b_i}{s} \tag{19}$$

where

R^*_m calculated capacity for the fasteners according to EC 5 by using the mean values of the material properties

b_i length of the wall element

s spacing of the fasteners

Wall elements of test series IV are tested with an eccentric anchorage, thus, the test results are not completely comparable with the test results of other test series. Therefore, the factor γ_{mech} was determined for every single test for this series. For the other test series, $\gamma_{0.95}$ was determined according to EC 0 based on the assumption of a normal distribution and of a known standard deviation.

Table 4.2: Test results and over-strength factors for wall elements

test series	specimen	R_k kN	R^*_m kN	$R_{exp,m}$ kN	S_x kN	k_n	γ_{mech}	$\gamma_{0.95}$
I	WL-1.1 WL-1.2 WL-1.3 WL-1.4	54.5	69.3	91.4	14.8	1.83	1.32	1.30
II	WL-2.1 WL-2.2 WL-2.3 WL-2.4	51.2	53.7	72.2	10.4	1.83	1.34	1.26
III	WL-3.1 WL-3.2	20.7	28.6	37.4	5.3	2.01	1.31	1.28
	WL-3.3 WL-3.4	27.3	34.6	37.6	2.9	2.01	1.09	1.16
IV	WL-4.1	54.5	69.3	59.4			0.86	
	WL-4.2	51.2	53.7	68.3			1.27	
	WL-4.3	27.3	34.6	37.1			1.07	
	WL-4.4	25.6	26.9	40.0			1.49	
V	WL-5.1 WL-5.2	20.6	25.3	37.0	6.2	2.01	1.46	1.34
	WL-5.3 WL-5.4	25.6	26.9	47.0	8.2	2.01	1.75	1.35
						mean value	1.33	1.28

5 Proposal and outlook

Based on the experimental data, over-strength factors for connections and timber-framed wall elements can be defined to ensure ductile behaviour. The γ values are comparatively well distributed for all connection units and wall elements tested, hence, it seems acceptable to use the mean values as determined for the partial factors to define over-strength for connections and timber-framed wall elements.

In order to consider the spread between the capacity of the connection as calculated by using the characteristic or mean values of material properties, the partial over-strength factor is set as

$$\gamma_{mat} = 1.30 . \tag{20}$$

The "hidden reserves" based on mechanical effects which are not considered in design codes but increase the capacity of the structural elements are rated by γ_{mech}. Based on the results from wall testing (see Table 4.2), this factor can be defined as

$$\gamma_{mech} = 1.33 . \tag{21}$$

The factor considering the statistic effect to create 95% percentiles for the capacity of wall elements can be set as

$$\gamma_{0,95} = 1.28 . \tag{22}$$

Multiplication of partial over-strength factors leads to

$$\gamma_{Rd} = 1.3 \cdot 1.33 \cdot 1.28 \cong 2.20 . \tag{23}$$

The mechanical over-strength factor γ_{mech} can be decreased to 1.0 if the same mechanical over-strength is expected for the wall element and connection. The over-strength then decreases to

$$\gamma_{Rd} = 1.30 \cdot 1.0 \cdot 1.28 \cong 1.65\,. \tag{24}$$

This proposal is restricted to the sheathing materials and connections used for testing, documented in Chapter 3. Additional testing and statistical assessment of test results from literature will help to enlarge the application area.

It is possible that different over-strength factors could be set for different sheathing materials and connections by increasing the number of test results.

Acknowledgements

The testing programme was part of the European research project Optimberquake, which is currently being carried out with participants from Belgium, Italy and Germany. The project is funded under the Cornet Programme of the European Union. The German part is supported by the “aiF – Arbeitsgemeinschaft industrieller Gemeinschaftsförderung”. The “ivth – Internationaler Verein für technische Holzfragen” is in charge of the financial management. Co-funding comes from “Holzbau Deutschland”, “Qualitätsgemeinschaft Holzbau und Ausbau”, “Verband der deutschen Holzwerkstoffindustrie”, Bundesverband der Gipsindustrie”, “Deutscher Holzfertigbau-Verband” and the “Studiengemeinschaft Holzleimbau”.

6 References

[1] DIN EN 1998-1: Eurocode 8: *Design of structures for earthquake resistance – Part 1: General rules, seismic actions and rules for buildings; German version* EN 1998-1:2004. April 2006.

[2] DIN EN 1995-1-1: Eurocode 5: *Design of timber structures – Part 1-1: General – Common rules and rules for buildings; German version* EN 1995-1-1:2010-12. December 2012.

[3] Blass H.J., Bienhaus A., Krämer V.; *Effective bending capacity of dowel-type fasteners*. Proceedings PRO 22, International RILEM Symposium on Joints in Timber Structures, pp. 71-80, 2001.

[4] DIN EN 1990: Eurocode: *Basis of structural design; German version* EN 1990:2012. December 2012.

[5] Mitchell D., Tremblay R., Karacabeyli R., Pauetre P., Saatciouglu M., Anderson D.L.; *Seismic force modification factors for the proposed 2005 edition of National Building Code of Canada*, Canadian Journal of Civil Engineering, pp. 308-327, 2003.

[6] Jorissen A., Fragiacomo M.; *General notes on ductility in timber structures, Engineering Structures,* pp. 2987-2997, 2001.

[7] Brühl F., Kuhlmann U., *Requirements on ductility in timber structures*, CIB W18, Alghero, 2011.

[8] Sustersic I., Fragiacomo, M., Dujic B.; *Influence of connection properties on the ductility and seismic resistance of multi-storey cross-lam buildings*, CIB W18, Alghero, 2011.

[9] Kessel M.H., Huse; *Vergleichende Betrachtungen europäischer Bauproduktennormen mit nationalen Bestimmungen. Teilprojekt: Lochleibungsfestigkeit von OSB-Platten. Abschlussbericht 3/1998*, 1998.

[10] Polatschek T.M., Kessel M.H.; *Zur Erweiterung der allgemeinen bauaufsichtlichen Zulassung Z-9.1-434 von FERMACELL-Gipsfaserplatten – Expertise.* Not published, 2003.

[11] DIN EN 26891: *Timber structures – Joints made with mechanical fasteners – General principles for the deformation of strength and deformation characteristics (ISO 6891:1983) – German version* EN 26891:1991. July 1991.

[12] ISO 16670: *Timber structures – Joints made with mechanical fasteners – Quasi-static reversed-cyclic test method*, 2003.

[13] Seim W., Vogt T.; *Optimberquake - Deliverable 2A: Connection units – monotonic and cyclic testing*. Technical Report, University of Kassel, 2012.

[14] ISO 21581: *Timber structures – Static and cyclic lateral load test method for shear walls*, 2010.

[15] Krawinkler H., Parisi F., Ibarra L., Ayoub A., Medina R.; *Development of a Testing Protocol for Woodframe Structures*. CUREE Publication No. W-02, 2001.

[16] Seim W., Vogt T.; *Optimberquake – Deliverable 2B: Timber framed wall elements – monotonic and cyclic testing.* Technical Report, University of Kassel, 2013.

INTERNATIONAL COUNCIL FOR RESEARCH AND INNOVATION
IN BUILDING AND CONSTRUCTION

WORKING COMMISSION W18 - TIMBER STRUCTURES

ANALYTICAL FORMULATION BASED ON EXTENSIVE NUMERICAL SIMULATIONS OF BEHAVIOR FACTOR Q FOR CLT BUILDINGS

L Pozza
R Scotta
D Trutalli

University of Padova

A Ceccotti
A Polastri

Trees and Timber Institute, Italian Research Council (CNR-IVALSA)

ITALY

Keywords: CLT, q-factor, seismic response, over-strength factor, Non-Linear Static Analyses (NLSA), Non-Linear Dynamic Analyses (NLDA)

Presented by R Scotta
M Popovski agreed that using more joints can lead to higher ductility.

Analytical formulation based on extensive numerical simulations of behavior factor q for CLT buildings

L. Pozza, R. Scotta, D. Trutalli

Department of Civil, Environmental and Architectural Engineering, University of Padova, Italy

A. Ceccotti, A. Polastri

Trees and Timber Institute, Italian Research Council (CNR-IVALSA), Italy

This paper reports a parametric study of various CLT building configurations, to define the effects of some significant structural characteristics on their seismic response and therefore on appropriate q-factor values. An analytical procedure to calculate such values for CLT structures is proposed, starting from building geometry and wall composition. The effects of over-strength factors in designing joint types are also studied. Two independent validations demonstrate the reliability of the proposed method.

1 Introduction

Although Cross-Laminated Timber (CLT) technology is widespread in construction practice, there are few calculation guidelines in building codes, especially as regards seismic design. CLT structures are not specifically considered in Eurocode 8 (CEN 2004) as a building type and the reduction (or behavior) q-factor for buildings with glued timber elements is safely imposed as 2, regardless of construction method (number and arrangement of connectors in relation to building's size and geometry). Effects due to building slenderness and the over-strength ratio between the various types of connectors are not taken into account. In the available codes, this disadvantage is substantial, as CLT panels to build sometimes tall buildings are increasingly used.

Despite the considerable number of experimental tests and numerical simulations carried out on various CLT structures and typical connections in some European countries, in Canada and Japan no provisions consider the effect of the above characteristics of CLT buildings on the seismic response and hence on the q-factor for seismic design. The most comprehensive research analyzing the seismic behavior of low- and mid-rise CLT buildings was carried out by CNR–IVALSA (Trento, Italy) in the SOFIE Project [Ceccotti et al. (2006), Sandhaas et al. (2009), Dujic et al. (2010), Gavric at al. (2011)]. According to these studies and experimental tests, a q-factor of 3 is presented as a reasonable estimate for CLT buildings [Ceccotti (2008)]. Other studies were conducted at the University of Ljubljana, Slovenia [Dujic et al. (2005)] to determine the seismic behavior of 2-D CLT shear walls in various load and boundary conditions. FPInnovations-Forintek in Canada undertook research to determine the structural properties and seismic resistance of CLT structures [Popovski et al. (2010)] and the results were used by Pei et al. (2012) to define the most suitable q-factor for a six-storey CLT building, recommending R_d=2.5 and R_0=1.5. Lastly, in Japan, experiments on shear walls consisting of two panels studied the failure mechanism of CLT structures [Yasumura (2012)].

These researches, experimental tests and numerical simulations focus on the seismic response of single or a few CLT elements or buildings with particular geometric characteristics, building methodologies and connector arrangements. They do not present a comprehensive approach which may be generalized to building technology in itself.

2 Parameters influencing the q-factor value

The q-factor of a CLT building is defined as a complex function of a number of parameters, according to Equation 1:

$$q = q \text{ (Regularity, Storeys number, Wall joint density, Slenderness, Joint design criteria)} \qquad (1)$$

In-plan regularity influences the distribution of the horizontal force of an earthquake in the shear walls of the structure. Elevation regularity affects the transmission of seismic forces through each storey, down to the building's foundations. Storey number and slenderness have a direct effect on the main elastic period of the building and therefore on its seismic susceptibility. The number of panel-to-floor connections increases with storey number, and the overall dissipative capacity of the building consequently also increases with the number of connectors. This trend is reliable only for buildings of up to 7-8 storeys, after which additional storeys remain in the elastic field without particular effects on dissipative capacity. The density of panel-to-panel wall joints (i.e., construction methodology) strongly influences the building's dissipative and displacement capacities and its resulting ductility. Slenderness - defined as the ratio between the height and base dimensions of the building - determines its response: squat buildings are more prone to shear failure mechanisms, whereas greater slenderness induces flexural and rocking behavior. Various over-strength factors calculated for each type of joint may also induce or prevent the failure of certain connectors and therefore modify the structural failure mode. Accurate definition of the q-factor cannot disregard the influence of these parameters, which all affect the seismic behavior of buildings.

3 Analyses and results

This extensive study of CLT walls provided information about the relationship between q-factor values and the characteristic parameters of CLT buildings.

3.1 Definition and design of case-study configurations

A total of 24 two-dimensional configurations were set, identified as A1N, B1N etc.; with varying numbers of storeys, base dimensions (B) and wall compositions. All configurations were regular in plan and in height, so that the dependence of the q-factor on regularity was not taken into account. Four building heights were chosen, corresponding to 1, 3, 5 and 7 storeys, with an inter-storey height of 3.05 m. Three wall compositions were analyzed: walls made with single CLT panels (No vertical joints), ones with 4 or 2 CLT panels, for configurations with dimensions of 17.5 m and 8.75 m, respectively (Medium density of vertical joints), and walls with CLT panels 1.25 m wide (High density of vertical joints). Table 1 lists the 24 configurations, together with their seismic mass M and principal elastic period T_1.

The configurations were designed according to Linear Static Analysis (LSA), with the following common data, according to Eurocode 8 (CEN 2004): type 1 elastic response spectra and rock foundation (type A soil, corresponding to S=1.0, T_B=0.15 s, T_C=0.4 s, T_D=2.0 s), behavior factor q=1, lowest bound factor for design spectrum β=0.20. Design PGA was assumed to be 0.35g (the highest value for Italian territory) with a building importance factor of γ_I=1.

According to current engineering design practice for CLT buildings, in-plane shear forces in walls were assigned to angle brackets; hold-downs were placed for vertical continuity and also to avoid wall uplift [Pei et al. (2012)].

Table 1 Storey mass and main elastic period of 24 case-study configurations.

	NO VERTICAL JOINTS		MEDIUM DENSITY OF VERTICAL JOINTS		HIGH DENSITY OF VERTICAL JOINTS	
Storey number	B = 17.5m	B = 8.75m	B = 17.5m	B = 8.75m	B = 17.5m	B=8.75m
1	**A 1 N** M=18.0 t T_1=0.12 s	**B 1 N** M=12.0 t T_1=0.14 s	**A 1 M** M=18.0 t T_1=0.14 s	**B 1 M** M=12.0 t T_1=0.14 s	**A 1 H** M=18.0 t T_1=0.17 s	**B 1 H** M=12.0 t T_1=0.16 s
3	**A 3 N** M=92.0 t T_1=0.24 s	**B 3 N** M=60.0 t T_1=0.28 s	**A 3 M** M=92.0 t T_1=0.30 s	**B 3 M** M=60.0 t T_1=0.30 s	**A 3 H** M=92.0 t T_1=0.41 s	**B 3 H** M=60.0 t T_1=0.36 s
5	**A 5 N** M=166.0 t T_1=0.40 s	**B 5 N** M=108.0 t T_1=0.46 s	**A 5 M** M=166.0 t T_1=0.47 s	**B 5 M** M=108.0 t T_1=0.50 s	**A 5 H** M=166.0 t T_1=0.58 s	**B 5 H** M=108.0 t T_1=0.60 s
7	**A 7 N** M=240.0 t T_1=0.59 s	**B 7 N** M=156.0 t T_1=0.75 s	**A 7 M** M=240.0 t T_1=0.65 s	**B 7 M** M=156.0 t T_1=0.78 s	**A 7 H** M=240.0 t T_1=0.80 s	**B 7 H** M=156.0 t T_1=0.97 s

3.2 Numerical models for case-study configurations

Numerical simulations were carried out with open-source research FEM code Open SEES. The models used to study the non-linear behavior of the configurations applied the criteria reported in Ceccotti (2008): CLT panels were modeled as lattice modules composed of stiff elastic truss elements, and fasteners had non-linear springs reproduced with the hysteresis model of Elwood (2006). This model conforms to the classical design assumption that the non-linear behavior of a wall is concentrated on the connectors, whereas CLT panels remain in the elastic field. Model reliability is based on negligible panel shear and bending deformation. As an example, Figure 1-a shows the numerical model used to assess the seismic response of the three-storey configuration with modular CLT panels 1.25 m wide. Calibration of the behavior of non-linear elements was based on experimental results from various types of CLT wall specimens [Ceccotti et al. (2006)] and typical connections [Sandhaas et al. (2009)]. Figures 1-b and 1-c show experimental-numerical comparisons in terms of hysteresis loops for the basic hold-downs and angle brackets. For a detailed description of model calibration, see Pozza (2013).

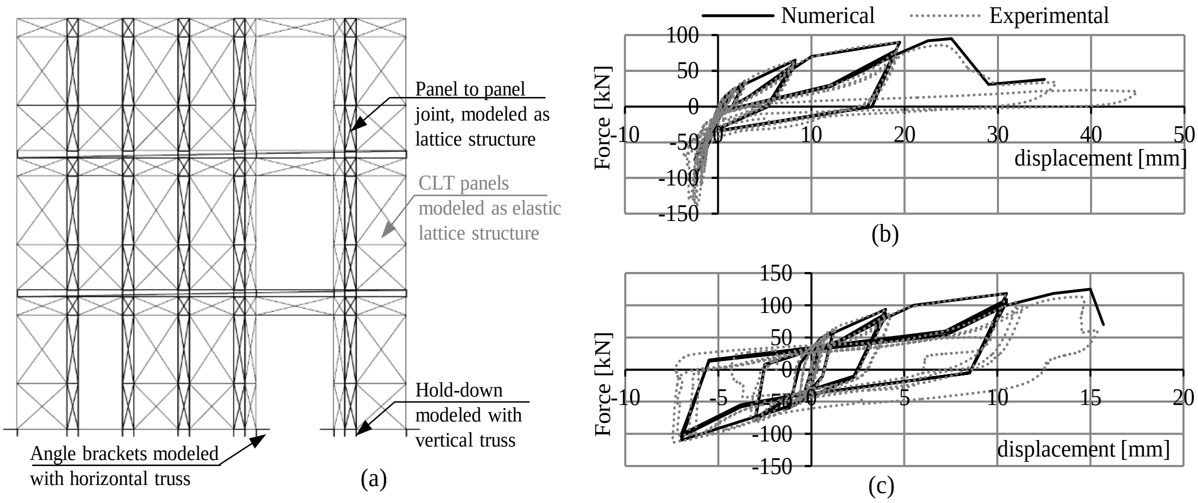

Figure 1 a) Scheme of numerical model for case study B3H; **b)** Example of calibration of hold-down spring; **c)** Example of calibration of angle bracket spring.

3.3 Non-linear analyses and q-factor evaluation

The 24 configurations were analyzed with both Non-Linear Static Analyses (NLSA) and Non-Linear Dynamic Analyses (NLDA), for a total of 120 analyses, 48 NLSA and 72 NLDA. NLSA yielded the capacity curves of the configurations. Two-storey horizontal force patterns were examined, one providing force distribution proportional to that of the first modal shape of the building ($NLSA_{\_1}$) and the second force distribution proportional to storey masses ($NLSA_{\_2}$). The failure displacement of the ultimate push-over curve corresponds to the moment of connector failure, according to Ceccotti (2008).

A series of NLDA was carried out with increasing PGA levels, starting from the design value, to define the failure value bringing the structure to the near-collapse condition. For the NLDA the near-collapse condition corresponds to the moment when a connector fails. Figures 1.b and 1.c show the failure conditions of fasteners, faithfully reproduced by the corresponding numerical models.

For configuration A3M, Figure 2 shows push-over curves overlapping the NLDA results with the increase in PGA, i.e., the points along the hysteresis curves represent the average values of maximum top displacements versus corresponding base shear ($NLDA_{\_1}$) and maximum base shear versus corresponding top displacements ($NLDA_{\_2}$). As Figure 2 shows, there is a good match between the NLSA and NLDA results. Their variability defines the range of possible responses of the building to seismic action.

The NLSA results were processed according to the standard push-over procedure [Fajfar (1996)] to define the reliable q-factor of the buildings. The PGA approach [Ceccotti (2010)] was also used, and estimates the q-factor as the ratio between near-collapse PGA calculated by NLDA and design PGA. As stressed in Pozza (2013), these approaches are code-dependent and the resulting q-factors already include the corrective factor of over-strength, defined as the ratio between yielding and the design force of the structure. Table 2 lists the q-factor values for each building configuration. Minimum, maximum and average q-factors are also listed.

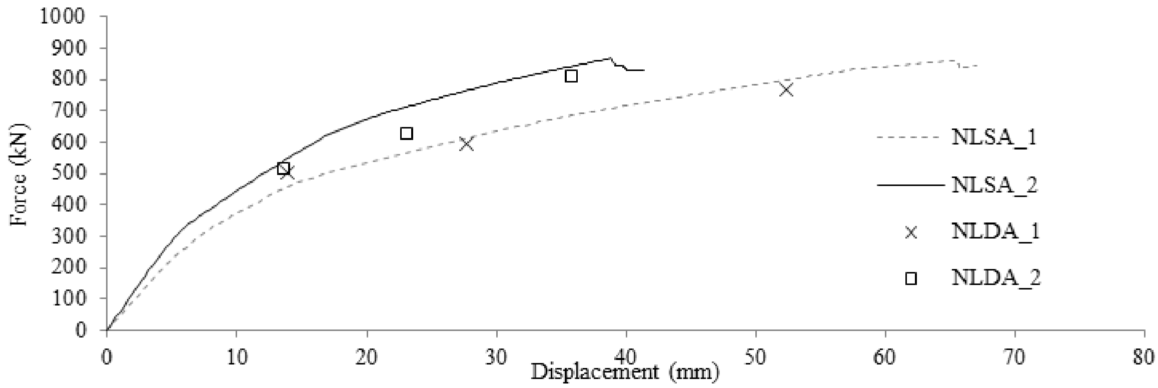

Figure 2 Results from NLSA and NLDA for building configuration A3M.

4 Analyses of results by synthetic indexes

The results shown in Table 2 indicate that the q-factor value strongly depends on specific building characteristics. In detail, the q-factor trend increases with number of storeys, number of panels used to compose walls (i.e., with the density of vertical joints) and slenderness.

In CLT structures, the connections to dissipate energy are arranged along the interfaces of panels with the foundation, floor, roof, and other panels. A specific index, α, is proposed to account for the joint density of the building, and is defined as the ratio between façade area A and the sum of connection line lengths P. Once wall dimensions (B and H), inter-storey height (h), façade area (A), storey number (n) and vertical panel-to-panel joint number (m) have all been defined, index α can be calculated according to Equation 2. The reference configuration of a hypothetical façade without any intermediate joint lines is characterized by index α_0, defined as the ratio between area (A) and perimeter (P_0), according to Equation 3. Figure 3 shows the synthetic indexes α and α_0 for a typical wall.

Current configuration	Reference configuration
$\alpha = A/P$ (2)	$\alpha_0 = A/P_0$ (3)

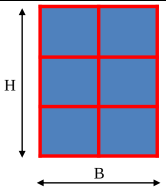

$\mathbf{A= B \cdot H}$

$\mathbf{P = (n + 1) \cdot B + (m + 2) \cdot H}$

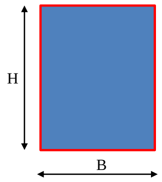

$\mathbf{A= B \cdot H}$

$\mathbf{P_0 = 2 \cdot (B + H)}$

Figure 3 Definition of actual (left) and reference (right) joint indexes.

The ratio between the two indexes in Equation 4 provides a-dimensional joint density index β, accounting for both number of vertical joints and number of storeys:

$$\beta = \alpha_0 / \alpha \tag{4}$$

Table 2 lists the values of joint density index β for each slenderness and configuration, together with q-factor range, average and 5% percentile values.
The results (Table 2) show how the q-factor increases with index β. For a given β value, a slender building has a higher q-factor, i.e., building slenderness λ also influences the q-factor. Accordingly, we may express the q-factor as a function of indexes β and λ. The relationship between them and the q-factor value can be studied by means of frequency distribution curves.

Table 2 Values of index β, q-factor range and slenderness for each case study.

Indexes			q-factor range								
	λ	β	NLSA_1	NLSA_2	NLDA_a	NLDA_b	NLDA_c	q_{min}	q_{max}	$\mathbf{q_{average}}$	$\mathbf{q_{k\text{-}5\%}}$
A1N		1.00	2.87	2.87	2.06	2.29	1.92	1.92	2.87	**2.40**	**1.95**
A1M	0.17	1.22	3.16	3.16	2.06	2.51	2.06	2.06	3.16	**2.59**	**2.04**
A1H		1.89	3.75	3.75	2.29	2.61	2.10	2.10	3.75	**2.90**	**2.10**
A3N		1.66	3.35	3.06	2.80	3.12	2.69	2.69	3.35	**3.00**	**2.74**
A3M	0.52	2.17	3.71	3.33	3.12	3.33	2.96	2.96	3.71	**3.29**	**3.01**
A3H		3.72	4.31	3.81	3.76	3.93	3.66	3.66	4.31	**3.89**	**3.64**
A5N		2.07	3.48	2.97	2.96	3.23	3.07	2.96	3.48	**3.14**	**2.92**
A5M	0.87	2.77	3.67	3.92	3.66	4.09	3.66	3.66	4.09	**3.80**	**3.60**
A5H		4.86	4.63	4.45	4.52	4.84	4.30	4.30	4.84	**4.55**	**4.35**
A7N		2.35	3.74	3.01	3.76	4.30	4.03	3.01	4.30	**3.77**	**3.29**
A7M	1.22	3.18	4.17	3.68	4.41	4.84	4.03	3.68	4.84	**4.23**	**3.79**
A7H		5.65	4.90	4.69	5.11	5.38	5.11	4.69	5.38	**5.04**	**4.78**
B1N		1.00	2.96	2.96	2.29	2.86	2.29	2.29	2.96	**2.67**	**2.32**
B1M	0.35	1.13	2.96	2.96	2.29	2.86	2.29	2.29	2.96	**2.67**	**2.32**
B1H		1.65	3.30	3.30	2.29	2.86	2.29	2.29	3.30	**2.81**	**2.30**
B3N		1.49	4.13	3.20	3.26	3.71	3.14	3.14	4.13	**3.49**	**3.06**
B3M	1.05	1.74	4.06	3.09	3.14	3.54	3.43	3.09	4.06	**3.45**	**3.06**
B3H		2.77	4.22	3.48	2.86	3.60	3.54	2.86	4.22	**3.54**	**3.06**
B5N		1.73	4.29	3.77	4.29	4.69	4.29	3.77	4.69	**4.27**	**3.94**
B5M	1.74	2.05	4.53	4.03	4.46	4.86	4.57	4.03	4.86	**4.49**	**4.19**
B5H		3.32	4.84	4.49	4.86	4.80	4.29	4.29	4.86	**4.66**	**4.40**
B7N		1.87	4.73	4.09	4.00	4.17	4.00	4.00	4.73	**4.20**	**3.89**
B7M	2.44	2.23	4.83	4.15	4.29	4.57	4.46	4.15	4.83	**4.46**	**4.20**
B7H		3.65	4.82	4.57	5.03	5.14	6.29	4.57	6.29	**5.17**	**4.51**

Figures 4 and 5 show the frequency histograms of the q-factor grouped with a class amplitude of 0.25. The corresponding normal distributions overlap the frequency histograms.
A first representation may be made by separating the values corresponding to two ranges of slenderness λ: 0< λ <1 and λ>1. Figure 4 clearly shows that configurations with higher slenderness have higher q-factor values.

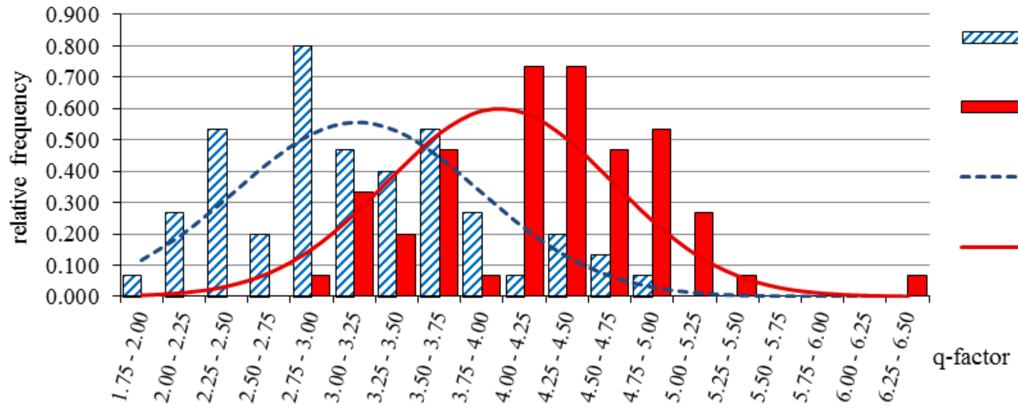

Figure 4 Histograms and normal distributions of 5% percentile q-factor for two ranges of slenderness.

The frequency histograms for increasing levels of coefficient β can also be calculated. Three ranges were examined: $1<\beta<2$; $2<\beta<3$; $\beta>3$. Figure 5 shows the histograms and corresponding normal distributions. The latter show that the q-factor strongly depends on index β. The average 5% percentile values range from about 3 for $1<\beta<2$ to 4.5 for $\beta>3$.

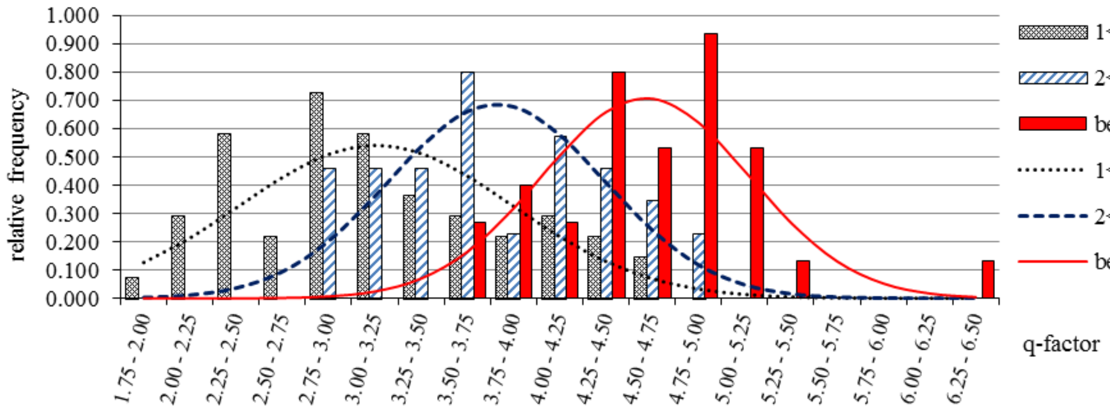

Figure 5 Histograms and normal distributions of 5% percentile q-factor for three ranges of joint density parameter β.

5 Proposed analytical formulations

Two analytical formulas for the q-factor and λ and β are proposed here. The first provides linear dependence between the q-factor and joint density β and the second is a power expression of β. Both formulas take into account the effect of slenderness λ by means of a correlation coefficient.
The linear formulation correlates the q-factor values with joint density β by a proportionality coefficient which depends on building slenderness through an exponential function, as shown in Equation 5:

$$q(\beta, \lambda) = q_0 + (k_0\, e^{k_0 \lambda})\, \beta \tag{5}$$

The second formulation proposes a power function of the q-factor with joint density β, according to Equation 6.

$$q(\beta, \lambda) = (q_0 + k_1 \lambda)\, \beta^{k_2} \tag{6}$$

In both formulations, the coefficients were calibrated to minimize the summation of the square difference between analytical values and numerical 5% percentile values of the q-factor (see Table 2). According to this minimization procedure, the parameters granting the best fit are k_0=0.36 and q_0=1.98 (linear formulation) and k_1=0.53, k_2=0.33, q_0 =1.97 (power formulation).

As a final remark, the proposed analytical laws do not pose any limit on the q-factor for high values of λ and β. An upper limit of q_{max}=5 of the q-factor was assumed.

The analytical formulations in Equations 5 and 6 lead to the abacus representations shown in Figure 6, which allow immediate estimation of the appropriate q-factor for a CLT building with specific slenderness λ and joint density β.

Lastly, it must be noted that the q-factor formulas developed here are valid under the following two assumptions: CLT buildings regular in plan and in height and connectors designed with a common over-strength for angle brackets, hold-downs and vertical panel-to-panel joints. If these two conditions are not met, suitable corrections must be applied (see section 7). Available seismic codes (e.g., CEN 2004) make some provision for the effects of building irregularity. However, numerical analyses of irregular 3-D structures must be performed in order to obtain better estimates for such corrections.

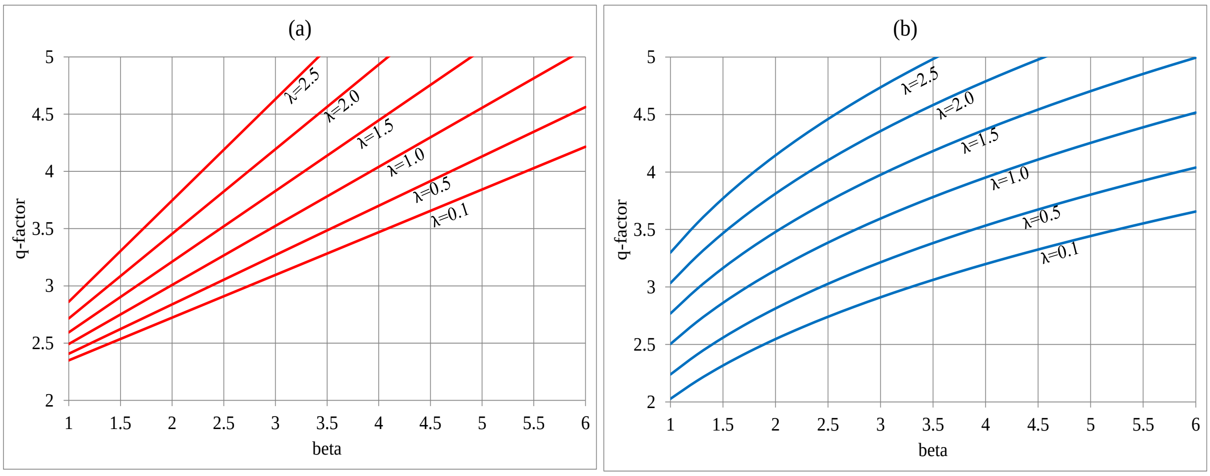

Figure 6 Linear (a) and power (b) abacus representations for q-factor estimation.

6 Validation of analytical procedure

The analytical procedure developed here was validated with reference to two case-study CLT buildings by means of independent numerical simulations.

The first case-study refers to the six-storey building designed by Pei et al. (2012), with CLT panels for walls and floors. This building has a regular, symmetrical rectangular plan, and is 18.3 m long and 12.2 m wide. The second case-study is the three-storey CLT building tested on a shake table in NIED, Japan, during the SOFIE project. It was built to a regular, symmetrical square plan, and each wall was composed of an assembly of three CLT panels. A detailed description of its geometric characteristics is given in Ceccotti (2008).

Table 3 lists the analytical evaluation of the q-factor for the two case-studies. In the first, the q-factor values obtained with the power and linear formulations match those obtained by Pei et al. (2012). In detail, the evaluation gives two q-values for the two wall directions of the

building. The average value is about 3.71 and is nearly equal to the R-factor = 3.75 of Pei et al. (2012), confirming the reliability of the procedure.
The calculated q-values for the second case-study also clearly match the value of q=3.00 estimated by Ceccotti (2008).

Table 3 Analytical evaluation of q-factor of case studies.

		Case-study 1		Case-study 2
		Direction 1	Direction 2	Quake Direction
Parameter α	$\alpha = A / P$	1.65 m	1.14 m	1.03 m
Parameter α_0	$\alpha_0 = A / P_0$	4.55 m	3.64 m	2.06 m
Parameter β	$\beta = \alpha_0 / \alpha = P/P_0$	2.76	3.20	2.00
slenderness	$\lambda = H / B$	0.98	1.48	1.43
q-factor	$q = (q_0 + k_1\lambda)\cdot \beta^{k2}$	3.48	4.04	3.43
q-factor	$q = q_0 + K_0 e^{k0\lambda} \beta$	3.39	3.94	3.18
	$q_{average}$	**3.44**	**3.99**	**3.31**

7 Effects of design over-strength of connectors

The described analytical procedures ensure accurate estimation of the q-factor only under the specific design hypothesis of common over-strengthening of fasteners with respect to earthquake action. In the case of hold-down (H) and angle brackets (A) only, this condition is ensured by Equation 7:

$$\gamma = \gamma_{O\_A} / \gamma_{O\_H} = (V_{rd} / V_{sd}) / (N_{rd}/N_{sd}) = 1 \qquad (7)$$

where γ is the overstrength ratio, γ_{O_A} is angle bracket over-strength, γ_{O_H} is hold-down over-strength, V_{rd} is angle bracket strength, V_{sd} is seismic action on the angle brackets, N_{rd} is hold-down strength, and N_{sd} is seismic action on the hold-downs.
Three additional design criteria were examined, in order to verify the influence of the over-strength (or under-strength) of angle brackets with respect to hold-downs on the seismic response of the building and hence on the q-factor value. Three configurations, with hold-downs strengths of 10% and 25% higher than that of angle brackets, and angle brackets strength 20% stronger than that of hold-downs were analyzed for configurations A3M, B3M, A5M and B5M. Figure 7 plots the results.

γ		$q_{\_average}$	$q/q_{(\gamma=1)}$		$q_{\_average}$	$q/q_{(\gamma=1)}$
0.8	**A 3 M**	2.53	0.77	**B 3 M**	2.69	0.78
0.9		2.96	0.90		3.08	0.89
1		**3.29**	**1.00**		**3.45**	**1.00**
1.2		3.30	1.00		3.40	0.98
0.8	**A 5 M**	3.09	0.81	**B 5 M**	3.64	0.81
0.9		3.47	0.91		4.06	0.90
1		**3.80**	**1.00**		**4.49**	**1.00**
1.2		3.79	1.00		4.44	0.99

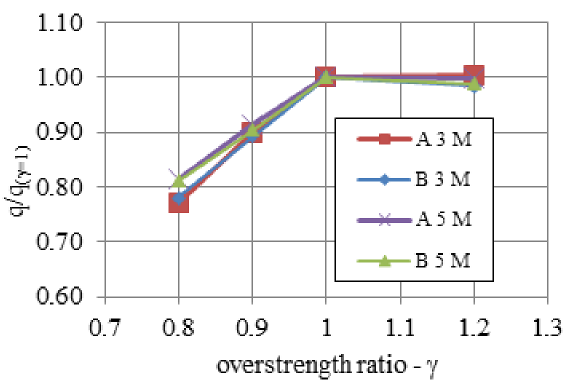

Figure 7 Variations in q-factor with design over-strength ratio between angle bracket and hold-down.

Results obtained with over-strength ratio $\gamma<1$ show that the q-factor values decrease almost linearly, thus suggesting that a correction index, K_O, should be added, to modify q-factor values obtained according to Equation 8:

$$K_O = \min (\gamma = (V_{rd} / V_{sd})/(N_{rd}/N_{sd}); 1) \quad (8)$$

When $\gamma \geq 1$, no correction of the q-factor is required.

8 Conclusions

The results presented here demonstrate that there is a strong correlation between the q-factor and some specific building characteristics. In addition, a q-factor value of 2, as proposed by current standards for CLT structures, is precautionary with respect to actual dissipative capacity. The studies and analyses described here define both the analytical formulation suitable for correlating future buildings with the q-factor value and the correction index, to account for the effects of over-strengthening of connectors.

These findings may be formalized into the proposal of a design formula to estimate the appropriate q-factor for CLT buildings of Equation 9.

$$q_E = K_R\, K_O\, q(\beta, \lambda) \quad (9)$$

where:

- q_E estimate of appropriate q-factor for seismic design of CLT buildings;
- K_R coefficient taking into account building regularity in plan and in height (according to available seismic codes, this may be assumed to be 1.0 for regular buildings and 0.8 for irregular ones);
- K_O coefficient taking into account connector over-strengthening (defined by Equation 8);
- $q(\beta, \lambda)$ reference q-factor (defined by linear or power relations in Equations 5 and 6).

The proposed expression for the q-factor of CLT buildings may be considered for possible implementation in a future review of seismic codes.

References

1. Ceccotti, A., Lauriola, M.P., Pinna, M. and Sandhaas, C. (2006). “SOFIE Project – Cyclic Tests on Cross-Laminated Wooden Panels.” Proceeding of the World Conference on Timber Engineering WCTE. Portland, USA, August 6-10, 2006, CD.

2. Ceccotti, A. (2008). “New technologies for construction of medium-rise buildings in seismic regions: the XLAM case”. IABSE Struct Eng Internat; 18:156–165. Tall Timber Buildings (special ed.).

3. Ceccotti, A. and Sandhaas, C. (2010). “A proposal for a standard procedure to establish the seismic behaviour factor q of timber buildings”. Proceeding of the World Conference on Timber Engineering WCTE. Riva del Garda, Italy, June 20–24, 2010, CD.

4. Dujic, B., Aicher, S. and Zarnic, R. (2005). “Investigation on in-plane loaded wooden elements – influence of loading on boundary conditions”. Otto Graf Journal, Materialprüfungsanstalt Universität. Otto-Graf-Institut, Stuttgart, Vol. 16.

5. Dujic, B., Strus, K., Zarnic, R. and Ceccotti, A. (2010). “Prediction of dynamic response of a 7-storey massive XLam wooden building tested on a shaking table”.

Proceeding of the World Conference on Timber Engineering WCTE. Riva del Garda, Italy, June 20–24, 2010, CD.

6. Elwood, K.J., and Moehle, J.P. (2006). “Idealized backbone model for existing reinforced concrete columns and comparisons with FEMA 356 criteria”. The Structural Design of Tall and Special Buildings, vol. 15, no. 5, pp. 553-569.
7. European Committee for Standardization (CEN). (2004). “Eurocode 8 - design of structures for earthquake resistance, part 1: General rules, seismic actions and rules for buildings”.
8. Fajfar, P. (1996) “Design spectra for new generation of code”. Proceeding 11th Word Conference on Earthquake Engineering, Acapulco, Mexico, 1996, paper No. 2127.
9. Gavric, I., Ceccotti, A. and Fragiacomo, M. (2011). “Experimental cyclic tests on cross-laminated timber panels and typical connections”. Proceeding of ANIDS, Bari Italy, 2011, CD.
10. Pei, S., Popovski, M. and van de Lindt, J.W. (2012). “Performance based design and force modification factors for CLT structures”. Proceeding of the meeting 45 of the Working Commission W18-Timber Structures, CIB. Växjö, Sweden, 2012, paper CIB-W18/45-15-1.
11. Popovski, M., Schneider, J. and Schweinstreiger, M. (2010). “Lateral load resistance of Cross-Laminated wood panels”. Proceeding of the World Conference on Timber Engineering WCTE. Riva del Garda, Italy, June 20–24, 2010, CD.
12. Pozza, L. (2013). “Ductility and behaviour factor of wood structural systems”. Ph.D. Thesis, University of Padova, Italy.
13. Sandhaas, C., Boukes, J., van de Kuilen, J.W. and Ceccotti, A. (2009). “Analysis of X-lam panel-to panel connections under monotonic and cyclic loading”. Proceeding of the meeting 42 of the Working Commission W18-Timber Structures, CIB. Dübendorf, Switzerland, 2009, paper CIB-W18/42-12-2.
14. Yasumura M. (2012). “Determination of failure mechanism of CLT shear walls subjected to seismic action”. Proceeding of the meeting 45 of the Working Commission W18-Timber Structures, CIB. Växjö, Sweden, 2012, paper CIB-W18/45-15-1.

INTERNATIONAL COUNCIL FOR RESEARCH AND INNOVATION IN BUILDING AND CONSTRUCTION

WORKING COMMISSION W18 - TIMBER STRUCTURES

PROPOSAL FOR THE Q-FACTOR OF MOMENT-RESISTING TIMBER FRAMES WITH HIGH DUCTILITY DOWEL CONNECTORS

D Wrzesniak

Claudio Amadio

Department of Engineering and Architecture, University of Trieste

G Rinaldin

M Fragiacomo

Department of Architecture, Design and Urban Planning, University of Sassari

ITALY

Keywords: beam-column joints, behaviour factor, FE modelling, high ductility dowel connectors, incremental dynamic analysis, moment-resisting frame, q-factor, seismic performance

---

Presented by M Fragiacomo

H Blass asked how to distinguish between single bay and multiple bay frames as there would be a huge difference in number of connections in the two cases. M Fragiacomo agreed that this could be an issue and will look into it further.

A Ceccotti discussed the issue of calculation of q factor. Two methods were presented in this study based on the definition of ductility. This was the approach he used in the past to find the "intrinsic" value of behaviour factor. Recently based on research of CLT buildings and shake table tests in Tsukuba and Miki, a different way of considering q as a ratio between PGA corresponding to ultimate limit state and PGA given by code seemed to be more rational. Also for designers, a single factor - Ceccotti calls it a "design" q factor - would be better without having to consider the ductility of the structure - that is always difficult to identify in wooden structures, differently from steel structures, for example. This q factor will be code-dependent of course, but this is what designers need. M Fragiacomo responded there were two concerns. For the portal frames the design was governed by snow instead of seismic loads. For a single DOF system, the two approaches will theoretically coincide. In multi-story buildings, he believed the base shear approach would be more appropriate.

A Buchanan raised a code related question as there were research based debates and code based debates. He questioned what the intent was and whether different q would be needed for different systems. He also asked whether similar issues exist for N. America.

M. Fragiacomo stated in Eurocode different q values would be needed for different systems. In Canadian code, R would be a product of several factors like R_d, R_o. Trying to split the q into different factors would involve large approximations. This would not be proposed for Eurocode as one has to consider different materials and systems.

Proposal for the q-factor of moment-resisting timber frames with high ductility dowel connectors

Daniela Wrzesniak
Department of Engineering and Architecture, University of Trieste

Giovanni Rinaldin
Department of Architecture, Design and Urban Planning, University of Sassari, Italy

Massimo Fragiacomo
Department of Architecture, Design and Urban Planning, University of Sassari, Italy

Claudio Amadio
Department of Engineering and Architecture, University of Trieste

1. Introduction

In recent years timber buildings have become a recognized alternative to reinforced concrete and steel structures in seismic areas. The huge amount of research carried out in Japan, North America, Italy and New Zealand has repeatedly proven the excellent performance of timber buildings under seismic loads (Ceccotti 2007, Buchanan et al. 2008, van De Lindt et al. 2010, Sartori et al. 2012,). Whereas the initial focus was on the seismic performance of the structure, nowadays architectural considerations have become more and more important. In contrast to load bearing walls, timber frames allow the architect to design a structure more freely. However, if timber frames are used as lateral load resisting system in multi-storey structures, horizontal deflections due to seismic and wind loads become the key aspect to be considered due to the flexibility of material.

It is then crucial to achieve stiff beam-column joints to limit the lateral deflection. However, this is challenging due to the anisotropy of timber (Fragiacomo and Batchelar 2012). Whilst for reinforced concrete structures the serviceability limit state requirements are generally fulfilled, for timber structures due to the flexibility of the material this becomes an issue. A connection system needs to be found which is able to provide enough stiffness to limit horizontal deflection but at the same time is sufficiently ductile to dissipate energy in the event of an earthquake.

Recent developments on moment resisting timber frames include the application of post-tensioned tendons or bars, which are located in the centre of beams or columns and provide in this way a self-centring moment resisting connection (Buchanan et al. 2008). Energy dissipaters in the form of mild steel damping elements are used to improve the seismic behaviour and provide the energy dissipation needed to control the lateral deflections. Other possibilities are the use of low level pre-stressed glued-in rods between column and beam elements. The rods can be bonded either into both the column and the beam ends or into one end only (Fragiacomo and Batchelar 2012; Tomasi et al. 2008).

Another option is the use of high energy dissipating dowel type connectors developed at Delft University, the Netherlands (Leijten 1998). With these dowel type connectors, a stiff, highly dissipative connection characterized by stable hysteresis loops without pinching can be achieved.

These characteristics make the tube fasteners a highly suitable solution for structures in seismic zones (Wrzesniak et al. 2013).

In the current version of Eurocode 8 (EN 1998-1:2005), a q-factor of 4 and 2.5 can be used for hyperstatic portal frames with dowelled and bolted joints if the connection deforms plastically for at least three fully reversed cycles at a static ductility ratio of 6 and 4, respectively, without more than a 20% reduction of their resistance (EC8, 8.3(3)P and 8.3(4)b). Preliminary non-linear numerical analyses were carried out by Ceccotti and Karacabeyli (1998) on portal frames using a set of different generated earthquake ground motions. Different glulam frames with the semi-rigid expanded tube fastener connections developed by Leijten (1998) were analyzed considering different values of the static ductility of the joint (4, 6 and 8). The lowest value of the behaviour factor (q-factor) obtained for a static ductility of the joint of 6, which is the typical value for expanded tube fastener connections, was 2. However, the average value was 5. Based on that, Leijten (1998) suggested a behavior factor of 4 for hyperstatic portal frames with expanded tube fastener connections.

The purpose of this study is to verify the above values of the q-factor for hyperstatic portal frames via extensive numerical analysis using an advanced model, and to determine the q-factor for multi-storey timber moment-resisting frames with the same type of beam-column connection, for a possible inclusion in the next generation of the Eurocode 8.

2. Conceptual design of frames

A three-story, five-bay frame has been analyzed in this paper, together with an industrial portal frame. A four-story, three-bay moment resisting frame with the expanded tube connection was analyzed in a previous paper (Wrzesniak et al. 2013).

The layout of the frames was chosen based on existing timber structures. Vertical permanent and imposed loads as well as horizontal wind and seismic loads have been calculated assuming the structures are located in Sant'Angelo dei Lombardi, Campania, Italy. The design is based on the Italian National Regulation for Construction (NTC) and Eurocode 5. The column-foundation connections have been designed as pinned. For ease of construction, the beams consist of two elements whereas the columns are single elements. The connectors are of 35 mm diameter, and they are arranged as presented in *Figure 1, left*. Tubes of this diameter have a characteristic shear capacity of 96 kN per tube and per shear plane (Leijten, 1998).

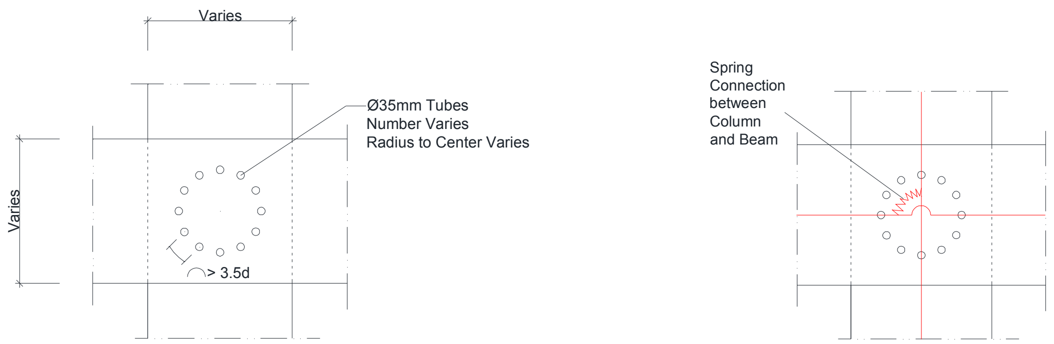

***Figure 1**: Typical layout of a beam-column joint with expanded tube fasteners (left) and numerical schematization of the connection (right).*

The numerical layout of this joint, where both beam and column are modelled as continuous through the connection is displayed in *Figure 1, right.* A global rotational spring with non-linear behaviour connects the beam and column elements. This global spring can then be calibrated on the results of experimental tests carried out on the connection, or obtained from the properties of the single connectors.

Based on the Italian Regulation NTC, different design spectra have to be considered for the ultimate and serviceability limit state design. A linear elastic analysis in accordance with the NTC has been carried out to design the frames, adopting a q-factor of 4 as suggested by Leijten. The chosen building site in Sant'Angelo dei Lombardi is characterized by a Peak Ground Acceleration a_g of 0.266g and by the parameters listed in *Table 1*, where F_0 = spectral amplification factor, S = Ground Type, V_N = reference Period, T_C*= factor depending on the ground type needed for the initial period.

***Table 1**: Values used to calculate the elastic spectrum on the base of NTC definition*

a_g [g]	F_0	T_C* [s]	S	V_N [$years$]
0.266	2.285	0.376	B	50

All required design verifications based on the Italian NTC and the Eurocode 5 were fulfilled. The layouts of the frames including span and inter-story heights are presented in *Figure 2*. Cross sectional dimensions and number of the tube connectors are summarized in *Table 2*, together with the governing limit state for each structural member.

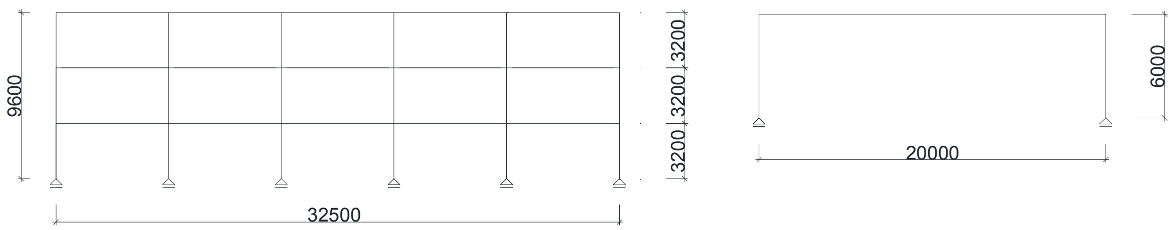

***Figure 2**: Layout of frames analyzed (dimensions in mm)*

***Table 2**: Summary of cross sectional dimensions, connection layout, and governing limit states*

Frame	Cross Sectional dimensions				Design of Joint		Governing design criteria		
No. Storeys × No. Bays	Single Column		Double Beam		No. of Tubes	R to Center	Column	Beam	Joint
	Width	Depth	Width	Depth					
3 x 5	240	655	2 x 100	655	8	275	U-E/U-W	U-E	U-E
1 x 1	300	800	2 x 120	900	10	347,5	U-E	S-S	U-S

Dimensions are in mm, the abbreviations stand for: U = ultimate limit state, S = serviceability limit state, E = seismic action, W = wind action, S = snow

3. Numerical model

3.1 Cyclic joint behaviour

To analyse the different frames under non-linear static and dynamic loads, the hysteretic behaviour of a joint with tube connectors under cyclic load has to be known, including parameters such as strength and stiffness degradation. Quasi static cyclic tests on connections with 28 mm and 18 mm diameter tubes were performed by Leijten et al. (2006) and the test results made available to the authors.

Since 35 mm diameter tubes were used for designs of the connections in both portal and multi-storey frames, the available test results had to be extrapolated to obtain the behaviour of a connection with 35 mm diameter tubes. To justify the extrapolation of the experimental data, the experimental values of the equivalent viscous damping ratio *v* of 18 and 28 mm diameter tubes were compared to each other. A difference of only 5% between the two values (30% for the 18 mm tube and 35% for the 28 mm tube) was found (Leijten et al., 2006), thus justifying the possibility to extrapolate experimental data to connectors of different diameters. The used extrapolation process is described in detail in Wrzesniak et al. (2013).

3.2 Model Calibration

Based on the cyclic moment-rotation curves obtained by the extrapolation of available experimental results, the properties of the rotational spring schematizing the connection were determined by fitting a previously developed hysteretic rule on the curves. The adopted hysteretic rule was developed by Rinaldin et al. (2013) and consists of a tri-linear backbone curve, loading and downloading curves with allowance for pinching effect, and strength and stiffness degradation (*Figure 3, left*). The best-fit approximating curve was found by using purposely developed software (Rinaldin 2011), which automatically alters the parameters of the backbone curve until the difference of the total energy values between the available input data and the approximating curve is less than 0.24%. A superposition of the input data (red, thin line) for the beam-column connection and the calibrated hysteretic approximating cycles (black, thick line) of the beam-column connection used in the 3-storey, 5-bay frame is presented in *Figure 3, right.*

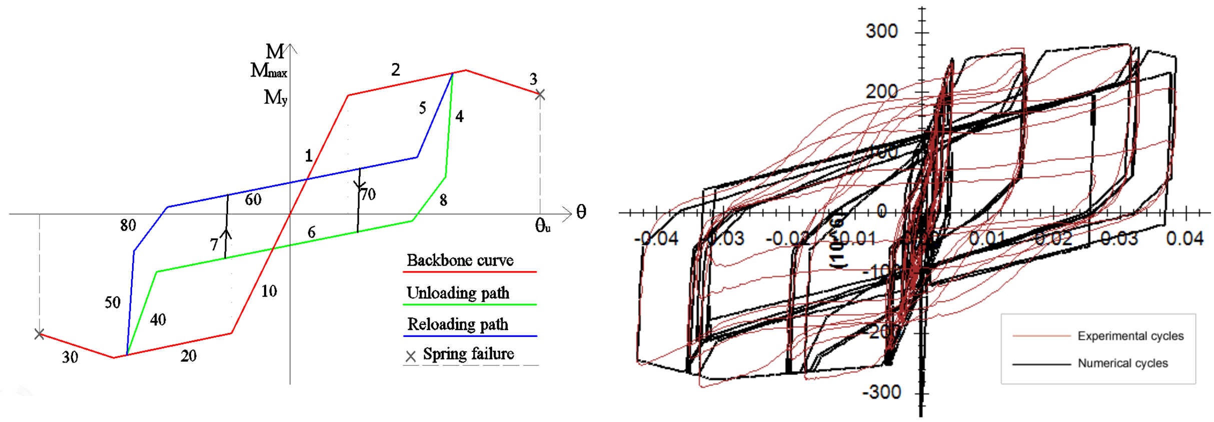

***Figure 3**: Hysteretic model adopted in the analyses (left) and superposition of data input and calibrated approximating curves for the beam-column connection with eight 35 mm diameter tube fasteners used in the 3-storey, 5-bay frame (right).*

The graph represents the moment rotation relationship with values measured in Nmm and rad, respectively. Elastic stiffness, yield force, and first inelastic stiffness which are calibrated in accordance with EN 12512 (2003) are then returned as output values. In addition, the peak and ultimate moment are provided as output assuming that the latter at the ultimate rotation is 80% of the peak moment.

The frames have then been modeled in Abaqus. The beam-column connections have been modeled as non-linear rotational springs as shown in *Figure 1, right*. The adopted hysteretic rule was implemented in Abaqus as an external subroutine. The beam and column elements were modeled with beam elements with linear elastic behaviour.

4. q-factor evaluation

The behaviour factor q was introduced to account for "…the capacity of the structure to dissipate energy, through mainly ductile behaviour of its elements and/or other mechanisms.." (EC8, 3.2.2.5). The q-factor allows the designer to carry out an elastic analysis, but taking into account the energy dissipation occurring in the structure. In the case of timber structures, most energy dissipation occurs in the metal fasteners or other connecting elements that are able to deform plastically and therefore dissipate energy, which results in a decreased seismic input energy in the structure.

The more appropriate method to evaluate the q-factor of a structural system is by using a non-linear dynamic approach. An incremental dynamic analysis (IDA) is carried out, where the structural system is analysed under a set of different accelerograms. The intensity of the accelerograms is incrementally increased until a certain limit state (for example a maximum rotation in the joint) is attained. The procedure followed in this paper to evaluate the q-factor of the frames is described herein after.

4.1 Background information

To evaluate the q-factor through an incremental dynamic analysis, two approaches can be applied: one is based on the evaluation of the base shear, whilst the other is based on the peak ground acceleration.

In the base shear approach, the sum of the base shear reactions when the frame responds elastically (V_{el}) is compared to the sum of the base shear reactions when the frame response is non-linear and a certain ultimate limit state is attained (V_{pl}):

$$q = \frac{V_{el}}{V_{pl}} \qquad \text{Eq.1}$$

Elastic and non-linear behaviour of the frame are controlled through the input parameters of the springs, which are the only non-linear elements in the model of the frame. To achieve a fully elastic response, the yield, maximum and ultimate moment and the rotation limits of the rotational springs are set to very large values to avoid any plasticization. For the base reactions of the frame in non-linear conditions, the actual spring parameters are used.

For the q-factor evaluation based on the peak ground acceleration, the value of the PGA which causes the attainment of a certain ultimate limit state, PGA_{inel}, is compared to the PGA of the structure at the attainment of the yielding point, PGA_{el}. In the analyses, the yielding point of the system has been assumed to be attained once the yielding point of the first rotational spring is reached:

$$q = \frac{PGA_{inel}}{PGA_{el}} \qquad \text{Eq.2}$$

Since the q-factor was found to depend upon the limit state considered, four limit states have been considered:

1) Occupancy Limit State (OLS):	when 2/3 of yielding rotation is attained in the first spring;
2) Damage Limit State (DLS):	when the yield rotation is attained in the first spring;
3) Life Safety Limit State (LLS):	when ¾ of the rotation at CLS (which is 25.5 mrad for the 3-storey, 5-bay frame and 21 mrad for the portal frame) is attained;
4) Near Collapse Limit State (CLS):	when the ultimate rotation as defined in Section 3.2 (which is 34 mrad for the 3-storey, 5-bay frame and 28 mrad for the portal frame) is attained.

Whilst the rotational limits for OLS and DLS are based on the yielding points of the connection, the rotational limits for CLS and LLS are based on experimental results: the ultimate rotation is taken at the point in which 15% of the maximum resistance is lost, and the LLS limit is 3/4 of that.

4.2 IDA – Results and discussion

To characterize the seismic response of the analysed frames, two pushover analyses have been performed for each structural system: one with a uniformly distributed load pattern which is proportional to the story masses, and a second one with a lateral load pattern proportional to the first mode eigenvector. The results of the pushover analysis of each frame are presented in *Figure 4*.

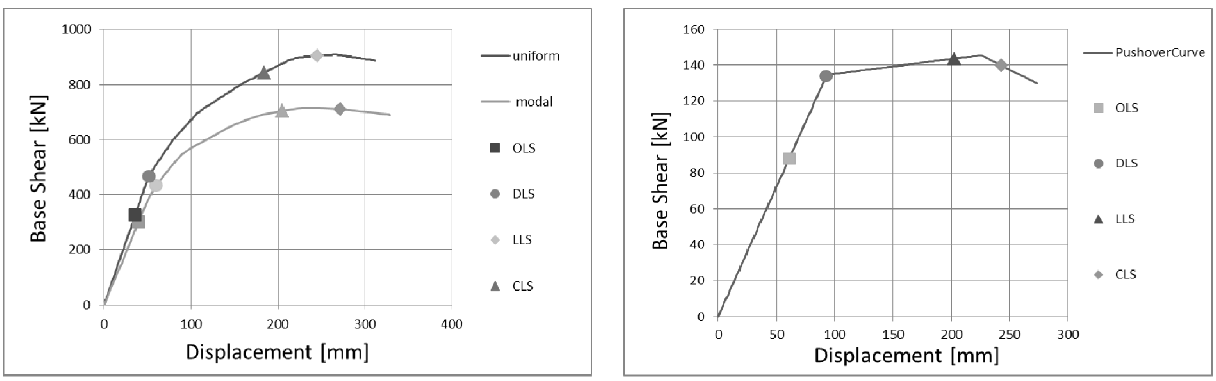

Figure 4: *Pushover curves based on uniform and modal load pattern; Left Graph: 3x5 Frame, Right Graph: Portal Frame.*

The top curve indicates the pushover results based on a uniform distribution of the forces whereas the bottom curve shows the results based on the modal distribution of the forces. Also highlighted are the points which are representative of the different limit states in the following order starting from left: OLS, DLS, LLS and CLS. Since the joint rotation corresponding to every Limit State has been previously defined, the four Limit States in the pushover curve can be detected as the points in which one spring (or more springs simultaneously) attains the rotation limits previously set.

In the next step, non-linear dynamic analyses have been carried out. Seven different accelerograms have been generated with the software SIMQKE (Gelfi 2012). The council of Sant'Angelo dei Lombardi, Campania (Italy) has been taken as the reference site. To obtain representative results it is important to choose a large variety of accelerograms since the response of a structure is not only dependent upon the intensity of an accelerograms but also on its properties such as frequency content and duration (Ceccotti and Karacabeyli 1998). The accelerograms have been generated accordingly to the Italian NTC recommendations.

The objective of an IDA is to find the PGA of an accelerogram which causes the attainment of the reference rotations at different limit states in the first spring or group of springs. This has been done by incrementally increasing the intensity of the generated accelerograms. Once the PGA value is found, the corresponding maximum base shear reaction at that limit state is recorded. Both base shear and PGA's are then used to evaluate the q-factor as described in Eqs. 1 and 2. This procedure was repeated for each frame and each type of generated earthquake ground motion.

Figures 5 and *6* plot the q-factors of each frame and each generated earthquake ground motion versus the PGA, based on the PGA (Eq. 2) and base shear (Eq. 1) approach, respectively. For every curve, the q-factors corresponding to the attainment of the different limit states are also highlighted. A summary of the q-factors based on the different approaches for the different structural systems is presented in *Table 3*.

The plots show a significant scatter of the behaviour factor depending on the type of generated earthquake ground motions. For example, the q-factor at CLS ranges from 2.3 to 4.0 for the multi-storey frame if the base shear approach is followed. This observation was also made by other researchers (Ceccotti and Vignoli 1988, 1990). Therefore, it is suggested to use a large variety of accelerograms to obtain representative values of the q-factor.

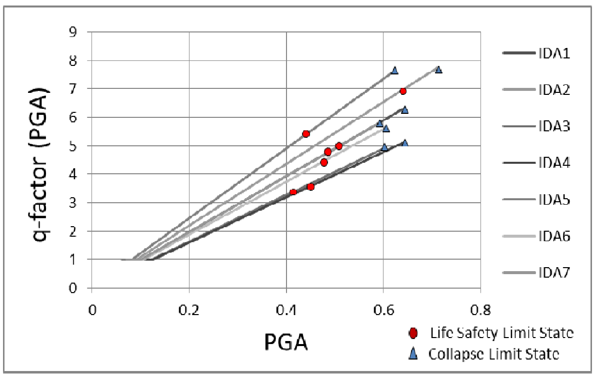

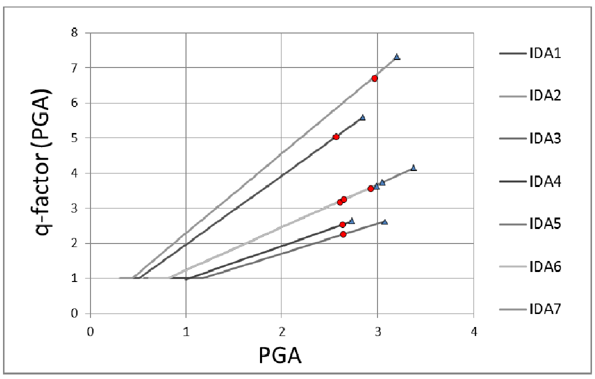

Figure 5*: Behaviour factor q in dependency of the PGA, evaluated based on the peak ground acceleration approach, for different generated earthquake ground motions. Left Graph: 3x5 Frame, Right Graph: 1x1 Frame.*

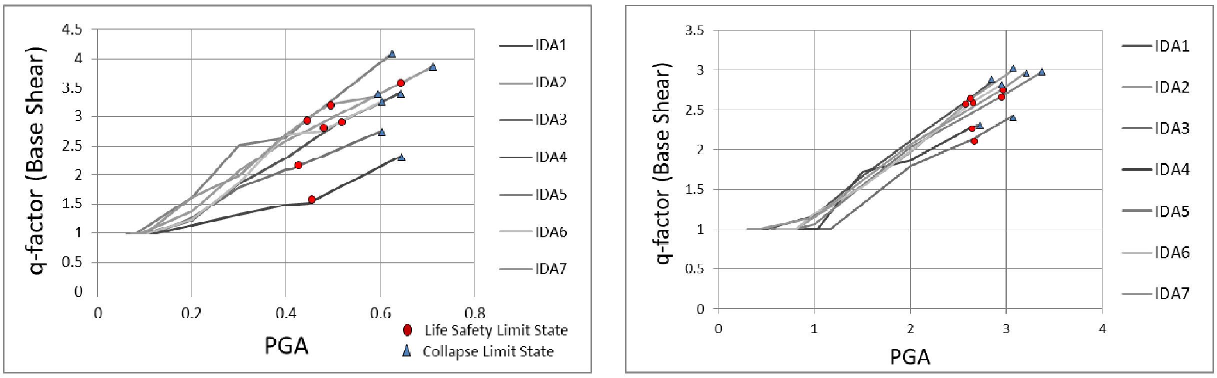

***Figure 6**: Behaviour factor q in dependency of the PGA, evaluated based on the base shear approach, for different generated earthquake ground motions. Left Graph: 3x5 Frame, Right Graph: 1x1 Frame.*

***Table 3**: Summary of q-factor values for different systems computed using the two different approaches*

q-factor value	3-storey, 5-bay frame (Joint ductility μ = 7.49)		Portal Frame (Joint ductility μ = 7.91)	
	Average	Minimum	Average	Minimum
q_{PGA}	6.16	4.23	4.23	2.60
q_V	3.29	2.32	2.76	2.31

In addition to that, there is a strong dependency of the q-factor on the PGA, with values ranging from 1 to 4 for the multi-storey frame and the base shear approach when the limit state changes from OLS to CLS. However in the current version of the Eurocode 8 only one value for the q-factor is provided irrespective of the type of limit state (near collapse or life safety).

The approach followed to calculate the q-factor has also an important influence on the results, with the PGA leading to higher and more scattered values compared to the base shear approach. The analysis based on the base shear values gives more conservative values for the q-factor.

The type of structural systems has also been found to affect quite significantly the value of the q-factor. The values for the portal frame compared to the multi-storey moment resisting frame are significantly lower. This can be explained by the higher hyperstaticity which allows the formation of more plastic hinges and, hence, higher energy dissipation.

Based on the results of the numerical analyses, the values of the q-factor recommended for the design of hyperstatic portal frames and multi-storey moment resisting frame with high ductility expanded tube connections are 2.5 and 3, respectively. These values have been calculated by slightly reducing the average of the q-factors at near collapse limit state obtained considering the different recorded earthquake ground motions.

According to Eurocode 8, for a high ductility class H, the connection has to be able to deform plastically for at least three fully reversed cycles at a static ductility ratio of at least 6. This means that the connection has to be able to perform three fully reversed cycles at no less than six times their yield displacement. In addition the decrease in strength has to be less than 20%. These conditions were found to be fulfilled by Cruz and Ceccotti (1996) who performed quasi static tests on this type of expanded tube connections. If this condition is fulfilled, a q-factor of 4 can be used for hyperstatic portal frames according to Eurocode 8. Otherwise, if the static ductility ratio is lower than 6 but greater than or equal to 4, the behaviour factor should be reduced to 2.5. In order to check the validity of this relationship between ductility at the beam-column connection and the q-factor, analyses have been carried out for the two analyzed structural systems by varying the static ductility of the joint μ. Obtained values of the behaviour factor have then been plotted versus the static ductility of the joint (*Figure 7*), defined as the ratio of the hypothesized ultimate rotation θ_{ult} over the yield rotation θ_{yield}. The results of all analyses are displayed in *Figure 7*.

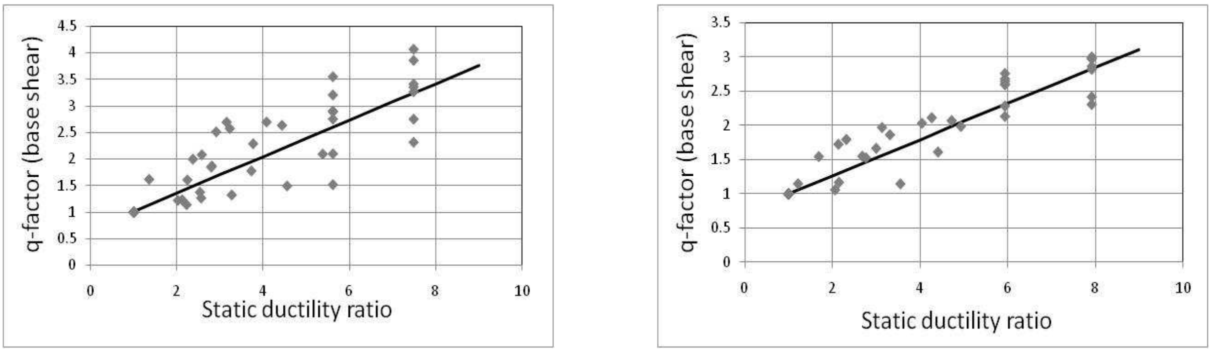

***Figure** 7: q-factor versus static ductility of joint based on the base shear approach, and their linear regression law; Left Graph: 3x5 Frame, Right Graph: 1x1 Frame.*

The plots above also display a linear regression curve obtained on the data collected, which represents the relationship between the behaviour factor q and the maximum static ductility if the joint μ during the seismic analysis. For the portal frames, the regression is expressed by:

$q = 0.263\mu + 0.737$ Eq.3

and for the 3-storey, 5-bay frame by:

$q = 0.3448\mu + 0.656$ Eq.4

The results show that the behaviour factor q is significantly lower than the static ductility of the joint μ. The suggestions made by Eurocode 8 to apply a q-factor of 4 for hyperstatic portal frames when the static ductility ratio of 6 is reached was found to be not applicable for this type of structure using the expanded tube connectors. On the contrary, based on the analyses results, for a joint ductility ratio of at least 6 and 4, q-factors of respectively 2 and 1.5 are suggested for the portal frame, while the recommended q-factor values are 2.5 and 2 for the 3-storey, 5-bay frame. These values are markedly different from the ones currently suggested in the Eurocode 8.

5. Conclusions

The behavior factor q describes the ability of a structure to dissipate energy through plasticization, which mainly occurs in the connection regions of timber systems. A high q-factor is desirable since the seismic forces in a structure will be significantly reduced. In order to ensure plasticization of the fasteners, the timber members have to be either overdesigned or reinforced. The excellent ductile behavior of the expanded tube fasteners and the high strength of the densified veneer wood which acts reinforcing the timber members, make this connection a suitable solution for structures in seismic areas. This is the reason why an investigation on the q-factor of timber systems using this type of connection was undertaken and is presented in this paper.

A non-linear dynamic approach was used to determine the q-factor. Two different frames, a hyperstatic portal frame and a three-storey, five-bay moment resisting frame, were analyzed using a set of seven different generated accelerograms. The cyclic behaviour of the connection was approximated using an advanced numerical model that can account for hysteretic behaviour with pinching effect, post-peak softening, and strength and stiffness degradation. The primary conclusions are reported herein after.

- A notable scatter of q-factor values was obtained when different spectrum-compatible generated earthquake ground motions were used. This supports the evidence that several accelerograms have to be used to obtain representative values.
- The values of the q-factor varied significantly when the Peak Ground Acceleration (PGA), the type of approach used to calculate the q-factor (the use of the PGA or the use of the base shear values), and the type of structural system was changed.
- The value of 4 recommended for the q-factor of hyperstatic portal frames with beam-column connections made of expanded tube fasteners was found too high. A conservative value of 2.5 can be proposed for this type of structural system, whilst an increase to 3 can be suggested for multi-storey moment resisting joints with the same type of connection.
- A simple relationship between static ductility of the joint and behavior factor has been proposed for hyperstatic portal frames and multi storey timber frames based on the data resulting from the numerical analyses.
- At a static ductility of at least 6, a conservative value of the q-factor of 2.5 and 2.0 can be recommended, for multi-storey moment resisting frames and hyperstatic portal frames respectively. If the static ductility of the joint reduces to 4, the recommended values of the q-factors should be decreased by 0.5 in both cases.

Further experimental tests are necessary to provide a solid and robust verification of the preliminary results discussed above. Additional numerical analyses will be carried out on a different, taller moment resisting frame with expanded tube fasteners, and on moment-resisting frames with different types of beam-column connection to find whether a conservative relationship between the q-factor and the joint ductility can be found and proposed for the new revision of the Eurocode 8, as the current relationship seems non-conservative.

Acknowledgements

The authors would like to thank Adrian Lejten from the Technical University of Eindhoven who provided the information and laboratory results which were needed to carry out the numerical analysis. His kind support and technical advice are very much appreciated.

References

Buchanan A., Deam B., Fragiacomo M., Pampanin S., Palermo A., 2008. Multi-storey prestressed timber buildings in New Zealand, IABSE Structural Engineering International, 2, 166-173.

Ceccotti A., Karacabeyli E., 1998. Seismic performance of moment resisting timber frames, World Conference on Timber Engineering, Lausanne, Switzerland.

Ceccotti A., Vignoli A., 1988. The effects of seismic events on the behaviour of semirigid-joint timber structures: A simulation of the influence of structural scheme and of joint characteristic, International Conference on Timber Engineering, Seattle, USA.

Ceccotti A., Vignoli A., 1990. On a better evaluation of the seismic behaviour factor of low dissipative timber structures, CIB Working Commission W18, Lisbon, Portugal.

Ceccotti A., 1996. Earthquake resistance of timber frame building systems, Cost Action E5 Meeting, Stuttgart, Germany.

Cruz H., Ceccotti A., 1996. Cyclic tests of DVW reinforced joints and portal frames with expanded tubes, International Timber Engineering Conference, New Orleans, USA.

Eurocode 8, 2005. Design of structures for earthquake resistance - Part 1, General rules, seismic actions and rules for buildings. EN 1998-1:2005.

EN 12512 – Timber structures - Test methods – Cyclic testing of joints made with mechanical fasteners, 2003.

Fragiacomo M., Batchelar M., 2012. Timber frame moment joints with glued-in steel rods. I: Design, ASCE Journal of Structural Engineering, 138(6), 789-801.

Gelfi P., 2012. SIMQKE_GR, version 2.7, University of Brescia website, http://dicata.ing.unibs.it/gelfi/, Italy.

Leijten A.J.M., 1998. Densified veneer wood reinforced timber connections with expanded tube fasteners, Doctoral Thesis, Delft University Press, the Netherlands.

Leijten A.J.M., Ruxton S., Prion H., and Lam F., 2006. Reversed-cyclic behavior of a novel heavy timber tube connection, ASCE Journal of Structural Engineering, **132(**8), 1314-1319.

NTC - Norme Tecniche per le Costruzioni (Italian National Regulation for Cosntruction), 2008. Decree of the Ministry of Infrastructures and Transportations.

Rinaldin G., 2011. So.ph.i. software version 4, http://giovanni.rinaldin.org/.

Rinaldin G., Amadio C., Fragiacomo M., 2013. A component approach for the hysteretic behaviour of connections in cross-laminated wooden structures, Earthquake Engineering and Structural Dynamics, printed online, DOI: 10.1002/eqe.2310.

Sartori T., Casagrande D., Tomasi R., Piazza M., 2012. Shake table test on 3-storey light-frame timber building, World Conference of Timber Engineering WCTE2012, Auckland, New Zealand.

Tomasi R., Zandonini R., Piazza M., Andreolli M., 2008. Ductile end connections for glulam beams, IABSE Structural Engineering International, 18(3), 290-296.

Van de Lindt J.W., Pei S., Pryor S. E., Shimizu H., Isoda H., 2010. Experimental seismic response of a full-scale six-story light-frame wood building, ASCE Journal of Structural Engineering, 136(10), 1262-1272.

Wrzesniak D., Rinaldin G., Fragiacomo M., Amadio C., 2013. Non-linear cyclic modelling of moment-resisting timber frames, Italian National Association of Earthquake Engineering ANIDIS - Conference, Padova, Italy.

INTERNATIONAL COUNCIL FOR RESEARCH AND INNOVATION IN BUILDING AND CONSTRUCTION

WORKING COMMISSION W18 - TIMBER STRUCTURES

WIND TUNNEL TESTS FOR WOOD STRUCTURAL PANELS USED AS NAILABLE SHEATHING

B Yeh

A Cope

E Keith

APA – The Engineered Wood Association

U.S.A.

Keywords: wood structural panels, nailable sheathing, wood siding, wind tunnel tests, critical wind angles

Presented by BJ Yeh

H Blass received confirmation that no foam was used as outer thermal insulation of the building. He commented that if foam was used nails would have to bridge and question whether the nails would then have to carry vertical loads also. BJ Yeh responded that these could be next stages of the research. For example, heavier siding could be considered which might be able to resist higher wind loads. H Blass stated calculation model for laterally loaded dowel-type fasteners with interlayer was available. Also heavier cladding could impose a higher vertical load.

S Winter received clarification that smooth shanked instead of ring shanked nails were used. S Winter stated nailing through OSB normally causes break out on the other side of OSB and discussed possible increase of capacity with other types of fasteners. BJ Yeh agreed that other types of fasteners could achieve higher capacity; however, contractors do not like screw guns and screw shank nails and prefer using normal nail guns.

J Munch Andersen commented that the wind pressure between the inside and outside of the siding would be different and whether such issues were considered. BJ Yeh agreed that this was an interesting point. They have information based on pressure tape but information was not reported here.

A Ceccotti asked how much was the test cost. BJ Yeh responded the test cost ~US$20k for two walls. The project was a collaborative effort, so there was a discount. A Ceccotti asked what height could be reached in the test facility. BJ Yeh responded 18 m ~ 3 stories.

S Aicher asked whether loosening of the nail was considered as a result of reversed cyclic loads. BJ Yeh stated that this issue was considered and therefore rigid siding rather than more flexible vinyl siding was used.

U Hübner commented that dynamic loading on smooth shank nails would be more realistic. BJ Yeh explained that the applied wind load was not constant as turbulences were created and wind direction of 20 degree was found to be most critical.

Wind Tunnel Tests for Wood Structural Panels Used as Nailable Sheathing

Borjen Yeh, Ph.D., P.E.
APA – The Engineered Wood Association, U.S.A.
Anne Cope, Ph.D., P.E.
Insurance Institute for Business & Home Safety, U.S.A.
Ed Keith, P.E.
APA – The Engineered Wood Association, U.S.A.

Abstract

Wood structural panels, defined as plywood and oriented strand board (OSB), have been occasionally used as a nail-base in light-frame wood construction. The demand for improved energy conservation in the building construction recently has promoted the construction of the so-called "advanced framing", which requires the stud spacing be increased from the typical 406 mm (16 in.) on center to 610 mm (24 in.) on center to align with the roof trusses or framing. In some climate zones, foam plastic insulation of 25 to 51 mm (1 to 2 in.) is installed outside of the wood structural panel sheathing (i.e., between wood structural panels and exterior wall cladding) to provide the needed thermal insulation required by the energy conservation code, which makes the installation of exterior wall cladding challenging due to the difficulties in accurately hitting the studs with nails that are required to be longer than typical. As a result, there is an interest by the construction industry to use wood structural panels as nailable sheathing, which can serve as the nail-base to facilitate the installation of exterior wall cladding at wider stud spacing without the concern on missing nails into wood studs when installing exterior wall cladding.

APA – The Engineered Wood Association has undertaken a series of studies to investigate the use of wood structural panels as nailable sheathing for lap siding, which includes an engineering analysis using single nail withdrawal capacity from wood studs and nailhead pull through capacity from the lap siding. However, due to the small thickness of the wood structural panel sheathing, there is a concern whether the single-nail withdrawal capacity could accurately predict the performance of walls subject to dynamic wind forces. To confirm the engineering calculation under wind dynamics, APA sponsored a study at the Insurance Institute for Business & Home Safety (IBHS) Research Center in South Carolina in September 2012 to provide full-scale wind tunnel test results. This paper describes the test details and results obtained from the study.

1. Introduction

In the wall applications, light-frame wood buildings in North America are typically sheathed with wood structural panels that are directly attached to wood studs with nails. By definition of the U.S. building codes, the term of wood structural panels is referred to plywood and oriented strand board (OSB). The exterior wall cladding, such as wood lap siding or vinyl siding, is then attached to wood studs over water-resistive barriers and wood structural panels. Rarely is the exterior wall cladding attached directly to wood structural panels as a nail-base, or so called "nailable sheathing" even though such practice exists in attaching roof shingles to roof sheathing and is permitted for wall applications in the U.S. building codes.

In recent years, the demand for improved energy conservation in the building construction has promoted the construction of light-frame wood construction with the so-called "advanced framing", which requires the stud spacing be increased from the typical 406 mm (16 in.) on center to 610 mm (24 in.) on center to align with the roof trusses or framing. In some climate zones, foam plastic insulation of 25 to 51 mm (1 to 2 in.) is installed outside of the wood structural panel sheathing (i.e., between wood structural panels and exterior wall cladding) to provide the needed thermal insulation required by the energy conservation code, which makes the installation of exterior wall cladding challenging due to the difficulties in accurately hitting the studs with nails that are required to be longer than typical. As a result, there is an interest by the construction industry to use wood structural panels as nailable sheathing, which can serve as the nail-base to facilitate the installation of exterior wall cladding at wider stud spacing without the concern on missing nails into wood studs when installing exterior wall cladding.

APA – The Engineered Wood Association has undertaken a series of studies to investigate the use of wood structural panels as nailable sheathing for lap siding, which includes an engineering analysis using single nail withdrawal capacity from wood studs and nailhead pull through capacity from the lap siding. However, due to the small thickness of the wood structural panel sheathing, there was a concern whether the single-fastener withdrawal capacity could accurately predict the performance of walls subject to dynamic wind forces. To confirm the engineering calculation under wind dynamics, APA sponsored a study at the Insurance Institute for Business & Home Safety (IBHS) Research Center in South Carolina in September 2012 to provide full-scale wind tunnel test results. This paper describes the test details and results obtained from the study.

2. Objectives

The main objectives of this study were to compare the engineering calculation with wind-tunnel test results when wood structural panels are used as nailable sheathing under wind loads at critical angles. Both the ultimate load and allowable load designs were to be examined.

3. Methods and Materials

3.1 Wind Tunnel Test Facility

The IBHS is a non-profit organization, which is wholly supported by the property insurance industry to conduct scientific research for identifying and promoting effective actions that strengthen homes, businesses, and communities against natural disasters and other causes of loss. The Research Center is a state-of-the-art, multi-hazard applied research and training facility in Richburg, South Carolina. The core facility at the center is a specially-designed open-jet wind tunnel, as shown in Figure 1, with an exceptionally large test chamber of 44 m (145 ft) wide by 44 m (145 ft) long with a clear interior height of 18 m (60 ft). The test chamber is large enough to subject full-scale, one- or two-story structures to a variety of wind-related or wind-influenced natural perils.

Figure 1. IBHS wind tunnel test facility

The unique wind flow capabilities inside the large test chamber are produced by 105 vane-axial fans. These 1.7 m (5.5 ft) diameter fans with 260 kW (350 hp) medium voltage electric motors push air through a 15-tube contraction structure. The flow through each tube in the structure is independently controlled using Rockwell medium voltage variable frequency drives, with active front-ends that allow precise control of acceleration and deceleration of the fans and hence the flow. The fans and controls are designed to allow simulation of gross flow characteristics of a variety of wind events including Category 1, 2 and 3 hurricanes, extra-tropical windstorms, and thunderstorm frontal winds. An illustration of a typical one-story structure in the test chamber identifying the location of the reference anemometer in relation to the fans, test structure on the turntable, and the direction of wind flow in the chamber is provided in Figure 2.

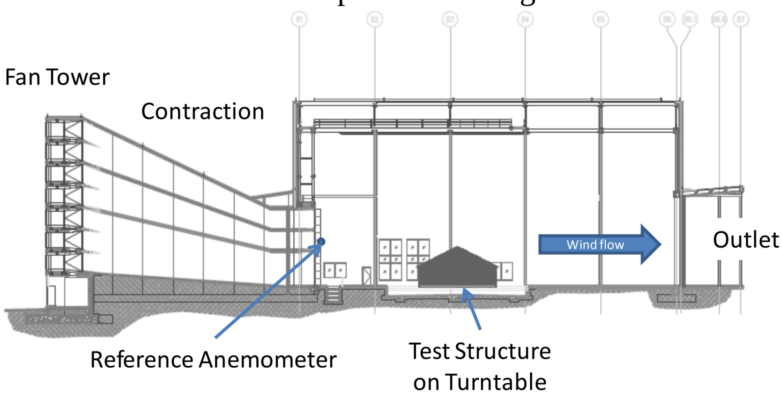

Figure 2. Elevation view of typical structure in test chamber; showing relative location of fans, contraction, outlet, and reference anemometer

Wind conditions for the testing conducted in this study consisted of a mean wind speed profile and turbulence characteristics profile typical of open country terrain, defined as Exposure C in ASCE 7-10 [1]. Validation of the Research Center's capability to replicate surface wind pressures on typical structures was accomplished by testing a replica of the Texas Tech Wind Engineering Research Field Laboratory building. Results of these validation studies are provided in Morrison, et al. [2].

3.2 Building Layout and Design

The test building consisted of a single-story steel foundation frame to which wall sections and a roof were attached. The roof on the test building had a 6 on 12 pitch with one gable end and one hip end. The structure was 9.1 m (30 ft) wide by 12.2 m (40 ft) long, with an additional 305 mm (1 ft) overhang on the roof. The mean roof height was 5.2 m (17 ft). Eight different wall assemblies were constructed for concurrent test programs, as shown in Figure 3. Two of the eight wall segments, i.e., Walls 5 and 6, were selected for this study.

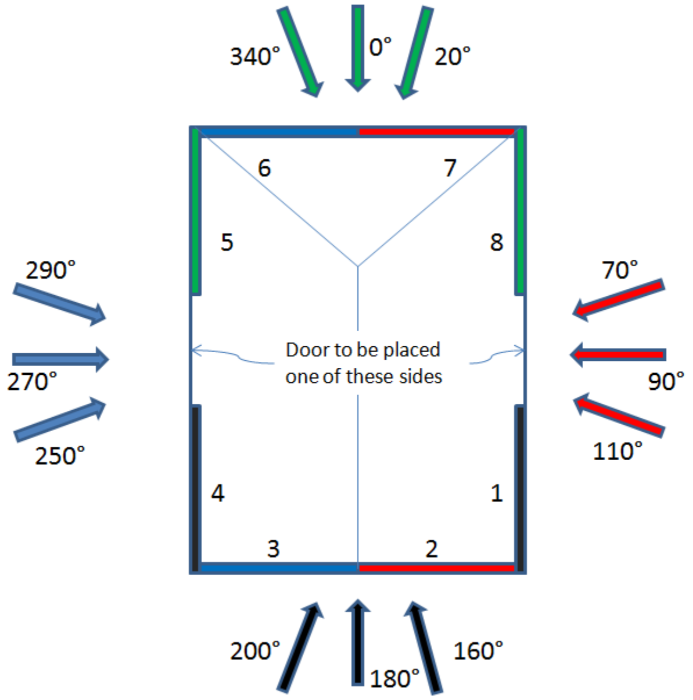

Figure 3. Sketch of wind angles and test wall locations

Based on previous wall pressure studies using this same frame and roof structure, IBHS researchers identified critical angles for each wall section as the wind direction parallel to the wall and 20 degrees from parallel. In the earlier studies, there was no discernible difference in external pressures or net loads across wall segments adjacent to the hip end versus the gable end. The location of the eight walls and critical wind angles are shown in Figure 3, where the wind directions in green are the most critical for Walls 5 and 8, and the wind directions in light blue are the most critical for Walls 3 and 6. As mentioned earlier, the walls used for this study were Walls 5 and 6. Hard stops were installed between Walls 4 and 5 on the side wall and between Walls 6 and 7 on the hip end wall to separate these configurations.

Wall 5 was used to evaluate the ultimate load capacities, i.e., the wall was designed to fail at a peak wind speed of 47 m/s (105 mph) in the wind tunnel, while Wall 6 was designed to sustain the same peak wind speed without failure by adjusting the nail spacing with a factor of safety. The peak wind speed of 47 m/s (105 mph) was selected as it is close to the 49 m/s (110 mph) covered in the U.S. residential code and based on the limitations of other materials used for the same building in the test plan. This wind speed is expected to impose a wind load of 1.8 kPa (37 psf) in Exposure C conditions (open terrain with scattered obstructions) based on the U.S. code.

Smooth-shank nails with 7.5 mm (0.297 in.) head diameter, 2.9 mm (0.113 in.) shank diameter, and 63.5 mm (2-1/2 in.) long were selected in conjunction with 2x4 (38 mm x 89 mm) Spruce-Pine-Fir studs spaced at 406 mm (16 in.) on center and 11 mm (7/16 in.) thick 1220 mm x 2440 mm (4 ft x 8 ft) OSB sheathing. The wall cladding was constructed with commercially available non-veneer lap siding of 11 mm (7/16 in.) thick, 203 mm (8 in.) wide, and 4.9 m (16 ft) long. The lap siding is overlapped with the next siding of 28.6 mm (1.125 in.). A house wrap was used as the water resistive barrier applied over the OSB sheathing. Commercially available R-13 unfaced fiber glass batt insulations were installed in the wall cavities between studs. Gypsum wall boards of 13 mm (1/2 in.) in thickness were installed in the interior of the building with seams taped and mudded. Figure 4 shows the wall-to-roof construction details.

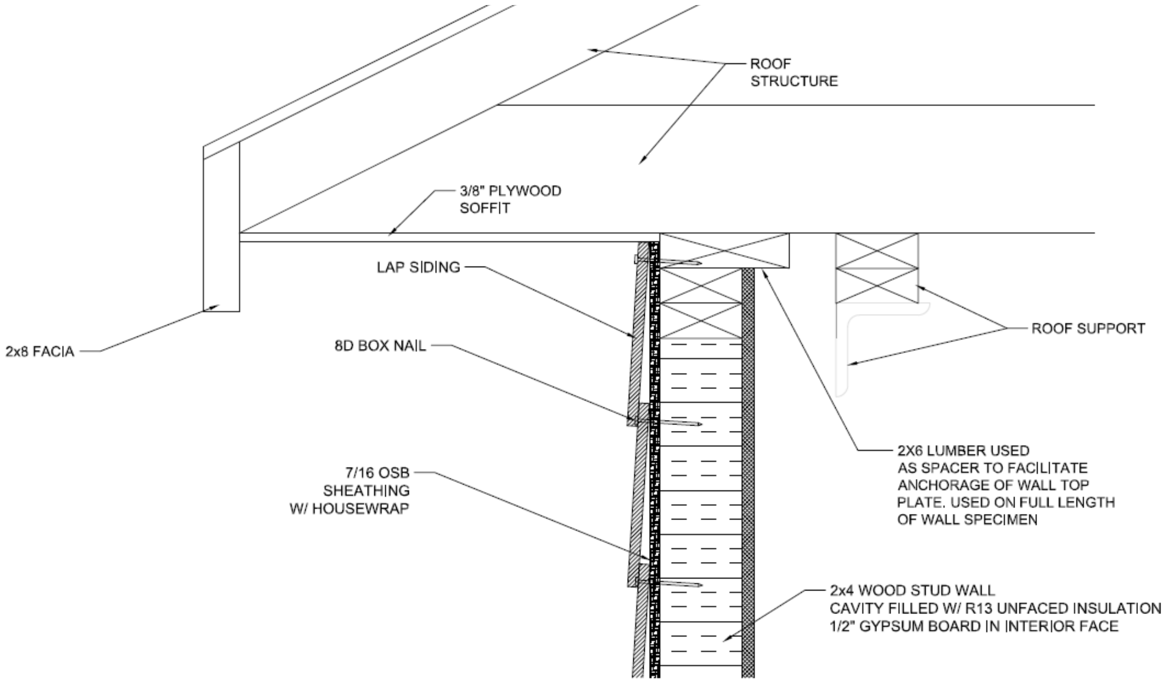

Figure 4. Wall-to-roof construction details (1 in. = 25.4 mm)

3.3 Nailing Spacing and Installation

For the experimental design, the engineering calculation for single nail withdrawal capacity under wind load was performed based on American Wood Council's National Design Specification for Wood Construction (NDS) [3]. According to APA Panel Design Specification (PDS) [4, 5], the "equivalent specific gravity" for wood structural panels is 0.40 for the purpose of determining the nail withdrawal resistance, which results in the average nail withdrawal capacity of about 246 N (55 lbf) when adjusting the published allowable nail withdrawal resistance in the NDS by a factor of 5 for 11 mm (7/16 in.) thick OSB sheathing under wind load duration (the load duration factor is 1.6 in accordance with the NDS). However, to ensure Wall 5 would fail at the expected peak wind speed of 47 m/s (105 mph), the experimental design took the upper bound of the equivalent specific gravity" for wood structural panels at 0.50, which resulted in the average nail withdrawal capacity of about 430 N (96 lbf).

This nail withdrawal capacity is substantially lower than the nailhead pull through capacities of the lap siding, as determined in accordance with ASTM D1037 [6] and published in APA Technical Topics TT-070, *Nailhead Pull-Through Strength of Wood Structural Panels* [7]. It is also lower than the lap siding bending and shear strength at the expected maximum nail spacing of 838 mm (33 in.). Therefore, this nail withdrawal capacity was used as the basis for the design of nailing schedules for Walls 5 and 6. For Wall 5, which was intended to fail at the peak wind speed of 47 m/s (105 mph), the calculated nail spacing was 838 mm (33 in.). For Wall 6, which was designed to sustain the same peak wind speed with a factor of safety, the calculated nail spacing was 254 mm (10 in.). In a simplistic way, this means that there is a factor of safety of 3.3 for Wall 5, as compared to the ultimate capacity from Wall 6.

The exposed height of the siding is 175 mm (6.875 in.) for both Walls 5 and 6. For Wall 6, the nail spacing of 254 mm (10 in.) on center results in a tributary area for each nail of 0.045 m^2 (0.48 ft^2). For Wall 5, the nail spacing of 838 mm (33 in.) on center for expected nail withdrawal failure results in a tributary area for each fastener of 0.15 m^2 (1.58 ft^2).

Figure 5 shows the installation details of the walls. Note that all nails for the lap siding were designed to directly attach to the OSB sheathing by intentionally missing the lumber studs except for the starter nails from each end of every lap siding run. The end joints of the lap siding were butted and staggered between lap siding runs.

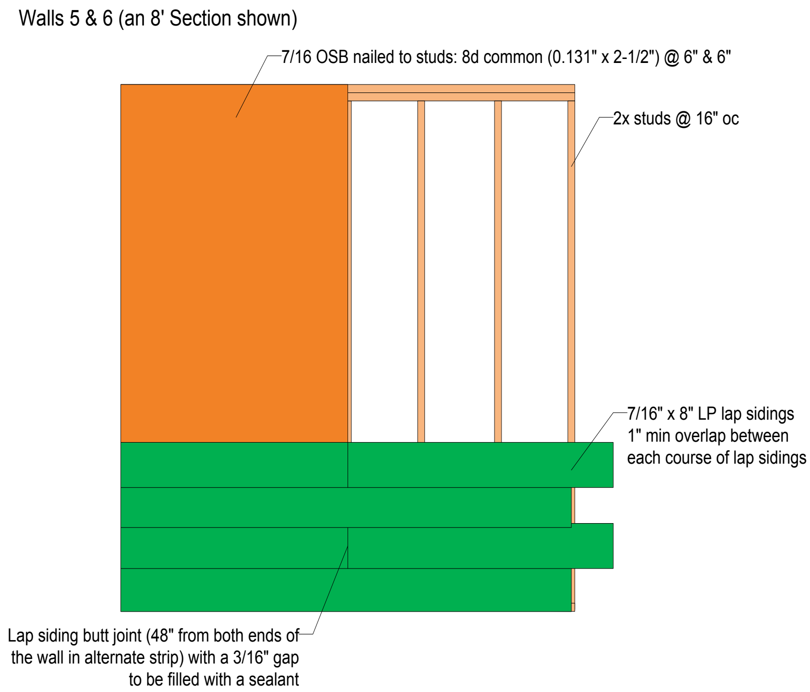

Figure 5. Installation details for the wall construction (1 in. = 25.4 mm)

3.4 Instrumentation

The test plan included measurement of wind pressures on the external wall surface, between each of the wall layers, and inside the test building. Each measurement location had three pressure taps installed, as shown in Figure 6. The pressure tap identified as P_1 in Figure 6 was mounted with its opening flush with the outside surface of the lap siding. P_2 was mounted to the inside surface of the lap siding such that it measures the pressure in the cavity between the siding and sheathing. P_3 was mounted such that it measures the pressure in the fiberglass-batt-filled cavity between the sheathing and the interior gypsum wallboard. Finally, internal pressures inside the building were measured at locations behind each of the wall segments. Pressure taps were strategically located on each wall. Pressure data was sampled at 100 Hz and filtered to 10 Hz to remove noise. The instrumentation was designed to facilitate the determination of the so-called “pressure equalization effect,” which is a phenomenon that occurs in multi-layer systems because openings in various layers allow the external wind pressures to be transmitted to interior layers, reducing the net wind loads across layers where equalization occurs, for the wall assemblies. Results of the pressure equalization effect expressed as the “pressure equalization factor” will be reported in a separate paper.

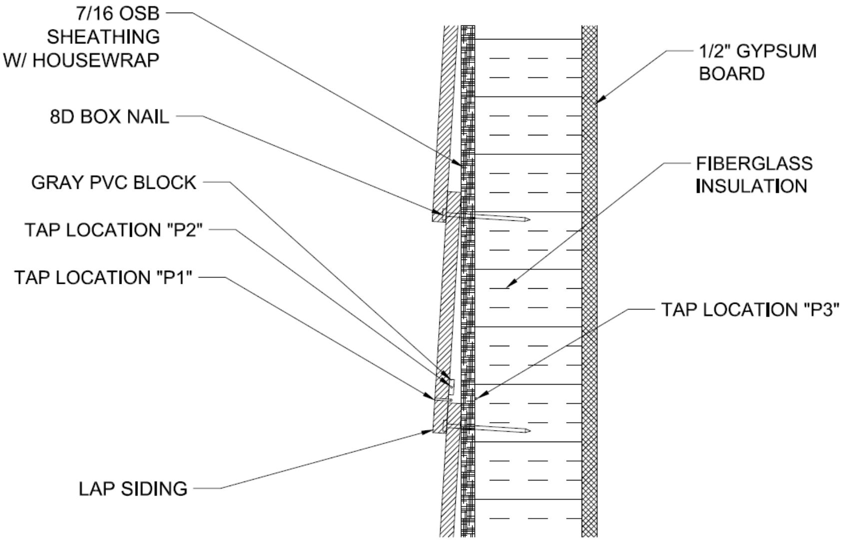

Figure 6. Configuration of pressure tapes in exterior wall system (1 in. = 25.4 mm)

3.5 Testing

Wall assemblies were tested at the critical angles identified to produce the worst wind loading effects from previous testing. These angles are shown in Figure 3 and Table 1. Wind pressure data are collected using an automated data acquisition system reading the output from the pressure sensors attached to each of the pressure taps. The test sequences in multiple-step wind speeds are described in Table 1. For each wind speed and wind angle combination, a 15-minute time history was applied. As these walls were part of the building that was subject to different wind angles, the overall cumulative test duration was about 2 hours at each wind speed.

Table 1: Test Sequence in Critical Wind Directions

Building rotation[1]		Gust wind speeds		
Wall #		Target gust at 5.5 m (18 ft)	Recorded gust[2] at 5.5 m (18 ft)	Equivalent gust at 10 m (33 ft)
5	6			
340°, 0°, 20°	250°, 270°, 290°	25 m/s (55 mph)	27 m/s (61.5 mph)	30 m/s (66.7 mph)
		34 m/s (77 mph)	35 m/s (78.8 mph)	38 m/s (85.4 mph)
		42 m/s (95 mph)	43 m/s (95.8 mph)	46 m/s (103.8 mph)
		48 m/s (108 mph)	49 m/s (110.5 mph)	54 m/s (119.8 mph)

1) Zero degrees is defined as the hip roof side of the building facing the fan inlet, and 180 degrees is defined at the gable end side of the building facing the fan inlet.
2) The same wind record results in slightly different maximum gust wind speeds in the test facility as a result of atmospheric conditions and variable frequency drive performance characteristics.

The achieved gust for each run varied slightly as a result of atmospheric conditions surrounding the test facility and variable frequency drive performance, thus a range of achieved gust wind speeds are reported with the results. The target values and typical 3-second peak gust wind speeds measured during the tests are provided in Table 1. Corresponding open country 3-second gust wind speeds at 10-m (33-ft) elevation in open terrain are also reported in Table 1.

4. Results

4.1 Siding Failure on Wall 5

Wall 5 was specifically designed with a nail spacing at the ultimate nail withdrawal capacity by assuming the full external wind pressure at the peak wind speed of 47 m/s (105 mph). However, during testing for wind speeds at a target gust of 42 m/s (95 mph) at 5.5 m (18 ft), a single piece of lap siding on Wall 5 experienced partial nail withdrawal. If testing had continued, the lap siding would have blown off. Upon inspection, it was noted that a single nail was omitted during construction from this piece of siding, leaving a 1676 mm (66 in.) nail spacing on this length of siding, instead of the designed spacing of 838 mm (33 in.) on center. The measured peak wind pressures experienced by this lap siding varied between approximately 0.9 kPa (19 psf) and 1.1 kPa (23 psf), depending on the wind direction.

Despite the fact that the nail was missing, this lap siding was still somewhat restrained by the siding directly above and the adjacent nails. For a 2515 mm (99 in.) long and two-panel tall segment of the lap siding centered on the location where the nail was missing, there were 5 nails providing restraint where 6 should have been installed. The area of these two siding would be 0.88 m^2 (9.45 ft^2) and the total peak wind load would have been between about 800 N (180 lbf) and 965 N (217 lbf). This would result in a peak wind load on each of the 5 nails of between 160 N (36 lbf) and 191 N (43 lbf), assuming the nail withdrawal loads were uniformly distributed among nails.

A review of the earlier sequence of tests with target gust wind speeds of 34 m/s (77 mph) that the wall survived without any observed withdrawal of the fasteners reveals that this section of siding would have been exposed to extreme peak wind pressures of between 0.62 kPa (13 psf) and 0.77 kPa (16 psf). The corresponding extreme loads on the nails using the same load distribution arguments discussed in the previous paragraph would have been between 111 N (25 lbf) and 133 N (30 lbf). It is possible that a longer duration of testing at the 34 m/s (77 mph) target wind speed might have resulted in withdrawal of nails in this area of the wall due to the missing nail.

Having encountered the failure reported in the previous section, the lap siding pieces in the area of the failure and above were removed and re-installed with nails shifted about 51 mm (2 in.) laterally to ensure that the new attachment points were not affected by the old attachment points. Testing was then resumed. The building was subjected to two tests where the target gust wind speed was 42 m/s (95 mph) without failure. This was followed by the sequence of testing with the target gust wind speed of 48 m/s (108 mph). During the first direction tested with the 48 m/s (108 mph) target gust wind speed, one lap siding was blown off the wall. Subsequent testing with wind records having a target gust of 48 m/s (108 mph) at 5.5 m (18 ft) resulted in a loss of the majority of lap siding on Wall 5. Failure of additional individual pieces of siding occurred during the 0° and 20° testing, as shown in Figure 7.

Figure 7. Wall 5 failure during testing at 20° with target gust speed of 48 m/s (108 mph)

At a nail spacing of 838 mm (33 in.) on center, the tributary area for each nail on Wall 5 was 0.15 m^2 (1.6 ft^2). The testing at a target gust wind speed of 42 m/s (95 mph) created peak loads between 0.9 kPa (19 psf) and 1.1 kPa (23 psf). The corresponding withdrawal forces on the nails would be peak values between 133 N (30 lbf) and 165 N (37 lbf). Consequently, it is likely that the two tests conducted with target 3-second gust winds of 42 m/s (95 mph) began to loosen up the re-attached lap siding. When the first test with a target wind speed of 48 m/s (108 mph) was conducted, the building was not oriented at the most critical wind direction for loading on this portion of the wall and the peak cyclic loads were likely once again weaken the over-stressed nailed joints in withdrawal. Therefore, the overall estimate of the Wall 5 performance at the failure between 42 m/s (95 mph) and 48 m/s (108 mph) must take the load duration and repeated loading history into account. Since the nail withdrawal is usually designed at a wind load that is about 1/3 of the ultimate withdrawal capacity, it is not expected that the accumulative damage experienced from these extreme wind load sequence will occur in reality.

4.2 Siding Performance on Wall 6

The siding installed on Wall 6 did not experience any signs of damage or nail backing out, despite of the repeated wind loads and long load duration, as compared to the assumed 10-minute load duration. It was exposed to a full battery of simulated open country winds with target peak gust wind speeds of 25 m/s (55 mph), 34 m/s (77 mph), 42 m/s (95 mph), and 48 m/s (108 mph). The simulated open country winds with a target of 48 m/s (108 mph) are expected to have applied peak wind pressures of between 1.2 kPa (25 psf) and 1.5 kPa (32 psf) to most areas of the siding on Wall 6.

The tributary area of the exposed siding with nails at 254 mm (10 in.) spacing is 0.045 m^2 (0.48 ft^2). The corresponding peak withdrawal forces on the nails would have been between 53 N (12 lbf) and 67 N (15 lbf). These forces are on the order of the allowable nail withdrawal resistance based on the APA Panel Design Specification (equivalent specific gravity of 0.40) with the load duration factor of 1.6. This confirms that the current design methodology for using wood structural panels as nailable sheathing can be justified under the wind loads at the most critical wind angles. It is also comfortable to confirm from these wind tunnel tests that the design methodology can be applied to wood structural panels with small nail penetration under the repeated wind loads at the full design wind speed from various wind angles.

5. Summary and Conclusions

The results obtained from this study clearly support the use of wood structural panels as nailable sheathing, which can be designed with single nail withdrawal resistance, even though the sheathing thickness might be small. On this basis, APA has published the Technical Topics TT-109, *Wood Structural Panels Used as Nailable Sheathing* [9], for use by design professionals. When the load duration factor of 1.6 is applied, the allowable withdrawal capacities used in the U.S. assure that the peak nail withdrawal loads at a design wind speed will be less than about 1/3 of the average ultimate nail withdrawal capacity (the allowable withdrawal capacity adjusted for the load duration is actually 1.6/5 = 32% of the average ultimate withdrawal capacity). Based on the IBHS wind tunnel tests provided in this report, an adequate factor of safety has been provided for the attachment of siding in real wind events.

6. Acknowledgements

This study is a joint research project of APA – The Engineered Wood Association, the Insurance Institute for Business & Home Safety (IBHS), and the USDA Forest Products Laboratory. This research was supported in part by funds provided by the USDA Forest Products Laboratory and the Engineered Wood Technology Association (EWTA), which is greatly appreciated.

7. References

[1] American Society of Civil Engineers. 2010. *Minimum Design Loads for Buildings and Other Structures*. ASCE 7-10. Reston, VA.

[2] Morrison, M., Brown, T., and Liu, Z. 2012. Comparison of Field and Full-Scale Laboratory Peak Pressures at the IBHS Research Center. *Proceedings of the ATC/SEI Advances in Hurricane Engineering Conference*, Miami, FL, October 24-26, 2012.

[3] American Wood Council. 2012. *National Design Specification for Wood Construction*. Leesburg, VA.

[4] APA – The Engineered Wood Association. 2012. *Panel Design Specification* (www.apawood.org/pdfs/download_pdf.cfm?PDFFilename=managed/D510.pdf), Tacoma, WA.

[5] Herzog, B. and Yeh, B. 2006. Nail Withdrawal and Pull-Through Strength of Structural-Use Panels. *Proceedings of the 9th World Conference on Timber Engineering*, Portland, OR. August 6-10, 2006

[6] ASTM International. 2012. *Standard Test Methods for Evaluating Properties of Wood-Base Fiber and Particle Panel Materials*. ASTM D1037-12. West Conshohocken, PA.

[7] APA – The Engineered Wood Association. 2010. *Nailhead Pull-Through Strength of Wood Structural Panels*. Technical Topics TT-070 (www.apawood.org/pdfs/download_pdf.cfm?PDFFilename=managed/TT-070.pdf), Tacoma, WA.

[8] APA – The Engineered Wood Association. 2010. *Wood Structural Panels Used as Nailable Sheathing*. Technical Topics TT-109 (www.apawood.org/pdfs/download_pdf.cfm?PDFFilename=managed/TT-109.pdf), Tacoma, WA.

INTERNATIONAL COUNCIL FOR RESEARCH AND INNOVATION IN BUILDING AND CONSTRUCTION

WORKING COMMISSION W18 - TIMBER STRUCTURES

COMPARISON OF THE FIRE RESISTANCE OF TIMBER MEMBERS IN TESTS AND CALCULATION MODELS

J Schmid

A Just

SP Technical Research Institute of Sweden

SWEDEN

M Klippel

A Frangi

ETH Zürich, Institute of Structural Engineering IBK, Zürich

SWITZERLAND

Keywords: fire design model, reduced cross section method, compression, tension, bending, timber, standard fire, fire resistance, fire testing

---

Presented by J Schmid

S Winter received clarification that the compression side lost most of the strength under fire. This was not their test results but based on backward calculations. It could be the compression side that was governing in bending and it could be more sensitive to steam and moisture transfer. S Winter commented that buckling would be the issue in compression. He questioned the assumed relationship between real strength and stiffness properties. Based on his experience and their test results, d_0= 7 mm fitted with the tabulated data more or less. Also in practice there are no damages or collapses in fire if this design process was correctly taken into consideration. J Schmid responded that standard fire is not likely to happen in reality. He further responded that just to say it never happened would not be a good excuse and one should look at the test data.

G Schickhofer and J Schmid discussed the negative value of the zero strength layer indicated that the prediction of material properties might be too variable. J Schmid agreed that the consideration is uncertain and more data is needed. As a next step there would be more work to consider test and analysis of members in compression.

A Buchanan questioned the zero strength layer increased with increase of member size. J Schmid explained that the use of 30% load ratio was connected to failure time. Larger member implies longer time before failure. A Buchanan asked about a slab with large width and stated that there was large variability therefore reliability of performance of timber members in real fire needs to be studied. J Schmid stated we are not there yet.

Comparison of the fire resistance of timber members in tests and calculation models

Joachim Schmid*
Michael Klippel**
Alar Just***
Andrea Frangi**

* SP Technical Research Institute of Sweden
** ETH Zürich, Institute of Structural Engineering IBK, Zürich, Switzerland
*** Tallinn University of Technology, Estonia

Keywords
Fire design model, Reduced cross section Method, Compression, Tension, Bending, Timber, standard fire, Fire resistance, Fire testing

Summary

For the design of timber members exposed to fire the "Reduced Cross-Section Method" provides a popular design method using an effective cross-section and mechanical properties at normal temperature. The method, originally developed for single span bending beams, has been further introduced in standards and handbooks for a large range of timber members including columns under compression and members under tension. Additionally, the method can be applied to cross-laminated panels or even I-joists. Recently, the method and its extended applications were discussed showing limitations as well as significant differences depending on the state of stress.

A total number of 110 fire tests were analysed and are discussed in this paper (79 members in bending, 6 members in compression and 25 members in tension). The results of the analysis of the fire tests show that the number of tests with reliable information is limited, among others, due to varying testing procedures and the lack of information reported. However, all results with adequate information content showed a significant variation of the zero-strength layer determined depending on the mode of stress. This is in agreement with advanced simulations presented in earlier research presented by the authors.

Introduction

While calculation methods provide a fast and cheap method to evaluate the load-bearing resistance of timber members, fire tests are time intensive and costly. Simulations of the fire performance of structural members are used for complex structures but even for the verification of easy-to-use models. In general, simulations use effective material properties to include effects such as cracks and degradation of the char layer as well as mass flow in the timber member. However, the use of effective thermal properties leads to a limited field of application. For the assessment of current design models of timber members for the fire situation, a large number of large-scale test results were evaluated in this paper: This paper compares fire test results in terms of the determined zero-strength layer d_0. Fire tests for members in compression, bending (single span beams) and tension were investigated. Since the main design procedure in EN 1995-1-2 [1] is based on the standard ISO-fire [2][3]; hence, only standard fire tests were evaluated in this study.

Recently a comparison of simulation results with the actual design procedure was published [4]; as a result, non-constant curves for the zero-strength layer for squared timber members was given, see Figure 1. Further, limitations and background of today's design procedure are summarized in [5].

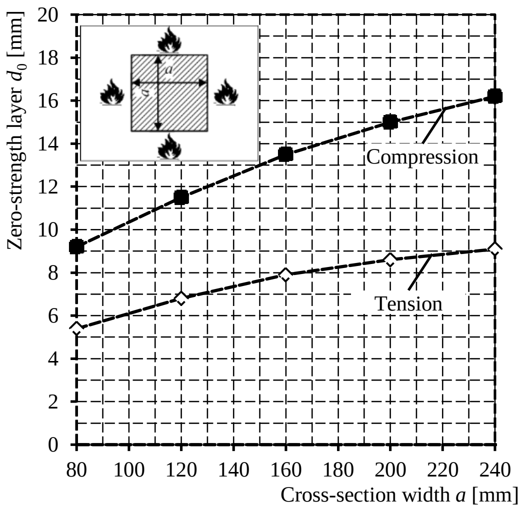

Figure 1. Determined zero-strength for squared timber members in compression and tension with dimensions $a \times a$ [4].

In general, the analysis of the fire tests is complex since the literature gives only limited information regarding the material tested. In case of lacking information, the fire tests were further analysed but evaluated separately. Test results presented here range from old results used to develop the basis for national design standards in Europe in the 1960s to tests performed by SP in Sweden in 2013 to conduct a comprehensive analysis of the zero-strength layer.

The requirements to consider a dataset as sufficient are, among others, reference tests at normal temperature, the standard fire exposure during loaded tests, the documentation of the failure time, the failure mode, and the residual cross-section. If the datasets were not complete, different scenarios were chosen and documented. The determined data were indicated as such and results were used separately. For the determination of all results, mean values were used and no safety factors were included in the analysis. For all members tested in a fire test, the zero-strength layer was calculated. For the determination of the zero-strength layer, results of the large-scale tests and design principals in terms of EN 1995-1-1 [6] were used, assuming ambient material properties in the fire situation and using effective cross-sections. In the following, the different fire tests are described shortly. The standards mentioned for each reference refer to the version at the time the reference was written and the tests were performed. Further, the results obtained from the fire tests were grouped in certain, uncertain and very uncertain results depending on the data reported in the different references.

Dorn et al. (1961) [7]

The authors present test results of 18 large-scale bending tests with glued-laminated (glulam) performed after a fire exposure according to the DIN 4102 standard fire temperature [8] for 30 minutes (16 tests) and 60 minutes (2 tests), respectively. Before the fire tests, the Young's Modulus (MOE) of the beams was determined and the moisture content measured. Limited preheating of the gas-fired furnace was done to follow the required temperature curve. Four test series with five different cross-sections and four different types of adhesives were tested. During the tests, temperature measurements within the four-sided exposed beams were performed. After the unloaded fire tests, the fire was extinguished using water or nitrogen and loaded in bending until failure about 90 to 120 minutes after the end of the fire test. Subsequently, the geometry and the moisture content of the residual cross-section were determined. The authors propose minimum widths for glulam beams to reach a fire resistance of 30 minutes for a defined design load (maximum allowed load given in the corresponding design standard). No influence of the adhesive was observed. The performed tests were not evaluated further in this study since the long delay between the end of the test and the determination of the bending resistance may influence the results considerably.

Hall (1968) [9]

The author performed one fire test on four glulam timber beams (139 mm × 228 mm, width × height) placed parallel to each other. The beams were simply supported (3650 mm span) and subjected to a constant bending moment achieved by weights. The tests were performed on a gas-fired furnace using the temperature fire curve according to the BS 476-1:1953 [10]. During the fire test, the temperatures were recorded in the timber cross-section as well as in the furnace by means of thermocouple readings. After the first beam had collapsed, the fire test had to be aborted. However, the second beam collapsed only 5 minutes after the first one. The material properties of the timber beams are given as grade LB, 9 laminations, and European whitewood. The actual timber grading uses a Knot Area Ratio (KAR) limiting the maximum allowed knot area to 20%. The failure stress in the fire situation in the actual test corresponds to 24,8 N/mm^2. For further calculation in this paper, it is assumed that the glulam beam was made of lamellas corresponding to a strength class of C24 according to EN 338 [11]. Using a JCSS [12] conversion factor of 1,56 a bending strength of 37,1 N/mm^2 was predicted. However, using these assumptions the data for the zero-strength layer is rated to be uncertain. Using a notional charring rate considering the corner roundings of β_n =0,7 mm/min as given in EN 1995-1-2 [1] and the above mentioned bending strength, a zero-strength layer of 2,1 mm was derived for the failed beam. For the second beam, which failed during the removal of the dead load (weights), a negative value for the zero-strength layer would be determined, likewise for the beams arranged close to the edge of the furnaces, for which the author supposed a lower fire load [9]. A negative result for the zero-strength layer may be explained by the high uncertainty of the material properties, i.e. a higher actual bending strength than assumed for the determination of the zero-strength layer.

Dorn et al. (1967) [13]

In total, 24 large-scale fire tests loaded in bending were performed with glulam beams of dimensions between 100 mm × 500 mm and 240 mm × 200 mm (width × height) and a length of 4500 mm and a span of 4000 mm. Two different adhesives, resorcinol-resin (PRF) and urea-resin (UF), were used to produce the beams with lamellas of between 20 and 25 mm thickness. Reference tests before the fire tests were performed to determine the stiffness of the glulam beams later tested in fire. Temperature measurements within some beams were performed in glue lines in depths of 6,0 to 34,1 mm. Four beams were impregnated with a fire retardant; two were protected from direct fire exposure by a fire protection system. Protected and impregnated beams were not evaluated in this study. The beams were exposed to fire according to the standard fire specified in DIN 4102:1940 [8] on all four sides. No significant influence of the adhesive used was observed regarding the load-bearing resistance. However, beams produced with the UF adhesive showed increased charring at the sides in areas of the glue lines. The fire exposure was 30 minutes in a gas-fired furnace. The load was applied prior to the fire test by means of two hydraulic jacks and kept constant until failure or 30 minutes fire exposure. The applied load corresponded to a bending stress of 12,75 N/mm^2. For some of the larger cross-sections ($h \geq 400$ mm), due to stability problems (lateral buckling) during the fire test, the load was applied only for 15 minutes and the next 15 minutes the timber member was only exposed to fire. Failure occurred during the fire tests in four cases. In the other cases, the load was increased after extinguishing about 35 minutes after the fire test had been terminated. Among others, it was observed that the decrease of flexural stiffness leading to the observed stability problems can be explained by an increased charring of about 1 mm/min instead of 0,66 mm/min, the determined charring rate. Since increasing the load until failure after the end of the fire test may be a questionable test procedure, all results determined from these tests were estimated to be uncertain but used for further investigations for this paper. For further analysis in this study, the residual cross-section was determined using a notional charring rate including the corner roundings of β_n = 0,7 mm/min as specified in EN 1995-1-2. This was done for either 30 minutes or, if the beam failed earlier, for the specific failure time. The reported specific stiffness measurements for every beam were used to predict the specific bending strength of the specimens resulting in a mean bending strength of about 37 N/mm^2. This value was estimated using today's strength classes for glued laminated timber of EN 1194 [14], a correction of the bending strength by means of EN 1995-1-1 [6] considering the actual depth and a conversion factor between the characteristic value and the mean value given by JCSS [12]. In general, the poor prediction method results only in an indication of the zero-strength layers. All beams with depths of 400 mm and above did not show bending failure but shear failure; corresponding results for the zero-strength layer are further reported as very uncertain since the results are expected to be lower for bending failure. A mean value for the zero-strength layer of the beams failed in bending in the investigation in [13] was derived to about 8,4 mm considering only uncertain results, see Table 1.

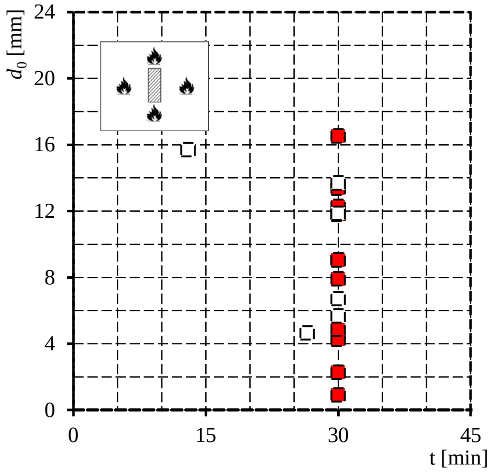

Figure 2. Determined zero-strength layer for tension tests [13]. Red squares indicate uncertain results; white squares indicate very uncertain results.

Table 1. Zero-strength layer results (minimum, maximum and mean) for all 24 evaluated results reported in [13] as well as for certain results only.

basis of calculation	$d_{0,min}$ [mm]	$d_{0,max}$ [mm]	$d_{0,mean}$ [mm]
all results	0,9	16,5	8,9
uncertain results	0,9	16,5	8,4

Dreyer, 1970 [15]

The author performed 14 large-scale fire tests in bending with glued laminated timber beams made from two different adhesives, resorcinol-resin and urea-resin. Beams were produced of lamella of different depths, 20 mm and 30 mm, respectively; however, neither the specific adhesives nor the build-up is given in the fire test result. The test program was intended to proof fire resistance for fire exposures longer than 60 minutes for three and four sided fire exposures. Fire tested beams had various rectangular cross-sections with areas from about 40.000 mm^2 (beams intended fire exposure of equal or more than 30 minutes) and up to about 120.000 mm^2 (beams intended fire exposure of equal or more than 60 minutes). Tests lasted from 35 to 79 minutes, all beams failed in bending. Images of residual cross-sections as well as measurements are reported. However, the time to extinguish the beams after the tests is specified to between 60 and 90 minutes. In the present study, the residual cross-section was estimated by the notional charring rate β_n (including the corner roundings) given in EN 1995-1-2 [1]. In [15], four tests were performed with three sided fire exposure. Very little information is given regarding the material properties. No reference tests at ambient temperature were performed; however, the densities of the beams were determined. To estimate a specific bending strength of every beams, in this study the density reported was used together with specified ratios between density and bending strength given in EN 1194 [14]. To estimate a mean strength by means of the derived characteristic value, a ratio of 1,29 given by JCSS [12] was used. To determine the zero-strength layer, a mean bending strength of 34 N/mm^2 was further used. Due to the assumptions of the residual cross-section as well as the material properties all results are considered as uncertain results. The zero-strength layer was determined separately for four-sided fire exposure (10 tests), see Figure 3, and three-sided fire exposure (4 tests), Figure 4.

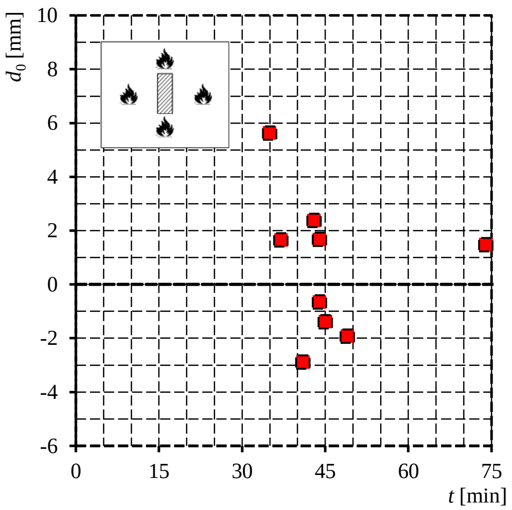

Figure 3. Determined zero-strength layer for bending tests and four sided fire exposure [15]. Red squares indicate uncertain results.

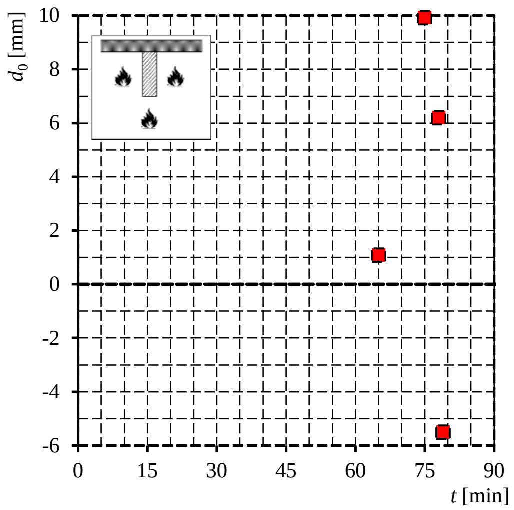

Figure 4. Determined zero-strength layer for bending tests and three sided fire exposure [15]. Red squares indicate uncertain results.

Table 2. Zero-strength layer results (minimum, maximum and mean) for all 14 evaluated results reported in [15] by means of two different material characterisation.

basis of material characterisation	ρ_{mean} [kg/m^3]	$f_{m,k}$ [N/mm^2]	$f_{m,mean}$ [N/mm^2]	$d_{0,min}$ [mm]	$d_{0,max}$ [mm]	$d_{0,mean}$ [mm]
reported specific beam densities	variable	variable	variable	-5,5	9,9	1,8
mean of reported densities	460	24,5	31,7	-6,2	16,9	2,0

For comparison reasons in Table 3 zero-strength values determined by means of the specific density and the mean batch density are given; differences are very limited. The in [15] reported charring depths at the top of the four-sided fire exposed beams are considerably lower than at the bottom side (up to 55% lower) most likely due to the very limited space of only 160 mm between the specimen and the furnace lock. Thus, the heating at the top side was limited. The observed mean charring rate β_n = 0,67 is slightly lower than specified in EN 1995-1-2; however the observed charring depths seem to be quite low considering the fact that the extinguishing work was finished about 30 to 60 minutes after the end of the fire test. Thus, the cross-section in the fire test is larger than assumed in this study and any calculated zero-strength layer is non-conservative.

Dreyer (1970) [16]

The author presents results of 19 large-scale fire tests with beams and roof sheathings whereas 14 were performed with glued-laminated timber beams. Lamella had a depth of about 30 mm; resorcinol-resin and urea-resin adhesives were used for the production of the beams. Four beam tests were performed with I-shaped beams and hollow core sections (four specimens). For comparison reasons, in this study only the fire tests with rectangular cross-sections were evaluated further (10 tests). Beams with rectangular section areas of about 45.000 mm^2 to 144.000 mm^2 were tested. The beams had a span of 4750 mm (5 specimens) or 7200 mm (5 specimens) and were subjected to bending. During the tests, one support was fire exposed; four tests were performed with a restrained support at one end. An oil-fired furnace was used; in general, two beams were tested at the same time with a distance of about 2100 mm between each other. In this investigation, the minimum cross-sectional area for a fire-rating of 30 minutes was studied for initially unprotected timber beams. Eight beams failed in bending, two in lateral buckling. No influence on the fire resistance for the two different types of adhesives was reported. The paper does not contain any information on the stiffness or strength properties of the material tested, however the density of each beam is reported. To estimate a bending strength of all beams, in this study the reported specific beam density between 395 and 475 kg/m^3 was used together with specified ratios between density and bending strength given in EN 1194 [14]. To estimate a mean bending strength values by means of the derived characteristic value a ratio of 1,29 given by JCSS [12] was used. To determine the zero-strength layer, a bending strength of in mean 30 N/mm^2 was used. In this study, the residual cross-sections were estimated by means of the reported charring depth values. Due to the assumptions of the material properties as well as the residual cross-section all results are considered as uncertain results, results for beams which showed lateral buckling failure are evaluated as very uncertain results (results B11b09 and B11b10 in Figure 5). The zero-strength layers were determined for all 10 tests and are given in Figure 5. However, test B11b05 (see Figure 5) is a result of the test with three-sided fire exposure. The reported charring depths at the top of the four-sided fire exposed beams are considerably lower than at the bottom side (up to 51% lower) most likely due to the very limited space of only 160 mm between the specimen and the furnace lock. Thus, the heating at the top side was limited. A significantly larger charring rate than given in EN 1995-1-2 [1] was observed at the bottom of the beams ($\beta_{n,mean}$ = 0,86 mm/min). Although fall-off of char was observed a delamination or an influence of the adhesive was not reported. Considering the lower charring at the top of the beams, the observed overall mean charring rate β_n = 0,66 mm/min is slightly lower than specified in EN 1995-1-2 [1]. Reported charring depths seem to be quite low considering the fact that the extinguishing work was finished about 30 to 60 minutes after the end of the fire test. Thus, the cross-section in the fire test is larger than assumed in this study and any calculated zero-strength layer is non-conservative. For comparison reasons in Table 3 zero-strength values determined by means of the specific density and by means of the mean batch density are given; differences are very limited. The conclusions reported in [16] include the assumption that the behaviour of the compression zone governs the overall fire performance of some beams.

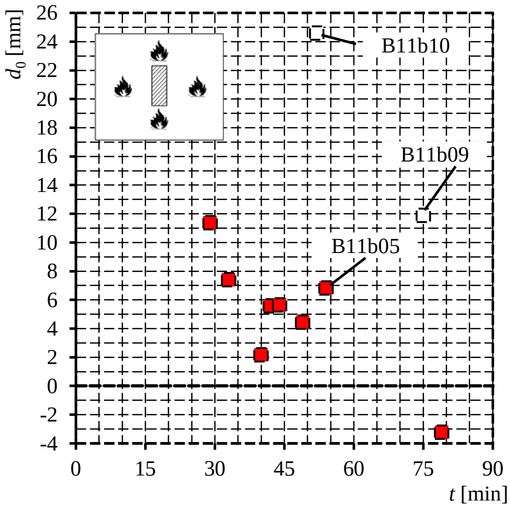

Figure 5. Determined zero-strength layer for bending tests and three sided fire exposure [15]. Red squares indicate uncertain results.

Table 3. Zero-strength layer results (minimum, maximum and mean) for all 14 evaluated results reported in [16] by means of two different material characterisation.

basis of material characterisation	ρ_{mean} [kg/m^3]	$f_{m,k}$ [N/mm^2]	$f_{m,mean}$ [N/mm^2]	$d_{0,min}$ [mm]	$d_{0,max}$ [mm]	$d_{0,mean}$ [mm]
reported specific beam densities	variable	variable	variable	-3,2	24,6	7,7
mean of reported densities	440	22,8	29,5	-3,7	21,2	7,8

White (1996) [17]

White [17] performed 15 large-scale fire tests with members in tension and applied constant load to specimens with four different cross-sections. Prior to the fire tests, White performed tensile tests at different elevated temperatures (constant). In the fire tests, solid timber as well as glulam was tested with an exposed length of 1800 mm. The smallest cross-section was 38 mm × 89 mm, the largest 217 mm × 222 mm (width × depth). Timber was Southern Pine (SP) and Douglas fir (DF) of different grades. Reference tests were determined for SP specimens, which showed that the factor between design value and tested mean value was about 1,5 times higher than given in general. No reference tests were performed to characterise the ultimate tensile strength of the DF specimens; for these tests a ratio of ultimate strength to allowable stress of 2,85 (general value, specified in [17]) was used for further calculations in the present investigation. Thus, results of the fire tests with DF specimens are rated uncertain in Figure 6. In the fire tests, the load was held constant until failure, which was observed between 10 and 124 minutes. Test T05t04, see Figure 6, was loaded intentionally with a lower load ratio and increased until failure after 120 minutes. For this test, a negative zero-strength layer (corresponding to a load-bearing char layer) was determined. The latter result is evaluated to be very uncertain but is included in Figure 6. The residual cross-section used for the determination of the zero-strength layer was calculated for the failure time by means of a notional charring rate of β_n = 0,7mm/min. The zero-strength layer for members in tension was determined for all results (15 tests) as well as for certain results (8 tests), see Table 4.

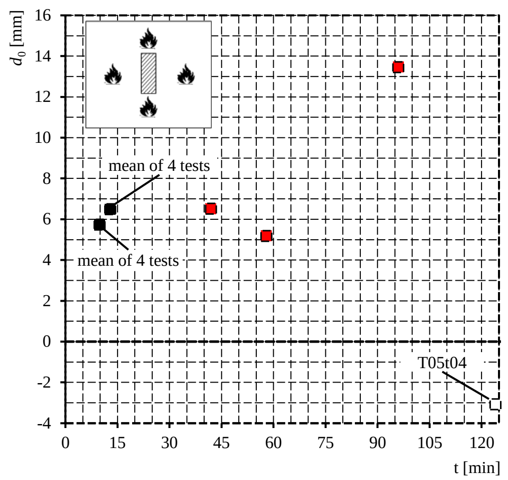

Figure 6. Determined zero-strength layer for tension tests [17]. Black squares indicate certain results, red squares indicate uncertain results, and white squares indicate very uncertain results.

Table 4. Zero-strength layer results (minimum, maximum and mean) for all 15 evaluated results reported in [17] as well as for certain results only.

basis of calculation	$d_{0,min}$ [mm]	$d_{0,max}$ [mm]	$d_{0,mean}$ [mm]
all results	-3,4	15,2	7,3
certain results	5,6	6,4	6,1

Peter et al. (2006) [18]

A very comprehensive test program was performed including fire tests in tension, compression and bending as well as reference test at normal temperature for the respective loading mode. All fire tests were conducted according to EN 1363-1 [3] with plate thermometers to control the test furnace. Reference tests at normal temperature were performed according to EN 408 [25]. In all fire tests, the load was kept constant until failure of the timber member. Beams made from solid timber members were graded according to EN 338 [11], glulam timber members were graded according to EN 1194 [14]. The charring depth and the geometry of the residual cross-section were evaluated on the basis of unloaded reference specimens exposed in the same fire test. These specimens were further instrumented with thermocouples to follow the charring rate. The residual cross-section was analysed by the authors and details specified; for most of the tests the residual-cross section is reported. If images were available, these were analysed for the present paper. This way, a notional charring rate β_n was calculated and used for the calculation of the zero-strength layer. The charring rate β_n reported in [18] deviates from the values determined in this study, it remains unclear if the definitions concur since no explanation of the determination performed by [18] was found.
Tension tests were performed with solid timber (grade C24) as well as glulam members (grade GL24h and GL36h). Dimensions from 120 mm × 120 mm to 220 mm × 220 mm (width × depth) were tested. Destructive

reference tests in tension were performed to determine the tensile strength between 19,1 and 27,3 N/mm^2, which were used to estimate the ultimate load-bearing resistance. The fire exposed length of the tested members was about 760 mm. The applied load was in the range of 0,18 to 0,54 of the predicted ultimate load-bearing resistance. Of six performed fire tests two failed in the connection area at the supports, for one specimen (C04t04, see Figure 7) a failure near the connection was observed after the test. All tests are included in this paper; however, the results for failure due to the connection are evaluated as uncertain since the timber members would have performed better. Thus, a lower zero-strength layer than determined here can be expected in these cases. One result of the zero-strength layer shows a negative value, which indicates that the material properties were better than predicted. The zero-strength layer for members in tension was determined in general to be lower than 7 mm as specified in EN 1995-1-2 [1], see Figure 7 and Table 5.

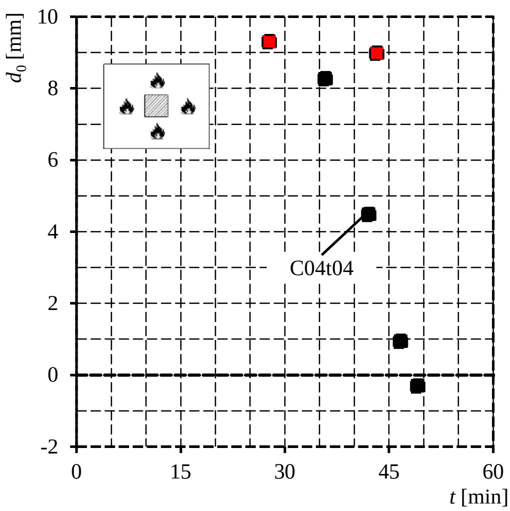

Figure 7. Determined zero-strength layer for tension tests [18]. Black squares indicate certain results, red squares indicate uncertain results.

Table 5. Zero-strength layer results (minimum, maximum and mean) for fire tests in tension reported in [18] as well as for certain results only.

basis of calculation	$d_{0,min}$ [mm]	$d_{0,max}$ [mm]	$d_{0,mean}$ [mm]
all results	-0,3	11,2	4,6
certain results	-0,3	5,8	1,7

Compression tests were performed with solid timber (grade C24) as well as glulam members (grade GL24h and GL36h). Dimensions from 120 mm × 120 mm to 220 mm × 220 mm (width × depth) were tested. The fire exposed length of the tested members was about 760 mm. Destructive reference tests in compression were used to determine the compression strength between 28,0 and 39,5 N/mm^2, which were used to predict the ultimate load-bearing resistance. Applied constant loads in the fire tests were in the range of 0,15 to 0,41 of the predicted ultimate load-bearing resistance. In all fire tests of this series, the specimens failed in compression. The zero-strength layer for members in compression was determined using a residual cross-sections computed by means of the notional charring rate β_n given in EN 1995-1-2 [1], see Figure 8 and Table 6 and for comparison reasons by means of β_n specified in [18], see Table 6.

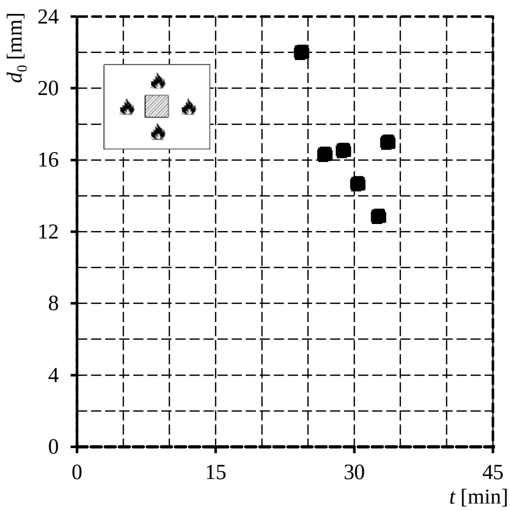

Figure 8. Determined zero-strength layer for compression tests [18].

Table 6. Zero-strength layer results (minimum, maximum and mean) for fire tests in compression in [18].

basis of calculation	$d_{0,min}$ [mm]	$d_{0,max}$ [mm]	$d_{0,mean}$ [mm]
reported charring β_n	15,5	23,7	18,1
β_n acc. to EN 1995-1-2	12,8	22,0	16,6

Bending tests with four sided exposed timber beams were performed with specimens of grade C24, GL24h and GL 32h. The test lasted from about 13 to about 52 minutes. Destructive reference tests in bending at normal temperature were performed with specimens from the same batch to predict the stiffness and the bending strength of the specimens tested in the fire situation. The fire tests were performed as 4-point bending tests with specimens of a length of 4000 mm exposed to fire on all sides. Dimensions varied from 120 mm to 140 mm in width and 278 mm to 600 mm in depth. The applied load was between 0,23 and 0,30 of the predicted ultimate load-bearing resistance. Due to the limited span of 3400 mm the absolute applied loads were rather high and resulted in unintended failure modes for beams with depths of 600 mm: shear failure was observed for both tests with specimens of higher grade GL32h; the determined zero-strength layers are evaluated as very uncertain and may be used to determine zero-strength layers for the shear capacity due to the observed failure mode. The specimen C04b03 (see Figure 9) resulted in a combined shear and bending failure and was evaluated further as uncertain result. Three residual cross-sections are reported by the authors. To estimate the moment of inertia of the residual cross-sections available images of the residual cross-sections were analysed in this study. If no images were available, the mean of before determined notional charring rates was used. The specimen C04b04 (see Figure 9) had an initial moisture content of 22,2% at the fire test, thus the result is evaluated as uncertain.

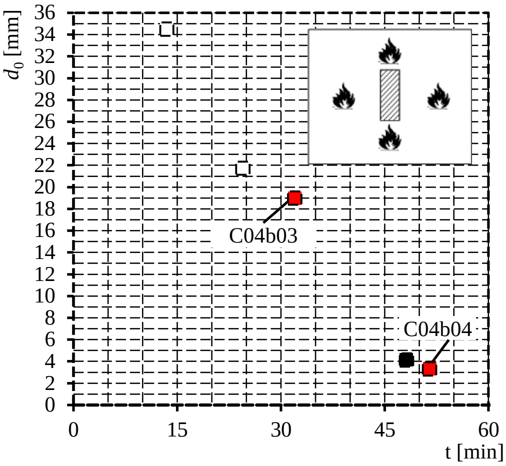

Figure 9. Determined zero-strength layer for bending tests [18]. Black squares indicate certain results, red squares indicate uncertain results, and white squares indicate very uncertain results.

Table 7. Zero-strength layer results (minimum, maximum and mean) for fire tests in bending reported in [18].

basis of calculation	$d_{0,min}$ [mm]	$d_{0,max}$ [mm]	$d_{0,mean}$ [mm]
all results	3,3	34,5	16,5

Fragiacomo et al. (2013) [19]

The authors conducted five fire tests in tension tests with LVL specimens with a cross-section of 150 mm × 63 mm and exposed length of 500 mm [19]. Tests were performed with constant loading between 0,12 and 0,22 of the predicted ultimate load-bearing resistance. The ultimate strength of about 37 N/mm^2 was predicted in [19] using a ratio of the characteristic value of tensile strength and an appropriate conversion coefficient specified by the LVL producer, given in [19]. This results in a very rough prediction of the material properties. The electrical furnace was not able to follow the ISO 834 [2] temperature curve; however, the deviations were very limited. The residual cross-section was not reported in [19]; during the tests the charring depth was determined by thermocouple measurements. The tests lasted up to about 30 minutes. In this study, the residual cross- section was determined by a notional charring rate of β_n = 0,65 mm/min reported in [20] for the same product. Results of the determination of the zero-strength layer assuming two different notional charring rates are given in Table 8; the calculated mean values agree well with the range between 7 and 9 mm reported in [20].

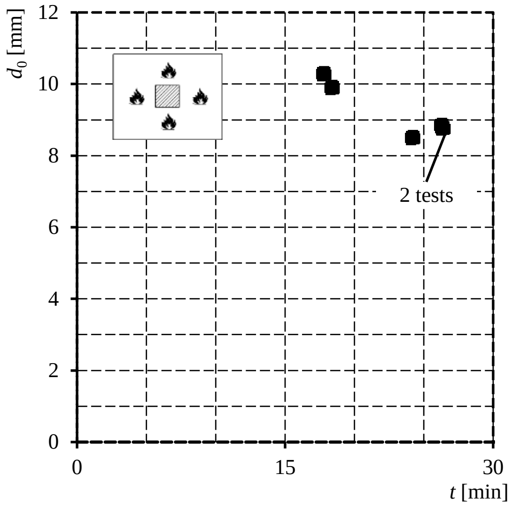

Figure 10. Determined zero-strength layer for tension tests [19].

Table 8. Zero-strength layer results (minimum, maximum and mean) for fire tests in tension reported in [19].

basis of calculation	$d_{0,min}$ [mm]	$d_{0,max}$ [mm]	$d_{0,mean}$ [mm]
reported charring β_n=0,65	8,5	10,3	9,3
β_n acc. to EN 1995-1-2	7,3	9,4	8,1

Klippel et al. (2013) [21],[22]

The investigation primarily investigates the influence of different adhesives on the load-bearing resistance of finger-jointed timber boards subjected to a tensile load and exposed to standard-ISO fire [2] on two sides. As a reference, four fire tests were performed on solid (unjointed) timber boards with dimensions of 140 mm × 40 mm (width × depth) which are further investigated in this study. The length of the tensile specimens was about 3500 mm; however for three of the four solid wood specimens the fire exposed length of 1000 mm was partly reduced by thermal insulation to reduce the risk of failure in the range of knots outside of the knot-free area of about 300 mm. Before the fire tests, reference tests at ambient temperature were performed with finger-jointed boards to obtain mean strength values of the material [23]. The density of each board as well as in general the residual cross-sections were determined after the test. The fire tests lasted between 55 and 73,5 minutes. In nearly all cases the fire tests with solid boards were performed with constant load-level of about 25% of the mean tensile strength at ambient temperature; however, for test specimen T01t02 (see Figure 11) the test load was increased after 40 minutes until failure. As already observed for tests performed by White [17], a small zero-strength layer of only about 2 mm was calculated for this test, in which the load was increased until failure after a certain time of fire exposure; this result is considered to be uncertain. Results of the determination of the zero-strength layers are given in Table 9.

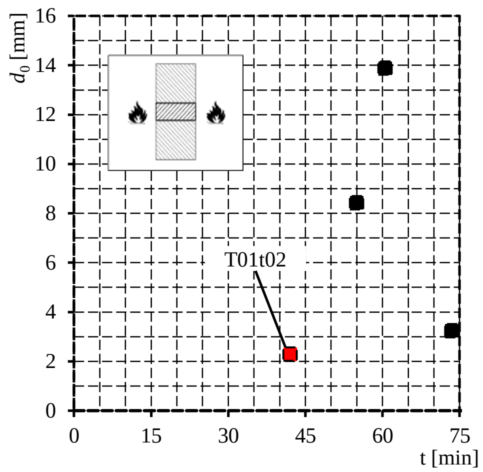

Figure 11. Determined zero-strength layer for tension tests [21], [22]. Black squares indicate certain results, and white squares indicate uncertain results.

Table 9. Zero-strength layer results (minimum, maximum and mean) for all 4 evaluated results reported in [21], [22] as well as for certain results only.

basis of calculation	$d_{0,min}$ [mm]	$d_{0,max}$ [mm]	$d_{0,mean}$ [mm]
all results	2,3	13,9	7,0
certain results	3,2	13,9	8,5

Lange et al. (2013) [24]

The authors performed a series of large-scale fire tests with one beam type (same batch, geometry and grade) and different fire exposures. In the present study, only fire tests performed with ISO 834 [2] fire exposure are evaluated. In the tests by Lange et al. (2013) [24], eight beams with a cross-section of 140 mm × 269 mm (width × height) were placed across the gas-fired horizontal furnace resulting in a span of 3300 mm. Prior to the fire tests, destructive reference tests in bending were performed according to EN 408 [25] at normal temperature to determine the mean ultimate bending resistance and to predict the resistance of the beams tested in the fire situation. A mean value of 42,7 N/mm^2 was derived for the bending strength of all beams, which was used for the prediction of the failure load of all beams tested in the fire situation. Beams tested in fire were instrumented with internal thermocouples in different depths along the centre line. In the fire tests, the beams were loaded pairwise with a constant load which was kept constant until failure. Due to the pairwise loading, the load had to be removed from the pair when one of the two beams failed to avoid integrity risks during the proceeding fire test. However, for the last pair an individual failure was allowed. After failure of any beam, the load was removed from the pair and the beams were left at the furnace until the last beam failed. Subsequently, the beams were removed from the furnace and extinguished. Following this procedure, five beams failed during the fire test. The results of fire tests are plotted in Figure 12 as a function of the predicted bending moment resistance at normal temperature.

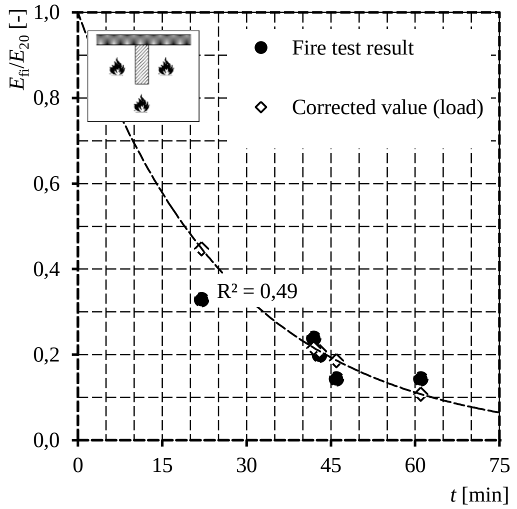

Figure 12. Test results of [24]. Load ratio E_{fi}/E_{20} versus time of failure.

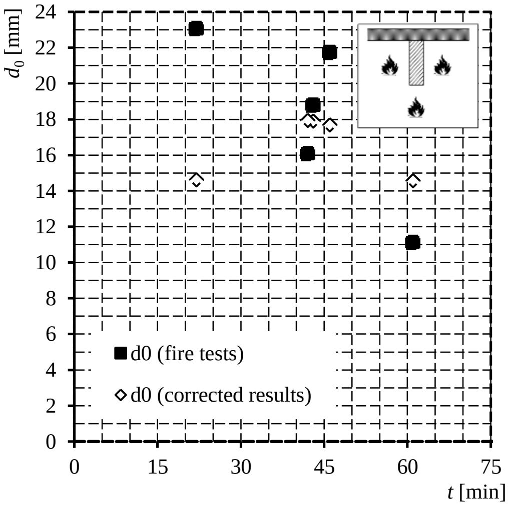

Figure 13. Determined zero-strength layer for bending tests [24].

In Figure 12, an exponential correlation was fitted to the fire test results to consider the scatter of the material properties of the glulam beams. In a next step, corrected values were determined to represent fire test results with perfect fit to the before mentioned correlation function; the failure time was kept constant but the load-level E_{fi}/E_{20} (ratio of effect of loads in the fire situation and at normal temperature) was modified. Results of the corrected values were then used for further evaluation but treated separately. The residual cross-section at specific failure could not be investigated due to the test set-up. For this study, the notional charring rate β_n was determined using images of the residual beams considering a fire exposure of 60 minutes when the fire test was terminated after the failure of the last beam. A mean value was found to be β_n = 0,71 mm/min, which is in good agreement with β_n specified in EN 1995-1-2 [1]. The determined zero-strength layer results for five fire tests as well as the corrected results are shown in Figure 13, the mean values for a determination by means of the fire test results and the corrected fire test results respectively are given in Table 10.

Table 10. Zero-strength layer results (minimum, maximum and mean) for all 5 evaluated results reported in [24]. Zero-strength layers derived from the fire tests as well as corrected values are specified.

basis of calculation	$d_{0,min}$ [mm]	$d_{0,max}$ [mm]	$d_{0,mean}$ [mm]
fire tests	11,1	23,1	18,2
corrected results	14,6	17,9	16,6

Conclusions

In this paper, results are presented as zero-strength layers determined by fire tests whereby most of the tests are large-scale fire tests. On the basis of extensive experimental investigations, the large variation of the zero-strength layer determined could be shown. The paper extends the analysis of the zero-strength layer significantly by a comprehensive evaluation of 110 fire tests under standard-fire exposure. However, due to the lack of the characterisation of the material later tested in fire, in many references an uncertainty regarding the determined zero-strength layer has to be mentioned. Figure 14 gives the mean values for the zero-strength layer depending on the state of stress for all references analysed. The number of fire tests considered for the calculation of the shown value are indicated.

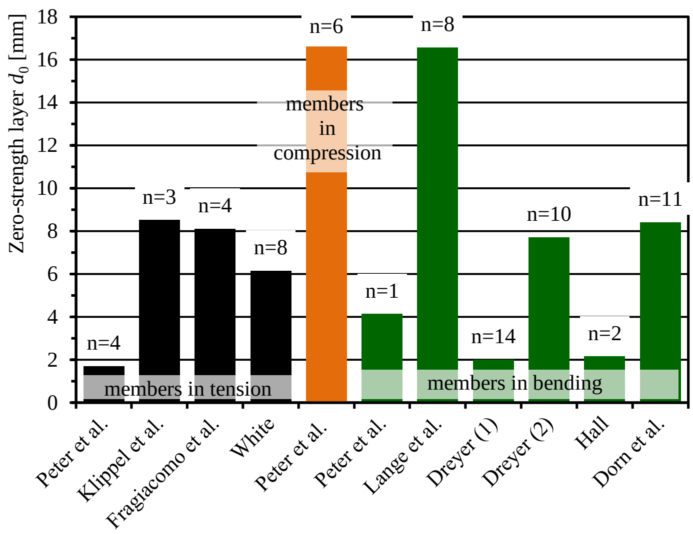

Figure 14. Determined zero-strength layer corresponding to fire test results reported in literature.

Fire exposed members in tension

Although truss construction elements are very commonly used, e.g. in attics, only few fire tests with members in tension are available. The evaluated tests of White [17] and Fragiacomo et al. [19] show a mean value which agrees very well with the today's general rule for the zero-strength layer in EN 1995-1-2 [1]; however, uncertain results indicate a higher value for longer fire exposures. Results of [18] and [21] show higher scatter but are in general in agreement with the other authors. Further, results are in good agreement with advanced calculations as given in [4].

Fire exposed members in compression

Limited literature with focus on the compression strength in the fire situation is available. However, the presented tests represent high reliability since tests were performed according to present European testing standards as well as offering comprehensive reference tests to describe the material properties of the tested members. Results show a mean value considerably larger than given in EN 1995-1-2 [1]. This was earlier indicated by Klippel et al. [4] based on advanced calculation with timber material properties given in [1].

Fire exposed members in bending

For bending tests, a very large variation of the results for the zero-strength layer can be observed. References using obsolete test procedures show either low results or values which agree fairly well with rules given in EN 1995-1-2 [1]. Although many fire tests were performed in the past, results are uncertain due to the lack of material characterisation. Further, the test methods are often deviating from today's standard testing requirements regarding the heat flux and the loading of the specimens.

Results

Based on the analysis of fire test, the today's design model in EN 1995-1-2 [1] seems to fit well for tension members while for compression members the design model is non-conservative. For members in bending, further investigation and comparison with advanced calculation is needed; a large scatter for the zero-strength layer was determined, most likely due to the assumptions of the material properties.

It seems that the existing simplified reduced cross-section method with a constant zero-strength layer was introduced in EN 1995-1-2 [1] without sufficient investigations and documentation of the reliability and uncertainties for different loading situations.

Acknowledgements

This study was carried out at and funded by SP Wood Technology (formerly SP Trätek), a division of SP Technical Research Institute of Sweden as well as ETH Zürich. The authors thank the European Societal Fund and postdoctoral program Mobilitas for funding. The authors would like to thank R. White and P. Steer for their help in evaluating some fire tests.

References

[1] EN 1995-1-2:2004, Eurocode 5: Design of timber structures – Part 1-2: General – Structural fire design. European Standard.
[2] ISO 834-1 Fire-resistance tests – Elements of building construction – Part 1: General requirements. International Organization for Standardization, Genève, Switzerland, 1999.
[3] EN 1363-1, Fire resistance tests - Part 1: General requirements, 1999.
[4] Klippel, M., Schmid, J., Frangi, A.: The Reduced Cross-Section Method for timber members subjected to compression, tension and bending in fire; CIB W18. Meeting 45; Växjö, Sweden; Lehrstuhl für Ingenieurholzbau, University of Karlsruhe, Karlsruhe, Germany; 2012.
[5] Schmid, J., König, J.: The Reduced Cross-Section Method for the design of timber structures exposed to fire – Background, limitations and new developments; Structural Engineering International; 22 (4); 2012.
[6] EN 1995-1-1:2010, Eurocode 5: Design of timber structures – Part 1-2: General design. European Standard.
[7] Dorn, H., Egner, K.: Fire Tests on Glued Laminated Structural Timber (Glulam Beams); original in Holz-Zentralblatt Stuttgart, (28): 435-438/1961, NRC TT-1131. Ottawa, Canada, 1964.
[8] DIN 4102, Widerstandsfähigkeit von Baustoffen und Bauteilen gegen Feuer und Wärme. DIN Deutsches Institut für Normung e. V., Berlin, Germany, 1940.
[9] Hall, G.S.: Fire Resistance Tests of Laminated Timber Beams. Timber Research and Development Association, High Wycombe, U.K. 1968.
[10] BS 476-1, Fire tests on Building materials and structures – part 1: Test conditions. British standard. BSI, British standards institution. London, UK, 1953.
[11] EN 338 Structural timber – Strength classes. European Standard. European Committee for Standardization. Brussels. 2003.
[12] JCSS, Joint Committee on Structural Safety, "Probabilistic Model Code"; www.jcss.byg.dtu.dk.
[13] Dorn, H., Egner. K.: Brandversuche an brettschichtverleimten Holzträgern unter Biegebeanspruchung - Flame Tests on Laminated Trusses under Bending Load. Mitteilung aus der Amtl. Forschung und Materialprüfanstalt für das Bauwesen der T.H. Stuttgart; (in German). 1967.
[14] EN 1194, Timber structures - Glued laminated timber - Strength classes and determination of characteristic values, 1999.
[15] Dreyer, R.: Brettschichtverleimte Binder unter Biege- und Feuerbeanspruchung, Institut für Baustoffkunde und Stahlbetonbau der technischen Universität Braunschweig, 1970.
[16] Dreyer, R.: Träger, Binder und Decken aus Holz unter Biege- und Feuerbeanspruchung, Institut für Baustoffkunde und Stahlbetonbau der technischen Universität Braunschweig, 1970.
[17] White, R.H., Tensile Strength of Fire-Exposed Wood Members, 1996.
[18] Peter, M., Göckerl, T.: Bemessung von Voll- und Brettschichtholzbauteilen aus maschinell sortiertem Schnittholz für den Brandfall – Teil 2: Brandversuche zur Bestätigung der theoretischen Ergebnisse. (in German) Institut des Zimmerer- und Holzbaugewerbes e.V., Berlin, 2006.
[19] Fragiacomo, M., Menis, A., Moss, P.J., Clemente, I., Buchanan, A.H., Nicolo, B. Predicting the fire resistance of timber members loaded in tension, Fire and Materials, Fire Mater, John Wiley & Sons, Ltd, 37:114-129, 2013.
[20] Lane, W., Buchanan, A., Moss, P., Fire Performance of Laminated Veneer Lumber (LVL). EWPA, Engineered Wood Products Association, Madison, United States, 2004.
[21] Klippel M., Frangi A., Hugi E.: Experimental analysis on the fire behaviour of finger-jointed timber members Journal of Structural Engineering (ASCE), URL: http://ascelibrary.org/doi/abs/10.1061/%28ASCE%29ST.1943-541X.0000851, 2013.
[22] Klippel M., Frangi A.: Fire tests on finger-jointed timber boards - Test report, Institut of Structural Engineering, ETH Zurich, IBK-Report, under preparation, Zurich, Switzerland, 2013.
[23] Frangi, A., Bertocchi, M., Clauß, S., Niemy, P., Mechanical behaviour of finger joints at elevated temperatures. Wood Science Technology, DOI: 10.1007/s00226-011-0444-9. 2011.
[24] Lange, D. et al.: Assessment of the impact of different fire scenarios on structural timber performance and reliability – Part 1: Fire tests; SP Report 2013, under preparation. Borås, Sweden, 2013.
[25] EN 408, Timber structures - Structural timber and glued laminated timber - Determination of some physical and mechanical properties, 2010.

CIB-W18/46-20-1

**INTERNATIONAL COUNCIL FOR RESEARCH AND INNOVATION
IN BUILDING AND CONSTRUCTION**

WORKING COMMISSION W18 - TIMBER STRUCTURES

CLT AND FLOOR VIBRATIONS: A COMPARISON OF DESIGN METHODS

A Thiel
S Zimmer
M Augustin
Competence Centre holz.bau forschungs gmbh

G Schickhofer
Graz University of Technology, Institute of Timber Engineering and Wood Technology

AUSTRIA

Keywords: floor vibration, cross laminated timber, design method, Eurocode 5, natural frequency, stiffness criterion, damping ratio, in-situ measurement

---

Presented by A Thiel
JW van de Kuilen received clarification that static MOE values instead of dynamic MOE was used.
T Reynolds asked about the relationship between amplitude of vibration and damping and whether this could explain the difference observed from heel drop tests. A Thiel stated in heel drop tests, the person was on the floor and the person also acted as a damper to the system. P Dietsch asked about the difference between sandbag and heel drop tests. A Thiel stated results from Hamm/Ritcher did consider this issue.
K Ranasinghe questioned the usefulness of standard heel drop tests.
M Fragiacomo suggested the use of dynamic shaker.
H Blass stated this might not be an issue as vibration affects people and people need to be on the floor to be affected.

CLT and floor vibrations:

A comparison of design methods

A Thiel, S Zimmer, M Augustin

Competence Centre holz.bau forschungs gmbh, Austria

G Schickhofer

Graz University of Technology, Institute of Timber Engineering and Wood Technology, Austria

1 Abstract

In the last years the engineered building product cross laminated timber (CLT) has become very common in particular as floor and wall element in single- and multi-storey buildings. Used as floor element the verification at serviceability limit state (SLS) generally controls the design, and especially for larger spans the floor vibration is crucial. For the verification of vibration a variety of methods exist, for example the standardised method described in EN 1995-1-1 [2], the suggestions of Hamm and Richter (2009) [9] and the Canadian approaches of Hu (2010, 2012) [4]. Application of these methods leads to decisively different results. In this paper the differences of these methods are discussed and a comparison of measured and calculated values is shown.

2 Introduction

For CLT used as floor elements with spans larger than 4 m, vibration usually governs the design. Currently there are a variety of methods and limit values. In frame of a research project [10] at the Centre of Competence holz.bau forschungs gmbh, the following methods were analysed and compared: (i) the method for verifying vibration of residential floors according to Eurocode 5 [2][7], (ii) the suggestions of Hamm / Richter (e.g. see [9]), (iii) a modified version of (ii) (e.g. see [10]), and (iv) the Canadian approach of Hu [4]. Added to this, on the basis of a parametric study on a single-span beam (with spans ranging from 3 m to 7 m under self weight, permanent load and exposed to imposed load of category A) the influence of significant parameters is investigated. Applying these procedures decisively different results occur. This is because the limit values are based on the highly subjective opinion of the person conducting the test. Therefore, it is currently impossible to define which approach would be best suited to verifying vibrations. Thus, it is considered worthwhile to compare available results from measurements with the prevailing methods and their limit values. Another highly important aspect is seen in quantifying the influence of support conditions (e.g. hinged, partly clamped, clamped, slabs supported by a floor beam, the influence of the upper floor loads transmitted through walls on the degree of clamping). Currently investigations in this regard are in progress at the Centre of Competence holz.bau forschungs gmbh.

3 Basic principles

Primarily, the methods mentioned before check the natural frequency and the stiffness criterion. Some of them also check the vibration acceleration if the natural frequency is below a critical frequency. Following [2], the vibration velocity should also be checked, but this verification is mainly required for light floors and thus of minor importance for CLT floors.

3.1 Natural frequency

The natural frequency of a single-span beam $f_{m,beam}$ follows eq. (1).

$$f_{m,beam} = \frac{k_m}{2\pi \cdot l^2} \sqrt{\frac{(EI)_{l,ef}}{\bar{m}}} \; [Hz] \tag{1}$$

The effective bending stiffness in longitudinal direction $(EI)_{l,ef}$ consists of the bending stiffness of the CLT element K_{CLT} and the bending stiffness of a possible final screed, but without the composite action (just adding its own moment of inertia). Furthermore, the shear flexibility in the CLT element may be taken into account by using the effective apparent bending stiffness (based on bending and shear deformations) instead of K_{CLT}.

The factor k_m takes different support conditions and Eigenmodes into consideration. In Fig. 1 the values for the 1st Eigenmode (m = 1) are shown.

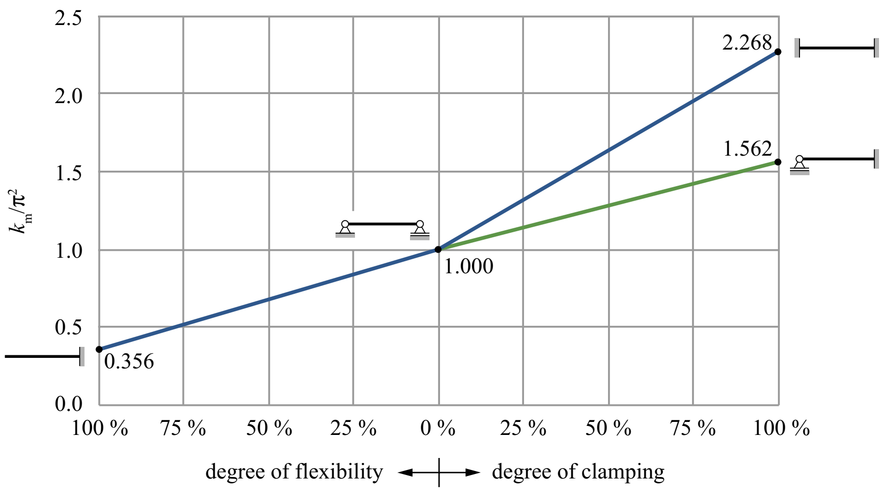

Fig. 1: Faktor k_m for the 1st Eigenmode depending on the structural system

For multi-span systems, the continuous beam effect can be considered. For example factor $k_{f,2}$ according eq. (2), can be used. Depending on the ratio l_{min} / l_{max}, this factor is between 1.0 and 1.5.

$$\begin{aligned} k_{f,2} = & -5.3828\left(\frac{l_{min}}{l_{max}}\right)^6 + 16.6637\left(\frac{l_{min}}{l_{max}}\right)^5 - 19.7305\left(\frac{l_{min}}{l_{max}}\right)^4 + 10.3840\left(\frac{l_{min}}{l_{max}}\right)^3 \\ & -1.9017\left(\frac{l_{min}}{l_{max}}\right)^2 - 0.5879\left(\frac{l_{min}}{l_{max}}\right) + 1.5537 \end{aligned} \tag{2}$$

Another possibility is to calculate the natural frequency according to the method of Morleigh, see [8]. Additionally to the continuous beam effect, this method also includes influences such as shear flexibility or elastic clamping. As, in context of CLT, the shear flexibility is of crucial importance, it is highly advisable to also take it into consideration in the context of vibrations.

If the slab is hinged at four sides, the transverse load-carrying effect can be taken into account. Therefore the natural frequency is calculated with eq. (3). Both, the twisting stiffness D_{xy}^{*} and the effective bending stiffness in the transverse direction $(EI)_{t,ef}$, can be considered. The increase of the natural frequency highly depends on the span-to-width ratio of the slab, l / b.

$$f_{1,\text{plate}} = f_{1,\text{beam}} \cdot \sqrt{1 + \frac{2 \cdot D_{xy}^{*}}{(EI)_{l,\text{ef}}} \cdot \frac{l^2}{b^2} + \frac{(EI)_{t,\text{ef}}}{(EI)_{l,\text{ef}}} \cdot \frac{l^4}{b^4}} \; [Hz] \tag{3}$$

The calculated natural frequency should be higher than the critical frequency f_{crit}. The critical frequencies for normal and high requirements of the different methods are shown in Tab. 5.

3.2 Stiffness criterion

In the examination of the criterion for stiffness, the maximum instantaneous vertical deflection, caused by a vertical concentrated static force $F = 1$ kN at any point of the floor taking the load distribution into account, has to be calculated and compared with the limit value $w_{crit,1kN}$ of Tab. 5.

Again, the shear flexibility should be taken into account when calculating the deflection. For a single-span beam, the maximum deflection $w(F,b_F)$ follows eq. (4). Eq. (5) considers the distribution of load by the effective width b_F.

$$w(F,b_F) = \frac{F \cdot l^3}{48 \cdot (EI)_{l,\text{ef}} \cdot b_F} + \frac{F \cdot l}{4 \cdot (GA)_{\text{ef}} \cdot b_F} \tag{4}$$

$$b_F = \frac{l}{1.1} \cdot \sqrt[4]{\frac{(EI)_{t,\text{ef}}}{(EI)_{l,\text{ef}}}} \tag{5}$$

3.3 Vibration acceleration

In cases where the natural frequency f_1 is between the critical frequency f_{crit} and the minimum frequency $f_{min} = 4.5$ Hz, the vibration acceleration a has to be checked also. This value has to be less than a critical acceleration a_{crit}. The critical accelerations for normal and high requirements are shown in Tab. 5.

$$a = \frac{0.4 \cdot \left(\frac{F_0 \cdot \alpha_{i,f_1}}{M_{\text{gen}}} \right)}{\sqrt{\left(\left(\frac{f_1}{f_f} \right)^2 - 1 \right)^2 + \left(2 \cdot \zeta \cdot \frac{f_1}{f_f} \right)^2}} \; [m/s^2] \tag{6}$$

The vibration acceleration is calculated according to eq. (6). It depends on the effective (generalised) mass M_{gen} of the slab, the excitation frequency f_f, the natural frequency f_1, the Fourier coefficient of the prevailing harmonic partial oscillation $\alpha_{i,f1}$, the self weight of the excitatory person F_0 = 700 N and on the modal damping ratio ζ.

The calculation of modal (generalised) mass M_{gen} is diverse described in literature. For consideration of the influence of the orthotropic material the use of eq. (7), with b_F from eq. (5), is proposed. However, for a more realistic consideration of the orthotropic material further research is needed.

$$M_{\text{gen}} = M \cdot \frac{l}{2} \cdot b_{\text{F}} \left[\text{kg/m}^2\right] \quad \text{with } b_{\text{F}} \leq \text{half room width } \frac{b}{2} \tag{7}$$

In fact, published values of Fourier coefficients and excitation frequencies do not coincide. Tab. 1 shows the values as given in [6].

Tab. 1: Fourier coefficients and excitation frequencies according to [6]

natural frequency f_1 [Hz]	Fourier coefficient $\alpha_{i,f1}$	excitation frequency f_f [Hz]
$4.5 < f_1 \leq 5.1$	0.20	f_1
$5.1 < f_1 \leq 6.9$	0.06	f_1
$6.9 < f_1 \leq 8.0$	0.06	6.9

The damping ratio ζ for CLT floors is found to be between 2.0 % and 3.5 %, depending on the type of floor construction and the support conditions, see [3].

Tab. 2: Recommended values for damping ratio ζ dependent on the type of floor construction

type of floor construction	damping ratio ζ	
	supported on 2 sides	supported on 4 sides
CLT floors with a light or without floor construction	2.0 %	2.5 %
CLT floors with heavy floor construction	2.5 %	3.5 %

4 Comparison of design methods

As already mentioned before, the design methods primarily check the frequency and the stiffness criterion. Some of them also proof the vibration velocity and acceleration. Tab. 3 gives a brief overview of the checks to be carried out for the different design methods.

Tab. 3: Checks to be carried out depending on the applied method

method	frequency	stiffness criterion	vibration velocity	vibration acceleration
Eurocode base document [2]	✓	✓	✓	×
Eurocode national annex of Austria (NA AT) [7] [1]	✓	✓	✓	✓
Hamm/Richter [9]	✓	✓	×	✓
Hamm/Richter modified [10][6]	✓	✓	×	✓
Hu [4]	✓	✓	×	×

Although all methods have in common the check of the frequency and the stiffness criterion, they do not lead to the same results. This is because of differences in considered parameters. An overview is provided in Tab. 4.

Tab. 4: Overview of methods and considered parameters like different support conditions, continuous beam effect, shear flexibility, transverse load-carrying effect, effective width b_F and part of loads as mass

method	k_m	continuous beam effect	shear flexibility	transverse load-carrying effect	effective width b_F	mass
Eurocode base document [2]	✗	✗	✗	✗	✓[1)]	$g_0 + g_1$
Eurocode NA AT [7]	✗	✗	✗	✓	✓	$g_0 + g_1 + \psi_2 \cdot q$
Eurocode NA AT - new proposal [1]	✓	✓	✗	✓	✓	$g_0 + g_1$
Hamm/Richter [9]	✗	✗	✗	✓	✓	$g_0 + g_1$
Hamm/Richter modified [10][6]	✗	✓	✗	✗	✓	$g_0 + g_1$
Hu [4]	✗	✗	✓	✗	✗	g_0 [2)]

1) Following EN 1995-1-1 [2], in calculating the deflection w(1kN) the load distribution has to be considered; the method is not specified.

2) The frequency is always calculated on the bare CLT element, but there are different limit values for slabs with light topping and slabs with heavy topping (see Tab. 5).

The influence of these parameters is discussed next.

As already stated in chapter 3.1, there is a significant influence of the support conditions on the natural frequency. If the floor element is partly clamped instead of hinged supported, than higher frequencies (up to a factor of 2.26 when fully clamped on both sides) are expected and give a positive effect. Partly clamping can be the result of load from the upper floor transferred by the walls. Consequently, higher wall loads cause higher clamping. In the frame of an ongoing research project at the Competence Centre holz.bau forschungs gmbh the dependency between wall loads and degree of clamping is investigated. However, partly clamping will also have a positive effect on the deflection w(1kN).

The consideration of the shear flexibility leads to lower frequencies and higher deflections. The influence highly depends on the ratio span to depth. Disregarding of shear flexibility in common span-to-depth ratios of 15 to 30 gives a bias on the frequency in the range of 3 % to 13 %. The bias in deflection w(1kN) is between 6 % and 25 %. As the shear flexibility in CLT is of crucial importance and its consideration is already required in calculating the deflections, it is mandatory to take it also into account in the context of vibrations.

For floor elements supported at all four sides, the transverse load-carrying effect can be considered for calculation of the frequency. This raises the fundamental natural frequency. The increase highly depends on the ratio of the bending stiffnesses in longitudinal and transverse direction as well as on the aspect ratio of room width to span. For common ratios used in practice an improvement of at most 10 % can be achieved.

The ratio of bending stiffnesses and also the span influence the effective width b_F. In most methods the effective width is used for calculating the deflection w(1kN). Consideration of b_F may reduce the deflection significantly, depending on the prevailing cross section and span. Therefore, it has to be clearified if the effective width has to be taken into account when the proposed limit values are applied.

The mass influences the frequency and the vibration acceleration. A higher mass reduces the frequency (which is negative) and also the vibration acceleration (which is positive). The permanent loads have to be considered in any case, but in certain cases it is reasonable to include the quasi-permanent part of the imposed loads.

When comparing the method according to Hamm/Richter with the modified version, it becomes evident, that for the determination of the vibration acceleration different parameters are considered. There are differences concerning the generalised mass, the Fourier-coefficients and the frequency of excitation. The consequence of using different values for these parameters is shown in Fig. 7.

Tab. 5: Critical values of frequency, stiffness criterion, vibration velocity and acceleration for normal and high requirements depending on the applied method

method	$f_{1,crit}$ [Hz]		$w(1kN)_{crit}$ [mm]		v_{crit} [m/(Ns)^2]		a_{crit} [m/s^2]	
	normal	high	normal	high	normal	high	normal	high
Eurocode base document [2]	8		2.00[1)]	1.00[1)]	$v_{crit} = b^{(f_1\zeta-1)}$		-	-
Eurocode NA AT [7]	8		1.50	1.00	$v_{crit} = b^{(f_1\zeta-1)}$		not specified	
Eurocode NA AT - new proposal [1]	6	8	0.50	0.25	-	-	0.10	0.05
Hamm/Richter [9]	6	8	0.50	0.25	-	-	0.10	0.05
Hamm/Richter modified [10][6]	6	8	0.50	0.25	-	-	0.10	0.05
Hu [4]	$\frac{f_1}{w(1kN,1m)^{0.7}} \geq \begin{cases} 13.0^{2)} \\ 20.0^{3)} \end{cases}$				-	-	-	-

1) EN 1995-1-1 allows variable limit values for the stiffness criterion, but it is highly advisable to stay within the limit values

2) for bare CLT-slabs or a CLT-slabs with light topping

3) for CLT-slabs with heavy topping (> 100 kg/m^2)

5 In-situ measurements "_massive_living"

In the frame of a master thesis [11] at the Institute of Timber Engineering and Wood Technology at Graz University of Technology in-situ measurements at the building project "_massive_living" were carried out. This building project consists of two separate three-storey buildings made of CLT. Fig. 2 shows the ground plan of the buildings and the chosen CLT elements for the measurements. These elements were selected because of their different support conditions. The conditions are shown in Fig. 3. The first measurements were carried out in the construction phase 2 (BP2; CLT floor elements ready mounted) or 3 (BP3; finished CLT construction). The second measurements were done at construction phase 4 (BP4; finished floor screed, but no floor covering).

Fig. 2: Ground plan and CLT elements chosen for the measurements [11]

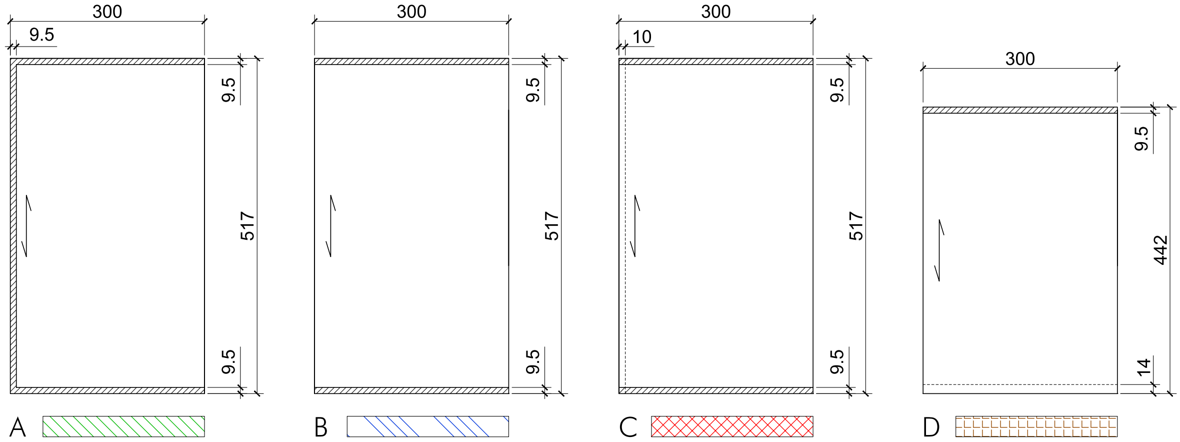

Fig. 3: Support conditions of the measured CLT elements: (A) wall support at three sides; (B) wall support at two sides; (C) wall support at two opposite sides and support on ceiling joist at the third side; (D) wall support and ceiling joist support on opposite sides [11]

Used notation:

BR1, BR2	…	building
BP2, BP3, BP4	…	construction phase
G0, G1, G2	…	floor level
W1, W2, W3, W4	…	flat
P1, P2, P3, P4, P5, P6	…	CLT element
M1, M2, M3	…	measurement position on the CLT element

5.1 1st natural frequency

At construction phase 2 and 3 the measured and calculated values according to eq. (3), considering shear flexibility ($f_{1,plate,flex}$; see Fig. 4 left) but ignoring the different support conditions (assumption of a single-span beam with hinged supports on both ends; $k_m = \pi^2$), match very well. The differences are, with one exception, below 12.5 %. The calculated values (only when the shear flexibility is considered!) lie on the safe side. The exception concerns the elements P6 of flat W4 of the second (BR1_BP3_G1_W4_P6) and also of the third floor (BR1_BP3_G2_W4_P6). Here the calculated values are 23.5 % higher than the measured ones. The reason is the flexible support by ceiling joists (see Fig. 3 support condition D). If the differences expressed as existing degrees of clamping and degrees of flexibility of the support according to Fig. 1, the values shown on the right side in Fig. 4 will be the result of that.

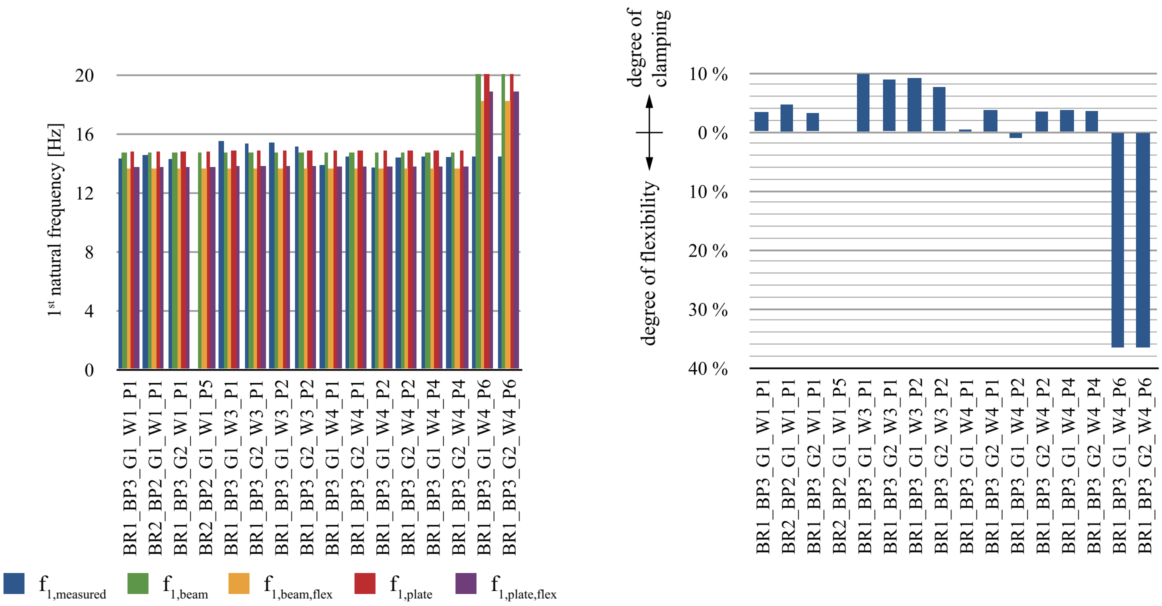

Fig. 4: Construction phase 2 and 3: measured and calculated ($k_m = \pi^2$) values of the 1st natural frequency (left); differences expressed as degrees of clamping and degrees of flexibility of the support (right)

The differences between measured and calculated frequencies at construction phase 4 are much higher and up to 150 % (see Fig. 5). However, the calculated values are always on the safe side.

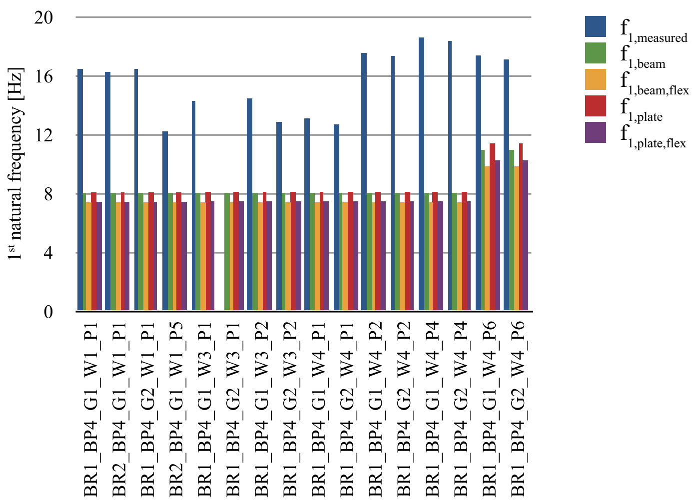

Fig. 5: Construction phase 4: measured and calculated values of the 1st natural frequency

Beside the disregarded degree of clamping several additional reasons can cause the observed significant differences, e.g.:

- The model of a one-degree-of-freedom system (mass – stiffness – damping) is not longer accurate, because the finished floor consists of a system of masses, springs and dampers acting together.
- The assumed mass is higher than the present one.
- The assumption of a hinged support is not longer accurate, because of a higher degree of clamping enforced by the higher upper floor loads transmitted through the walls.
- The influence of intermediate walls, which is not considered in the calculation, is higher than assumed.
- The intensity of the 1st natural frequency is too low for measuring.
- The heel drop could not excite the system, but rather only the floor screed.
- A superposition of vibrations/oscillations can occur and influence the measurement.

5.2 Subjective rating and limit values from design methods

The subjective rating is done according to Kreuzinger and Mohr [5].

At construction phase 2 and 3 all elements got the grade 1 with the exception of the elements of flat W4, which are supported on ceiling joists. P4 got the grade 1-2 and P6 the grade 2. At construction phase 4 all elements got grade 1.

The comparison of natural frequency and stiffness criterion of measured and calculated cases with the limit values from the different design methods are shown in Fig. 6.

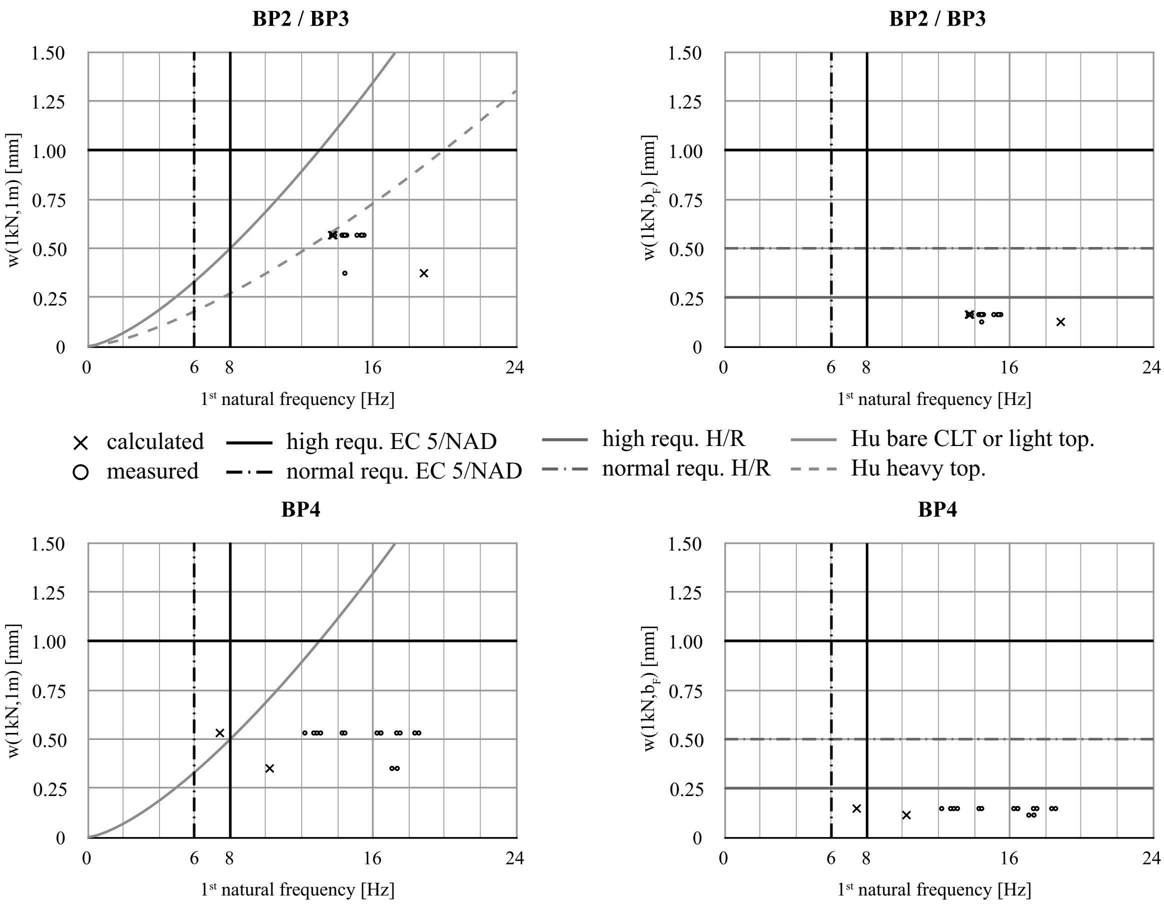

Fig. 6: Measured and calculated frequency, depending on calculated deflections w(1kN,1m) and w(1kN,b_F), in comparison with the limit values of the different design methods

It can be seen, that at construction phase 2 and 3 all cases fulfil the high requirements of all methods, although the subjective rating was 1-2 and 2 in some cases. At construction phase 4 the calculated frequencies of the elements with the span of 5.17 m are around 7.45 Hz. If high requirements are expected, the critical frequency of most methods (see Tab. 5) is 8 Hz. For frequencies below that value, the vibration acceleration has to be checked. The accelerations according to the suggestions of Hamm/Richter and the modified version are shown in Fig. 7. The application of the modified Hamm/Richter method leads to accelerations below the critical values and fulfilment of the high requirements. Applying the suggestions of Hamm/Richter on the examined floors only normal requirements are fulfilled, although the subjective rating was first class. According to Hu, the calculated cases lay near the limit curve for floors with heavy topping (see Fig. 6, top-left) or even exceed the limit curve in cases where the mass of the finish is considered in calculation and compared to the limit curve of bare CLT or light topping (see Fig. 6, bottom-left).

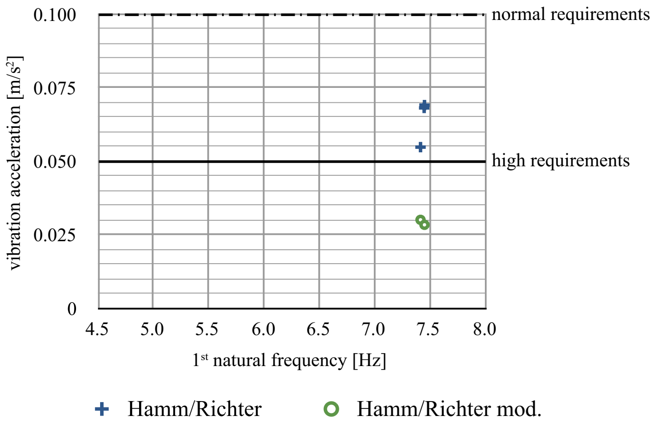

Fig. 7: Vibration acceleration for cases with frequencies below the critical frequency, calculated according to the suggestions of Hamm/Richter and the modified version

6 Evaluation of the damping ratio

In literature different values for the damping ratio of CLT floor elements can be found. In [3] (see also Tab. 2) the damping ratios of bare CLT floor elements are between 2 % and 2.5 %, in [4] the ratio is given with around 1 %. These differences are caused by applying different excitation methods.

As part of the laboratory research on dynamic behaviour of CLT floor-elements, seven five-layer CLT elements with the dimensions 8,250 mm / 800 mm / 140 mm were investigated. In the basic configuration the CLT element was simply supported at a total span of eight meters. Fig. 8 shows the modal damping ratio of the fundamental frequency (first order bending mode), which is determined with the decay curve after the excitation methods initial displacement, hammer and heeldrop.

The first two excitation methods were performed without any additional loading of the floor plate, while the heeldrop requires a person standing on the floor centre, which adds damping to the system. Another description of the results throughout the first two excitation methods can be stated as material damping, while the results of the Heeldrop are seen as a system damping (floor – person). The mean material damping of 0.5 % (coefficient of variation CoV = 10.3 %) is a result of inner friction of the material itself, while the system damping contains some additional damping of the present person, which leads to a mean damping of 4.3 % (CoV = 22.2 %) with a 5 %-fractile of 3.0 %. The system damping benefits from the low bending stiffness in comparison to the high span length, as well as from the low mass of the CLT element. Both factors raise the influence of the person on damping. Beside these facts a minimum system damping ratio of 2.5 %, as proposed in the BSPhandbuch [9], seems to be justified for vibrations of residential floors, where a person is exciting the vibration.

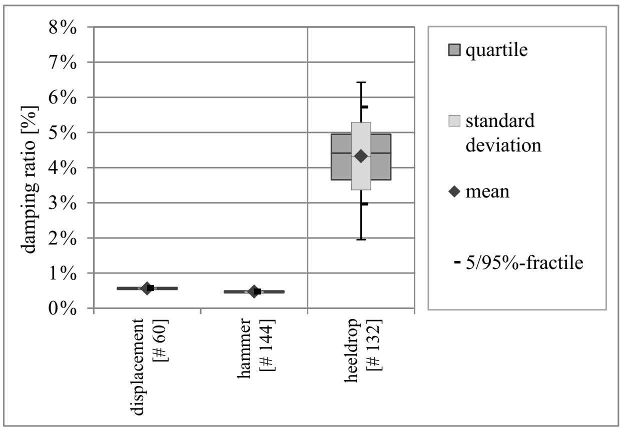

Fig. 8: First modal damping ratios of a single span beam (CLT element) obtained from different excitation methods

7 Conclusions

This paper focuses on the basic principles for the vibration design of residential floors made of cross laminated timber (CLT). A comparison of some available design methods is made as parameter study and with in-situ measurements.

Each of the methods gives significant different results. This can be explained by the limit values, which base on the highly subjective opinion of the test person. However, differences are also in the consideration of some parameters. Due to the fact that, in the context of cross laminated timber, the shear flexibility is of crucial importance and hence has to be considered already in calculating the deflections, it is highly advised to take them into account also in the context of vibrations. Another highly important aspect on vibration is seen in the influence of the support conditions, e.g. hinged, partly clamped, clamped and for example supported by a ceiling joist, and in the influence caused by the degree of clamping, e.g. in cases where upper floor loads are transmitted through the walls. Especially the support on ceiling joists has to be considered.

With regard to the comparison of calculated and measured values at the finished building, it must be said, that there are many influences, which are not considered in current design methods and therefore the calculated values are too conservative. Further and future research is needed.

8 Acknowledgement

The research work within the project 'focus_sts' is financed by the Competence Centre holz.bau forschungs gmbh and performed in collaboration with the Institute of Timber Engineering and Wood Technology of Graz University of Technology.

The project is fostered through the funds of the Federal Ministry of Economics, Family and Youth, the Federal Ministry of Transport, Innovation and Technology, the Styrian Business Promotion Agency Association and the province of Styria (A12), the Carinthian Economic Promotion Fund (KWF), the province of Lower Austria department economy, tourism and technology as well as the Business Location Tirol.

9 References

[1] Augustin M.: Personeninduzierte Schwingungen von Deckenkonstruktionen aus Holz. Manuskript erstellt für den Fachnormenausschuss FNA 012-02 des Austrian Standards Institute, Graz, 2013 (German).

[2] EN 1995-1-1:2004-11, Eurocode 5: Design of timber structures – Part 1-1: General – Common rules and rules for buildings.

[3] Fitz M.: Untersuchung des Schwingverhaltens von Deckensystemen aus Brettsperrholz (BSP). Diploma Thesis, Graz University of Technology, 2008 (German).

[4] Gagnon S., Pirvu C. (editors): CLT Handbook: cross-laminated timber. Library and Archives Canada Cataloguing in Publication, Canadian Edition 2011.

[5] Kreuzinger H., Mohr B.: Gebrauchstauglichkeit von Wohnungsdecken aus Holz. Abschlussbericht, Technische Universität München, 1999, ISBN: 3-8167-5487-2 (German).

[6] Lignum Holzwirtschaft Schweiz (editor): *Holzbau*: Bemessungsbeispiele zur Norm SIA 265. Schweiz 2003 (German).

[7] ON B 1995-1-1:2010-08, Eurocode 5: Bemessung und Konstruktion von Holzbauten – Teil 1-1: Allgemeines – Allgemeine Regeln für den Hochbau, (German).

[8] Petersen C.: Dynamik der Baukonstruktionen. Friedr. Vieweg & Sohn Verlagsgesellschaft mbH, Braunschweig / Wiesbaden, 2000 (German).

[9] Schickhofer G., Bogensperger T., Moosbrugger T. (editors): BSPhandbuch: Holz-Massivbauweise in Brettsperrholz – Nachweise auf Basis des neuen europäischen Normenkonzepts. Verlag der Technischen Universität Graz, 2010, ISBN 978-3-85125-109-8 (German).

[10] Thiel A., Schickhofer G.: Design Methods of Cross Laminated Timber concerning Floor Vibrations: A Comparability Study. Research Report, holz.bau forschungs gmbh, 2012.

[11] Zimmer S.: Ein Beitrag zur Aufarbeitung der Schwingungsthematik für die Holz-Massivbauweise in Brettsperrholz. Master Thesis, Graz University of Technology, 2013 (German).

6 CIB-W18 Notes, Vancouver, Canada 2013

Structural elements made of beech LVL **- P Kobel, L Boccadoro, A Frangi, R Steiger**

Fasteners and connections in the next Eurocode 5 **- J Munch-Andersen, S Svensson**

Structural elements made of beech LVL

Peter Kobel*
Lorenzo Boccadoro*
Prof. Dr. Andrea Frangi*
Dr. René Steiger**

*ETH Zurich, Institute of Structural Engineering IBK

**Empa, Structural Engineering Research Laboratory

1 WHY STRUCTURAL ELEMENTS MADE OF BEECH

Timber as natural resource is highly complex due to its anisotropic nature and natural inhomogeneities. The mechanical and physical properties are influenced by duration of load, moisture and temperature. As a consequence, the reliability of structural timber elements is often inadequate and the full potential of timber in the building and construction sector has not been exploited yet.

Tab. 1. Mechanical properties parallel to the grain of beech-laminated veneer lumber (LVL) with some cross veneers (Van de Kuilen 2012).

Bending strength	$f_{m,mean}$	78	N/mm^2
Tensile strength	$f_{t,0,mean}$	59	N/mm^2
Compressive strength	$f_{c,0,mean}$	46	N/mm^2
Modulus of elasticity	$E_{0,mean}$	13'800	N/mm^2

Fig. 1. Laminated veneer lumber (LVL) made of beech.

The higher strength and stiffness properties of beech wood as compared to most softwood species are well known (Kolb 1968; Ehlbeck and Colling 1985; Aydin et al. 2004; Burdurlu et al. 2007; Van de Kuilen 2012). In Switzerland and other European countries beech is available in large quantities. However, beech wood is today almost entirely used for energetic purposes or non-structural applications (e.g. in the wood furniture industry). In Switzerland, for example, almost 60% of the harvested hardwood is used directly for energetic purposes without adding value to it by considering other applications. A current research project at ETH Zurich and Empa aims at developing sustainable innovative and reliable timber structures using Laminated Veneer Lumber (LVL) made of beech wood (Fig. 1 and Tab. 1). Due to its industrialised production, reliable and high strength and stiffness properties, improved dimensional and form stability, structural elements made of beech LVL have a great potential to be "strong and reliable as steel and sustainable as wood". The project aims at developing beam-type (e.g. trusses) as well as plate-type (e.g. timber-concrete composite slabs) elements. Particular attention will be paid to the reliable characterisation of selected mechanical properties of beech LVL, the development of reliable, efficient and economic connections and the development of safe and economic design methods for elements and connections.

2 BEAM-TYPE STRUCTURAL ELEMENTS MADE OF BEECH LVL

With its large ratio between weight and strength timber in general is very suitable for large span structures. For large spans, usually truss structures are applied. However, due to the brittle behaviour of timber, the connections in timber truss structures generally become expansive and complex, which can lead to overdesigned timber members. In order to improve the performance of timber truss structures, the presented project focuses on developing more efficient connections by applying LVL made of beech. In a first step, dowel-type connections were investigated, as this is a very common type of connection for truss structures.

To provide a basis for the design of dowel-type connections using LVL made of beech, a series of 30 tensile embedment tests was carried out according to the test standard EN 383:2007, using dowel diameters of 8, 12,16, and 20 mm. Additionally, the influence of a reduced end distance l_3 was studied.

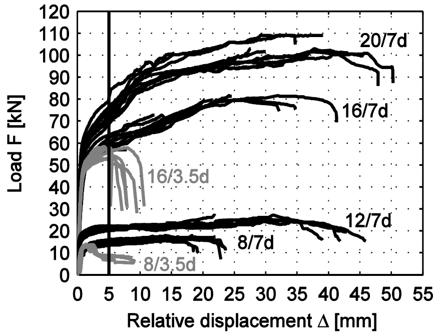

Fig. 2. Load-displacement behaviour of all conducted embedment tests. Limit displacement acc. to EN 383: Δ=5mm. Labels: (dowel diameter d)/(end distance l_3).

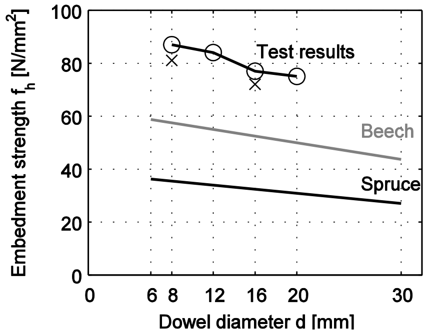

Fig. 3. Comparison of embedment test results. According to Eurocode 5: $f_{h,m}=0.082\cdot(1-0.01)\cdot\rho_m$ with ρ_m(spruce)=470kg/m^3 , ρ_m(beech)=760kg/m^3. ○: l_3= 7d; x: l_3=3.5d.

Fig. 3 shows that the mean embedment strength (f_h) values obtained in beech LVL are significantly higher compared to corresponding values for solid Norway spruce and beech timber. This confirms the advantage of beech compared to Norway spruce (as the embedment strength is a function of the timber density) and the beneficial effect of the cross-layers. Given an adequate spacing, a very ductile behaviour was observed in the embedment tests (Fig. 2), along with a very low scatter (CoV < 5%).

In current design codes (e.g. Eurocode 5) the load-carrying capacity of dowel-type connections is calculated according to the Johansen theory (Johansen 1949) and additional design criteria. The validity of these design criteria for LVL made of beech was verified in a preliminary tensile test series of eight specimens, each specimen being equipped with two connections of four dowels and two slotted-in steel plates each. Dowel diameters *d* = 20 mm (rigid dowels) and *d* = 8 mm (slender dowels) were used, and spacing according to EC 5 was applied, as well as a reduced spacing with only half the distances.

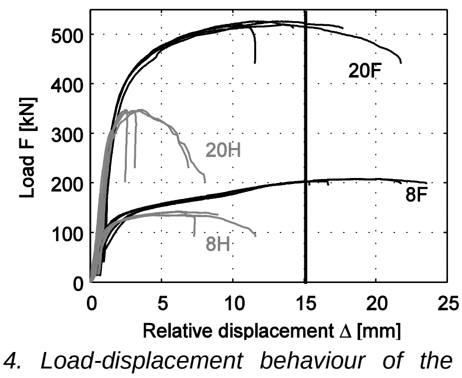

Fig. 4. Load-displacement behaviour of the tested connections.

Fig. 5. Failure modes for d=20mm. Left: full spacing; right: half spacing.

The results have shown that a notable ductility can be provided by the beech LVL material, as even connections with rigid dowels (d = 20 mm) showed a ductile overall behaviour (Fig. 4). Furthermore, the problem of premature splitting failure could be eliminated by the cross-layers, so the adequate spacing should be determined with regard to shear plug failure (Fig. 5). The observed ductile behaviour indicates that the negative group effect should be small ($n_{ef} \rightarrow n$). However, further experimental and numerical analysis has to be conducted in order to validate this hypothesis.

The experimental investigation has shown the potential for efficient connections in LVL made of beech. This, along with the high strength and stiffness values, confirms the suitability of beech LVL for high performance timber structures, such as large span trusses.

3 TIMBER-CONCRETE COMPOSITE SLABS MADE OF BEECH LVL

In recent times, the refurbishment of old buildings with timber floors has drawn attention to the timber-concrete composite slab. As a result of the several advantages over traditional timber floors, the composite structure is also used in new constructions. However, the current timber-concrete composite slab systems, which consist of spruce wood, are not competitive in comparison with traditional reinforced concrete slabs because of the cost of the timber material and the connection systems.

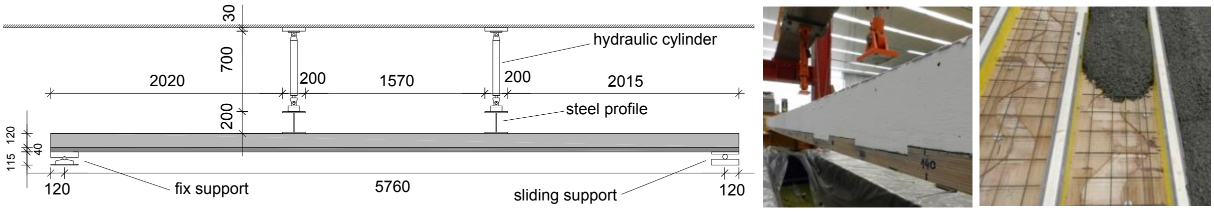

Fig. 6. Timber-concrete composite slabs made of beech-LVL: test setup (left), specimen with rectangular notches (middle), specimen with notched waves (right).

The presented work studies the structural behaviour of timber-concrete composite slabs made of beech LVL with a series of six bending tests (Fig. 6, left). This innovative composite slab concept has a slender layout and consists of a thin beech LVL plate (thickness t = 40 mm), which acts as tensile reinforcement and lost formwork, and a concrete layer (t = 120 mm). Timber and concrete are connected with notches (depth 15 mm) in the LVL plate which transmit the shear force thanks to the compressive contact between the two materials. Two types of notched shear connections were tested. One connection transfers the shear force with rectangular notches in the beech plate (Fig. 6, middle) and the other connections by means of notched waves (Fig. 6, right). No steel fasteners were used. The significantly better quality of the wood material allows a more slender layout and a reduced timber thickness in comparison to the current timber-concrete composite slab systems.

The first main difference between the connection systems is that in the specimens with rectangular notches the connection remained intact and the failure took place in the cross section (Fig. 7, left), whereas in the specimens with notched waves the failure took place in the interface area between timber and concrete and, as consequence, the load carrying capacity was smaller (Fig. 7, right). The influence of the opening of the gap was analysed during two additional bending tests with reinforcement: if the opening is completely avoided, the failure load increases by 25%. Furthermore, the rectangular notches show a very stiff behaviour which corresponds to the trend of several research works (e.g. Frangi and Fontana 2000). A satisfying aspect of the results of the bending tests is the load carrying capacity. The highest load carrying capacity was measured in the specimens with rectangular notches (maximal force per cylinder of 55 kN ≈ 34 kN/m^2).

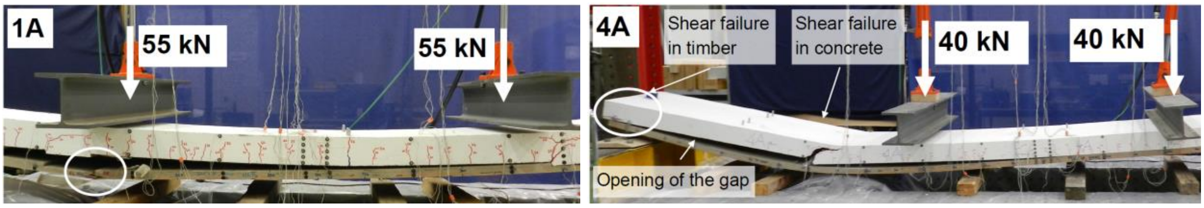

Fig. 7. Failure modes: combined bending and tensile failure in the beech LVL plate of a specimen with rectangular notches (left); horizontal shear failure in timber close to the support and opening of the gap in a specimen with notched wave connection (right).

The basic idea of the notched wave is a more homogeneous and continuous transmission of shear force, however the geometry of the notches has to be optimised to avoid brittle shear failures in the connection and vertical gap opening between timber and concrete. Analytical calculations and numerical simulations will give the basis to model the structural behaviour and to develop an optimised form of the notched connection, in order to be able to exploit the potential of beech LVL as tensile reinforcement.

4 LITERATURE

1. Aydin, I., Colak, S., Colakoglu, G., Salih, E. (2004). “A comparative study on some physical and mechanical properties of laminated veneer lumber (LVL) produced from Beech (Fagus orientalis Lipsky) and Eukalyptus (eucalyptus camalduleius Dehn.) veneers”, *Holz Roh Werkst*, **62**, 218–220.
2. Burdurlu, E., Kilic, M., Ilce, A. C., Uzunkavak, O. (2007). “The effects of ply organisation and loading direction on bending strength and modulus of elasticity in laminated veneer lumber (LVL) obtained from beech and Lombardy poplar”, *Construction and building materials*, **21**(8), 1720–1725.
3. DIN EN 1995-1-1:2010-12. “Eurocode 5: Design of timber structures - Part 1-1: General - Common rules and rules for buildings”. DIN German Institute for Standardization.
4. DIN EN 383:2007. “Timber Structures - Test methods - Determination of embedment strength and foundation values for dowel type fasteners”. DIN German Institute for Standardization.
5. Ehlbeck, J., Colling, F. (1985). “Scherfestigkeit rechtwinklig zur Plattenebene und Schubmodul von Bau-Furniersperrholz aus Buche”, *Holz Roh Werkst*, **43**(4), 143–147
6. Frangi, A., and Fontana, M. (2000). “Experimental tests on timber-concrete composite slabs at room temperature and under ISO-fire exposure.” *Rep. No. 249,* Institute of Structural Engineering, ETH Zurich, Switzerland (in German).
7. Gehri, E. (1993). “Holzwerkstoffe auf Furnierbasis.” Das Grafik Werk, Zurich, Switzerland.
8. Johansen, K. W. (1949). “Theory of Timber Connections”. IABSE, Publication No. 9, Bern, Switzerland, pp. 56-69.
9. Kolb, H. (1968). “Biegeversuche und Prüfung des Brandverhaltens an Trägern aus verleimten Buchenschälfurnieren.” *Holz Roh Werkst*, **26**(8), 277–283.
10. Krackler, V., Keunecke, D., Niemz, P (2010). “Verarbeitung und Verwendungsmöglichkeiten von Laubholz und Laubholzresten.” Institute of Building Materials, ETH Zurich, Switzerland.
11. Krackler, V., Niemz, P. (2011). “Schwierigkeiten und Chancen in der Laubholzverarbeitung, Teil 1”, *Holztechnologie*, **52**(2), 5–11.
12. Van de Kuilen, J. W. (2012). “Ergebnisse der Zulassungsversuche für eine allgemeine bauaufsichtliche Zulassung von Furnierschichtholz aus Buche”, Prüfbericht, Technische Universität München, Germany.

Fasteners and connections in the next Eurocode 5

Jørgen Munch-Andersen, Danish Timber Information

Staffan Svensson, Dept. of Civil Eng., Technical University of Denmark

Introduction

The present Eurocode for timber, EC5, requires testing for most combinations of fasteners and timber material. Only the most traditional combinations are fully covered. Further, many rules and limitations are inconsistent and non-physical. There is therefore a strong need to improve the code, which requires a coordinated action in order to identify the existing knowledge and acquire the missing information. An idea to link new experimental research together is presented.

Vision for new code

1. Transparent and comprehensive design criteria together with accurate design equations for the load-carrying capacities of all common steel fasteners in all relevant timber materials, including engineered products like LVL, timber panels etc. The equations should be based on geometry, steel strength and perhaps density as far as possible.
2. Simple and flexible methods to determine the load-carrying capacity of a group of fasteners. The methods might be based on a necessary timber area per fastener for full capacity and a reduction if the area is smaller.

Both statements apply to axial load as well as lateral load.

Benefits of better code

There are numerous benefits of a new code fulfilling the vision for industry, contractors and designers:

- Similar products will have same load-carrying capacity
- The design engineer can specify fasteners independent on which brand of fasteners the contractor will use
- The contractor can use the product he prefers and still satisfy the engineer's design requirements
- Straight forward design procedures will positively contribute to the competiveness of timber on the construction market
- Manufactures of fasteners and timber materials will, in contrary to the present case, only as exceptions and for very special cases need to conduct type testing (ITT's)
- Accurate design equations will increase safety and in many cases also the load-carrying capacity of connections

Shortcomings of present EC 5

Present rules in Eurocode 5 are not comprehensive, accurate or transparent. The following examples illustrate the need for improvement.

EC5 is not comprehensive since the design equations mainly cover old fashioned fasteners like smooth nails, lag screws and bolts in structural timber and glulam. Almost all other combinations of fasteners and timber materials requires type testing to determine a number of parameters for the actual fastener product applied to the specific timber product.

Further, the requirement to European certification (CE-marking) of fasteners - and thereby the type testing results available in practice - focus on structural timber. This is obviously not satisfying when engineered wood products are widely used.

Various geometrical minimum requirements cause the load-carrying capacity to vanish completely when the requirement are not met. This causes problems, especially when the laws of physics are violated and hence 'engineering judgment' cannot be applied.

EC5 is not accurate regarding the load-bearing capacity, especially for laterally loaded fasteners. The so-called European Yield Model used to estimate the capacity underestimates in many cases the capacity significantly when compared to test results.

The present and very old criteria for minimum spacing of fasteners and edge distances are solely based on the diameter of the fastener. They were presumably conservative for the fasteners they were developed for, but the increased capacity of modern fasteners is only accounted for in some supplementary rules adding row-effects and plug shear failure. Further, the old criteria suffer from discontinuities.

EC5 is not transparent and treats various types of fasteners quite differently, e.g. nails and screws. The missing transparency, accompanied by inaccuracy, is very obvious for screws since small screws are treated as nails and larger screws as lag screws. Very significant discontinuities appear when the limit between small and large screws is crossed, which makes it obvious that at least some equations are very inaccurate. The combination of discontinuities and unclear rules, which in some cases violates fundamental laws of physics, is most discouraging when designing timber structures.

Research need

In order to fill in the gaps the existing knowledge should be collected and supplemented by new experimental work. It can be foreseen that the need for new work is huge if the vision should be met. However, if the experimental work is planned and coordinated carefully the outcome can be enhanced very significantly.

The most valuable experiments are those where a number of parameters have been varied in a systematic way such that the influence of these parameters can be deduced. With adequate planning and systematic variation of parameters proper statistical treatment of data is possible with very few repetitions when many parameters dealt with in the same test series.

The principles for determining characteristic values given in the Eurocode for safety (EC 0) can be used. It is possible to take advantage of the fact that there are many degrees of freedom available for estimating the global coefficient of variation when many parameters are combined, even without repetitions, see Munch-Andersen et al (2010). It is easy to handle both incomplete data sets and data with a bias, e.g. due to the timber material.

Linking experimental research

The great variability of timber and engineered products make it almost impossible to repeat tests at a later time or in another place and get the same results. Reliable design equations should therefore in principle be based on results from similar tests repeated independently numerous times in various places.

This is not a realistic way to fill in all the gaps, so a mean identify the timber properties is needed. A simple method that makes it easy to compare tests from different laboratories etc. will be to , parallel to the planed test, also conduct tests with reference fasteners.

In Denmark there was recently chosen two reference fasteners, a 3.1 x 90 mm profiled nail and a 4.5 x 80 mm screw with raised thread, see Figure 1. The idea is that testing laboratories should include some tests with the reference fasteners parallel with ordinary test in all experiment with timber and/or engineered wood products connections. It could be any type of test e.g. simple tests for embedment strength, withdrawal strength, pull-through strength and lateral capacity carried out with the reference fasteners and the fasteners used in the individual project at the same time and using the timber material investigated. The results will tell something about both the timber material and the fasteners which cannot be expressed by measurable properties as density and moisture content.

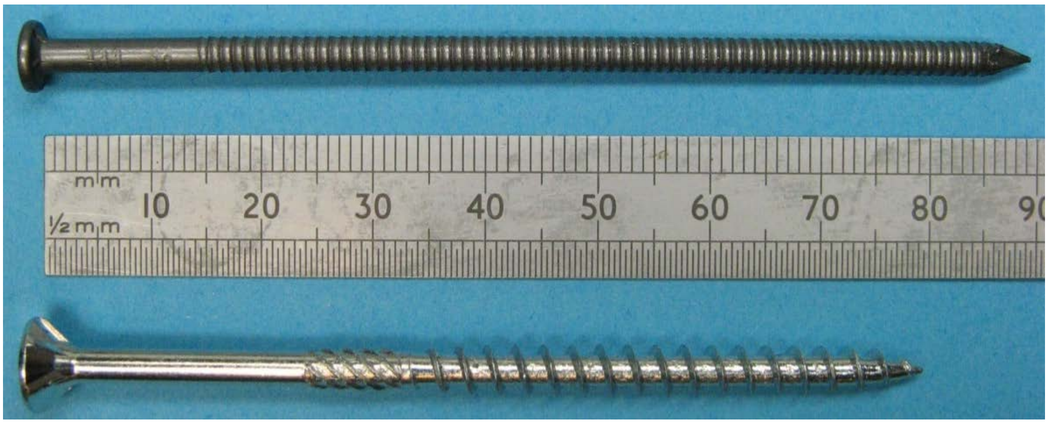

Figure 1. Reference fasteners, top 3.1 x 90 mm profiled nail and bottom 4.5 x 80 mm raised thread screw.

The intention and hope are that other research institutions will understand the meaning and advantage with a set of reference fasteners and therefore use them. We will be happy to send you a sample (nss@byg.dtu.dk) and hope to receive a copy of your report. It could be expanded to a real Round Robin test if a reference timber material could also be supplied.

Acknowledgement

A fairly large amount of reference fasteners supplied by ITW Construction Products is considered utterly important for this work and appreciated.

References

[1] Munch-Andersen, J, Sørensen, J D & Sørensen, F: Estimation of load-bearing capacity of timber connections. Proc. of CIB-W18 Timber Structures (Paper 43-21-1). Nelson, New Zealand. 2010.